VEGF IMMOBILIZATION AND

VEGFR2 TRAFFICKING AND PHOSPHORYLATION:

IN VITRO AND *IN VIVO* IMPLICATIONS

by

Lindsay Clegg

A dissertation submitted to Johns Hopkins University in conformity with the

requirements for the degree of Doctor of Philosophy

Baltimore, Maryland

June, 2017

Abstract

Modern drug development is marked by high failure rates in translation to the clinic. Further, many drugs that succeed in clinical trials work for only a fraction of patients. Systems pharmacology attempts to address these challenges by improving our understanding of the disease-therapy system, integrating detailed molecular interactions, cellular signaling, tissue architecture, and whole body physiology. I built cutting-edge, molecularly-detailed, multi-scale computational models to study the effects of immobilization of growth factors on signaling in angiogenesis, focusing in particular on the binding of vascular endothelial growth factor (VEGF) family members to the ECM. While most studies of VEGF signaling use only VEGF presented in solution, there is evidence that a large potion of VEGF may be ECM-bound *in vivo*, and relative expression of isoforms binding to ECM vs. found only in solution varies by tissue and changes in disease, motivating further study of this question. Starting at the *in vitro* level, we showed that differential signaling of VEGF-receptor 2 (VEGFR2) in response to soluble vs. immobilized VEGF can be explained by reduced internalization of ECM-VEGF-VEGFR2 complexes. Moving *in vivo*, we predicted differences in both growth factor distribution and receptor activation by VEGF family ligands, as a function of their ECM-binding properties. These predictions are consistent with observed vascular phenotypes in mice expressing single VEGF isoforms. Next, we explored how VEGF splicing changes in peripheral artery disease lead to impaired angiogenic responses to ischemia. Our model showed that the $VEGF_{165b}$ isoform, which does not bind to ECM or to the coreceptor NRP1, is a weak activator of VEGFR2 *in vivo*, and competes for binding to VEGF-receptor 1, but not VEGF-receptor 2. Finally, we used this model to screen potential therapeutic strategies designed to promote VEGF-mediated revascularization in ischemic disease and tissue engineering applications. Within a single system, we compared failed and promising biomaterial-based VEGF delivery systems, antibody-based therapeutics, and gene therapy strategies to identify key rules for design, optimization, and translation of these pro-angiogenic therapies.

Thesis Advisor: Feilim Mac Gabhann, PhD

Second Thesis Reader: Hai-Quan Mao, PhD

Additional Committee Members: Kalina Hristova, PhD & Brian Annex, MD (University of Virginia)

Acknowledgments

It simply isn't possible to make it through a 6-year PhD journey without having far more people to thank than can be acknowledged in a brief note tucked into the front matter of a thesis. That said, I would be incredibly amiss if I didn't do my best to briefly yet sincerely thank all of those that have a claim in this accomplishment, whether they are passionate about VEGF or not!

I have to start with most heartfelt thanks to my advisor, Feilim, who has seen every up and down along the way, and provided so much thoughtful, meaningful, and constructive guidance during my time at Johns Hopkins. I would not have had near as productive or enjoyable a time with any other advisor, and I would not have grown near as much as a scientist, a communicator, and a person (and a maker of aesthetically pleasing plots, and a frequent user of semi-colons…) without him. Feilim provided so much support and guidance, but also let me undertake many more far-fetched side-schemes (and teaching!) along the way than any normal advisor would have. He gave me the resources and connected me with the people I needed to work past roadblocks, and let me explore wherever the science ended up taking me, even if that wasn't quite the direction I meant to go when I set out… So, many, many sincere thanks. I assure you that this won't be the last you see of me!

The friendly, supportive, and Christmas-decorating culture of the Mac Gabhann lab has made this a great home for the last six years. Thank you to all of those who have helped to make it such a wonderful environment, and for all the questions on one topic or another you've helped with over the years- Liz, Yas, Iraj, Laura, and Joe. To the current lab members (Sarvenaz, Inez, Christy), thanks for listening to my VEGF spiel so many times, and for happily continuing to make the lab a wonderful place − I have no doubts that the lab community and science will only keep getting better! A special thanks to Sarvenaz (and Feilim), who spent many hours showing a computational modeler how to navigate a wet lab. Thanks also to several undergrads and high schools students who have left their marks on this project over the years: Luis Milburn did some of the earliest work on finding useful ways to visualize complicated model outputs, Amanda Bertsch worked on a mouse version of this giant model, and Seleste Villalon was a great sport about running my wet lab experiments while I disappeared off to Gaithersburg for the summer.

Many thanks as well to my wonderful committee members: Brian Annex, Hai-Quan Mao, and Kalina Hristova, for their unique and valuable expertise, which has helped to make this work more accurate

Table of Contents

List of Tables

List of Figures

Section I: Background & Motivation

Chapter 1. Introduction

Modern drug development is marked by high failure rates in translation to the clinic [1, 2]. Further, many approved drugs work for only a fraction of patients. Using systems pharmacology, we aim to incorporate decades of hard-won prior knowledge of molecular interactions, cellular signaling, and cellular behavior into the context of human physiology and pharmacology to improve understanding of human ischemic disease and facilitate design, optimization, and translation of growth factor-based therapies in regenerative medicine applications.

Angiogenesis, the growth of new blood vessels from the existing vasculature, is critical for maintenance of health and response to injury. In ischemic disease, this process is impaired, but therapies targeting vascular endothelial growth factor (VEGF) have failed to translate clinically [3], despite success in animal models. This failure highlights the need for more mechanistic understanding to design a next generation of more effective therapies [4, 5]. Engineering of thick (>1-2mm) tissues also requires growth of a functional, hierarchical vascular network, a challenge that has not yet been effectively addressed [6].

Angiogenesis is regulated by expression of the splice isoforms of VEGF, which have different affinities for the extracellular matrix (ECM) and the co-receptor Neuropilin-1 (NRP1). These differences lead to distinct vascular phenotypes in mice expressing a single VEGF isoform; non-ECM-binding isoforms lead to signaling that promotes cell proliferation, while strong ECM-binding promotes migration and branching [7]. *In vitro*, VEGF immobilization (e.g. to ECM proteins) alters VEGF receptor-2 (VEGFR2) signaling, increasing phosphorylation on tyrosine 1214 more than on Y1175 [8, 9], but the connection between this signaling change and the phenotypes observed *in vivo* had not been elucidated. Understanding this signaling is key to identify the role of VEGF splicing changes in diseases such as peripheral artery disease (PAD), and to design biomaterials with tunable VEGF delivery that induce formation of functional, perfused vascular networks in native tissue and engineering tissue constructs.

PAD is characterized by insufficient angiogenesis in response to ischemia in the limbs [10]. Intriguingly, VEGF levels are normal or elevated in PAD patients [11, 12], and multiple clinical trials targeting VEGF delivery for PAD have failed [3]. However, VEGF splicing changes in PAD; $VEGF_{165a}$ protein is reduced, while expression of $VEGF_{165b}$ is increased [11, 13]. Unlike $VEGF_{165a}$, $VEGF_{165b}$ does not bind to the ECM or NRP1, and is a weak inducer of VEGFR2 phosphorylation and angiogenesis [14-

16], motivating study of VEGF$_{165b}$ as a potential therapeutic target. The prevailing hypothesis is that VEGF$_{165b}$ competes with VEGF$_{165a}$ for binding to VEGFR2, reducing VEGFR2 phosphorylation [11]. This hypothesis is supported by *in vitro* observations [14-16], but is challenging to test *in vivo*. Here, we leverage our modeling framework to overcome this barrier, bridging from *in vitro* observations to *in vivo* signaling to provide insight into these difficult-to-measure quantities in diseased human tissue.

In this thesis, I describe the first computational model to capture differences in signaling by VEGFR2 bound to ECM-binding and non-ECM binding VEGF isoforms *in vitro* and *in vivo*, accounting for VEGF-ECM binding, regulation of VEGFR2 trafficking by NRP1, and changes in proliferative vs. migratory signaling of VEGFR2 as a function of receptor trafficking and ligand immobilization. By understanding the underlying biological complexity across multiple scales, we can overcome the challenge of translating pro-angiogenic therapies for ischemic disease, as well as biomaterials and engineered tissues, into the clinic. Specifically, incorporation of this mechanistic detail enabled the model to capture VEGF isoform-specific changes in signaling *in vivo*, elucidate splicing-induced changes in VEGF signaling in peripheral artery disease, and provide novel quantitative insight into design of both biomaterial- and antibody-based pro-angiogenic therapies targeting the VEGF system.

My overall research objective was to build multi-scale mechanistic computational models of growth factor-ECM interactions; these models are firmly grounded on and validated against experimental data. I used two differential equation-based modeling approaches to bridge from molecular mechanism to therapy design:

(1) cell-level models of molecular interactions and signaling built on and validated against multiple types of *in vitro* data (Chapter 5); and

(2) whole body pharmacological models that examine growth factor distribution in the human body, incorporate detailed signaling based on (1), and serve as a platform to study the impact of patient variability on therapy response (Chapters 6-8).

First, in Chapters 2-4, I will discuss blood vessel physiology and pathology, therapeutic angiogenesis, and the role of computational models in drug development, to place this work in context. Then, in Chapters 5-9 I will discuss the development and application of these computational models.

1.1 A Note on Published Work

Content from the following chapters has been peer-reviewed and published, and is included with permission:

Chapter 2: Systems Biology of the Microvasculature, as L. E. Clegg & F. Mac Gabhann, "Systems Biology of the Microvasculature," *Integrative Biology*, vol. 7, pp. 498-512, Mar. 2015. DOI: 10.1039/C4IB00296B.

Chapter 3. Therapeutic Angiogenesis: The Role of Growth Factors and Extracellular Matrix, as P. S. Briquez*, L. E. Clegg*, M. M. Martino*, F. Mac Gabhann, & J. A. Hubbell, "Design principles for therapeutic angiogenic materials," *Nature Reviews Materials*, vol. 1, January 2016. DOI: 10.1038/natrevmats.2015.6. http://palgrave.nature.com/articles/natrevmats20156

Chapter 4. Computational Modeling in Therapy Design and Translation, as L. E. Clegg & F. Mac Gabhann, "Molecular mechanism matters: Benefits of mechanistic computational models for drug development," *Pharmacological Research*, vol. 99, pp. 149-154, June 2015. DOI: 10.1016/j.phrs.2015.06.002.

Chapter 5. Modeling Molecular Mechanism: Signaling by Soluble vs. Immobilized VEGF *in vitro*, as L. W. Clegg & F. Mac Gabhann, "Site-specific phosphorylation of VEGFR2 is mediated by receptor trafficking: insights from a computational model," *PLoS Computational Biology*, vol. 11, no 6, pp. e1004158, June 2015. DOI: 10.1371/journal.pcbi.1004158. PMCID: PMC4466579. http://journals.plos.org/ploscompbiol/article?id=10.1371/journal.pcbi.1004158

Chapter 6. VEGF Isoform Distribution and Signaling in Healthy Humans, as L. Clegg & F. Mac Gabhann, "A Computational Analysis of *in vivo* VEGFR Activation by Multiple Co-Expressed Ligands," *PLoS Computational Biology*, vol. 13, no 3, pp. e1005445, March 2017. DOI: 10.1371/journal.pcbi.1005445. https://doi.org/10.1371/journal.pcbi.1005445.

Content from the following chapters will be submitted for publication:

Chapter 7. The Role of VEGF Splicing in Human Peripheral Artery Disease, as L. E. Clegg, V. C. Ganta, B. H. Annex, & F. Mac Gabhann, "Systems pharmacology of VEGF165b in peripheral artery disease."

Chapter 8. A Computational Analysis of Pro-angiogenic Therapies, as L. E. Clegg & F. Mac Gabhann, "A computational analysis of pro-angiogenic therapies for peripheral artery disease."

1.2 References

1.   Scannell JW, Blanckley A, Boldon H, Warrington B. Diagnosing the decline in pharmaceutical R&D efficiency. Nature Reviews Drug Discovery. 2012;11(3):191-200. doi: 10.1038/nrd3681. PubMed PMID: WOS:000300940200021.

2.   Clegg LE, Mac Gabhann F. Molecular mechanism matters: Benefits of mechanistic computational models for drug development. Pharmacological Research. 2015;99(0):149-54. doi: http://dx.doi.org/10.1016/j.phrs.2015.06.002.

3.   Grochot-Przeczek A, Dulak J, Jozkowicz A. Therapeutic angiogenesis for revascularization in peripheral artery disease. Gene. 2013;525(2):220-8. doi: 10.1016/j.gene.2013.03.097. PubMed PMID: WOS:000322416200014.

4.   Clegg LE, Mac Gabhann F. Systems biology of the microvasculature. Integrative Biology. 2015. doi: 10.1039/C4IB00296B.

5.   Mac Gabhann F, Qutub AA, Annex BH, Popel AS. Systems biology of pro-angiogenic therapies targeting the VEGF system. Wiley Interdisciplinary Reviews-Systems Biology and Medicine. 2010;2(6):694-707. doi: 10.1002/wsbm.92. PubMed PMID: WOS:000283713500006.

6.   Briquez PS, Clegg LE, Martino MM, Gabhann FM, Hubbell JA. Design principles for therapeutic angiogenic materials. Nature Reviews Materials. 2016;1:15006. doi: 10.1038/natrevmats.2015.6.

7.   Vempati P, Popel AS, Mac Gabhann F. Extracellular regulation of VEGF: Isoforms, proteolysis, and vascular patterning. Cytokine & Growth Factor Reviews. 2014;25(1):1-19. doi: http://dx.doi.org/10.1016/j.cytogfr.2013.11.002.

8.   Anderson SM, Shergill B, Barry ZT, Manousiouthakis E, Chen TT, Botvinick E, et al. VEGF internalization is not required for VEGFR-2 phosphorylation in bioengineered surfaces with covalently linked VEGF. Integrative Biology. 2011;3(9):887-96. doi: 10.1039/c1ib00037c. PubMed PMID: WOS:000294448600002.

9.   Chen TT, Luque A, Lee S, Anderson SM, Segura T, Iruela-Arispe ML. Anchorage of VEGF to the extracellular matrix conveys differential signaling responses to endothelial cells. Journal of Cell Biology. 2010;188(4):595-609. doi: Doi 10.1083/Jcb.200906044. PubMed PMID: ISI:000274723800016.

10.   Annex BH. Therapeutic angiogenesis for critical limb ischaemia. Nature Reviews Cardiology. 2013;10(7):387-96. doi: 10.1038/nrcardio.2013.70. PubMed PMID: WOS:000320763800006.

11.   Kikuchi R, Nakamura K, MacLauchlan S, Doan Thi-Minh N, Shimizu I, Fuster JJ, et al. An antiangiogenic isoform of VEGF-A contributes to impaired vascularization in peripheral artery disease. Nature Medicine. 2014;20(12):1464-71. doi: 10.1038/nm.3703. PubMed PMID: WOS:000345817900023.

12.   Hoier B, Walker M, Passos M, Walker PJ, Green A, Bangsbo J, et al. Angiogenic response to passive movement and active exercise in individuals with peripheral arterial disease. Journal of Applied Physiology. 2013;115(12):1777-87. doi: 10.1152/japplphysiol.00979.2013. PubMed PMID: WOS:000328847900006.

13.   Ganta VC, Choi M, Kutateladze A, Annex BH. VEGF165b Modulates Endothelial VEGFR1-STAT3 Signaling Pathway and Angiogenesis in Human and Experimental Peripheral Arterial Disease. Circulation Research. 2016.

14.   Suarez SC, Pieren M, Cariolato L, Arn S, Hoffmann U, Bogucki A, et al. A VEGF-A splice variant defective for heparan sulfate and neuropilin-1 binding shows attenuated signaling through VEGFR-2. Cellular and Molecular Life Sciences. 2006;63(17):2067-77. doi: 10.1007/s00018-006-6254-9. PubMed PMID: WOS:000240377300012.

15.   Kawamura H, Li X, Harper SJ, Bates DO, Claesson-Welsh L. Vascular endothelial growth factor (VEGF)-A165b is a weak in vitro agonist for VEGF receptor-2 due to lack of coreceptor binding and deficient regulation of kinase activity. Cancer Research. 2008;68(12):4683-92. doi: 10.1158/0008-5472.can-07-6577. PubMed PMID: WOS:000256855700026.

16.   Delcombel R, Janssen L, Vassy R, Gammons M, Haddad O, Richard B, et al. New prospects in the roles of the C-terminal domains of VEGF-A and their cooperation for ligand binding, cellular signaling and vessels formation. Angiogenesis. 2013;16(2):353-71. doi: 10.1007/s10456-012-9320-y. PubMed PMID: WOS:000316199200007.

17.   Tan WH, Popel AS, Mac Gabhann F. Computational model of VEGFR2 pathway to ERK activation and modulation through receptor trafficking. Cellular Signalling. 2013;25(12):2496-510. doi: 10.1016/j.cellsig.2013.08.015. PubMed PMID: MEDLINE:23993967.

18.   Wan Hua T, Popel AS, Mac Gabhann F. Computational Model of Gab1/2-Dependent VEGFR2 Pathway to Akt Activation. Plos One. 2013;8(6). doi: 10.1371/journal.pone.0067438. PubMed PMID: WOS:000320846500140.

19.   Wu FTH, Stefanini MO, Gabhann FM, Popel AS. A Compartment Model of VEGF Distribution in Humans in the Presence of Soluble VEGF Receptor-1 Acting as a Ligand Trap. Plos One. 2009;4(4). doi: 10.1371/journal.pone.0005108. PubMed PMID: WOS:000265505700013.

20.   Wu FT, Stefanini MO, Mac Gabhann F, Kontos CD, Annex BH, Popel AS. VEGF and soluble VEGF receptor-1 (sFlt-1) distributions in peripheral arterial disease: an in silico model. Am J Physiol Heart Circ Physiol. 2010;298(6):H2174-91. Epub 2010/04/13. doi: ajpheart.00365.2009 [pii]10.1152/ajpheart.00365.2009. PubMed PMID: 20382861; PubMed Central PMCID: PMC2886617.

21.   Clegg LW, Mac Gabhann F. Site-Specific Phosphorylation of VEGFR2 Is Mediated by Receptor Trafficking: Insights from a Computational Model. PLoS Comput Biol. 2015;11(6):e1004158. doi: 10.1371/journal.pcbi.1004158.

22.   Ballmer-Hofer K, Andersson AE, Ratcliffe LE, Berger P. Neuropilin-1 promotes VEGFR-2 trafficking through Rab11 vesicles thereby specifying signal output. Blood. 2011;118(3). doi: 10.1182/blood-2011-01-328773. PubMed PMID: WOS:000292967300045.

23.   Mellberg S, Dimberg A, Bahram F, Hayashi M, Rennel E, Ameur A, et al. Transcriptional profiling reveals a critical role for tyrosine phosphatase VE-PTP in regulation of VEGFR2 activity and endothelial cell morphogenesis. Faseb Journal. 2009;23(5). doi: 10.1096/fj.08-123810. PubMed PMID: WOS:000266651700025.

24.   Mattila E, Auvinen K, Salmi M, Ivaska J. The protein tyrosine phosphatase TCPTP controls VEGFR2 signalling. Journal of Cell Science. 2008;121(21):3570-80. doi: 10.1242/jcs.031898. PubMed PMID: WOS:000260266700010.

25.   Anderson SM, Siegman SN, Segura T. The effect of vascular endothelial growth factor (VEGF) presentation within fibrin matrices on endothelial cell branching. Biomaterials. 2011;32(30):7432-43. doi: 10.1016/j.biomaterials.2011.06.027. PubMed PMID: WOS:000294829300015.

26.   Martino MM, Tortelli F, Mochizuki M, Traub S, Ben-David D, Kuhn GA, et al. Engineering the Growth Factor Microenvironment with Fibronectin Domains to Promote Wound and Bone Tissue Healing.

Science Translational Medicine. 2011;3(100). doi: 10.1126/scitranslmed.3002614. PubMed PMID: WOS:000294841400004.

27.   Clegg LE, Mac Gabhann F. A Computational Analysis of *in vivo* VEGFR Activation by Multiple Co-Expressed Ligands. in review.

28.   Ngo DTM, Farb MG, Kikuchi R, Karki S, Tiwari S, Bigornia SJ, et al. Antiangiogenic Actions of Vascular Endothelial Growth Factor-A(165)b, an Inhibitory Isoform of Vascular Endothelial Growth Factor-A, in Human Obesity. Circulation. 2014;130(13):1072-80. doi: 10.1161/circulationaha.113.008171. PubMed PMID: WOS:000342685100012.

29.   Martino MM, Briquez PS, Güç E, Tortelli F, Kilarski WW, Metzger S, et al. Growth Factors Engineered for Super-Affinity to the Extracellular Matrix Enhance Tissue Healing. Science. 2014;343(6173):885-8. doi: 10.1126/science.1247663.

30.   Sacchi V, Mittermayr R, Hartinger J, Martino MM, Lorentz KM, Wolbank S, et al. Long-lasting fibrin matrices ensure stable and functional angiogenesis by highly tunable, sustained delivery of recombinant VEGF(164). Proceedings of the National Academy of Sciences of the United States of America. 2014;111(19):6952-7. doi: 10.1073/pnas.1404605111. PubMed PMID: WOS:000335798000054.

31.   Ozawa CR, Banfi A, Glazer NL, Thurston G, Springer ML, Kraft PE, et al. Microenvironmental VEGF concentration, not total dose, determines a threshold between normal and aberrant angiogenesis. Journal of Clinical Investigation. 2004;113(4):516-27. doi: 10.1172/jci200418420. PubMed PMID: WOS:000189008000007.

32.   von Degenfeld G, Banfi A, Springer ML, Wagner RA, Jacobi J, Ozawa CR, et al. Microenvironmental VEGF distribution is critical for stable and functional vessel growth in ischemia. Faseb Journal. 2006;20(14):2657-+. doi: 10.1096/fj.06-6568fje. PubMed PMID: WOS:000242490700056.

33.   Salmeron-Sanchez M, Dalby MJ. Synergistic growth factor microenvironments. Chemical Communications.   2016;52(91):13327-36.   doi: 10.1039/c6cc06888j.   PubMed   PMID: WOS:000388102800002.

Chapter 2: Systems Biology of the Microvasculature

2.0 Summary

The vascular network carries blood throughout the body, delivering oxygen to tissues and providing a pathway for communication between distant organs. The network is hierarchical and structured, but also dynamic, especially at the smaller scales. Remodeling of the microvasculature occurs in response to local changes in oxygen, gene expression, cell-cell communication, and chemical and mechanical stimuli from the microenvironment. These local changes occur as a result of physiological processes such as growth and exercise, as well as acute and chronic diseases including stroke, cancer, and diabetes, and pharmacological intervention. While the vasculature is an important therapeutic target in many diseases, drugs designed to inhibit vascular growth have achieved only limited success, and no drug has yet been approved to promote therapeutic vascular remodeling. This highlights the challenges involved in identifying appropriate therapeutic targets in a system as complex as the vasculature. Systems biology approaches provide a means to bridge current understanding of the vascular system, from detailed signaling dynamics measured *in vitro* and pre-clinical animal models of vascular disease, to a more complete picture of vascular regulation *in vivo*. This will translate to an improved ability to identify multi-component biomarkers for diagnosis, prognosis, and monitoring of therapy that are easy to measure *in vivo*, as well as better drug targets for specific disease states. In this review, we summarize systems biology approaches that have advanced our understanding of vascular function and dysfunction *in vivo*, with a focus on computational modeling.

2.1 Introduction

2.1.1 Motivation for a Systems Approach to the Vasculature

Systems biology is an integrative approach that synthesizes our current understanding of molecular, physiological and pathological mechanisms to reconcile experimental data from multiple perturbations with the predictions of detailed computational models. By integrating detailed experimental data (e.g. from hi-throughput experiments) with mechanistic information (e.g. from multi-scale computational models and bioinformatics), we can formulate a more complete understanding of a system across multiple scales and at higher spatial and temporal resolution than would otherwise be possible. In addition, modeling the interconnectedness of the system from gene to protein to pathway, and from cell to tissue to organism, allows systems biology simulations to predict the system-wide response to perturbation, for example the change in blood supply to a tumor following delivery of drugs.

Systems biology is well-suited to studying vascular function and dysfunction because the vasculature and its regulation are highly complex. The insides of all blood vessels – from the smallest to the largest; arteries, veins, capillaries; newly sprouting or mature – are lined with endothelial cells (ECs). This cell type must therefore be sufficiently flexible to survive and thrive in diverse environments, and to perform different specialized functions in many tissues [1]. In particular, moving from *in vitro* systems in which perturbations to endothelial cues can be controlled to *in vivo* vascularized tissues necessitates a quantitative understanding of these complex systems. Whether following exercise [2] or in a growing tumor [3], there can be changes to the expression of many or all of the ligands and receptors regulating endothelial cell behavior, and not all in the same direction. The outcome of all of these changes would be impossible to calculate without a detailed quantitative model of the system.

Because of the number of potential levers and drivers of vascular changes, there are many possible quantitative metrics to measure, including potentially informative quantities that are difficult to measure *in vivo*. By incorporating detailed *in vitro* measurements, computational models can be validated and used to identify which *in vivo* measurements would be most informative – as diagnostics, prognostics, or as indicators of therapy effectiveness either before or after treatment.

2.1.2   Vascular Development and Remodeling

The vasculature supplies oxygen to tissues. Maintenance of homeostasis requires the vascular system to adapt in response to local stimuli (e.g. oxygen tension) sensed by endothelial and other cells. The smallest vessels, directly involved in delivery and transport of oxygen to tissues, develop new branches, expand in diameter, or are pruned as a result of these dynamic molecular, cellular, and tissue microenvironmental cues (**Fig.2-1**).. Vascular network development, maintenance, and remodeling can occur through multiple distinct morphogenic processes. Each requires complex molecular and multicellular regulation, though the regulatory details are not completely understood for any of these forms of vascular remodeling.

Early in development, blood islands coalesce and lacunae form, resulting in a network of interconnected endothelial cords [4]. This process, by which whole networks can be formed simultaneously, is known as vasculogenesis. The tendency of ECs to coalesce and form cords in this way has been leveraged for *in vitro* assays [5], and studied using computational models of early vascular network formation by the Glazier group [4,6].

Following vasculogenesis, the blood vessel networks in developing organs must be refined and expanded as tissues grow and differentiate. The process of angiogenesis increases vascular density by sprouting new vascular branches or splitting existing vessels in two. Sprouting angiogenesis takes two forms: first, expansion of vascular networks into currently avascular tissue – for example, the perinatal expansion of the retinal vasculature [7,8], or the investment of new vessels into small tumors; second, the dynamic sprouting and pruning/regression of vessels within an existing network [9], for example due to exercise or within a growing organ. In both forms of sprouting angiogenesis, endothelial cells become activated by stimuli secreted from distant cells and undergo phenotypic differentiation to migratory, vessel-sprout-leading 'tip' cells. These cells degrade local extracellular matrix and lead proliferative stalk ECs to form sprouts that may ultimately anastamose and become part of the blood flow circuit. Intussusceptive angiogenesis is different to sprouting: existing endothelial tubes form internal pillars that lead to splitting of one vessel into two. This form of vascular expansion can result from changes to shear stress [10,11]. Vasculogenesis and angiogenesis are both typically processes of microvessel development. To obtain hierarchical vascular networks, growth (diameter expansion) is required. Arteriogenesis is the process of

expansion of existing arterioles into larger vessels [12], permitting the vessel to carry more blood flow. Capillary arterialization [13], also known as arteriolargenesis [14], is the process by which capillaries can, under specific circumstances, expand beyond typical capillary dimensions and acquire the characteristics of arterioles. Diameter expansion is typically accompanied by the acquisition of arterial/venous phenotype, including the investment of perivascular smooth muscle cells (SMCs) [14].

Incorporating current understanding of the different vascular remodeling processes (**Fig.2-1**) into systems biology approaches is important for identifying proper strategies to promote or prevent vascularization in disease applications with distinct vascular network morphologies. The main drivers of these processes vary, including different local mechanical and chemical cues sensed by ECs. This suggests that multiple types of therapeutic targets may be combined to selectively activate or inhibit one or more of these remodeling processes. In this review, we focus primarily on non-developmental vascular remodeling, specifically discussing sprouting and intussusceptive angiogenesis. To date, arteriogenesis and capillary arterialization have not been the subjects of significant systems biology efforts; these provide opportunities for future work. Section 2.2 will provide more detail on the types of models used to study different vascular remodeling processes, and the components included in these models. Section 2.3 will discuss the use of systems biology to identify effective therapeutic approaches to stimulating or inhibiting the vasculature. Section 2.4 will highlight challenges and bottlenecks that must be addressed to translate advances in microvascular systems biology into improved clinical outcomes.

Figure 2-1. Vascular development and remodeling processes. The six distinct types of *in vivo* blood vessel formation or remodeling, described in the text, are prevalent in different tissues and situations. Both the emergence and the dynamic adaptation of a functional hierarchical vascular system depend on the coordinated regulation of all these processes. Vasculogenesis results in *de novo* vessel formation, which is critical for development, while angiogenesis involves expansion of the existing network via sprouting or vessel splitting, and is required for network expansion. Arteriogenesis and capillary arterialization allow for remodeling of the vascular network in response to stressors such as ischemia, to alter blood flow within existing tissues. Examples of *in vivo* situations in which each process is particularly relevant are given.

VASCULOGENESIS
Developmental network formation

ANGIOGENESIS
Expanding network vascular front

ANGIOGENESIS
Remodeling network sprouting & pruning

ANGIOGENESIS
Intussusception splitting

ARTERIOGENESIS
Diameter expansion
Collateral expansion

CAPILLARY ARTERIALIZATION
Arteriolargenesis

Canonical Examples

Early organ development

Perinatal Retina
Corneal assay
Embryoid body
Tumor investment

Organ growth
Tumor growth
Exercise training

Exercise

Organ growth
Ischemia response

Ischemia response

Figure 2-1

2.2 Microvascular Systems Physiology and Pharmacology

Vascular development and remodeling *in vivo* comprises several multicellular, multi-scale morphogenic processes. A systems approach is required to understand these processes and the effect of physiological and pathological changes to the system. In this section, we will describe the multiple scales of integrated regulation involved in vascular remodeling (**Fig. 2-2**). While the goal is to improve clinical outcomes in disease, our ability to measure systems changes *in vivo* is often limited. As such, computational studies of molecular and cellular regulation rely heavily on *in vitro* experimental studies for validation. These results must then be interpreted or translated to an *in vivo* context to be used for biomarker development and prediction of therapeutic responses. Appropriate computational models can provide this bridge between *in vitro* and *in vivo* measurements. For a detailed review of the mathematics underlying many of the modeling techniques presented here, see [15].

Figure 2-2. Vascular remodeling is a system-wide response to various perturbations at different scales. Vascular homeostasis can be perturbed by disease, therapy, exercise, injury, or aging (left column). While some of the perturbations introduced by disease are relatively well-characterized (cancer, cardiovascular disease & hypoxia), others represent opportunities for future systems biology research (diabetes, age-related changes). These perturbations directly alter one or more of the scales regulating the vascular system (center box, discussed in Sections 2.2.1-2.2.4 as indicated), and propagate due to the connectedness of the system, inducing indirect changes at the other levels of regulation as well. As the vascular system adapts to the perturbation via remodeling (See Fig. 2-1), a new homeostasis is established (right column). This new homeostatic state may have different blood flow and gene expression than the pre-perturbation system, depending on the effectiveness of the physiological or therapy-induced remodeling. While perturbation/dysfunction can occur at any of the levels, most therapies target molecular regulation mechanisms (Section 2.2.2).
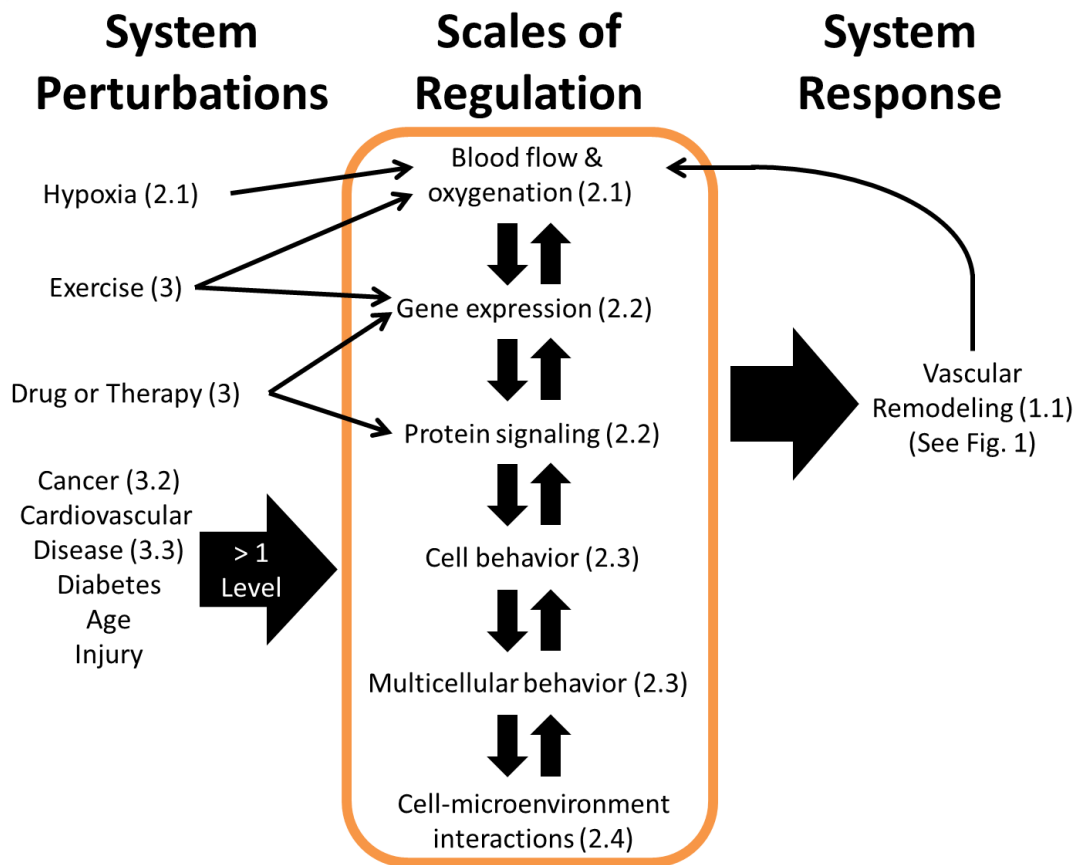
2.2.1 Blood flow and oxygen distribution: a system of delivery and consumption

The vasculature comprises a hierarchical network of interconnected endothelium-lined tubes. The flow of blood distributes oxygen to tissues, with local blood flow matching metabolic demand [16]. Mismatches in blood flow and tissue oxygen consumption can arise from normal processes such as growth and exercise, as well as pathological conditions including stroke, diabetes, respiratory disease, and myocardial infarction [17]. Mathematical models of blood flow fall into two categories: (a) three-dimensional models of blood flow, particularly potentially turbulent flow at sites of atherosclerosis in large vessels [18,19]; (b) network models of blood flow in systems of smaller vessels, in which laminar flow permits the use of Poiseuille-based algebraic models. One example of the first category of models is work by the Diamond group, which integrates hemodynamics with signaling cascades in platelets [20] and stochastic models of coagulation initiation [21] to study the effect of hemodynamics on blood components, including red blood cells and platelets. These models allow for prediction of clot formation and drug sensitivity under varying platelet signaling and flow conditions [22]. The network models in the second category can incorporate experimental measurements of heterogeneous and dynamic microvessel diameters, pressure, flow rates, shear stress, and oxygen exchange [23]. Shear stress and local oxygen availability in particular are key stimuli for angiogenesis and remodeling of the vessel wall, for which predictive models have been developed by the Secomb and Pries groups [24,25]. Combined experimental-computational systems studies such as these can produce interesting predictions with implications for *in vivo* physiology and pathology, such as that the vascular wall must be capable of sensing oxygen levels in order match experimental observations after changes in blood flow and oxygen distribution [26].

The biomechanics of blood flow are important for intussusceptive angiogenesis. While this form of angiogenesis has not been studied as extensively as sprouting angiogenesis [11], intussusception is thought to be the primary form of vascular remodeling in animal models with VEGF overexpression [27], chronic shear stress [28], or colitis [29]. Computational models have demonstrated that hemodynamics and shear stress [30-32], along with oxygen consumption [33] contribute to vessel splitting and pillar formation, which are requirements for intussusceptive angiogenesis. Szczerba *et al.* generated the first model incorporating the combined effects of hemodynamics, chemical agents, and vessel wall stiffness on intussusceptive angiogenesis [10]. In this model framework, increasing vessel wall stiffness during development (a result of

pericyte investment and/or basement membrane deposition) was required to produce realistic predictions of vessel splitting [10]. Interestingly, another computational model (of skeletal muscle) predicted that intussusceptive angiogenesis can more effectively maintain oxygen levels than sprouting angiogenesis when oxygen consumption is high [33]. Tumor vessels have also been shown to undergo intussusceptive angiogenesis after treatment with angiogenesis inhibitors, but a model of these processes has not yet been developed [34].

Other computational models focus on oxygen distribution in tissues, which is regulated by blood flow, oxygen consumption, and by chemical signal molecules such as nitric oxide. By integrating a blood flow model with an oxygen diffusion/consumption model, the Popel group created a multi-scale model of oxygen transport in skeletal muscle, demonstrating the influence of muscle fiber type on oxygen distribution [35]. The simulations predicted that the distribution of muscle fiber sizes has a larger impact on O_2 distribution than O_2 consumption, myoglobin concentration or oxygen diffusivity [35]. Regulation of oxygen by nitric oxide, which stimulates vascodilation and is required for normal endothelial function, has been simulated [36], but this has not been modeled in the context of angiogenesis. The effect of tissue oxygenation on wound healing has also been modeled [37]. More detail on the modeling of oxygen distribution in the microvascular circulation can be found in [38] and [39].

In a later section, we will discuss the importance of blood as a communication route for key proteins and drugs regulating vascular remodeling, as well as the centrality of blood measurements as clinically-relevant, reproducible biomarkers.

2.2.2 Molecular regulators of endothelial cell behavior and vascular remodeling

In the adult, mismatch of oxygen supply and demand can result in changes to the vascular network (**Fig. 2-3**), typically through the transcription factor hypoxia inducible factor (HIF) and the vascular endothelial growth factor (VEGF) family of extracellular ligands [40], though other transcription factors and ligands are known to regulate vascular remodeling [41,42]. Cancer, ischemia, diabetes, and other diseases alter gene regulation, protein expression, and signaling pathway function in angiogenesis, but these changes and their effects on vascular homeostasis are not yet completely understood [3,43]. As examples, expression of cell surface receptors becomes heterogeneous in many solid tumors due to non-uniform oxygen pressure

(resulting from structural abnormalities in tumor vessels) [44]; and changes in shear stress (e.g. due to elevated blood pressure) can alter endothelial gene expression [11].

Normal oxygen levels (normoxia) enable the hydroxylation of the transcription factor HIF1α by prolyl hydroxylases, resulting in HIF degradation [40]. Low oxygen (hypoxia) stabilizes HIF1α, which moves to the nucleus and activates transcription after binding HIF1β/ARNT [45,46]. There are hundreds of downstream targets of HIF, notably members of the VEGF ligand and VEGF receptor families [46]. Multiple microenvironment-dependent HIF-1α signaling profiles (switch-like or gradual) have been demonstrated using computational models of HIF-1α regulation [40,47]. Such divergent system behaviors are difficult to couch in a single framework without the use of computational methods. Models of HIF-1 have also been used to: determine the mechanisms through which HIF-1α senses oxygen [40,48]; study the regulation of HIF-1α [49,50]; and examine differences in HIF-1α regulation in cancer and ischemia [51] with the goal of identifing promising therapeutic targets for different disease states.

While a wide variety of growth factors, adhesion molecules, and cell-cell communication proteins are involved in angiogenesis, including integrins, cadherins, Delta-Notch and semaphorins, we focus here on VEGF and fibroblast growth factor (FGF); as diffusible proteins that can be measured in the blood, they hold promise for validating predictive models of their transport and impact on vascular behavior. The VEGF family of growth factors are critical regulators of both physiological and pathological angiogenesis, promoting endothelial cell survival, proliferation, and migration. There are five ligand genes, each with splice isoforms. These ligand genes and splice isoforms have varying affinity for the three VEGF receptors (which can hetero- or homo-dimerize upon ligand binding), two main VEGF coreceptors (the neuropilins), and the extracellular matrix (ECM) [52]. The VEGF receptors (VEGFRs) also exist as soluble and membrane-bound isoforms [53]. Recent work has demonstrated that post-translational modification (glycosylation, acetylation, methylation) can also modulate the activity of VEGFR2 [54,55]. The multiplicative complexity of these ligands and receptors make understanding the spatial and temporal dynamics of the system and predicting reponse to VEGF-based therapies extremely difficult, as is highlighted by the lack of of success to date in VEGF-based pro-angiogenesis clinical trials [56].

VEGF family members are secreted by parenchymal cells experiencing hypoxia, including: skeletal myocytes in exercise; neural and glial cells in retinal development; bone marrow-derived dendridic

cells in wound repair; and hypoxic tumor cells [57]. VEGF isoforms diffuse through the extracellular matrix to bind VEGF receptors on endothelial cells. ECM-binding isoforms also become sequestered in tissues, where they can still activate VEGF receptors [52,58]. The simulation of VEGF-VEGFR interactions and VEGFR-VEGFR coupling has been developed using biophysically-detailed ordinary differential equation models that are first vaildated against *in vitro* experimental data and then applied to *in vivo* scenarios. This allows for much more detailed understanding than would be possible using only *in vivo* data, which typically consists of plasma protein concentrations, plus some genetic and gene expression data. The scenarios examined to date include competition between ligands for binding to multiple receptors [59]; coupling and enhancement of VEGF binding by Neuropilin co-receptors [60-62]; dimerization of VEGF receptors [63]; downstream signaling of the Akt and ERK pathways [64,65]; matrix-immobilized growth factors and VEGFR trafficking and phosphorylation [66,67]. In addition to these detailed models of VEGF dynamics, models have been developed to directly predict VEGF production in skeletal muscle based on oxygen levels, both after exercise and in peripheral artery disease [33,68-70]. These models allow comparison of disparate therapeutic strategies including exercise and VEGF delivery. Here, exercise was predicted to improve VEGFR ligation and VEGF gradients in ischemic tissue better than therapeutic delivery of VEGF; we will discuss the models of VEGF and exercise as therapies more in Section 3. More detail on the systems biology of VEGF can be found in [52,71].

The fibroblast growth factor (FGF) family has also been implicated in control of angiogenesis. FGFR signaling is complicated by the existence of multiple FGF ligands and the requirement for cell surface heparin sulfate proteoglycans (HSPGs) to stabilize FGF ligand-receptor complexes. A variety of computational models have been developed to study FGF ligand-receptor binding and regulation by HSPGs *in vitro* [72-74], showing that HSPGs able to form active FGF2-HSPG-FGFR signaling complexes are required for effective downstream signaling [75]. FGF binding to EC receptors and to the vascular basement membrane under physiological flow conditions has also been simulated, both *in vivo* [76,77] and in the context of a bioreactor [78,79]. These models have quantified variation in FGF-receptor binding as a function of flow conditions, FGF delivery method (bolus or continuous flow), HSPG and FGF receptor density, and binding affinities [76,78,79]. In particular, Filion et. al. showed that after intracoronary administration, myocardial deposition and retention of FGF2 is limited by the time required for FGF to bind cell surface receptors, and

not by diffusion [77]. Additionally, they showed that the production and internalization rates of FGF receptors are important in regulating FGF distribution. These results have implications for the therapeutic delivery of FGF, and can be used to predict clinically relevant measurements that are difficult to obtain *in vivo*. While the majority of systems biology techniques leverage computational methods, the use of systems biology principles in experimental data collection is increasing, and greatly enhances our understanding of the regulation of complex systems. In one example of such work, the lab of George Davis performs high-throughput experimental assays on endothelial cells cultured in the absence of serum [80-82]. This allows for the comparison of many experimental conditions in a well-controlled system, without the variability and background signaling generated by serum typical of most *in vitro* experiments. The angiogenesis and vasculogenesis assays performed by this group [5] have clearly identified the minimal factors required for endothelial tube formation, identifying the key nodes in these complex regulatory networks. Such assays can be compared directly to computational models of *in vitro* sprouting angiogenesis and vasculogenesis, and then scaled to an *in vivo* context.

2.2.3 Vascular remodeling is a multicellular process

In translating extensive experimental results from ECs studied *in vitro* to understanding how endothelial cells behave *in vivo*, we must recognize the different environment that cells have in tissues – a multicellular environment where heterotypic neighbor interactions are key. Vascular remodeling requires the coordinated action of many endothelial cells and their neighbors. In sprouting angiogenesis, VEGF stimulation upregulates tip cell expression of Delta-like ligand 4 (Dll4) [83]. This results in activation of Notch in trailing stalk cells, reducing the sensitivity of these cells to VEGF by altering VEGF receptor expression [84], and producing a non-uniform population of endothelial cells. This Delta-Notch system can be dysregulated in cancer [85]. Cell-cell adhesions (mediated by VE-Cadherin) can reduce VEGF-mediated EC migration [86]. Shear stress resulting from blood flow also regulates sprouting angiogenesis when blood flow is present [23]. Additionally, pericytes control angiogenesis and vessel stabilization by regulating EC proliferation and migration, along with contributing to formation of the vessel basement membrane [87,88]. Pericytes express angiopoietin-1 (Ang1) and Ang2, which bind to Tie2 on endothelial cells [87]. Ang1 promotes vessel stabilization, while Ang2 destabilizes vessels. Endothelial cell-pericyte association is

disrupted in many cancers, contributing to the formation of structurally and functionally abnormal vascular networks [44].

Due to the critical coordination of cells during sprouting angiogenesis, agent-based models (ABMs) are commonly used to study the evolution of sprouting in space and time. ABMs represent each cell individually, with specific logic rules dictating cell behavior, which may be time- or location-dependent [89,90]. Rule-based ABMs can also be coupled with ODE- or PDE- based models, for instance of VEGF distribution in tissues [91,92]. Such models can recapitulate directional sprouting in response to VEGF gradients, and capture emergent differences in sprout morphology under varying conditions [91]. Cellular Potts Models (CPM), also known as Glazier-Graner-Hogeweg (GGH) models, are lattice-based ABMs in which each cell can evolve in shape, size, and interactions with other cells. As such, CPMs are used to study adhesion, cell elongation, and cell-cell signaling that alters EC behavior in angiogenesis and vasculogenesis [4,6,93,94].

ABM cell behavior rules can be relatively simple, such as growth and movement based directly on experimental observations of dynamic cell behavior data in zebrafish [95]. ABM rules can also be more complex, basing cell behavior on detailed ligand-receptor dynamics and signaling, e.g. filopodia extension, migration, and proliferation, leading to tip and stalk cell behaviors, based on the Dll4, Notch, and VEGFR2 network by Bentley and colleagues [96,97]. This model predicted that ECs in a nascent sprout can continuously compete for tip position, resulting in dynamic changes in tip and stalk cell specification, which has been experimentally validated [97]. This and other models and experimental data indicate that the Notch system may be an interesting potential therapeutic target [97-99]. In another study, the Glazier group has shown using CPMs that contact inhibition of cell proliferation or migration in response to extracellular stimuli can regulate vascular patterning [4]. Other ABMs have studied sprouting in response to combinations of VEGF and brain-derived neurotropic factor [100], and examined clean behavioral changes or knock-outs (e.g. tip and stalk cell proliferation and migration) that are not possible *in vivo* or even *in vitro* [101,102], which is a key advantage of computational modeling as a tool to enhance drug design. Taking an alternate approach, a Boolean model links activation of combinations of VEGF receptors, integrins, and cadherins to cell behaviors such as migration and proliferation [103]. Together, these models improve our understanding of

how combinations of extracellular cues regulate vascular remodeling, allowing for identification of new ways to modulate these processes *in vivo*.

As angiogenesis progresses, sprouts form lumens and anastomose onto existing vessels, facilitating blood flow and introducing these ECs to shear stress. Anastomosis requires the tip cell to become quiescent, a transition that has been studied by Bentley and colleagues using a Spring-Agent model, a type of ABM where each agent is a collection of smaller entities connected by spring-like tensions [104]. This allows for cell shape and cell-cell contacts to change, altering Notch signaling between cells. A multi-scale model of exercise response in skeletal muscle from the Popel group includes sprout formation, branching, and anastomosis in a single framework integrating blood flow, oxygen distribution, and VEGF transport (continuous processes) with cell behavior (discrete ABM) [105]. In this model, anastomoses occur when tip cells come within close proximity to other vessels, but molecular detail of anastomoses is not included. Simulations of tumor angiogenesis and blood flow incorporating shear stress-induced vessel branching [106], varying vessel morphology [107], and vessel pruning in response to therapy [108] suggest that vascular network morphology strongly influences delivery of both nutrients and chemotherapy drugs to tumors.

Some multi-scale models of vascular remodeling include other cell types, such as pericytes [109-112]. Pericytes must dissociate from vessels to permit sprouting, and their recruitment is required for vessel stabilization following remodeling. An ABM including pericyte recruitment in response to gradients of EC-secreted platelet-derived growth factor B (PDGF-B) and differentiation of interstitial cells into pericytes as a function of contact with endothelial sprouts can predict the portion of capillary coverage by smooth muscle α-actin-positive pericytes [110]. A separate computational model captured vessel stabilization and destabilization in response to VEGF, PDGF, Ang1, and Ang2 by integrating modules for tumor growth, endothelial angiogenesis, and vessel stabilization (by pericytes) [111]. Vessel stabilization was predicted to result in slower tumor growth. This growth model predicted that anti-VEGF therapy is more effective when the portion of immature vessels is high, and that co-application of anti-VEGF and anti-Ang1 resulted in prolonged inhibition of tumor growth [111], in line with another model of metastatic ovarian cancer *in vivo* [112]. While many of these agent-based models consider only a small number of cells, understanding the initiation, extension, and anastomosis of angiogenic sprouts is essential to predicting structural and

functional characteristics of developing vascular networks *in vivo*. Even on this small scale, differences can be observed between the behaviors of sprouts forming due to physiological and pathological angiogenesis. The ABMs presented here describe angiogenesis in healthy tissue [105], tumors [91,93,106-109,111], the cornea [102,112], and *in vitro* or developmental scenarios [4,6,97,100], as well as studying sprouting in a generalized context [94,96,101,103,104,110]. Some incorporate expression levels of cell surface receptors or protein concentrations [96,97,105], in order to understand how changes to these quantities alter sprout morphology in disease. Others integrate discrete models of angiogenesis with blood flow simulations [105,107], increasing our understanding of the crosstalk between these differing regulatory mechanisms.

2.2.4 Microenvironment of the microvasculature: high-resolution molecular biology

Not only do ECs receive guidance cues from soluble factors and neighboring cells, but also from mechanical and chemical interactions with their microenvironment [113]. Spatial and temporal patterning of these cues is required for formation of functional vascular networks that effectively oxygenate the surrounding tissue [113]. The extracellular matrix provides a scaffold for tissues; changes in its stiffness are sensed by endothelial and other cells. Additionally, EC signaling is altered by integrin adhesion to ECM proteins [113]. ECs alter their microenvironment by secreting ECM proteins and proteases that degrade ECM components, clearing a path for vessel growth and remodeling. One family of proteases implicated in angiogenesis are the matrix metalloproteinases (MMPs), inhibitors of which are also expressed by ECs [114]. In addition to degrading ECM, proteases can also cleave VEGF, releasing previously immobilized VEGF into the interstitial fluid [113]. The microenvironment in solid tumors is much different than in normal tissue, with perturbed ECM organization and high vascular permeability [44,115], while in peripheral artery disease the endothelial basement membranes are much thicker than in normoxic skeletal muscle [116]. Certain aspects of molecular regulation and cell-cell interactions can be studied *in vitro*, where detailed measurements are possible, but it is not feasible to exactly replicate the complete tissue microenvironment in which vascular remodeling occurs. Thus, multi-scale computational models are necessary to integrate the cues endothelial cells receive from their microenvironment and translate this information into predicted cellular behaviors.

A variety of modeling techniques have been used to study the influence of the microenvironment on vascular remodeling at higher spatial and temporal resolution than is feasible experimentally. For

example, a CPM (Cellular Potts Model, discussed in the previous section) of tumor angiogenesis can predict vascular branching and anastomosis of adjacent sprouts using rules based on molecular, cellular, and local tissue environment dynamics (VEGF gradients, proliferation rates, ECM composition) instead of observed cellular behavior [91]. In this model by the Jiang group, inhomogeneities in the extracellular environment were required to obtain realistic predictions. Additional study with this model demonstrated regulation by ECM fiber density and orientation of sprout extension and branching, suggesting that the ECM itself is a therapeutic target [94]. Other computational models, ranging from ABMs to multi-phase models, have demonstrated regulation of vascularization by pore size in porous scaffolds [117], collagen fiber orientation [118], and a combination of expression of soluble and matrix-bound growth factors, EC proliferation rate, and MMP activity [119].

In addition to the composition of the microenvironment, the local geometry surrounding an angiogenic sprout can significantly alter the availability of diffusible proteins to cell surface receptors. As such, the effect of distance between adjacent angiogeneic sprouts was studied in a 2D reaction-diffusion model by the Mac Gabhann group [120]. The model showed that decreased distance between two sprouts increased the probability that the sprouts would diverge. This study also demonstated that the VEGF-sequesting soluble VEGFR1 isoform, which is secreted by endothelial cells increases the gradient of VEGF-VEGFR2 along the length of sprouts [120]. These behaviors hold in extending the model to three-dimensional sprouts in tissues, and these models can provide molecular explanations for the observed behaviors of perturbed systems such as VEGFR1-knockouts [121]. These models are developed using high-resolution imaging of developing sprouts, enabling true image-based simulations that are specific to the different anatomical outcomes of the molecular perturbations.

Other computational models have focused on modification of the ECM due to endothelial secretion of proteases. Detailed models of the production, activation, and inhibition of several MMPs in the context of angiogenesis have been developed by the Popel group [122-124]. These models have been incorporated into larger 2D and 3D reaction-diffusion models of VEGF ligand-receptor binding and transport, and consider the release of HSPG-bound VEGF from the ECM via cleavage by proteases [125,126]. It was shown that endothelial cells alone do not produce enough proteases to release a significant amount of VEGF, suggesting involvement of other neighboring cell types [125]. Additionally, simulation of the tissue

distribution and gradient formation of HSPG-binding and non-HSPG-binding VEGF isoforms showed that isoform-specific degradation is necessary to match experimental measurements of VEGF localization, and is involved in vascular patterning [126]. These results are of particular relevance to tissue engineering, where the properties of the microenvironment can be tuned to promote proper vascular network formation. In addition to computatational modeling, high-throughput experiments and proteomic analysis have been used to understand the activity of MMPs and identify promising therapeutic targets [127-129]. The data generated by such studies can improve computational models of MMP activity in vascular remodeling and cancer [126,130,131].

2.2.5 Homeostasis requires coordination of multiple scales of regulation

While we have presented distinct levels of vascular regulation in this section, it is vital for understanding *in vivo* physiology to recall that all of these levels are interconnected. Diseases can alter any of these regulatory mechanisms, while drugs typically target gene expression and/or protein signaling networks within cells. Systems biology can aid in identifying the regulatory levels perturbed in specific disease states, which are not fully established for many diseases. After any perturbation (**Fig. 2-2**), the system can adapt using the outlined regulatory mechanisms, resulting in vascular remodeling and reaching a new homeostatic state. A specific example of a homeostatic cycle relevant to altered blood flow/oxygenation is shown in **Fig. 2-3**, along with the types of computational models that are used to study each process in the system. An example of multiscale modeling applied to skeletal muscle to simulate this entire homeostatic cycle will be discussed in Section 2.3.3. Other tissue-specific multiscale models with multiple cell types are emerging, including a study of oxygen and growth factors in healing bone defects [132-134]. While it is not computationally feasible to unite all of these modeling techniques in a detailed 3D model of the complete human body, we use a subset of these tools (application-dependent), the insights resulting from other models, and quantities that are experimentally measureable (*in vivo* and *in vitro*) to understand regulation of vascular remodeling at multiple scales, and how perturbations at any of these levels alters both local and system-wide behavior. This is turn will lead to improved ability to identify biomarkers and potential therapeutic targets.

Figure 2-3. An example of vascular homeostasis and regulation by VEGF. The many different computational model types employed to simulate the flow of information through the integrated multi-scale physiological models is indicated in italics. In general, *in vivo* models often incorporate key elements of tissue physiology: vascular network geometry, blood flow, and/or oxygen distribution. Detailed models of molecular and cellular regulation, for example of the VEGF family, are often constructed and validated with *in vitro* experimental data, and then integrated into *in vivo* models and coupled to the other scales of regulation (**Fig. 2-2**) to predict the vascular remodeling and other physiological changes resulting from molecular perturbations (such as therapeutics). In diseases such as cancer, the homeostatic regulatory mechanisms can become non-functional or function in altered ways, leading to different vessel morphology than observed under physiological conditions.
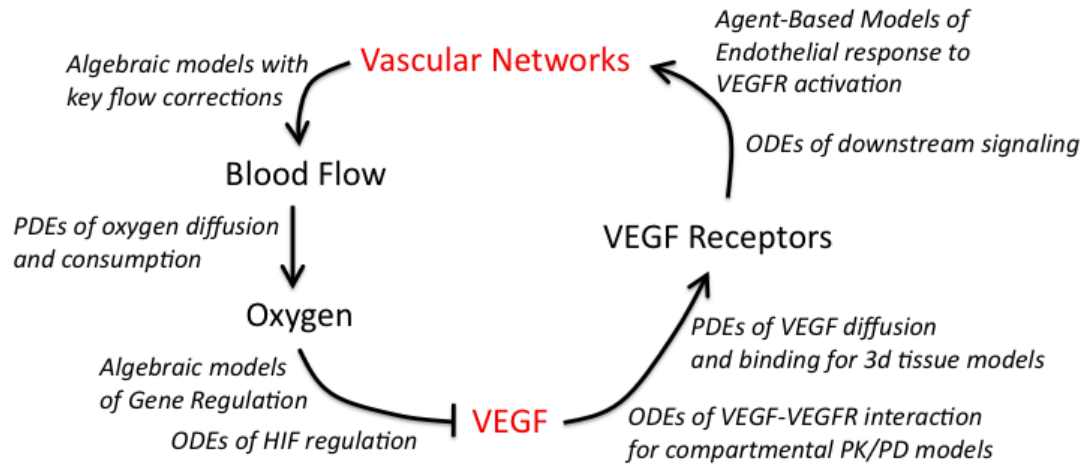
2.3 Microvascular Systems Pharmacology

Vascular remodeling plays key roles, beneficial or detrimental, in many diseases [9]. Angiogenesis is a hallmark of cancer [135,136], and ectopic vascularization drives retinopathies and other leading causes of blindness. In contrast, for diseases characterized by hypovascularization and/or ischemia, such as atherosclerosis, pre-eclampsia, Crohn's disease or hypertension, amelioration by the induction of angiogenesis or arteriogenesis continues to be an active area of therapeutic research. We focus here on cancer and peripheral artery disease as canonical diseases requiring anti-angiogenesis and pro-angiogenesis treatment, respectively.

Drugs, gene vectors, exercise, and other vascular-targeted therapeutic approaches can be studied using systems approaches. For example, the repeated lack of success in human clinical trials of proteins and genes encoding vascular-targeting growth factors suggests that scaling from mice and other pre-clinical models to humans is not trivial. The variability from person to person in responses to all drugs further complicates matters. Understanding the pharmacokinetics and pharmacodynamics of vascular-targeting agents is particularly difficult since the target cells for many of these – endothelial cells – have two active surfaces: one facing the blood stream where many of the drugs are delivered, and one facing the interstitial space of the tissue [137]. These two surfaces are not the same, and the effects of drugs at each surface are not the same.

Systems Pharmacology is crucial to improving the extremely low success rate in clinical trials generally. Clinical trials are very expensive, and using them we cannot try every target, drug combination, dose, or schedule. Systems Pharmacology enables us to virtually explore the therapeutic space. Thus, we call on computational models to test and compare multiple drugs, drug combinations, doses, schedules and routes of administration. We can also go further than drugs to include non-drug therapeutics, including mechanical and electrical stimulation, exercise, or the implantation of engineered or transplanted cells and tissues. In this way we can efficiently eliminate therapies unlikely to be successful and focus on optimizing approaches predicted to show success for at least a subset of the patient population.

Clinical data – gene and protein expression, but also height, weight and other measurements – can be incorporated into well-designed models to build individualized simulations and populations of predictive patient models. On the other side, predictive models need to make clinically testable and measureable

predictions, for example the dynamics of change to concentrations of key molecules in the blood. Only by validating such pharmacological models can we hope to make them useful in the clinic. These models can also help in prospective design of clinical trials by identifying key biomarkers, including complex or nonlinear biomarkers that would not be obvious from a linear analysis of the data.

2.3.1 Whole-body compartment models: pharmacokinetics and pharmacodynamics

As a consistent framework for the analysis of therapies – not just small molecule drugs and biologics, but also gene therapies, physiological changes, and tissue transplants – we must integrate the molecular and cellular understanding outlined in **Section 2.2** into a whole-body model that simulates the transport of key vascular regulatory proteins such as VEGF as well as their cellular targets. Clearly this cannot currently be done at the whole-body scale with the same level of three-dimensional anatomical detail and spatial resolution described in the models of **Section 2.2.4**; however, much of the anatomical specificity can be retained – for example, the multicellular nature of tissues; the heterogeneity of gene and protein expression between cell types; the volumes and surface areas associated with different cell types; the complex molecular interaction networks; and the dynamic nature of cells in responding to extracellular stimulus. By assuming each tissue compartment is well mixed, we can trade partial differential equations for ordinary differential equations [71,138], significantly speeding up computation without losing much of the key biology regulating vascular remodeling.

In **Section 2.2**, we discussed the importance of blood in delivering oxygen to tissues and the importance of computational models in building a quantitative understanding of tissue physiology and pathology. The blood compartment also plays a central role in any systems biology perspective of disease and treatment, because blood-based measurements are the most common type of *in vivo* data available for validation of computational models. Accessibility, reproducibility, low invasiveness and the ability to do sequential measurements make blood biomarkers highly sought after. Simple one-component blood-based biomarkers can have clear population-level changes in pathology, but not be informative for an individual [139], suggesting that more complex biomarkers based on understanding of molecular mechanisms may be more informative. For example, a ratio of VEGF and sFlt1 protein levels in blood may be an important predictor of pre-eclampsia [140], better than either metric alone. Going beyond detection and diagnosis,

prediction of blood-based biomarkers for disease progression and therapeutic response is an area of high interest that opens the door to predictive, responsive and adaptive personalized medicine. Thus, understanding the relation between blood-based measurements (e.g. of soluble proteins) and disease state is an important goal that can be addressed using systems biology techniques.

2.3.2 Targeting angiogenesis in cancer: virtual clinical trials

Tumors can cause a perturbation to vascular homeostasis (Fig.2-2). At first, without vascular ingrowth, the tumor is oxygen limited. However, acquisition of pro-angiogenesis characteristics, such as the constitutive activation of HIF by oncogenic kRAS, can result in perfusion by new vessels. Because of the broken homeostatic cycle, hypervascularization and atypical vessels result – tortuous, inefficient and leaky. Tumor vascularization permits growth beyond the oxygen diffusion limit, and provides tumor cells a route for metastasis. Drugs developed to inhibit angiogenesis in cancer have targeted the key receptor tyrosine kinase pathways in vascular remodeling, including the VEGF receptors, EGF receptors (ErbB/HER) and FGF receptors on endothelial cells. These drugs include antibodies to ligands (e.g. bevacizumab) or to receptors (e.g. DC101) and tyrosine kinase inhibitors (e.g. sunitinib).

By building pharmacokinetic-pharmacodynamic (PK/PD) models of these growth factor-RTK systems, direct testing of multiple RTK-targeting drugs has been possible. These models can incorporate specific current drugs with known interactions and kinetics, but can also be used as a drug design tool by introducing molecules with different interactions. These models can give insight into whole classes of drugs and functions; for example, inhibiting receptor-receptor interactions has emerged from simulation of the VEGF/VEGFR system [61,141-144] as a strategy potentially superior to ligand targeting [61]. This is being borne out in recent experimental results for drugs targeting receptor dimerization [145]. More recently, the tendency of tumors to favor the expression of specific VEGF isoforms was identified using computational simulation to be a critical vulnerability and improve the predicted efficacy of anti-tumor VEGF-targeting [143]. The predicted impact of isoform-specific anti-VEGF agents are not as might be expected based on our understanding of physiological angiogenesis, in part because the regulation of isoforms is very different in tumors [146].

An alternate model of VEGFR pharmacodynamics goes beyond the ligand-receptor interactions by incorporating VEGFR2's downstream signaling pathways [147]. By doing this, the Birtwistle and Gallo groups were able to run sensitivity analyses of dosing for multiple drugs targeting VEGF, VEGF receptors and downstream signal molecules such as PLCγ. They then used optimization algorithms to define potential multidrug regimens with different dosing and scheduling [147].

Validation of pharmacological models is crucial to developing helpful predictive simulations. For models of human pharmacology, the detail and complexity of the models results in many outputs that are not easily measurable, e.g. cell-type-specific activation of multiple receptor families, but also several that are. In particular, the models can predict the effect of multiple perturbations in different cells in different tissues on key proteins in the blood. For example, a multi-compartment PK/PD model of VEGF in humans was used to investigate dynamic changes in the tumor and in the blood following treatment with systemic infusion bevacizumab (anti-VEGF antibody). Counterintuitively, and without any fitting of data, the model predicted that the concentration of VEGF in blood would increase following anti-VEGF treatment [144]; this surprising effect has indeed been clinically observed [148-150]. Because of the highly detailed and mechanistic nature of the model, we could go further and determine that this emergent property resulted from a shuttling mechanism of the VEGF-antibody complex [144]. Such mechanistic hypothesis testing can result in strong and actionable therapeutic predictions.

Another key requirement of models – to be populated with high-quality, detailed experimental data – becomes a benefit of taking an integrated (experimental and computational) systems approach. Models can help us to identify which experimental measurements (target, type, location, spatial resolution and temporal resolution) are the most important or informative. For example, pharmacological models have identified that cell-specific receptor expression plays an important role in the response to therapy – many RTKs are expressed on multiple cell types and not just on the target cell type [151] and the potential for synergistic or antagonistic side effects is clear. Model-based quantification of these multi-cellular (and multi-tissue) effects is clearly important to prediction of therapeutic outcome. Based on simulations, delivery of a VEGF-neutralizing agent can result in available VEGF in the tumor going either up or down depending on the variability in both ligand and receptor expression [141,143]; even the difference between the

apical and basolateral expression of VEGF receptors was predicted to play a major role in pharmacodynamics [152] and this prediction of a systems biology model is now being borne out [137].

2.3.3 Promoting vascularization in peripheral artery disease: from rodent to human

While therapies targeting hypervascularity in cancer and age-related macular degeneration have come to market, no pro-angiogenesis therapeutic agents have been approved. Indeed, multiple trials have failed [56,153,154], including proteins or gene therapy targeting VEGF, HIF-1 or FGF. These failures occurred despite successes in pre-clinical animal models of ischemic disease. Thus, there is an urgent need for systems biology techniques to help predict which treatments would be successful, providing a better bridge from pre-clinical to human clinical trials.

To study the *in vivo* pharmacodynamics of angiogenesis-targeting treatments, we have developed two types of multi-scale models. First, a fully three-dimensional model, that uses image-based anatomical information to simulate a portion of tissue at micron resolution – for example, skeletal muscle (**Fig.2-4A**). While simulations using this model are confined to a particular volume of tissue, the pharmacodynamics of key treatments can still be tested – for example: local effects of gene delivery, which will alter the cell-specific expression rates in the model; or cell-based therapy, in which augmented stem cells can differentiate and integrate into the tissue; or exercise, which will impact gene expression but also blood flow and oxygen demand [68,69,155,156]. These three-dimensional simulations identified key drivers of the VEGF concentration in the tissue as well as of VEGFR activation. Even at rest, without disease or external perturbation, there is heterogeneity in oxygen, VEGF expression, and VEGF and VEGFR concentration gradients. This was further studied using a more detailed anatomical model that included realistic muscle fiber type distributions [35]. The expression of VEGF receptors, and thus the location of the blood vessels, was identified as the key driver of VEGF gradients (which are thought to provide chemotactic guidance to nascent sprouts). We noted that exercise, which is encouraged therapeutically for PAD patients but is often difficult especially in more severe disease, results in up-regulation of both VEGF ligands and VEGF receptors. We were then able to identify using our models that therapeutics delivering only ligands are less effective at increasing the concentration gradients in tissues, and can induce these increases for a shorter time, than receptor expression changes. This, then, provides a possible path forward in developing the next

generation of PAD therapeutics. Based on these models, we added an agent-based model of cell behavior to 'complete the circle' (**Fig.2-3**) and enable the simulation of chronic disease and treatment, or repeated bouts of exercise training [92].

Building a whole-body three-dimensional model with the resolution needed to deal with the molecular gradients described above is not currently feasible. Instead, a second kind of model is needed – a compartmental PK/PD model [157], similar to that described in the previous section for cancer, but now with a target 'disease' tissue of the ischemic calf muscle (**Fig.2-4B**). Although concentration gradients cannot now be simulated at this scale, we can test systemic organism-wide perturbations, such as sleep/wake and exercise cycles, which impact lymphatic flow as well as molecular expression [70,158] (**Fig.2-4B**), the impact of therapeutics on non-target not-diseased normal tissues, and the intravascular delivery of therapeutic molecules.

Figure 2-4. Multi-scale models of microvascular physiology and pathology *in vivo*. A, Three-dimensional multi-scale model of vascular regulation in skeletal muscle *in vivo*. By integrating multiple model types (**Fig.2-3**), we can simulate the links from three-dimensional tissue anatomy and heterogeneity to blood flow, to oxygen distribution, to hypoxia-dependent VEGF secretion by parenchymal cells, to VEGF diffusion, to ligation of VEGF receptors on endothelial cells. The output is heterogeneous VEGF receptor activation across the vasculature, which can then be coupled to cell behavior models such as ABMs [92,105] to complete the homeostatic cycle and remodel the vascular network. This integrated model has been used to study peripheral ischemia disease and to test potential treatments. Simulation results figures adapted from [156]. **B, Multi-compartment PK/PD model of the VEGF family.** This model has multiple compartments, including calf muscle to enable studying the effects of PAD which results in significant pathological changes to that muscle. The model predicts the distribution of VEGF and soluble VEGFR1 and VEGF receptor activation throughout the body, including the blood concentrations of the diffusible proteins. The compartments of the PK/PD model can communicate via physiological processes such as vessel wall permeability and lymphatic drainage. An example application of the PK/PD model is also shown, a simulation of the dynamic effects of diurnal changes in lymphatic drainage (as a result of changes in posture and activity) on plasma soluble VEGFR1 and VEGF levels in a healthy patient. Purple background represents bed rest days, yellow represents active days, and aqua shows calf rest days. Models of this form allow for prediction of tissue VEGF concentrations, and net flows of VEGF between multiple tissues and the blood, and are also druggable – small molecule, protein and gene therapies can be added, as can therapeutic alterations to exercise scheduling. Schematic and simulation results figure adapted from [158].
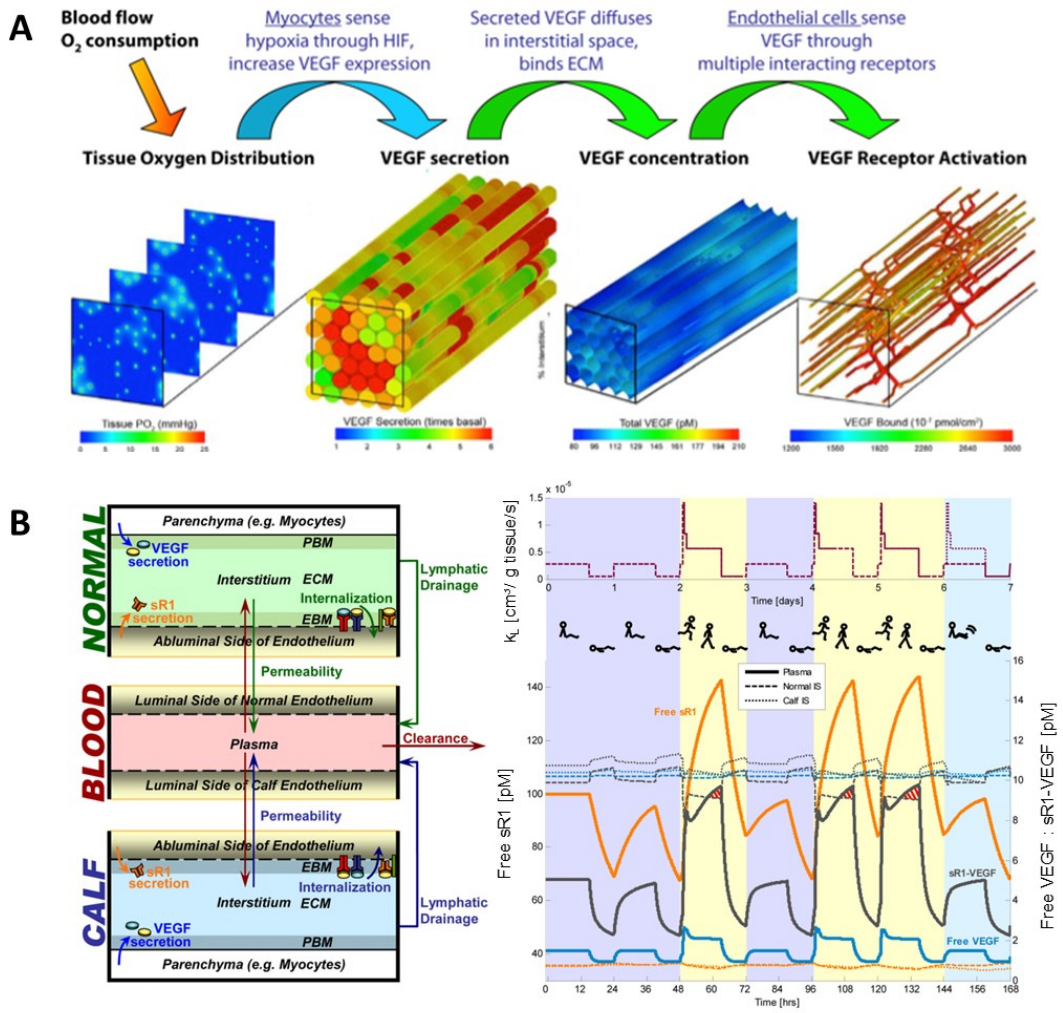
Figure 2-4

These two model types – 3D high-resolution models of tissue and the compartmental PK/PD models – can be directly compared because the interstitial concentrations in the compartments will be the same as the average concentrations adjacent to the interstitial surface of VEGFR-expressing ECs; the average VEGFR activation in the 3D model will be the same as the compartment-level VEGFR activation in endothelial cells.

Lastly, we note that a key issue in the treatment of peripheral artery disease is the failure in humans of treatments that work in rodents. This is a common problem and one for which systems biology is well suited. The parallel development of mouse-specific and human-specific computational models, with a common framework and species-specific parameters, will enable the translation of findings in one to predictions of successful approaches in the other.

2.4 Challenges and Future Directions

A wide variety of computational and experimental techniques have been harnessed to expand our knowledge of microvascular function in health and disease. Computational models are invaluable in their ability to integrate multiple experimental results into a single, often mechanistically-based framework. Progress has been made in integrating across multiple model types, biological regulation mechanisms, and geometric scales to provide a systems-level, dynamic view of the microvasculature and of its remodeling processes. And yet much remains to be done to meet the challenge of making these models, and our resultant understanding of this complex dynamic system, capable of bridging insights from the lab to the clinic.

Areas of potential growth include the development of species-specific and personalized models. Mouse-specific and human-specific models, parameterized with species-specific experimental data, can be used side-by-side to assist in successful translation from pre-clinical to clinical trials. Patient-specific models can incorporate not only individualized pharmacokinetic parameters but also the high variability in gene and protein expression that greatly affect pharmacodynamics. Such models can advance identification of biomarkers for specific subpopulations, and identify specific therapeutic strategies as being effective (or ineffective) for each group [159].

It is crucial, as increasingly complex computational models are developed, to validate model outputs against quantities that are measurable *in vivo*, while leveraging non-measurable model outputs to predict changes in cellular signaling and behavior that may be important for disease prognosis and response to therapy. In parallel with continued model development, systematic collection of quantitative experimental measurements to characterize vascular growth and remodeling in healthy and diseased tissue, both before and after treatment, is critical to develop a sufficient mechanistic understanding of microvascular dynamics to provide meaningful clinical decision support. And as these models and experimental data are produced, it is essential to perform failure analysis – to probe the molecular mechanisms behind the failure of unsuccessful pro-angiogenic drugs. There is so much to learn from previous preclinical and clinical trials that can inform future therapeutic design.

There is also a need for further study of the less well-understood forms of vascular remodeling, such as arteriogenesis and capillary arterialization. In addition, more must be done to understand the

layered and complex effects on vascular remodeling and therapeutics of key co-morbidities such as diabetes and hypertension. In the clinic, patient presentation is rarely single-factor, and a systems approach to multi-disease interactions could greatly improve outcomes.

While there remain many challenges to be met in microvascular systems biology, the progress of recent years highlights the value of systems computational and experimental approaches, and promises advances in clinical outcomes in the years to come.

2.5 References

1   Chi, J. T. *et al.* Endothelial cell diversity revealed by global expression profiling. *Proceedings of the National Academy of Sciences of the United States of America* **100**, 10623-10628, doi:10.1073/pnas.1434429100 (2003).

2   Lloyd, P. G., Prior, B. M., Yang, H. T. & Terjung, R. L. Angiogenic growth factor expression in rat skeletal muscle in response to exercise training. *American Journal of Physiology-Heart and Circulatory Physiology* **284**, H1668-H1678, doi:10.1152/ajpheart.00743.2002 (2003).

3   Loureiro, R. M. B. & D'Amore, P. A. Transcriptional regulation of vascular endothelial growth factor in cancer. *Cytokine & Growth Factor Reviews* **16**, 77-89, doi:10.1016/j.cytogfr.2005.01.005 (2005).

4   Merks, R. M., Perryn, E. D., Shirinifard, A. & Glazier, J. A. Contact-inhibited chemotaxis in de novo and sprouting blood-vessel growth. *PLoS Comput Biol* **4**, e1000163, doi:10.1371/journal.pcbi.1000163 (2008).

5   Koh, W., Stratman, A. N., Sacharidou, A. & Davis, G. E. In vitro three dimensional collagen matrix models of endothelial lumen formation during vasculogenesis and angiogenesis. *Angiogenesis: in Vitro Systems* **443**, 83-101, doi:10.1016/s0076-6879(08)021105-3 (2008).

6   Merks, R. M., Brodsky, S. V., Goligorksy, M. S., Newman, S. A. & Glazier, J. A. Cell elongation is key to in silico replication of in vitro vasculogenesis and subsequent remodeling. *Dev Biol* **289**, 44-54, doi:10.1016/j.ydbio.2005.10.003 (2006).

7   Connolly, S. E., Hores, T. A., Smith, L. E. H. & Damore, P. A. CHARACTERIZATION OF VASCULAR DEVELOPMENT IN THE MOUSE RETINA. *Microvascular Research* **36**, 275-290, doi:10.1016/0026-2862(88)90028-3 (1988).

8   De Smet, F., Segura, I., De Bock, K., Hohensinner, P. J & Carmeliet, P. Mechanisms of Vessel Branching Filopodia on Endothelial Tip Cells Lead the Way. *Arteriosclerosis Thrombosis and Vascular Biology* **29**, 639-649, doi:10.1161/atvbaha.109.185165 (2009).

9   Logsdon, E. A., Finley, S. D., Popel, A. S. & Mac Gabhann, F. A systems biology view of blood vessel growth and remodelling. *Journal of Cellular and Molecular Medicine* **18**, 1491-1508, doi:10.1111/jcmm.12164 (2014).

10   Szczerba, D., Kurz, H. & Szekely, G. A computational model of intussusceptive microvascular growth and remodeling. *J Theor Biol* **261**, 570-583, doi:10.1016/j.jtbi.2009.09.018 (2009).

11   Styp-Rekowska, B., Hlushchuk, R., Pries, A. R. & Djonov, V. Intussusceptive angiogenesis: pillars against the blood flow. *Acta Physiol* **202**, 213-223 (2011).

12   Schaper, W. & Scholz, D. Factors regulating arteriogenesis. *Arteriosclerosis Thrombosis and Vascular Biology* **23**, 1143-1151, doi:10.1161/01.atv.0000069625.11230.96 (2003).

13   Mac Gabhann, F. & Peirce, S. M. Collateral Capillary Arterialization following Arteriolar Ligation in Murine Skeletal Muscle. *Microcirculation* **17**, 333-347, doi:10.1111/j.1549-8719.2010.00034.x (2010).

14   Benest, A. V. *et al.* Arteriolar genesis and angiogenesis induced by endothelial nitric oxide synthase overexpression results in a mature vasculature. *Arteriosclerosis Thrombosis and Vascular Biology* **28**, 1462-1468, doi:10.1161/atvbaha.108.169375 (2008).

15   Scianna, M., Bell, C. G. & Preziosi, L. A review of mathematical models for the formation of vascular networks. *Journal of Theoretical Biology* **333**, 174-209, doi:10.1016/j.jtbi.2013.04.037 (2013).

16   Zakrzewicz, A., Secomb, T. W. & Pries, A. R. Angioadaptation: Keeping the vascular system in shape. *News in Physiological Sciences* **17**, 197-201, doi:10.1152/nips.01395.2001 (2002).

17   Semenza, G. L. Hypoxia-inducible factor 1: oxygen homeostasis and disease pathophysiology. *Trends in Molecular Medicine* **7**, 345-350, doi:10.1016/s1471-4914(01)02090-1 (2001).

18   Antonova, N., Dong, X., Tosheva, P., Kaliviotis, E. & Velcheva, I. Numerical analysis of 3D blood flow and common carotid artery hemodynamics in the carotid artery bifurcation with stenosis. *Clinical Hemorheology and Microcirculation* **57**, 159-173, doi:10.3233/ch-141827 (2014).

19   Xiong, G., Figueroa, C. A., Xiao, N. & Taylor, C. A. Simulation of blood flow in deformable vessels using subject-specific geometry and spatially varying wall properties. *International Journal for Numerical Methods in Biomedical Engineering* **27**, 1000-1016, doi:10.1002/cnm.1404 (2011).

20   Purvis, J. E., Chatterjee, M. S., Brass, L. F. & Diamond, S. L. Amolecular signaling model of platelet phosphoinositide and calcium regulation during homeostasis and P2Y(1) activation. *Blood* **112**, 4069-4079, doi:10.1182/blood-2008-05-157883 (2008).

21   Lo, K., Denney, W. S. & Diamond, S. L. Stochastic modeling of blood coagulation initiation. *Pathophysiology of Haemostasis and Thrombosis* **34**, 80-90, doi:10.1159/000089929 (2005).

22   Flamm, M. H. *et al.* Multiscale prediction of patient-specific platelet function under flow. *Blood* **120**, 190-198, doi:10.1182/blood-2011-10-388140 (2012).

23   Pries, A. R., Reglin, B. & Secomb, T. W. Modeling of angioadaptation: insights for vascular development. *Int J Dev Biol* **55**, 399-405, doi:103218ap [pii] 10.1387/ijdb.103218ap (2011).

24   Pries, A. R., Reglin, B. & Secomb, T. W. Remodeling of blood vessels: responses of diameter and wall thickness to hemodynamic and metabolic stimuli. *Hypertension* **46**, 725-731, doi:10.1161/01.HYP.0000184428.16429.be (2005).

25   Pries, A. R., Secomb, T. W. & Gaehtgens, P. Structural adaptation and stability of microvascular networks: theory and simulations. *Am J Physiol* **275**, H349-360 (1998).

26   Reglin, B., Secomb, T. W. & Pries, A. R. Structural adaptation of microvessel diameters in response to metabolic stimuli: where are the oxygen sensors? *Am J Physiol Heart Circ Physiol* **297**, H2206-2219, doi:00348.2009 [pii] 10.1152/ajpheart.00348.2009 (2009).

27   Gianni-Barrera, R. *et al.* VEGF over-expression in skeletal muscle induces angiogenesis by intussusception rather than sprouting. *Angiogenesis* **16**, 123-136, doi:10.1007/s10456-012-9304-y (2013).

28   Brown, M. D. & Hudlicka, O. Modulation of physiological angiogenesis in skeletal muscle by mechanical forces: involvement of VEGF and metalloproteinases. *Angiogenesis* **6**, 1-14, doi:5128107 [pii] (2003).

29   Konerding, M. A. *et al.* Inflammation-induced intussusceptive angiogenesis in murine colitis. *Anatomical record* **293**, 849-857, doi:10.1002/ar.21110 (2010).

30   Filipovic, N. *et al.* Computational flow dynamics in a geometric model of intussusceptive angiogenesis. *Microvasc Res* **78**, 286-293, doi:10.1016/j.mvr.2009.08.004 (2009).

31   Lee, G. S. *et al.* Blood flow shapes intravascular pillar geometry in the chick chorioallantoic membrane. *Journal of angiogenesis research* **2**, 11-11, doi:10.1186/2040-2384-2-11 (2010).

32   Godde, R. & Kurz, H. Structural and biophysical simulation of angiogenesis and vascular remodeling. *Developmental Dynamics* **220**, 387-401, doi:10.1002/dvdy.1118 (2001).

33   Ji, J. W., Tsoukias, N. M., Goldman, D. & Popel, A. S. A computational model of oxygen transport in skeletal muscle for sprouting and splitting modes of angiogenesis. *Journal of Theoretical Biology* **241**, 94-108, doi:10.1016/j.jtbi.2005.11.019 (2006).

34   Ribatti, D. & Djonov, V. Intussusceptive microvascular growth in tumors. *Cancer Lett* **316**, 126-131, doi:10.1016/j.canlet.2011.10.040 (2012).

35   Liu, G., Mac Gabhann, F. & Popel, A. S. Effects of fiber type and size on the heterogeneity of oxygen distribution in exercising skeletal muscle. *PLoS One* **7**, e44375, doi:10.1371/journal.pone.0044375 (2012).

36   Kavdia, M. Mathematical and computational models of oxidative and nitrosative stress. *Crit Rev Biomed Eng* **39**, 461-472, doi:4513fb4953b8ab42,5df7de0d6436343b [pii] (2011).

37   Schugart, R. C., Friedman, A., Zhao, R. & Sen, C. K. Wound angiogenesis as a function of tissue oxygen tension: a mathematical model. *Proc Natl Acad Sci U S A* **105**, 2628-2633, doi:10.1073/pnas.0711642105 (2008).

38   Goldman, D. Theoretical models of microvascular oxygen transport to tissue. *Microcirculation* **15**, 795-811, doi:10.1080/10739680801938289 (2008).

39   Toma-Dasu, I. & Dasu, A. Modelling tumour oxygenation, reoxygenation and implications on treatment outcome. *Comput Math Methods Med* **2013**, 141087, doi:10.1155/2013/141087 (2013).

40   Qutub, A. A. & Popel, A. S. A computational model of intracellular oxygen sensing by hypoxia-inducible factor HIF1 alpha. *Journal of Cell Science* **119**, 3467-3480, doi:10.1242/jcs.03087 (2006).

41   Dow, J. K. & White, R. W. D. Fibroblast growth factor 2: Its structure and property, paracrine function, tumor angiogenesis, and prostate-related mitogenic and oncogenic functions. *Urology* **55**, 800-806, doi:10.1016/s0090-4295(00)00457-x (2000).

42   Mizukami, Y. *et al.* Hypoxia-inducible factor-1-independent regulation of vascular endothelial growth factor by hypoxia in colon cancer. *Cancer Research* **64**, 1765-1772, doi:10.1158/0008-5472.can-03-3017 (2004).

43   Warren, C. M., Ziyad, S., Briot, A., Der, A. & Iruela-Arispe, M. L. A Ligand-Independent VEGFR2 Signaling Pathway Limits Angiogenic Responses in Diabetes. *Science Signaling* **7**, doi:10.1126/scisignal.2004235 (2014).

44   Carmeliet, P. & Jain, R. K. Angiogenesis in cancer and other diseases. *Nature* **407**, doi:10.1038/35025220 (2000).

45   Powell, F. L. Functional genomics and the comparative physiology of hypoxia. *Annual Review of Physiology* **65**, 203-230, doi:10.1146/annurev.physiol.65.092101.142711 (2003).

46   Semenza, G. L. Hydroxylation of HIF-1: Oxygen sensing at the molecular level. *Physiology* **19**, 176-182, doi:10.1152/physiol.00001.2004 (2004).

47   Yu, Y. *et al.* Pathway switching explains the sharp response characteristic of hypoxia response network. *Plos Computational Biology* **3**, 1657-1668, doi:10.1371/journal.pcbi.0030171 (2007).

48   Dayan, F., Monticelli, M., Pouyssegur, J. & Pecou, E. Gene regulation in response to graded hypoxia: The non-redundant roles of the oxygen sensors PHD and FIH in the HIF pathway. *Journal of Theoretical Biology* **259**, 304-316, doi:10.1016/j.jtbi.2009.03.009 (2009).

49   Yucel, M. A. & Kurnaz, I. A. An in silico model for HIF-alpha regulation and hypoxia response in tumor cells. *Biotechnology and Bioengineering* **97**, 588-600, doi:10.1002/bit.21247 (2007).

50   Nguyen, L. K. *et al.* A dynamic model of the hypoxia-inducible factor 1 alpha (HIF-1 alpha) network. *Journal of Cell Science* **126**, 1454-1463, doi:10.1242/jcs.119974 (2013).

51   Qutub, A. A. & Popel, A. S. Reactive oxygen species regulate hypoxia-inducible factor 1alpha differentially in cancer and ischemia. *Mol Cell Biol* **28**, 5106-5119, doi:MCB.00060-08 [pii] 10.1128/MCB.00060-08 (2008).

52   Mac Gabhann, F. & Popel, A. S. Systems biology of vascular endothelial growth factors. *Microcirculation (New York, N.Y. : 1994)* **15**, 715-738 (2008).

53   Tugues, S., Koch, S., Gualandi, L., Li, X. & Claesson-Welsh, L. Vascular endothelial growth factors and receptors: anti-angiogenic therapy in the treatment of cancer. *Mol Aspects Med* **32**, 88-111, doi:10.1016/j.mam.2011.04.004 (2011).

54   Hartsough, E. J. *et al.* Lysine Methylation Promotes VEGFR-2 Activation and Angiogenesis. *Science Signaling* **6**, doi:10.1126/scisignal.2004289 (2013).

55   Rahimi, N. & Costello, C. Emerging roles of post-translational modifications in signal transduction and angiogenesis. *Proteomics* **00**, 1-10, doi:10.1002/pmic.201400183 (2014).

56   Mac Gabhann, F., Qutub, A. A., Annex, B. H. & Popel, A. S. Systems biology of pro-angiogenic therapies targeting the VEGF system. *Wiley Interdisciplinary Reviews-Systems Biology and Medicine* **2**, 694-707, doi:10.1002/wsbm.92 (2010).

57   Folkman, J. Role of angiogenesis in tumor growth and metastasis. *Seminars in Oncology* **29**, 15-18, doi:10.1053/sonc.2002.37263 (2002).

58   Ferrara, N. Binding to the extracellular matrix and proteolytic processing: two key mechanisms regulating vascular endothelial growth factor action. *Mol Biol Cell* **21**, 687-690, doi:21/5/687 [pii] 10.1091/mbc.E09-07-0590 (2010).

59   Mac Gabhann, F. & Popel, A. S. Model of competitive binding of vascular endothelial growth factor and placental growth factor to VEGF receptors on endothelial cells. *American Journal of Physiology-Heart and Circulatory Physiology* **286**, doi:10.1152/ajpheart.00254.2003 (2004).

60   Mac Gabhann, F. & Popel, A. S. Differential binding of VEGF isoforms to VEGF receptor 2 in the presence of neuropilin-1: a computational model. *American Journal of Physiology-Heart and Circulatory Physiology* **288**, H2851-H2860, doi:10.1152/ajpheart.01218.2004 (2005).

61   Mac Gabhann, F. & Popel, A. S. Targeting neuropilin-1 to inhibit VEGF signaling in cancer: Comparison of therapeutic approaches. *Plos Computational Biology* **2**, doi:10.1371/journal.pcbi.0020180 (2006).

62   Mac Gabhann, F. & Popel, A. S. Interactions of VEGF isoforms with VEGFR-1, VEGFR-2, and neuropilin in vivo: a computational model of human skeletal muscle. *American Journal of Physiology-Heart and Circulatory Physiology* **292**, doi:10.1152/ajpheart.00637.2006 (2007).

63   Mac Gabhann, F. & Popel, A. S. Dimerization of VEGF receptors and implications for signal transduction: A computational study. *Biophysical Chemistry* **128**, 125-139, doi:10.1016/j.bpc.2007.03.010 (2007).

64   Tan, W. H., Popel, A. S. & Mac Gabhann, F. Computational model of VEGFR2 pathway to ERK activation and modulation through receptor trafficking. *Cellular Signalling* **25**, 2496-2510, doi:10.1016/j.cellsig.2013.08.015 (2013).

65   Wan Hua, T., Popel, A. S. & Mac Gabhann, F. Computational Model of Gab1/2-Dependent VEGFR2 Pathway to Akt Activation. *Plos One* **8**, doi:10.1371/journal.pone.0067438 (2013).

66   Clegg, L. E. W. & Mac Gabhann, F. Intracellular trafficking mediates site-specific phosphorylation of VEGFR2 induced by soluble vs. immobilized VEGF. *Angiogenesis* **17**, 948-948 (2014).

67   Clegg, L. & Mac Gabhann, F. Site-specific phosphorylation of VEGFR2 is mediated by receptor trafficking: insights from a computational model. *PLOS Computational Biology* **11**, e1004158, June 2015. DOI: 10.1371/journal.pcbi.1004158 (2015).

68   Mac Gabhann, F., Ji, J. W. & Popel, A. S. Multi-scale computational models of pro-angiogenic treatments in peripheral arterial disease. *Ann Biomed Eng* **35**, 982-994, doi:10.1007/s10439-007-9303-0 (2007).

69   Mac Gabhann, F., Ji, J. W. & Popel, A. S. Computational model of vascular endothelial growth factor spatial distribution in muscle and pro-angiogenic cell therapy. *PLoS Comput Biol* **2**, e127, doi:10.1371/journal.pcbi.0020127 (2006).

70   Wu, F. T. *et al.* VEGF and soluble VEGF receptor-1 (sFlt-1) distributions in peripheral arterial disease: an in silico model. *Am J Physiol Heart Circ Physiol* **298**, H2174-2191, doi:ajpheart.00365.2009 [pii] 10.1152/ajpheart.00365.2009 (2010).

71   Wu, F. T., Stefanini, M. O., Mac Gabhann, F. & Popel, A. S. Modeling of growth factor-receptor systems from molecular-level protein interaction networks to whole-body compartment models. *Methods Enzymol* **467**, 461-497, doi:10.1016/S0076-6879(09)67018-X S0076-6879(09)67018-X [pii] (2009).

72   Filion, R. J. & Popel, A. S. A reaction-diffusion model of basic fibroblast growth factor interactions with cell surface receptors. *Annals of Biomedical Engineering* **32**, 645-663, doi:10.1023/b:abme.0000030231.88326.78 (2004).

73   Forsten, K. E., Fannon, M. & Nugent, M. A. Potential mechanisms for the regulation of growth factor binding by heparin. *Journal of Theoretical Biology* **205**, 215-230, doi:10.1006/jtbi.2000.2064 (2000).

74   Forsten-Williams, K., Chua, C. C. & Nugent, M. A. The kinetics of FGF-2 binding to heparan sulfate proteoglycans and MAP kinase signaling. *Journal of Theoretical Biology* **233**, 483-499, doi:10.1016/j.jtbi.2004.10.020 (2005).

75   Ibrahimi, O. A., Zhang, F. M., Hrstka, S. C. L., Mohammadi, M. & Linhardt, R. J. Kinetic model for FGF, FGFR, and proteoglycan signal transduction complex assembly. *Biochemistry* **43**, 4724-4730, doi:10.1021/bi0352320 (2004).

76   Shen, W., Zhang, C., Fannon, M. W., Forsten-Williams, K. & Zhang, J. A Computational Model of FGF-2 Binding and HSPG Regulation Under Flow. *Ieee Transactions on Biomedical Engineering* **56**, 2147-2155, doi:10.1109/tbme.2008.2002109 (2009).

77   Filion, R. J. & Popel, A. S. Intracoronary administration of FGF-2: a computational model of myocardial deposition and retention. *American Journal of Physiology-Heart and Circulatory Physiology* **288**, H263-H279, doi:10.1152/ajpheart.00205.2004 (2005).

78   Zhao, B., Zhang, C., Forsten-Williams, K., Zhang, J. & Fannon, M. Endothelial Cell Capture of Heparin-Binding Growth Factors under Flow. *Plos Computational Biology* **6**, doi:10.1371/journal.pcbi.1000971 (2010).

79   Patel, N. S., Reisig, K. V. & Clyne, A. M. A Computational Model of Fibroblast Growth Factor-2 Binding to Endothelial Cells Under Fluid Flow. *Annals of Biomedical Engineering* **41**, 154-171, doi:10.1007/s10439-012-0622-4 (2013).

80   Smith, A. O., Bowers, S. L. K., Stratman, A. N. & Davis, G. E. Hematopoietic Stem Cell Cytokines and Fibroblast Growth factor-2 Stimulate Human Endothelial Cell-Pericyte Tube Co-Assembly in 3D Fibrin Matrices under Serum-Free Defined Conditions. *Plos One* **8**, doi:10.1371/journal.pone.0085147 (2013).

81   Stratman, A. N., Davis, M. J. & Davis, G. E. VEGF and FGF prime vascular tube morphogenesis and sprouting directed by hematopoietic stem cell cytokines. *Blood* **117**, 3709-3719, doi:10.1182/blood-2010-11-316752 (2011).

82   Bowers, S. L. K., Meng, C.-X., Davis, M. T. & Davis, G. E. Investigating Human Vascular Tube Morphogenesis and Maturation Using Endothelial Cell-Pericyte Co-cultures and a Doxycycline-Inducible Genetic System in 3D Extracellular Matrices. *Tissue Morphogenesis: Methods and Protocols* **1189**, 171-189, doi:10.1007/978-1-4939-1164-6_12 (2015).

83   Hellstroem, M. *et al.* Dll4 signalling through Notch1 regulates formation of tip cells during angiogenesis. *Nature* **445**, 776-780, doi:10.1038/nature05571 (2007).

84   Jakobsson, L., Bentley, K. & Gerhardt, H. VEGFRs and Notch: a dynamic collaboration in vascular patterning. *Biochemical Society Transactions* **37**, 1233-1236, doi:10.1042/bst0371233 (2009).

85   Bray, S. J. Notch signalling: a simple pathway becomes complex. *Nature Reviews Molecular Cell Biology* **7**, 678-689, doi:10.1038/nrm2009 (2006).

86   Dejana, E. Endothelial cell-cell junctions: happy together. *Nat Rev Mol Cell Biol* **5**, 261-270, doi:10.1038/nrm1357 (2004).

87   Ribatti, D., Nico, B. & Crivellato, E. The role of pericytes in angiogenesis. *Int J Dev Biol* **55**, 261-268, doi:10.1387/ijdb.103167dr (2011).

88   Gaengel, K., Genove, G., Armulik, A. & Betsholtz, C. Endothelial-mural cell signaling in vascular development and angiogenesis. *Arterioscler Thromb Vasc Biol* **29**, 630-638, doi:10.1161/atvbaha.107.161521 (2009).

89   Guidolin, D., Rebuffat, P. & Albertin, G. Cell-oriented modeling of angiogenesis. *ScientificWorldJournal* **11**, 1735-1748, doi:10.1100/2011/586475 (2011).

90   Qutub, A. A., Mac Gabhann, F., Karagiannis, E. D., Vempati, P. & Popel, A. S. Multiscale models of angiogenesis. *IEEE Eng Med Biol Mag* **28**, 14-31, doi:10.1109/memb.2009.931791 (2009).

91   Bauer, A. L., Jackson, T. L. & Jiang, Y. A cell-based model exhibiting branching and anastomosis during tumor-induced angiogenesis. *Biophys J* **92**, 3105-3121, doi:10.1529/biophysj.106.101501 (2007).

92   Liu, G., Qutub, A. A., Vempati, P., Mac Gabhann, F. & Popel, A. S. Module-based multiscale simulation of angiogenesis in skeletal muscle. *Theoretical Biology and Medical Modelling* **8**, doi:6 10.1186/1742-4682-8-6 (2011).

93   Shirinifard, A. *et al.* 3D multi-cell simulation of tumor growth and angiogenesis. *PLoS One* **4**, e7190, doi:10.1371/journal.pone.0007190 (2009).

94   Bauer, A. L., Jackson, T. L. & Jiang, Y. Topography of extracellular matrix mediates vascular morphogenesis and migration speeds in angiogenesis. *PLoS Comput Biol* **5**, e1000445, doi:10.1371/journal.pcbi.1000445 (2009).

95   Shirinifard, A. *et al.* 3D quantitative analyses of angiogenic sprout growth dynamics. *Dev Dyn*, doi:10.1002/dvdy.23946 (2013).

96   Bentley, K., Gerhardt, H. & Bates, P. A. Agent-based simulation of notch-mediated tip cell selection in angiogenic sprout initialisation. *J Theor Biol* **250**, 25-36, doi:10.1016/j.jtbi.2007.09.015 (2008).

97   Jakobsson, L. *et al.* Endothelial cells dynamically compete for the tip cell position during angiogenic sprouting. *Nat Cell Biol* **12**, 943-953, doi:10.1038/ncb2103 (2010).

98   Kuhnert, F., Kirshner, J. R. & Thurston, G. Dll4-Notch signaling as a therapeutic target in tumor angiogenesis. *Vascular Cell* **3**, 20 (2011).

99   Gurney, A. & Hoey, T. Anti-DLL4, a cancer therapeutic with multiple mechanisms of action. *Vascular Cell* **3**, 18 (2011).

100   Long, B. L., Rekhi, R., Abrego, A., Jung, J. & Qutub, A. A. Cells as state machines: Cell behavior patterns arise during capillary formation as a function of BDNF and VEGF. *J Theor Biol* **326**, 43-57, doi:10.1016/j.jtbi.2012.11.030 (2013).

101   Qutub, A. A. & Popel, A. S. Elongation, proliferation & migration differentiate endothelial cell phenotypes and determine capillary sprouting. *BMC Syst Biol* **3**, 13, doi:10.1186/1752-0509-3-13 (2009).

102   Jackson, T. & Zheng, X. A cell-based model of endothelial cell migration, proliferation and maturation during corneal angiogenesis. *Bull Math Biol* **72**, 830-868, doi:10.1007/s11538-009-9471-1 (2010).

103   Bauer, A. L., Jackson, T. L., Jiang, Y. & Rohlf, T. Receptor cross-talk in angiogenesis: mapping environmental cues to cell phenotype using a stochastic, Boolean signaling network model. *J Theor Biol* **264**, 838-846, doi:10.1016/j.jtbi.2010.03.025 (2010).

104   Bentley, K., Mariggi, G., Gerhardt, H. & Bates, P. A. Tipping the balance: robustness of tip cell selection, migration and fusion in angiogenesis. *PLoS Comput Biol* **5**, e1000549, doi:10.1371/journal.pcbi.1000549 (2009).

105   Qutub, A. A., Liu, G., Vempati, P. & Popel, A. S. INTEGRATION OF ANGIOGENESIS MODULES AT MULTIPLE SCALES: FROM MOLECULAR TO TISSUE. *Pacific Symposium on Biocomputing 2009*, 316-327 (2009).

106   McDougall, S. R., Anderson, A. R. & Chaplain, M. A. Mathematical modelling of dynamic adaptive tumour-induced angiogenesis: clinical implications and therapeutic targeting strategies. *J Theor Biol* **241**, 564-589, doi:10.1016/j.jtbi.2005.12.022 (2006).

107   McDougall, S. R., Anderson, A. R. A., Chaplain, M. A. J. & Sherratt, J. A. Mathematical modelling of flow through vascular networks: implications for tumour-induced angiogenesis and chemotherapy strategies. *Bull Math Biol* **64**, 673-702 (2002).

108   Stephanou, A., McDougall, S. R., Anderson, A. R. A. & Chaplain, M. A. J. Mathematical modelling of flow in 2D and 3D vascular networks: Applications to anti-angiogenic and chemotherapeutic drug strategies. *Math Comput Model* **41**, 1137-1156 (2005).

109   Plank, M. J., Sleeman, B. D. & Jones, P. F. A mathematical model of tumour anglogenesis, regulated by vascular endothelial growth factor and the angiopoietins. *Journal of Theoretical Biology* **229**, 435-454, doi:10.1016/j.jtbi.2004.04.012 (2004).

110   Peirce, S. M., Van Gieson, E. J. & Skalak, T. C. Multicellular simulation predicts microvascular patterning and in silico tissue assembly. *FASEB J* **18**, 731-733, doi:10.1096/fj.03-0933fje (2004).

111   Arakelyan, L., Vainstein, V. & Agur, Z. A computer algorithm describing the process of vessel formation and maturation, and its use for predicting the effects of anti-angiogenic and anti-maturation therapy on vascular tumor growth. *Angiogenesis* **5**, 203-214 (2002).

112   Zheng, X., Koh, G. Y. & Jackson, T. A continuous model of angiogenesis: Initiation, extension, and maturation of new blood vessels modulated by vascular endothelial growth factor,

angiopoietins, platelet-derived growth factor-B, and pericytes. *Discrete and Continuous Dynamical Systems - Series B* **18**, 1109-1154 (2013).

113   Eming, S. A. & Hubbell, J. A. Extracellular matrix in angiogenesis: dynamic structures with translational potential. *Experimental Dermatology* **20**, 605-613, doi:10.1111/j.1600-0625.2011.01309.x (2011).

114   Kessenbrock, K., Plaks, V. & Werb, Z. Matrix metalloproteinases: regulators of the tumor microenvironment. *Cell* **141**, 52-67, doi:S0092-8674(10)00288-6 [pii] 10.1016/j.cell.2010.03.015 (2010).

115   Quail, D. F. & Joyce, J. A. Microenvironmental regulation of tumor progression and metastasis. *Nature Medicine* **19**, 1423-1437, doi:10.1038/nm.3394 (2013).

116   Baum, O., Djonov, V., Ganster, M., Widmer, M. & Baumgartner, I. Arteriolization of capillaries and FGF-2 upregulation in skeletal muscles of patients with chronic peripheral arterial disease. *Microcirculation* **12**, 527-537, doi:10.1080/10739680591003413 (2005).

117   Artel, A., Mehdizadeh, H., Chiu, Y. C., Brey, E. M. & Cinar, A. An agent-based model for the investigation of neovascularization within porous scaffolds. *Tissue Eng Part A* **17**, 2133-2141, doi:10.1089/ten.TEA.2010.0571 (2011).

118   Edgar, L. T., Sibole, S. C., Underwood, C. J., Guilkey, J. E. & Weiss, J. A. A computational model of in vitro angiogenesis based on extracellular matrix fibre orientation. *Computer Methods in Biomechanics and Biomedical Engineering* **16**, 790-801, doi:10.1080/10255842.2012.662678 (2013).

119   Travasso, R. D., Corvera Poire, E., Castro, M., Rodriguez-Manzaneque, J. C. & Hernandez-Machado, A. Tumor angiogenesis and vascular patterning: a mathematical model. *PLoS One* **6**, e19989, doi:10.1371/journal.pone.0019989 (2011).

120   Hashambhoy, Y. L., Chappell, J. C., Peirce, S. M., Bautch, V. L. & Mac Gabhann, F. Computational modeling of interacting VEGF and soluble VEGF receptor concentration gradients. *Front Physiol* **2**, 62, doi:10.3389/fphys.2011.00062 (2011).

121   Chappel, J. C. *et al.* Flt-1 (VEGFR-1) Coordinates Discrete Stages of Blood Vessel Branching and Coalescence. (in review).

122   Karagiannis, E. D. & Popel, A. S. Distinct modes of collagen type I proteolysis by matrix metalloproteinase (MMP) 2 and membrane type I MMP during the migration of a tip endothelial cell: insights from a computational model. *J Theor Biol* **238**, 124-145, doi:10.1016/j.jtbi.2005.05.020 (2006).

123   Karagiannis, E. D. & Popel, A. S. A theoretical model of type I collagen proteolysis by matrix metalloproteinase (MMP) 2 and membrane type 1 MMP in the presence of tissue inhibitor of metalloproteinase 2. *J Biol Chem* **279**, 39105-39114, doi:10.1074/jbc.M403627200 (2004).

124   Vempati, P., Karagiannis, E. D. & Popel, A. S. A biochemical model of matrix metalloproteinase 9 activation and inhibition. *J Biol Chem* **282**, 37585-37596, doi:10.1074/jbc.M611500200 (2007).

125   Vempati, P., Mac Gabhann, F. & Popel, A. S. Quantifying the proteolytic release of extracellular matrix-sequestered VEGF with a computational model. *PLoS One* **5**, e11860, doi:10.1371/journal.pone.0011860 (2010).

126   Vempati, P., Popel, A. S. & Mac Gabhann, F. Formation of VEGF isoform-specific spatial distributions governing angiogenesis: computational analysis. *BMC Syst Biol* **5**, 59, doi:10.1186/1752-0509-5-59 1752-0509-5-59 [pii] (2011).

127   Miller, M. A. *et al.* Proteolytic Activity Matrix Analysis (PrAMA) for simultaneous determination of multiple protease activities. *Integrative Biology* **3**, 422-438 (2011).

128   Chen, C. H. *et al.* Multiplexed protease activity assay for low-volume clinical samples using droplet-based microfluidics and its application to endometriosis. *J Am Chem Soc* **135**, 1645-1648, doi:10.1021/ja307866z (2013).

129   Morrison, C. J., Butler, G. S., Rodriguez, D. & Overall, C. M. Matrix metalloproteinase proteomics: substrates, targets, and therapy. *Curr Opin Cell Biol* **21**, 645-653 (2009).

130   Ribba, B. *et al.* A multiscale mathematical model of avascular tumor growth to investigate the therapeutic benefit of anti-invasive agents. *J Theor Biol* **243**, 532-541 (2006).

131   Billy, F. *et al.* A pharmacologically based multiscale mathematical model of angiogenesis and its use in investigating the efficacy of a new cancer treatment strategy. *J Theor Biol* **260**, 545-562, doi:10.1016/j.jtbi.2009.06.026 (2009).

132   Carlier, A., van Gastel, N., Geris, L., Carmeliet, G. & Van Oosterwyck, H. Size does matter: an integrative in vivo-in silico approach for the treatment of critical size bone defects. *PLoS computational biology* **10**, e1003888-e1003888, doi:10.1371/journal.pcbi.1003888 (2014).

133   Carlier, A., Geris, L., van Gastel, N., Carmeliet, G. & Van Oosterwyck, H. Oxygen as a critical determinant of bone fracture healing-A multiscale model. *Journal of Theoretical Biology* **365**, 247-264, doi:10.1016/j.jtbi.2014.10.012 (2015).

134   Carlier, A. *et al.* MOSAIC: A Multiscale Model of Osteogenesis and Sprouting Angiogenesis with Lateral Inhibition of Endothelial Cells. *Plos Computational Biology* **8**, doi:10.1371/journal.pcbi.1002724 (2012).

135   Hanahan, D. & Weinberg, R. A. The hallmarks of cancer. *Cell* **100**, 57-70, doi:10.1016/s0092-8674(00)81683-9 (2000).

136   Hanahan, D. & Weinberg, R. A. Hallmarks of Cancer: The Next Generation. *Cell* **144**, 646-674, doi:10.1016/j.cell.2011.02.013 (2011).

137   Hudson, N. *et al.* Differential Apicobasal VEGF Signaling at Vascular Blood-Neural Barriers. *Developmental Cell* **30**, 541-552, doi:10.1016/j.devcel.2014.06.027 (2014).

138   Stefanini, M. O., Qutub, A. A., Mac Gabhann, F. & Popel, A. S. Computational models of VEGF-associated angiogenic processes in cancer. *Mathematical Medicine and Biology-a Journal of the Ima* **29**, 85-94, doi:10.1093/imammb/dqq025 (2012).

139   Kut, C., Mac Gabhann, F. & Popel, A. S. Where is VEGF in the body? A meta-analysis of VEGF distribution in cancer. *British Journal of Cancer* **97**, 978-985, doi:10.1038/sj.bjc.6603923 (2007).

140   Rana, S. *et al.* Angiogenic Factors and the Risk of Adverse Outcomes in Women With Suspected Preeclampsia. *Circulation* **125**, 911-U199, doi:10.1161/circulationaha.111.054361 (2012).

141   Finley, S. D., Engel-Stefanini, M. O., Imoukhuede, P. I. & Popel, A. S. Pharmacokinetics and pharmacodynamics of VEGF-neutralizing antibodies. *BMC Syst Biol* **5**, 193 (2011).

142   Stoll, B. R., Migliorini, C., Kadambi, A., Munn, L. L. & Jain, R. K. A mathematical model of the contribution of endothelial progenitor cells to angiogenesis in tumors: implications for antiangiogenic therapy. *Blood* **102**, 2555-2561, doi:10.1182/blood-2003-02-0365 2003-02-0365 [pii] (2003).

143   Finley, S. D. & Popel, A. S. Effect of Tumor Microenvironment on Tumor VEGF During Anti-VEGF Treatment: Systems Biology Predictions. *Jnci-Journal of the National Cancer Institute* **105**, 802-811 (2013).

144   Stefanini, M. O., Wu, F. T. H., Mac Gabhann, F. & Popel, A. S. Increase of Plasma VEGF after Intravenous Administration of Bevacizumab Is Predicted by a Pharmacokinetic Model. *Cancer Research* **70**, 9886-9894, doi:10.1158/0008-5472.can-10-1419 (2010).

145   Tvorogov, D. *et al.* Effective Suppression of Vascular Network Formation by Combination of Antibodies Blocking VEGFR Ligand Binding and Receptor Dimerization. *Cancer Cell* **18**, 630-640, doi:10.1016/j.ccr.2010.11.001 (2010).

146   Vempati, P., Popel, A. S. & Mac Gabhann, F. Extracellular regulation of VEGF: Isoforms, proteolysis, and vascular patterning. *Cytokine & Growth Factor Reviews* **25**, 1-19, doi:http://dx.doi.org/10.1016/j.cytogfr.2013.11.002 (2014).

147   Zhang, X. Y., Birtwistle, M. R. & Gallo, J. M. A General Network Pharmacodynamic Model-Based Design Pipeline for Customized Cancer Therapy Applied to the VEGFR Pathway. *CPT: pharmacometrics & systems pharmacology* **3**, e92-e92, doi:10.1038/psp.2013.65 (2014).

148   Segerstrom, L. *et al.* The anti-VEGF antibody bevacizumab potently reduces the growth rate of high-risk neuroblastoma xenografts. *Pediatr Res* **60**, 576-581, doi:01.pdr.0000242494.94000.52 [pii] 10.1203/01.pdr.0000242494.94000.52 (2006).

149   Willet, C. G. *et al.* Surrogate markers for antiangiogenic therapy and dose-limiting toxicities for bevacizumab with radiation and chemotherapy: continued experience of a Phase I trial in rectal cancer patients. *J Clin Oncol* **23**, 8136-8139 (2005).

150   Yang, J. C. *et al.* A randomized trial of bevacizumab, an anti-vascular endothelial growth factor antibody, for metastatic renal cancer. *N Engl J Med* **349**, 427-434, doi:10.1056/NEJMoa021491 349/5/427 [pii] (2003).

151   Imoukhuede, P. I. & Popel, A. S. Quantitative fluorescent profiling of VEGFRs reveals tumor cell and endothelial cell heterogeneity in breast cancer xenografts. *Cancer medicine* **3**, 225-244, doi:10.1002/cam4.188 (2014).

152   Stefanini, M. O., Wu, F. T. H., Mac Gabhann, F. & Popel, A. S. The Presence of VEGF Receptors on the Luminal Surface of Endothelial Cells Affects VEGF Distribution and VEGF Signaling. *Plos Computational Biology* **5**, doi:10.1371/journal.pcbi.1000622 (2009).

153   Mac Gabhann, F., Annex, B. H. & Popel, A. S. Gene therapy from the perspective of systems biology. *Curr Opin Mol Ther* **12**, 570-577 (2010).

154   Annex, B. H. Therapeutic angiogenesis for critical limb ischaemia. *Nature Reviews Cardiology* **10**, 387-396, doi:10.1038/nrcardio.2013.70 (2013).

155   Ji, J. W., Mac Gabhann, F. & Popel, A. S. Skeletal muscle VEGF gradients in peripheral arterial disease: Simulations of rest and exercise. *Am J Physiol Heart Circ Physiol* **293**, H3740-H3749 (2007).

156   Mac Gabhann, F., Ji, J. W. & Popel, A. S. VEGF gradients, receptor activation, and sprout guidance in resting and exercising skeletal muscle. *J Appl Physiol* **102**, 722-734 (2007).

157   Wu, F. T. H. *et al.* A systems biology perspective on sVEGFR1: its biological function, pathogenic role and therapeutic use. *Journal of Cellular and Molecular Medicine* **14**, 528-552, doi:10.1111/j.1582-4934.2009.00941.x (2010).

158   Wu, F. T. H., Stefanini, M. O., Gabhann, F. M. & Popel, A. S. A Compartment Model of VEGF Distribution in Humans in the Presence of Soluble VEGF Receptor-1 Acting as a Ligand Trap. *Plos One* **4**, doi:10.1371/journal.pone.0005108 (2009).

159   Bender, R. J. & Mac Gabhann, F. Expression of VEGF and Semaphorin Genes Define Subgroups of Triple Negative Breast Cancer. *Plos One* **8**, doi:10.1371/journal.pone.0061788 (2013).

Chapter 3. Therapeutic Angiogenesis: The Role of Growth Factors and Extracellular Matrix

3.0 Summary

Despite extensive research, pro-angiogenic drugs have failed to translate clinically, and therapeutic angiogenesis, which has the potential in the treatment of various cardiovascular diseases, remains a major challenge. Physiologically, angiogenesis—the process of blood-vessel growth from existing vasculature—is regulated by a complex interplay of biophysical and biochemical cues from the extracellular matrix (ECM), angiogenic factors and multiple cell types. The ECM can be regarded as the natural three-dimensional material regulating angiogenesis. Here, we leverage knowledge of ECM properties to derive design rules for engineering pro-angiogenic materials. We propose that pro-angiogenic materials should be biomimetic, incorporate angiogenic factors and mimic cooperative interactions between growth factors and the ECM.

3.1 Introduction

Angiogenesis is a multicellular morphogenetic process in which new blood vessels sprout from existing ones, penetrating a three-dimensional milieu—the extracellular matrix (ECM)—and generating a new vascular network to support a local metabolic demand for oxygen[1-3]. This process is controlled by an intricate interplay of biomolecular and biophysical signals[4]. The expression of angiogenic factors is triggered by hypoxia under the influence of hypoxia-sensitive transcription factors[5-7]. Angiogenic growth factors interact with the ECM through complex binding interactions, which depend on the particular sequence and structure of the growth factor that is expressed[8-11]. Receptors on endothelial cell (EC) surfaces bind growth factors in concert with binding of adhesion proteins in the ECM by integrins, leading to synergistic signaling as ECs integrate both adhesion signals and growth factor signals from the milieu[12-17]. Other cells (pericytes and smooth muscle cells (SMCs)) in the angiogenic microenvironment also signal to the endothelium to stabilise the angiogenic vessels and yield a mature, functional vascular network[7, 18-20]. Moreover, the ECM[8, 21] provides biomechanical signaling and is proteolytically remodeled to accommodate the nascent vascular network[22-24].

Here, we seek to describe the morphogenetic process of angiogenesis from two perspectives: (i) understanding angiogenesis and (ii) harnessing this understanding to engineer therapeutic angiogenesis. In the first case, we consider the ECM as a dynamic material system, providing the biomolecular context in which angiogenesis takes place, as well as controlling and regulating multiple aspects of angiogenesis. We then translate this insight into design rules for therapeutic angiogenesis. Recently developed biological and completely synthetic matrices have exemplified at least some of these design rules, engineering adhesion ligands, growth-factor-binding domains and protease-sensitive domains into the matrix, allowing for growth factor release and matrix remodeling, all within the context of controllable biomechanics[16, 25-30]. These design rules also include approaches for modifying the growth factors themselves, for use either in engineered ECMs or using endogenous ECM, to induce more effective therapeutic angiogenesis[27, 31, 32]. Thus, we highlight that the physiological material system provides design rules that can guide mimicry by biomaterials scientists.

3.2 Clinical Significance

Cardiovascular diseases are the leading cause of mortality worldwide[33]. Coronary artery disease (CAD), peripheral arterial disease (PAD) and cerebrovascular disease result from insufficient blood supply, and lead to major deficiencies of the heart, limb and brain, respectively. Therapeutic angiogenesis, or generation of new blood vessels from the existing vasculature, is an appealing strategy to treat these diseases, as well as chronic wounds and diabetic ulcers[34] **(Fig. 3-1A)**. In spite of major efforts to develop angiogenic drug-based therapies in recent decades[37], there is only one approved pro-angiogenic drug[38]. The lack of approved therapeutics indicates the slow pace of clinical translation in this field and highlights an unmet clinical need. This slow pace is not due to a lack of potential drug targets **(Fig. 3-1B)**; many promising results have been observed in animal models. However, these results have failed to translate clinically[34, 39, 40], leading to over 70 clinical trials of pro-angiogenic therapies[41] **(Fig. 3-1C)**, including delivery of recombinant growth factor, or the associated genes[40, 41], without a single new approval since 2007, or even a positive outcome in a late-phase clinical trial[40, 41].

These trials likely result in part from poor delivery and/or poor retention at the target site, limiting effectiveness and duration, increasing dose (and cost), and leading to potential safety-related issues with subsequent high dosing[39]. Studies suggest than slow, sustained release of growth factors may lead to more successful outcomes[42]. It may also be important to consider the complex interplay of multiple cues involved in physiological healing and regeneration, as opposed to focusing on delivery of a single cue[39]. Our limited understanding of physiological angiogenesis has limited our ability to effectively mimic this process therapeutically. To improve angiogenic factor-based therapies, we must leverage all we do know about the physiological ECM to design new materials that will efficiently control the effectiveness of angiogenic factors.

Figure 3-1. Clinical overview of cardiovascular diseases and pro-angiogenic factor-based therapies.

A| Common cardiovascular diseases. **B|** Number of hits on PubMed database (National Center for Biotechnology Information, U.S. National Library of Medicine, USA) for publications on cardiovascular diseases, and on pro-angiogenic factors per year, between 2004 and 2014. **C|** Estimated number of clinical trials on pro-angiogenic growth factors registered in the International Clinical Trials Registry Platform (ICTRP, World Health Organization) for the treatment of cardiovascular diseases, displayed by year between 2004 and 2014, and by angiogenic factor families. CSF: colony-stimulating factor; IGF: insulin growth factor, HIF: hypoxia-induced factor.

a Common cardiovascular diseases

Cerebral ischaemia

Coronary artery disease

Ischaemic wounds, diabetic ulcers

Peripheral arterial disease
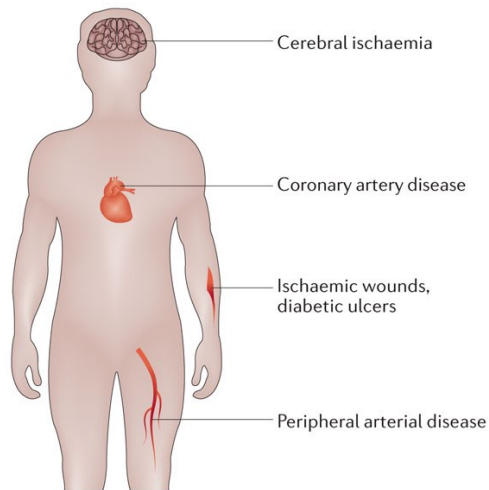
b Increasing research interest in cardiovascular diseases and pro-angiogenic factors between 2004 and 2014

- Number of research publications on cardiovascular diseases in the PubMed database
- Number of research publications on pro-angiogenic factors in the PubMed database
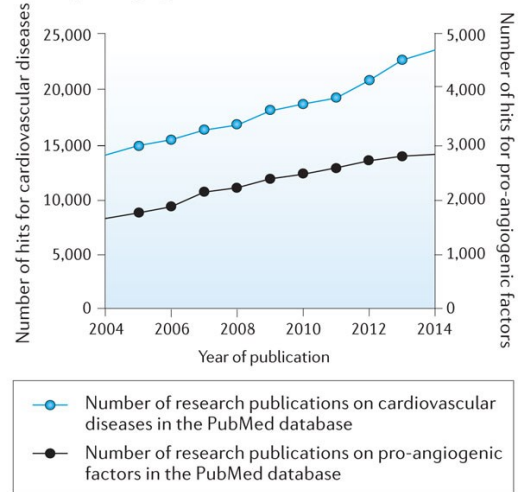
c Clinical trials on pro-angiogenic factors for the treatment of cardiovascular diseases between 2004 and 2014

Distribution per year

Distribution per pro-angiogenic factor

Nature Reviews | Materials
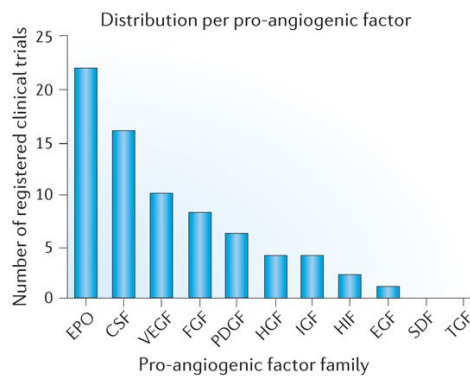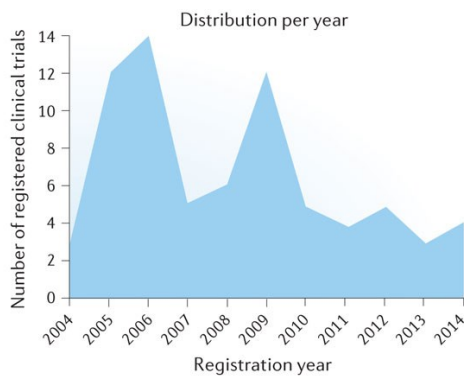
3.3 The Physiological ECM as a Material in Angiogenesis

During angiogenesis, cells interact dynamically with the ECM and are regulated in turn by local microenvironmental cues **(Fig. 3-2A–C)**. The ECM serves as a mechanical scaffold and provides survival and growth signals to cells. The ECM is also a platform for intricate spatiotemporal coordination of the biochemical and biophysical cues presented to cells during angiogenesis[17]. In this section, we detail the molecular mechanisms that drive the material characteristics and biological actions of the ECM in physiological and pathological angiogenesis.

Figure 3-2. Multiscale microenvironmental regulation of angiogenesis. A| Tissue-scale regulation: response to hypoxia. When blood flow is compromised owing to disease or injury (arrows), hypoxia induces release of growth factors, which form gradients within the tissue. **B|** Multicellular-scale: angiogenic sprout. Growth factors bind to receptors, resulting in angiogenic sprouting towards the source of growth factor production (hypoxic cells; shown in (**A**)). Cell–cell communication is critical for proper sprout formation and outgrowth. To clear a path for invasion into the ECM, the sprout and surrounding cells release proteases and express other proteases on the cell surface. **C|** Protein-scale: ECM proteins promote complex formation between the growth factor, its receptor and integrins at the cell surface, inducing synergistic signalling and resulting in gene expression changes. ECM-bound growth factor can bind to and activate its receptor, but the receptor cannot internalise without either the ECM-growth factor bond or the growth factor-receptor bond breaking, resulting in altered RTK trafficking and downstream signaling. Integrins also transduce mechanical cues to the cell cytoskeleton.

a Tissue-scale regulation

Vessel narrowing
Protease
Hypoxic cell
ECM
Growth factor concentration gradient
Growth factor
Vessel sprout
vSMC
Basement membrane
Capillary

b Multicellular-scale regulation

Growth factor
Protease
Basement membrane
ECM
Tip cell
ANG2
Pericyte
TIE2
Stalk cells
ANG1
Ephrin

c Protein-scale regulation

Growth factor
Growth factor immobilization
Integrin
ECM
RTK
Ligand and receptor clustering
Integrin activation
Mechanical force transduction
Plasma membrane
Synergistic signalling
Receptor internalization
Gene expression changes
Cytoskeleton

Figure 3-2

3.3.1 ECM is a dynamic biomolecular scaffold for cells.

ECM composition dictates the biomechanical properties of the cell microenvironment, including stiffness and viscoelasticity. Quiescent blood vessels are surrounded by a dense basement membrane (BM) mainly composed of type IV collagen and the adhesive protein laminin-1. During angiogenesis, cell-secreted proteases degrade the BM, exposing sprouting ECs to an interstitial ECM rich in type collagen I and elastin[21, 43, 44]. This environment promotes cell migration and proliferation[21]. Adhesive glycoproteins found in the interstitial ECM, such as fibronectin and vitronectin, connect type I collagen to cell surface integrins, and are essential for vascular development[45]. The interstitial ECM and vascular BM are also rich in proteoglycans and glycosaminoglycans (GAGs), including heparan sulphate proteoglycans (HSPGs) and hyaluronan, which are composed of very hydrophilic polysaccharide chains that allow high water retention in the matrix.

Changes in ECM structure and composition alter cell behaviour and angiogenesis through cell surface integrins **(Fig. 3-2C)**[17], as studied using both experimental techniques and computational models[3, 46]. Integrins transduce mechanical forces from the ECM to the actin cytoskeleton via multiple adaptor proteins, leading to changes in cellular signaling[17], protein splicing[47], and regulation of other integrins[48]. Integrin cytoplasmic tails also interact directly with signaling molecules, including focal adhesion kinase (FAK) and Src, which are considered to be critical points of crosstalk between integrin and growth factor receptor signaling[21, 49]. Integrins are usually expressed at only low levels in quiescent ECs, and are present in their inactive conformation. The profile of expressed integrins shifts and activation increases with the loss of pericyte investment and the onset of angiogenesis[50]. Of the integrins expressed on ECs, $\alpha_5\beta_1$ binds to fibronectin and $\alpha_v\beta_5$ preferentially binds vitronectin, whereas $\alpha_1\beta_1$ and $\alpha_2\beta_1$ bind collagen, $\alpha_3\beta_1$, $\alpha_6\beta_1$ and $\alpha_6\beta_4$ bind laminin, and $\alpha_v\beta_3$ binds to multiple ECM substrates including vitronectin[13, 51]. This allows ECs to sense multiple changes in the local ECM and alter their behaviour accordingly[21].

3.3.2 ECM regulates angiogenic factors.

Secreted growth factors and cell–cell communication proteins are key contributors to new vessel formation. Although many growth factors involved in angiogenesis (*e.g.* epidermal growth factor (EGF), hepatocyte growth factor (HGF), transforming growth factor (TGF)-β) can be sequestered by ECM

components and released according to precise spatiotemporal kinetics, we focus here on a few important families, highlighting the impact of immobilisation in the matrix on their biological functions.

VEGFs are critical regulators of angiogenesis[52, 53]. VEGF levels in healthy humans are low (*e.g.* 1–3 pM in plasma and tissue interstitial fluid), with production increasing in response to hypoxia (1–2-fold in diseased tissue[54], 5–10-fold in exercising skeletal muscle[54, 55] and 10-fold in wounds[56]). VEGF diffuses through the interstitial space, binding to the ECM and cell surface receptors, producing VEGF gradients[57], and attracting endothelial sprouts towards hypoxic regions. The five VEGF ligand genes can be spliced into multiple isoforms. The three VEGF receptor tyrosine kinases (RTKs) dimerise and activate upon ligand binding, and two main co-receptors (the neuropilins) alter ligand–receptor affinity and receptor trafficking[58, 59]. Alternative soluble splice isoforms of the RTKs can bind and sequester growth factors extracellularly. Most studies have focussed on VEGF-A binding to the RTK VEGFR2 on ECs. Longer VEGF-A splice isoforms (VEGF-A$_{165}$ and VEGF-A$_{189}$) contain heparin-binding domains, allowing for ECM binding, and domains for binding to the co-receptor neuropilin-1 (NRP1)[58]. In contrast, the shorter isoform VEGF-A$_{121}$ does not bind to the ECM. VEGF-A$_{165}$ and VEGF-A$_{189}$ form steep gradients within the extracellular space, remaining in close proximity to the site of production (*e.g.* VEGF$_{189}$ accumulation in the BM)[60], whereas VEGF-A$_{121}$ forms shallow gradients[57], as illustrated in **Fig. 3-3**. This spatial organisation has physiological impact: mice and tumours expressing only shorter, non-ECM binding VEGF-A isoforms produce small numbers of leaky, wide-diameter blood vessels[22, 61, 62], whereas mice and tumors expressing only longer, ECM-binding isoforms exhibit large numbers of thin, highly branched vessels[60, 63]. The mechanisms by which changes in the relative expression of these ECM-binding and non-ECM-binding splice isoforms, which varies with tissue type[11] and ECM stiffness[47], alters VEGFR2 signaling and vascular morphology, and are not completely understood.

Figure 3-3. Molecular changes directly regulate spatial cues within tissue. Changes in expression of VEGF splice isoforms with varying affinity for the ECM alters growth factor gradients within tissues and the resulting vascular morphology. $VEGF_{121}$ does not bind to the ECM, creating shallow VEGF gradients in tissue and resulting in formation of wide diameter vessels with low branching density. Conversely, $VEGF_{189}$ binds strongly to the ECM, resulting in short, steep VEGF gradients and formation of networks of thick, highly branched vessels.
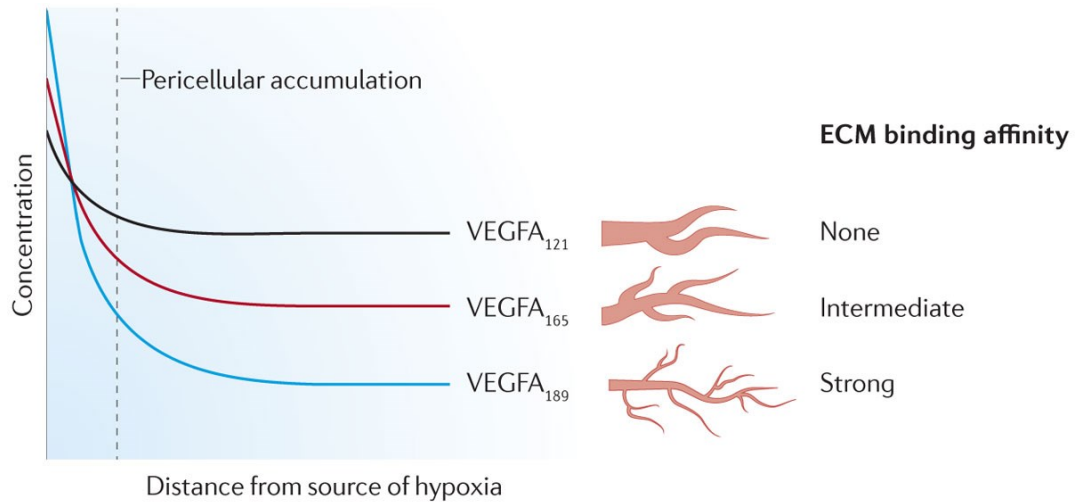
FGF family growth factors are also potent inducers of angiogenesis. FGF-1 and FGF-2 are expressed by endothelial and other cells[64] and bind to the receptor FGFR1. FGF is present in the body at similar concentrations to VEGF (0.6 pM in healthy blood and up to 6 pM in disease[65]) and FGF-2 is upregulated in response to hypoxia[66, 67]. FGFs regulate many steps of angiogenesis, from BM degradation and integrin expression to EC proliferation and migration, vessel maturation and reformation of the BM[68]. FGF-2 binds to the ECM and vascular BM[64] and to cell-surface HSPGs. Maximal signaling by FGF-FGFR complexes requires stabilisation of the ligand–receptor complex by cell-surface HSPGs[69-71]. Signaling and gene expression crosstalk has been observed between the FGF and VEGF systems[68].

The heparin-binding ligand PDGF-BB and RTK PDGFR-β are also implicated in vascular remodeling[72]. PDGF-BB is produced by vascular ECs following cues including hypoxia and other growth factors, binds to PDGFR-β expressed on vascular SMCs (vSMCs) and pericytes[72], and is found in the body at similar levels to VEGF and FGF[73]. Capture of EC-secreted PDGF-BB in the vascular BM is thought to aid in pericyte recruitment to maturing vessels[74, 75]. Indeed, mice with the heparin-binding domain from PDGF-B deleted or with reduced heparin sulphate N-sulphation showed pericyte detachment from microvessels[76, 77].

Cell–cell communication is also critical for angiogenesis **(Fig. 3-2B)**; in particular, EC–EC, EC–vSMC and EC–pericyte interactions maintain or interrupt the stability of mature vessels. Angiopoietin1 (Ang1) is produced by pericytes, vSMC and stalk ECs of an angiogenic sprout. Ang1 promotes vessel quiescence and pericyte recruitment (along with PDGF-BB). Ang1 has a critical role in cell–cell junction stabilisation and cell–matrix adhesion; ECs tend to dissociate from one another and from the BM in Ang1 conditional knockout mice[78]. In the extracellular space, Ang1 interacts with matrix proteins, notably vitronectin, as well as with cell-surface integrin $\alpha_5\beta_1$ and Ang1's receptor Tie2[78]. Ang1 and Tie2 interactions with integrin $\alpha_5\beta_1$ modulate the sensitivity of Tie2 to Ang1[78, 79]. Interestingly, Tie2 activates the Notch signaling pathway[80], which is involved in EC–EC communication, specifying tip and stalk cells by regulating expression of the VEGF receptors[81]. In contrast to Ang1, its antagonist Ang2 is expressed primarily by tip ECs and promotes vessel destabilisation[82] upon binding to Tie2 at the onset of angiogenesis. EphrinB2 and EphB4 are critical for assembly of mature vessel walls[83]. This bi-directional

signaling also controls cell–cell attraction and repulsion between ECs and neighboring vSMCs or ECs in small vessels, and regulates VEGFR2 internalisation[84] and $\alpha_5\beta_1$ clustering[85].

The total amount of ECM-immobilised growth factor *in vivo* and its physiological impact are difficult to measure. Computational models estimate 30 to 100 times more VEGF-A is electrostatically bound to the ECM than is free in skeletal muscle[86]. Another model predicts that 98% of interstitial FGF-2 is bound to ECM and BM HSPGs after intracoronary FGF-2 administration[87]. The large number of available growth factor binding sites within the ECM and on soluble molecules[68] can buffer local free growth-factor concentrations. ECM–growth-factor binding sites also affect cell-surface reactions; extracellular HSPGs compete effectively with cell-surface HSPGs for binding to FGF-2 and VEGF-A[70, 88]. Buffering may maintain growth-factor concentrations within tightly regulated physiological bounds, a requirement highlighted by VEGF-A's lethal haploinsufficiency[89, 90] and the fact that even in disease or after injury, VEGF and FGF levels generally stay within an order of magnitude of baseline levels[56]. Computational models predict that in tissues, VEGF receptor binding is ligand-limited rather than receptor-limited[91], again suggesting an important role for ECM-mediated regulation of local VEGF-A concentration in VEGF receptor signaling.

VEGF-A$_{165}$ immobilised to a surface or hydrogel can bind to and activate VEGFR2[92, 93] *in vitro*, inducing VEGFR2 phosphorylation of similar magnitude to equivalent amounts of soluble VEGF-A. However, the pattern of tyrosine site-specific phosphorylation, and the resulting EC behaviour, is altered. In one study, VEGF-A immobilisation increased phosphorylation of tyrosine Y1214 on VEGFR2, upstream of p38 and cell migration, whereas phosphorylation of Y1175, upstream of ERK1/2 and cell proliferation[92] was not increased compared with soluble VEGF-A. This parallels the vascular phenotypes mentioned above: thin, highly branched vessel networks in response to matrix-binding isoforms via cell migration signaling pathways; and sparsely branched, high-diameter vessels in response to soluble isoforms primarily via cell proliferation. Thus, ECM-bound VEGF has direct effects on vascular physiology and remodeling; however, the mechanism underlying this differential signaling was unclear. To address this, a computational model of VEGF-A binding to ECM proteins, NRP1, and VEGFR2, as well as VEGFR2 trafficking and site-specific phosphorylation was built[94]. This model showed that reduced internalisation of ECM-VEGF-A-VEGFR2 complexes (owing to VEGF immobilization via multiple protocols) was

sufficient to explain all relevant experimental data to date. Immobilised VEGF-A alters VEGFR2 trafficking and therefore its exposure to phosphatases, resulting in different downstream signaling. FGF2 and PDGF-BB are also biologically active when immobilised on a surface and exposed to 3T3 cells[95], suggesting that this is a common feature of heparin-binding growth factors. The large quantities of ECM-bound growth factors, which owing to ECM heterogeneity are not uniformly distributed *in vivo*, suggest that ECM-bound VEGF-A may have an important role in angiogenesis, perhaps aiding in tip-cell selection and migration. However, ECM–growth-factor affinity, mode of presentation (*e.g.* ECM *vs* nanoparticle), and region of the growth factor bound to the substrate may be different *in vivo* than *in vitro*. This, combined with the difficulty of experimentally determining the relative contributions of direct RTK ligation by immobilised growth factors and ECM-mediated spatiotemporal regulation of growth factor availability[31] to observed improvements in angiogenic responses, highlight the need for further study of ECM-bound VEGF in the body.

3.3.3 ECM coordinates microenvironmental signaling.

Growth factors and their receptors (soluble and cell-surface) do not regulate angiogenesis in isolation. They regulate, are regulated by, and/or signal synergistically with ECM proteins, proteases, cell-surface integrins and cell-surface HSPGs.

In addition to altering ECM protein properties[21, 50], cell-derived proteases regulate local growth factor availability by cleaving ECM components to which growth factors are bound, or by cleaving matrix-binding growth factors and releasing shorter isoforms that do not bind to the ECM. For example, FGF is released via cleavage of HSPGs by heparinase[96] or plasmin[97]. VEGF-A can also be released by matrix metalloproteinases (MMPs)[11, 23]. Cleavage of VEGF itself, particularly by plasmin and the MMPs, can have pro- or anti-angiogenic effects[11, 98]. For example, cleavage of VEGF-A$_{165}$ reduces its bioactivity, removing the domains required for ECM- and NRP1-binding, whereas VEGF-A$_{189}$ binds to VEGFR2 poorly in some cell lines until being cleaved by urokinase-type plasminogen activator (uPA) or plasmin[11]. Computational models predict that ECs cannot produce enough protease to account for all VEGF-A cleavage, suggesting contributions by other local cells[99]. PDGF-BB is also cleaved, by thrombin[75], releasing it from the endothelial BM[74]. Protease expression is also regulated by growth factors; FGF upregulates multiple MMPs

and uPA[68], aiding in the initiation of angiogenesis. When present at high levels (*e.g.* in a chronic wound), proteases can alter not only the local growth factor concentrations and ECM structure over short times (*e.g.* at the tip of an angiogenic sprout), but also tissue-level properties.

Growth-factor–receptor and integrin–substrate interactions must be considered as a system. Growth-factor ligation of RTKs promotes integrin activation, increasing integrin affinity for ECM substrates and enhancing cell signaling. Similarly, integrin ligation is necessary for maximal and extended signaling by VEGFR2, FGFR1 and PDGFR-β[93, 100]. These interactions require clustering of RTKs and integrins, which is facilitated by the multivalency of integrin- and heparin-binding sites on crosslinked ECM proteins. Simultaneous activation of RTKs and integrins leads to Src-mediated synergistic signaling in their overlapping pathways[12]. For example, the integrin $\alpha_v\beta_3$, which is strongly upregulated in ECs during angiogenesis[101], binds promiscuously to ECM proteins, and interacts with both VEGFR2 and FGFR1. Notably, $\alpha_v\beta_3$ is required for VEGFR2-dependent activation of p38 and FAK[102]. Although VEGFR2 and $\alpha_v\beta_3$ interact via the β_3 extracellular domain, perturbations of β_3 have not produced consistent results, suggesting that $\alpha_v\beta_3$ may be pro- or anti-angiogenic depending on the context[103, 104]. In contrast, the fibronectin-binding integrin $\alpha_5\beta_1$ is critical during vascular development[105] and is consistently pro-angiogenic. The fibronectin-mediated presentation of VEGF-A or PDGF-BB to VEGFR2 or PDGFRβ, respectively, co-activates the integrin $\alpha_5\beta_1$, resulting in a synergistic increase in and prolongation of growth-factor-receptor phosphorylation and downstream ERK1/2 signaling[15, 16].

RTKs and integrins mutually regulate their expression. For example, culture of microvascular ECs on vitronectin, a ligand for $\alpha_v\beta_3$ and $\alpha_v\beta_5$, increases expression of FGF and VEGF receptors[106]. Additionally, stimulation of microvascular EC with FGF-2 upregulates α_2, α_5, β_1, and β_3 integrins[107, 108], while stimulation of cells with VEGF-A results in activation of $\alpha_v\beta_3$, $\alpha_v\beta_5$, $\alpha_5\beta_1$, and $\alpha_2\beta_1$[109]. Adding another layer of complexity, the VEGF co-receptor NRP1 interacts with $\alpha_5\beta_1$[110], and $\alpha_v\beta_3$ prevents NRP1–VEGF–VEGFR2 interactions[111]. Teasing out the contributions of this mutual regulation to RTK–integrin interactions **(Fig. 2C)** is often difficult.

3.3.4 ECM is dynamically regulated in health and disease.

Extracellular biochemical and biomechanical cues, along with cell–cell communication, form a complex, interwoven regulatory network. Each component must be activated to the correct extent, in the correct place, and at the correct time, to promote appropriate vascular growth. First, ECs must sense a pro-angiogenic cue. Then, proteases must degrade the BM, and EC interactions with support cells must be broken. As an endothelial sprout grows through interstitial space, it senses complex and dynamic gradients of soluble and immobilised growth factors, ECM proteins and cytokines. These sprouts must anastomose with existing vessels, lumenise to provide blood flow, and mature into stabilised vessels with BMs, invested support cells and appropriate permeability. In each step, microenvironmental regulation is critical and is mediated by the ECM.

Understanding the molecular drivers of this complex system, and how each feature that is perturbed in a given disease fits into the larger regulatory picture, will make appropriate therapeutic strategies easier to identify. For example, in properly healing wounds **(Fig. 3-4A)** the provisional matrix is rich in cytokines, growth factors, fibronectin and fibrin, whereas, an ulcer or chronic wound (**Fig. 3-4B**) is characterised by a perturbed ECM and high protease levels[49]. In PAD **(Fig. 3-4C)**, BMs thicken[112], capillary density decreases, endothelial FGF-2 expression increases[112], and the production of matrix-binding and non-matrix-binding VEGF-A splice isoforms changes[113]. Inflammation and atherosclerosis lead to changes in ECM degradation[8] and increased PDGFR-β expression, whereas altered VEGF-A splice isoform expression is observed in obese patients[114]. Although each of these diseases involves or may lead to ischemia, the proper treatment depends on the specific molecular changes in the material environment of the ECM, as well as the time-course of disease. There are still many important, complex open questions about spatial and temporal extracellular regulation of angiogenesis **(Table 3-1)**. Answering these questions requires use of multiple tools and platforms, including traditional cell culture experiments leveraging novel perturbations and measurement techniques, *in vitro* systems providing a 3D context for angiogenesis, *in vivo* systems and computational models. These efforts will continue to advance our understanding of and ability to emulate or circumvent regulation of angiogenesis by the material properties of the ECM.

Table 3-1. Open questions about microenvironmental regulation of angiogenesis.

Topic	Open Questions	Tools to Address	Implications for Therapy
Complexity of angiogenic signaling	What are the minimal microenvironmental requirements for development of a functional vascular network? (*e.g.* ECM proteins, growth factors, physical cues, proteolysis) How are signals from multiple growth factor receptors and integrins integrated? Which combinations are synergistically pro-angiogenic in a given context?	Angiogenesis assays (screen combinations of cues) *In vitro* experiments leveraging genetic perturbations (e.g. site-directed mutagenesis, CRISPR/Cas), novel measurement tools (e.g. high resolution imaging and single cell measurements), and high-throughput screening of combinations of cues Molecularly-detailed computational models Genetically modified mice & mouse disease models	Determine the combinations of angiogenic growth factors and biomechanical signals that should be delivered.
Spatio-temporal control of growth factors	What temporal profiles of multi-growth factor therapy result in effective sprouting followed by stabilisation? What is the dynamic (concentration) range of cell response to growth factor? Is concentration, presentation (soluble *vs* immobilised), and/or gradient most important? How do the ECM and proteases alter the growth factor pharmacokinetics? How does growth factor source (cell type-specific endogenous expression *vs* exogenous delivery) affect spatial distribution and vessel integrity?	Microdialysis in humans (measure free/soluble protein concentrations) Mouse models of ischemic disease Computational models of growth factor pharmacology and distribution in realistic tissues Systematic experiments in microfluidic and organ-on-a-chip systems Knock-in/knock-out experiments High-resolution microscopy	Establish therapeutic doses and molecular presentation strategies to implement in angiogenic materials. Effectively implement sequential delivery, sustained release, and spatial patterning of growth factors in angiogenic materials. Maximise effective induction of therapeutic angiogenesis while minimising side-effects.
ECM changes in disease	How does expression of ECM proteins, proteases, and growth factor splice isoforms change in ischemia, diabetes and obesity? What are the resulting changes in integrin and RTK signaling? What are the key drivers of impairment to overcome in each disease?	Gene & protein measurements in humans Computational models of growth factor pharmacology and distribution in tissues Mouse disease models Human cell-based organ-on-a-chip systems	Design angiogenic materials to target key causes of functional impairment and restore "normal" signaling in diseased tissue. Optimise angiogenic material properties to match the environment in which it will be delivered.

Figure 3-4. Perturbation of ECM-mediated regulation of angiogenesis in disease. Disease-specific changes in the ECM likely contribute to vascular dysfunction. **A|** The provisional fibrin clot acts as a reservoir of growth factors and cytokines in healthy wounds. **B|** Chronic wounds are highly proteolytic environments, which impairs the ECM integrity in the wound. **C|** Basement membrane thickness increases and the capillary density decreases in peripheral artery disease.

a Healthy, acute wound

Growth factor

ECM

Fibrin clot

Cytokine

Protease

b Chronic wound (for example, diabetic ulcers)

Protease overexpression

Collagen fragment

c Peripheral arterial disease or chronic ischaemia

Hypoxia

Vessel narrowing

Basement membrane thickening
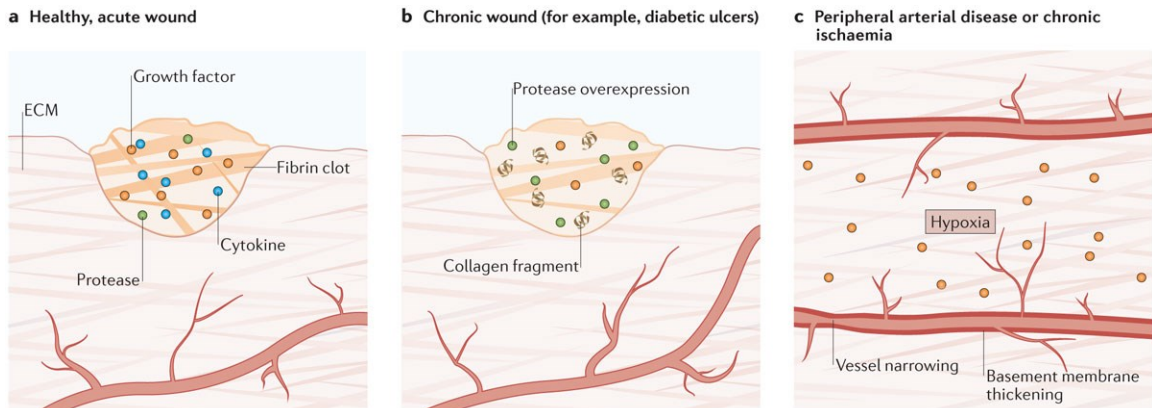
Nature Reviews | Materials

3.4 ECM-Inspired Design Rules for Pro-Angiogenic Biomaterials

A detailed discussion of engineered constructs that leverage the biological insights outlined in the previous section can be found in Ref. [121]. Briefly, these systems have evolved along with our understanding of the biology underlying wound healing and ischemic disease, as well as technological advancements in protein synthesis and production of tunable hydrogels. Some approaches leverage processed natural materials, to provide the complexity of native extracellular matrix, but with concerns about immunogenicity[115, 116]. Others develop simpler, highly controlled synthetic materials[118], which do not recapitulate this natural complexity[119], but are more defined and well-characterized[120]. Overall, three main rules for effective angiogenic rules were proposed (**Fig. 3-5**):

Rule 1: The material should be biomimetic.

*Rule 2: The material should deliver angiogenic factors (see **Fig. 3-6** for a summary of strategies).*

Rule 3: The material should leverage synergy between the matrix or gel, growth factors and cells.

Figure 3-5. Design rules for the development of pro-angiogenic materials. Pro-angiogenic materials can be engineered **(A)** to be cell-compatible and **(B)** to control the spatio-temporal delivery of single or multiple essential angiogenic factors. The material design can also consider **(C)** collaborative interactions between its different components to leverage its angiogenic properties.

The material should be biomimetic (that is, biocompatible, non-immunogenic, and include proteolytic and cell-adhesion sites).

The material should incorporate single or multiple angiogenic factors, the release of which can be spatiotemporally controlled.

The material should take advantage of collaborative interactions between cells, factors and the material to enable cell-mediated release of angiogenic factors and synergistic signalling between integrins and angiogenic factor receptors.

Nature Reviews | Materials

Figure 3-6. Delivery systems for angiogenic factors. A| Delivery of angiogenic factors based on biophysical and biochemical interactions with exogenous materials. **B|** Materials engineered with heparin and heparin-like moieties for the retention of heparin-binding angiogenic factors. Delivery of angiogenic factors with high-affinity GAGs to prolonged receptor signaling. **C|** Material engineered with ECM protein domains displaying affinity for angiogenic factors, or recombinant fusion domains for co-binding to integrins and angiogenic factors to induce synergistic signaling. Materials engineered with angiogenic factor high-affinity domain isolated from its receptor. **D|** Material and/or angiogenic factor modified for chemical or enzymatic covalent immobilization. Angiogenic factor engineered for protease sensitivity and release upon cell-demand. **E|** Angiogenic factors engineered for high-affinity toward endogenous matrix components, such as glycosaminoglycans and collagens, or for promiscuous affinity toward various endogenous ECM glycoproteins.

a Physicochemical-based factor retention

Natural or augmented material
affinity to angiogenic factor

Encapsulation

Electrostatic
interactions

Angiogenic factors

Exogenous material
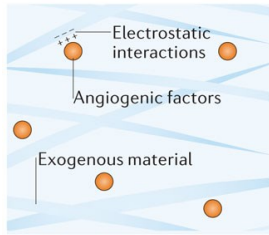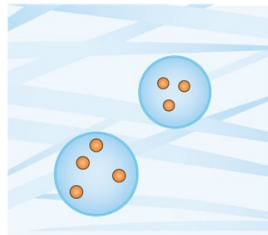
b Heparin- or GAG-based material engineering

Affinity mediated by heparin
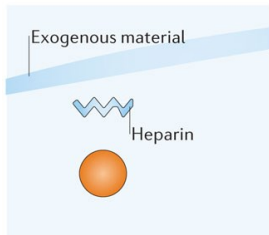
Affinity mediated by immobilized
heparin
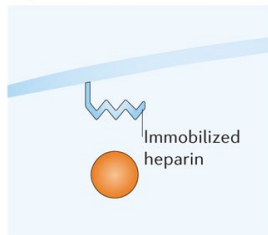
Prolonged signalling by high-
affinity GAGs

Exogenous material

Heparin

Immobilized
heparin

High-affinity GAG

Angiogenic factor
receptor

Cell
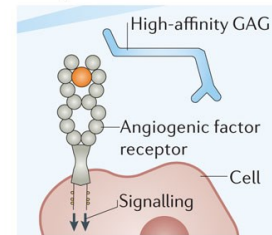
Signalling

c ECM protein- and receptor-based material engineering

Affinity mediated by ECM proteins
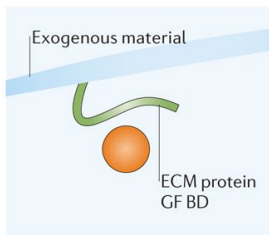
Synergistic signalling between integrins
and angiogenic factor receptors
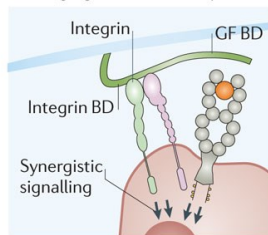
High affinity mediated by
receptor domains

Exogenous material

ECM protein
GF BD

Integrin

GF BD

Integrin BD

Synergistic
signalling

Angiogenic factor BD
(derived from receptor)
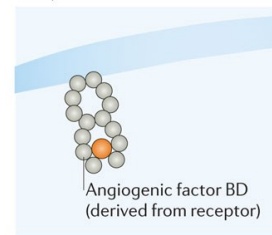
d Engineering of angiogenic factors along with the material

Direct conjugation
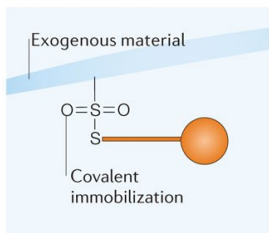
Enzymatic crosslinking

Cell-mediated release

Exogenous material

O=S=O
S

Covalent
immobilization

Factor XIIIa
substrate sequence

Factor XIIIa
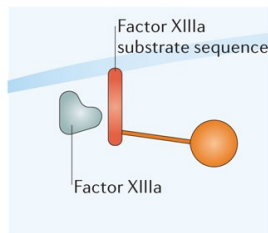
Protease

Proteolytic site
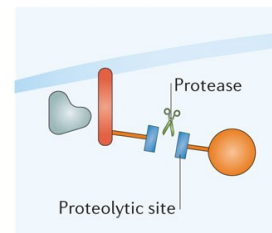
e Engineering of angiogenic factors to target endogenous ECM

Binding to endogenous GAGs
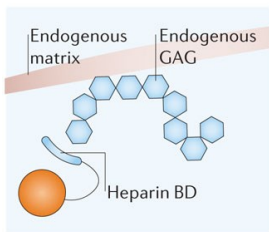
Binding to endogenous collagens
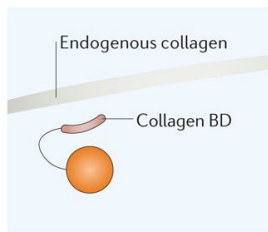
Promiscuous binding to various
ECM proteins

Endogenous
matrix

Endogenous
GAG

Heparin BD

Endogenous collagen

Collagen BD

ECM BD

Endogenous ECM protein

Nature Reviews | Materials

76
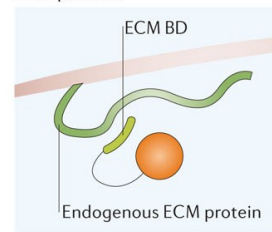
3.5 Conclusion and Outlook

Therapeutic angiogenesis remains a major clinical challenge. Given the lack of success following non-physiological delivery of angiogenic factors, future effects should emphasize the rules outlines here to better mimic physiological angiogenic conditions **(Box 3-1)**. Angiogenesis takes place in a highly dynamic 3D milieu that provides the instructive biomechanical and biomolecular microenvironment in which morphogenesis proceeds. The ECM regulates the sprouting of new blood vessels and the formation of vessel lumens and vessel stabilisation, to ultimately restore functional blood circulation into ischemic tissues. We detailed the molecular mechanisms involved in the reciprocal crosstalk between cells and the ECM during angiogenesis, highlighting the essential role of the ECM in controlling the spatiotemporal presentation and release of angiogenic growth factors. These molecular mechanisms can be used to identify key design rules for biomimetic angiogenic materials: biocompatibility, physiological delivery of angiogenic factors, and leveraging synergy between chemical and mechanical cues. These rules will help the next generation of biomaterials to become more effective in induction of stable angiogenic responses.

Box 3-1. Summary of design rules for therapeutic angiogenesis

Translation of angiogenic factors into clinical therapeutics has been strongly limited by both efficacy- and safety-related issues; the delivery of supra-physiological doses of angiogenic factors in a non-physiological context has failed to restore proper tissue vascularisation and may increase the risk of cancer in patients.

The extracellular matrix is the physiological material system in which angiogenesis naturally takes place; it displays key biophysical and biomolecular signals that can be mimicked or incorporated into angiogenic materials.

Angiogenic biomatrices should contain cell-adhesion and cell-degradable sites to allow cell migration and matrix remodeling, both central mechanisms in angiogenesis.

Angiogenic materials should incorporate essential angiogenic growth factors and control their spatio-temporal delivery to achieve sustained therapeutic angiogenesis.

Angiogenic materials should leverage cooperative interactions between the materials components, such as synergistic receptor signaling, to reduce the dose of angiogenic factors to be delivered.

It is critical to reduce the complexity of angiogenic materials to facilitate the regulatory process and make them suitable for clinical applications.

3.6 References

1.   Potente, M., Gerhardt, H. & Carmeliet, P. Basic and therapeutic aspects of angiogenesis. *Cell* **146**, 873-87 (2011).

2.   Carmeliet, P. Angiogenesis in life, disease and medicine. *Nature* **438**, 932-6 (2005).

3.   Clegg, L.E. & Mac Gabhan, F. Systems biology of the microvasculature. *Integrative Biology* (2015).

4.   Eming, S.A. & Hubbell, J.A. Extracellular matrix in angiogenesis: dynamic structures with translational potential. *Exp Dermatol* **20**, 605-13 (2011).

5.   Krock, B.L., Skuli, N. & Simon, M.C. Hypoxia-induced angiogenesis: good and evil. *Genes Cancer* **2**, 1117-33 (2011).

6.   Semenza, G.L. Hydroxylation of HIF-1: Oxygen sensing at the molecular level. *Physiology* **19**, 176-182 (2004).

7.   Herbert, S.P. & Stainier, D.Y. Molecular control of endothelial cell behaviour during blood vessel morphogenesis. *Nat Rev Mol Cell Biol* **12**, 551-64 (2011).

8.   Arroyo, A.G. & Iruela-Arispe, M.L. Extracellular matrix, inflammation, and the angiogenic response. *Cardiovasc Res* **86**, 226-35 (2010).

9.   Schultz, G.S. & Wysocki, A. Interactions between extracellular matrix and growth factors in wound healing. *Wound Repair Regen* **17**, 153-62 (2009).

10.   Ruhrberg, C. et al. Spatially restricted patterning cues provided by heparin-binding VEGF-A control blood vessel branching morphogenesis. *Genes & Development* **16**, 2684-2698 (2002).

11.   Vempati, P., Popel, A.S. & Mac Gabhann, F. Extracellular regulation of VEGF: isoforms, proteolysis, and vascular patterning. *Cytokine Growth Factor Rev* **25**, 1-19 (2014).

12.   Mahabeleshwar, G.H., Feng, W., Reddy, K., Plow, E.F. & Byzova, T.V. Mechanisms of integrin-vascular endothelial growth factor receptor cross-activation in angiogenesis. *Circ Res* **101**, 570-80 (2007).

13.   Somanath, P.R., Ciocea, A. & Byzova, T.V. Integrin and Growth Factor Receptor Alliance in Angiogenesis. *Cell Biochemistry and Biophysics* **53**, 53-64 (2008).

14.   Streuli, C.H. & Akhtar, N. Signal co-operation between integrins and other receptor systems. *Biochem J* **418**, 491-506 (2009).

15.   Wijelath, E.S. et al. Heparin-II domain of fibronectin is a vascular endothelial growth factor-binding domain: enhancement of VEGF biological activity by a singular growth factor/matrix protein synergism. *Circ Res* **99**, 853-60 (2006).

16.   Martino, M.M. et al. Engineering the growth factor microenvironment with fibronectin domains to promote wound and bone tissue healing. *Sci Transl Med* **3**, 100ra89 (2011).

17.   Kim, S.H., Turnbull, J. & Guimond, S. Extracellular matrix and cell signalling: the dynamic cooperation of integrin, proteoglycan and growth factor receptor. *J Endocrinol* **209**, 139-51 (2011).

18.   Armulik, A., Abramsson, A. & Betsholtz, C. Endothelial/pericyte interactions. *Circ Res* **97**, 512-23 (2005).

19.   Gaengel, K., Genove, G., Armulik, A. & Betsholtz, C. Endothelial-mural cell signaling in vascular development and angiogenesis. *Arterioscler Thromb Vasc Biol* **29**, 630-8 (2009).

20.   Ribatti, D., Nico, B. & Crivellato, E. The role of pericytes in angiogenesis. *Int J Dev Biol* **55**, 261-8 (2011).

21.   Davis, G.E. & Senger, D.R. Endothelial extracellular matrix: biosynthesis, remodeling, and functions during vascular morphogenesis and neovessel stabilization. *Circ Res* **97**, 1093-107 (2005).

22.   Lee, S., Jilani, S.M., Nikolova, G.V., Carpizo, D. & Iruela-Arispe, M.L. Processing of VEGF-A by matrix metalloproteinases regulates bioavailability and vascular patterning in tumors. *J Cell Biol* **169**, 681-91 (2005).

23.   Roy, R., Zhang, B. & Moses, M.A. Making the cut: protease-mediated regulation of angiogenesis. *Exp Cell Res* **312**, 608-22 (2006).

24.   van Hinsbergh, V.W. & Koolwijk, P. Endothelial sprouting and angiogenesis: matrix metalloproteinases in the lead. *Cardiovasc Res* **78**, 203-12 (2008).

25.   Ehrbar, M. et al. The role of actively released fibrin-conjugated VEGF for VEGF receptor 2 gene activation and the enhancement of angiogenesis. *Biomaterials* **29**, 1720-9 (2008).

26.   Martino, M.M. & Hubbell, J.A. The 12th-14th type III repeats of fibronectin function as a highly promiscuous growth factor-binding domain. *FASEB J* **24**, 4711-21 (2010).

27.   Lin, Y.-D. et al. Instructive nanofiber scaffolds with VEGF create a microenvironment for arteriogenesis and cardiac repair. *Sci Transl Med* **4**, 146ra109 (2012).

28.   Martino, M.M., Briquez, P.S., Ranga, A., Lutolf, M.P. & Hubbell, J.A. Heparin-binding domain of fibrin(ogen) binds growth factors and promotes tissue repair when incorporated within a synthetic matrix. *Proc Natl Acad Sci U S A* **110**, 4563-8 (2013).

29.   Phelps, E.A., Landazuri, N., Thule, P.M., Taylor, W.R. & Garcia, A.J. Bioartificial matrices for therapeutic vascularization. *Proc Natl Acad Sci U S A* **107**, 3323-8 (2010).

30.   Silva, E.A. & Mooney, D.J. Spatiotemporal control of vascular endothelial growth factor delivery from injectable hydrogels enhances angiogenesis. *J Thromb Haemost* **5**, 590-8 (2007).

31.   Martino, M.M. et al. Growth factors engineered for super-affinity to the extracellular matrix enhance tissue healing. *Science* **343**, 885-8 (2014).

32.   Sacchi, V. et al. Long-lasting fibrin matrices ensure stable and functional angiogenesis by highly tunable, sustained delivery of recombinant VEGF164. *Proc Natl Acad Sci U S A* **111**, 6952-7 (2014).

33.   World Health Organization. Cardiovascular diseases (CVDs), Fact Sheet n°317, www.who.int/mediacentre/factsheets/fs317/en/ (2015).

34.   Yoo, S.Y. & Kwon, S.M. Angiogenesis and its therapeutic opportunities. *Mediators Inflamm* **2013**, 127170 (2013).

35.   Martino, M.M. et al. Extracellular matrix and growth factor engineering for controlled angiogenesis in regenerative medicine. *Front Bioeng Biotechnol* **3**, 45 (2015).

36.   Foundation, T.A. (2015).

37.   Prabhu, V.V., Chidambaranathan, N. & Gopal, V. A Historical Review on Current Medication and Therapies for Inducing and Inhibiting Angiogenesis. *J. Chem. Pharm. Res.* **2**, 526-533 (2011).

38.   U.S. Food and Drug Administration (FDA). Safety warning on becaplermin in Regranex®. *Silver Spring*, 1-10 (2008).

39.   Simons, M. & Ware, J.A. Therapeutic angiogenesis in cardiovascular disease. *Nat Rev Drug Discov* **2**, 863-71 (2003).

40.   Tongers, J., Roncalli, J.G. & Losordo, D.W. Therapeutic angiogenesis for critical limb ischemia: microvascular therapies coming of age. *Circulation* **118**, 9-16 (2008).

41.   World Health Organization. International Clinical Trials Registry Platform (ICTRP) database, www.who.int/ictrp/search/en/ (2015).

42.   Ruel, M. et al. Long-term effects of surgical angiogenic therapy with fibroblast growth factor 2 protein. *The Journal of Thoracic and Cardiovascular Surgery* **124**, 28-34 (2002).

43.   Briquez, P.S., Hubbell, J.A. & Martino, M.M. Extracellular Matrix-Inspired Growth Factor Delivery Systems for Skin Wound Healing. *Advances in Wound Care*, 150127064149004 (2015).

44.   Rhodes, J.M. & Simons, M. The extracellular matrix and blood vessel formation: not just a scaffold. *J Cell Mol Med* **11**, 176-205 (2007).

45.   George, E.L., Georges-Labouesse, E.N., Patel-King, R.S., Rayburn, H. & Hynes, R.O. Defects in mesoderm, neural-tube and vascular development in mouse embryos lacking fibronectin. *Development* **4**, 1079-91 (1993).

46.   Edgar, L.T., Hoying, J.B. & Weiss, J.A. In Silico Investigation of Angiogenesis with Growth and Stress Generation Coupled to Local Extracellular Matrix Density. *Ann Biomed Eng* **43**, 1531-42 (2015).

47.   Bordeleau, F. et al. Tissue stiffness regulates serine/arginine-rich protein-mediated splicing of the extra domain B-fibronectin isoform in tumors. *Proc Natl Acad Sci U S A* **27**, 8314-9 (2015).

48.   Kim, S., Harris, M. & Varner, J.A. Regulation of integrin alpha vbeta 3-mediated endothelial cell migration and angiogenesis by integrin alpha5beta1 and protein kinase A. *J Biol Chem* **275**, 33920-8 (2000).

49.   Davis, G.E., Bayless, K.J. & Mavila, A. Molecular basis of endothelial cell morphogenesis in three-dimensional extracellular matrices. *Anat Rec* **268**, 252-75 (2002).

50.   Grainger, S. & Putnam, A. in Mechanical and Chemical Signaling in Angiogenesis. Studies in Mechanobiology, Tissue Engineering and Biomaterials. (ed. CA, R.-K.) 185-209 (Springer Berlin Heidelberg, 2013).

51.   Hodivala-Dilke, K.M., Reynolds, A.R. & Reynolds, L.E. Integrins in angiogenesis: multitalented molecules in a balancing act. *Cell Tissue Res* **314**, 131-44 (2003).

52.   Koch, S., Tugues, S., Li, X., Gualandi, L. & Claesson-Welsh, L. Signal transduction by vascular endothelial growth factor receptors. *Biochem J* **437**, 169-83 (2011).

53.   Olsson, A.K., Dimberg, A., Kreuger, J. & Claesson-Welsh, L. VEGF receptor signalling - in control of vascular function. *Nat Rev Mol Cell Biol* **7**, 359-71 (2006).

54.   Hoier, B. et al. Angiogenic response to passive movement and active exercise in individuals with peripheral arterial disease. *J Appl Physiol* **115**, 1777–1787 (2013).

55.   Hoier, B. et al. Pro- and anti-angiogenic factors in human skeletal muscle in response to acute exercise and training. *J Physiol* **590**, 595-606 (2012).

56.   Kut, C., Mac Gabhann, F. & Popel, A.S. Where is VEGF in the body? A meta-analysis of VEGF distribution in cancer. *Br J Cancer* **97**, 978-85 (2007).

57.   Vempati, P., Popel, A.S. & Mac Gabhann, F. Formation of VEGF isoform-specific spatial distributions governing angiogenesis: computational analysis. *BMC Syst Biol* **5**, 59 (2011).

58.   Mac Gabhann, F. & Popel, A.S. Systems biology of vascular endothelial growth factors. *Microcirculation* **15**, 715-38 (2008).

59.   Ballmer-Hofer, K., Andersson, A.E., Ratcliffe, L.E. & Berger, P. Neuropilin-1 promotes VEGFR-2 trafficking through Rab11 vesicles thereby specifying signal output. *Blood* **118**, 816-26 (2011).

60.   Park, J.E., Keller, G.A. & Ferrara, N. Vascular endothelial growth-factor (VEGF) isoforms - differential deposition into the subepithelial extracellular-matrix and bioactivity of extracellular matrix-bound VEGF. *Molecular Biology of the Cell* **4**, 1317-1326 (1993).

61.   Ruhrberg, C. et al. Spatially restricted patterning cues provided by heparin-binding VEGF-A control blood vessel branching morphogenesis. *Genes & Development* **16**, 2684-2698 (2002).

62.   Grunstein, J., Masbad, J.J., Hickey, R., Giordano, F. & Johnson, R.S. Isoforms of vascular endothelial growth factor act in a coordinate fashion to recruit and expand tumor vasculature. *Molecular and Cellular Biology* **20**, 7282-7291 (2000).

63.   Grunstein, J., Masbad, J.J., Hickey, R., Giordano, F. & Johnson, R.S. Isoforms of Vascular Endothelial Growth Factor Act in a Coordinate Fashion To Recruit and Expand Tumor Vasculature. *Molecular and Cellular Biology* **19**, 7282-91 (2000).

64.   Cordon-Cardo, C., Vlodavsky, I., Haimovitz-Friedman, A.H., D. & Fuks, Z. Expression of basic fibroblast growth factor in normal human tissues. *Lab Invest* **6**, 832-40 (1990).

65.   Jin-No, K., Tanimizu, M., Hyodo, I., Kurimoto, F. & Yamashita, T. Plasma level of basic fibroblast growth factor increases with progression of chronic liver disease. *J Gastroenterol* **1**, 119-21 (1997).

66.   Kuwabara, K. et al. Hypoxia-mediated induction of acidic/basic fibroblast growth factor and platelet-derived growth factor in mononuclear phagocytes stimulates growth of hypoxic endothelial cells. *Proc Natl Acad Sci U S A* **92**, 4606-4610 (1995).

67.   Wang, L. et al. The effect of hypoxia on expression of basic fibroblast growth factor in pulmonary vascular pericytes. *J Tongji Med Univ.* **4**, 265-7 (2000).

68.   Presta, M. et al. Fibroblast growth factor/fibroblast growth factor receptor system in angiogenesis. *Cytokine Growth Factor Rev* **16**, 159-78 (2005).

69.   Forsten, K.E., Fannon, M. & Nugent, M.A. Potential mechanisms for the regulation of growth factor binding by heparin. *J Theor Biol* **205**, 215-30 (2000).

70.   Forsten-Williams, K., Chua, C.C. & Nugent, M.A. The kinetics of FGF-2 binding to heparan sulfate proteoglycans and MAP kinase signaling. *J Theor Biol* **233**, 483-99 (2005).

71.   Delehedde, M. et al. Fibroblast growth factor-2 stimulation of p42/44(MAPK) phosphorylation and I kappa B degradation is regulated by heparan sulfate/heparin in rat mammary fibroblasts. *Journal of Biological Chemistry* **275**, 33905-33910 (2000).

72.   Andrae, J., Gallini, R. & Betsholtz, C. Role of platelet-derived growth factors in physiology and medicine. *Genes & Development* **22**, 1276-1312 (2008).

73.   Cenni, E. et al. Plasma levels of platelet-derived growth factor BB and transforming growth in patients with failed hip prostheses. *Acta Orthopaedica* **76**, 61-66 (2005).

74. Kelly, J.L., Sanchez, A., Brown, G.S., Chesterman, C.N. & Sleigh, M.J. Accumulation of PDGF-BB and cell-binding form of PDGF-A in the extracellular matrix. *Journal of Cell Biology* **121**, 1153-1163 (1993).

75. Soyombo, A.A. & Dicorleto, P.E. Stable expression of human platelet-derived growth factor-B chain by bovin aortic endothelial cells - matrix association and selective proteolytic cleavage by thrombin. *Journal of Biological Chemistry* **269**, 17734-17740 (1994).

76. Lindblom, P. et al. Endothelial PDGF-B retention is required for proper investment of pericytes in the microvessel wall. *Genes & Development* **17**, 1835-1840 (2003).

77. Abramsson, A. et al. Analysis of mural cell recruitment to tumor vessels. *Circulation* **105**, 112-117 (2002).

78. Carlson, T.R., Feng, Y.Z., Maisonpierre, P.C., Mrksich, M. & Morla, A.O. Direct cell adhesion to the angiopoietins mediated by integrins. *Journal of Biological Chemistry* **276**, 26516-26525 (2001).

79. Cascone, I., Napione, L., Maniero, F., Serini, G. & Bussolino, F. Stable interaction between alpha 5 beta 1 integrin and Tie2 tyrosine kinase receptor regulates endothelial cell response to Ang-1. *Journal of Cell Biology* **170**, 993-1004 (2005).

80. Zhang, J. et al. Angiopoietin-1/Tie2 signal augments basal Notch signal controlling vascular quiescence by inducing delta-like 4 expression through AKT-mediated activation of beta-catenin. *J Biol Chem* **286**, 8055-66 (2011).

81. Kofler, N.M. et al. Notch signaling in developmental and tumor angiogenesis. *Genes & cancer* **2**, 1106-16 (2011).

82. Augustin, H.G., Koh, G.Y., Thurston, G. & Alitalo, K. Control of vascular morphogenesis and homeostasis through the angiopoietin-Tie system. *Nature Reviews Molecular Cell Biology* **10**, 165-177 (2009).

83. Mosch, B., Reissenweber, B., Neuber, C. & Pietzsch, J. Eph receptors and ephrin ligands: important players in angiogenesis and tumor angiogenesis. *Journal of oncology* **2010**, 135285-135285 (2010).

84. Sawamiphak, S. et al. Ephrin-B2 regulates VEGFR2 function in developmental and tumour angiogenesis. *Nature* **465** (2010).

85. Marston, D.J., Dickinson, S. & Nobes, C.D. Rac-dependent trans-endocytosis of ephrinBs regulates Eph-ephrin contact repulsion. *Nature Cell Biology* **5**, 879-888 (2003).

86. Mac Gabhann, F. & Popel, A.S. Interactions of VEGF isoforms with VEGFR-1, VEGFR-2, and neuropilin in vivo: a computational model of human skeletal muscle. *American Journal of Physiology-Heart and Circulatory Physiology* **292** (2007).

87. Filion, R.J. & Popel, A.S. Intracoronary administration of FGF-2: a computational model of myocardial deposition and retention. *American Journal of Physiology-Heart and Circulatory Physiology* **288**, H263-H279 (2005).

88. Fannon, M. et al. Binding inhibition of angiogenic factors by heparan sulfate proteoglycans in aqueous humor: potential mechanism for maintenance of an avascular environment. *Faseb Journal* **17**, 902-+ (2003).

89. Ferrara, N. et al. Heterozygous embryonic lethality induced by targeted inactivation of the VEGF gene. *Nature* **380**, 439-442 (1996).

90. Carmeliet, P. et al. Abnormal blood vessel development and lethality in embryos lacking a single VEGF allele. *Nature* **380**, 435-439 (1996).

91. Stefanini, M.O., Wu, F.T., Mac Gabhann, F. & Popel, A.S. A compartment model of VEGF distribution in blood, healthy and diseased tissues. *BMC Systems Biology* **2** (2008).

92. Anderson, S.M. et al. VEGF internalization is not required for VEGFR-2 phosphorylation in bioengineered surfaces with covalently linked VEGF. *Integrative Biology* **3**, 887-896 (2011).

93. Chen, T.T. et al. Anchorage of VEGF to the extracellular matrix conveys differential signaling responses to endothelial cells. *Journal of Cell Biology* **188**, 595-609 (2010).

94. Clegg, L.W. & Mac Gabhann, F. Site-Specific Phosphorylation of VEGFR2 Is Mediated by Receptor Trafficking: Insights from a Computational Model. *PLoS Comput Biol* **11**, e1004158 (2015).

95. Smith, J.C., Singh, J.P., Lillquist, J.S., Goon, D.S. & Stiles, C.D. Growth factors adherent to cell substrate are mitogenically active in situ. *Nature* **296**, 154-156 (1982).

96.   Baird, A. & Ling, N. Fibroblast growth factors are present in the extracellular-matrix produced by endothelial cells in vitro - implications for a role of heparinase-like enzymes in the neovascular response. *Biochemical and Biophysical Research Communications* **142**, 428-435 (1987).

97.   Saksela, O. & Rifkin, D.B. Release of basic fibroblast growth factor-heparan sulfate complexes from endothelial cells by plasminogen activator-mediated proteolytic activity. *Journal of Cell Biology* **110**, 767-775 (1990).

98.   Ferrara, N. Binding to the extracellular matrix and proteolytic processing: two key mechanisms regulating vascular endothelial growth factor action. *Mol Biol Cell* **21**, 687-90 (2010).

99.   Vempati, P., Mac Gabhann, F. & Popel, A.S. Quantifying the Proteolytic Release of Extracellular Matrix-Sequestered VEGF with a Computational Model. *Plos One* **5** (2010).

100.   Miyamoto, S., Teramoto, H., Gutkind, J.S. & Yamada, K.M. Integrins can collaborate with growth factors for phosphorylation of receptor tyrosine kinases and MAP kinase activation: Roles of integrin aggregation and occupancy of receptors. *Journal of Cell Biology* **135**, 1633-1642 (1996).

101.   Sepp, N.T. et al. Basic fibroblast growth factor increases expression of the alpha(v) beta(3) integrin complex on human microvascular endothelial cells. *Journal of Investigative Dermatology* **103**, 295-299 (1994).

102.   Masson-Gadais, B., Houle, F., Laferriere, J. & Huot, J. Integrin alpha(v)beta(3) requirement for VEGFR2-mediated activation of SAPK2/p38 and for Hsp90-dependent phosphorylation of focal adhesion kinase in endothelial cells activated by VEGF. *Cell Stress & Chaperones* **8**, 37-52 (2003).

103.   Hodivala-Dilke, K. Alpha v beta 3 integrin and angiogenesis: a moody integrin in a changing environment. *Current Opinion in Cell Biology* **20**, 514-519 (2008).

104.   Somanath, P.R., Malinin, N.L. & Byzova, T.V. Cooperation between integrin alpha(nu)beta(3) and VEGFR2 in angiogenesis. *Angiogenesis* **12**, 177-185 (2009).

105.   Francis, S.E. et al. Central roles of alpha(5)beta(1) integrin and fibronectin in vascular development in mouse embryos and embryoid bodies. *Arteriosclerosis Thrombosis and Vascular Biology* **22**, 927-933 (2002).

106.   Tsou, R. & Isik, F.F. Integrin activation is required for VEGF and FGF receptor protein presence on human microvascular endothelial cells. *Molecular and Cellular Biochemistry* **224**, 81-89 (2001).

107.   Enenstein, J., Waleh, N.S. & Kramer, R.H. Basic FGF and TGF-beta differentially modulate integrin expression of microvascular endothelial cells. *Experimental Cell Research* **203**, 499-503 (1992).

108.   Klein, S. et al. Basic fibroblast growth-factor modulates integrin expression in microvascular endothelial cells. *Molecular Biology of the Cell* **4**, 973-982 (1993).

109.   Byzova, T.V. et al. A mechanism for modulation of cellular responses to VEGF: Activation of the integrins. *Molecular Cell* **6**, 851-860 (2000).

110.   Valdembri, D. et al. Neuropilin-1/GIPC1 Signaling Regulates alpha 5 beta 1 Integrin Traffic and Function in Endothelial Cells. *Plos Biology* **7**, 115-132 (2009).

111.   Robinson, S.D. et al. alpha v beta 3 Integrin Limits the Contribution of Neuropilin-1 to Vascular Endothelial Growth Factor-induced Angiogenesis. *Journal of Biological Chemistry* **284**, 33966-33981 (2009).

112.   Baum, O., Djonov, V., Ganster, M., Widmer, M. & Baumgartner, I. Arteriolization of capillaries and FGF-2 upregulation in skeletal muscles of patients with chronic peripheral arterial disease. *Microcirculation* **12**, 527-537 (2005).

113.   Kikuchi, R. et al. An antiangiogenic isoform of VEGF-A contributes to impaired vascularization in peripheral artery disease. *Nature Medicine* **20**, 1464-1471 (2014).

114.   Ngo, D.T.M. et al. Antiangiogenic Actions of Vascular Endothelial Growth Factor-A(165)b, an Inhibitory Isoform of Vascular Endothelial Growth Factor-A, in Human Obesity. *Circulation* **130**, 1072-1080 (2014).

115.   Zisch, A.H., Lutolf, M.P. & Hubbell, J.A. Biopolymeric delivery matrices for angiogenic growth factors. *Cardiovascular Pathology* **12**, 295-310 (2003).

116.   Rice, J.J. et al. Engineering the regenerative microenvironment with biomaterials. *Adv Healthc Mater* **2**, 57-71 (2013).

117.   Hoganson, D.M. et al. The retention of extracellular matrix proteins and angiogenic and mitogenic cytokines in a decellularized porcine dermis. *Biomaterials* **31**, 6730-7 (2010).

118.   Hern, D.L. & Hubbell, J.A. Incorporation of adhesion peptide into nonadhesive hydrogels useful for tissue resurfacing. *Journal of Biomedical Materials Research* (1998).

119.   Seliktar, D., Zisch, A.H., Lutolf, M.P., Wrana, J.L. & Hubbell, J.A. MMP-2 sensitive, VEGF-bearing bioactive hydrogels for promotion of vascular healing. *J Biomed Mater Res A* **68**, 704-16 (2004).

120.   Turturro, M.V. et al. MMP-sensitive PEG diacrylate hydrogels with spatial variations in matrix properties stimulate directional vascular sprout formation. *PLoS One* **8**, e58897 (2013).

121.   Briquez, P. S., Clegg, L. E., Martino, M. M., Gabhann, F. M. & Hubbell, J. A. Design principles for therapeutic angiogenic materials. *Nature Reviews Materials* **1**, 15006, doi:10.1038/natrevmats.2015.6 (2016).

Chapter 4. Computational Modeling in Therapy Design and Translation

4.0 Summary

Making drug development a more efficient and cost-effective process will have a transformative effect on human health. A key, yet underutilized, tool to aid in this transformation is mechanistic computational modeling. By incorporating decades of hard-won prior knowledge of molecular interactions, cellular signaling, and cellular behavior, mechanistic models can achieve a level of predictiveness that is not feasible using solely empirical characterization of drug pharmacodynamics. These models can integrate diverse types of data from cell culture and animal experiments, including high-throughput systems biology experiments, and translate the results into the context of human disease. This provides a framework for identification of new drug targets, measurable biomarkers for drug action in target tissues, and patient populations for which a drug is likely to be effective or ineffective. Additionally, mechanistic models are valuable in virtual screening of new therapeutic strategies, such as gene or cell therapy and tissue regeneration, identifying the key requirements for these approaches to succeed in a heterogeneous patient population. These capabilities, which are distinct from and complementary to those of existing drug development strategies, demonstrate the opportunity to improve success rates in the drug development pipeline through the use of mechanistic computational models.

Fig. 4-G1. Graphical Abstract

Cell Culture Data

Animal Model Data

Mechanistic Computational Models

Transform experimental data into mechanistic insight

Translate mechanistic insight into the context of human disease

Human Patients

Novel Drug Targets
Virtual Drug Screening
Predictive Biomarkers
Patient-Specific Regimens
Increase Knowledge of Disease
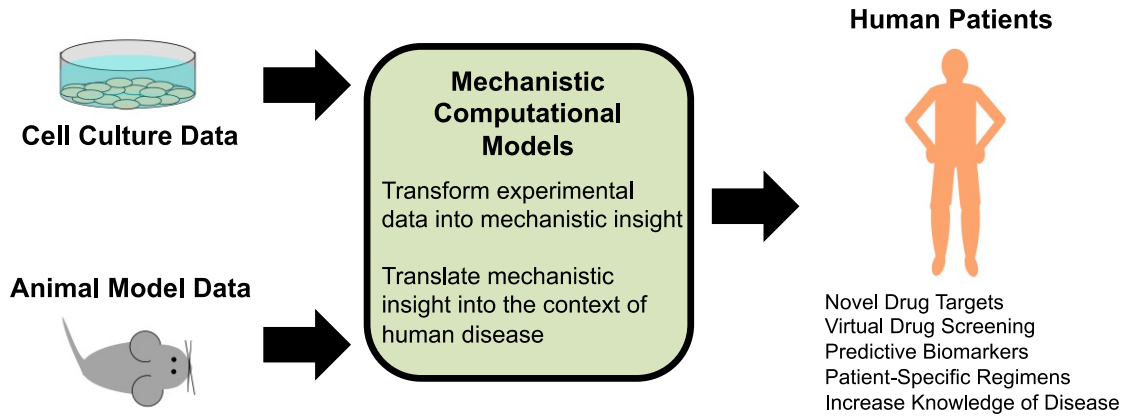
4.1 Current Strategies for Drug Development

It is well established that traditional drug development is a long and increasingly costly process, due in large part to high attrition of drugs throughout the development pipeline [1, 2]. As of 2010, the estimated cost to develop a single new molecular entity (novel active ingredient) was $1.8 billion dollars [3]. In addition, only about 5-6 mechanistically innovative (first-in-class) drugs are approved in the US per year [3, 4]. The most common reasons for drug failure, particularly in Phase 2 trials, are lack of efficacy and toxicity due to off-target drug effects, which were not apparent in cellular and animal systems [5-7]. A better understanding of potential drug targets and mechanisms of action promises to aid in earlier identification of ineffective drugs, or drugs with unsafe off-target effects, as well as to inform the necessary properties (e.g. precise targets and binding affinities) for more effective compounds.

Traditionally, drug efficacy and safety are assayed by characterizing the pharmacokinetics (PK) and pharmacodynamics (PD) of the drug. PK describes what the body does to a drug (e.g. drug absorption, clearance, and distribution throughout the body), while PD characterizes what a drug does to the body (i.e. drug action in target tissue). Drug PK and PD are typically estimated using a combination of cell culture and animal models, along with human data for similar, previously-developed drugs. This empirical PK and PD characterization allows drug developers to estimate drug half-life in the body and uptake within tissues. Computational models incorporating both PK and PD (PK/PD models) are used to simulate drug distribution in the body, predicting the time delay from administration to drug action in the target tissue, and potential issues such as drug accumulation leading to toxicity. As such, these simulations have the potential to aid in establishing safety margins [8]. While PK/PD work is a critical component of drug development, traditional PK/PD studies do not identify the most effective targets for new drugs, or account for complex biological compensation mechanisms. This lack of predictiveness is a result of the data-driven nature of these studies, which makes extrapolation to other dosing ranges or to related drugs, as well as prediction of patient-specific responses, difficult. The missing piece is a detailed understanding of the molecular mechanisms of action underlying pharmacodynamic responses. Mechanistic models (**Box 4-1**) can incorporate this understanding into PK/PD models.

Box 4-1. What is a mechanistic computational model?

A **mechanistic computational model** simulates interactions between the key molecular entities (e.g. proteins, ATP, RNA), and the processes they undergo (e.g. expression, subcellular trafficking, degradation, phosphorylation, deactivation), explicitly by solving a set of mathematical equations that represent the underlying chemical reactions (e.g. $[A]+[B]\rightleftharpoons[A\cdot B]$). The **key distinguishing feature** of a mechanistic model is incorporation of detail **based on prior knowledge** of the regulatory network, as opposed to inferring interactions using a data-driven approach.

The sequencing of the human genome brought hope that newly identified genetic components of health and disease would clearly guide advances in therapies for a wide variety of conditions. While bioinformatics approaches have identified new therapeutic targets for some diseases, in many cases there is no clear disease-associated genetic signature that is consistent across patients. Even when a disease-related molecule is identified, it does not necessarily represent an effective drug target; thus far, target-based screening has not been more effective than traditional phenotypic drug screening [9]. As such, many researchers interested in drug development have turned to systems biology, which combines high-throughput experiments and mechanistic computational modeling to better understand the interactions of the molecules that regulate cell behavior.

Systems biology approaches have deepened our understanding of the pathways involved in cellular survival & behavior, and how cellular signaling changes in disease [10]. One particularly valuable benefit of mechanistic computational models is their ability to incorporate the specifics of different experimental protocols (e.g. drug/ligand concentration, measurement time, cell line), allowing for reconciliation of apparent discrepancies in experimental results from different groups, protocols, or cell types. Along with deriving more insight from experimental results, these models can be used to design the next sets of experiments, in order to answer key unsolved questions. A second key strength of mechanistic computational models is the ability to examine the sensitivity of individual signaling pathway components to perturbation (e.g. change in receptor expression or ligand concentration). Proteins to which the model is highly sensitive likely represent key nodes and promising drug targets. Despite these advantages, translation of systems biology into the context of the human body for use in the drug development pipeline has been limited [5, 11], due in part to the prevalence of empirical PK/PD modeling in industry, while mechanistic computational modeling occurs primarily in academic research laboratories (with some notable exceptions).

The emerging field of systems pharmacology aims to bridge systems biology and PK/PD modeling, translating the mechanistic insight emerging from systems biology into a therapeutically relevant context [12, 13]. To do this, mechanistic models (**Box 4-1**) are used to describe the pharmacodynamics in quantitative detail, and are integrated with drug pharmacokinetics in a PK/PD model. Several excellent examples of systems pharmacology models incorporating mechanistic intracellular signaling detail have

been published in recent years [12, 14, 15]. However, such models remain the minority; it is more common for drug pharmacodynamics to be represented by empirical drug-tissue binding curves (e.g. Hill equation) [16, 17]. While useful, such data-driven binding curves have limited ability to reliably extrapolate to other species, to humans with different genetics and body mass, to related drugs, to combination therapies, or even to different dosing schedules and administration routes for the same drug [11]. One reason for a semi-mechanistic representation of PD in many models to date is a lack of sufficient mechanistic information available from experiments. While this is a challenge, the amount of useful information increases quickly, e.g. due to high-throughput experiments using new molecular imaging and gene expression measurement techniques [18-20]. Additionally, because computational models can integrate diverse data types into a single framework, data from experiments designed for very different purposes, or obtained from different groups using different protocols, can be leveraged [21]. For example, in our PK/PD models, the geometric parameters for the PK component are obtained from histological studies, while the PD are based on a combination of binding assays, receptor trafficking studies, and measurements of receptor phosphorylation under different conditions, from experiments performed in multiple cells lines by different research groups [22, 23].

One of the areas where systems pharmacology holds the most promise is in accounting for changes in PK and PD between animal models and humans, both due to geometric differences, and to species-specific genes and gene expression patterns (**Fig. 4-1**) [13]. Detailed systems pharmacology models can be built and validated using *in vitro* data and pharmacokinetic studies in animals, and then converted into human- and disease-specific models [10, 24]. In order for these models to make clinically-relevant predictions, they must then be validated against human data to the maximum extent possible. While human data is limited, levels of drug and other biomarkers in plasma can be measured with relative ease. Mechanistically-detailed systems pharmacology models can then connect predictions of important but difficult-to-measure quantities, such as drug concentration, occupancy of receptors with drug versus native ligand, and cellular signaling at the target site, to measureable biomarkers [10]. By providing a window into the site of disease, these models have great promise to improve our understanding of both disease and therapy in the human body.

Figure 4-1. Mechanistic computational models bridge gaps in translation. Due to the difficulty and invasiveness of obtaining direct human measurements of disease and drug action, we often rely on data from other systems. However, translating experimental results from cell culture and animal models into useful predictions in human patients is difficult (dashed boxes). Experimental conditions in cell culture (top) do not match the *in vivo* site of drug action. Similarly, there is mismatch between animal models (bottom) and human patients. Mechanistic computational models can explicitly account for these differences, integrating data from diverse sources into a single framework, and providing mechanistic insight into drug action. Human disease-specific computational models (PK/PD of the whole body or 3D models or particular tissues) can then be used to predict the effects of drugs in human patients, incorporating patient-specific information (e.g. genetic mutations and gene expression changes).
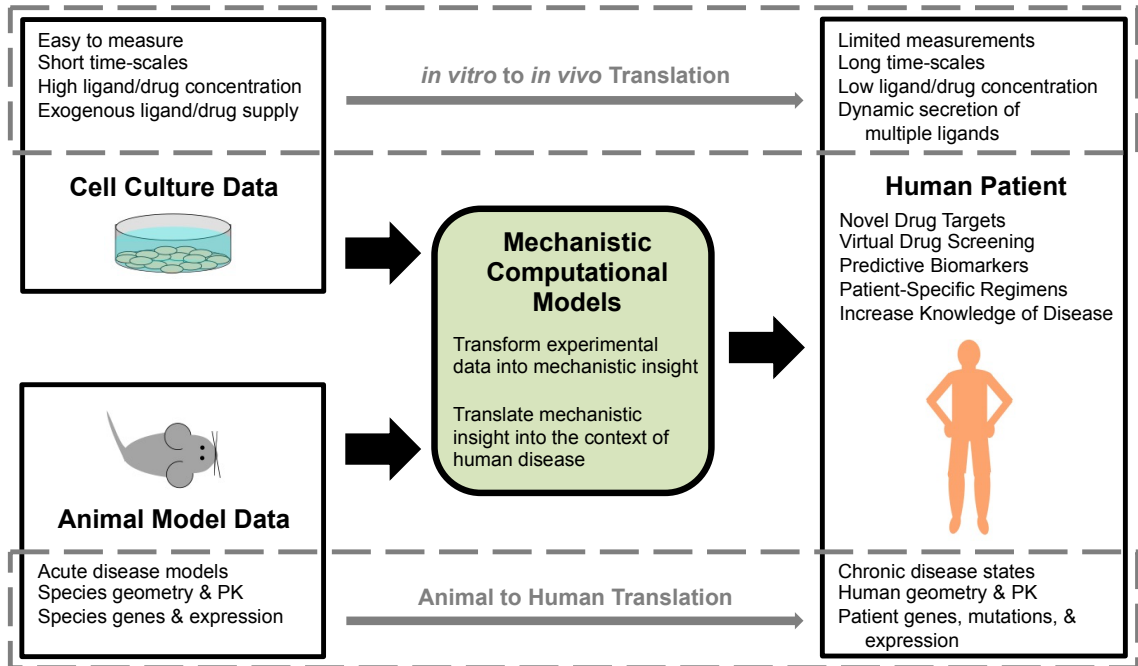
In light of the capabilities of mechanistic computational models (**Box 4-2**), we propose that inclusion of detailed mechanistic information into pharmacodynamic models is critical to understand drug PD in an insightful and predictive way. We present three brief examples where inclusion of mechanistic detail was necessary to: (1) meaningfully discriminate between effective and ineffective drugs, (2) identify promising new drug targets, or (3) understand why existing therapeutic approaches have been ineffective. We chose case studies that focus on mechanistic modeling of receptors and channels, as they are subject to complex regulation, but provide targets more specific than downstream signaling pathways, which are common to many cellular processes. These examples involve different biological systems, highlight different advantages of mechanistic models, and use different techniques to translate the mechanistic insight into the human body. All, however, demonstrate the promise of mechanistic computational models to aid in drug development for a wide range of diseases (**Box 4-2**).

Box 4-2. Capabilities of mechanistic computational models.

New Drug Design
- Integrate data from diverse sources
- Identify key, highly sensitive nodes in a signaling network
- Inform optimal properties of new drugs (e.g. binding affinity)

Drug Discrimination
- Predict effective vs. ineffective therapeutic strategies based on mechanism & properties that emerge in humans but not in experimental systems
- Predict off-target drug effects that may lead to toxicity or drug failure
- Predict optimal dosing, scheduling, route of administration, & drug combinations
- Design experiments to better discriminate between drug candidates or existing & repurposed drugs

Translation to Diverse Human Population
- Develop better understanding of human disease states
- Translate results from experimental & animal systems into a human patient- and disease-specific context
- Improve extrapolation between similar drugs, between experimental systems, and between patients, due to predictive, mechanism-based framework
- Identify biomarkers for subpopulation inclusion or exclusion from clinical trials, e.g. based on patient-specific gene expression
- Link measurable blood biomarkers to disease state at drug site-of-action

Establish Requirements for Success of Emerging Therapeutic Approaches
- Gene Therapy (e.g. transfection efficiency)
- Cell Therapy (e.g. cell type & delivery method)
- Organ Transplant (e.g. drug regimens, predictive markers of rejection)
- Engineered Tissue Constructs (e.g. requirements for functional vascularization)

4.2 Case Study 1: Drug Discrimination for Cardiac Arrhythmia

A promising application for mechanistic computational models is to perform virtual drug screening, eliminating candidate drugs that appear to work in single-cell systems, but have emergent properties in the context of human physiology that may result in adverse effects. The multi-scale mechanistic computational models built by Colleen Clancy and collaborators to compare anti-arrhythmia drugs, both in the context of a single cell and within tissues, provide an elegant example. Cardiac arrhythmia is a complex condition involving the (dis)coordinated electrical excitation of a large number of cells in the heart, which can cause sudden death. Based on single-cell experiments, blocking Na^+ channels in cardiac myocytes was identified as a promising therapeutic strategy. However, clinical trials have demonstrated that, instead of suppressing arrhythmia, some of these drugs actually increase the incidence of sudden cardiac death by 2-3 fold in patients with a history of myocardial infarction [25]. Specifically, the class 1B anti-arrhythmia drug lidocaine, which has fast association-dissociation kinetics, has no known safety issues, but the class 1C anti-arrhythmia drug flecainide, with slow drug-channel association & dissociation, is known to cause conduction block at high physiological doses. As the pharmacokinetics of these drugs are well-characterized [26, 27], this study focused specifically on modeling drug pharmacodynamics within cardiac tissue.

The Clancy group model, which integrates decades of experimental study on the mechanisms of action of ion channels, represents the active and inactive states of the cardiac Na^+ channel using a Markov model [28, 29]. To incorporate Na^+-channel-blocking drugs, they used experimental data to estimate the affinity of both charged and neutral fractions of multiple drugs for each of the possible Na^+ channel conformations [29]. The resulting model captured the ability of both drugs to slow conduction in single cardiac cells. To translate these observations to a clinically-relevant framework, the Clancy group and their collaborators simulated the actions of the same drugs in groups of coupled cells. The computational model — applied to both simulated 2D tissue sheets and 3D models of the human ventricle — was able to replicate the clinically-observed conduction block and increased sensitivity to early or late heart beats (which can lead to sudden cardiac death) after treatment with a high clinical dose of flecainide at fast pacing rates (160 bpm), but not with lidocaine [29]. This prediction, which emerged in organized tissues as a result of molecular-level differences in drug properties, was then validated in an animal model. In

addition to discriminating between effective and ineffective drugs, this model allows for identification of safe dosing ranges and physiological counter-indications (tachycardia) for use. The Clancy group is now expanding this work to other drugs and personalized medicine applications [30, 31], including a study of sex-driven differences in susceptibility to arrhythmia as a result of sex-specific gene expression and sex hormones [32].

4.3 Case Study 2: Drug Target Identification for Cancer

Sensitivity analysis of mechanistic computational models allows for identification of key nodes in signaling pathways, which can be promising drug targets, as well as predicting changes in signaling resulting from the tuning of drug properties. This is of particular interest in fields where existing drugs have limited efficacy or are susceptible to resistance, as mechanistic models can also predict which patients will benefit from a particular drug. An excellent application of mechanistic computational models for cancer drug development is the work of Birgit Schoeberl and colleagues at Merrimack Pharmaceuticals. This group built detailed models of ligand-binding, receptor dimerization, and downstream signaling in the ErbB family, the receptors of which are commonly overexpressed or constitutively active in cancer [33, 34]. To build these models, they performed extensive screening of ErbB family receptor phosphorylation and Akt activation in diverse cancer cell lines. They then fit kinetic parameters in the model using this experimental data. They found that Akt signaling resulting from treatment with betacellulin or heregulin1-β was more sensitive to perturbation of ErbB3/HER3, a kinase-dead receptor tyrosine kinase, than the more commonly targeted ErbB1/EGFR or ErbB2/HER2 [34]. Without such modeling efforts, ErbB3 was unlikely to be identified as a promising drug target, due to its lack of an active kinase domain.

As a result of this work, Merrimack Pharmaceuticals designed an antibody (MM-121) specifically to inhibit phosphorylation of ErbB3, with an affinity for ErbB3 informed by the mechanistic computational modeling effort [34, 35]. In addition to drug design, the team was able to identify potential molecular biomarkers for response to MM-121. This has had a direct impact on the development process: high heregulin expression, predicted to be indicative of a positive response to MM-121 treatment, is an inclusion criteria for a current phase II clinical trial for MM-121 in combination with chemotherapy for non-small cell lung cancer [36]. Similar work has led to additional candidate antibodies currently in development. This example demonstrates the value of detailed computational models in not only discriminating between previously-developed and characterized drugs, but also in optimizing the targets and properties of future drugs.

4.4 Case Study 3: Better Therapeutic Approaches for Ischemic Disease

Mechanistic computational models are valuable both for screening potential drug targets in stand-alone pharmacodynamic models, and in the context of systems pharmacology-style PK/PD models, where diverse therapeutic delivery routes can be compared. We apply these strategies to study angiogenesis, the growth of new blood vessels from the existing vasculature. A promising approach to treat ischemic disease is to promote angiogenesis by targeting one of its key regulators, vascular endothelial growth factor (VEGF). However, despite multiple clinical trials, no VEGF-based pro-angiogenic therapies have yet been approved [10, 37, 38], and success in promoting vascularization of engineered tissue constructs has also been limited [39]. This suggests that our current understanding of the underlying processes is insufficient to effectively promote vascular growth or remodeling.

To address this barrier, we build detailed mechanistic computational models of VEGF binding to its receptors, coreceptors, and the extracellular matrix (ECM), as well as the dimerization, intracellular trafficking and phosphorylation of the primary signaling VEGF receptor, VEGFR2. Such models can be used to study how changes in VEGF presentation (i.e. in solution or bound to the ECM) and the distribution of splice isoforms (which changes in disease), can alter endothelial cell signaling and the resulting vascular morphology [22]. As such, regulation of these properties is important to ensure proper perfusion and to control the permeability of developing vessels [40]. In addition to increasing our understanding of the pharmacodynamics of VEGF action in tissues, these biophysically-detailed models allow for comparison of many potential therapies, such as antibodies that target VEGF or block coreceptor binding, or gene therapy approaches [41-43]. We build these models upon detailed measurements of VEGF-induced signaling in cultured endothelial cells following various perturbations. However, the conditions for cell culture experiments are quite different than those in the human body (**Fig. 4-1**).

One of the strategies we use to translate this mechanistic insight into the context of the human body is by seeding these detailed endothelial cell signaling reactions (PD) into a PK model to form a mechanistically-detailed systems pharmacology model [23]. Our PK framework includes blood, healthy tissue, and diseased tissue (e.g. mouse or human calf muscle with peripheral artery disease), parameterized using histological and physiological data. These models allow us to predict how VEGF-mediated signaling changes in diseased tissue (compared to healthy tissue), which is very difficult to measure in patients.

Additionally, we can predict how therapeutically-relevant quantities, such as the phosphorylation of VEGFR2, relate to measurable biomarkers, for example plasma levels of different VEGF isoforms [44], as we have previously done in cancer [43]. These whole-body models allow for screening of different delivery methods for therapies, such as intravenous or intramuscular antibody delivery, as well as gene, protein, or cell-based therapies and exercise [45]. While it is expected that these different therapy delivery methods (e.g. protein versus gene therapy) will result in different magnitudes & durations of effect in the target tissue, it is unclear without simulation which approaches may be most or least effective. Additionally, by incorporating mouse- and human-specific geometry and molecular (e.g. gene expression) changes, we can predict differences in therapy effectiveness between animal and human models [6]. This powerful framework provides great promise both to understand why previous therapeutic strategies have failed, and to identify promising future drug targets and delivery strategies.

4.5 Mechanistic Computational Models: A Way Forward for Drug Development

The body's response to a drug is often an emergent property of the complex system. As such, drug design is not simply a problem of maximizing binding of a single drug to a single target. The case studies presented here demonstrate the unique ability of computational models including receptor- or channel-level mechanistic detail to improve selection of the right drug targets, properties, dosing & delivery route, and patient populations. The most effective way to implement mechanistic computational models of drug pharmacodynamics depends on the disease application. By linking predictions of important but difficult-to-measure markers of disease state to measureable plasma biomarkers, mechanistic models coupled to PK/PD frameworks (parameterized for specific disease applications) can give clinicians and drug designers a window into disease-driven changes on a patient-specific basis (**Box 4-2**). In other cases, where spatial patterning and cell-cell communication are known to play an important role, 3D tissue-scale computational models have a critical ability to capture emergent behaviors in healthy and diseased tissues. To incorporate pharmacokinetics into these 3D models, PK/PD model predictions can provide the local drug concentration (due to delivery and average consumption by the target tissue) and help parameterize the 3D pharmacodynamic model. Regardless of approach, the mechanistic detail is what makes these models predictive, conferring the ability to identify critical drug design requirements and patient counter-indications.

As highlighted by the diverse applications in the case studies, mechanistic computational models can be applied to any disease state, be it acute or chronic, and regardless of whether the disease stems from infection, genetic factors, and/or environmental or behavior factors. The only requirement is sufficient experimental information to build a mechanistic model of the underlying molecular changes. Computational models can also be used to test the feasibility of promising, but not yet widely successful, therapeutic strategies (**Box 4-2**). For example, models can predict the transfection efficiency required for gene and cell therapy to be effective across a heterogeneous patient population [46, 47]. In addition to drug design, mechanistic computational models, paired with traditional drug development tools, can be used to identify better biomarkers for disease progression and therapy response [48], better predict differences in response in animal models and human patients [49, 50], and to perform failure analysis on ineffective drugs [3, 29], informing the next generation of therapeutics. Personalized medicine approaches can also benefit

from the use of mechanistic models, for example in predicting dosing regimes and drug combinations based on the molecular markers of individual patients or disease sub-types [12, 14]. Because mechanistic computational models can address some of the key shortcomings of the drug development process, they hold promise, used hand-in-hand with experimental approaches, to reduce clinical trial failure, reduce the average per-drug time and cost investment for development, and ultimately, improve patient outcomes.

4.6 References

1.   Pammolli F, Magazzini L, Riccaboni M. The productivity crisis in pharmaceutical R&D. Nature Reviews Drug Discovery. 2011;10(6):428-38. doi: 10.1038/nrd3405. PubMed PMID: WOS:000291165000020.

2.   Scannell JW, Blanckley A, Boldon H, Warrington B. Diagnosing the decline in pharmaceutical R&D efficiency. Nature Reviews Drug Discovery. 2012;11(3):191-200. doi: 10.1038/nrd3681. PubMed PMID: WOS:000300940200021.

3.   Paul SM, Mytelka DS, Dunwiddie CT, Persinger CC, Munos BH, Lindborg SR, et al. How to improve R&D productivity: the pharmaceutical industry's grand challenge. Nature Reviews Drug Discovery. 2010;9(3):203-14. doi: 10.1038/nrd3078. PubMed PMID: WOS:000275357500021.

4.   Leil TA, Bertz R. Quantitative Systems Pharmacology can reduce attrition and improve productivity in pharmaceutical research and development. Frontiers in Pharmacology. 2014;5. doi: 10.3389/fphar.2014.00247. PubMed PMID: WOS:000347151200001.

5.   Sorger PK, Allerheiligen SRB, Abernethy DR, Altman RB, Brouwer KLR, Califano A, et al. Quantitative and Systems Pharmacology in the Post-genomic Era: New Approaches to Discovering Drugs and Understanding Therapeutic Mechanisms. National Institutes of Health. Bethesda 2011.

6.   Agoram BM, Martin SW, van der Graaf PH. The role of mechanism-based pharmacokinetic-pharmacodynamic (PK-PD) modelling in translational research of biologics. Drug Discovery Today. 2007;12(23-24):1018-24. doi: 10.1016/j.drudis.2007.10.002. PubMed PMID: WOS:000251913200005.

7.   Gobburu JVS, Lesko LJ. Quantitative Disease, Drug, and Trial Models. Annual Review of Pharmacology and Toxicology. 2009;49:291-301. doi: 10.1146/annurev.pharmtox.011008.145613. PubMed PMID: WOS:000263565900013.

8.   Van der Graaf PH, Gabrielsson J. Pharmacokinetic-pharmacodynamic reasoning in drug discovery and early development. Future Medicinal Chemistry. 2009;1(8):1371-4. doi: 10.4155/fmc.09.124. PubMed PMID: WOS:000276094100001.

9.   Swinney DC, Anthony J. How were new medicines discovered? Nature Reviews Drug Discovery. 2011;10(7):507-19. doi: 10.1038/nrd3480. PubMed PMID: WOS:000292287200016.

10.   Clegg LE, Mac Gabhann F. Systems biology of the microvasculature. Integrative Biology. 2015. doi: 10.1039/C4IB00296B.

11.   van der Graaf PH, Benson N. Systems Pharmacology: Bridging Systems Biology and Pharmacokinetics-Pharmacodynamics (PKPD) in Drug Discovery and Development. Pharmaceutical Research. 2011;28(7):1460-4. doi: 10.1007/s11095-011-0467-9. PubMed PMID: WOS:000291357700003.

12.   Iyengar R, Zhao S, Chung S-W, Mager DE, Gallo JM. Merging Systems Biology with Pharmacodynamics. Science Translational Medicine. 2012;4(126). doi: 10.1126/scitranslmed.3003563. PubMed PMID: WOS:000302129100001.

13.   Kleiman LB, Maiwald T, Conzelmann H, Lauffenburger DA, Sorger PK. Rapid Phospho-Turnover by Receptor Tyrosine Kinases Impacts Downstream Signaling and Drug Binding. Molecular Cell. 2011;43(5):723-37. doi: 10.1016/j.molcel.2011.07.014. PubMed PMID: WOS:000294593300008.

14.   Zhang XY, Birtwistle MR, Gallo JM. A General Network Pharmacodynamic Model-Based Design Pipeline for Customized Cancer Therapy Applied to the VEGFR Pathway. CPT: pharmacometrics & systems pharmacology. 2014;3:e92-e. doi: 10.1038/psp.2013.65. PubMed PMID: MEDLINE:24429593.

15.   Lindner AU, Concannon CG, Boukes GJ, Cannon MD, Llambi F, Ryan D, et al. Systems Analysis of BCL2 Protein Family Interactions Establishes a Model to Predict Responses to Chemotherapy. Cancer Research.   2013;73(2):519-28.   doi: 10.1158/0008-5472.can-12-2269.   PubMed   PMID: WOS:000313739500012.

16.   Ploeger BA, van der Graaf PH, Danhof M. Incorporating Receptor Theory in Mechanism-Based Pharmacokinetic-Pharmacodynamic (PK-PD) Modeling. Drug Metabolism and Pharmacokinetics. 2009;24(1):3-15. PubMed PMID: WOS:000263905100002.

17.   Holford NHG, Sheiner LB. Understanding the dose-effect relationship- clinical application of pharmacokinetic-pharmacodynamic models. Clinical Pharmacokinetics. 1981;6(6):429-53. PubMed PMID: WOS:A1981MT63600002.

18.   Niepel M, Hafner M, Pace EA, Chung M, Chai DH, Zhou L, et al. Profiles of Basal and Stimulated Receptor Signaling Networks Predict Drug Response in Breast Cancer Lines. Science Signaling. 2013;6(294). doi: 10.1126/scisignal.2004379. PubMed PMID: WOS:000324863000004.

19.   Niepel M, Hafner M, Pace EA, Chung M, Chai DH, Zhou L, et al. Analysis of growth factor signaling in genetically diverse breast cancer lines. Bmc Biology. 2014;12. doi: 10.1186/1741-7007-12-20. PubMed PMID: WOS:000334366400001.

20.   Bagci-Onder T, Agarwal A, Flusberg D, Wanningen S, Sorger P, Shah K. Real-time imaging of the dynamics of death receptors and therapeutics that overcome TRAIL resistance in tumors. Oncogene. 2013;32(23):2818-27. doi: 10.1038/onc.2012.304. PubMed PMID: WOS:000320369100002.

21.   Gallo JM, Birtwistle MR. Network pharmacodynamic models for customized cancer therapy. Wiley Interdisciplinary Reviews: Systems Biology and Medicine. 2015:n/a-n/a. doi: 10.1002/wsbm.1300.

22.   Clegg L, Mac Gabhann F. Site-specific phosphorylation of VEGFR2 is mediated by receptor trafficking: insights from a computational model. PLoS Computational Biology. in press. doi: 10.1371/journal.pcbi.1004158.

23.   Stefanini MO, Wu FT, Mac Gabhann F, Popel AS. A compartment model of VEGF distribution in blood, healthy and diseased tissues. BMC Systems Biology. 2008;2. doi: 10.1186/1752-0509-2-77. PubMed PMID: WOS:000259952700001.

24.   Ballesta A, Zhou Q, Zhang X, Lv H, Gallo JM. Multiscale design of cell-type-specific pharmacokinetic/pharmacodynamic models for personalized medicine: application to temozolomide in brain tumors. CPT: pharmacometrics & systems pharmacology. 2014;3:e112-e. doi: 10.1038/psp.2014.9. PubMed PMID: MEDLINE:24785551.

25.   Preliminary Report: Effect of Encainide and Flecainide on Mortality in a Randomized Trial of Arrhythmia Suppression after Myocardial Infarction. New England Journal of Medicine. 1989;321(6):406-12. doi: doi:10.1056/NEJM198908103210629. PubMed PMID: 2473403.

26.   Perry JC, McQuinn RL, Smith RT, Gothing C, Fredell P, Garson A. Flecainide acetate for resistant arrhythmias in the young- efficacy and pharmacokientics. Journal of the American College of Cardiology. 1989;14(1):185-91. PubMed PMID: WOS:A1989AG41500024.

27.   Nolan PE. Pharmacokinetics and pharmacodynamics of intravenous agents for ventricular arrhythmias. Pharmacotherapy. 1997;17(2):S65-S75. PubMed PMID: WOS:A1997WP08600003.

28.   Clancy CE, Rudy Y. Linking a genetic defect to its cellular phenotype in a cardiac arrhythmia. Nature. 1999;400(6744):566-9. PubMed PMID: WOS:000081854800056.

29.   Moreno JD, Zhu ZI, Yang P-C, Bankston JR, Jeng M-T, Kang C, et al. A Computational Model to Predict the Effects of Class I Anti-Arrhythmic Drugs on Ventricular Rhythms. Science Translational Medicine. 2011;3(98). doi: 10.1126/scitranslmed.3002588. PubMed PMID: WOS:000294462100005.

30.   Romero L, Trenor B, Yang P-C, Saiz J, Clancy CE. In silico screening of the impact of hERG channel kinetic abnormalities on channel block and susceptibility to acquired long QT syndrome. Journal of Molecular and Cellular Cardiology. 2014;72:126-37. doi: 10.1016/j.yjmcc.2014.02.018. PubMed PMID: WOS:000337119700014.

31.   Moreno JD, Yang P-C, Bankston JR, Grandi E, Bers DM, Kass RS, et al. Ranolazine for Congenital and Acquired Late I-Na -Linked Arrhythmias In Silico Pharmacological Screening. Circulation Research.   2013;113(7):E50-E61.   doi: 10.1161/circresaha.113.301971.   PubMed   PMID: WOS:000329479600001.

32.   Yang P-C, Clancy CE. In silico prediction of sex-based differences in human susceptibility to cardiac ventricular tachyarrhythmias. Frontiers in Physiology. 2012;3. doi: 10.3389/fphys.2012.00360. PubMed PMID: WOS:000209173000354.

33.   Chen WW, Schoeberl B, Jasper PJ, Niepel M, Nielsen UB, Lauffenburger DA, et al. Input-output behavior of ErbB signaling pathways as revealed by a mass action model trained against dynamic data. Molecular Systems Biology. 2009;5. doi: 10.1038/msb.2008.74. PubMed PMID: WOS:000263167600002.

34.	Schoeberl B, Pace EA, Fitzgerald JB, Harms BD, Xu L, Nie L, et al. Therapeutically Targeting ErbB3: A Key Node in Ligand-Induced Activation of the ErbB Receptor-PI3K Axis. Science Signaling. 2009;2(77). doi: 10.1126/scisignal.2000352. PubMed PMID: WOS:000275475800003.

35.	Schoeberl B, Faber AC, Li D, Liang M-C, Crosby K, Onsum M, et al. An ErbB3 Antibody, MM-121, Is Active in Cancers with Ligand-Dependent Activation. Cancer Research. 2010;70(6):2485-94. doi: 10.1158/0008-5472.can-09-3145. PubMed PMID: WOS:000278485900036.

36.	Merrimack Pharmaceuticals. A Study of MM-121 in Combination With Chemotherapy Versus Chemotherapy Alone in Heregulin Positive NSCLC ClinicalTrials.gov [Internet]: National Library of Medicine (US); [cited 2015 05/20]. Available from: http://www.clinicaltrials.gov/ct2/show/NCT02387216?term=MM-121&rank=7.

37.	Mac Gabhann F, Qutub AA, Annex BH, Popel AS. Systems biology of pro-angiogenic therapies targeting the VEGF system. Wiley Interdisciplinary Reviews-Systems Biology and Medicine. 2010;2(6):694-707. doi: 10.1002/wsbm.92. PubMed PMID: WOS:000283713500006.

38.	Grochot-Przeczek A, Dulak J, Jozkowicz A. Therapeutic angiogenesis for revascularization in peripheral artery disease. Gene. 2013;525(2):220-8. doi: 10.1016/j.gene.2013.03.097. PubMed PMID: WOS:000322416200014.

39.	Briquez PS, Hubbell JA, Martino MM. Extracellular Matrix-Inspired Growth Factor Delivery Systems for Skin Wound Healing. Advances in Wound Care. 2015.

40.	Vempati P, Popel AS, Mac Gabhann F. Extracellular regulation of VEGF: Isoforms, proteolysis, and vascular patterning. Cytokine & Growth Factor Reviews. 2014;25(1):1-19. doi: http://dx.doi.org/10.1016/j.cytogfr.2013.11.002.

41.	Mac Gabhann F, Popel AS. Targeting neuropilin-1 to inhibit VEGF signaling in cancer: comparison of therapeutic approaches. PLoS Comput Biol. 2006;2(12):e180.

42.	Mac Gabhann F, Ji JW, Popel AS. Multi-scale computational models of pro-angiogenic treatments in peripheral arterial disease. Ann Biomed Eng. 2007;35(6):982-94. Epub 2007/04/17. doi: 10.1007/s10439-007-9303-0. PubMed PMID: 17436110.

43.   Stefanini MO, Wu FTH, Mac Gabhann F, Popel AS. Increase of Plasma VEGF after Intravenous Administration of Bevacizumab Is Predicted by a Pharmacokinetic Model. Cancer Research. 2010;70(23):9886-94. doi: 10.1158/0008-5472.can-10-1419. PubMed PMID: WOS:000285045900038.

44.   Clegg L, Mac Gabhann F. Regulation of VEGFR2 Activation in Skeletal Muscle by VEGF Isoforms with Differential ECM- and NRP1-Binding: a Computational Study. The FASEB Journal. 2015;29(1 Supplement).

45.   Wu FTH, Stefanini MO, Gabhann FM, Popel AS. A Compartment Model of VEGF Distribution in Humans in the Presence of Soluble VEGF Receptor-1 Acting as a Ligand Trap. Plos One. 2009;4(4). doi: 10.1371/journal.pone.0005108. PubMed PMID: WOS:000265505700013.

46.   Hosseini I, Mac Gabhann F. APOBEC3G-Augmented Stem Cell Therapy to Modulate HIV Replication: A Computational Study. Plos One. 2013;8(5). doi: 10.1371/journal.pone.0063984. PubMed PMID: WOS:000320362700088.

47.   Hosseini I, Mac Gabhann F. Designing Stem-Cell Based Anti-HIV Therapies using Molecular-Detailed Multiscale Models. Biophysical Journal. 108(2):314a. doi: 10.1016/j.bpj.2014.11.1707.

48.   Bender RJ, Mac Gabhann F. Personalized medicine of VEGF-targeting therapies: a multiscale modeling approach for developing predictive biomarkers from gene expression data. 2015 Interagency Modeling and Analysis Group MSM Consortium Meeting; NIH 2014.

49.   Mager DE, Woo S, Jusko WJ. Scaling Pharmacodynamics from In Vitro and Preclinical Animal Studies to Humans. Drug Metabolism and Pharmacokinetics. 2009;24(1):16-24. PubMed PMID: WOS:000263905100003.

50.   Finley SD, Dhar M, Popel AS. Compartment model predicts VEGF secretion and investigates the effects of VEGF trap in tumor-bearing mice. Frontiers in oncology. 2013;3:196-. doi: 10.3389/fonc.2013.00196. PubMed PMID: MEDLINE:23908970.

Section II: Multi-scale Computational Models of Angiogenesis

Chapter 5. Modeling Molecular Mechanism: Signaling by Soluble vs. Immobilized VEGF *in vitro*

5.0 Summary

Matrix-binding isoforms and non-matrix-binding isoforms of vascular endothelial growth factor (VEGF) are both capable of stimulating vascular remodeling, but the resulting blood vessel networks are structurally and functionally different. Here, we develop and validate a computational model of the binding of soluble and immobilized ligands to VEGF receptor 2 (VEGFR2), the endosomal trafficking of VEGFR2, and site-specific VEGFR2 tyrosine phosphorylation to study differences in induced signaling between these VEGF isoforms. In capturing essential features of VEGFR2 signaling and trafficking, our model suggests that VEGFR2 trafficking parameters are largely consistent across multiple endothelial cell lines. Simulations demonstrate distinct localization of VEGFR2 phosphorylated on Y1175 and Y1214. This is the first model to clearly show that differences in site-specific VEGFR2 activation when stimulated with immobilized VEGF compared to soluble VEGF can be accounted for by altered trafficking of VEGFR2 without an intrinsic difference in receptor activation. The model predicts that Neuropilin-1 can induce differences in the surface-to-internal distribution of VEGFR2. Simulations also show that ligated VEGFR2 and phosphorylated VEGFR2 levels diverge over time following stimulation. Using this model, we identify multiple key levers that alter how VEGF binding to VEGFR2 results in different coordinated patterns of multiple downstream signaling pathways. Specifically, simulations predict that VEGF immobilization, interactions with Neuropilin-1, perturbations of VEGFR2 trafficking, and changes in

expression or activity of phosphatases acting on VEGFR2 all affect the magnitude, duration, and relative strength of VEGFR2 phosphorylation on tyrosines 1175 and 1214, and they do so predictably within our single consistent model framework.

5.1 Introduction

Members of the vascular endothelial growth factor (VEGF) family are critical regulators of angiogenesis and are implicated as cause or as potential therapy in over 70 diseases, including ischemic diseases of the heart and brain and many cancers. To date, only limited success has been achieved in promoting development of functional vascular networks for tissue engineering [1-3], regeneration [4], and wound healing [5-7]. To harness the VEGF family for tissue vascularization, we must improve our understanding of the mechanisms by which the mode of presentation of VEGF to endothelial cells alters endothelial cell response.

Some VEGF isoforms can bind to proteins and proteoglycans in the extracellular matrix as well as to their cognate cell surface receptors. This matrix-bound VEGF was previously thought to represent a relatively inert pool of sequestered VEGF held in reserve until proteolytic release. Recent work has demonstrated that matrix-bound VEGF can directly ligate and activate VEGF receptors [8-10], and that VEGF and platelet-derived growth factor (PDGF) engineered to have increased affinity for the extracellular matrix promote wound healing and angiogenesis better than the wild-type growth factors [11]. Computational models of VEGF transport predict that the amount of matrix-bound VEGF in normal human tissue (e.g. skeletal muscle) is 30 to 100-fold higher than the amount of free (soluble, unbound) VEGF [12,13]. However, almost all *in vitro* studies of VEGF receptor signaling have examined only soluble presentation of VEGF. Better mechanistic understanding of how VEGF immobilization alters VEGF receptor 2 (VEGFR2) signaling (and the resulting cellular behavior) will greatly improve our ability to design VEGF-based therapies and to pattern cues for vascular networks in tissue engineering applications.

Multiple isoforms of VEGFA (herein referred to as VEGF) exist, the most common in humans being $VEGF_{121}$, $VEGF_{165}$, and $VEGF_{189}$ ($VEGF_{120}$, $VEGF_{164}$, and $VEGF_{188}$ in mice) [14]. $VEGF_{165}$ and $VEGF_{189}$ include basic heparin-binding domains through which they can bind to extracellular matrix (ECM) proteins such as fibronectin and collagen, and also heparin [15-19]. Tissues express distinct ratios of VEGF isoforms, possibly inducing tissue-specific vascular architecture [20]. Mouse tumors expressing only $VEGF_{188}$ or modified protease-resistant VEGF isoforms exhibit dense, highly branched networks of small diameter blood vessels [21,22]. In contrast, tissues or tumors secreting primarily $VEGF_{120/121}$ (purely soluble) exhibit wide, tortuous vessels with low branching density and high permeability [22,23].

115

There are 3 receptor tyrosine kinases (RTKs) for the VEGF ligands. We focus here on VEGFR2, the RTK most strongly associated with VEGF-induced angiogenesis. VEGF, a constitutive dimer, binds and dimerizes two VEGFR2 monomers, resulting in receptor autophosphorylation of multiple intracellular tyrosines. Each phosphotyrosine recruits distinct sets of adaptor proteins, leading to distinct downstream signaling [24,25] (**Fig.1D**). Generally, phosphorylation on tyrosine 951 (Y951) promotes Akt activation (via PI3K) and cell survival [1,26]. Phosphorylation of Y1175 leads to activation of ERK1/2 (via PLCγ) and proliferation, as well as activation of Akt [27,28], while phosphorylation of Y1214 leads to activation of p38 MAPK and migration [1,29,30].

The isoform-specific coreceptor Neuropilin-1 (NRP1) does not bind directly to VEGFR2; NRP1-binding VEGF isoforms bridge VEGFR2 and NRP1 to form a ternary complex [31]. NRP1 increases the effective affinity of VEGF for VEGFR2 [32], as well as influencing VEGFR2 trafficking [33,34]. NRP1 may have other VEGF-induced, VEGFR2-independent signaling capabilities [35,36], but these effects are excluded from this analysis.

While many aspects of trafficking are conserved across RTK systems [24,25,37] [38,39], there are significant differences between the well-studied EGF system and the VEGF system [40,41]. Similar to other RTKs, VEGFR2 is constantly being produced, internalized, recycled, and degraded in endothelial cells, resulting in continuous turn-over of the receptor population even in the absence of VEGF [42] (**Fig. 5-1B**). Upon internalization, VEGFR2 is initially found in early endosomes, identified by the marker Rab5. From the early endosome, VEGFR2 can be recycled directly via Rab4-positive endosomes, degraded via Rab7-positive late endosomes, or transferred to Rab11-positive recycling endosomes [40,43,44]. Constitutive recycling of VEGFR2 in endothelial cells occurs primarily through the Rab4 pathway [40,41], while NRP1 promotes routing of VEGF-VEGFR2 complexes through the Rab11–positive recycling pathway [40,45].An increasing body of evidence suggests that trafficking of VEGFR2 regulates receptor phosphorylation, downstream signaling, and the resulting cell behavior [24,30,46,47]. VEGFR2 signaling can be attenuated by receptor degradation or by tyrosine phosphatase-mediated dephosphorylation of intracellular residues [9,48,49]. Significant gaps exist in current understanding of phosphatases acting on VEGFR2, but the subcellular localization and tyrosine residue specificity of some phosphatases is known.

Vascularization is critical for the viability of thick tissue-engineered constructs. As such, there is significant interest in immobilizing VEGF in tissue scaffolds or on surfaces. Though a variety of different techniques for immobilization of VEGF have been explored, a clear understanding of the mechanism through which immobilized VEGF results in different cellular signaling and vascular phenotypes than soluble VEGF has not yet emerged. We and others have previously developed models to study the trafficking of VEGFR2 [8,24,25] and other growth factor receptors (most notably EGF receptors [50-52]), as well as the impact of growth factor sequestration in the extracellular matrix on distribution and availability to cells [53-55]. However, these models have only considered matrix-bound VEGF, VEGFR2 trafficking, and receptor phosphorylation events in a limited way, if at all.

The purpose of this study is to quantitatively connect trafficking and localization of VEGFR2 to tyrosine site-specific VEGFR2 phosphorylation patterns, which have been implicated in regulating signaling downstream of VEGFR2. Specifically, this model was developed to test the hypothesis that control of site-specific VEGFR2 dephosphorylation by receptor trafficking is sufficient to explain experimental observations following stimulation of endothelial cells with soluble or immobilized VEGF. We also study the effect of NRP1 expression on VEGFR2 trafficking and phosphorylation.

Figure 5-1. Model Schematics. A. Biochemical Reactions. Interactions between VEGF, VEGFR2, NRP1, and an extracellular matrix proteoglycan (M) are summarized. VEGF can bind VEGFR2, NRP1, and M. NRP1 and M cannot be present in the same complex (as they bind to the same surface of VEGF), and VEGFR2 and NRP1 cannot form a complex without VEGF. **B.** Trafficking Pathways. Surface molecular complexes can be internalized with rate constant k_{intn}. Rab4/5-resident molecular complexes can be degraded (rate constant k_{degr}), recycled (rate constant k_{rec4}), or transferred to the Rab11 compartment (rate constant k_{4to11}). Rab11 endosome-resident complexes are recycled with rate constant k_{rec11}. New surface receptors are produced at rate s. **C.** Phosphorylation Reactions. Intracellular tyrosine residues Y951, Y1175, and Y1214 are phosphorylated and dephosphorylated independently. **D.** Overview of signaling pathways and cellular behaviors downstream of tyrosine residues Y951, Y1175, and Y1214 on VEGFR2.
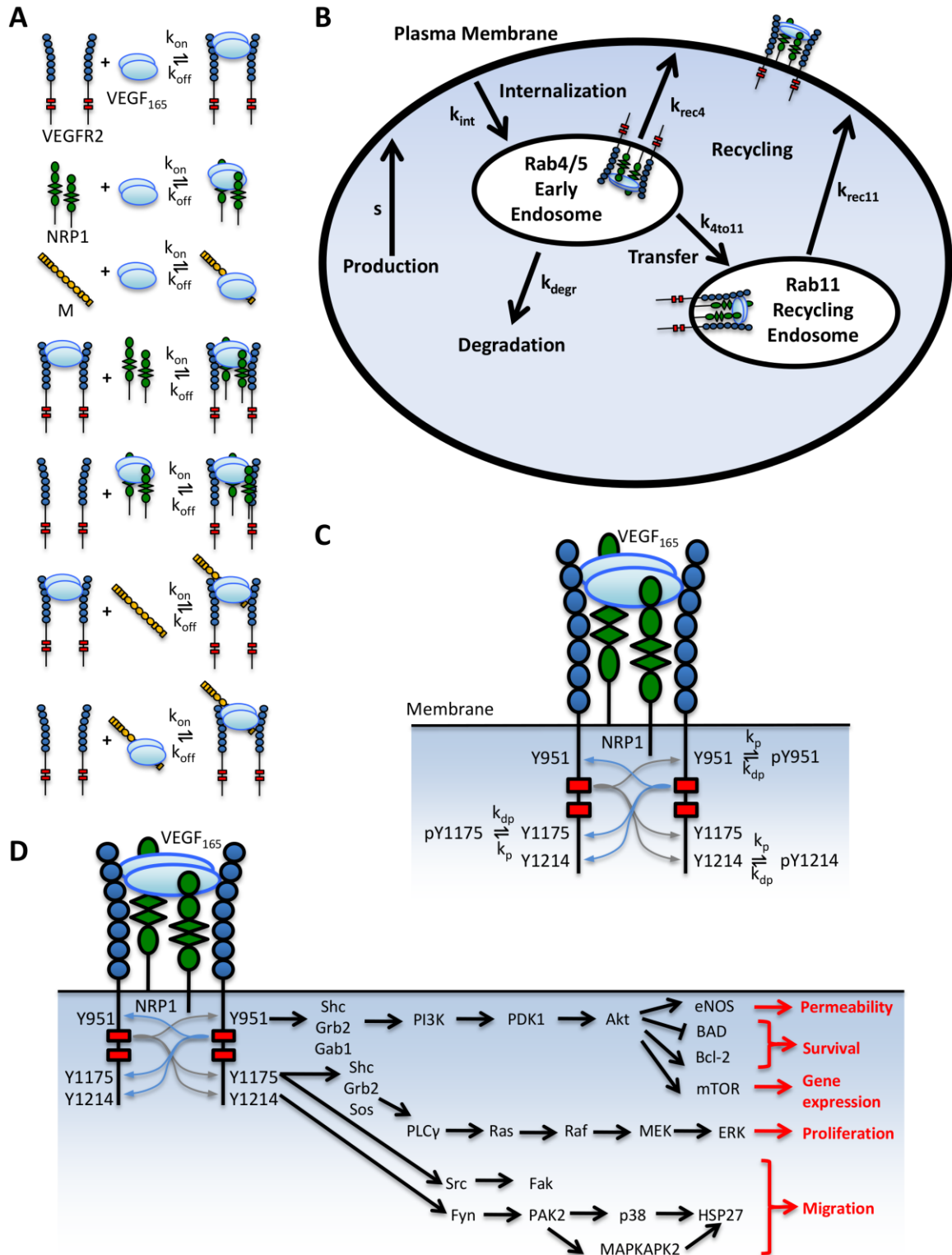
Figure 5-1

5.2 Materials and Methods

5.2.1 Computational Model Overview

We developed a model to simulate *in vitro* experiments in which monolayers of endothelial cells are exposed to exogenous soluble or immobilized VEGF. The model uses a large set of coupled, nonlinear, deterministic, ordinary differential equations to simulate key biochemical reactions (**Fig. 5-1A**), trafficking processes (**Fig. 5-1B**), and phosphorylation reactions (**Fig. 5-1C**). The model uses experimentally-derived kinetics (**Tables 5-1, 5-2, & 5-3**) and incorporates geometry and initial concentrations specific to the experimental protocols being simulated (**Table 5-4**). In the model, we assume that VEGF and VEGFR2 are pre-dimerized, though we have examined the implications of including dimerization reactions in the past [56]. Both soluble VEGF (V) and ECM-bound or immobilized VEGF (V·M) can bind to VEGFR2 (R2). V·M can dissociate and reassociate. NRP1 (N1) can bind to V or V·R2, but not to M·V·R2, as N1 and M bind to the same heparin-binding domain on VEGF. We exclude for now the possibility of one NRP1 and one M binding to opposite sides of the same VEGF dimer simultaneously, though this assumption was tested. These reactions occur in every model compartment (described below) in which the corresponding species are present.

Table 5-1. Model Parameters for Biochemical Reactions

Species 1	Species 2	k_{on}	k_{off}	K_D	Reference
External					
V	M	Varies	Varies	Varies	Fit
Surface					
V	R2	1.0×10^7 M^{-1}s^{-1}	1.0×10^{-3} s^{-1}	1.0×10^{-10} M	[85]
M	V·R2	4.2×10^5 M^{-1}s^{-1}	1.0×10^{-2} s^{-1}	2.4×10^{-8} M	Assumed same as V·M
V·M	R2	1.0×10^7 M^{-1}s^{-1}	1.0×10^{-3} s^{-1}	1.0×10^{-10} M	Assumed same as V·R2
V	N1	4.8×10^4 M^{-1}s^{-1}	1.0×10^{-4} s^{-1}	2.1×10^{-9} M	[86]
N1	V·R2	3.1×10^{13} (mol/cm^2)$^{-1}$ s^{-1}	1.0×10^{-3} s^{-1}	3.2×10^{-17} mol/cm^2	[85]
V·N1	R2	1.0×10^{14} (mol/cm^2)$^{-1}$ s^{-1}	1.0×10^{-3} s^{-1}	1.0×10^{-17} mol/cm^2	[85]
V·M	N1	0 M^{-1}s^{-1}	-	-	Assumed
V·M·R2	N1	0 M^{-1}s^{-1}	-	-	Assumed
M	V·N1	0 M^{-1}s^{-1}	-	-	Assumed
Internal (same in Rab4/5 and Rab11 endosomes)[a]					
V	R2	1.0×10^7 M^{-1}s^{-1}	1.0×10^{-3} s^{-1}	1.0×10^{-10} M	[85]
V	N1	4.8×10^4 M^{-1}s^{-1}	1.0×10^{-4} s^{-1}	2.1×10^{-9} M	[86]
N1	V·R2	3.1×10^{13} (mol/cm^2)$^{-1}$ s^{-1}	1.0×10^{-3} s^{-1}	3.2×10^{-17} mol/cm^2	[85]
V·N1	R2	1.0×10^{14} (mol/cm^2)$^{-1}$ s^{-1}	1.0×10^{-3} s^{-1}	1.0×10^{-17} mol/cm^2	[85]

[a] All rates for internal reactions were assumed to be the same as on the cell surface. Unit conversion was required (not shown) for k_{on} and K_D in internal compartments (from M^{-1}s^{-1} to (#/cm^2)$^{-1}$s^{-1} for k_{on} and from M to #/cm^2 for K_D) using the total volume of the specified endosomal compartment per unit surface area (See Table S2- not assumed to be spherical). Note that all rates are effective rates; diffusion considerations are lumped into these effective rates.

Table 5-2. Model Parameters for Trafficking

Parameter	Species	Value (s^{-1})	Reference
k_{int}	R2	2.6×10^{-3}	[24,25]
	V·R2	3.12×10^{-2}	[24,25]
	M·V·R2	0	Assumed
	V	0	Assumed
	N1	2.6×10^{-3}	Assumed same as R2
	V·N1	2.6×10^{-3}	Assumed same as N1
	V·N1·R2	3.12×10^{-2}	Assumed same as V·R2
k_{rec4}	**$R2_{rab45}$**	**3.8×10^{-3}**	Fit
	$V·R2_{rab45}$	3.8×10^{-3}	Held equal to k_{rec4} for $R2_{rab45}$ during fitting
	V_{rab45}	0	Assumed
	$N1_{rab45}$	3.8×10^{-5}	Held equal to $1/100 * k_{rec4}$ for $R2_{rab45}$ during
	$V·N1_{rab45}$	3.8×10^{-5}	Held equal to k_{rec4} for $N1_{rab45}$ during fitting
	$V·N1·R2_{rab45}$	3.8×10^{-5}	Held equal to k_{rec4} for $N1_{rab45}$ during fitting
k_{rec11}	$R2_{rab11}$	1.4×10^{-4}	Held equal to $1/100 * k_{rec11}$ for $N1_{rab11}$ during
	$V·R2_{rab11}$	1.4×10^{-4}	Held equal to $1/100 * k_{rec11}$ for $N1_{rab11}$ during
	V_{rab11}	0	Assumed
	$N1_{rab11}$	**1.4×10^{-2}**	Fit
	$V·N1_{rab11}$	1.4×10^{-2}	Held equal to k_{rec4} for $N1_{rab11}$ during fitting
	$V·N1·R2_{rab11}$	1.4×10^{-2}	Held equal to k_{rec4} for $N1_{rab11}$ during fitting
k_{4to11}	$R2_{rab45}$	1.0×10^{-5}	Assumed
	$V·R2_{rab45}$	1.0×10^{-5}	Assumed
	V_{rab45}	0	Assumed
	$N1_{rab45}$	**1.9×10^{-2}**	Fit
	$V·N1_{rab45}$	1.9×10^{-2}	Held equal to k_{4to11} for $N1_{rab45}$ during fitting
	$V·N1·R2_{rab45}$	1.9×10^{-2}	Held equal to k_{4to11} for $N1_{rab45}$ during fitting
k_{degr}	$R2_{rab45}$	3.6×10^{-6}	Held equal to $1/10 * k_{degr}$ for $V·R2_{rab45}$ during
	$V·R2_{rab45}$	**3.6×10^{-5}**	Fit
	V_{rab45}	1.2×10^{-2}	Assumed
	$N1_{rab45}$	**1.6×10^{-4}**	Fit
	$V·N1_{rab45}$	1.6×10^{-4}	Held equal to k_{degr} for $N1_{rab45}$ during fitting
	$V·N1·R2_{rab45}$	**6.8×10^{-4}**	Fit
s	R2	Calculated	Calculated (Units: #/(cm^2s))
	N1	Calculated	Calculated (Units: #/(cm^2s))

Bold: Value fit directly in this study

Table 5-3. Model Parameters for VEGFR2 Phosphorylation

Species	k_p (All	$k_{dp,Y951}$ (s^{-1})	$k_{dp,Y1175}$ (s^{-1})	$k_{dp,Y1214}$ (s^{-1})
R2	0	30	30	30
R2$_{rab45}$	0	30	30	30
R2$_{rab11}$	0	30	30	30
V·R2	1	**0.043**	**4.98**	**1.06**
V·R2$_{rab45}$	1	**75.0**	**0.00972**	**0.0307**
V·R2$_{rab11}$	1	30	30	30
V· N1·R2	1	6	5	1
V·	1	15	0.01	6
V·	1	30	30	30

All units s^{-1}: **Bold = fit**. References: See Methods.

Table 5-4. Initial Conditions and Parameters that vary by Study

Parameter	Trafficking Study[40]	2011 Presentation Study[8]	2010 Presentation Study[29]	Other Simulations
Cell Type	PAEC	HUVEC	HUVEC	HUVEC
Initial Conditions				
[V]	50 ng/mL	2 ng/mL	200 ng/mL	Varies
[M]	-	1500 ng/mL	3 mg/mL	3 mg/mL
$[R2]_{surf}$	37,400/108,000 per cell	6,000 per cell	6,000 per cell	6,000 per cell
$[N1]_{surf}$	0/113,000 per cell	35,000 per cell	35,000 per cell	35,000 per cell
Geometry				
Total Surface Area	1 cm^2	3 cm$^{2\,b}$	1 cm^2	1 cm^2
Solution/Matrix Depth[a]	0.5 cm	0.05 cm (Vb)/ 0.5 cm (Vs)	0.5 cm	0.5 cm
Trafficking Parameters (factor change from values in Table 2)				
$k_{int}(V \cdot R2)$	-	-	/6	-[c]
k_{degr}	-	x 2.4	x 2.4	x 2.4
V·M Binding Parameters				
$k_{off,V \cdot M}$	-	3.3×10^{-3} s^{-1} (Ve) / 1.1×10^{-3} s^{-1} (Vc)	1.0×10^{-2} s^{-1}	1.0×10^{-2} s^{-1}
$k_{on,V \cdot M}$	-	4.2×10^5 M^{-1}s^{-1}	4.0×10^3 M^{-1}s^{-1}	4.0×10^3 M^{-1}s^{-1}
$K_{D,V \cdot M}$	-	7.9×10^{-9} M (Ve)[d] / 2.6×10^{-9} M (Vc)	2.5×10^{-6} M	2.5×10^{-6} M

[a] Calculated from information in [8] on surface densities and VEGF concentration, and used to calculate [M].

[b] Tuned so total surface Vs·R2 + internal VEGF matches data in [8].

[c] The original k_{int} value was used for [V] < 50 ng/mL (trafficking study [40], 2011 presentation study [8], Anderson et al. 2011 Validation study [58], Mellberg et al. [61]), as well as for all model predictions. $k_{int}/6$ was used for [V] > 50 ng/mL (2010 presentation study [29], Martino et al. Validation study [59], and Mattila et al. [60]). In cases where [V] = 50 ng/mL, the value that resulted in better fits was used.

[d] References: [12,63]

5.2.2 Trafficking Processes

The model includes five compartments: extracellular (media and matrix); cell surface; early endosomes (combining Rab4- and Rab5-positive endosomes); recycling endosomes (Rab11-positive); and degraded (late/Rab7-positive endosomes and lysosomes). The concentration of soluble or immobilized VEGF in the extracellular compartment is assumed to be uniform, but not constant. Newly synthesized VEGFR2 and NRP1 are inserted into the cell surface compartment at a constant rate, resulting in constant surface VEGFR2 and NRP1 populations in the absence of VEGF. The initial quantity of VEGFR2 and NRP1 in each endosomal compartment was set based on the trafficking parameters to obtain a steady distribution in the absence of VEGF. R2, V·R2, N1, V·N1, and V·N1·R2 are internalized from the surface to the early endosome compartment. M·V·R2 is not internalized in our model; we assume it is anchored to the gel or surface to which VEGF is immobilized. All receptor complexes in the Rab4/5 compartment can be recycled directly, degraded, or trafficked to the Rab11 compartment for recycling. We assume that free (non-receptor-bound) VEGF in Rab4/5 endosomes does not recycle or travel to Rab11 endosomes; quantitative analysis showed that these processes were negligible compared to degradation of free VEGF. We assumed that no degradation occurs from the Rab11 compartment, as Rab11 endosomes have an outward-directed motor (for recycling). The trafficking processes are summarized in **Fig. 5-1B**. Examples of the equations describing the biochemical reactions and trafficking of each species are given below. The complete set of biochemical and trafficking reactions (not including all phosphorylation states of VEGFR2) can be found in the Supplemental Information.

Extracellular Molecular Complexes:

$$\frac{d[V]}{dt} = -k_{on,V\cdot M}[V][M] + k_{off,V\cdot M}[V\cdot M] - k_{on,V\cdot R2}[V][R2] + k_{off,V\cdot R2}[V\cdot R2] - k_{on,V\cdot N1}[V][N1]$$
$$+ k_{off,V\cdot N1}[V\cdot N1]$$

Cell Surface Molecular Complexes:

$$\frac{d[V \cdot R2]}{dt} = k_{on,V \cdot R2}[V][R2] - k_{off,V \cdot R2}[V \cdot R2] - k_{on,M \cdot (V \cdot R2)}[M][V \cdot R2]$$
$$+ k_{off,M \cdot (V \cdot R2)}[M \cdot V \cdot R2] - k_{on,(V \cdot R2) \cdot N1}[V \cdot R2][N1]$$
$$+ k_{off,(V \cdot R2) \cdot N1}[V \cdot N1 \cdot R2] - k_{intn,V \cdot R2}[V \cdot R2] + k_{rec4,V \cdot R2}[(V \cdot R2)_{rab45}]$$
$$+ k_{rec11,V \cdot R2}[(V \cdot R2)_{rab11}]$$

Rab4/5 Molecular Complexes:

$$\frac{d[R2_{rab45}]}{dt} = -k_{on,V \cdot R2_{rab45}}[V_{rab45}][R2_{rab45}] + k_{off,V \cdot R2_{rab45}}[(V \cdot R2)_{rab45}]$$
$$- k_{on,(V \cdot N1) \cdot R2_{rab45}}[(V \cdot N1)_{rab45}][R2_{rab45}] + k_{off(V \cdot N1) \cdot R2_{rab45}}[(V \cdot N1 \cdot R2)_{rab45}]$$
$$+ k_{intn,R2}[R2] - k_{rec4,R2_{rab45}}[R2_{rab45}] - k_{4to11,R2_{rab45}}[R2_{rab45}] - k_{degr,R2_{rab45}}[R2_{rab45}]$$

5.2.3 Phosphorylation Reactions

Phosphorylation and dephosphorylation of ligated VEGFR2 (V·R2) and free VEGFR2 (R2) take place on the cell surface and in the endosomes. We assume that the intrinsic phosphorylation and dephosphorylation rates for V·R2 are the same whether VEGF is immobilized or soluble. We also assume that NRP1 does not affect the intrinsic phosphorylation rates of VEGFR2, though it does increase the affinity of VEGF for VEGFR2. While some information about the subcellular locations and tyrosine specificities of phosphatases targeting VEGFR2 is available, there is insufficient information to develop detailed explicit phosphatase models. Thus, we assume first order phosphorylation and dephosphorylation kinetics, effectively assuming that the relevant phosphatases are present in excess. The phosphorylation and dephosphorylation rates for each tyrosine residue examined (Y951, Y1175, and Y1214) can be independent in the model, and vary with the ligation status and subcellular localization of VEGFR2. Thus, we do not assume that VEGFR2 is automatically phosphorylated upon binding of VEGF or dephosphorylated upon unbinding of VEGF; these are still first-order reactions. We assume that the trafficking rates in the model are controlled by the ligation status of VEGFR2, not by its phosphorylation

state. VEGFR2 internalization has been shown to be regulated by phosphorylation of Y1054/Y1059 [57]. However, as these are considered activation tyrosine residues, we assume that VEGFR2 ligation is a surrogate for pY1054/59, as done in previous models [24,25]. We assume that phosphorylation of all tyrosine sites on VEGFR2 is lost upon degradation, but that phosphorylation and ligation patterns are not directly changed by other trafficking processes.

Given the three tyrosine sites being considered, there are eight possible phosphorylation patterns for VEGFR2: R2 (no phosphorylation), $R2_{pY951}$, $R2_{pY1175}$, $R2_{pY1214}$, $R2_{pY951\text{-}pY1175}$, $R2_{pY951\text{-}pY1214}$, $R2_{pY1175\text{-}pY1214}$, and $R2_{pY951\text{-}pY1175\text{-}pY1214}$. The same patterns are possible for $V \cdot R2$, $M \cdot V \cdot R2$, $V \cdot N1 \cdot R2$, $R2_{rab45}$, $V \cdot R2_{rab45}$, $V \cdot N1 \cdot R2_{rab45}$, $R2_{rab11}$, $V \cdot R2_{rab11}$, and $V \cdot N1 \cdot R2_{rab11}$. We assume that all newly produced VEGFR2 is completely unphosphorylated. These reactions are shown schematically for $V \cdot R2$ on the cell surface in **Fig.1C**. A sample equation describing the complete set of biochemical reactions, trafficking processes, and phosphorylation events that affect the population of surface $R2_{pY1175}$ is given below:

$$
\begin{aligned}
\frac{d\left[R2_{pY1175}\right]}{dt} =\ & -k_{on,V \cdot R2}\left[V\right]\left[R2_{pY1175}\right] + k_{off,V \cdot R2}\left[V \cdot R2_{pY1175}\right] - k_{on,(M \cdot V) \cdot R2}\left[M \cdot V\right]\left[R2_{pY1175}\right] \\
& + k_{off,(M \cdot V) \cdot R2}\left[M \cdot V \cdot R2_{pY1175}\right] - k_{intn,R2_{pY1175}}\left[R2_{pY1175}\right] + k_{rec4,R2_{rab45,pY1175}}\left[R2_{rab45,pY1175}\right] \\
& + k_{rec11,R2_{rab11,pY1175}}\left[R2_{rab11,pY1175}\right] + k_{p,Y1175,R2}\left[R2\right] - k_{dp,Y1175,R2_{pY1175}}\left[R2_{pY1175}\right] \\
& - k_{p,Y951,R2_{pY1175}}\left[R2_{pY1175}\right] + k_{dp,Y951,R2_{pY951-pY1175}}\left[R2_{pY951-pY1175}\right] \\
& - k_{p,Y1214,R2_{pY1175}}\left[R2_{pY1175}\right] + k_{dp,Y1214,R2_{pY1175-pY1214}}\left[R2_{pY1175-pY1214}\right]
\end{aligned}
$$

5.2.4 Model Outputs

The outputs of this model are the concentrations of each molecule or molecular complex (summarized in **Table 5-S1**) over time. The concentrations of certain complexes were combined into lumped quantities of interest, which could be directly compared to experimental data. For example, the model allows prediction of pY951 VEGFR2 (pY951), pY1175, and pY1214 quantities over time under different simulation conditions. These quantities are obtained by summing the concentrations of all VEGFR2 (ligated and free) that are phosphorylated on the given site. These quantities are examined in total, and also partitioned into surface, Rab4/5, and Rab11 components. We assume that the total VEGFR2

phosphorylated on at least one of Y951, Y1175, and Y1214 in the model is a reasonable correlate to total

phosphorylated VEGFR2 (pR2) experimental data. As we do not include all tyrosine residues on VEGFR2

in our model, this is expected to underestimate the total percentage of VEGFR2 phosphorylated, but the

shape of the resulting curve is expected to be correct. Model outputs were normalized for parameter

estimation in the same way as the experimental data to which they were compared. For model predictions,

outputs are shown relative to the total VEGFR2 in the system in the absence of VEGF (100%) (*See* **Fig. 5-2C**). Note that, due to degradation, the total amount of VEGFR2 in the system after VEGF stimulation is

less than 100%.

5.2.5 Parameter Fitting Overview

Parameters in this model were taken from literature, calculated, assumed, or fit to data from one

study of VEGFR2 and NRP1 trafficking [40] (hereafter referred to as the "trafficking study") and two

studies of immobilized VEGF [8,29] (hereafter referred to as the "2010 presentation study" and the "2011

presentation study," together the "VEGF presentation studies"). The provenance of each parameter is

shown in **Tables 5-1, 5-2, & 5-3**. The experimental trafficking study provides the most detailed and

complete quantitative data on VEGFR2 and NRP1 trafficking from a single study to date [40]. The VEGF

presentation studies provide data on site-specific phosphorylation of VEGFR2 upon exposure to soluble

and immobilized VEGF [8,29], allowing us to study site- and location-specific phosphorylation patterns.

These studies have experimental outputs that can be directly compared to model outputs for parameter

estimation and validation. We simulated the experimental protocols from these studies by altering the

initial conditions and geometry in the model to fit the protocol used in each study, as summarized in **Table 5-4**.

The general protocol used to assemble a completely parameterized model was as follows. All

biochemical reaction rates, excepting V·M reaction parameters, were taken from literature or previous

experimentally-validated models of $VEGF_{165}$, VEGFR2, and NRP1, as summarized in **Table 5-1**. The

trafficking parameters were fit to data in the trafficking study [40] (soluble VEGF only). The assumptions

used to reduce the number of parameters fit are detailed in **Table 5-2** and in section 5.2.6 below. Next, we

fixed the dephosphorylation rates for all species in Rab11 endosomes at a sufficiently high value to

minimize phosphorylation in this compartment, as pY1175 and pY1212 (mouse equivalent of human Y1214) did not co-localize with Rab11 in the trafficking study. We then took the model, to this point parameterized solely with soluble VEGF data, and applied it to the VEGF presentation studies [8,29]. The M·V reaction parameters were fit to data in each study. We then fit phosphorylation parameters for the cell surface and Rab4/5 endosomes to data from both of the VEGF presentation studies simultaneously. We fixed the phosphorylation rates and fit the dephosphorylation rates in each compartment, as phosphorylation is assumed to be fast upon ligand binding. We then validated the complete model against data from four independent studies and additional data from the trafficking study [40,58-61]. This modular approach to parameter fitting was chosen to reduce the number of parameters being fit at each step, and because distinct types of data (cell lines and experimental set-ups) were used for each step. It does not reduce the utility of our model in determining whether trafficking-controlled dephosphorylation of VEGFR2 is sufficient to account for observed trends in experimental data.

5.2.6 Trafficking Parameters

We fixed the internalization rates in the model using values for free and ligated VEGFR2 estimated for previous models of VEGFR2 internalization, recycling, and degradation [24,25]. Our goal was to obtain a validated parameter set that gives correct VEGFR2 distributions, rather than validated, identifiable values for each individual parameter. Receptor distribution is controlled by internalization, recycling, and degradation (production rates for receptors are determined using these values). As such, fitting the recycling and degradation rates should be adequate to capture the trafficking dynamics in this system. We assumed relationships between some of the trafficking parameter values for different molecular species (based upon prior knowledge) to reduce the number of parameters to be fit, given the limited and noisy data available (**Table 5-2**). This set was sufficient to capture the trafficking processes of interest in this analysis. Each assumption was relaxed during parameter fitting, to verify that it was reasonable. The listed set of assumptions resulted in the parameter set that best described the data in the trafficking study. The trafficking study examined colocalization of NRP1 and VEGFR2 with over-expressed, fluorescently-tagged Rab4, Rab5, Rab7, and Rab11 in porcine aortic endothelial cells (PAECs) transfected with VEGFR2, NRP1, or both, and exposed to soluble VEGF [40]. Data was also given on

total VEGFR2 and NRP1 over time, and total cell-surface NRP1 over time [40]. We included an additional term in the optimization cost function to constrain the percent of total VEGFR2 on the cell surface to approximately 60% in the absence of VEGF, ensuring a biologically reasonably VEGFR2 distribution [41]. For this study, we assumed PAECs transfected with VEGFR2 had 37,400 surface VEGFR2/cell, and cells transfected with VEGFR2 and NRP1 had 108,000 cell surface VEGFR2/cell and 113,000 cell surface NRP1/cell, as previously reported [62].

The experimental data from the trafficking study [40] that was used to fit the trafficking parameters, the weights used on each piece of data in the cost function, and the corresponding simulated values for a representative set of parameters are shown in **Table 5-S4**. Data in that study is given for both Rab4- and Rab5-positive endosomes [40]. The maximum of these values was used to fit the data for the Rab4/5 compartment in the model. We fit parameter sets using the relative values of each molecular species in Rab4/5, Rab11, and Rab7 endosomes, normalized so that these three values summed to 100% of the internal population of that receptor. We also tried using the ratio of each quantity in Rab4/5 endosomes to Rab11 endosomes (Number in Rab4/5 endosomes / Number in Rab11 endosomes) to fit the trafficking parameters. This second strategy was considered because we compared Rab7 measures to internal degraded quantities in the model. While species routed for degradation in real cells pass through Rab7 endosomes, degraded species in our model are not removed from the system, and so these quantities increase over time. The resulting parameter sets were similar, and the first approach was pursued.

We fit the trafficking parameters using the Levenberg-Marquardt algorithm, a non-linear least squares optimization routine. Values of all fit parameters were constrained to the range $[10^{-5}, 1]$ s^{-1} to ensure physiologically reasonable parameter estimates. Initial parameter values were pulled randomly from a distribution that is uniform on a $\log_{10}$ scale constrained to the range $[10^{-4}, 10^{-2}]$ s^{-1}. This initial range resulted in approximately ½ of optimal parameter sets found being accepted, where a parameter set was accepted if the total cost for the set was within 15% of the value for the lowest cost set. From the resulting 23 acceptable parameter sets, a representative parameter set was selected for use in the remainder of this study (shown in **Table 5-2**).

The VEGF presentation studies were performed in human umbilical vein endothelial cells (HUVECs) [8,29]. For all studies using HUVECs, we assumed surface populations of 6,000 VEGFR2/cell

and 35,000 NRP1/cell [62]. Due to the differences in receptor numbers between PAECs and HUVECs, and the use of constitutively active, overexpressed Rab proteins in the trafficking study [40], some difference in trafficking parameters between the trafficking and VEGF presentation studies was anticipated. To adjust, the degradation rates for all molecular species were increased by a constant factor (2.4, **Table 5-4**), which was determined by minimizing the least square error between model simulations and experimental data in the 2010 presentation study for total VEGFR2 over the time range 0-60 minutes [29].

5.2.7 Matrix-Binding Parameters

With trafficking parameters set, we next manually fit the VEGF-matrix reaction parameters. The 2011 presentation study immobilized VEGF to a gold-coated slide using a modified heparin linker, using two different protocols to create either an electrostatic or covalent bond between the heparin surface and VEGF [8]. Here, we fixed K_D for the electrostatic case to be consistent with literature data on VEGF-heparin affinity [63], and fit $k_{off,V\cdot M}$. For the covalent case, $k_{off,V\cdot M}$ was tuned, also altering $K_{D,V\cdot M}$. After examination of the protocols used, we determined that the measurements of internalized VEGF presented in this study [8] (used to fit $k_{off,V\cdot M}$) likely also contain surface-bound quantities of VEGF. Thus, we compared these measurements to the total internal and soluble surface-bound VEGF quantity in our model. The 2010 presentation study immobilized VEGF in a collagen and fibrinogen gel [29]. VEGF in the collagen gel was assumed to be immobilized primarily through heparin, and the value of $k_{off,V\cdot M}$ was assumed to be 10^{-2} s^{-1}. $K_{D,V\cdot M}$ was then tuned to give acceptable fits for phosphorylation data in this study.

5.2.8 Phosphorylation Parameters

Since phosphorylation is assumed to be a fast process that quickly reaches quasi-static equilibrium upon ligation of VEGFR2, we assumed a constant value of k_p for V·R2 for all residues in all compartments, and tuned the dephosphorylation rates. We assume k_p is zero for free VEGFR2; thus, free VEGFR2 can transiently maintain its phosphorylation status if VEGF unbinds, but it cannot become phosphorylated without a preceding ligation event. Additionally, we assume a constant high value for k_{dp} for free VEGFR2 in all compartments. Sensitivity studies were performed to confirm that the chosen value was sufficiently high to result in efficient dephosphorylation of VEGFR2 following dissociation of ligand; thus the model

predictions were relatively insensitive to this parameter. We also assume that the same constant high k_{dp} value holds for all complexes in Rab11 endosomes, based on qualitative observations in the trafficking study that neither pY1175 nor pY1214 VEGFR2 colocalizes with Rab11 [40]. The remaining k_{dp} values, for Y951, Y1175, and Y1214 on the cell surface and in Rab4/5 endosomes, were fit using the Levenberg-Marquardt algorithm. The dephosphorylation rate constants were fit directly to a portion of the experimental data from the VEGF presentation studies, including Vb/Vs ratios (**Fig. 5-3B-C,H**). The fits were then checked against the remaining data from the VEGF presentation studies for reasonableness of fit (**Fig. 5-3D-G,I-K**) [8,29]. When fitting, we excluded early time-points, as our phosphorylation dynamics (controlled by receptor ligation and trafficking) cannot capture these early peaks, similar to models of EGFR [64], rendering optimization ineffective. A model that captures the full complexity of phosphorylation at very early times (<5 min) remains a task for future targeted studies; here we focus on the later time-points, which our model can achieve. Initial values for all parameters were pulled from a wide range [10^{-3}, 100], using a log-uniform distribution, and updated parameters were constrained to the same range. Parameter sets were accepted if the final cost was within 165% of the lowest cost set. Sets were excluded if the predicted number of phosphoVEGFR2 were too low to be realistic (<10 per cell at peak activation); this eliminates unrealistic scenarios and is necessary because the data used to fit is normalized, and so the total phosphorylation levels are not well-constrained. The lowest cost set found was selected as a representative parameter set, and used throughout the remained of this study (shown in **Table 5-3**)

5.2.9 Model Size

The complete model contains 97 molecular species, including all of the considered phosphorylation states for VEGFR2 and all of the locations each protein can exist in the model (surface, Rab4/5 endosomes, Rab11 endosomes, degraded). All biochemical reactions and trafficking processes are assumed to be independent of the phosphorylation state of VEGFR2 in this model. This results in a total of 15 reversible binding reactions that occur across all model compartments, all but one of which were parameterized using data from literature (**Table 5-1**). The model has 31 trafficking reactions, with 13 unique trafficking parameters. Two of these were taken from literature, 6 were fit directly, and 5 were

assumed or related to other parameter values (**Table 5-2**). There are 120 reversible phosphorylation

reactions in the model, with 9 unique phosphorylation parameters. Three of these parameters were

assumed, and the other 6 were fit directly (**Table 5-3**). Including all phosphorylation states of VEGFR2

considered, the model contains a total of 277 reactions, with 52 unique parameters, 13 of which were fit

directly, 31 taken from literature, and 8 of which were assumed or calculated based on relationships to

other values. Additionally, there are 8 geometric parameters in the model (**Tables 5-S2** and 5-**4**), two of

which are specific to the experimental set-up of each study (**Table 5-4**), and initial concentrations and

numbers of receptors per cell for each molecular species (**Table 5-4**). While this model is large in size,

previous work and simplifying assumptions (discussed in sections 5.2.5-5.2.8) reduce it to a tractable size.

5.2.10 Validation and Additional Model Simulations

        The complete, parameterized model was validated against additional data in the trafficking study

and against four independent studies [58,59]. The additional data in the trafficking study compared

colocalization of VEGFR2 with Rab proteins following stimulation with the isoform VEGF$_{165b}$ (V$_{165b}$),

which may account for a substantial portion of VEGF$_{165}$ present *in vivo* [65] but lacks the capability to bind

NRP1 [66], and VEGF$_{165a}$ (V), which does bind NRP1. The next two validation studies included both

soluble and immobilized VEGF. Outputs for the first of these validation studies are pY1175 and pY1214

[58]. The same k$_{off,V \cdot M}$ values were used here as for 2011 presentation study [8]. An assumption that the

concentration of immobilized VEGF was lower (by a factor of 3) than that reported for this particular study

was necessary to match experimental observations, in particular that pY1175 was lower with immobilized

VEGF than with soluble VEGF, and the magnitude of increase in pY1214 with immobilized compared to

soluble VEGF. We hypothesize that this reduction in apparent matrix-bound VEGF concentration is due to

reduced spatial availability/accessibility of this particular form of VEGF (immobilized on nanoparticles) to

endothelial cells. Such a correction was unnecessary for the VEGF presentation studies because the 2011

presentation study presented VEGF in a monolayer and the 2010 presentation study used a high VEGF

concentration, so depletion was negligible within the analyzed time-frame (not shown). For the second of

these validation studies, the output is total phosphorylated VEGFR2 (pR2) [59]. Here, M·V binding

parameters were taken from literature [18]. The initial conditions and geometry were tuned to the

experimental set-up, assuming that VEGF and fibronectin (FN) or FN fragments were pre-mixed and allowed to equilibrate before presentation to endothelial cells. We did not change any other model parameters. The third and fourth validation studies examined perturbations to VEGFR2 dephosphorylation [60,61] using only soluble VEGF. To mimic the experimental perturbations, we altered the relevant dephosphorylation parameters. See **Table 5-4** for a summary of parameters used in additional simulations to probe trafficking and phosphorylation.

5.2.11 Sensitivity Analysis

We performed a local sensitivity analysis to identify parameters that most strongly affect model outputs. Selected parameters were increased and decreased (one at a time) by a factor of 2, and the absolute value of the percent change in each output was calculated. The values resulting from upward and downward perturbations were averaged. These values were then averaged across a selected set of model outputs. We selected the following model outputs for our sensitivity analysis: pY1175 VEGFR2, pY1214 VEGFR2, and the ratio pY1214/pY1175, at 5, 15, and 30 minutes, for soluble and matrix-bound VEGF at concentrations of 2 ng/mL and 200 ng/mL.

5.2.12 Model Solution

The set of coupled ordinary differential equations that comprise this model were solved using a 5th order accurate Runge-Kutta scheme with an adaptive step-size. The algorithm was implemented in Fortran on a desktop PC. Simulation run-time was short for all cases.

5.3 Results

5.3.1 Trafficking parameter estimates appear consistent across cell lines and studies

Our primary goal was to quantify how changes in trafficking of VEGFR2 lead to altered patterns of site-specific phosphorylation. We first optimized the model trafficking parameters against data on VEGFR2 and NRP1 trafficking in PAECs [40] (**Table 5-S3**). The biochemical reaction parameters used are summarized in **Table 5-1**, and the initial conditions and geometry used are summarized in the first column of **Table 5-4**. The distributions of accepted parameter values (based on many parallel fits) are summarized in **Fig. 5-2A** and **Table 5-S4**. A representative parameter set was selected for use in the model (**Fig. 5-2A**, red dots). These values are shown in **Table 5-2**, along with assumptions made to reduce the number of parameters being fit. Based upon our analysis, we found that assuming a ratio of 1/100 for the relative recycling rates from Rab4/5 and Rab11 endosomes for several molecular species (as indicated in Table 2) produced optimal results. In general, the model captured the relative proportions of a molecule distributed between Rab4/5 and Rab11 endosomes well. The proportion of a species in Rab7 endosomes was typically lower in the experimental data than the degraded quantity in the model, but this was anticipated, as the model does not explicitly represent Rab7 endosomes separately from the degraded compartment. The relative agreement between simulated and experimental values (**Table 5-S3**) for this parameter set indicate that the model likely reproduces key elements of the underlying trafficking processes.

Using the obtained trafficking parameters, the model predicts that in the absence of NRP1, internalized V·R2 will be preferentially recycled via the Rab4 pathway or degraded ($k_{rec4} > k_{degr} > k_{4to11}$). Conversely, in the presence of NRP1, internalized V·R2 will be preferentially routed via the Rab11 pathway for recycling (k_{4to11} & $k_{rec11} > k_{degr} > k_{rec4}$). Interestingly, the degradation rate for V·N1·R2 was predicted to be an order of magnitude larger than the degradation rate for V·R2 (**Table 5-2**, **Fig. 5-2A**), suggesting a potential role for NRP1 in regulating VEGFR2 degradation. Our parameter set is also consistent with the Rab11 pathway being the "faster" recycling pathway, accessible only after stimulation with VEGF.

135

Figure 5-2. VEGF presentation and trafficking control the distribution of ligated VEGFR2. A.

Visualization of fit trafficking parameters. Red dots indicate a representative coherent set of parameters used throughout the rest of this study. (See Methods) **B.** Tuning of k_{degr} values to match data in 2010 presentation study. Dotted lines: fits using k_{degr} values fit in PAECs; solid lines: fits after k_{degr} values are increased by a factor of 2.4 to minimize the least squared error between simulations and this experimental data. Soluble VEGF (Vs), blue lines; bound VEGF (Vb), green lines. **C.** Summary of the distribution of VEGF-bound (V·R2) and unbound VEGFR2 (Free R2) over time, shown for Vb. Y-axis is shown in terms of the percentage of the steady-state (no VEGF) total VEGFR2 population. Note that, due to degradation, the total amount of VEGFR2 decreases after addition of VEGF. [V] = 20 ng/mL. **D.** Decrease in total VEGFR2 upon stimulation with VEGF. Solid line, [V] = 2 ng/mL; dashed line, [V] = 20 ng/mL; dotted line, [V] = 200 ng/mL. **E-M.** Distribution of V·R2 on the cell surface (E-G), in Rab4/5 endosomes (H-J), and in Rab11 endosomes (K-M) following stimulation with Vs (left column) or Vb (middle column). The right column shows the ratio of the first two columns.
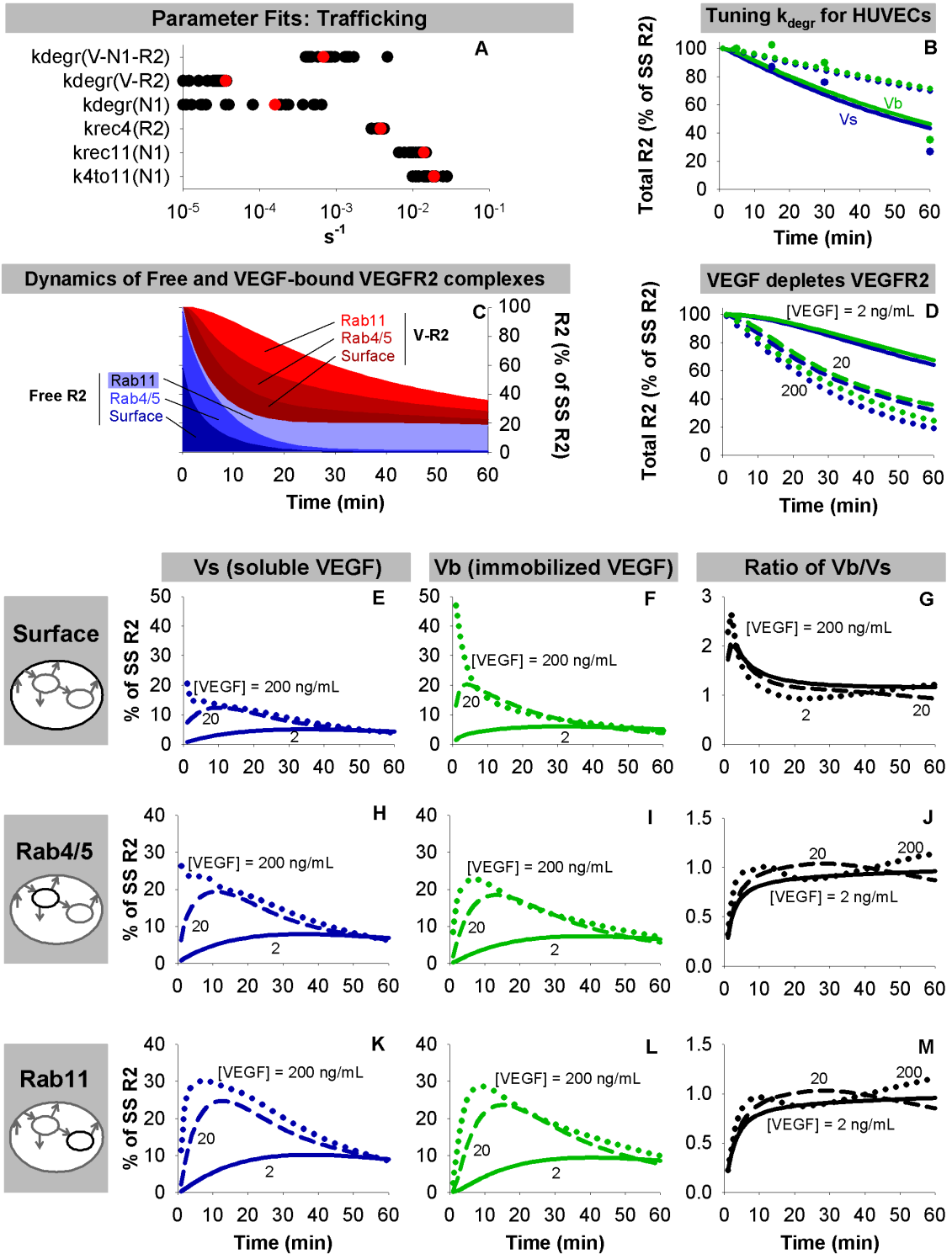
Figure 5-2

We next compared predictions using these trafficking parameters to data on VEGF presentation in a different endothelial cell type (HUVECs) [8,29]. The study-specific parameters for these VEGF presentation studies are shown in **Table 5-4**. The degradation rates for all species were increased by a constant factor (2.4) to match experimental measurements of total VEGFR2 loss from the 2010 presentation study [29] (**Fig. 5-2B**). In addition, the internalization rate for V·R2 was decreased slightly for the 2010 presentation study [29]. We hypothesize that this difference in internalization rates is due to the 100-fold difference in VEGF concentration between the experiments, as increasing the numbers of occupied receptors has been shown to decrease the measured internalization rate, likely due to saturation of endocytic pathways [50,67]. These modifications are summarized in **Table 5-4**.

Because obtaining good agreement between the simulated and experimental data in HUVECs did not require many changes in the parameters fit for PAECs, we propose that trafficking may be more consistent across endothelial cell lines than previously thought. Observed differences between cell lines may be the result of changes in absolute and relative receptor densities, along with the difference in degradation rates mentioned above. The obtained trafficking parameter values were also in reasonable agreement with previous estimates [8,24,25]. Our estimated degradation rates were lower than previous values, likely because this is the first model to consider dephosphorylation explicitly, allowing for decreases in phosphorylated VEGFR2 without receptor degradation or release of ligand.

The distribution of free and ligated VEGFR2 is predicted to vary as a function of both VEGF concentration and mode of VEGF presentation (**Fig.5-2 E-M**, **Fig. 5-S1**). Prior to stimulation with VEGF, the model predicts that most intracellular VEGFR2 is located in Rab4/5 endosomes (**Fig. 5-2C**), consistent with experimental observations [41]. Upon stimulation with VEGF, the proportion of VEGFR2 in Rab11 endosomes increases, while total and surface VEGFR2 decrease (**Fig. 5-2C**). Immobilized VEGF (Vb) results in increased magnitude and duration of V·R2 on the cell surface, and delayed peaks of decreased magnitude for V·R2 in both endosomal compartments compared to soluble VEGF (Vs) (**Fig. 5-2E-M**). The magnitude and width of the V·R2 peak was highly dependent upon VEGF concentration in all compartments (**Fig. 5-2E-M**). At 30 minutes, the majority of remaining VEGFR2 is predicted to be ligated at VEGF concentrations of 20 ng/mL and higher (**Fig. 5-2C**, **Fig. 5-S1**).

5.3.2 Parameterization of VEGF release from the matrix

We next estimated the VEGF-matrix reaction parameters for the VEGF presentation studies. For the 2011 presentation study using a modified heparin linker [8], the equilibrium dissociation constant (K_D) for VEGF and matrix in this study was taken from literature [12,63]. The off-rate constant, $k_{off,V\cdot M}$, was estimated to be 3.3×10^{-3} s^{-1} in the electrostatic case (Ve), which is within the range reported literature for VEGF and heparin [12,63] (**Fig. 5-3A**). For the covalent case (Vc), this value was decreased until a reasonable fit was obtained (**Table 5-4**). For the 2010 presentation study, we found that a surprisingly low value of $k_{off,V\cdot M}$ was necessary to fit the experimental release data. This value was too low to allow for sufficient internalization of V·R2 after stimulation with immobilized VEGF to be consistent with experimentally observed data (not shown). We believe therefore that $k_{off,V\cdot M}$ is being underestimated using this release data, as VEGF must both release and diffuse out of the gel to be measured in that assay. Instead, we assumed that VEGF was immobilized in the collagen gel in a heparin-mediated manner, and we used a $k_{off,V\cdot M}$ of 10^{-2} s^{-1}. This allowed us to estimate a $K_{D,V\cdot M}$ value for this study (**Table 5-4**).

Figure 5-3. Prediction of VEGFR2 binding and phosphorylation parameters. A. Total surface Vs·R2 + internal VEGF, used to fit $k_{off,M \cdot V}$ for the 2011 presentation study [8]. Lines indicate simulation results, dots indicate experiments. Soluble VEGF (Vs), blue; electrostatic bound VEGF (Ve), green; covalent bound VEGF (Vc), red. **B-C.** pY1175 and pY1214 data for 2011 presentation study [8], which was used to fit dephosphorylation rate constants, along with **H**. **D-F.** Phosphorylation data from the 2010 presentation study [29], which was used to confirm dephosphorylation rate fits. **D-E.** Western blot data. **F.** ELISA data. Soluble VEGF, blue; bound VEGF, green. **G-J.** Additional phosphorylated VEGFR2 (by residue) experimental data from 2010 presentation study with model predictions. **K.** Ratio of pR2 for Vb and Vs at various times, from 2010 presentation study.
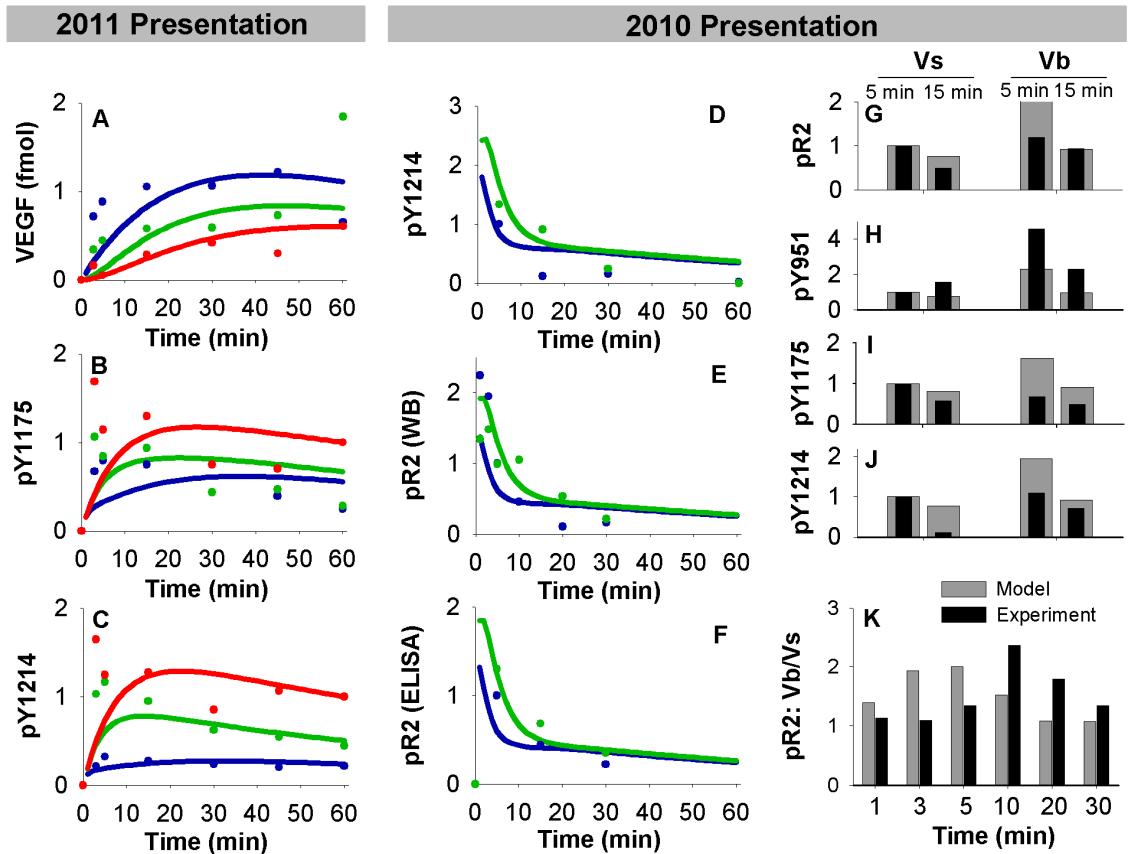
5.3.3 Parameterization of Phosphorylation Reactions

The final set of parameters we estimated were the dephosphorylation rate constants for Y951, Y1175, and Y1214 on the cell surface and in Rab4/5 endosomes. All other phosphorylation parameters (see **Table 5-3**) were fixed as described in the Methods. We fit the dephosphorylation rates to data from the two VEGF presentation studies simultaneously [8,29], with no study-specific changes in these values. The distribution of accepted parameters values from many fit sets are shown in **Fig. 5-S2A** and summarized in **Table 5-S4**. A representative parameter set (**Fig. 5-S2A**, red dots; **Table 5-3**) is used in the rest of this study. While a wide range of dephosphorylation parameter values resulted in acceptable fits of the data, the ratios of the surface and Rab4/5 dephosphorylation rate constants for Y1175 and Y1214 were more consistent (**Fig. 5-S2B**). The dephosphorylation rates for 1175 and 1214 were higher on the surface than in Rab4/5 endosomes, while the surface/Rab4/5 ratio was higher for Y1175 than Y1214 in 46 of the 47 accepted parameter sets (**Fig. 5-S2B**). Slightly better fits could be obtained if the parameters were permitted to be study-dependent, or if additional experimental set-up or cell line-specific changes were made; however, we used a consistent parameter set to keep the model as general as possible across multiple experimental set-ups (see **Table 5-3**). The fits for these studies are shown in **Fig. 5-3A-K** and **Fig. 5-S2C-D**. In general, important trends in dynamics and relative activation by soluble or matrix-bound VEGF were captured by the model, as were the original experimental values 10 minutes or more after stimulation with VEGF. Additionally, our estimated phosphorylation and dephosphorylation rate constants are consistent with those previously estimated for EGFR [64]. As the estimated dephosphorylation rate constants for Y951 were not well-constrained, and only one set of data was available for pY951, we have limited confidence in the Y951 dephosphorylation rate constants. We therefore focus on VEGFR2 phosphorylated on at least one of Y951, Y1175 and Y1214 (pR2), and VEGFR2 phosphorylated specifically on Y1175 (pY1175) or Y1214 (pY1214).

5.3.4 Validation of Complete Model

To validate our trafficking parameters, we used additional data from the trafficking study. Here, PAECS transfected with NRP1 and VEGFR2 were stimulated with the VEGF isoform V_{165b} [40], which does not bind NRP1 [68]. We used our model to predict whether the differences in VEGFR2 distribution

upon stimulation with V_{165a} (V) and V_{165b} can be accounted for solely by the inability of V_{165b} to bind

NRP1 (**Fig. 5-4A-B**) by comparing to simulations lacking NRP1. The ratio of VEGFR2 in Rab4/5

endosomes to VEGFR2 in Rab11 endosomes matched data for V_{165b} well (**Fig. 5-4A**). Thus, the model

predicts that the impact of V_{165b} on VEGFR2 localization in early and recycling endosomes (compared to

V_{165a}) can be accounted for solely by its inability to bind NRP1, and suggesting that our model framework

can capture differences in trafficking between VEGF isoforms. The model overestimates routing of

VEGFR2 for degradation (compared to Rab7 populations in the experimental data) for V_{165a} and

underestimates it for V_{165b} (**Fig. 5-4A**). This may indicate some error in the relative values of our

degradation rate constants for V·R2 and V·N1·R2, due to the limited and normalized data available to fit

these rate constants, but it does not affect model predictions when NRP1 is present.

Figure 5-4. Validation of complete model with trafficking and phosphorylation parameters. A. Validation of trafficking parameters by comparing model predictions for VEGFR2 in the absence of NRP1 in PAECs compared to Ballmer-Hofer data for V_{165b} (V_b), which does not bind NRP1. Data is compared to the normal case including NRP1 in the model and data for V_{165a} (V_a), which does bind NRP1, at 30 min in the trafficking study. The percent of internal VEGFR2 in Rab4/5 and Rab11 endosomes (left) and the ratio of total VEGFR2 in Rab4/5 endosomes to total VEGFR2 in Rab11 endosomes (right) is shown. Grey: model simulations; black, experimental data. **B-D.** Validation of complete model including trafficking and phosphorylation parameters. **B)** Data taken from Martino et. al. 2011 [59]. [V] = 50 ng/mL. Assumed VEGF and FN are pre-mixed. Soluble VEGF, blue; VEGF bound to wild type fibronectin, green; VEGF bound to rFNIII9-10/12-14 fragments, red ($k_{off,M\cdot V}$ values from Wijelath et. al. 2006 [18]). **C-D**. Data taken from an additional Anderson et. al. 2011 study [58]. **E-F.** Validation of phosphorylation parameters by comparing model predictions to data in cells with perturbations to specific phosphatases. **E.** Impact of siRNA against VEPTP on pY951, pY1175, and pY1214. Experimental data (black) taken from Mellberg et. al. 2006 [61]. TIME cells, [V] = 50 ng/mL, measurements taken at t = 5 min. In the model, the experimentally observed decrease in VEPTP expression to 20% of control values with VEPTP siRNA was simulated by decreasing the dephosphorylation rate for Y951 and Y1175 by a factor of 5 on the cell surface. HUVEC receptor numbers were used in model. **F.** Impact of exposing HEK 293 cells transfected with VEGFR2 to a constitutively active form of TCPTP on pR2, pY1175, and pY1214. Data taken from Mattila et. al. 2008 [60]. In the model, we simulated the constitutively active TCPTP by increasing the dephosphorylation rate for Y951 and Y1214 to match the rate for unligated R2 (30 s^{-1}) in all compartments. HUVEC receptor numbers were used in model.
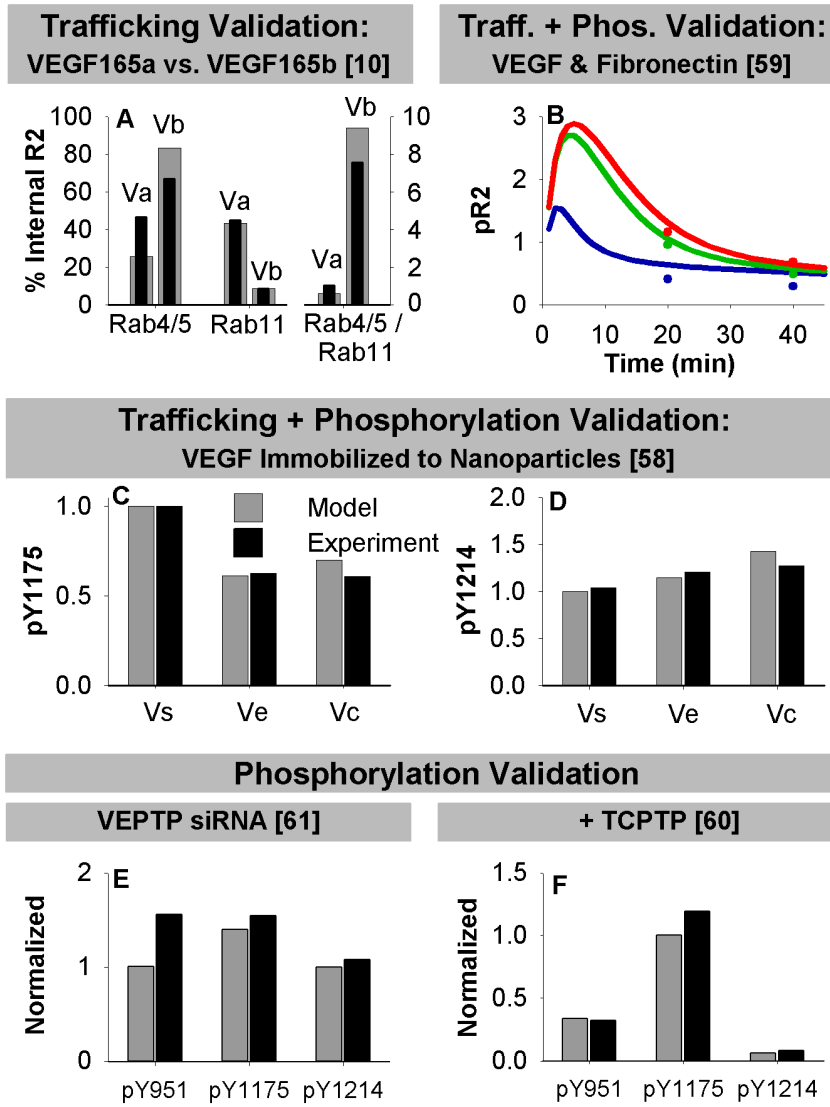
Figure 5-4

Next, we validated the complete model including biochemical reactions, trafficking processes, and phosphorylation reactions using two additional studies of soluble and immobilized VEGF (*See* Methods) [58,59] (**Fig. 5-4B-D**). We also validated our phosphorylation parameters by comparing model predictions to experimental measurements of VEGFR2 phosphorylation after perturbation of the expression or activity of phosphatases that are known to regulate VEGFR2. As we did not explicitly include these phosphatases in our model, we altered the dephosphorylation rate constants specifically for the tyrosine residues on which the specified phosphatase is known to act, and in the subcellular locations where the phosphatase is typically located. We examined two phosphatases known to act on VEGFR2, but that are not yet completely understood. VEPTP, which is found on the plasma membrane, dephosphorylates Y951 and Y1175, but not Y1214 [61]. TCPTP, which is found both at the plasma membrane and in the cytosol, dephosphorylates Y1214 and likely also Y951, but not Y1175 [60]. **Fig. 5-4E** shows model predictions and experimental data for change in pY951, pY1175, and pY1214 when TIME cells are treated with siRNA to VEPTP. Application of VEPTP siRNA was modeled as a decrease in the dephosphorylation rate constants for Y951 and Y1175 on the cell surface by a factor of 5, to match the experimental observation that VEPTP siRNA results in reduction of VEPTP expression to 20% of expression in the control. **Fig. 5-4F** shows model predictions of VEGFR2 phosphorylation in HEK 293 cells exposed to a constitutively active form of TCPTP, which was modeled by increasing the dephosphorylation rate constants for Y951 and Y1214 to the values for unligated VEGFR2 (30 s^{-1}) in all compartments. The model predicts that VEPTP siRNA only partially abrogates dephosphorylation of VEGFR2, while addition of constitutively active TCPTP results in strong dephosphorylation of Y1214. The consistency of model predictions and experimental data in these studies provides further validation for our model framework.

5.3.5 Trafficking-mediated regulation of site-specific phosphorylation is sufficient to capture experimental trends in VEGFR2 activation

In order to understand the influence of trafficking on phosphorylation of VEGFR2, we compared the relative amounts of pR2, pY1175, and pY1214 in each subcellular location and in total after stimulation with soluble and immobilized VEGF (**Fig. 50-5**, **Fig.5-S3**). While pY1175 and pY1214 are both split between the cell surface and Rab4/5 endosomes, Rab4/5 endosomes contain more pY1175 (**Fig. 5-S3H-I,**

Fig. 5-6B-C) and the cell surface has more pY1214 (**Fig. 5-S3E-F, Fig. 5-6F-G**). The peak magnitude of

total pY1214 (**Fig.5-5K**) is predicted to be more than twice the peak magnitude of pY1175 after stimulation

with immobilized VEGF (**Fig.5-5H**, due to the increased surface population of VEGF·VEGFR2), but the

peak magnitudes are more similar when stimulated with soluble VEGF (**Fig.5-5G,J**). Immobilization of

VEGF also leads to increased pR2 peak magnitude on the cell surface (**Fig. 5-S3D**), decreased pR2 peak

magnitude in Rab4/5 endosomes (**Fig.5- S3G**), and increased duration of total pR2 (**Fig. 5-5D-F**, **Fig.5-**

S3A). To test the hypothesis that multiple endosomal compartments with distinct properties are necessary

to capture experimentally observed trends in pY1175 and pY1214, we examined a case where the

dephosphorylation rate constants in Rab11 endosomes were assumed to be the same as those in Rab4/5

endosomes (**Fig.5-S4**). In this case, peak pY1214 remains essentially unchanged, but the duration

increases (**Fig.5-S4C**), while the peak magnitude and duration of pY1175 increases significantly (**Fig.5-**

S4B). The observed increase in duration is inconsistent with experimental data, emphasizing the need for

multiple internal compartments with independent dephosphorylation rates to reflect the cellular localization

of phosphatases.

Figure 5-5. VEGF presentation mode affects VEGFR2 phosphorylation more than VEGFR2 ligation.
The time-dependent response to soluble VEGF (Vs, blue, left column) and bound VEGF (Vb, green, middle column) of: VEGF-ligated VEGFR2 (V·R2, A-C); all phosphorylated VEGFR2 (pR2, D-F); and site-specific phosphorylated VEGFR2, pY1175 (G-I) and pY1214 (J-L). The ratios of responses to bound and soluble VEGF are shown at the right. Time-scale ends at 30 minutes, but pR2 curves are relatively flat after this time. Solid line, [V] = 2 ng/mL; dashed line, [V] = 20 ng/mL; dotted line, [V] = 200 ng/mL.

147
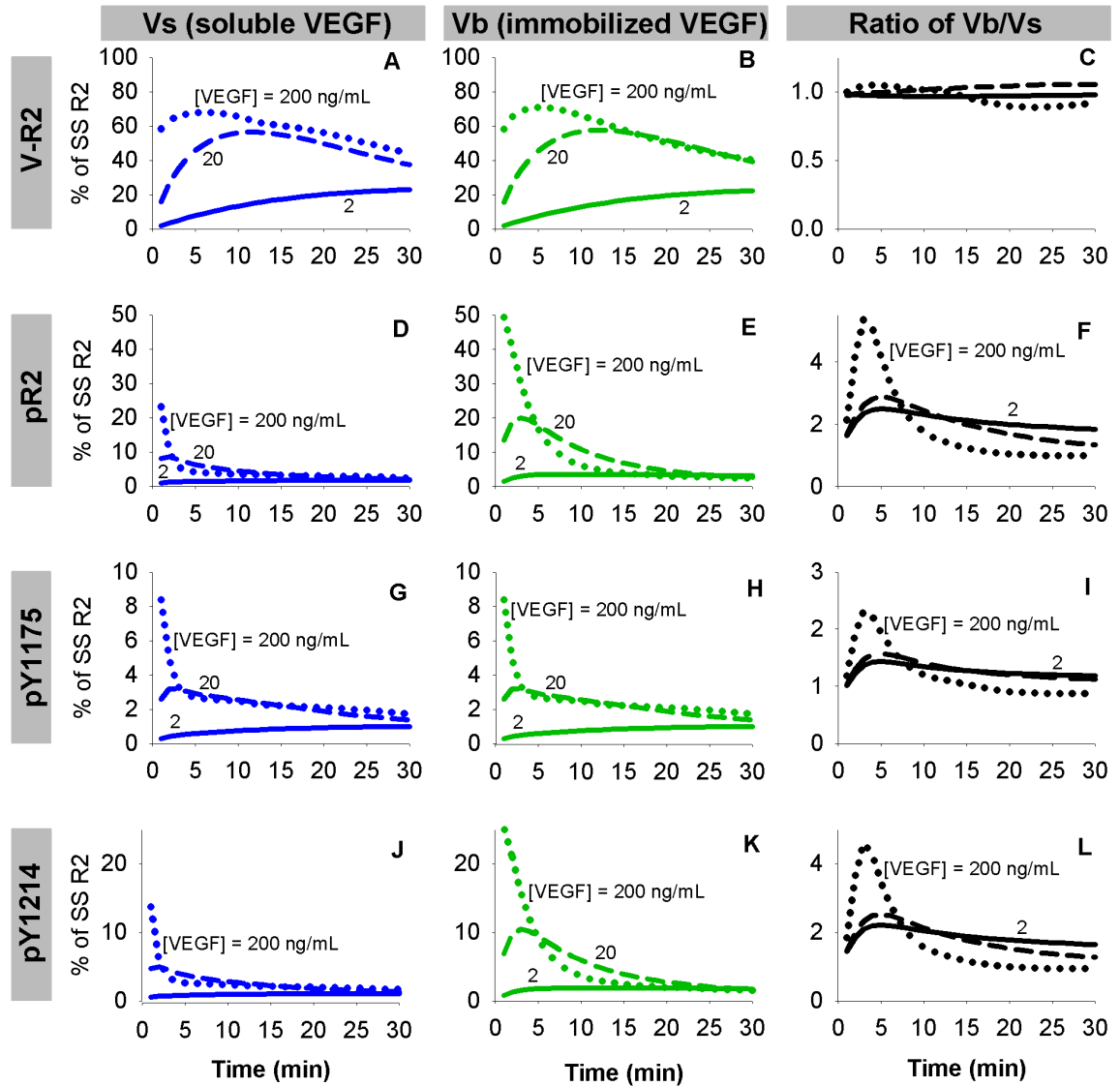
The model clearly predicts that ligated VEGFR2 (V·R2) is not an accurate representation of VEGFR2 phosphorylated on at least one of the considered residues (pR2) at all times; while V·R2 and pR2 are both elevated at early times, the durations are quite dissimilar (**Fig. 5-5A-F**). We found that only 33% of ligated VEGFR2 is phosphorylated on at least of one Y951, Y1175, and Y1214 at 5 minutes after stimulation with 20 ng/mL of immobilized VEGF (**Fig 5-.S5B**). By 30 minutes, only 7% of ligated VEGFR2 is phosphorylated on one of these residues (**Fig. 5-S5B**), though a significant amount of VEGFR2 is predicted to remain ligated (**Fig. 5-2E-M**, **Fig. 5-5A-B**). This model prediction is consistent with experimental observations that, while detectable pR2 is low by 30 minutes in most cases, total VEGF and VEGFR2 populations are still significant [29,58]. To test the robustness of this prediction, we increased our assumed phosphorylation rate constant. This did not substantially increase the percentage of VEGF-VEGFR2 phosphorylated at 30 minutes (not shown). The short duration of phosphorylation on ligated VEGFR2 results from recycling through Rab11 endosomes, where dephosphorylation rates are high.

To quantify the total amount of VEGFR2 activation in the first 60 minutes after stimulation with soluble or immobilized VEGF, we calculated the area under the pR2 vs. time curves (curves shown in **Fig. 5-S3**). The increase in total VEGFR2 activation observed after stimulation with Vb compared to Vs results primarily from increased pR2 on the surface (**Fig. 5-6A-C, Fig.5-S6C-E**). Note that the relative proportion of total surface VEGFR2 activation on Y1175 and Y1214 is similar for Vs and Vb (**Fig. 5-6D**); the difference in total signaling (**Fig. 5-6L**) arises from the relative sizes of the surface and internal populations (**Fig. 5-2E-M**). The simulations also predicted that the size of the increases in the pY1214/pY1175 ratio due to immobilized VEGF is higher at lower VEGF concentrations (**Fig. 5-S6R**), which is where the physiological range of VEGF concentrations lies [13].

Figure 5-6. Increased total VEGFR2 activation with immobilized VEGF is driven by the change in surface VEGFR2. All panels show area under the curve (AUC), a measure of total VEGFR2 activation, for the first 60 minutes after stimulation with soluble (Vs- blue) or immobilized (Vb- green) VEGF at a concentration of 2 ng/mL. AUCs are shown for surface VEGFR2 (A-D), Rab4/5 VEGFR2 (E-H), and total VEGFR2 (I-L). Activation on any considered tyrosine residue (pR2, 1st column), Y1175 (2nd column), and Y1214 (3rd column) are compared. The last column shows the AUC for the curve pY1214/pY1175 (total pY1214/pY1175 curves shown in Fig. 8F-G) for surface VEGFR2 (D), Rab4/5 VEGFR2 (H), and total VEGFR2 (L). Note that the difference in total pY1214/pY1175 for Vs and Vb emerges from the altered VEGFR2 distribution, not altered pY1214/pY1175 in each subcellular location.
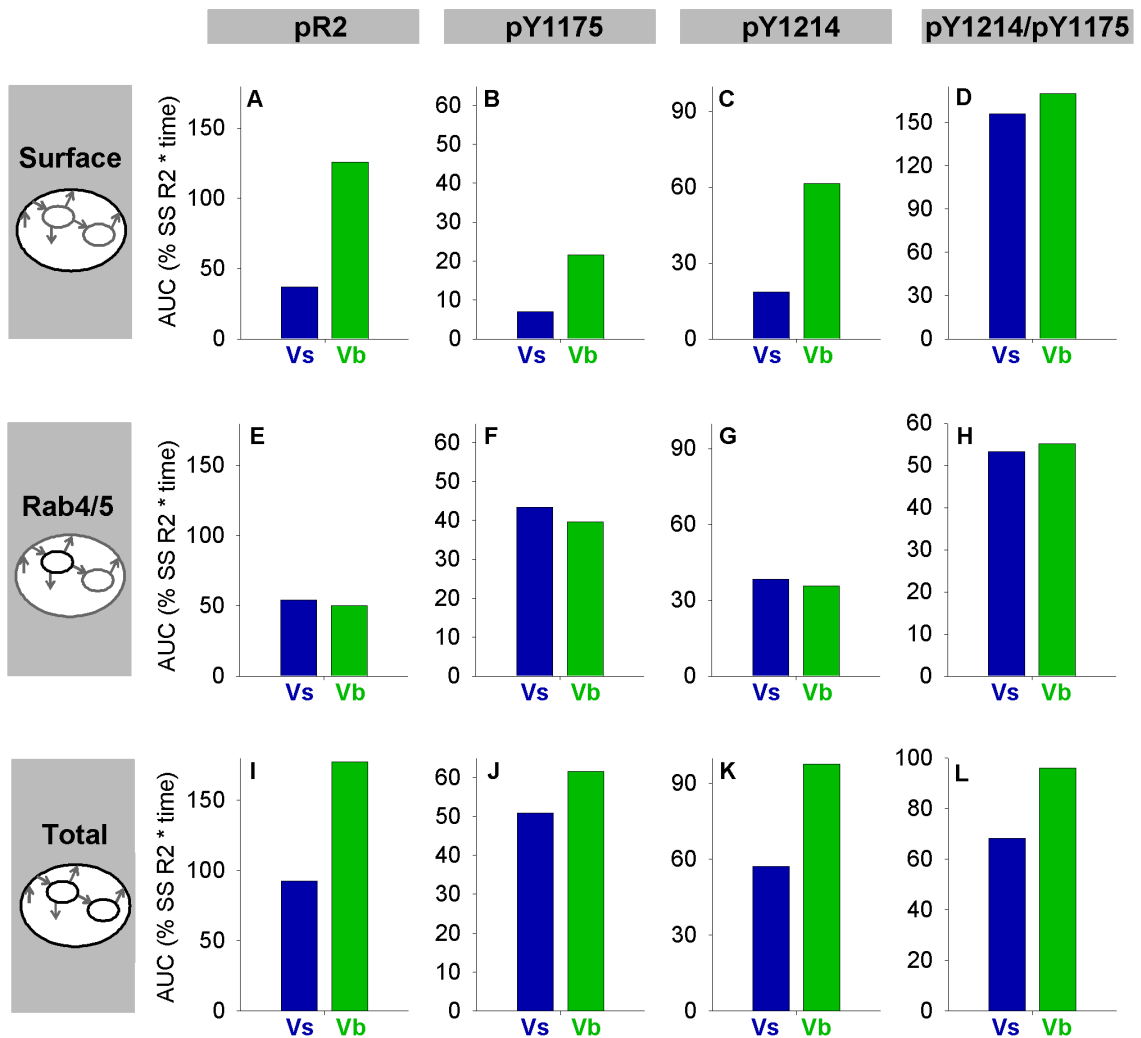
5.3.6 Neuropilin-1 modulates site-specific VEGFR2 phosphorylation due to altered recycling and degradation of VEGF-bound VEGFR2

In most endothelial cell types, NRP1 is present at cell surface densities higher than those of VEGFR2 [62]. Based on the strong receptor-receptor coupling effect, it is expected that the majority of cell surface V·R2 will be bound to NRP1 [12,32]. To probe the impact of NRP1 on VEGFR2 trafficking and phosphorylation, we simulated stimulation of HUVECs with VEGF in the presence or absence of NRP1 (**Fig.5-7A-G**). In the absence of NRP1 (e.g. through siRNA knockdown), the model predicts less total degradation of VEGFR2 (**Fig. 5-7G**) and an increase in the duration of VEGFR2 phosphorylation (**Fig. 5-7D-F**, due to decreased degradation and decreased localization to Rab11 endosomes, where efficient dephosphorylation occurs). NRP1 absence also results in a larger difference in VEGFR2 ligation after stimulation with soluble or immobilized VEGF (**Fig. 5-7A-C**). In the absence of NRP1, V·R2 (**Fig. 5-7A-C**) and unligated VEGFR2 (**Fig. 5-S7**) are predicted to accumulate in the Rab4/5 compartment (**Fig. 5-7B, Fig. 5-S7B**), as the "fast" Rab11 recycling pathway is not accessible (k_{4to11} and $k_{rec11} \gg k_{rec4}$). Thus, our model supports the hypothesis that NRP1 is necessary for the enhancement of VEGFR2 recycling observed upon stimulation with VEGF (by rerouting the ligated receptor through the Rab11 recycling pathway) [40]. This is also consistent with experimental observations that Rab11-dependent recycling of VEGFR2 leads to increased activation of p38 after stimulation with soluble VEGF, presumably due to the return of more VEGFR2 to the plasma membrane and subsequent reactivation [40,69]. Upon stimulation with immobilized VEGF in the absence of NRP1, surface VEGF-VEGFR2 is increased, as the matrix (M) does not have to compete with NRP1 for binding to VEGF (**Fig. 5-7A**). These changes have the potential to alter the balance of downstream signaling (**Fig. 5-7E-F**) differently than VEGF immobilization or NRP1 loss alone. By routing V·R2 through the Rab11 compartment to be dephosphorylated and recycled, NRP1 may be a strong regulator of pR2, and thus of interest as a therapeutic target.

As we assume that M and NRP1 cannot bind to VEGF simultaneously, we examined whether, for immobilized VEGF presentation, VEGF-bound VEGFR2 internalized following detachment from the matrix would be predicted to remain unbound to NRP1, potentially altering its recycling and degradation compared to soluble VEGF. The model predicts that almost all internal V·R2 complexes (Rab4/5 and Rab11) contain NRP1 after stimulation with either form of VEGF (**Fig. 5-S8**). Thus, it is predicted that

NRP1 joins the V·R2 complex shortly after dissociation of VEGF from M, so VEGF immobilization does

not alter V·R2 recycling and degradation *after* dissociation from the matrix and internalization.

Figure 5-7. Neuropilin-1 and phosphatases modulate site-specific VEGFR2 phosphorylation. A-C. Distribution of VEGF-bound VEGFR2 (sum of V·R2, V·N1·R2, and M·V·R2) in HUVECs. Solid lines: Baseline case with NRP1 present; dotted lines: no NRP1 present. Soluble VEGF (Vs), blue lines; bound VEGF (Vb), green lines. For all lines, [V] = 20 ng/mL, HUVEC receptor numbers. **D-G.** Total VEGFR2 phosphorylated on at least one of Y951, Y1175, and Y1214 (pR2, D), pY1175 (E), pY1214 (F), and total VEGFR2 (G) with NRP1 (solid lines) and without NRP1 (dotted lines). **H-I.** Model predictions for site-specific VEGFR2 phosphorylation under perturbation of phosphatase activity. **H.** Model predictions for the experiment in Fig. 4F (siRNA to VEPTP), with the addition of a constitutively active TCPTP (as described in Fig. 4G). **I.** Model predictions for exposure of HUVECs to a cell-surface phosphatase that dephosphorylates Y951, Y1175, and Y1214, similar to DEP-1. The impact of increasing phosphatase expression by a factor of 2, 5, or 10 is shown.

Figure 5-7

153
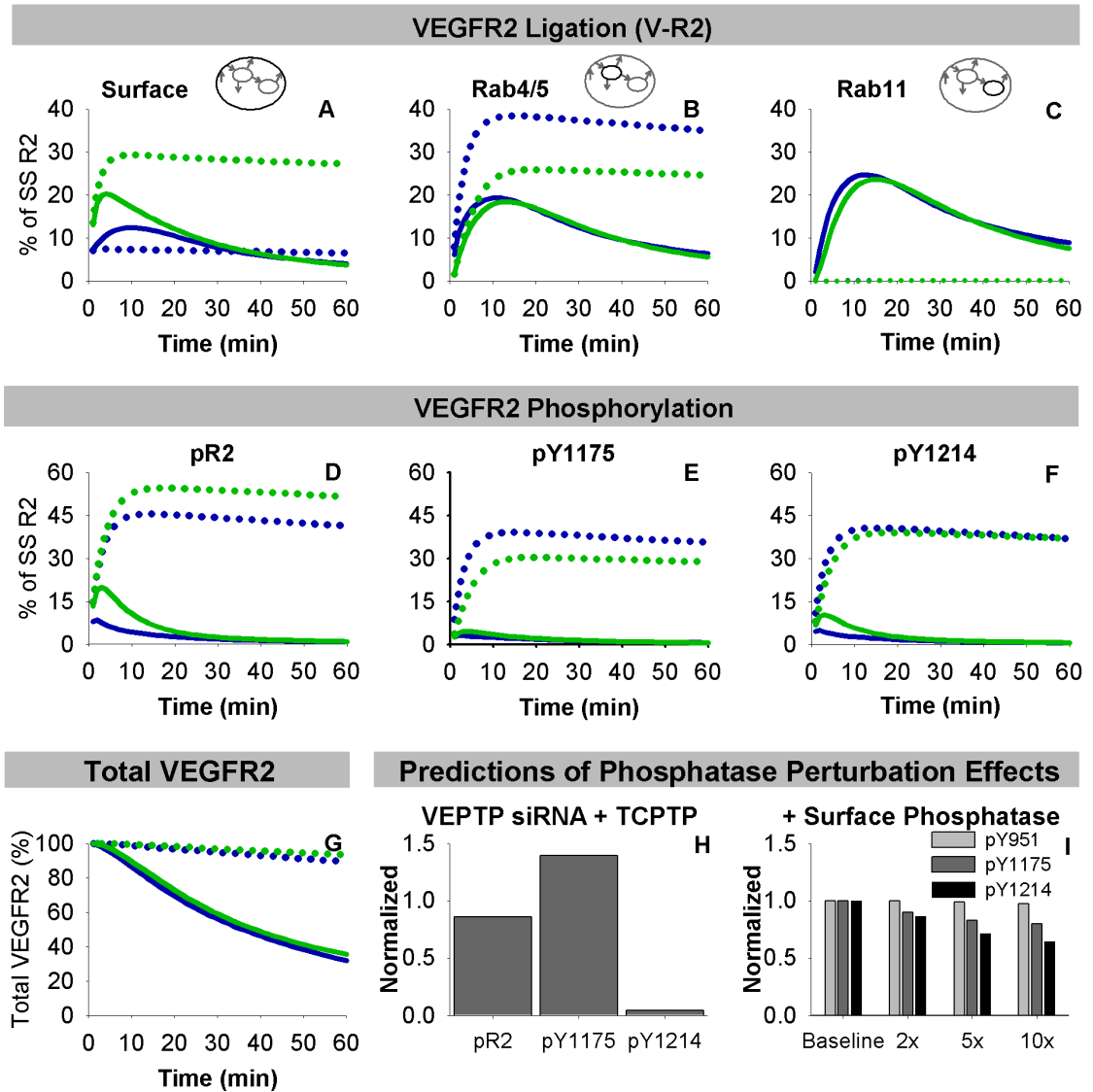
5.3.7 Integrated model can predict the impact of novel phosphatase perturbations on VEGFR2 phosphorylation

We also used the model to predict the impact of novel scenarios involving phosphatases. First, we predicted the impact of exposing HUVECs to VEGF after treatment with a combination of siRNA to VEPTP and a constitutively active form of TCPTP (**Fig. 5-7H**). The simulations show that pY1175 would be elevated, due to the VEPTP siRNA, while pY1214 would be decreased, due to the constitutively active TCPTP. This produces a situation where the balance of pY1175 and pY1214 is strongly shifted, while total phosphorylated VEGFR2 (pR2) remains close to baseline levels. We also explored the impact of a cell surface-localized phosphatase that dephosphorylated Y951, Y1175, and Y1214 (**Fig. 5-7I**). This phosphatase is similar to DEP-1, except that DEP-1 is also implicated in inhibition of VEGFR2 internalization [46], which our theoretical phosphatase does not do. We examined the impact of this phosphatase by increasing the rate constant for cell surface dephosphorylation of all three residues in this model, in order to mimic increased expression of this phosphatase (**Fig. 5-7I**). We found that pY1214 was decreased most by the phosphatase, while pY1175 was affected less because this phosphatase cannot access VEGFR2 in Rab4/5 endosomes. These model predictions are examples of specific mechanistic hypotheses that could be tested experimentally.

5.3.8 VEGF immobilization alters surface vs. internal distribution of VEGFR2 and balance of pY1175 and pY1214

There is significant interest in how specific immobilization techniques will alter activation of VEGFR2. As a first step, we examined the influence of varying the rate constant for VEGF release from the matrix, $k_{off,V \cdot M}$ (**Fig. 5-8A-E**). Assuming all immobilized VEGF is spatially available to bind VEGFR2, a significant portion of cell surface V·R2 is bound to the matrix (M) (**Fig. 5-8E**). Total peak pY1175 magnitude and distribution across subcellular locations (**Fig. 5-8A-B**), is significantly altered by increasing $k_{off,V \cdot M}$. pY1214 remains primarily surface-localized for all cases with immobilized VEGF (**Fig. 5-8C**), but the magnitude decreases with increasing $k_{off,V \cdot M}$, altering the relative magnitudes of pY1175 and pY1214 (**Fig. 5-8D**). While total ligated VEGFR2 is not dramatically different after stimulation with soluble or immobilized VEGF (**Fig. 5-5A-C**), the ratio pY1214/pY1175 is greater than two at early times after

stimulation with immobilized VEGF, favoring p38 activation and migration (**Fig. 5-8G**), while the ratio is closer to one for soluble VEGF, favoring ERK activation and proliferation (**Fig. 5-8F**). Increasing $k_{off,V \cdot M}$ decreases the difference in pR2 after stimulation with soluble or immobilized VEGF (**Fig. 5-8A**) by allowing for more internalization of VEGF·VEGFR2 complexes in the Vb case.

Figure 5-8. Relative activation pY1175 and pY1214 varies as a function of VEGF immobilization and concentration. A-C. Total VEGFR2 phosphorylated on at least one of Y951, Y1175, and Y1214 (pR2, A) and site-specific phosphorylation (pY1175, B and pY1214, C) at 5 min with varying $k_{off,V\cdot M}$. Note quantities of VEGFR2 phosphorylated on any residues in Rab11 endosomes are negligible. **D.** Ratio of pY1214 to pY1175 at 5 minutes with varying $k_{off,V\cdot M}$. **E.** Percent of surface V·R2 complexes that are bound to the matrix at t = 5 minutes. **F-H.** The ratio of pY1214-VEGFR2 to pY1175-VEGFR2 for Vs (F) and Vb (G). The ratio of this quantity for bound VEGF and soluble VEGF (Vb/Vs) is shown in (H). Solid line, [V] = 2 ng/mL; dashed line, [V] = 20 ng/mL; dotted line, [V] = 200 ng/mL. Soluble VEGF (Vs), blue lines; bound VEGF (Vb), green lines. For all lines, HUVEC receptor numbers were used.
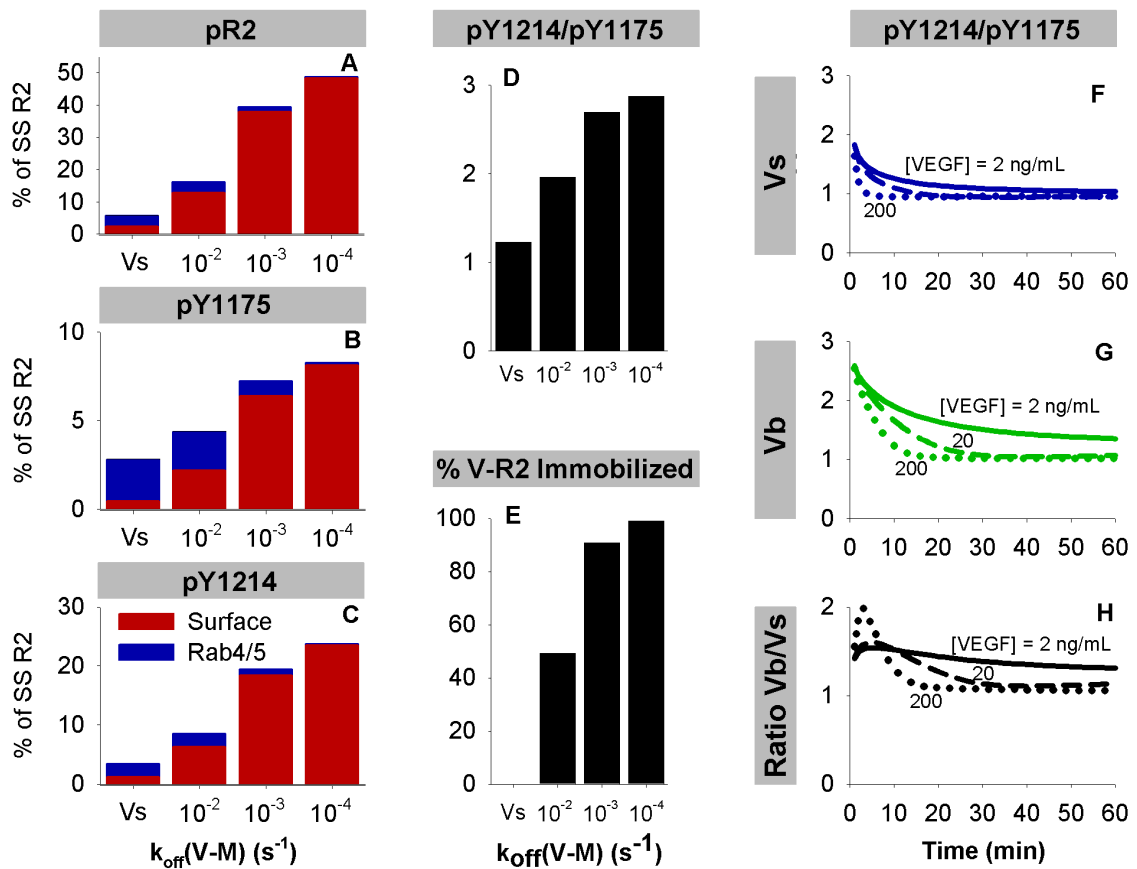
5.3.9 pY1175 and pY1214 are predicted to be more sensitive to trafficking parameters than to

phosphorylation parameters

We performed a local sensitivity analysis to investigate which initial conditions and rate constants impact model outputs the most (**Fig. 5-S9**). The outputs considered were pY1175, pY1214, and the ratio pY1214/pY1175 after stimulation with soluble or immobilized VEGF at 5, 15, or 30 minutes. We found that sensitivities are notably different at low (2 ng/mL, **Fig. 5-S9A**) and high (200 ng/mL, **Fig. 5-S9B**) VEGF concentrations. Specifically, at low VEGF concentrations, outputs are more sensitive to initial conditions ([V] and receptor numbers) and to dephosphorylation parameters (**Fig. 5-S9A**); while at high VEGF concentrations, outputs are more sensitive to trafficking parameters (**Fig. 5-S9B**). Almost all outputs are quite sensitive to VEGFR2 and NRP1 levels. In general, model outputs (pY1175, pY1214, pY1214/pY1175) are less sensitive to the phosphorylation parameters than the trafficking parameters, reinforcing that, in our model, trafficking is an strong regulator of phosphorylation patterns. Stimulation with immobilized VEGF decreased the sensitivity of the model to trafficking parameters compared to soluble VEGF.

5.4 Discussion

5.4.1 Computational model of VEGFR2 ligation, trafficking, and phosphorylation

In this study we developed a computational model that quantitatively relates VEGF-VEGFR2 binding and trafficking of VEGFR2-to patterns of site-specific phosphorylation. Our model was parameterized using data from three separate studies [8,29,40], and validated against data from four additional independent studies [58-61]. We identified trafficking parameters that describe experimental data in multiple endothelial cell lines, suggesting that trafficking processes may be more conserved than previously thought. Our simulations predict that the relative surface and endosomal populations of ligated VEGFR2 (V·R2) are affected by the coreceptor NRP1. By routing V·R2 through Rab11 endosomes to be dephosphorylated and recycled, NRP1 may be a strong regulator of VEGFR2 phosphorylation. Our model further indicates that immobilization of VEGF leads to decreased internalization, but does not affect recycling or degradation of internalized receptors because ligated VEGFR2 (V·R2) is predicted to bind NRP1 quickly after unbinding from the matrix. The model predicts that the durations of ligated VEGFR2 (V·R2) and phosphorylated VEGFR2 (pR2) curves are quite dissimilar, providing a good rationale for simulating phosphorylation and dephosphorylation separately from receptor ligation. Additionally, the pR2 pool represents only a fraction of ligated VEGFR2 (<35% by 5 minutes after VEGF stimulation), and is altered by perturbations to dephosphorylation of specific residues.

In enabling us for the first time to predict VEGFR2 phosphorylation patterns in response to receptor ligation and trafficking, without assuming that phosphorylation of VEGFR2 is synonymous with ligation and dimerization, this study represents an advance over existing models. In our previous models of VEGF-NRP1-VEGFR2 interactions [12,32,84], we had not included the effect of NRP1 on VEGFR2 trafficking. The observed differences in duration of ligated (V·R2) and phosphorylated VEGFR2 (pR2) captured by our model cannot be replicated by a model with a single endosomal compartment. An early compartment where significant amounts of phosphorylated VEGFR2 can accumulate is necessary, while a second, later compartment is required where ligated VEGFR2 is dephosphorylated before recycling to the cell surface. This model is also the first to include site-specific activation of VEGFR2 by immobilized VEGF. Importantly, our model accurately captures *relative* trends in phosphorylation of Y1175 and Y1214 between soluble and immobilized VEGF (**Fig. 5-S2C-D**) at multiple VEGF concentrations (2-200 ng/mL)

and under a variety of experimental conditions. A computational model developed by the authors of the 2011 presentation study captured trends in VEGF internalization between soluble and immobilized VEGF, but does not contain the level of detail in trafficking and phosphorylation included in our model, and cannot replicate trends in pY1175 and pY1214 (**Fig. 5-3B-C**) [8]. Most of the phosphorylation data used to fit our model was normalized and semi-quantitative; as such, we cannot validate model predictions of the total percentage of VEGFR2 phosphorylated, but we can make and validate predictions about the relative phosphorylation of VEGFR2 on Y1175 and Y1214, and how these curves change under various conditions. The detail in our model allows us to demonstrate that trafficking (and immobilization), coreceptor expression, and phosphatase activity all affect the balance of VEGFR2 phosphorylation on tyrosines 1175 and 1214. This in turn alters the recruitment of signaling complexes, and regulates downstream signaling and resultant cellular behavior. As such, changes to any combination of these could have therapeutic value, and all need to be considered in an integrated fashion when designing tissue constructs to promote development of a functional vascular network.

5.4.2 Does trafficking regulate phosphorylation, or does phosphorylation regulate trafficking?

Our simulations show how one ligand, VEGF, can elicit different cellular responses simply via changes in its mode of presentation. Differences in trafficking resulting from immobilization of VEGF are sufficient to account for differences in activation of VEGFR2 by soluble and matrix-bound VEGF. It is not necessary that there be a different activating VEGFR2 conformational change following soluble versus immobilized ligation. The link between immobilized/soluble ligands, receptor trafficking, and site-specific receptor tyrosine phosphorylation could be due to: (a) control of site-specific phosphorylation of VEGFR2 by receptor trafficking (e.g. via localization of site-specific phosphatases); or (b) conformational changes in VEGFR2 in response to ligation by matrix-bound ligands that result in altered site-specific phosphorylation of VEGFR2 compared to soluble ligands, which in turn alters trafficking of the receptor; or a combination of these mechanisms. Because phosphorylation is a fast process compared to trafficking, in line with previous estimates for EGFR [64] (*See* kinetics in Tables 2 and 3), receptor location and site-specific phosphorylation are highly correlated. This makes distinguishing between mechanisms (a) and (b) difficult. There are experimental results to date that support both (a) [8,29,40,43] and (b) [46,57,70,71].

Our model simulation results show that mechanism (a) is sufficient to explain all current experimental phosphorylation and trafficking data after stimulation with $VEGF_{165a}$. This does not exclude (b), but suggests that it is not necessary. Alteration of the conformation of VEGFR2 in response to ligation with immobilized VEGF would be difficult to prove or disprove with current experimental techniques. However, the observation that immobilized VEGF effectively activates VEGFR2 whether it is coupled to different matrix molecules or even directly to a surface strongly suggests that the immobilized ligand is not specifically altered in conformation and that the receptor is not binding to an epitope that includes both the ligand and the matrix/surface. This reduces the likelihood of a 'matrix-specific' altered VEGFR2 conformation. An additional possibility is that immobilization of VEGF may interfere sterically with VEGFR2 coupling to regulatory molecules (e.g. integrins, VE-Cadherin and DEP-1), which may alter the phosphorylation pattern and/or trafficking of VEGFR2. Although internalization is known to be phosphorylation-dependent [57], complex control of trafficking by site-specific phosphorylation seems unlikely because it would require active sorting of VEGFR2 into vesicles by multi-tyrosine site phosphorylation pattern and specific internalization mechanics for each phospho-form of the receptor. Mechanism (a), on the other hand, relies only on passive sorting because matrix-binding VEGF retains VEGFR2 at the surface.

We propose an experiment that could, with the aid of our computational model, distinguish between (a) and (b) for specific trafficking steps and tyrosine residues on VEGFR2. The subcellular distribution of wild type VEGFR2 and VEGFR2 tyrosine mutants (e.g. Y1214F) could be compared in a manner similar to that in the trafficking study [40]. Differences in the localization of wild type (WT) and mutant VEGFR2 would suggest that phosphorylation on the mutated residue is required for the trafficking step where a change is observed. Computational modeling could predict whether additional changes are occurring downstream of the primary observed trafficking change. It would be important to verify that these mutants have equivalent ligand-binding and NRP1-coupling behaviors as WT VEGFR2. This proposed experiment would help to determine in more detail which mechanisms control each step of trafficking and phosphorylation, and to further refine our model.

The role of NRP1 is a confounding factor; it has been shown that treatment with a tyrosine kinase inhibitor (TKI) reduces VEGFR2-NRP1 complex formation in the presence of $VEGF_{165}$ [72], which would

in turn affect trafficking (and possibly also phosphorylation directly). This could imply that phosphorylation of VEGFR2 is required for complex formation with NRP1, or that TKIs interfere with interactions between the cytoplasmic domains of VEGFR2 and NRP1. The NRP1 cytoplasmic domain is required for binding of synectin and myosin VI, which are required for movement into EEA1-positive early endosomes and Rab4-to-Rab11 transfer, and thus NRP1-mediated control of VEGFR2 trafficking [33]. It is also possible that NRP1-binding could affect the phosphorylation pattern of VEGFR2 directly, which could then induce the trafficking changes mediated by NRP1. This is supported by evidence that $VEGF_{165b}$, which does not bind Neuropilin-1, results in differential site-specific phosphorylation of VEGFR2 [68]. We suggest that additional experiments should be performed to clarify whether NRP1 directly alters phosphorylation of VEGFR2, and whether specific tyrosine residues are necessary for VEGFR2-NRP1 coupling.

5.4.3 Model insights for in vivo therapeutic applications

The majority of VEGF in normal tissues is sequestered in the ECM, so elucidating how immobilization alters site-specific phosphorylation of VEGFR2 is key to understanding VEGF behavior in tissues [12]. While the *in vitro* experimental studies examined here used equivalent concentrations of soluble and immobilized VEGF, the differences in concentrations and spatial availability of soluble and immobilized VEGF *in vivo* may result in a different balance of signaling in the body. $VEGF_{165}$ is the most highly expressed isoform in normal tissue (though a significant portion of this may be $VEGF_{165b}$ [65]), but $VEGF_{188/189}$, which binds even more strongly to ECM species, represents a significant portion of the local VEGF in the mouse lung, heart, and liver, and in certain human tumors [20,21]. The results of this study suggest that many of the differences in cell behavior and vascular morphology resulting from stimulation with different splice isoforms of VEGF may be direct effects of differences in interactions with Neuropilin-1 and the extracellular matrix (**Fig. 5-9**). $VEGF_{121}$ (**Fig. 5-9A**) does not bind to NRP1 and VEGFR2 simultaneously, or to the matrix (M), resulting in slower ligand-receptor binding and faster internalization. We predict $VEGF_{121}$-ligated VEGFR2 will localize to Rab4/5 endosomes, leading to increased Y1175 phosphorylation, ERK activation, and proliferation. The result would be a network of vessels with large diameters and little branching, as is seen in V_{121} isoform-specific mice [22,23] . $VEGF_{165}$ (**Fig. 5-9B**),

examined in this study, binds to both NRP1 and the matrix, resulting in fast VEGFR2 ligation and slower internalization compared to $VEGF_{121}$. $VEGF_{165}$ leads to a more even balance of surface and Rab4/5-located VEGF·VEGFR2, depending upon the strength of VEGF immobilization. This leads to a balance of pY1175 and pY1214, mixed ERK and p38 signaling, and a mix of cell proliferation and migration. $VEGF_{189}$ (**Fig. 5-9C**) binds strongly to the matrix and to NRP1. Competition between NRP1 and the matrix for VEGF slows VEGFR2 ligation and internalization. This increases pY1214 relative to pY1175, increasing p38 signaling and cell migration, and creating a highly branched vascular network, as is observed in $VEGF_{189}$-specific mice [21,22].

Figure 5-9. Differences in molecular interactions of VEGF isoforms are predicted to account for changes in observed vascular phenotype. A. $VEGF_{121}$ does not bind NPR1 or extracellular matrix proteins (M), leading to slow VEGFR2 ligation (due to lack of NRP1-mediated VEGF-VEGFR2 binding), fast internalization (no immobilization of $VEGF_{121}$), and a lack of recycling via the Rab11 pathway. **B.** $VEGF_{165}$ binds both NRP1 and extracellular matrix species, leading to faster VEGFR2 ligation, but slower internalization of VEGFR2 compared to stimulation with $VEGF_{121}$. The Rab11 recycling pathway is accessible to $VEGF_{165}$-NRP1-VEGFR2 complexes. **C.** $VEGF_{189}$ binds to extracellular matrix species and NRP1 more strongly than $VEGF_{165}$. This results in moderate VEGFR2 ligation speed (NRP1 must compete with matrix species (M) for VEGF) and slow VEGFR2 internalization.
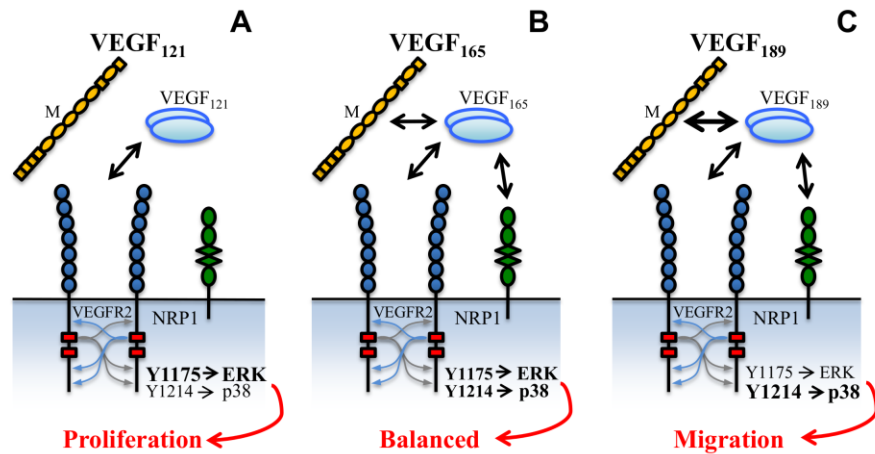
	$VEGF_{121}$	$VEGF_{165}$	$VEGF_{189}$
V·R2 Binding	Slow	Fast	Medium
Internalization	Fast	Medium	Slow
Rab11 Recycling	Low	High	High
V·R2 Location	Increased Rab4/5 V·R2	Surface and Rab4/5	Increased Surface V·R2
VEGFR2 Activation	pY1175	pY1175 and pY1214	pY1214
Downstream Signaling	ERK	ERK and p38	p38
Cell Behavior	Proliferation	Proliferation and Migration	Migration

VEGF has potential utility in tissue engineering applications, where vascularization is necessary for the viability of thick tissue constructs. The ability to spatially organize the impetus to endothelial cells to proliferate and migrate could be used to effectively induce hierarchical networks with diverse diameters and branching properties. Current platforms for VEGF immobilization include tunable heparin-functionalized gold surfaces [8] , collagen and PLGA hydrogels functionalized with VEGF [8,29,58], fibrin gels with active and passive growth factor release mechanisms, and presentation of VEGF with fibronectin fragments, VEGF binding peptides, and ECM proteins [11,59,73]. Cell lines, VEGF concentrations, quantities measured, time-points, and immobilization techniques vary across these studies. In aggregate, these experiments have demonstrated that immobilized VEGF promotes increased and extended phosphorylation of VEGFR2 [18,29,59,74], specifically on Y1214 [8,29,58], activation of p38 [29,58] and ERK [16,18,59,75], and increased migration and proliferation [16,18,59,74]. Results are less consistent regarding the impact of VEGF immobilization on phosphorylation of VEGFR2 on Y1175 [8,29,58] and activation of Akt [29,75]. These conflicting results, combined with the limited success in producing functional vascular networks to date, make it clear that a better understanding of how VEGF immobilization alters cellular response to VEGF is essential to design effective scaffolds for regenerative application requiring vascularization. In addition to reducing internalization, VEGF immobilization alters VEGFR2 cell surface interactions with co-receptors (NRP1, integrins, etc.). We begin to describe the impact of NRP1 on VEGFR2 trafficking, but more work remains to develop a quantitative understanding of VEGFR2-integrin interactions [77,78], and how these interactions are altered by immobilization of VEGF. In the future, we can also examine the impact of ephrin B2 [79], epsins [80], dynamin2 [81], synectin and myosin VI [82], and NRP1 presentation *in trans* [83] on VEGFR2 activation by simulating their effects on VEGFR2 trafficking and phosphorylation.

Tyrosine phosphatases represent a pool of potential therapeutic targets that are not yet well-understood [49]. Targeting phosphatases to selectively control dephosphorylation of specific VEGFR2 tyrosine residues is appealing for anti-angiogenic therapies, which are currently focused mostly on antagonists to VEGF or to the receptor tyrosine kinases, but also for the control of therapeutic vascularization. Our model accurately captures the impact of perturbations to TCPTP and VEPTP on site-specific VEGFR2 phosphorylation (**Fig. 5-4E-F**). While many other phosphatases are implicated in

164

regulation of VEGFR2 phosphorylation (**Table 5-S5**), these two examples support our model's structure of site- and location-specific dephosphorylation, and its ability to make therapeutically-relevant predictions.

Using this experimentally-validated model, we identified multiple key levers that can be manipulated to produce the desired multi-pathway signaling profile in endothelial and other cells. We identify VEGF presentation, trafficking, co-receptors (including NRP1), and regulatory molecules (such as phosphatases) as important levers that together control site-specific phosphorylation of VEGFR2 in a predictable way. While all of these facets are interconnected, we create a framework to study how perturbations to one or more of these levers alters VEGFR2 signaling. Future work is needed to tie changes in site-specific phosphorylation of Y951, Y1175, and Y1214 to activation of downstream signaling molecules. This work will continue to move us towards a more complete view of the VEGF system, improving our ability to design and predict the outcomes of novel vascular therapies.

5.5 References

1. Eming SA, Hubbell JA (2011) Extracellular matrix in angiogenesis: dynamic structures with translational potential. Experimental Dermatology 20: 605-613.

2. Lovett M, Lee K, Edwards A, Kaplan DL (2009) Vascularization Strategies for Tissue Engineering. Tissue Engineering Part B-Reviews 15: 353-370.

3. Auger FA, Gibot L, Lacroix D (2013) The Pivotal Role of Vascularization in Tissue Engineering. Annual Review of Biomedical Engineering, Vol 15 15: 177-200.

4. Mac Gabhann F, Qutub AA, Annex BH, Popel AS (2010) Systems biology of pro-angiogenic therapies targeting the VEGF system. Wiley Interdisciplinary Reviews-Systems Biology and Medicine 2: 694-707.

5. Galiano RD, Tepper OM, Pelo CR, Bhatt KA, Callaghan M, et al. (2004) Topical vascular endothelial growth factor accelerates diabetic wound healing through increased angiogenesis and by mobilizing and recruiting bone marrow-derived cells. American Journal of Pathology 164: 1935-1947.

6. Bao P, Kodra A, Tomic-Canic M, Golinko MS, Ehrlich HP, et al. (2009) The Role of Vascular Endothelial Growth Factor in Wound Healing. Journal of Surgical Research 153: 347-358.

7. Wilgus TA, Ferreira AM, Oberyszyn TM, Bergdall VK, DiPietro LA (2008) Regulation of scar formation by vascular endothelial growth factor. Laboratory Investigation 88: 579-590.

8. Anderson SM, Shergill B, Barry ZT, Manousiouthakis E, Chen TT, et al. (2011) VEGF internalization is not required for VEGFR-2 phosphorylation in bioengineered surfaces with covalently linked VEGF. Integrative Biology 3: 887-896.

9. Simons M (2012) An Inside View: VEGF Receptor Trafficking and Signaling. Physiology 27.

10. Berger P, Ballmer-Hofer K (2011) The reception and the party after how vascular endothelial growth factor receptor 2 explores cytoplasmic space. Swiss Medical Weekly 141.

11. Martino MM, Briquez PS, Güç E, Tortelli F, Kilarski WW, et al. (2014) Growth Factors Engineered for Super-Affinity to the Extracellular Matrix Enhance Tissue Healing. Science 343: 885-888.

12. Mac Gabhann F, Popel AS (2007) Interactions of VEGF isoforms with VEGFR-1, VEGFR-2, and neuropilin in vivo: a computational model of human skeletal muscle. American Journal of Physiology-Heart and Circulatory Physiology 292.

13. Kut C, Mac Gabhann F, Popel AS (2007) Where is VEGF in the body? A meta-analysis of VEGF distribution in cancer. British Journal of Cancer 97: 978-985.

14. Mac Gabhann F, Popel AS (2008) Systems biology of vascular endothelial growth factors. Microcirculation (New York, NY : 1994) 15: 715-738.

15. Yao C, Roderfeld M, Rath T, Roeb E, Bernhagen J, et al. (2006) The impact of proteinase-induced matrix degradation on the release of VEGF from heparinized collagen matrices. Biomaterials 27: 1608-1616.

16. Wijelath ES, Murray J, Rahman S, Patel Y, Ishida A, et al. (2002) Novel vascular endothelial growth factor binding domains of fibronectin enhance vascular endothelial growth factor biological activity. Circulation Research 91: 25-31.

17. Tabata Y, Miyao M, Ozeki M, Ikada Y (2000) Controlled release of vascular endothelial growth factor by use of collagen hydrogels. Journal of Biomaterials Science-Polymer Edition 11: 915-930.

18. Wijelath ES, Rahman S, Namekata M, Murray J, Nishimura T, et al. (2006) Heparin-II domain of fibronectin is a vascular endothelial growth factor-binding domain - Enhancement of VEGF biological activity by a singular growth factor/matrix protein synergism. Circulation Research 99: 853-860.

19. Wijelath E, Namekata M, Murray J, Furuyashiki M, Zhang S, et al. (2010) Multiple Mechanisms for Exogenous Heparin Modulation of Vascular Endothelial Growth Factor Activity. Journal of Cellular Biochemistry 111: 461-468.

20. Vempati P, Popel AS, Mac Gabhann F (2013) Extracellular regulation of VEGF: Isoforms, proteolysis, and vascular patterning. Cytokine & Growth Factor Reviews In Press.

21. Ng YS, Rohan R, Sunday ME, Demello DE, D'Amore PA (2001) Differential expression of VEGF isoforms in mouse during development and in the adult. Developmental Dynamics 220: 112-121.

22. Grunstein J, Masbad JJ, Hickey R, Giordano F, Johnson RS (2000) Isoforms of vascular endothelial growth factor act in a coordinate fashion to recruit and expand tumor vasculature. Molecular and Cellular Biology 20: 7282-7291.

23. Lee S, Jilani SM, Nikolova GV, Carpizo D, Iruela-Arispe ML (2005) Processing of VEGF-A by matrix metalloproteinases regulates bioavailability and vascular patterning in tumors. Journal of Cell Biology 169: 681-691.

24. Tan WH, Popel AS, Mac Gabhann F (2013) Computational model of VEGFR2 pathway to ERK activation and modulation through receptor trafficking. Cellular signalling 25: 2496-2510.

25. Wan Hua T, Popel AS, Mac Gabhann F (2013) Computational Model of Gab1/2-Dependent VEGFR2 Pathway to Akt Activation. Plos One 8.

26. Fujio Y, Walsh K (1999) Akt mediates cytoprotection of endothelial cells by vascular endothelial growth factor in an anchorage-dependent manner. Journal of Biological Chemistry 274: 16349-16354.

27. Sase H, Watabe T, Kawasaki K, Miyazono K, Miyazawa K (2009) VEGFR2-PLC gamma 1 axis is essential for endothelial specification of VEGFR2(+) vascular progenitor cells. Journal of Cell Science 122: 3303-3311.

28. Takahashi T, Yamaguchi S, Chida K, Shibuya M (2001) A single autophosphorylation site on KDR/Flk-1 is essential for VEGF-A-dependent activation of PLC-gamma and DNA synthesis in vascular endothelial cells. Embo Journal 20: 2768-2778.

29. Chen TT, Luque A, Lee S, Anderson SM, Segura T, et al. (2010) Anchorage of VEGF to the extracellular matrix conveys differential signaling responses to endothelial cells. Journal of Cell Biology 188: 595-609.

30. Lamalice L, Houle F, Huot J (2006) Phosphorylation of Tyr(1214) within VEGFR-2 triggers the recruitment of Nck and activation of Fyn leading to SAPK2/p38 activation and endothelial cell migration in response to VEGF. Journal of Biological Chemistry 281: 34009-34020.

31. Koch S (2012) Neuropilin signalling in angiogenesis. Biochemical Society Transactions 40: 20-25.

32. Mac Gabhann F, Popel AS (2005) Differential binding of VEGF isoforms to VEGF receptor 2 in the presence of neuropilin-1: a computational model. American Journal of Physiology-Heart and Circulatory Physiology 288: H2851-H2860.

33. Lanahan A, Zhang X, Fantin A, Zhuang Z, Rivera-Molina F, et al. (2013) The Neuropilin 1 Cytoplasmic Domain Is Required for VEGF-A-Dependent Arteriogenesis. Developmental Cell 25: 156-168.

34. Salikhova A, Wang L, Lanahan AA, Liu M, Simons M, et al. (2008) Vascular endothelial growth factor and semaphorin induce neuropilin-1 endocytosis via separate pathways. Circulation Research 103: E71-E79.

35. Herzog B, Pellet-Many C, Britton G, Hartzoulakis B, Zachary IC (2011) VEGF binding to NRP1 is essential for VEGF stimulation of endothelial cell migration, complex formation between NRP1 and VEGFR2, and signaling via FAK Tyr407 phosphorylation. Molecular Biology of the Cell 22: 2766-2776.

36. Shraga-Heled N, Kessler O, Prahst C, Kroll J, Augustin H, et al. (2007) Neuropilin-1 and neuropilin-2 enhance VEGF(121) stimulated signal transduction by the VEGFR-2 receptor. Faseb Journal 21: 915-926.

37. Bruns AF, Herbert SP, Odell AF, Jopling HM, Hooper NM, et al. (2010) Ligand-Stimulated VEGFR2 Signaling is Regulated by Co-Ordinated Trafficking and Proteolysis. Traffic 11: 161-174.

38. Wang Y, Pennock S, Chen XM, Wang ZX (2002) Endosomal signaling of epidermal growth factor receptor stimulates signal transduction pathways leading to cell survival. Molecular and Cellular Biology 22: 7279-7290.

39. Wang Y, Pennock SD, Chen XM, Kazlauskas A, Wang ZX (2004) Platelet-derived growth factor receptor-mediated signal transduction from endosomes. Journal of Biological Chemistry 279: 8038-8046.

40. Ballmer-Hofer K, Andersson AE, Ratcliffe LE, Berger P (2011) Neuropilin-1 promotes VEGFR-2 trafficking through Rab11 vesicles thereby specifying signal output. Blood 118.

41. Gampel A, Moss L, Jones MC, Brunton V, Norman JC, et al. (2006) VEGF regulates the mobilization of VEGFR2/KDR from an intracellular endothelial storage compartment. Blood 108: 2624-2631.

42. Jopling HM, Howell GJ, Gamper N, Ponnambalam S (2011) The VEGFR2 receptor tyrosine kinase undergoes constitutive endosome-to-plasma membrane recycling. Biochemical and Biophysical Research Communications 410: 170-176.

43. Jopling HM, Odell AF, Hooper NM, Zachary IC, Walker JH, et al. (2009) Rab GTPase Regulation of VEGFR2 Trafficking and Signaling in Endothelial Cells. Arteriosclerosis Thrombosis and Vascular Biology 29: 1119-U1206.

44. Sadowski L, Pilecka I, Miaczynska M (2009) Signaling from endosomes: Location makes a difference. Experimental Cell Research 315.

45. Nakayama M, Berger P (2013) Coordination of VEGF receptor trafficking and signaling by coreceptors. Experimental Cell Research 319: 1340-1347.

46. Lampugnani MG, Orsenigo F, Gagliani MC, Tacchetti C, Dejana E (2006) Vascular endothelial cadherin controls VEGFR-2 internalization and signaling from intracellular compartments. Journal of Cell Biology 174: 593-604.

47. Goh LK, Sorkin A (2013) Endocytosis of Receptor Tyrosine Kinases. Cold Spring Harbor Perspectives in Biology 5: 17.

48. Dobrowolski R, De Robertis EM (2012) Endocytic control of growth factor signalling: multivesicular bodies as signalling organelles. Nature Reviews Molecular Cell Biology 13.

49. Kappert K, Peters KG, Bohmer FD, Ostman A (2005) Tyrosine phosphatases in vessel wall signaling. Cardiovascular Research 65.

50. Hendriks BS, Opresko LK, Wiley HS, Lauffenburger D (2003) Coregulation of epidermal growth factor receptor/human epidermal growth factor receptor 2 (HER2) levels and locations: Quantitative analysis of HER2 overexpression effects. Cancer Research 63: 1130-1137.

51. Resat H, Ewald JA, Dixon DA, Wiley HS (2003) An integrated model of epidermal growth factor receptor trafficking and signal transduction. Biophysical Journal 85: 730-743.

52. Hendriks BS, Opresko LK, Wiley HS, Lauffenburger D (2003) Quantitative analysis of HER2-mediated effects on HER2 and epidermal growth factor receptor endocytosis - Distribution of homo- and heterodimers depends on relative HER2 levels. Journal of Biological Chemistry 278: 23343-23351.

53. Vempati P, Popel AS, Mac Gabhann F (2011) Formation of VEGF isoform-specific spatial distributions governing angiogenesis: computational analysis. Bmc Systems Biology 5.

54. Forsten-Williams K, Kurtagic E, Nugent MA (2011) Complex receptor-ligand dynamics control the response of the VEGF system to protease injury. Bmc Systems Biology 5.

55. Vempati P, Mac Gabhann F, Popel AS (2010) Quantifying the Proteolytic Release of Extracellular Matrix-Sequestered VEGF with a Computational Model. Plos One 5.

56. Mac Gabhann F, Popel AS (2007) Dimerization of VEGF receptors and implications for signal transduction: A computational study. Biophysical Chemistry 128: 125-139.

57. Dougher M, Terman BI (1999) Autophosphorylation of KDR in the kinase domain is required for maximal VEGF-stimulated kinase activity and receptor internalization. Oncogene 18: 1619-1627.

58. Anderson SM, Siegman SN, Segura T (2011) The effect of vascular endothelial growth factor (VEGF) presentation within fibrin matrices on endothelial cell branching. Biomaterials 32: 7432-7443.

59. Martino MM, Tortelli F, Mochizuki M, Traub S, Ben-David D, et al. (2011) Engineering the Growth Factor Microenvironment with Fibronectin Domains to Promote Wound and Bone Tissue Healing. Science Translational Medicine 3.

60. Mattila E, Auvinen K, Salmi M, Ivaska J (2008) The protein tyrosine phosphatase TCPTP controls VEGFR2 signalling. Journal of Cell Science 121: 3570-3580.

61. Mellberg S, Dimberg A, Bahram F, Hayashi M, Rennel E, et al. (2009) Transcriptional profiling reveals a critical role for tyrosine phosphatase VE-PTP in regulation of VEGFR2 activity and endothelial cell morphogenesis. Faseb Journal 23.

62. Imoukhuede PI, Popel AS (2011) Quantification and cell-to-cell variation of vascular endothelial growth factor receptors. Experimental Cell Research 317: 955-965.

63. Zhao W, McCallum SA, Xiao Z, Zhang F, Linhardt RJ (2012) Binding affinities of vascular endothelial growth factor (VEGF) for heparin-derived oligosaccharides. Bioscience Reports 32: 71-81.

64. Kleiman LB, Maiwald T, Conzelmann H, Lauffenburger DA, Sorger PK (2011) Rapid Phospho-Turnover by Receptor Tyrosine Kinases Impacts Downstream Signaling and Drug Binding. Molecular Cell 43: 723-737.

65. Nowak DG, Woolard J, Amin EM, Konopatskaya O, Saleem MA, et al. (2008) Expression of pro- and anti-angiogenic isoforms of VEGF is differentially regulated by splicing and growth factors. Journal of Cell Science 121: 3487-3495.

66. Cebe-Suarez S, Gruenewald FS, Jaussi R, Li X, Claesson-Welsh L, et al. (2008) Orf virus VEGF-E NZ2 promotes paracellular NRP-1/VEGFR-2 coreceptor assembly via the peptide RPPR. Faseb Journal 22: 3078-3086.

67. Wiley HS (1988) Anomalous binding of the epidermal growth factor to A431 cells is due to the effect of high receptor densities and a saturable endocytic system. Journal of Cell Biology 107: 801-810.

68. Kawamura H, Li X, Harper SJ, Bates DO, Claesson-Welsh L (2008) Vascular endothelial growth factor (VEGF)-A165b is a weak in vitro agonist for VEGF receptor-2 due to lack of coreceptor binding and deficient regulation of kinase activity. Cancer Research 68: 4683-4692.

69. Kawamura H, Li X, Goishi K, van Meeteren LA, Jakobsson L, et al. (2008) Neuropilin-1 in regulation of VEGF-induced activation of p38MAPK and endothelial cell organization. Blood 112: 3638-3649.

70. Rosa Santos SC, Miguel C, Domingues I, Calado A, Zhu Z, et al. (2007) VEGF and VEGFR-2 (KDR) internalization is required for endothelial recovery during wound healing. Experimental Cell Research 313: 1561-1574.

71. Ewan LC, Jopling HM, Jia H, Mittar S, Bagherzadeh A, et al. (2006) Intrinsic tyrosine kinase activity is required for vascular endothelial growth factor receptor 2 ubiquitination, sorting and degradation in endothelial cells. Traffic 7: 1270-1282.

72. Prahst C, Heroult M, Lanahan AA, Uziel N, Kessler O, et al. (2008) Neuropilin-1-VEGFR-2 complexing requires the PDZ-binding domain of neuropilin-1. Journal of Biological Chemistry 283: 25110-25114.

73. Ehrbar M, Zeisberger SM, Raeber GP, Hubbell JA, Schnell C, et al. (2008) The role of actively released fibrin-conjugated VEGF for VEGF receptor 2 gene activation and the enhancement of angiogenesis. Biomaterials 29: 1720-1729.

74. Martino MM, Hubbell JA (2010) The 12th-14th type III repeats of fibronectin function as a highly promiscuous growth factor-binding domain. Faseb Journal 24.

75. Porter AM, Klinge CM, Gobin AS (2011) Covalently grafted VEGF(165) in hydrogel models upregulates the cellular pathways associated with angiogenesis. American Journal of Physiology-Cell Physiology 301: C1086-C1092.

76. Gourlaouen M, Welti JC, Vasudev NS, Reynolds AR (2013) Essential Role for Endocytosis in the Growth Factor-stimulated Activation of ERK1/2 in Endothelial Cells. Journal of Biological Chemistry 288: 7467-7480.

77. Streuli CH, Akhtar N (2009) Signal co-operation between integrins and other receptor systems. Biochemical Journal 418: 491-506.

78. Serini G, Napione L, Arese M, Bussolino F (2008) Besides adhesion: new perspectives of integrin functions in angiogenesis. Cardiovascular Research 78: 213-222.

79. Sawamiphak S, Seidel S, Essmann CL, Wilkinson GA, Pitulescu ME, et al. (2010) Ephrin-B2 regulates VEGFR2 function in developmental and tumour angiogenesis. Nature 465.

80. Tessneer KL, Pasula S, Cai X, Dong Y, McManus J, et al. (2014) Genetic Reduction of Vascular Endothelial Growth Factor Receptor 2 Rescues Aberrant Angiogenesis Caused by Epsin Deficiency. Arteriosclerosis Thrombosis and Vascular Biology 34: 331-337.

81. Lee MY, Skoura A, Park EJ, Landskroner-Eiger S, Jozsef L, et al. (2014) Dynamin 2 regulation of integrin endocytosis, but not VEGF signaling, is crucial for developmental angiogenesis. Development 141: 1465-1472.

82. Lanahan AA, Hermans K, Claes F, Kerley-Hamilton JS, Zhuang ZW, et al. (2010) VEGF Receptor 2 Endocytic Trafficking Regulates Arterial Morphogenesis. Developmental Cell 18.

83. Koch S, van Meeteren LA, Morin E, Testini C, Westrom S, et al. (2014) NRP1 Presented in trans to the Endothelium Arrests VEGFR2 Endocytosis, Preventing Angiogenic Signaling and Tumor Initiation. Developmental Cell 28: 633-646.

84. Mac Gabhann F, Popel AS (2006) Targeting neuropilin-1 to inhibit VEGF signaling in cancer: Comparison of therapeutic approaches. Plos Computational Biology 2.

85. Stefanini MO, Wu FT, Mac Gabhann F, Popel AS (2008) A compartment model of VEGF distribution in blood, healthy and diseased tissues. Bmc Systems Biology 2.

86. Whitaker GB, Limberg BJ, Rosenbaum JS (2001) Vascular endothelial growth factor receptor-2 and neuropilin-1 form a receptor complex that is responsible for the differential signaling potency of VEGF(165) and VEGF(121). Journal of Biological Chemistry 276: 25520-25531.

5.6 Supplemental Figures

Figure 5-S1. Free and ligated VEGFR2 are not uniformly distributed between cell compartments.
These panels expand on the results shown in Figure 5-2. Plots show the distribution of VEGF- bound VEGFR2 (V·R2, top row) and unbound VEGFR2 (Free R2, bottom row) on the cell surface (A,D), in Rab4/5 endosomes (B,E), and in Rab11 endosomes (C,F). In each case, the Y axis depicts the percentage of the VEGFR2 distributed to each compartment relative to the total VEGFR2 present at steady state (100%). After VEGF stimulation, percentages add up to less than 100, as a portion of the VEGFR2 has been degraded. Note that while peak levels of VEGFR2 ligation increase monotonically with VEGF concentration (solid line, [V] = 2 ng/mL; dashed line, [V] = 20 ng/mL; dotted line, [V] = 200 ng/mL), the temporal response is delayed at lower concentrations. Soluble VEGF (Vs), blue lines; bound VEGF (Vb), green lines.
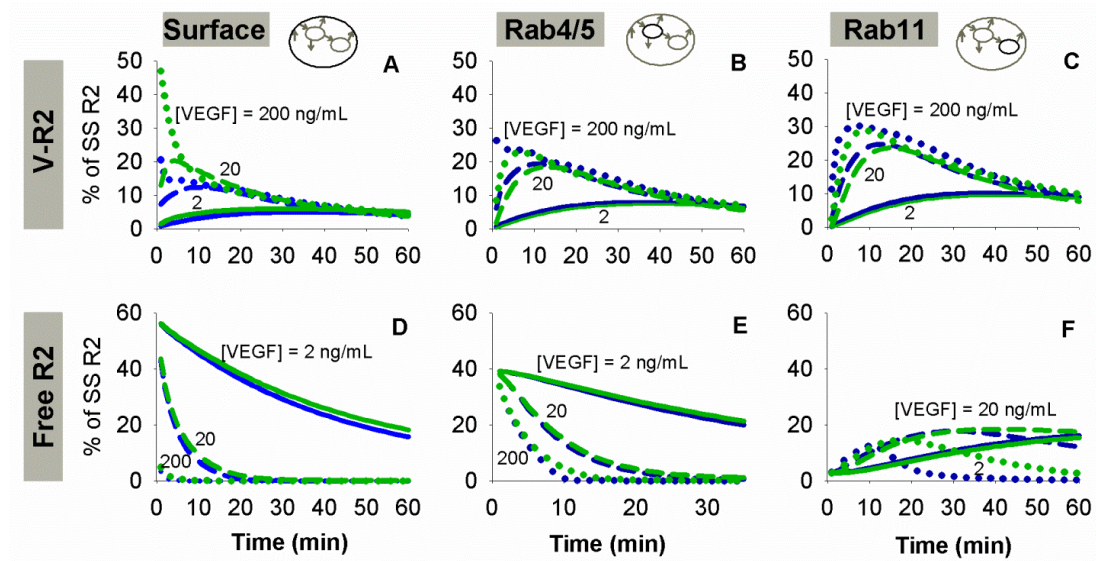
Figure 5-S2. Distribution of Phosphorylation Parameters. These panels expand on the results shown in Figure 5-3. **A.** Dephosphorylation parameters fit to experimental data. 47 sets of parameters were accepted as achieving good fit. Red dots indicate a representative coherent set of parameters used throughout the rest of this study. *See* Methods. **B.** Ratios of surface-to-internal dephosphorylation rates (panel A) for Y951, Y1175, and Y1214. The ratio of these ratios for Y1175 and Y1214 is also shown. The surface-to-internal dephosphorylation ratio is consistently higher for Y1175 than for Y1214.
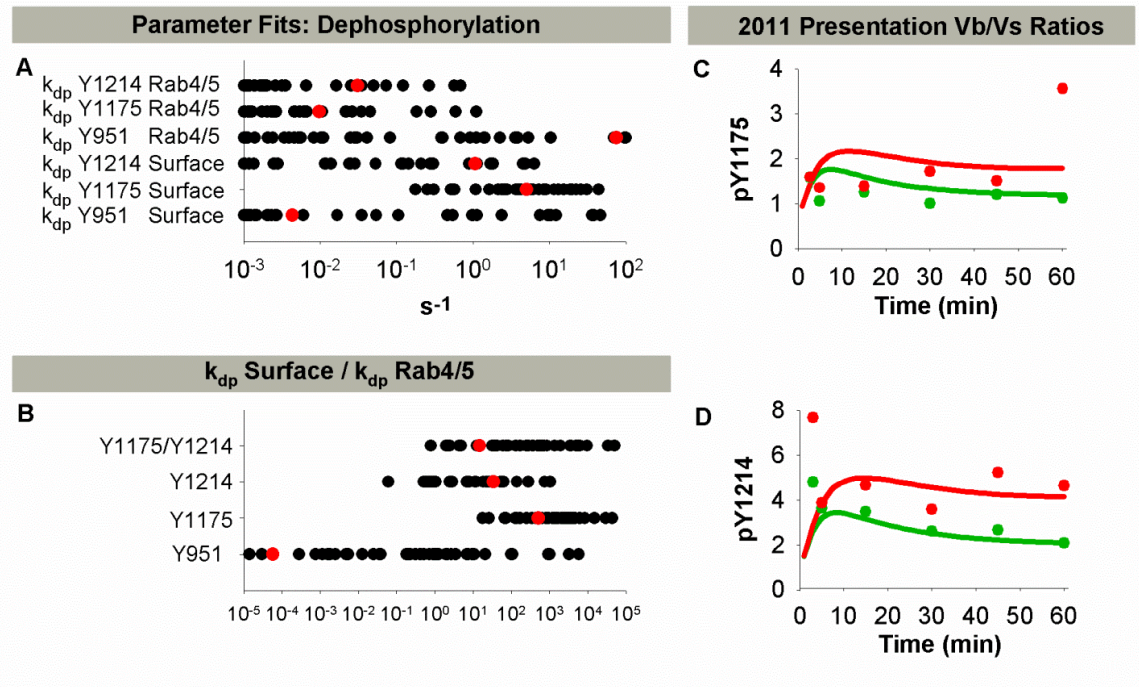
Figure 5-S3. Altered trafficking of VEGFR2 regulates site-specific phosphorylation of VEGFR2.
These panels expand on the results show in Figure 5-5. Distribution of VEGFR2 phosphorylated on at least one of Y951, Y1175, and Y1214 (pR2, left), pY1175 (middle), or pY1214 (right) in total (top row), on the cell surface only (2nd row), in Rab4/5 endosomes (3rd row), and in Rab11 endosomes (4th row) in HUVECs. Inset figures are included where the larger scale prevents clear distinction between lines. Time-scale ends at 30 minutes, but pR2 curves are relatively flat after this time. Soluble VEGF (Vs), blue line; bound VEGF (Vb), green line. Solid line, [V] = 2 ng/mL; dashed line, [V] = 20 ng/mL; dotted line, [V] = 200 ng/mL.
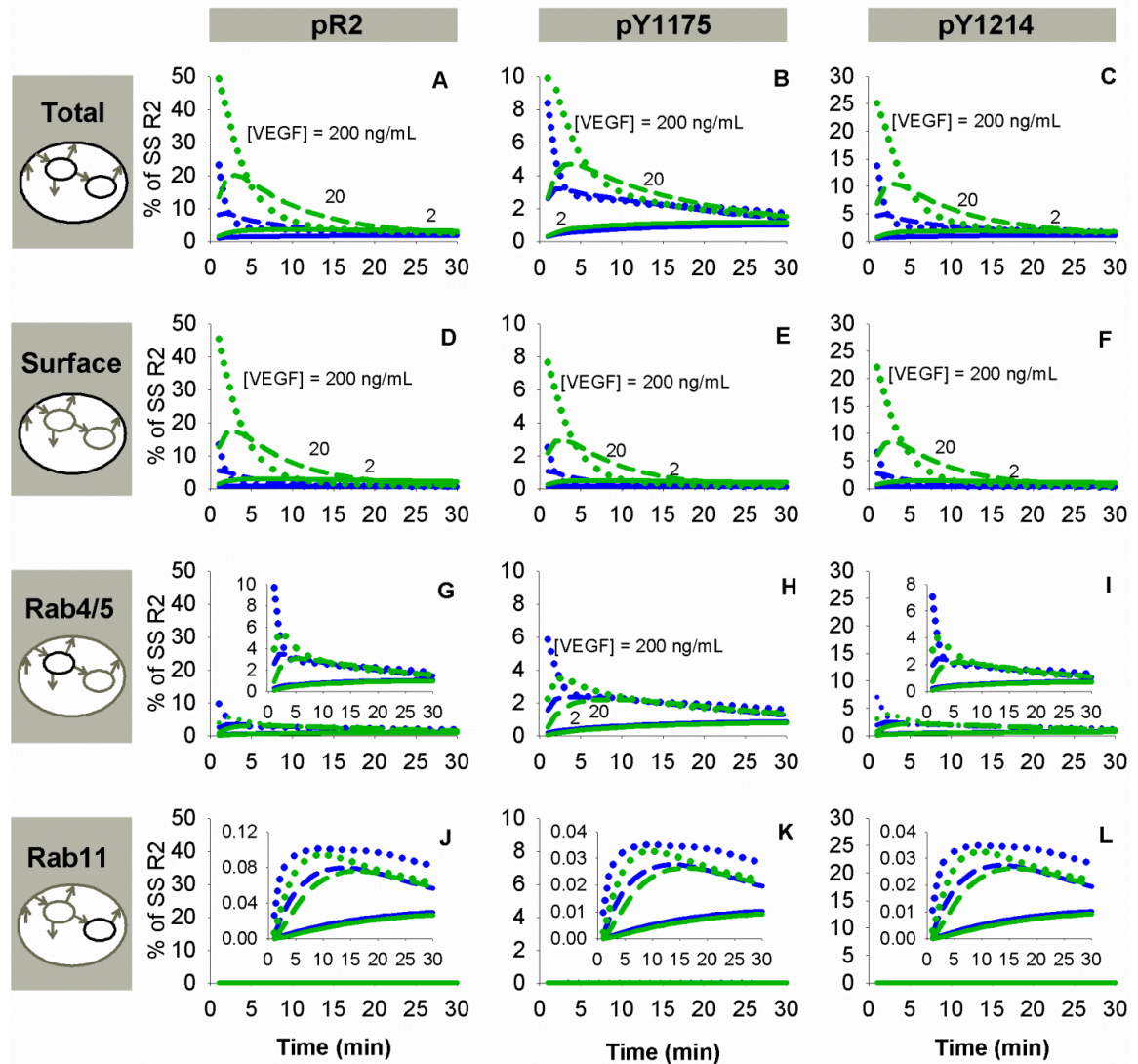
Figure 5-S4. Independent receptor dephosphorylation rates in multiple internal compartments result in decreased pY1175-VEGFR2. These panels expand on the results shown in Figure 5-5. Impact on total phosphorylated VEGFR2 (pR2, A), pY1175-VEGFR2 (B), and pY1214-VEGFR2 (C) if k_{dp} in Rab11 endosomes is the same as in Rab4/5 endosomes. Solid Lines: Baseline case with dephosphorylation rates in each compartment as specified in Table 3 of the main manuscript; dotted lines: dephosphorylation rates in Rab11 endosomes set to the same values as for Rab4/5 endosomes. Soluble VEGF (Vs), blue lines; bound VEGF (Vb), green lines. For all lines, [V] = 20 ng/mL, HUVEC receptor numbers.
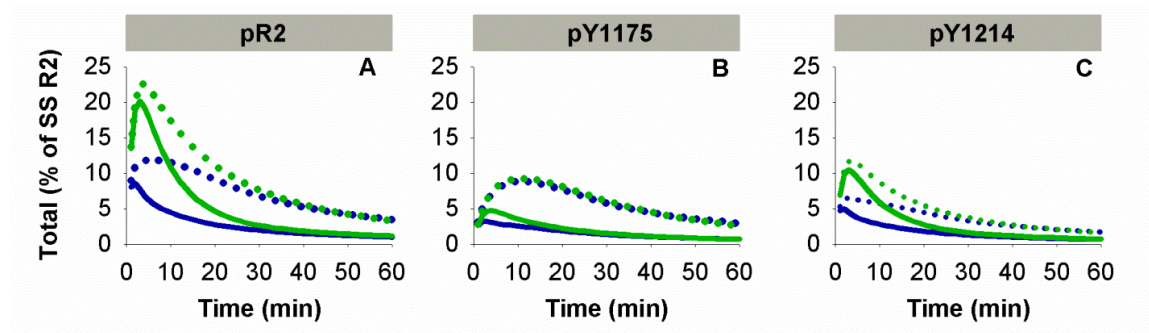
Figure 5-S5. Only a fraction of ligated VEGFR2 is phosphorylated. These panels expand on the results shown in Figure 5-5. Percentage of ligated VEGFR2 is that is phosphorylated on at least one tyrosine residue for soluble VEGF (Vs, A) and matrix-bound VEGF (Vb, B). Quantities are broken down into cell surface, Rab4/5 endosome, and Rab11 endosome components. Quantities of phosphorylated VEGFR2 are negligible in Rab11 endosomes. For all lines, [V] = 20 ng/mL, HUVEC receptor numbers.
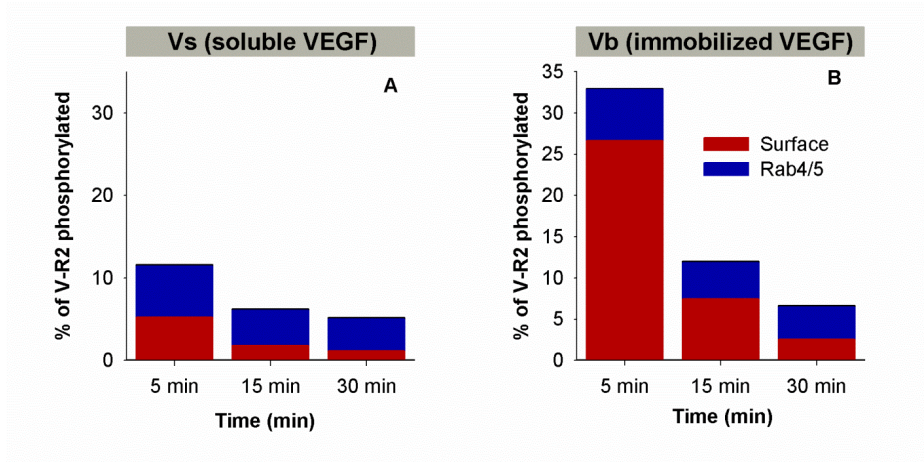
Figure 5-S6. Trends in ligated and phosphorylated VEGFR2 are consistent across VEGF concentrations. These panels expand on the results show in Figure 5-6. All panels show area under the curve (AUC), for the first 60 minutes after stimulation with soluble (Vs- blue) or immobilized (Vb- green) VEGF at concentrations of 2, 20, and 200 ng/mL. AUCs are shown for cell surface quantities (A-F), Rab4/5 quantities (G-L), and total quantities (M-R). AUCs are shown for total VEGFR2 (1st column), ligated VEGFR2 (2nd column), VEGFR2 phosphorylation on any considered tyrosine residue (pR2, 3rd column), pY1175 (4th column), and pY1214 (5th column). The last column shows the AUC for the curve pY1214/pY1175 (not the ratio AUC for pY1175 / AUC for pY1214) for surface VEGFR2 (F), Rab4/5 VEGFR2 (L), and total VEGFR2 (R).
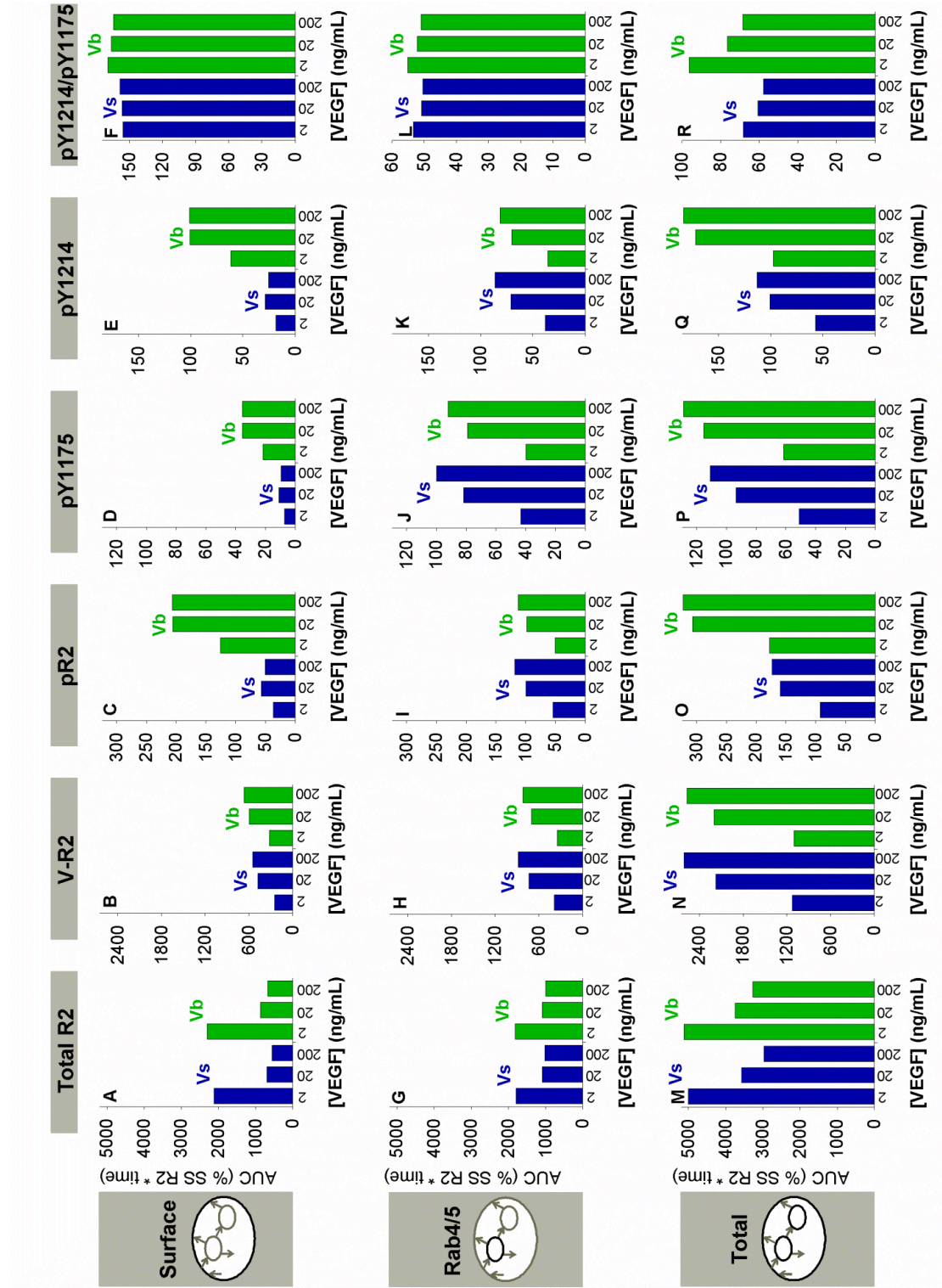
Figure 5-S6

Figure 5-S7. Loss of NRP1 increases levels of free VEGFR2 on the cell surface and in Rab4/5 endosomes. These panels expand on the results shown in Figure 5-7. Distribution of unligated VEGFR2. Solid lines: Baseline case with NRP1 present; dotted lines: no NRP1 present. Soluble VEGF (Vs), blue lines; bound VEGF (Vb), green lines. For all lines, [V] = 20 ng/mL, HUVEC receptor numbers.
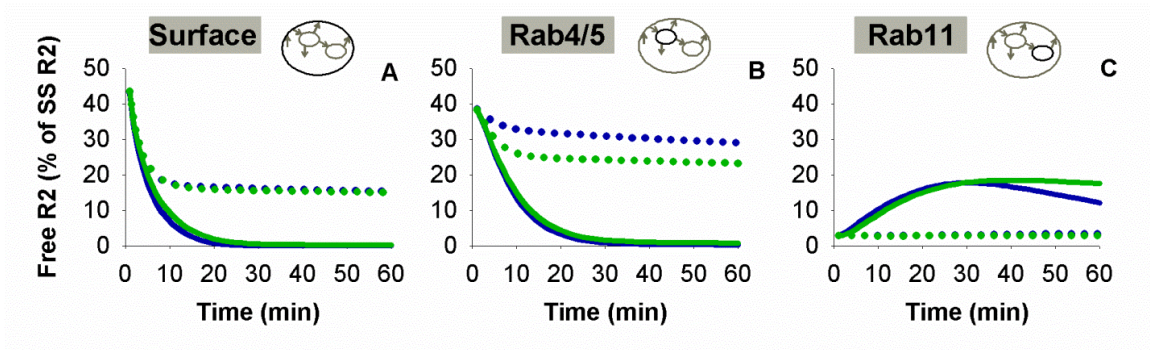
Figure 5-S8. The majority of ligated VEGFR2 is complexed with NRP1. These panels expand on the results shown in Figure 5-7. Percentages of VEGFR2 that are ligated and immobilized (M·V·R2, green), bound to NRP1 (V·N1·R2, blue), or bound to neither M nor NRP1 (V·R2, red), upon stimulation with soluble VEGF (Vs, left) or immobilized VEGF (Vb, right) at 5 minutes (top) and 15 minutes (bottom). Values shown are percentages of the total steady-state VEGFR2 population in the specified compartment and at the given times. Note that even upon stimulation with matrix-bound VEGF, essentially all internal ligated VEGFR2 is complexed with NRP1, due to the excess of NRP1. [V] = 20 ng/mL, HUVEC receptor numbers.
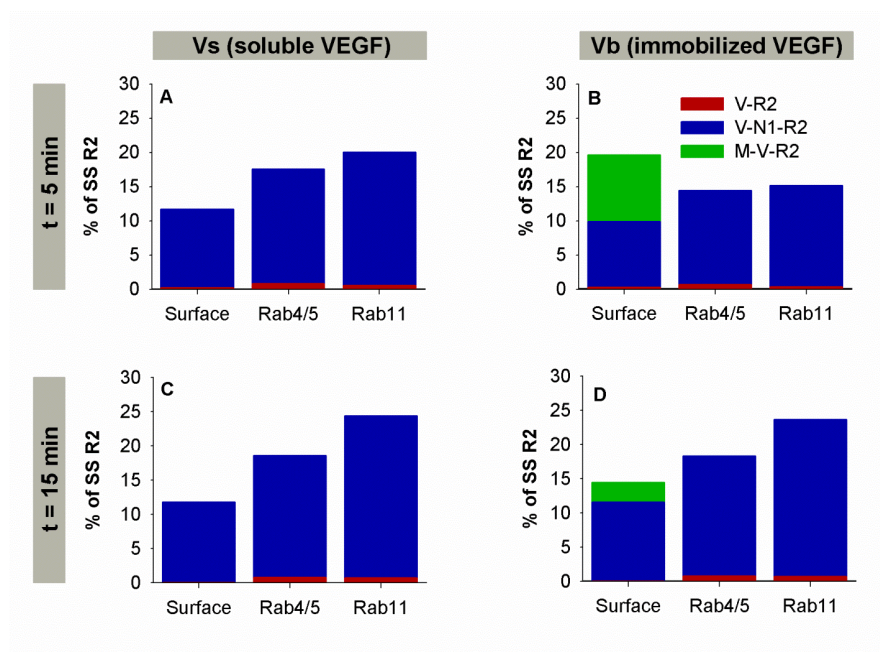
Figure 5-S9. Sensitivity of model outputs varies with VEGF concentration. Sensitivity of outputs to small changes in parameters and initial conditions. Values are average fold change in selected outputs for a 1-fold change in the specified parameter. **A.** [V] = 2 ng/mL. Scale: Black = 0, Bright red (maximum) = 0.77 **B.** [V] = 200 ng/mL. Scale: Black = 0, Bright red = 1.03 (maximum).
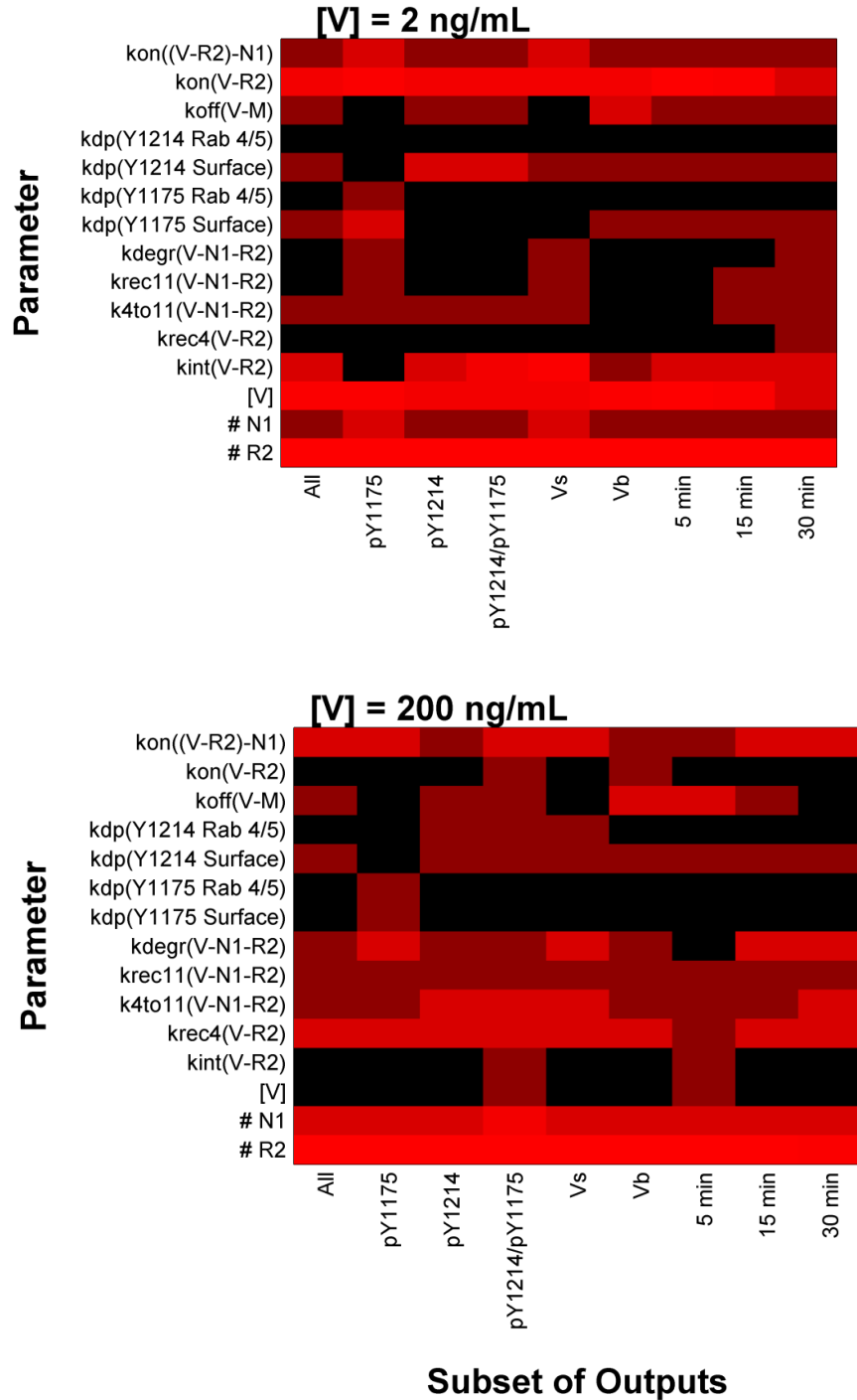
5.7 Supplemental Tables

Table 5-S1. Molecules included in the model and simulations.

Species	Description	Units
[V]	Free VEGF in extracellular compartment	M
[M]	ECM or VEGF-binding sites in extracellular compartment	M
[V·M]	Immobilized VEGF (bound to the ECM or surface)	M
[R2]	Free VEGFR2 on the cell surface	mol/cm^2
[V·R2]	Soluble VEGF bound to VEGFR2 on the cell surface	mol/cm^2
[M·V·R2]	Matrix-bound VEGF bound to VEGFR2 on the cell surface	mol/cm^2
[N1]	Free NRP1 on the cell surface	mol/cm^2
[V·N1]	NRP1-bound VEGF on the cell surface	mol/cm^2
[V·N1·R2]	VEGF-NRP1-VEGFR2 complex on the cell surface	mol/cm^2
[V$_{rab45}$]	Free VEGF in Rab 4/5 endosomes	mol/cm^2
[R2$_{rab45}$]	VEGFR2 in Rab 4/5 endosomes	mol/cm^2
[V·R2$_{rab45}$]	V·R2 complex in Rab 4/5 endosomes	mol/cm^2
[N1$_{rab45}$]	Free NRP1 in Rab 4/5 endosomes	mol/cm^2
[V·N1$_{rab45}$]	NRP1-bound VEGF in Rab 4/5 endosomes	mol/cm^2
[V·N1·R2$_{rab45}$]	VEGF-NRP1-VEGFR2 complex in Rab 4/5 endosomes	mol/cm^2
[V$_{rab11}$]	Free VEGF in Rab 11 endosomes	mol/cm^2
[R2$_{rab11}$]	VEGFR2 in Rab 11 endosomes	mol/cm^2
[V·R2$_{rab11}$]	V·R2 complex in Rab 11 endosomes	mol/cm^2
[N1$_{rab11}$]	NRP1 in Rab 11 endosomes	mol/cm^2
[V·N1$_{rab11}$]	NRP1-bound VEGF in Rab 11 endosomes	mol/cm^2
[V·N1·R2$_{rab11}$]	VEGF-NRP1-VEGFR2 complex in Rab 11 endosomes	mol/cm^2
[V$_{deg}$]	Degraded VEGF	mol/cm^2
[R2$_{deg}$]	Degraded VEGFR2	mol/cm^2
[V·R2$_{deg}$]	Degraded V·R2	mol/cm^2
[N1$_{deg}$]	Degraded free NRP1	mol/cm^2
[V·N1$_{deg}$]	Degraded NRP1-bound VEGF	mol/cm^2
[V·N1·R2$_{deg}$]	Degraded VEGF-NRP1-VEGFR2 complex	mol/cm^2

Note: For all reactions, units on surface and internal species are converted to M as needed. Surface species units are mol/cm^2 of well plate surface area (not cell surface area). Internal species are also in mol/cm^2 of well plate surface area.

Table 5-S2. Cell Geometry Parameters

Dimension	Value	Units	Reference
Cell Surface Area (top only)	1000	μm^2	Jaffe 1987 [1]
Cell Volume	1000	μm^3	Jaffe 1987 [1]
Total Rab 4/5 Surface Area per Cell	100	μm^2	Steinman 1976 [2] (assume ½ endosomal surface area)
Total Rab 4/5 Volume per Cell	2.5	μm^3	Griffiths 1989 [3] (assume ½ endosomal volume)
Total Rab 11 Surface Area per Cell	100	μm^2	Steinman 1976 [2] (assume ½ endosomal surface area)
Total Rab 11 Volume per Cell	2.5	μm^3	Griffiths 1989 [3] (assume ½ endosomal volume)

1. Jaffe EA (1987) Cell Biology of Endothelial Cells. Human Pathology 18.

2. Steinman RM, Brodie SE, Cohn ZA (1976) Membrane flow during pinocytosis- stereologic analysis. Journal of Cell Biology 68: 665-687.

3. Griffiths G, Back R, Marsh M (1989) A quantitative analysis of the endocytic pathway in baby hamster kidney cells. Journal of Cell Biology 109: 2703-2720.

Table 5-S3. Representative Fits to Experimental Trafficking Data

Species Measured	Location	Time (min)	Transfected Receptors	[VEGF] (ng/mL)	Simulation Value	Data Value	Weight
R2	Rab 4/5	-	R2	0	**93**	**81**	1
R2	Rab 11	-	R2	0	**6.6**	**2.7**	1
N1	Rab 4/5	-	N1	0	**37**	**48**	1
N1	Rab 11	-	N1	0	**51**	**46**	1
V·N1·R2	Rab 4/5	30	R2 + N1	50	**27**	**47**	1
V·N1·R2	Rab 11	30	R2 + N1	50	**37**	**45**	1
V·N1·R2	Rab 4/5	180	R2 + N1	50	**4.6**	**47**	1
V·N1·R2	Rab 11	180	R2 + N1	50	**6.2**	**46**	1
R2	Rab 4/5	30	R2	50	**91**	**79**	1
R2	Rab 11	30	R2	50	**3.7**	**4.5**	1
R2	Rab 4/5	180	R2	50	**66**	**78**	1
R2	Rab 11	180	R2	50	**4.8**	**2.6**	1
N1	Surface	30	R2 + N1	50	**22**	**21**	1
N1	Surface	180	R2 + N1	50	**7.1**	**90**	1
R2	Total	10	R2 + N1	50	**38**	**64**	3
R2	Total	30	R2 + N1	50	**32**	**44**	3
R2	Total	180	R2 + N1	50	**11**	**33**	3
N1	Total	10	R2 + N1	50	**91**	**74**	3
N1	Total	30	R2 + N1	50	**72**	**66**	3
N1	Total	180	R2 + N1	50	**18**	**45**	3
% R2 on Surface		-	R2 + N1	0	**58**	**60**	5

Note: Simulated values and experimental data in Rab4/5 and Rab11 endosomes are expressed as a percentage of the internalized molecule of interest in the indicated compartment. Rab7 data (not shown) is compared to the degraded compartment in the model. Rab7 was not used for parameter fitting, as percentages in the Rab7 compartment are fully specified if the percentages in Rab4/5 and Rab11 endosomes are known. Total values are given as a percentage of the value in unstimulated cells. Receptors included in the count can be free or bound to VEGF.

1. Ballmer-Hofer K, Andersson AE, Ratcliffe LE, Berger P (2011) Neuropilin-1 promotes VEGFR-2 trafficking through Rab11 vesicles thereby specifying signal output. Blood 118.

Table 5-S4. Summary of Distribution of Accepted Parameter Sets

Parameter	Mean (s^{-1})	Median (s^{-1})	σ (s^{-1})	CV
Trafficking				
k_{degr}(V·N1·R2)	9.26 x 10^{-4}	6.90 x 10^{-4}	9.06 x 10^{-4}	0.98
k_{degr}(V·R2)	2.72 x 10^{-5}	2.80 x 10^{-5}	7.58 x 10^{-6}	0.28
k_{degr}(N1)	1.55 x 10^{-4}	4.00 x 10^{-5}	1.92 x 10^{-4}	1.24
k_{rec4}(R2)	3.73 x 10^{-3}	3.70 x 10^{-3}	2.93 x 10^{-4}	0.08
k_{rec11}(N1)	1.19 x 10^{-2}	1.30 x 10^{-2}	2.60 x 10^{-3}	0.22
k_{4to11}(N1)	1.65 x 10^{-2}	1.60 x 10^{-2}	4.18 x 10^{-3}	0.25
Phosphorylation				
$k_{dp, Y951, surface}$	4.986	0.0027	11.9	2.39
$k_{dp, Y1175, surface}$	7.267	3.97	8.94	1.23
$k_{dp, Y1214, surface}$	0.580	0.0118	1.35	2.33
$k_{dp, Y951, rab45}$	9.523	0.0413	25.8	2.71
$k_{dp, Y1175, rab45}$	0.051	0.00172	0.184	3.61
$k_{dp, Y1214, rab45}$	0.041	0.00119	0.133	3.24
Surface/Internal Ratios: k_{dp}				
Y951	266	0.719	989	3.72
Y1175	3440	940	7750	2.25
Y1214	64.9	6.84	190	2.93
Y1175/Y1214	2760	252	8810	3.19

σ: Standard Deviation; CV: coefficient of variation.

Table 5-S5. Summary of Phosphatases Acting on VEGFR2

Name	Location(s)	Interactions	Residues Dephosphorylated	Residues Not Dephosphorylated	Refs.
TCPTP (PTPN2)	PM (focal adhesions), N, C	VEGFR2, α_1 integrins	Y996, Y1054, Y1059, Y1214	Y1175	[1]
VEPTP (PTPRB)	PM (cell junctions)	VEGFR2, Tie2, VE-Cadherin	Y951, Y1175	Y1214	[2,3]
DEP-1 (CD148, PTPRJ)	PM (cell junctions)	VEGFR2, VE-Cadherin	Y801, Y951, Y996, Y1054, Y1059, Y1175, Y1214		[4-6]
SHP-1 (PTPN6)	PM	VEGFR2, Src, eNOS	Y996, Y1059, Y1175	Y951	[7,8]
SHP-2 (PTPN11)	PM	VEGFR2, Tie2, collagen I, D2DR	Y951, Y996, Y1059	Y1175	[9-11]
PTP1B (PTPN1)	PM/EE, ER	VEGFR2, VE-cadherin	Y1175		[12-14]
PTP-MEG2 (PTPN9)	PM, C (peri-nuclear & vesicular)	VEGFR2	Y1175		[15]
HCPTPA	C	VEGFR2			[16]

PM: Plasma Membrane; N: Nucleus; C: Cytosol; EE: Early Endosomes; ER: endoplasmic reticulum

1. Mattila E, Auvinen K, Salmi M, Ivaska J (2008) The protein tyrosine phosphatase TCPTP controls VEGFR2 signalling. Journal of Cell Science 121: 3570-3580.

2. Mellberg S, Dimberg A, Bahram F, Hayashi M, Rennel E, et al. (2009) Transcriptional profiling reveals a critical role for tyrosine phosphatase VE-PTP in regulation of VEGFR2 activity and endothelial cell morphogenesis. Faseb Journal 23.

3. Hayashi M, Majumdar A, Li X, Adler J, Sun Z, et al. (2013) VE-PTP regulates VEGFR2 activity in stalk cells to establish endothelial cell polarity and lumen formation. Nature Communications 4.

4. Chabot C, Spring K, Gratton JP, Elchebly M, Royal I (2009) New Role for the Protein Tyrosine Phosphatase DEP-1 in Akt Activation and Endothelial Cell Survival. Molecular and Cellular Biology 29: 241-253.

5. Lampugnani MG, Zanetti A, Corada M, Takahashi T, Balconi G, et al. (2003) Contact inhibition of VEGF-induced proliferation requires vascular endothelial cadherin, beta-catenin, and the phosphatase DEP-1/CD148. Journal of Cell Biology 161.

6. Lampugnani MG, Orsenigo F, Gagliani MC, Tacchetti C, Dejana E (2006) Vascular endothelial cadherin controls VEGFR-2 internalization and signaling from intracellular compartments. Journal of Cell Biology 174: 593-604.

7. Bhattacharya R, Kwon J, Wang E, Mukherjee P, Mukhopadhyay D (2008) Src homology 2 (SH2) domain containing protein tyrosine phosphatase-1 (SHP-1) dephosphorylates VEGF Receptor-2 and attenuates endothelial DNA synthesis, but not migration*. Journal of molecular signaling 3: 8-8.

8. Cai J, Jiang WG, Ahmed A, Boulton M (2006) Vascular endothelial growth factor-induced endothelial cell proliferation is regulated by interaction between VEGFR-2, SH-PTP1 and eNOS. Microvascular Research 71.

9. Sinha S, Vohra PK, Bhattacharya R, Dutta S, Sinha S, et al. (2009) Dopamine regulates phosphorylation of VEGF receptor 2 by engaging Src-homology-2-domain-containing protein tyrosine phosphatase 2. Journal of Cell Science 122: 3385-3392.

10. Mitola S, Brenchio B, Piccinini M, Tertoolen L, Zammataro L, et al. (2006) Type I collagen limits VEGFR-2 signaling by a SHP2 protein-tyrosine phosphatase-dependent mechanism 1. Circulation Research 98: 45-54.

11. Huang LW, Turck CW, Rao P, Peters KG (1995) Grb2 and SH-PTP2- Potentially important endothelial signaling molecules downstream of the TEK/Tie2 receptor tyrosine kinase. Oncogene 11: 2097-2103.

12. Lanahan A, Zhang X, Fantin A, Zhuang Z, Rivera-Molina F, et al. (2013) The Neuropilin 1 Cytoplasmic Domain Is Required for VEGF-A-Dependent Arteriogenesis. Developmental Cell 25: 156-168.

13. Lanahan AA, Hermans K, Claes F, Kerley-Hamilton JS, Zhuang ZW, et al. (2010) VEGF Receptor 2 Endocytic Trafficking Regulates Arterial Morphogenesis. Developmental Cell 18.

14. Nakamura Y, Patrushev N, Inomata H, Mehta D, Urao N, et al. (2008) Role of protein tyrosine phosphatase 1B in vascular endothelial growth factor signaling and cell-cell adhesions in endothelial cells. Circulation Research 102.

15. Hao Q, Samten B, Ji H-L, Zhao ZJ, Tang H (2012) Tyrosine phosphatase PTP-MEG2 negatively regulates vascular endothelial growth factor receptor signaling and function in endothelial cells. American Journal of Physiology-Cell Physiology 303.

16. Huang LW, Sankar S, Lin C, Kontos CD, Schroff AD, et al. (1999) HCPTPA, a protein tyrosine phosphatase that regulates vascular endothelial growth factor receptor-mediated signal transduction and biological activity. Journal of Biological Chemistry 274: 38183-38188.

Chapter 6. VEGF Isoform Distribution and Signaling in Healthy Humans

6.0 Summary

The splice isoforms of vascular endothelial growth A (VEGF) each have different affinities for the extracellular matrix (ECM) and the coreceptor NRP1, which leads to distinct vascular phenotypes in model systems expressing only a single VEGF isoform. ECM-immobilized VEGF can bind to and activate VEGF receptor 2 (VEGFR2) directly, with a different pattern of site-specific phosphorylation than diffusible VEGF. To date, the way in which ECM binding alters the distribution of isoforms of VEGF and of the related placental growth factor (PlGF) in the body and resulting angiogenic signaling is not well-understood. Here, we extend our previous validated cell-level computational model of VEGFR2 ligation, intracellular trafficking, and site-specific phosphorylation, which captured differences in signaling by soluble and immobilized VEGF, to a multi-scale whole-body framework. This computational systems pharmacology model captures the ability of the ECM to regulate isoform-specific growth factor distribution distinctly for VEGF and PlGF, and to buffer free VEGF and PlGF levels in tissue. We show that binding of immobilized growth factor to VEGF receptors, both on endothelial cells and soluble VEGFR1, is likely important to signaling *in vivo*. Additionally, our model predicts that VEGF isoform-specific properties lead to distinct profiles of VEGFR1 and VEGFR2 binding and VEGFR2 site-specific phosphorylation *in vivo*, mediated by Neuropilin-1. These predicted signaling changes mirror those observed in murine systems expressing single VEGF isoforms. Simulations predict that, contrary to the 'ligand-shifting hypothesis,' VEGF and PlGF do not compete for receptor binding at physiological concentrations, though PlGF is

predicted to slightly increase VEGFR2 phosphorylation when over-expressed by 10-fold. These results are critical to design of appropriate therapeutic strategies to control VEGF availability and signaling in regenerative medicine applications.

Figure 6-G1. Graphical Abstract
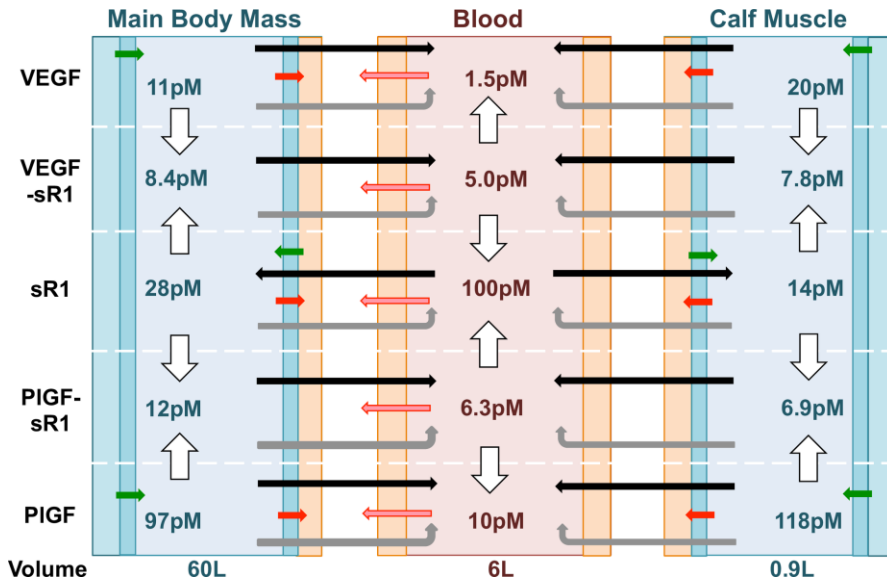
6.1 Introduction

Angiogenesis, the growth of new capillaries from the existing vasculature, is critical for maintenance of health and response to injury, as well as being a component of many diseases. However, regulation of angiogenesis is highly complex [1], and not fully understood. This complexity is a key reason for the lack of approved, effective therapies to promote angiogenesis for tissue engineering applications [2-4], for wound healing [5], or for ischemic diseases such as peripheral artery disease (PAD) [6], despite much research and multiple clinical trials [7]. Thus, a more complete, mechanistic understanding of the regulation of angiogenesis is crucial to designing more effective pro-angiogenic therapies.

Key to angiogenesis is the vascular endothelial growth factor (VEGF) family, including VEGF-A, VEGF-B, VEGF-C, VEGF-D, and placental growth factor (PlGF). VEGF-A (hereafter referred to as VEGF), considered the primary pro-angiogenesis VEGF ligand, has multiple splice isoforms, the most prevalent in humans being $VEGF_{121}$, $VEGF_{165}$, and $VEGF_{189}$. Constitutive dimers of these splice isoforms bind to VEGF-receptor 1 (VEGFR1) and VEGF-receptor 2 (VEGFR2). Upon ligand binding, VEGF receptors dimerize, transphosphorylate, and initiate downstream signaling [8-10].

The longer two prevalent human VEGF isoforms ($VEGF_{165}$ and $VEGF_{189}$) contain heparin-binding domains, allowing for binding to heparan sulfate proteoglycans (HSPGs) in the extracellular matrix (ECM). These isoforms also have binding sites for the coreceptor Neuropilin-1 (NRP1), which regulates VEGF affinity for VEGFR2 and influences VEGFR2 trafficking, though the less-common heparin-binding $VEGF_{145}$ does not bind to NRP1 [11, 12]. These isoform-specific properties have physiological significance; upon secretion into the extracellular space, $VEGF_{121}$, which does not bind to the ECM or to NRP1, forms shallow gradients and diffuses away from the source of production, while $VEGF_{189}$, which binds strongly to the ECM and also binds NRP1, forms steep interstitial gradients and remains close to the site of production [13].

In addition, mice and tumors expressing single VEGF isoforms have distinct phenotypes. Expression of only $VEGF_{121}$ leads to formation of high diameter vessels with low branching density, while expression of only $VEGF_{189}$ results in highly branched networks of very thin vessels. By contrast, expression of $VEGF_{165}$ alone results in a phenotypically normal vasculature, with balanced branching and diameters [14-17]. In addition to regulating VEGF distribution, it has recently been shown that the

immobilization of VEGF to ECM proteins or to a surface alters the site-specific phosphorylation profile of VEGFR2 *in vitro*. While phosphorylation of tyrosine Y1175, which leads to ERK1/2 activation and cell proliferation, is similar whether VEGF is immobilized or presented in solution, phosphorylation of Y1214, which leads to phosphorylation of p38 and cell migration, increases when VEGF is immobilized [18, 19]. This shift in signaling, which parallels the phenotypes seen with single VEGF isoform expression, can be explained by reduced internalization of VEGFR2 bound to immobilized VEGF, altering the exposure of VEGFR2 to specific phosphatases, as we recently demonstrated via a computational model of VEGFR2 signaling *in vitro* [20].

PlGF is not as well-studied as VEGF-A, in part because it is not required for normal murine development and homeostasis [21], and in part because PlGF binds only to VEGFR1, and not to VEGFR2, which is often considered to be the primary signaling receptor [22]. Like VEGF, PlGF has multiple splice isoforms, namely PlGF1 and PlGF2, with only the longer isoform (PlGF2) binding to ECM proteins strongly, and also to NRP1 [23, 24]. Despite being dispensable for murine development, PlGF expression is different in humans than mice [25], and increasing evidence implicates PlGF in disease [26]. Structural similarity also allows VEGF and PlGF to form heterodimers when produced in the same cells [27, 28]. There is high inter-study and intra-study variability in measurements of PlGF in human plasma and serum [29-41], many of which are from pregnant women, but levels of PlGF in healthy subjects are generally higher than those of VEGF-A (in 6 of 8 studies reviewed in [42] where both VEGF and PlGF in plasma or serum were measured [29-36]), and lower than those of soluble VEGFR1 (in 4 of 5 studies reviewed in [42] measuring both PlGF and sR1 in human plasma or serum [32, 34-37]).

VEGFR1 is also understudied compared to VEGFR2. VEGFR1 kinase activity appears to be weaker than that of VEGFR2, but VEGFR1 binds to VEGF more strongly than VEGFR2 [10]. While VEGFR1 kinase activity is not required for normal murine development [43], it appears to be important in the adult vasculature [44-46]. Like the VEGF ligands, VEGF receptors have alternative splice forms. Specifically, soluble VEGFR1 (sR1) is a naturally-occurring splice isoform lacking the transmembrane and intracellular domains but maintaining the ligand-, NRP1-, and HSPG-binding sites of VEGFR1. sR1 is secreted by endothelial cells into the extracellular space [47, 48]. There, sR1 can bind to the ECM [49] and/or bind to VEGF and PlGF, potentially preventing these growth factors from binding to cell surface

receptors. Additionally, sR1 may heterodimerize with cell surface receptor monomers, forming non-signaling complexes [50]. While VEGF binding to VEGFR1 is thought by some to be anti-angiogenic, PlGF-induced VEGFR1 activation is generally considered to be pro-angiogenic [2]; the tyrosine phosphorylation patterns on VEGFR1 induced by VEGF and PlGF are different [44], and PlGF-VEGFR1 signaling is pro-angiogenic in zebrafish [51]. It has been hypothesized, based on *in vitro* data and overexpression studies, that PlGF and VEGFB binding to VEGFR1 induces pro-angiogenic effects by occupying VEGFR1, shifting VEGF from VEGFR1 to VEGFR2 [44, 52-54].

Though the contributions of VEGF, PlGF, growth factor immobilization, sR1, NRP1, VEGFR1, and VEGFR2 to VEGF-mediated signaling have all been studied *in vitro* (and to a limited extent *in vivo*), the combined regulation of these cues in the context of the human body is not well-understood. Compared to *in vitro* studies, physiological ligand concentrations are very low, many different growth factors are constantly being produced, consumed, and transported throughout the body, and the time-scales of interest are far longer [55]. Computational models provide a key tool to study the combined effects of many forms of regulation within a single framework, and to scale between model systems and human patients.

6.1.1 Objectives

The primary objectives of this study were: (1) to predict the distribution of VEGF and PlGF within the body, (2) to understand the effect of VEGF and PlGF on the balance of VEGFR1 and VEGFR2 ligation and VEGFR2 phosphorylation, (3) to quantify the effect of matrix-bound VEGF & PlGF binding to endothelial and soluble receptors on VEGFR signaling, and (4) to study the impact of changes in VEGF & PlGF isoform expression on absolute and relative VEGFR1 & VEGFR2 activation and site-specific phosphorylation of VEGFR2, as a result of isoform-specific matrix- and NRP1-binding properties, all within the context of a healthy human body.

The computational systems pharmacology model developed in this study is based on previously-developed computational models of VEGF distribution and receptor binding *in vivo*. These models have included $VEGF_{165}$, $VEGF_{121}$, VEGFR1, VEGFR2, soluble VEGFR1 (sR1), NRP1, and sites in the interstitial matrix to which some growth factors and sR1 can bind [56-58]. The distribution of these proteins and their complexes has been examined in tissues of therapeutic interest (healthy or PAD calf [58],

197

or tumor [59, 60]), the blood, and non-diseased tissue (main body mass) [56, 57], in humans or mice [61, 62], incorporating transport between these compartments via vascular permeability and lymphatic drainage of tissues, and clearance of proteins from the plasma. By including multiple tissue compartments, we can compare quantities in a tissue of interest to those in the bulk of body tissue.

In the present study, we greatly expand upon previous models to further capture the complexity of VEGF distribution and VEGF receptor activation in the body. For the first time, we include two isoforms of placental growth factor (PlGF1 & PlGF2), and the VEGF isoform $VEGF_{189}$. Additionally, we account for binding of matrix-immobilized ligands in the endothelial basement membrane (EBM) to cell-surface receptors (VEGFR1 & VEGFR2), binding of immobilized ligands throughout the interstitial space to soluble sR1, and the ability of sR1, when sequestered in the interstitial matrix, to bind some VEGF isoforms. To capture these effects, we simulate receptor trafficking and VEGFR2 tyrosine site-specific phosphorylation following ligand binding or unbinding explicitly, implementing the reactions in a previously-developed *in vitro* computational model that captures differences in VEGFR2 phosphorylation following stimulation with soluble or matrix-bound $VEGF_{165}$ [20]. Finally, we leverage recent measurements to update endothelial cell surface receptor densities [63].

6.2 Methods

6.2.1 Compartmental Model Formulation

To capture the pharmacokinetics of VEGF, PlGF, and sR1 distribution in the human body, we divide the body into three compartments: a healthy calf muscle (gastrocnemius + soleus muscles), blood, and the main body mass (the rest of the tissues), approximated with the properties of skeletal muscle (**Fig 6-1A**). Transport between compartments occurs via bi-directional vascular permeability and lymphatic drainage of tissues (into the blood), while growth factors and sR1 are cleared from the blood (via the liver and kidneys), using rates previously determined (**Table 6-S10**). Each tissue compartment includes physiological proportions of interstitial space, extracellular matrix (ECM), endothelium, other parenchymal cells, and basement membranes for both the endothelium and parenchyma (endothelial- EBM, and parenchymal- PBM).

Figure 6-1: Schematics of molecular detail and structure of multi-scale computational model. (A) Whole-body compartmental model structure and mass flow. VEGF and PlGF are secreted from parenchymal cells, and sR1 is secreted by endothelial cells into the tissue interstitial space. Ligands and sR1 can then bind to EC receptors (leading to internalization and degradation), and can be transported between the tissue and blood via bi-directional vascular permeability or lymphatic draining of tissues into the circulation. Soluble species in the blood can be directly cleared from the blood. **(B)** Molecular interactions in tissue interstitial space between $VEGF_{121}$, $VEGF_{165}$, $VEGF_{189}$, PlGF1, PlGF2, NRP1, sR1, and extracellular HSPGs/GAGs (M). It is assumed that, similar to NRP1-VEGFR1 complexes, $VEGF_{121}$ and PlGF1 can bind to sR1-M. ECM-bound $VEGF_{165}$, $VEGF_{189}$, and PlGF2 can also bind to sR1. **(C)** Trafficking processes simulated in endothelial cells. **(D)** Site-specific phosphorylation and dephosphorylation of VEGFR2. **(E)** Abluminal (tissue-side) endothelial cell-surface molecular interactions between $VEGF_{121}$, $VEGF_{165}$, $VEGF_{189}$, PlGF1, PlGF2, VEGFR1, VEGFR2, NRP1, sR1, and extracellular HSPGs/GAGs in the endothelial basement membrane (EBM).

Figure 6-1
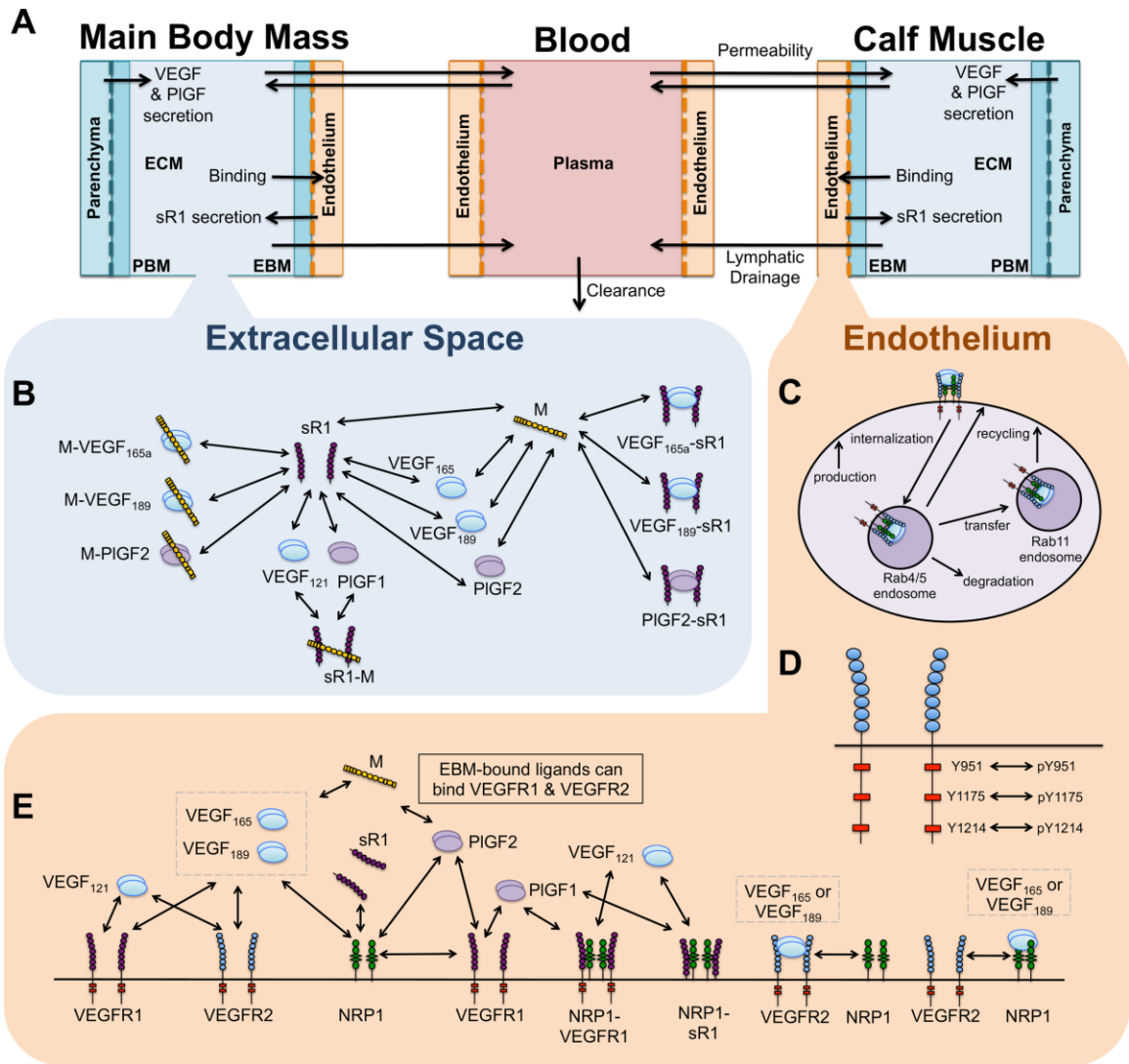
Within each tissue, we incorporate molecularly-detailed pharmacodynamics, including secretion into the interstitial space of VEGF and PlGF by parenchymal cells and sR1 by endothelial cells. In the interstitium, these diffusible proteins can then bind to heparan sulfate proteoglycans (HSPGs) in the ECM and basement membranes (see **Fig 6-1B, Table 6-S11**), bind to receptors on endothelial cells (ECs), or be removed from the compartment via physiological transport processes (**Fig 6-1A**). VEGF and PlGF isoforms have different affinities for matrix sites and for the coreceptor NRP1, which are included (**Table 6-1**), to account for isoform-specific ligand distribution and receptor activation. On the surface of and within endothelial cells, we simulate binding of sR1 to NRP1, binding of PlGF to VEGFR1 and/or NRP1, and binding of VEGF to VEGFR1, VEGFR2, and/or NRP1, based on the binding properties of each protein (summarized in **Tables 6-1, 6-2, & 6-3** and **Fig 6-1E**).

Table 6-1. Binding/Unbinding Reactions: K_D.

K_D	Description	VEGF$_{165}$	VEGF$_{121}$	VEGF$_{189}$	PlGF1	PlGF2	Units	Ref
L-R1	Ligand binding to VEGFR1	3.3 x 10⁻¹¹	3.3 x 10⁻¹¹	3.3 x 10⁻¹¹	2.3 x 10⁻¹⁰	2.3 x 10⁻¹⁰	M	[45, 57]
L-R2	Ligand binding to VEGFR2	1.0 x 10⁻¹⁰	1.0 x 10⁻¹⁰	1.0 x 10⁻¹⁰	-	-	M	[45, 57]
L-N1	Ligand binding to NRP1	1.2 x 10⁻⁹	-	1.2 x 10⁻¹⁰	-	1.0 x 10⁻⁷	M	[64, 65]
L-sR1	Ligand binding to sR1	3.3 x 10⁻¹¹	3.3 x 10⁻¹¹	3.3 x 10⁻¹¹	2.3 x 10⁻¹⁰	2.3 x 10⁻¹⁰	M	[57]
L-M	Ligand binding to M (ECM/BM)	6.1 x 10⁻⁸	-	6.1 x 10⁻⁹	-	4.6 x 10⁻⁹	M	[66]
(M-L)-R1	M-bound ligand binding to R1	3.3 x 10⁻¹¹	-	3.3 x 10⁻¹¹	-	2.3 x 10⁻¹⁰	M	
(M-L)-R2	M-bound ligand binding to R2	1.0 x 10⁻¹⁰	-	1.0 x 10⁻¹⁰	-	-	M	
(M-L)-sR1	M-bound ligand binding to sR1	3.3 x 10⁻¹¹	-	3.3 x 10⁻¹¹	-	2.3 x 10⁻¹⁰	M	
M-(L-R1)	M binding to ligand-R1 complex	6.1 x 10⁻⁸	-	6.1 x 10⁻⁹	-	4.6 x 10⁻⁹	M	
M-(L-R2)	M binding to ligand-R2 complex	6.1 x 10⁻⁸	-	6.1 x 10⁻⁹	-	-	M	
M-(L-sR1)	M binding to L in L-sR1 complex	6.1 x 10⁻⁸	-	6.1 x 10⁻⁹	-	4.6 x 10⁻⁹	M	
(L-sR1)-M	M binding to sR1 in L-sR1	-	2.4 x 10⁻⁸	-	2.4 x 10⁻⁸	-	M	
(M-sR1)-L	Ligand binding to sR1 in M-sR1	-	3.3 x 10⁻¹¹	-	2.3 x 10⁻¹¹	-	M	
(N1-L)-R2	VEGFR2 binding to ligand-NRP1	1.0 x 10⁻¹⁷	-	1.0 x 10⁻¹⁷	-	-	moles/cm²	
N1-(L-R2)	NRP1 binding to ligand-VEGFR2	3.2 x 10⁻¹⁷	-	3.2 x 10⁻¹⁷	-	-	moles/cm²	
(L-R1)-N1	NRP1 binding to ligand VEGFR1	-	1.0 x 10⁻¹⁶	-	1.0 x 10⁻¹⁶	-	moles/cm²	
(L-sR1)-N1	NRP1 binding to ligand-sR1	-	1.0 x 10⁻¹⁶	-	1.0 x 10⁻¹⁶	-	M	
(N1-R1)-L	Ligand binding to NRP1-R1	-	3.3 x 10⁻¹¹	-	2.3 x 10⁻¹⁰	-	M	
(N1-sR1)-L	Ligand binding to NRP1-sR1	-	3.3 x 10⁻¹¹	-	2.3 x 10⁻¹¹	-	M	

Other								
	NRP1-VEGFR1 coupling	N1-R1	1.0 x 10⁻¹⁶	moles/cm²				[57]
	NRP1-sR1 coupling	sR1-N1	1.8 x 10⁻⁹	M				[64, 65]
	M binding to sR1	sR1-M	2.4 x 10⁻⁸	M				

Notes:

1. L: ligand, column-specific

2. Ordering shows where the bond is. For example: in M-(L-sR1): M binding to L for $VEGF_{165}$, $VEGF_{189}$, & PlGF2. Whereas, in (L-sR1)-M, M binding to sR1 for $VEGF_{121}$, PlGF1.

3. All rates are the same inside endosomes as on cell surface. Unit conversions (see [20]) were required to convert all k_{on} (and thus K_D) into context-specific units, as in previous compartment models. K_D in moles/cm^2 = K_D in moles/L * (1 L/ 1000 cm^3) * (1/ESAV) where ESAV is the endothelial surface area to volume ratio, given in S7 Table.

Bold: new parameters (to compartment model)

Table 6-2. Binding/Unbinding Reactions: k_{on}

$\underline{k_{on}}$	VEGF$_{165}$	VEGF$_{121}$	VEGF$_{189}$	PlGF1	PlGF2	Units
L-R1	3.0×10^7	3.0×10^7	3.0×10^7	**1.5×10^6**	**1.5×10^6**	$M^{-1} s^{-1}$
L-R2	1.0×10^7	1.0×10^7	1.0×10^7	-	-	$M^{-1} s^{-1}$
L-N1	5.0×10^5	-	**1.4×10^6**	-	**1.0×10^4**	$M^{-1} s^{-1}$
L-sR1	3.0×10^7	3.0×10^7	3.0×10^7	**1.5×10^6**	**1.5×10^6**	$M^{-1} s^{-1}$
L-M	**1.6×10^5**	-	**1.6×10^5**	-	**2.2×10^5**	$M^{-1} s^{-1}$
(M-L)-R1	**3.0×10^7**	-	**3.0×10^7**	-	**1.5×10^6**	$M^{-1} s^{-1}$
(M-L)-R2	**1.0×10^7**	-	**1.0×10^7**	-	-	$M^{-1} s^{-1}$
(M-L)-sR1	**3.0×10^7**	-	**3.0×10^7**	-	**1.5×10^6**	$M^{-1} s^{-1}$
M-(L-R1)	**1.6×10^5**	-	**1.6×10^5**	-	**2.2×10^5**	$M^{-1} s^{-1}$
M-(L-R2)	**1.6×10^5**	-	**1.6×10^5**	-	-	$M^{-1} s^{-1}$
M-(L-sR1)	**1.6×10^5**	-	**1.6×10^5**	-	**2.2×10^5**	$M^{-1} s^{-1}$
(L-sR1)-M	-	**4.2×10^5**	-	**4.2×10^5**	-	$M^{-1} s^{-1}$
(M-sR1)-L	-	**3.0×10^7**	-	**1.5×10^6**	-	$M^{-1} s^{-1}$
(N1-L)-R2	1.0×10^{14}	-	1.0×10^{14}	-	-	$(moles/cm^2)^{-1} s^{-1}$
N1-(L-R2)	3.1×10^{13}	-	3.1×10^{13}	-	-	$(moles/cm^2)^{-1} s^{-1}$
(L-R1)-N1	-	1.0×10^{14}	-	**1.0×10^{14}**	-	$(moles/cm^2)^{-1} s^{-1}$
(L-sR1)-N1	-	1.0×10^{14}	-	**1.0×10^{14}**	-	$M^{-1} s^{-1}$
(N1-R1)-L	-	3.0×10^7	-	**1.5×10^6**	-	$M^{-1} s^{-1}$
(N1-sR1)-L	-	3.0×10^7	-	**1.5×10^6**	-	$M^{-1} s^{-1}$
Other	N1-R1	1.0×10^{14}	$(moles/cm^2)^{-1} s^{-1}$			
	sR1-N1	5.6×10^6	$M^{-1} s^{-1}$			
	sR1-M	4.2×10^5	$M^{-1} s^{-1}$			

Bold: new parameters (to compartment model)

Table 6-3. Binding/Unbinding Reactions: k_{off}

$\underline{k_{off}}$	$VEGF_{165}$	$VEGF_{121}$	$VEGF_{189}$	PlGF1	PlGF2	Units
L-R1	1.0×10^{-3}	1.0×10^{-3}	1.0×10^{-3}	**3.5×10^{-4}**	**3.5×10^{-4}**	s^{-1}
L-R2	1.0×10^{-3}	1.0×10^{-3}	1.0×10^{-3}	-	-	s^{-1}
L-N1	6.0×10^{-4}	-	**1.7×10^{-4}**	-	**1.0×10^{-3}**	s^{-1}
L-sR1	1.0×10^{-3}	1.0×10^{-3}	1.0×10^{-3}	3.5×10^{-4}	3.5×10^{-4}	s^{-1}
L-M	**1.0×10^{-2}**	-	**1.0×10^{-3}**	-	**1.0×10^{-3}**	s^{-1}
(M-L)-R1	**1.0×10^{-3}**	-	**1.0×10^{-3}**	-	**3.5×10^{-4}**	s^{-1}
(M-L)-R2	**1.0×10^{-3}**	-	**1.0×10^{-3}**	-	-	s^{-1}
(M-L)-sR1	**1.0×10^{-3}**	-	**1.0×10^{-3}**	-	**3.5×10^{-4}**	s^{-1}
M-(L-R1)	**1.0×10^{-2}**	-	**1.0×10^{-3}**	-	**1.0×10^{-3}**	s^{-1}
M-(L-R2)	**1.0×10^{-2}**	-	**1.0×10^{-3}**	-	-	s^{-1}
M-(L-sR1)	**1.0×10^{-2}**	-	**1.0×10^{-3}**	-	**1.0×10^{-3}**	s^{-1}
(L-sR1)-M	-	**1.0×10^{-2}**	-	**1.0×10^{-2}**	-	s^{-1}
(M-sR1)-L	-	**1.0×10^{-3}**	-	**3.5×10^{-4}**	-	s^{-1}
(N1-L)-R2	1.0×10^{-3}	-	1.0×10^{-3}	-	-	s^{-1}
N1-(L-R2)	1.0×10^{-3}	-	1.0×10^{-3}	-	-	s^{-1}
(L-R1)-N1	-	**1.0×10^{-2}**	-	**1.0×10^{-3}**	-	s^{-1}
(L-sR1)-N1	-	**1.0×10^{-2}**	-	**1.0×10^{-3}**	-	s^{-1}
(N1-R1)-L	-	**1.0×10^{-3}**	-	**3.5×10^{-4}**	-	s^{-1}
(N1-sR1)-L	-	**1.0×10^{-3}**	-	**3.5×10^{-4}**	-	s^{-1}
Other	N1-R1	1.0×10^{-2}	s^{-1}			
	sR1-N1	1.0×10^{-2}	s^{-1}			
	sR1-M	1.0×10^{-2}	s^{-1}			

Bold: new parameters (to compartment model)

Endothelial cell surface receptors are continually produced, internalized, recycled, and degraded, with trafficking rates that depend on ligation status and complex formation with NRP1 (**Fig 6-1C**). We include detailed VEGFR2 trafficking based on a previous *in vitro* computational model (**Table 6-S8**). Surface receptor production rates were tuned to match experimental measurements of cell surface receptor levels in human umbilical vein endothelial cells (**Table 6-4**). We also explicitly include phosphorylation and site-specific dephosphorylation of VEGFR2 (**Fig 6-1D**), which is dependent on receptor trafficking, with higher net activation at Y1214 than Y1175 on the cell surface, and higher Y1175 phosphorylation in early (Rab4/5) endosomes (**Table 6-S9**), as a result of differential dephosphorylation of Y1175 and Y1214 on the cell surface and in early endosomes [20]. This allows us to study phosphorylation explicitly, instead of using receptor occupancy as a surrogate, and to look at relative activation of downstream signaling pathways leading to proliferation (pY1175 via ERK1/2) and migration (pY1214 via p38).

Table 6-4. Targets & Secretion/Production Rates at Steady-State

Species	Target Location	Target Value	Target Units	Fit Production/ Secretion Rates	Production Units	Ref
VEGFR1	Main Body Mass	1800	Surface receptors/EC	**1.162**	Change from No VEGF SS	[67]
	Calf	1800	Surface receptors/EC	**1.32**	Change from No VEGF SS	[67]
VEGFR2	Main Body Mass	5800	Surface receptors/EC	**32.09**	Change from No VEGF SS	[67]
	Calf	5800	Surface receptors/EC	**53.95**	Change from No VEGF SS	[67]
NRP1	Main Body Mass	70,000	Surface receptors/EC	**1.295**	Change from No VEGF SS	[63]
	Calf	70,000	Surface receptors/EC	**1.502**	Change from No VEGF SS	[63]
sR1	Plasma	100	pM	0.0893	molec/EC/s	[57]
PlGF	Plasma	10	pM	**0.0146**	molec/MD/s	[42]
PlGF1				**15%**	% of Prod	[68]
PlGF2				**85%**	% of Prod	[68]
VEGF	Plasma	1.5	pM	0.2830	molec/MD/s	[57]
VEGF$_{165}$				77%	% of Prod	[69]
VEGF$_{121}$				8%	% of Prod	[69]
VEGF$_{189}$				**15%**	% of Prod	[69]

Bold: new parameters (to compartment model)

SS: steady-state

MD: myonuclear domain (portion of a skeletal muscle myocyte associated with a single nucleus)

Due to the spatially-averaged nature of this model, gradients and heterogeneity in growth factor, soluble receptor, and cell surface receptor patterning are neglected. Instead, we examine the tissue-averaged behavior within the context of the human body. We neglect secretion of sR1 directly into the bloodstream, receptors present on the luminal side of ECs, and degradation of growth factors by proteases. All parameters are based on or fit to experimental data, either newly here or previously for other computational models. By building on previous modeling efforts, we have built more molecular detail into our models, while adding only a modest number of new parameters (indicated in bold in **Tables 6-1, 6-2, 6-4 & 6-4** and **Table 6-S7**).

To simulate the time-course of each molecular species in each tissue and the blood, this model includes 635 nonlinear ordinary differential equations that are solved simultaneously. The model equations can be found in the **Supplemental Equations**. The full set of differential equations was solved in Fortran using the Livermore Solver for Ordinary Differential Equations with Automatic method switching for stiff and nonstiff problems (LSODA), on a laptop PC, with a relative error tolerance of 10^{-6}.

6.2.2 Model Parameterization

Geometry. The geometric parameterization is taken, without modification, from a previous 3-compartment model of a healthy 70 kg human [57], and is detailed in S7 Table. Briefly, histological cross-sections of human gastrocnemius muscle and vastus lateralis muscle were used to parameterize the "calf muscle" and "main body mass" compartments, respectively. These cross-sections and other measurements were used to estimate the relative fractions of muscle volume occupied by myocytes, capillaries (separated into vascular space and endothelium), and interstitial space. Estimates of endothelial and myocyte basement membrane thickness, cell surface areas and volumes, and the volume fractions of ECM protein and fluid in interstitial space were also used to parameterize the tissue compartments. For full details, see [57]. The blood is taken to be 5L, with 60% of that volume being plasma.

Binding and Coupling Kinetics. In this model, we include five growth factor ligands (L), each with different receptor-binding, matrix-binding, and NRP1-binding properties (**Fig 6-1B and 6-1E**). Our goal is to understand how these isoform-specific properties lead to differential ligation and activation of VEGFR1 and VEGFR2. We assume all ligands and receptors are pre-dimerized, neglecting the formation of ligand or

receptor heterodimers, and assume the same binding properties for sR1 as endothelial VEGFR1 [70]. NRP1 can bind directly to VEGFR1 (and we assume sR1) [71], while VEGF is required to bridge NRP1 and VEGFR2. While VEGF binds to both VEGFR1 and VEGFR2, PlGF binds to only VEGFR1. The shorter PlGF1 does not bind to NRP1 or to the matrix (M), but we assume that PlGF1, like $VEGF_{121}$, does bind to VEGFR1 and NRP1 simultaneously. $VEGF_{121}$ does not bind to the matrix, and its ability to bind NRP1 [72] alone is neglected, as it has previously been shown to have very little effect on VEGFR signaling *in vivo* [57]. For both PlGF and VEGF, the longer isoforms ($VEGF_{165}$, $VEGF_{189}$, and PlGF2) bind to the matrix, PlGF2 more strongly than $VEGF_{165}$ [66]. These longer isoforms also bind NRP1, but not NRP1-VEGFR1 complexes (though this remains unproven for PlGF2). Reflecting our previous *in vitro* computational model, we account for binding of matrix-bound ligands to VEGFR2 (previously demonstrated [18, 19]) and VEGFR1 (assumed to occur). We assume that endothelial basement membrane-bound growth factor within 25nm of the cell surface is accessible to cell surface receptors, based on the length of the extracellular domain of the related RTKs ErbB2 and ErbB3 (11.3-16.4nm) [73-75], and assuming some flexibility in cell position and shape. We calculated the resulting fraction of EBM accessible to cell surface receptors (S7 Table), and scaled the corresponding reaction on-rates (**Table 6-2, see Supplemental Equations**). Similarly, we allow matrix-immobilized $VEGF_{165}$, $VEGF_{189}$, or PlGF2 to bind to sR1, creating matrix-ligand-sR1 (M-L-sR1) complexes, which cannot bind cell surface receptors, and are therefore effectively sequestered. As VEGFR1 can bind to NRP1 without ligand, and the NRP1- and heparin-binding domains of VEGFR1 overlap, we also examine the impact of allowing matrix-bound sR1 to bind $VEGF_{121}$ and PlGF1 in the interstitial space, allowing these non-matrix-binding ligands to be sequestered. In all cases, in the absence of evidence to the contrary, we assume that matrix-immobilization does not affect the affinity of any interactions.

The binding and unbinding rates for VEGF and PlGF to VEGFR1, VEGFR2, and sR1 are kept the same as in previous models [45, 57], as summarized in **Tables 6-1, 6-2, & 6-3** (new parameters in bold). Though we have not previously included PlGF in a compartment model, PlGF binding to VEGFR1 has been modeled *in vitro* [45], and the parameter values are matched to this study. The affinity of PlGF2 for NRP1 is based on experimental measurements of PlGF2 binding to the NRP1 extracellular domain [65]. Slightly different affinities are used for VEGF binding to matrix sites and to NRP1 than in previous

compartment models, in order to use measurements from a single source for both $VEGF_{165}$ and $VEGF_{189}$ (NRP1-binding) [64], or for VEGF and PlGF (matrix-binding) [66]. Since $VEGF_{189}$ is known to bind the ECM more strongly than $VEGF_{165}$, but an affinity is not available, we assume 10x stronger binding, similar to the difference in $VEGF_{165}$ and $VEGF_{189}$ affinity for NRP1 [64]. As in previous models [57], lacking a measured affinity for sR1 binding to matrix, we assume a value similar to that for VEGF, as both interactions occur via heparin-binding domains.

Receptor Trafficking and VEGFR2 Phosphorylation. We added receptor trafficking and VEGFR2 phosphorylation to the model, in order to track site-specific phosphorylation of VEGFR2 explicitly, rather than simply receptor occupancy. This is more accurate, as *in vitro* VEGFR2 phosphorylation decreases faster than can be accounted for by ligand depletion or receptor degradation [20]. We implemented these reactions as previously described in an *in vitro* model [20] for VEGFR2, accounting for ligand-induced changes in internalization, recycling, and degradation, as well as preferential recycling of VEGFR2 complexes containing NRP1 via a Rab11-dependent pathway. The trafficking rate constants are given in **Table 6-S8**. Though VEGFR1 trafficking is known to be distinct from that of VEGFR2 [76, 77], we lack sufficient data to build or validate a model of VEGFR1 trafficking. As such, a structure for VEGFR1 trafficking was incorporated for future use, but results are presented only for cell surface VEGFR1. Site-specific phosphorylation of VEGFR2 on three tyrosine sites is included: Y951, Y1175, and Y1214. We approximate phosphorylation and dephosphorylation as first order processes, and assume that these processes occurred independently on each tyrosine. The phosphorylation rate is assumed to be zero for unoccupied VEGFR2, and fast (1 s^{-1}) for ligated VEGFR2. The dephosphorylation rates do not depend directly on the VEGF isoform, but vary by tyrosine site and subcellular location (**Table 6-S9**), as previously fit and validated [20] using experimental observations of increased pY1214 following stimulation with immobilized VEGF compared to free VEGF in solution [18], and enabling site-specific phosphorylation patterns to depend on the mixture of matrix- binding and non-matrix-binding isoforms available to VEGFR2. Given limited data available for phosphorylation of Y951 upon which to fit the model, this analysis focuses on VEGFR2 activation on Y1175 and Y1214.

Transport. Inter-compartmental transport parameters are taken from a previous model [57] (see **Table 6-S10**). Vascular permeability was estimated based on the Stokes-Einstein radii for each protein. Here, we

assume the same permeability for PlGF as VEGF, as they have similar molecular weights and are structurally related. Lymphatic drainage transports proteins from tissue compartments to the blood in a tissue-mass-dependent and a protein-size-independent fashion. We use the estimated lymphatic flow rates for a supine, awake 70 kg human [57].

Protein Expression Levels. We assume the same densities of interstitial matrix sites available to bind VEGF, PlGF, and sR1 in the ECM and basement membranes as used in previous models [57] (see S11 Table). Briefly, ECM binding-site density is based on measured FGF binding sites [78, 79], while basement membrane binding site densities are estimated based on Engelbreth-Holm-Swarm sarcomas in diabetic mice [80]. Endothelial cell surface VEGFR1, VEGFR2, and NRP1 target levels were chosen to match median experimental (FACS) measurements in human umbilical vein endothelial cells [63, 67], which represented our best information to date on receptor levels in humans; these values are summarized in **Table 6-4**. Total receptor levels are not directly controlled, but remain within a reasonable range. The VEGF and PlGF secretion rates by myocytes and endothelial secretion of sR1 into the interstitial space were adjusted to match experimentally measured plasma protein levels (**Table 6-4**). Plasma levels are used as targets because no interstitial measurements of sR1 or PlGF levels are available, and plasma VEGF levels are better characterized than tissue interstitial levels. Target levels of plasma VEGF and sR1 are unchanged from previous models [57], and a plasma PlGF target concentration of 10pM was selected. The secretion of different VEGF isoforms and PlGF isoforms are maintained at fixed ratios, based on experimental measurements in mice (VEGF) and humans (PlGF) [68, 69]. Production rates for VEGFR1, VEGFR2, and NRP1 were adjusted independently in the calf muscle and the main body mass to meet target values in each tissue while also meeting plasma ligand targets. As VEGF, PlGF, and sR1 secretion are fit only to plasma measurements, we assume the same secretion rates per cell in both tissue compartments. .

6.3 Results

6.3.1 Ligand secretion and receptor production rates for baseline typical healthy human

The ligand secretion and receptor production rates necessary to hit baseline (healthy) targets had to be fit simultaneously, due to the highly non-linear nature of the system. At our baseline steady-state, the VEGF production rate is 0.2830 molecules/myonuclear domain/s, the PlGF production rate is 0.0146 molecules/myonuclear domain/s, and the sR1 production rate is 0.0893 molecules/EC/s (see **Table 6-4**). The VEGF and sR1 production rates here are higher than previous estimates. This is unsurprising, given the changes in receptor levels, trafficking, and growth factor isoforms. Surprisingly, the PlGF production rate is lower than that for VEGF, despite a higher target plasma level (see Flux Analysis section for the mechanism by which this occurs).

To illustrate the nonlinearity of our model, we perturbed each ligand secretion and receptor production rate slightly (2%), and examined changes in plasma ligand and tissue receptor levels. As shown in **Fig 6-2A**, plasma VEGF and tissue VEGFR2 are highly sensitive to changes in either VEGF secretion or VEGFR2 production in the main body mass, with changes of 11-25% per percent change in input. As VEGF levels increase, more VEGFR2 becomes occupied, internalized, and degraded, reducing VEGFR2 levels and decreasing VEGF consumption (**Fig 6-2B and Fig 6-S1**). Similarly, as VEGFR2 production increases, more VEGF is bound to VEGFR2, internalized, and degraded, reducing VEGF levels and thus increasing EC surface VEGFR2. This super-sensitivity was not present in previous models, where surface VEGFR2 levels were fixed (see **Fig 6-S1**). This new, emergent result suggests that, lacking upregulation of VEGFR2 in response to VEGF, VEGFR2 levels would be highly sensitive to even small fluctuations in local VEGF concentration (**Fig 6-2**), highlighting the importance of dynamic adjustments to ligand and receptor expression *in vivo*. In the calf muscle, perturbing VEGFR2 production has a large impact on EC surface VEGFR2, but little effect on plasma VEGF, due to the smaller size of the compartment. Changes in receptor production in one tissue compartment have little effect on receptor levels in the other tissue compartment.

Figure 6-2: Nonlinearity of ligand & sR1 secretion and EC receptor production rates in the model.

(A) One at a time, each baseline ligand secretion or receptor production rate (inputs- listed across the top), was increased by 2%, then decreased by 2%. For each perturbation, the change in plasma ligand and EC surface receptor levels (outputs- listed on the left) in in both the main body mass ("Body") and calf muscle ("Calf") were obtained. The average change in output from baseline levels was calculated, and divided by the change in input (+/-2%) to give the relative change in output per % change in input. **(B)** Schematic of positive feedback in VEGF gene and protein levels in the model. An increase in VEGF expression increases local VEGF protein, increasing VEGF binding to VEGFR2, and subsequent internalization and degradation. This decreases total VEGFR2 protein levels, leading to reduced VEGF-VEGFR2 complex formation, which reduces net endothelial consumption of VEGF protein. To accommodate, in the model, VEGFR2 expression was increased until target baseline levels were achieved for all ligands and receptors. A similar positive feedback loop exists for changes in VEGFR2 expression.
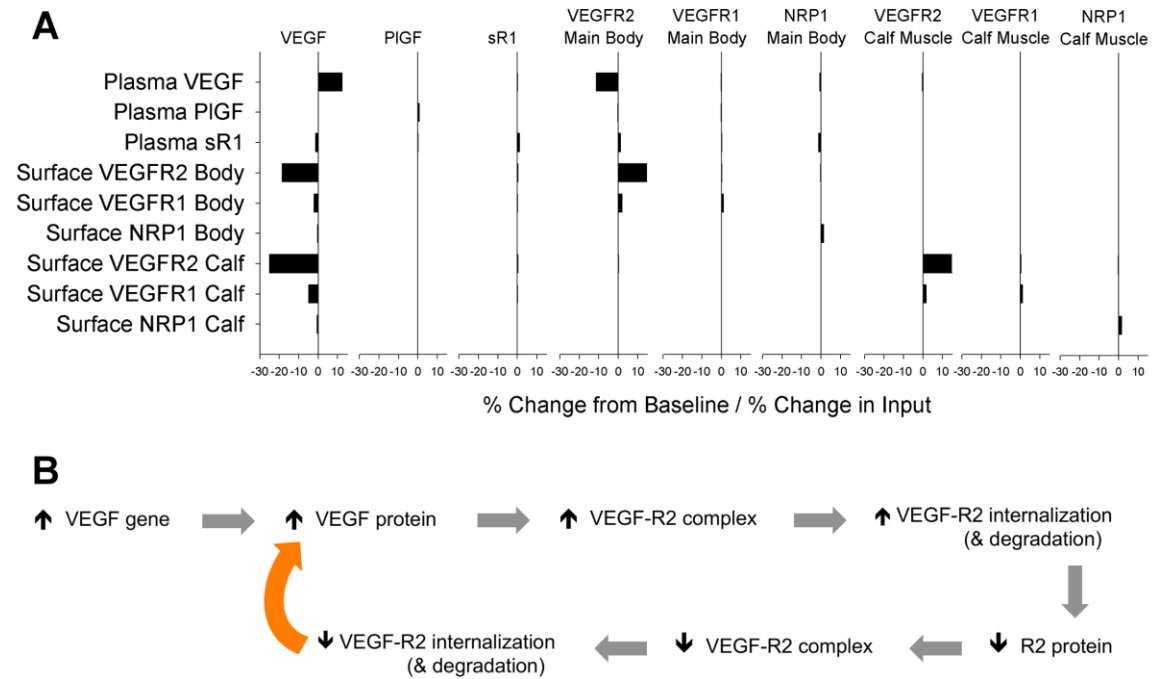
In this model, we assume the same rates for ligand production in both the healthy calf muscle and the main body mass. As such, perturbing the VEGF secretion rate (in both compartments) alters the receptor levels in both tissues (**Fig 6-2**). Due to differences in the geometric parameterizations of the calf and other tissues (**Table 6-S7**), using the same ligand secretion rates results in different interstitial VEGF, sR1, and PlGF levels (**Fig 6-3D**). We focus primarily on quantities measured in the "Main Body Mass" compartment, which, due to its larger size, represents the primary determinant of plasma VEGF, sR1, and PlGF levels.

6.3.2 Pharmacokinetics: Where are VEGF, PlGF, and sR1 in the body?

After establishing the secretion and production rates required to achieve basal targets, we next examined the steady-state distribution of VEGF, PlGF, and sR1.

Plasma: differential isoform representation compared to relative expression levels. In the plasma, free VEGF protein is predicted to be 84% $VEGF_{165}$, 7% $VEGF_{121}$, and 9% $VEGF_{189}$; thus $VEGF_{189}$ (the strongest ECM-binding isoform) is underrepresented compared to the production fractions of 77%, 8%, and 15%, respectively (Fig 3A and 3E). Conversely, the ECM-binding PlGF2 isoform is overrepresented in plasma (98% of free plasma PlGF), compared to its production (85% of PlGF production), reflecting its overrepresentation in the tissue extracellular space (see Fig 3). In agreement with previous models, 77% of plasma VEGF and 39% of PlGF are bound to sR1. A total of 10% of plasma sR1 is bound to ligand, with 44% of this bound to VEGF and 56% bound to PlGF, suggesting that PlGF interacts with sR1 to a comparable extent as VEGF.

Figure 6-3: Pharmacokinetics of VEGF, PlGF, and sR1 at steady-state. (A) Predicted free and sR1-bound ligands, and free and ligand-bound sR1 in plasma. **(B)** Predicted VEGF, PlGF, and sR1 distribution in healthy tissue in "Main Body Mass" compartment, shown in pM of tissue. **(C)** Extracellular (not bound to or inside ECs) VEGF, PlGF, and sR1 in "Main Body Mass" compartment, in pM of tissue. **(D)** Steady-state net flow profiles for VEGF, PlGF, sR1, and sR1-ligand complexes between the calf muscle, blood, and main body mass. All VEGF isoforms are aggregated, as are both PlGF isoforms. Green arrows represent production, red arrows EC consumption, black arrows bi-directional vascular permeability, gray arrows lymphatic drainage, and pink arrows with red outlines direct clearance from blood. The white arrows show the net association or dissociation of VEGF-sR1 and PlGF-sR1 complexes in each compartment. Displayed concentrations are free ligand, sR1, or complex in interstitial fluid or plasma. The numbers under each compartment are the respective compartment volumes. Flows are given in pmoles/day. **(E)** Comparison of VEGF and PlGF isoform distribution with relative isoform production rates demonstrates locations and complexes where each isoform is under- or over-represented relative to the fraction of total VEGF or PlGF production. **(F)** Matrix site occupancy in the EBM, ECM, and PBM.
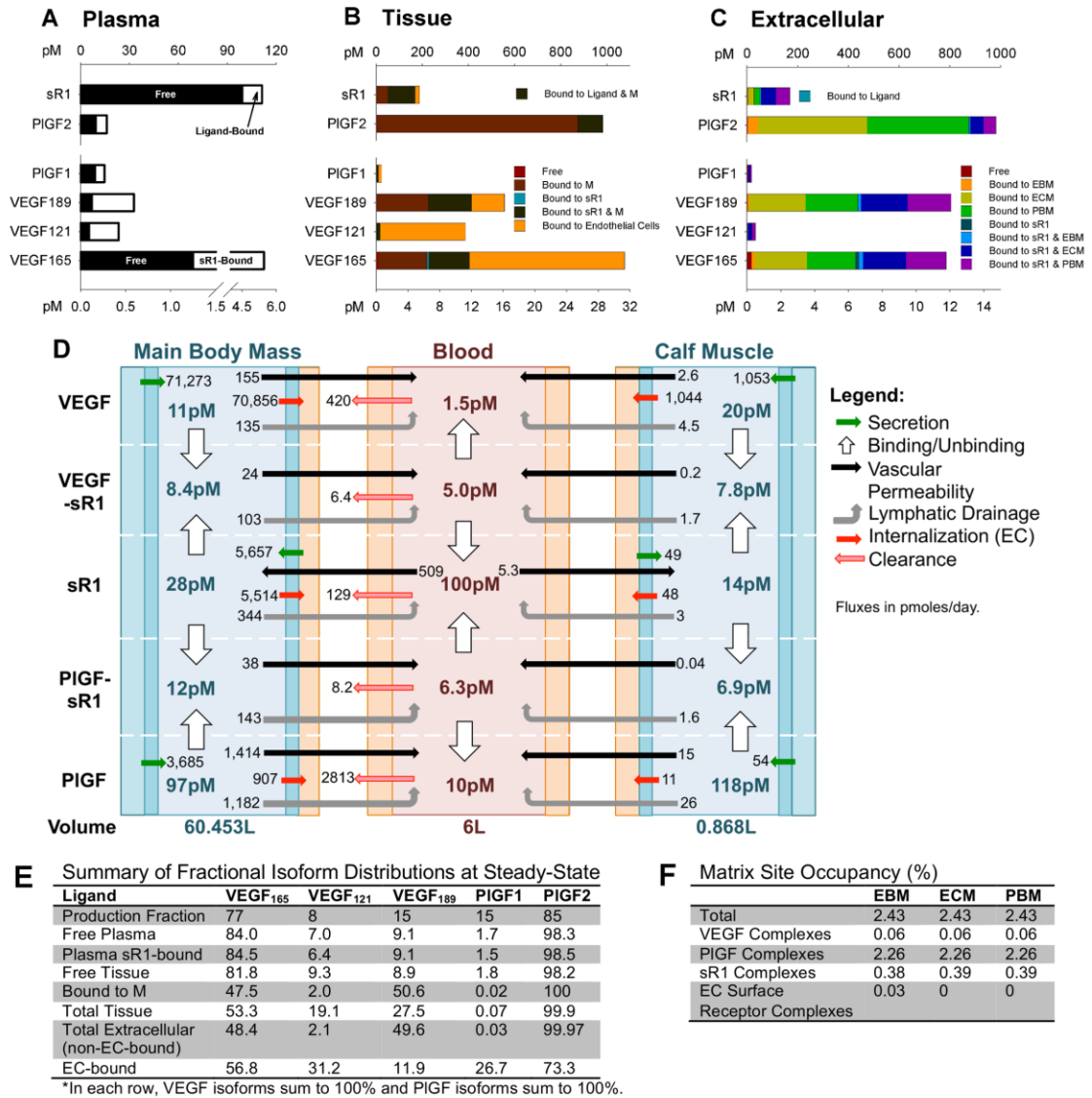
Figure 6-3

Tissue (Main Body Mass): ECM-binding drives distinct VEGF & PlGF isoform distribution. The

model predicts that the total and relative levels of matrix-bound and free growth factor are dictated by ECM

binding properties (**Fig 6-3C**). While the model predicts that the majority of VEGF121, VEGF165, and

PlGF1 are bound to endothelial cells (96%, 62%, and 58%, respectively- see **Fig 6-3B**) in the main body

mass, large portions of the heparin-binding isoforms, VEGF165, VEGF189, and PlGF2, are bound to the

ECM and basement membranes (36%, 74%, and 99.6% of total in tissue, respectively), alone or in complex

with sR1 (**Fig 6-3B**). Most of the immobilized growth factor is in the ECM and parenchymal BM (**Fig 6-

3C**), inaccessible to EC receptors, but available for proteolytic release. Total extracellular (non-EC-bound)

VEGF is 48% VEGF165, only 2% VEGF121, and 50% VEGF189, while extracellular PlGF is 99.97%

PlGF2 (Fig 6-3E). As these percentages suggest, most extracellular heparin-binding growth factor is matrix

bound (alone or in complex with sR1): 96% of VEGF165, 99.6% of VEGF189, and 99.7% of PlGF2.

However, 93% of VEGF121 and 80% of PlGF1 are also sequestered (via immobilized sR1) in our

simulations. The total amount of sequestered VEGF121 and PlGF1 is small (**Fig 6-3C**), but still significant

compared to the corresponding free growth factor concentrations in solution. Indeed, only 7.8% of tissue

PlGF1 and <1% of every other isoform is predicted to be "free" in solution. This is consistent with previous

results [57] in suggesting that, unlike cell culture experiments, ligand-receptor binding is limited by ligand

availability in the body. The model predicts that 90% of sR1 in tissue is matrix-bound (**Fig 6-3B**), while

only 0.45% is free (bound to neither matrix nor ligand), and 0.32% bound to ligand alone, implicating the

ECM in regulation of sR1 distribution as well.

　　　　While a large fraction of growth factor is immobilized, predicted matrix site occupancy is low

(2.4%- see **Fig 6-3F**). This is higher than in previous models, as a result of the inclusion of PlGF and

immobilized complexes containing both growth factor and sR1. In the endothelial BM, most (93%)

occupied sites contain PlGF; 16% contain sR1, and 2.3% VEGF. While only 1.1% of occupied EBM sites

include ligand bound to cell surface receptors, the large number of binding sites in the endothelial BM

makes even this small fraction physiologically relevant (see **Fig 6-4**).

Flux analysis: differential transport of VEGF & PlGF. By calculating the net transport, consumption,

and clearance of each protein or complex (**Fig 6-3D**), we can examine the contributions of each dynamic

process to the steady-state distribution. At steady-state, the model predicts a concentration of 11pM VEGF

in the available interstitial fluid of the main body mass, similar to previous models. The levels in the calf muscle are higher (20pM), due to a higher myocyte volume fraction and resulting higher production per unit tissue volume. While other quantities also varied between the two compartments, all trends and net flux directions were the same. In agreement with previous model predictions, free sR1 levels are higher in plasma than in tissue, while PlGF levels, like VEGF levels, are higher in tissue. These concentration differences lead to predicted transendothelial intravasation (net transfer from tissue to blood) of VEGF and PlGF, while free sR1 is predicted to extravasate (net transfer from blood to tissue). The fraction of sR1 bound to ligand is similar in plasma and tissue interstitial fluid (42% in the main body mass, 51% in calf muscle), with substantial contributions by both VEGF and PlGF. The large majority of VEGF and sR1 produced are consumed locally by endothelial cells (99% of VEGF and 98% of sR1 in the "Main Body Mass"), accounting for the high sensitivity of interstitial VEGF to VEGFR2 production (see **Fig 6-2**). Conversely, the model predicts that only 25% of PlGF is consumed by ECs, due to much lower total binding to EC receptors than VEGF. This accounts for the low PlGF production rate required to match target plasma levels, and suggests that PlGF may be primarily cleared via transendothelial transport and lymphatic drainage into plasma, followed by clearance from the blood, or by cell types not included in this model (e.g. monocytes & macrophages).

6.3.3 Pharmacodynamics: What controls VEGFR1 and VEGFR2 activation?

Having examined the distribution of VEGF, PlGF, and sR1, we next zoomed in to examine the effect of these proteins and their distributions on the binding and activation of endothelial VEGFR1 and VEGFR2 within healthy tissue.

Growth factors levels are limiting for in vivo EC receptor activation. At steady state, cell surface ligation of VEGFR2 is predicted to be close to an order of magnitude higher than cell surface ligation of VEGFR1 (**Fig 6-4D**), due in part to higher levels of EC surface VEGFR2 (5800 VEGFR2/cell vs. 1800 VEGFR1/cell). As a result, the majority of EC consumption of VEGF occurs via VEGFR2, explaining why VEGF levels are more sensitive to changes in production of VEGFR2 than VEGFR1 (**Fig 6-2**). Overall, the model predicts low cell surface receptor occupancies of 3.4% for VEGFR1 and 8.7% for VEGFR2 (4.5% VEGFR1 and 14% VEGFR2 in calf muscle), and somewhat higher but still low total (surface + endosomal)

VEGFR2 occupancy (20%), suggesting that ligands do not compete for receptor binding (**Fig 6-4C**). This prediction is conservative; model VEGF levels are in fact higher than estimates of free interstitial VEGF via microdialysis, and plasma target levels for VEGF and PlGF assume that no sR1-bound ligand was detected. While sR1 is known to interfere with VEGF ELISA measurements, likely at least a portion of this bound VEGF is in fact detected, thus placing our calibrated model at the top of the possible VEGF range.

Figure 6-4: Pharmacodynamics of ligand binding to VEGFR1 and VEGFR2. (A) Total soluble growth factor (in available interstitial fluid) and immobilized growth factor (in innermost 25nm of EBM) accessible to ECs. Growth factor bound to EC receptors is not included in this plot. **(B)** Break-down of EC surface-bound ligand, by isoform. Note the difference in quantities of total ligated VEGFR2, VEGFR1, and NRP1 (**panel C**). **(C)** Occupancy of VEGFR2, VEGFR1, and NRP1 on ECs, broken down by ligand and NRP1-binding. VEGFR2 occupancy is shown on the cell surface, in early signaling endosomes (Rab4/5), and in recycling endosomes (Rab11), while VEGFR1 and NRP1 are shown only on the cell surface. Quantities are given in pM of total tissue in the "Main Body Mass" compartment. **(D)** VEGFR2, VEGFR1, and NRP1 ligation on ECs, excluding receptor not bound to ligand. Complexes not listed in the legend are present at levels too low to be seen in the figure. **(E)** Break-down of percentage of EC surface VEGFR1 and VEGFR2 ligation comprised by each isoform, compared to the relative production of each isoform. Production fractions are calculated separately for VEGF and PlGF, while for receptor binding the combined distribution is shown.

A Ligand Amounts Seen by ECs

PlGF2, PlGF1, VEGF189, VEGF121, VEGF165a

Free
sR1-bound
EBM-bound
sR1 & EBM-bound

pmoles 0 10 20 30 400 800

B Surface Receptor-Bound

sR1, PlGF2, PlGF1, VEGF189, VEGF121, VEGF165a

NRP1
VEGFR1
VEGFR2
NRP1-VEGFR1
NRP1 & VEGFR2
M & VEGFR1
M & VEGFR2

pM 0 1 2 3 4 5 12 13

C VEGFR2

pM 0 20 40 60 80

Subcellular Location

Rab11, Rab4/5, Surface

Free VEGFR2
Ligated

VEGFR1

Surface

Free VEGFR1
NRP1-VEGFR1
Ligated

pM 0 5 10 15 20 25

NRP1

Surface

Free NRP1
NRP1-VEGFR1
sR1-NRP1

pM 0 200 400 600 800 1000

D VEGFR2

pM 0 2 4 6 8 10 12 14

Subcellular Location

Rab11, Rab4/5, Surface

VEGF165-NRP1
VEGF165-M
VEGF121
VEGF189-NRP1
VEGF189-M

VEGFR1

Surface

VEGF121-NRP1
PlGF1-NRP1
PlGF2
PlGF2-M

pM 0.0 0.2 0.4 0.6 0.8

NRP1

Surface

PlGF2
sR1

pM 0 2 4 6 8 10 12 14

E Fractional Isoform Receptor Binding at Steady-state (%)

Ligand	VEGF$_{165}$	VEGF$_{121}$	VEGF$_{189}$	PlGF1	PlGF2
Production Fraction	77	8	15	15	85
Surface R1-bound	1.0	69.8	0.6	9.1	19.6
Surface R2-bound	71.5	9.8	18.7	-	-

Figure 6-4

222

NRP1- & ECM-binding drive VEGF & PlGF isoform binding to VEGFR1 and VEGFR2. The

majority of non-ligand-bound VEGFR1 is predicted to be in complex with NRP1 (99.1%). NRP1 remains

mostly free (95.3%) (Fig 6-4C), with some binding to sR1 and PlGF2 to form non-signaling complexes

(Fig 6-4D). The isoform-specific NRP1 binding properties of VEGF and PlGF make NRP1 a strong

regulator of ligand-binding to VEGFR1 and VEGFR2. The model predicts that VEGF165 and VEGF189,

which bind to VEGFR2 and NRP1 simultaneously, bind almost exclusively to VEGFR2 (**Fig 6-4D**).

Conversely, VEGF121, which binds to NRP1-VEGFR1 complexes, comprise 70% of ligand bound to

VEGFR1 (**Fig 6-4D**), while PlGF makes up only 29% of the ligand bound to VEGFR1 at steady-state (**Fig

6-4E**). This result explains the lower predicted occupancy of VEGFR1 than VEGFR2; VEGF121 and

PlGF1, the only ligands to bind VEGFR1 and NRP1 simultaneously, represent a small fraction of total

ligand (**Fig 6-4A**). The dominance of VEGF121 binding to endothelial VEGFR1 is in contrast to the

relatively even binding of VEGF and PlGF to sR1 (**Fig 6-2**), and occurs because most tissue PlGF is

PlGF2, which cannot bind to NRP1-VEGFR1 complexes on endothelial cells.

While all soluble growth factors are accessible to EC receptors in this model (assuming a well

mixed compartment, i.e. nonlimiting fast diffusion), cell surface receptors are only allowed to bind to

immobilized ligands in the innermost 25nm of endothelial BM. A substantial fraction of both soluble and

endothelial BM-bound growth factor is bound to sR1, and thus inaccessible to EC receptors (**Fig 6-4A**). Of

the remaining growth factor, the model predicts that the amount of available free growth factor exceeds the

amount of available immobilized growth factor for all VEGF isoforms, but not for PlGF2 (**Fig 6-4A**)

However, within the 25nm space adjacent to endothelial cells, the concentration of available immobilized

growth factor far exceeds the predicted concentration of free growth factor for all matrix-binding isoforms

(**Fig 6-S2A**).

Of the 0.03% of basement membrane sites bound to ligand-cell surface receptor complexes, 23%

are immobilized PlGF2 bound to VEGFR1, 20% are $VEGF_{165}$-R2 complexes, and 56% are $VEGF_{189}$-R2

complexes. While more of these complexes are bound to VEGFR2, VEGFR1 has a higher fraction of

ligand-receptor complexes bound to immobilized ligands (18% versus 6.9%- see **Fig 6-4D**). This is due the

lower total number of ligand-VEGFR1 complexes, combined with higher tissue levels and stronger matrix

binding by PlGF2 compared to VEGF. If we assumed all endothelial BM-bound growth factors were

accessible to receptors (as opposed to the closest 25nm), 50% of ligated VEGFR1 would be bound to immobilized PlGF, and 17% of ligated VEGFR2 would be bound to immobilized $VEGF_{165}$ or $VEGF_{189}$.

NRP1 regulates isoform-specific trafficking and phosphorylation of VEGFR2. In addition to guiding receptor ligation, NRP1 also regulates VEGFR2 trafficking [11], speeding up recycling of ligated VEGFR2. This leads to predicted accumulation of $VEGF_{121}$-VEGFR2 complexes in early signaling (Rab4/5) endosomes, while $VEGF_{165}$-VEGFR2 and $VEGF_{189}$-VEGFR2 are recycled back to the cell surface, leading to a more even distribution between the cell surface and early endosomes (**Fig 6-4D**). As such, changes in relative levels of VEGF isoforms are predicted to alter not only the tissue distribution of ligand and the balance of VEGFR1 and VEGFR2 activation, but also the subcellular localization of VEGFR2.

We previously showed that changes in site-specific phosphorylation of VEGFR2 as a function of $VEGF_{165}$ immobilization to a surface or in a gel could be explained by prolonged retention of immobilized VEGF-VEGFR2 complexes at the cell surface [20], increasing net phosphorylation on Y1214 and promoting pro-migratory signaling. Here, we examined whether this translated to VEGF isoform-specific trends in site-specific phosphorylation of VEGFR2 in a physiological context. Indeed, we see that the faster dephosphorylation of tyrosine Y1175 than Y1214 on the cell surface, and vice versa in early (Rab4/5) signaling endosomes (**Fig 6-5B**), leads to different relative levels of VEGFR2 activation on Y1175 and Y1214 as a function of the bound ligand; the heparin-binding VEGF isoforms ($VEGF_{165}$ and $VEGF_{189}$) lead to higher net activation on Y1214, while $VEGF_{121}$ shifts relative activation towards Y1175 (**Fig 6-5C**).

Figure 6-5: VEGF isoform-specific trafficking and site-specific phosphorylation of VEGFR2 *in vivo*.

(A) VEGF isoform-specific NRP1-binding properties result in isoform-specific trafficking of VEGFR2. **(B)** Subcellular location-specific dephosphorylation rates for Y1175 and Y1214 (**Table 6-S9**) lead to preferential activation of tyrosine 1214 on the EC surface, compared to signaling in endosomes. **(C)** Isoform-specific trafficking and location-specific dephosphorylation combine to result in isoform-specific trends in relative activation of VEGFR2 on tyrosine 1175 and tyrosine 1214. **(D)** Total VEGFR2 phosphorylation, on at least one tyrosine (pR2) and specifically on Y1175 or Y1214, across all subcellular locations. **(E-F)** Distribution of pY1175 (**E**) and pY1214 (**F**), by VEGF isoform and location.
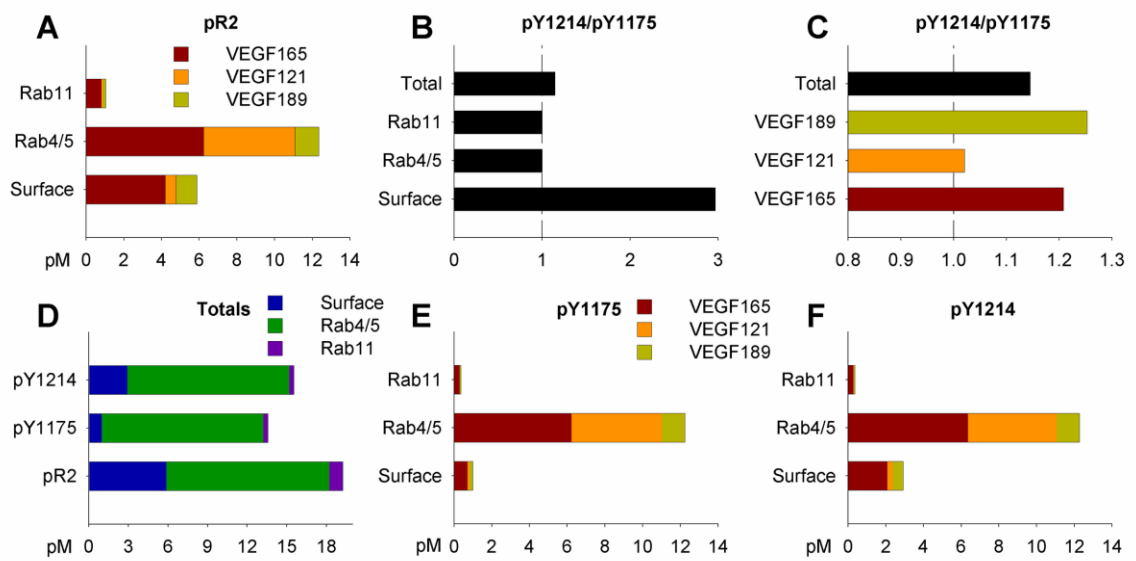
6.3.4 Complex, coordinated regulation of VEGFR1 and VEGFR2 signaling.

It is clear that the different proteins – ligands, soluble receptors, and co-receptors – regulating VEGFR1 and VEGFR2 activation do not act in isolation. Changes to any single feature affect the total multi-factor system in a way that is difficult to predict without the use of a computational model. Here, we perturb several interactions that are of interest therapeutically, and/or are included in this model for the first time.

PlGF does not displace VEGF from VEGFR1 to increase VEGFR2 signaling *in vivo*. To test the 'ligand-shifting hypothesis,' i.e. that PlGF induces pro-angiogenic effects *in vivo* by shifting VEGF binding from VEGFR1 to VEGFR2, we altered the amount of PlGF production in tissue, and quantified the resulting changes in cell surface VEGFR1 ligation and total VEGFR2 phosphorylation. To control for changes in cell surface VEGFR1 and total VEGFR2, we normalized these quantities by the relevant receptor population. We found, across a wide range of PlGF production (from zero to 10x baseline levels), that despite large changes in free PlGF levels in tissue (**Fig 6-6A**), only modest changes in VEGFR2 ligation and phosphorylation (pR2/R2) were observed (**Fig 6-6B**). Conversely, VEGFR1 ligation changes much more (varying from 69% to 389% of baseline VEGFR1 ligation) with PlGF levels. The shift in VEGFR1 ligation is almost entirely due to PlGF; VEGFR1 ligation by VEGF remains approximately constant (Fig 6C). These results suggest that, while at supraphysiologic concentrations (>10x baseline), PlGF may increase VEGFR2 phosphorylation, PlGF and VEGF do not compete for VEGFR1 binding in physiological conditions. This is consistent with the low predicted receptor occupancies, and our previous *in vitro* simulations [45, 46], but is demonstrated here for the first time for *in vivo* scenarios.

Figure 6-6: Complex regulation of VEGF family signaling by PlGF, EBM binding sites, and sR1. (A-C) Changes in free ligand levels in tissue interstitial fluid (**A**), EC surface VEGFR1 ligation and VEGFR2 phosphorylation (**B**), and the breakdown of VEGF and PlGF bound to EC surface VEGFR1 (**C**), in response to varying PlGF production. Quantities shown are normalized to baseline cases. **(D-F)** Effect of endothelial basement membrane (EBM) binding site density on EBM site occupancy (**D**), fraction of occupied EBM sites bound to different ligands and receptors (**E**), and VEGFR1 and VEGFR2 ligation by immobilized VEGF or PlGF (**F**). **(G-I)** Total activation of VEGFR1 and VEGFR2 (**F**), and break-down of relative ligation by each VEGF and PlGF isoform (**G-H**) with varying sR1 production.
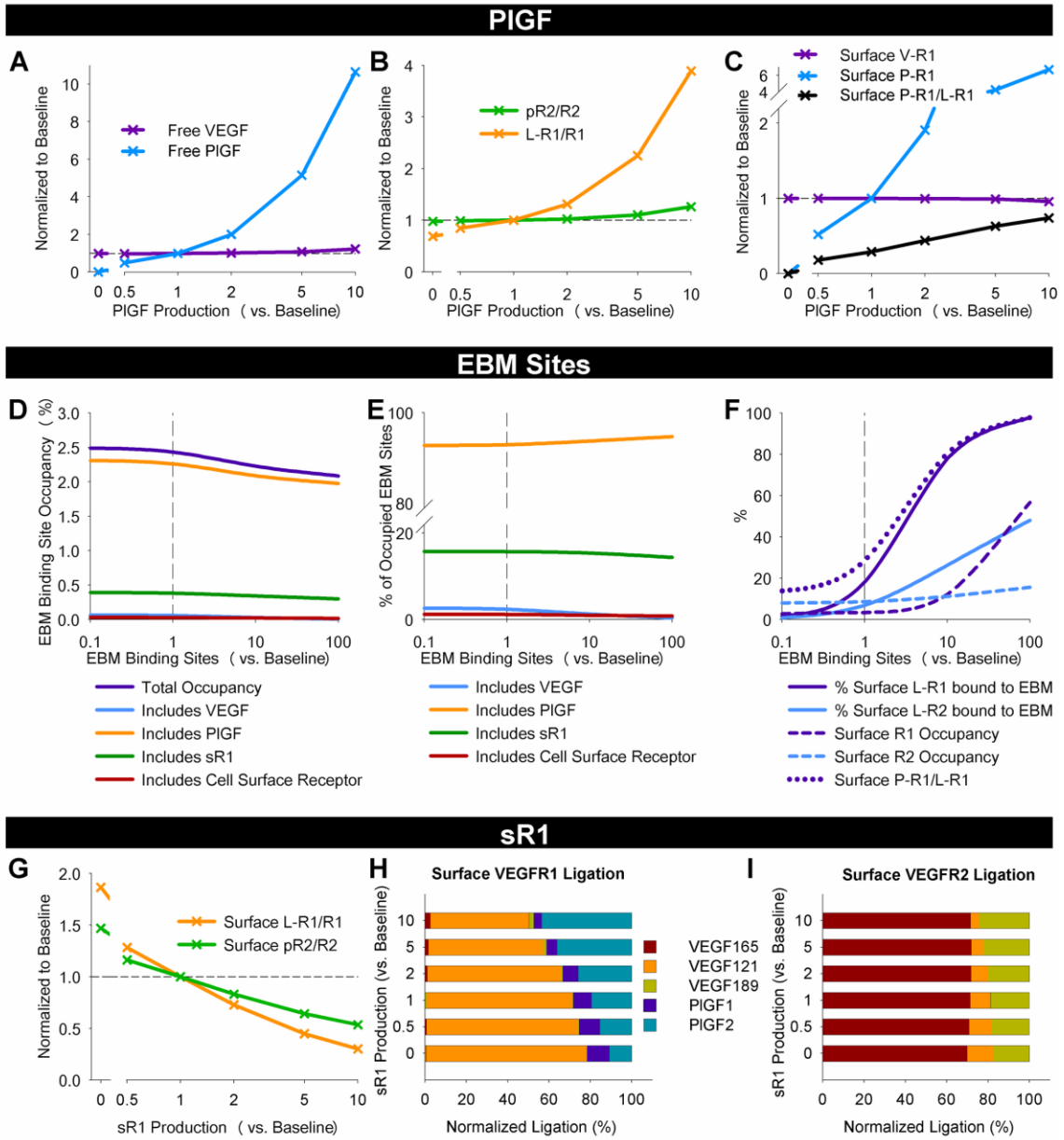
Figure 6-6

VEGFR1 ligation is more sensitive than VEGFR2 ligation to matrix site density. While the model predicts that less than 20% of ligated endothelial cell surface receptors are bound to immobilized ligand, the total number of accessible binding site in the endothelial BM is not well-characterized, nor is the fraction of the basement membrane accessible to EC surface receptors. Thus, we examined whether, if growth factor binding sites in the endothelial BM are present at higher or lower density than estimated, a difference in cell surface receptor ligation would be predicted. As we increased the density of accessible sites from baseline levels by factors of 10 and 100, the fraction of cell surface ligated VEGFR2 bound to immobilized VEGF increased, reaching 48% (compared to 6.9% at baseline) with a 100-fold increase in binding site density (**Fig 6-6F**). Interestingly, the fraction of ligated cell surface VEGFR1 bound to immobilized ligand (largely PlGF2) increases more quickly with endothelial BM site density, reaching 76% with 10x, and 97% with 100x, compared to 17% at baseline. These results suggest that immobilized ligand-receptor complexes may be important in vivo (**Fig 6-6F**).

sR1 alters the magnitude of receptor activation more than the profile of receptor-bound ligands. Since plasma sR1 levels are known to change in disease, we examined the extent to which sR1 can act in an anti-angiogenic manner to modulate endothelial VEGFR1 and VEGFR2 activation. To do this, we simulated knockdown or overexpression of sR1. As expected, free tissue VEGF and PlGF and ligation of both VEGFR1 and VEGFR2 increases (1.9- and 1.5-fold increases in ligation, respectively) with complete sR1 knockout (**Fig 6-6G**). Similarly, overexpression of sR1 reduces EC receptor ligation substantially, but does not completely block binding. Interestingly, the effect is more pronounced on VEGFR1 than VEGFR2, shifting the overall balance of signaling by VEGFR1 vs. VEGFR2 (**Fig 6-6G**). We examined whether sR1 perturbation would affect the profiles of ligands bound to VEGFR1 and VEGFR2 (**Fig 6-6H-I**). We observed little change in the ligand bound to VEGFR2. Changes to VEGFR1 ligation are larger, with relative PlGF binding increasing and relative VEGF121 binding decreasing with increasing sR1 production.

Immobilized ligand binding to sR1 regulates ligand distribution, binding to EC receptors regulates EC signaling. Next, we examined the relative contribution of immobilized complexes containing sR1 versus EC receptors to our observed results. We compared four cases: (1) the baseline case where 3-element complexes of matrix, VEGF or PlGF, and either sR1 or EC VEGFR1 and VEGFR2 were allowed

to form, (2) a case excluding all such reactions (No MLR), (3) a case allowing these reactions on sR1 but not EC receptors (sR1 Only), and (4) a case allowing these reactions on EC receptors but not sR1 (Cell Only). For each case, we re-fit the secretion and production rates to hit our plasma and cell surface receptor targets (**Table 6-S12**). We found that sR1 binding to immobilized ligands has a large impact on the amounts of free and total growth factor in tissue (**Fig 6-7**). Conversely, EC receptor binding to immobilized ligand increases receptor ligation and phosphorylation. Combined, these effects produce the observed differences between the baseline and No MLR cases.

Figure 6-7: Immobilized ligand binding to sR1 alters tissue distribution, while immobilized ligand binding to EC receptors alters activation state. Panels show percent change from baseline. Thus, the smallest bars indicate little impact of the removed reactions on a given output, while large bars indicate large change when the reactions are removed. **Cell Only:** Immobilized ligand allowed to bind to EC receptors, but not sR1. Binding of ligand to immobilized sR1 is also not allowed. **sR1 Only:** Immobilized ligand allowed to bind to sR1, and ligand to immobilized sR1, but binding of immobilized ligand to EC receptors is not included. **No MLR:** No matrix-ligand-receptor or matrix-ligand-sR1 complexes are allowed to form. **Top:** Changes in fit ligand secretion and receptor production rates to match plasma ligand and sR1 targets and tissue EC surface receptor targets. **Middle:** Distribution of free, total, and matrix-bound VEGF and PlGF. **Bottom:** EC receptor activation.
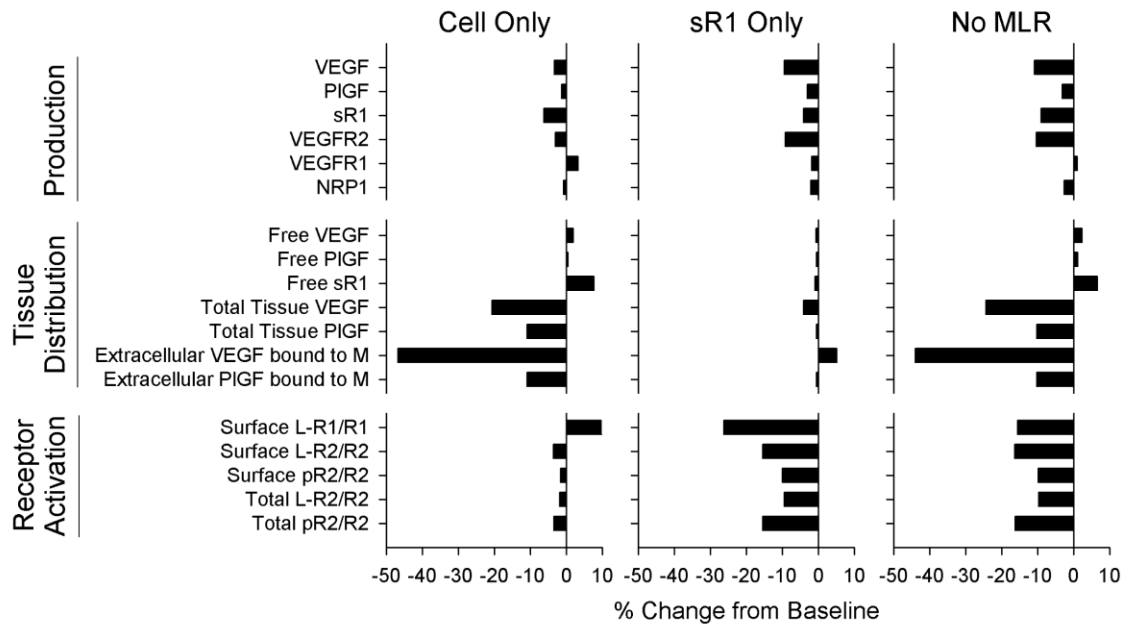
6.3.5 Model predictions of signaling in human body with expression of only single VEGF isoforms are consistent with observed murine vascular phenotypes

The most convincing evidence to date of differential signaling by VEGF isoforms is the distinct vascular phenotypes of mice or human tumors (implanted in mice) expressing only single isoforms of VEGF, with $VEGF_{121}$-only tissues producing high diameter, sparsely branched networks, $VEGF_{165}$-only tissue a relatively normal phenotype, and $VEGF_{189}$-only tissues networks of thin, highly branched vessels. Endothelial cells isolated from these single isoform-expressing mice also display distinct signaling and behavior in cell culture [81]. It is assumed that similar regulation occurs in humans. To better understand VEGF isoform-specific signaling in the context of the human, as well as to qualitatively validate our model, we simulated expression of a single VEGF isoform in the human body. While no significant changes in VEGFR1 or VEGFR2 mRNA were observed in the muscle of mice expressing only $VEGF_{120}$ [82] (equivalent to human $VEGF_{121}$), we re-fit our model for each case, in order to maintain target ligand and receptor levels (**Table 6-S13**). The need for these changes in receptor production and ligand secretion rates may be a result of differences between humans and mice, or underlying compensation mechanisms and physiological changes in the engineered mice [82] not included in this model. Consistent with observations in mice, ligand distribution and VEGFR2 activation are more similar to wild type (baseline) in the $VEGF_{165}$-only than the $VEGF_{121}$-only or $VEGF_{189}$-only cases (**Fig 6-8A-B**). Similar to the baseline case (**Fig 6-5**), where all three isoforms are expressed, with single VEGF isoform expression the ratio of migratory to proliferative signaling downstream of VEGFR2 (pY1214/pY1175) is predicted to increase with isoform length, paralleling the observed phenotypes (**Fig 6-8C**). The model's ability to capture this trend provides qualitative validation of our isoform-specific signaling predictions *in vivo*. Interestingly, the model also predicts other changes, in free VEGF levels in tissue interstitium (**Fig 6-8A**) and in relative activation of VEGFR1 and VEGFR2 (**Fig 6-8B,D, Supplemental Results**).

Figure 6-8: Predicted signaling changes in the human body with expression of single VEGF isoforms mirror experimentally observed murine phenotypes. (A) Levels of free VEGF, PlGF, and sR1 in tissue interstitial fluid, normalized to baseline, when all VEGF production is $VEGF_{121}$, $VEGF_{165}$, or $VEGF_{189}$. **(B)** Endothelial cell surface ligation of VEGFR1 and phosphorylation of VEGFR2. Changes in pR2 and ligated VEGFR2 were very similar. **(C)** Ratio of total VEGFR2 phosphorylation on tyrosine Y1214 to phosphorylation of tyrosine Y1175. **(D)** Percent of ligated EC surface VEGFR1 and VEGFR2 bound to EBM-immobilized ligand.
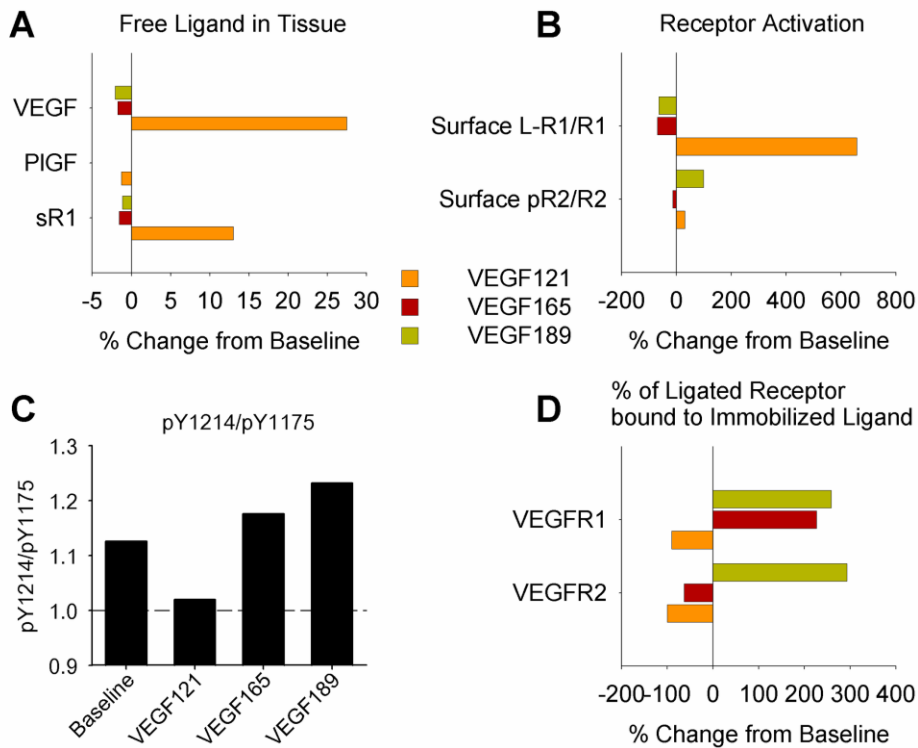
6.4 Discussion

We constructed this computational systems pharmacology model to probe the complexity of VEGF family distribution and signaling in the body, for the first time accounting for the impact of PlGF and of receptor binding by basement membrane-immobilized ligands. In demonstrating the contribution of multiple specific mechanisms to regulation of VEGF family signaling, this model explores the sometimes non-intuitive effects these complex interactions have on VEGFR1 and VEGFR2 activation. This model is based on previously-developed compartment models, leveraging the same structure and geometric parameterization. Despite this commonality, adding to and improving the molecular-level detail resulted in changes to some model predictions, as well as the ability to predict VEGFR2 signaling in more detail than was previously possible (see **Fig 6-9A**).

Figure 6-9: Summary of key model predictions. (A) Overview of key predictions. **(B)** Due to differences in NRP1- and ECM-binding, VEGF isoform-VEGFR2 complexes are trafficked differently, leading to distinct downstream signaling, cellular behavior, and vascular network architecture. **(C)** Summary of predicted ligand binding to VEGFR1 and VEGFR2. All ligands in the respective boxes can bind to VEGFR1 or VEGFR2. The size of the ligands represents the predicted contribution to receptor binding *in vivo*. The model suggests that, for each receptor, a subset of the ligands dominate.

A

Topic	Prediction	Therapeutic Implications
Pharmacokinetics	• ECM-binding properties regulate VEGF, PlGF, and sR1 distribution • sR1 modulates the magnitude of EC receptor activation	• Need to consider isoform properties to predict impact of VEGF, PlGF, or sR1 delivery.
Pharmacodynamics	• Receptor activation is limited by available ligand • NRP1 regulates isoform-specific binding to VEGFR1 vs VEGFR2 and site-specific phosphorylation of VEGFR2 • Substantial VEGFR1 and VEGR2 binding by immobilized ligand	• Increasing receptor levels alone may not be effective • For therapy, precise control of growth factor concentration is critical • Receptor ligation by immobilized ligand may be important *in vivo*
PlGF	• PlGF does not have a substantial impact on VEGFR2 activation; its pro-angiogenic effects are likely via VEGFR1 activation • PlGF & VEGF distribution are distinct	• VEGFR1 may be important for angiogenesis in adults • PlGF is not a good target for altering VEGFR2 activation.
Vascular phenotypes	• Predictions of relative VEGFR2 activation on Y1214 versus Y1175 in human model mirror observed phenotypes in mice	• Better prediction of effects of disease- and therapy-induced changes in VEGF isoforms

B

Isoform	VEGFR2	Signal	Behavior	Vascular Network
VEGF$_{121}$ →	pY1175 →	pERK1/2 →	Proliferation →	High diameter vessels, low branching
VEGF$_{165}$ →	Balanced →	Balanced →	Balanced →	Normal network architecture
VEGF$_{189}$ →	pY1214 →	p-p38 →	Migration →	Low diameter vessels, highly branched

C

VEGFR1

VEGFR2

VEGF$_{121}$
VEGF$_{165}$
VEGF$_{189}$
PlGF1
PlGF2

VEGF$_{121}$
VEGF$_{165}$
VEGF$_{189}$
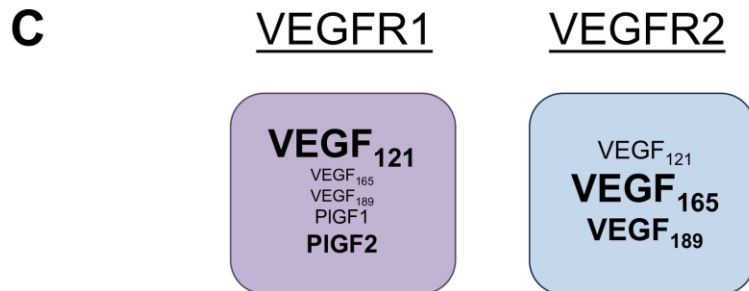
6.4.1 Model provides novel insight into PlGF transport and potential for VEGFR1-dependent PlGF signaling

Our model predicts that, based on their binding properties and *in vivo* concentrations, PlGF and VEGF have distinct distributions within the body. PlGF2, binding to the ECM more strongly than VEGF, is bound to interstitial matrix sites at very high levels (~1 nM in tissue: soluble + ECM-bound + EC-bound predicted, **Fig 6-3C**), forming a large reservoir available for proteolytic release. Despite high tissue PlGF levels, our simulations predict that only about 30% of ligated EC surface VEGFR1 is bound to PlGF. As a result, while most VEGF removal from tissue is predicted to occur via binding to endothelial receptors, only 25% of PlGF was predicted to bind to and be subsequently degraded by endothelial cells. PlGF also binds VEGFR1 on other cells, e.g. monocytes and macrophages, that are implicated in arteriogenesis [26, 83]. We found that removing PlGF or increasing PlGF secretion has only a modest effect on predicted VEGFR2 phosphorylation, while substantially altering VEGFR1 activation (**Fig 6-6A**). This result suggests that observed physiological PlGF-dependent pro-angiogenic effects are likely mediated directly by VEGFR1, either on ECs or other cells, and not via changes in VEGFR2 signaling, contrary to the 'ligand-shifting hypothesis'. This result implicates VEGFR1 in the impaired angiogenic responses to ischemia, wound healing, and cancer [21] observed in mice lacking PlGF. It also implicates VEGFR1 in diseases where PlGF levels are known to change or to be predictive of prognosis, e.g. pre-eclampsia [42] and breast cancer [84]. The pro-angiogenic effects of PlGF likely also rely on its ability to up-regulate other growth factors, including VEGF, FGF2, and PDGF [85, 86].

This result is not inconsistent with recent work by the Alitalo group showing that therapeutic over-expression of VEGFB (which like PlGF binds only VEGFR1) in mice improves metabolic health even following endothelial Flt1 gene deletion, and inhibits doxorubicin-induced cardiotoxicity [54, 87]. Competition between ligands is concentration-dependent, and in these studies, VEGFB protein levels were elevated 20-fold or more in serum, heart, liver, and white adipose tissue. Our model predicts that competition is not a driver of PlGF signaling in physiological conditions, but does not preclude the existence of competition following supraphysiologic therapy. Indeed, at 10-fold PlGF over-expression, outside of the concentration range likely to be observed in untreated healthy or diseased tissue [42], the model does begin to predict an effect on VEGFR2 signaling.

6.4.2 Growth factor immobilization and binding to soluble VEGFR1 predicted to be important for VEGF family signaling in vivo

Both the ECM and sR1 regulate tissue levels of free interstitial VEGF and PlGF, the amount of growth factor available to bind ECs, and the steady-state distribution of ligand throughout the body (**Fig 6-3**). The model predicts that sR1 modulates the magnitude of EC receptor ligation, potentially also altering the balance of signaling via VEGFR1 vs. VEGFR2 (**Fig 6-6G**). This is of therapeutic interest because ratios of VEGF or PlGF to sR1 levels in plasma are increasingly of interest as a biomarker (e.g. in pre-eclampsia) [70], and sR1 levels increase in diabetic mice following hindlimb ischemia [88]. Including binding of immobilized ligands to sR1, and binding of immobilized sR1 to $VEGF_{121}$ and PlGF1, increases total extracellular VEGF and PlGF stored in tissue (**Fig 6-7**). While there is not yet evidence to prove the existence of such complexes, the heparin- and ligand-binding sites on sR1 are distinct, as are the heparin- and receptor-binding domains on VEGF and PlGF, and therefore these complexes are likely.

Unlike matrix-ligand-sR1 complexes, VEGF immobilized to both surfaces and ECM proteins has been shown to bind and activate VEGFR2 *in vitro*, preferentially increasing VEGFR2 activation of tyrosine Y1214, upstream of p38 phosphorylation and migratory cell behavior, demonstrating an important role for physical immobilization of VEGF in signal regulation *in vitro* [18, 19, 89]. However, whether VEGFR2 ligation by immobilized VEGF would occur to any notable extent *in vivo*, and what the physiological impact on EC receptor signaling would be, have been unknown. Here, we saw that including these reactions increased EC receptor ligation and altered VEGFR2 signaling (**Fig 6-7**). While the number of available sites in the EBM is not well-established, our model suggests that these M-L-R complexes may make up a small but significant portion of ligated EC receptors (**Fig 6-4D**). To improve our estimates of the extent of EC receptor ligand by EBM-bound growth factor, it is necessary to obtain better estimates of heparin-binding sites in basement membranes. Interestingly, the fraction of ligated VEGFR1 bound to immobilized ligand was predicted to be higher than that for VEGFR2, owing largely to the strong M-PlGF2 affinity (**Fig 6-6F**). To date, the impact of VEGFR1 ligation by immobilized ligand has not been studied. However, as these are largely PlGF2-VEGFR1 complexes (**Fig 6-6F**), EBM binding site density may shift relative ligation of VEGFR1 by VEGF versus PlGF, which is known to alter VEGFR1-mediated signaling [44]. Spatial patterning of receptor ligation by soluble and immobilized ligand is also likely to be

important, but cannot be examined with this model. Additionally, the potential roles for HSPGs and NRP1 expressed on other cells engaging with VEGFR2 *in trans* [90, 91] are of interest for future study.

6.4.3 Model predicts VEGF isoform-specific activation of VEGFR1 and VEGFR2

We were interested in differences in signaling between VEGF isoforms upon binding to VEGFR1 and VEGFR2. Explicitly simulating VEGFR2 trafficking and site-specific phosphorylation, placed in the context of physiological geometry and transport processes, allowed us to predict isoform-specific VEGFR2 signaling *in vivo* (**Fig 6-5**). Immobilization in the matrix alters VEGF distribution and the resulting signaling, while NRP1 alters VEGF-receptor binding and trafficking. By including these isoform-specific properties, the model predicts that $VEGF_{121}$ induces a shift in VEGFR2 distribution towards early signaling endosomes, decreasing the signaling ratio pY1214/pY1175, and shifting the net cellular signaling towards proliferation. Conversely, a larger portion of VEGFR2 bound to $VEGF_{189}$ was localized on the EC surface at steady-state, increasing pY1214/pY1175, and shifting the balance towards pro-migratory signaling (**Fig 6-5C**). This isoform-specific patterning in VEGFR2 signaling was seen in both the baseline case (**Fig 5C**), with all three VEGF isoforms present, and in cases where only single isoforms of VEGF were expressed (**Fig 6-8C**). This is key validation, as our simulated signaling predictions in humans match the observed vascular phenotypes in mice or tumors expressing single VEGF isoforms (**Fig 6-9B**). Interestingly, in the single isoform cases, change in relative activation of VEGFR1 and VEGFR2 were also predicted (**Fig 6-8B**), which may contribute to these phenotypes [92, 93].

This is in line with another interesting model prediction; while all VEGF isoforms can bind to both VEGFR1 and VEGFR2, physiologically it appears that $VEGF_{165}$ and $VEGF_{189}$ bind almost exclusively to VEGFR2, while $VEGF_{121}$ comprises a large portion of the ligand on VEGFR1, and also binds VEGFR2 to an extent (**Fig 6-4D**). This segregation of ligands suggests that, while ligand levels are limiting for receptor binding, VEGFR1 and VEGFR2 don't directly compete for VEGF *in vivo*, instead binding to largely distinct subsets of ligands dictated primarily by isoform-specific NRP1-binding properties (**Fig 6-9C**). The relative levels of VEGF isoforms are not yet extensively-characterized, but they are known to vary by tissue and to change in disease [69, 82, 94, 95]. As such, this model can be used to understand splicing-induced tissue- and disease-specific changes in VEGF receptor signaling.

6.4.4 Considerations for interpretation of model predictions

Our model is built upon experimental data and a validated model of VEGFR2 signaling *in vitro*, and provides new insight into distribution of and signaling by VEGF and PlGF isoforms *in vivo*. However, when interpreting the results, it is important to acknowledge mismatch between model predictions and experimental measurements, which may result from limitations of our modeling approach, uncertainly in interpretation of experimental measures, and/or missing understanding of underlying biological mechanism. Similar to previous models, our predicted interstitial VEGF concentrations when fitting the model to measured plasma VEGF levels are higher than those measured in tissues using microdialysis. This discrepancy could be due to: difficulty in obtaining accurate measurements for high molecular weight proteins using microdialysis; production of VEGF by blood sources (e.g. PBMCs, platelets) or specific organs (e.g. highly fenestrated tissue), reducing the requisite VEGF production by skeletal muscle; or degradation of VEGF by tissue-resident proteases and/or other cell types expressing VEGF receptors (modeled in [96, 97]). Inclusion of proteases in the model would reduce immobilized growth factor stores at steady state**.** Additionally, as in previous models, the predicted fraction of plasma sR1 bound to ligand was higher than the experimentally-measured fraction. There are other soluble receptors that may be important to consider and are not included here. There may also be limitations with the experimental method that make these *in vivo* measurements inaccurate. To quantify the importance of some difficult-to-measure parameters, as well as reactions included in this model for the first time (some of which have not been explicitly demonstrated experimentally), we analyzed the sensitivity of many new or poorly characterized parameters (see **Fig 6-S3** and **Supplemental Results**).

In order to achieve simulation at the whole body scale, compartment models neglect spatial effects, instead predicting only average values for tissue. The interstitial space of the tissue, the cell surface of endothelial cells and the cell surface of myocytes are still independent entities in this case and each is treated as well-mixed. Detailed study of gradients in interstitial space and along cell surfaces, which are difficult to measure *in vivo* but are likely key to angiogenic signaling, requires development of detailed 2- and 3-dimensional models of tissue and experimental set-ups, calibrated to match predicted average concentrations from compartment models [98-101] such as the one presented here. Much work remains to

fully understand the role of spatial gradients of VEGF distribution and receptor activation in health, disease, and response to therapy.

6.4.5 Conclusions

This model integrates detailed regulation of VEGF and PlGF distribution and binding to EC VEGFR1 and VEGFR2 by sR1, the ECM, and NRP1 into a multi-scale pharmacokinetic/pharmacodynamic (PK/PD) framework. The resulting model predicts that all of these features interact, and contribute to regulation of tissue-level VEGF family signaling. While many model predictions are difficult to validate *in vivo*, the mechanisms included were first modeled using detailed *in vitro* measurements, and validated in many cases on the cellular level, before being put in a physiological context using an existing PK/PD framework. By progressively adding complexity, we can study the impact of each contribution, and compare simulation results to quantities that are measurable and to observable phenotypes, such as the vascular morphologies in mice expressing single isoforms of VEGF. By the same turn, this model provides a window into details of growth factor distribution and signaling that are essentially impossible to measure (especially on the protein level), though in many cases implicated in disease-related impairment in angiogenic response, or targeted by potential therapies. The lack of approved pro-angiogenic therapies to date makes it clear that a better understanding of the molecular mechanisms driving disease is critical to identify more effective drug targets, optimize drug properties (e.g. affinity), and avoid off-target effects leading to toxicity and drug failure [55]. This work can be extended to disease applications with changes in VEGF splicing, and to compare results in humans versus mice, to aid in translation of therapeutics targeting the VEGF system and to further validate the model against data obtained in mice.

6.5 References

1.   Clegg LE, Mac Gabhann F. Systems biology of the microvasculature. Integrative Biology. 2015. doi: 10.1039/C4IB00296B.

2.   Mac Gabhann F, Qutub AA, Annex BH, Popel AS. Systems biology of pro-angiogenic therapies targeting the VEGF system. Wiley Interdisciplinary Reviews-Systems Biology and Medicine. 2010;2(6):694-707. doi: 10.1002/wsbm.92. PubMed PMID: WOS:000283713500006.

3.   Lovett M, Lee K, Edwards A, Kaplan DL. Vascularization Strategies for Tissue Engineering. Tissue Engineering Part B-Reviews. 2009;15(3):353-70. doi: 10.1089/ten.teb.2009.0085. PubMed PMID: WOS:000269621100010.

4.   Auger FA, Gibot L, Lacroix D. The Pivotal Role of Vascularization in Tissue Engineering. Annual Review of Biomedical Engineering, Vol 15. 2013;15:177-200. doi: 10.1146/annurev-bioeng-071812-152428. PubMed PMID: WOS:000323896000009.

5.   Briquez PS, Hubbell JA, Martino MM. Extracellular Matrix-Inspired Growth Factor Delivery Systems for Skin Wound Healing. Advances in Wound Care. 2015.

6.   Grochot-Przeczek A, Dulak J, Jozkowicz A. Therapeutic angiogenesis for revascularization in peripheral artery disease. Gene. 2013;525(2):220-8. doi: 10.1016/j.gene.2013.03.097. PubMed PMID: WOS:000322416200014.

7.   Briquez PS, Clegg LE, Martino MM, Gabhann FM, Hubbell JA. Design principles for therapeutic angiogenic materials. Nature Reviews Materials. 2016;1:15006. doi: 10.1038/natrevmats.2015.6.

8.   Mac Gabhann F, Popel AS. Systems biology of vascular endothelial growth factors. Microcirculation (New York, NY : 1994). 2008;15(8):715-38. PubMed PMID: MEDLINE:18608994.

9.   Koch S, Tugues S, Li X, Gualandi L, Claesson-Welsh L. Signal transduction by vascular endothelial growth factor receptors. Biochemical Journal. 2011;437:169-83. doi: 10.1042/bj20110301. PubMed PMID: WOS:000293156500001.

10.   Koch S, Claesson-Welsh L. Signal Transduction by Vascular Endothelial Growth Factor Receptors. Cold Spring Harbor Perspectives in Medicine. 2012;2(7). doi: 10.1101/cshperspect.a006502. PubMed PMID: WOS:000314279100013.

11.   Ballmer-Hofer K, Andersson AE, Ratcliffe LE, Berger P. Neuropilin-1 promotes VEGFR-2 trafficking through Rab11 vesicles thereby specifying signal output. Blood. 2011;118(3). doi: 10.1182/blood-2011-01-328773. PubMed PMID: WOS:000292967300045.

12.   Gluzman-Poltorak Z, Cohen T, Herzog Y, Neufeld G. Neuropilin-2 and neuropilin-1 are receptors for the 165-amino acid form of vascular endothelial growth factor (VEGF) and of placenta growth factor-2, but only neuropilin-2 functions as a receptor for the 145-amino acid form of VEGF. Journal of Biological Chemistry. 2000;275(24):18040-5. doi: 10.1074/jbc.M909259199. PubMed PMID: WOS:000087659400020.

13.   Vempati P, Popel AS, Mac Gabhann F. Extracellular regulation of VEGF: Isoforms, proteolysis, and vascular patterning. Cytokine & Growth Factor Reviews. 2014;25(1):1-19. doi: http://dx.doi.org/10.1016/j.cytogfr.2013.11.002.

14.   Park JE, Keller GA, Ferrara N. Vascular endothelial growth factor (VEGF) isoforms- Differential deposition into the subepithelial extracellular-matrix and bioactivity of extracellular matrix-bound VEGF. Molecular Biology of the Cell. 1993;4(12):1317-26. PubMed PMID: WOS:A1993MU41300008.

15.   Ruhrberg C, Gerhardt H, Golding M, Watson R, Ioannidou S, Fujisawa H, et al. Spatially restricted patterning cues provided by heparin-binding VEGF-A control blood vessel branching morphogenesis. Genes & Development. 2002;16(20):2684-98. doi: 10.1101/gad.242002. PubMed PMID: WOS:000178645700010.

16.   Grunstein J, Masbad JJ, Hickey R, Giordano F, Johnson RS. Isoforms of vascular endothelial growth factor act in a coordinate fashion to recruit and expand tumor vasculature. Molecular and Cellular Biology. 2000;20(19):7282-91. doi: 10.1128/mcb.20.19.7282-7291.2000. PubMed PMID: WOS:000089268700025.

17.   Lee S, Jilani SM, Nikolova GV, Carpizo D, Iruela-Arispe ML. Processing of VEGF-A by matrix metalloproteinases regulates bioavailability and vascular patterning in tumors. Journal of Cell Biology. 2005;169(4):681-91. doi: 10.1083/jcb.200409115. PubMed PMID: WOS:000229305400016.

18.   Anderson SM, Shergill B, Barry ZT, Manousiouthakis E, Chen TT, Botvinick E, et al. VEGF internalization is not required for VEGFR-2 phosphorylation in bioengineered surfaces with covalently linked VEGF. Integrative Biology. 2011;3(9):887-96. doi: 10.1039/c1ib00037c. PubMed PMID: WOS:000294448600002.

19.   Chen TT, Luque A, Lee S, Anderson SM, Segura T, Iruela-Arispe ML. Anchorage of VEGF to the extracellular matrix conveys differential signaling responses to endothelial cells. Journal of Cell Biology. 2010;188(4):595-609. doi: 10.1083/jcb.200906044. PubMed PMID: WOS:000274723800016.

20.   Clegg LW, Mac Gabhann F. Site-Specific Phosphorylation of VEGFR2 Is Mediated by Receptor Trafficking: Insights from a Computational Model. PLoS Comput Biol. 2015;11(6):e1004158. doi: 10.1371/journal.pcbi.1004158.

21.   Carmeliet P, Moons L, Luttun A, Vincenti V, Compernolle V, De Mol M, et al. Synergism between vascular endothelial growth factor and placental growth factor contributes to angiogenesis and plasma extravasation in pathological conditions. Nature Medicine. 2001;7(5):575-83. doi: 10.1038/87904. PubMed PMID: WOS:000169961100037.

22.   De Falco S. The discovery of placenta growth factor and its biological activity. Experimental and Molecular Medicine. 2012;44(1):1-9. doi: 10.3858/emm.2012.44.1.025. PubMed PMID: WOS:000299765300001.

23.   Migdal M, Huppertz B, Tessler S, Comforti A, Shibuya M, Reich R, et al. Neuropilin-1 is a placenta growth factor-2 receptor. Journal of Biological Chemistry. 1998;273(35):22272-8. doi: 10.1074/jbc.273.35.22272. PubMed PMID: WOS:000075616600019.

24.   Yang W, Ahn H, Hinrichs M, Torry RJ, Torry DS. Evidence of a novel isoform of placenta growth factor (PlGF-4) expressed in human trophoblast and endothelial cells. Journal of Reproductive

Immunology. 2003;60(1):53-60. doi: 10.1016/s0165-0378(03)00082-2. PubMed PMID: WOS:000186441800005.

25. Persico MG, Vincenti V, DiPalma T. Structure, expression and receptor-binding properties of placenta growth factor (PlGF). Vascular Growth Factors and Angiogenesis. 1999;237:31-40. PubMed PMID: WOS:000077725200002.

26. Dewerchin M, Carmeliet P. PlGF: A Multitasking Cytokine with Disease-Restricted Activity. Cold Spring Harbor Perspectives in Medicine. 2012;2(8). doi: 10.1101/cshperspect.a011056. PubMed PMID: WOS:000314279800013.

27. Cao YH, Chen H, Zhou L, Chiang MK, AnandApte B, Weatherbee JA, et al. Heterodimers of placenta growth factor vascular endothelial growth factor - Endothelial activity, tumor cell expression, and high affinity binding to Flk-1/KDR. Journal of Biological Chemistry. 1996;271(6):3154-62. PubMed PMID: WOS:A1996TU69100044.

28. Eriksson A, Cao RH, Pawliuk R, Berg SM, Tsang M, Zhou D, et al. Placenta growth factor-1 antagonizes VEGF-induced angiogenesis and tumor growth by the formation of functionally inactive PlGF-1/VEGF heterodimers. Cancer Cell. 2002;1(1):99-108. doi: 10.1016/s1535-6108(02)00028-4. PubMed PMID: WOS:000178347800014.

29. Reuvekamp A, Velsing-Aarts FV, Poulina IEJ, Capello JJ, Duits AJ. Selective deficit of angiogenic growth factors characterises pregnancies complicated by pre-eclampsia. British Journal of Obstetrics and Gynaecology. 1999;106(10):1019-22. doi: 10.1111/j.1471-0528.1999.tb08107.x. PubMed PMID: WOS:000083214800004.

30. Livingston JC, Chin R, Haddad B, McKinney ET, Ahokas R, Sibai BM. Reductions of vascular endothelial growth factor and placental growth factor concentrations in severe preeclampsia. American Journal of Obstetrics and Gynecology. 2000;183(6):1554-7. doi: 10.1067/mob.2000.108022. PubMed PMID: WOS:000165952000049.

31. Taylor RN, Grimwood J, Taylor RS, McMaster MT, Fisher SJ, North RA. Longitudinal serum concentrations of placental growth factor: Evidence for abnormal placental angiogenesis in pathologic

pregnancies. American Journal of Obstetrics and Gynecology. 2003;188(1):177-82. doi: 10.1067/mob.2003.111. PubMed PMID: WOS:000180676900030.

32.   Maynard SE, Min JY, Merchan J, Lim KH, Li JY, Mondal S, et al. Excess placental soluble fms-like tyrosine kinase 1 (sFlt1) may contribute to endothelial dysfimction, hypertension, and proteinuria in preeclampsia. Journal of Clinical Investigation. 2003;111(5):649-58. doi: 10.1172/jci200317189. PubMed PMID: WOS:000181346600013.

33.   Madazli R, Aydin S, Uludag S, Vildan O, Tolun N. Maternal plasma levels of cytokines in normal and preeclamptic pregnancies and their relationship with diastolic blood pressure and fibronectin levels. Acta Obstetricia Et Gynecologica Scandinavica. 2003;82(9):797-802. doi: 10.1034/j.1600-0412.2003.00206.x. PubMed PMID: WOS:000184719900004.

34.   Tsatsaris V, Goffin F, Munaut C, Brichant JFO, Pignon MR, Noel A, et al. Overexpression of the soluble vascular endothelial growth factor receptor in preeclamptic patients: Pathophysiological consequences. Journal of Clinical Endocrinology & Metabolism. 2003;88(11):5555-63. doi: 10.1210/jc.2003-030528. PubMed PMID: WOS:000186393900077.

35.   Levine RJ, Maynard SE, Qian C, Lim KH, England LJ, Yu KF, et al. Circulating angiogenic factors and the risk of preeclampsia. New England Journal of Medicine. 2004;350(7):672-83. doi: 10.1056/NEJMoa031884. PubMed PMID: WOS:000188869500008.

36.   Muy-Rivera M, Vadachkoria S, Woelk GB, Qiu C, Mahomed K, Williams MA. Maternal plasma VEGF, sVEGF-R1, and PlGF concentrations in preeclamptic and normotensive pregnant Zimbabwean women. Physiological Research. 2005;54(6):611-22. PubMed PMID: WOS:000234481000006.

37.   Staff AC, Braekke K, Harsem NK, Lyberg T, Holthe MR. Circulating concentrations of sFlt1 (soluble fins-like tyrosine kinase 1) in fetal and maternal serum during pre-eclampsia. European Journal of Obstetrics Gynecology and Reproductive Biology. 2005;122(1):33-9. doi: 10.1016/j.ejogrb.2004.11.015. PubMed PMID: WOS:000232419400004.

38.   Krauss T, Pauer HU, Augustin HG. Prospective analysis of placenta growth factor (PIGF) concentrations in the plasma of women with normal pregnancy and pregnancies complicated by

preeclampsia. Hypertension in Pregnancy. 2004;23(1):101-11. doi: 10.1081/prg-120028286. PubMed PMID: WOS:000220710600010.

39.   D'Audigier C, Gautier B, Yon A, Alili JM, Evrard S, Inguimbert N, et al. Targeting VEGFR1 on endothelial progenitors modulates their differentiation potential. Journal of Thrombosis and Haemostasis. 2013;11:332-. PubMed PMID: WOS:000331833602080.

40.   DePrimo SE, Bello CL, Smeraglia J, Baum CM, Spinella D, Rini BI, et al. Circulating protein biomarkers of pharmacodynamic activity of sunitinib in patients with metastatic renal cell carcinoma: modulation of VEGF and VEGF-related proteins. Journal of Translational Medicine. 2007;5. doi: 10.1186/1479-5876-5-32. PubMed PMID: WOS:000248652100001.

41.   Okamoto T, Saito C, Yamada S. Levels of placenta growth factor in gestational trophoblastic diseases. Placenta. 2004;25(10):A5-A. PubMed PMID: WOS:000224487300024.

42.   Bates DO. An unexpected tail of VEGF and PlGF in pre-eclampsia. Biochemical Society Transactions. 2011;39:1576-82. doi: 10.1042/bst20110671. PubMed PMID: WOS:000298200000006.

43.   Hiratsuka S, Minowa O, Kuno J, Noda T, Shibuya M. Flt-1 lacking the tyrosine kinase domain is sufficient for normal development and angiogenesis in mice. Proceedings of the National Academy of Sciences of the United States of America. 1998;95(16):9349-54. doi: 10.1073/pnas.95.16.9349. PubMed PMID: WOS:000075246600053.

44.   Autiero M, Waltenberger J, Communi D, Kranz A, Moons L, Lambrechts D, et al. Role of PIGF in the intra- and intermolecular cross talk between the VEGF receptors Flt1 and Flk1. Nature Medicine. 2003;9(7):936-43. doi: 10.1038/nm884. PubMed PMID: WOS:000183979300036.

45.   Mac Gabhann F, Popel AS. Model of competitive binding of vascular endothelial growth factor and placental growth factor to VEGF receptors on endothelial cells. American Journal of Physiology-Heart and Circulatory Physiology. 2004;286(1). doi: 10.1152/ajpheart.00254.2003. PubMed PMID: WOS:000187350500021.

46.   Mac Gabhann F, Popel AS. Differential binding of VEGF isoforms to VEGF receptor 2 in the presence of neuropilin-1: a computational model. American Journal of Physiology-Heart and Circulatory

Physiology. 2005;288(6):H2851-H60. doi: 10.1152/ajpheart.01218.2004. PubMed PMID: WOS:000229139900040.

47.   Cebe-Suarez S, Zehnder-Fjallman A, Ballmer-Hofer K. The role of VEGF receptors in angiogenesis; complex partnerships. Cellular and Molecular Life Sciences. 2006;63(5):601-15. doi: 10.1007/s00018-005-5426-3. PubMed PMID: WOS:000236203300008.

48.   Park M, Lee ST. The fourth immunoglobulin-like loop in the extracellular domain of FLT-1, a VEGF receptor, includes a major heparin-binding site. Biochemical and Biophysical Research Communications. 1999;264(3):730-4. doi: 10.1006/bbrc.1999.1580. PubMed PMID: WOS:000083666200022.

49.   Orecchia A, Lacal PM, Schietroma C, Morea V, Zambruno G, Failla CM. Vascular endothelial growth factor receptor-1 is deposited in the extracellular matrix by endothelial cells and is a ligand for the alpha 5 beta 1 integrin. Journal of Cell Science. 2003;116(17):3479-89. doi: 10.1242/jcs.00673. PubMed PMID: WOS:000187394900004.

50.   Kendall RL, Wang G, Thomas KA. Identification of a natural soluble form of the vascular endothelial growth factor receptor, FLT-1, and its heterodimerization with KDR. Biochemical and Biophysical Research Communications. 1996;226(2):324-8. doi: 10.1006/bbrc.1996.1355. PubMed PMID: WOS:A1996VJ52500005.

51.   Rossi A, Gauvrit S, Marass M, Pan LY, Moens CB, Stainier DYR. Regulation of Vegf signaling by natural and synthetic ligands. Blood. 2016;128(19):2359-66. doi: 10.1182/blood-2016-04-711192. PubMed PMID: WOS:000388100700013.

52.   Tjwa M, Luttun A, Autiero M, Carmeliet P. VEGF and PlGF: two pleiotropic growth factors with distinct roles in development and homeostasis. Cell and Tissue Research. 2003;314(1):5-14. doi: 10.1007/s00441-003-0776-3. PubMed PMID: WOS:000186541800003.

53.   Park JE, Chen HH, Winer J, Houck KA, Ferrara N. Placenta growth-factor - Potentiation of Vascular Endothelial Growth-Factor Bioactivity, in-vitro and in-vivo, and high-affinity binding to the FLT-

1 but not to FLK-1/KDR. Journal of Biological Chemistry. 1994;269(41):25646-54. PubMed PMID: WOS:A1994PQ49100064.

54.   Robciuc MR, Kivela R, Williams IM, de Boer JF, van Dijk TH, Elamaa H, et al. VEGFB/VEGFR1-Induced Expansion of Adipose Vasculature Counteracts Obesity and Related Metabolic Complications. Cell Metabolism. 2016;23(4):712-24. doi: 10.1016/j.cmet.2016.03.004. PubMed PMID: WOS:000374123200018.

55.   Clegg LE, Mac Gabhann F. Molecular mechanism matters: Benefits of mechanistic computational models for drug development. Pharmacological Research. 2015;99(0):149-54. doi: http://dx.doi.org/10.1016/j.phrs.2015.06.002.

56.   Stefanini MO, Wu FT, Mac Gabhann F, Popel AS. A compartment model of VEGF distribution in blood, healthy and diseased tissues. BMC Systems Biology. 2008;2. doi: 10.1186/1752-0509-2-77. PubMed PMID: WOS:000259952700001.

57.   Wu FTH, Stefanini MO, Gabhann FM, Popel AS. A Compartment Model of VEGF Distribution in Humans in the Presence of Soluble VEGF Receptor-1 Acting as a Ligand Trap. Plos One. 2009;4(4). doi: 10.1371/journal.pone.0005108. PubMed PMID: WOS:000265505700013.

58.   Wu FT, Stefanini MO, Mac Gabhann F, Kontos CD, Annex BH, Popel AS. VEGF and soluble VEGF receptor-1 (sFlt-1) distributions in peripheral arterial disease: an in silico model. Am J Physiol Heart Circ Physiol. 2010;298(6):H2174-91. Epub 2010/04/13. doi: ajpheart.00365.2009 [pii]

10.1152/ajpheart.00365.2009. PubMed PMID: 20382861; PubMed Central PMCID: PMC2886617.

59.   Finley SD, Popel AS. Effect of Tumor Microenvironment on Tumor VEGF During Anti-VEGF Treatment: Systems Biology Predictions. Jnci-Journal of the National Cancer Institute. 2013;105(11):802-11. PubMed PMID: CCC:000320134100011.

60.   Stefanini MO, Wu FTH, Mac Gabhann F, Popel AS. Increase of Plasma VEGF after Intravenous Administration of Bevacizumab Is Predicted by a Pharmacokinetic Model. Cancer Research. 2010;70(23):9886-94. doi: 10.1158/0008-5472.can-10-1419. PubMed PMID: WOS:000285045900038.

61.   Finley SD, Dhar M, Popel AS. Compartment model predicts VEGF secretion and investigates the effects of VEGF trap in tumor-bearing mice. Frontiers in oncology. 2013;3:196-. doi: 10.3389/fonc.2013.00196. PubMed PMID: MEDLINE:23908970.

62.   Yen P, Finley SD, Engel-Stefanini MO, Popel AS. A Two-Compartment Model of VEGF Distribution in the Mouse. Plos One. 2011;6(11). doi: 10.1371/journal.pone.0027514. PubMed PMID: WOS:000297349700055.

63.   Imoukhuede PI, Popel AS. Quantification and cell-to-cell variation of vascular endothelial growth factor receptors. Experimental Cell Research. 2011;317(7):955-65. doi: 10.1016/j.yexcr.2010.12.014. PubMed PMID: WOS:000288822600006.

64.   Vintonenko N, Pelaez-Garavito I, Buteau-Lozano H, Toullec A, Lidereau R, Perret GY, et al. Overexpression of VEGF189 in breast cancer cells induces apoptosis via NRP1 under stress conditions. Cell Adhesion & Migration. 2011;5(4):332-43. doi: 10.4161/cam.5.4.17287. PubMed PMID: WOS:000300713300008.

65.   Hoffmann DC, Willenborg S, Koch M, Zwolanek D, Mueller S, Becker A-KA, et al. Proteolytic Processing Regulates Placental Growth Factor Activities. Journal of Biological Chemistry. 2013;288(25):17976-89. doi: 10.1074/jbc.M113.451831. PubMed PMID: WOS:000320721900005.

66.   Martino MM, Briquez PS, Güç E, Tortelli F, Kilarski WW, Metzger S, et al. Growth Factors Engineered for Super-Affinity to the Extracellular Matrix Enhance Tissue Healing. Science. 2014;343(6173):885-8. doi: 10.1126/science.1247663.

67.   Imoukhuede PI, Popel AS. Expression of VEGF Receptors on Endothelial Cells in Mouse Skeletal Muscle. Plos One. 2012;7(9). doi: 10.1371/journal.pone.0044791. PubMed PMID: WOS:000308738500085.

68.   Nucci M, Poon LC, Demirdjian G, Darbouret B, Nicolaides KH. Maternal Serum Placental Growth Factor (PIGF) Isoforms 1 and 2 at 11-13 Weeks' Gestation in Normal and Pathological Pregnancies. Fetal Diagnosis and Therapy. 2014;36(2):106-16. doi: 10.1159/000357842. PubMed PMID: WOS:000340815100004.

69.   Ng YS, Rohan R, Sunday ME, Demello DE, D'Amore PA. Differential expression of VEGF isoforms in mouse during development and in the adult. Developmental Dynamics. 2001;220(2):112-21. doi: 10.1002/1097-0177(2000). PubMed PMID: WOS:000166693000003.

70.   Wu FTH, Stefanini MO, Mac Gabhann F, Kontos CD, Annex BH, Popel AS. A systems biology perspective on sVEGFR1: its biological function, pathogenic role and therapeutic use. Journal of Cellular and Molecular Medicine. 2010;14(3):528-52. doi: 10.1111/j.1582-4934.2009.00941.x. PubMed PMID: WOS:000276950100006.

71.   Fuh G, Garcia KC, de Vos AM. The interaction of neuropilin-1 with vascular endothelial growth factor and its receptor Flt-1. Journal of Biological Chemistry. 2000;275(35):26690-5. PubMed PMID: WOS:000089144800005.

72.   Pan Q, Chathery Y, Wu Y, Rathore N, Tong RK, Peale F, et al. Neuropilin-1 binds to VEGF(121) and regulates endothelial cell migration and sprouting. Journal of Biological Chemistry. 2007;282(33):24049-56. doi: 10.1074/jbc.M703554200. PubMed PMID: WOS:000248686600030.

73.   Hu S, Sun Y, Meng Y, Wang X, Yang W, Fu W, et al. Molecular architecture of the ErbB2 extracellular domain homodimer. Oncotarget. 2015;6(3):1695-706. PubMed PMID: WOS:000352689800031.

74.   Cho HS, Leahy DJ. Structure of the extracellular region of HER3 reveals an interdomain tether. Science. 2002;297(5585):1330-3. doi: 10.1126/science.1074611. PubMed PMID: WOS:000177573900042.

75.   Cho HS, Mason K, Ramyar KX, Stanley AM, Gabelli SB, Denney DW, et al. Structure of the extracellular region of HER2 alone and in complex with the Herceptin Fab. Nature. 2003;421(6924):756-60. doi: 10.1038/nature01392. PubMed PMID: WOS:000180938000047.

76.   Bruns AF, Bao L, Walker JH, Ponnambalam S. VEGF-A-stimulated signalling in endothelial cells via a dual receptor tyrosine kinase system is dependent on co-ordinated trafficking and proteolysis. Biochemical Society Transactions. 2009;37:1193-7. doi: 10.1042/bst0371193. PubMed PMID: WOS:000272646000008.

77.   Mittar S, Ulyatt C, Howell GJ, Bruns AF, Zachary I, Walker JH, et al. VEGFR1 receptor tyrosine kinase localization to the Golgi apparatus is calcium-dependent. Experimental Cell Research. 2009;315(5):877-89. doi: 10.1016/j.yexcr.2008.12.020. PubMed PMID: WOS:000263859200013.

78.   Filion RJ, Popel AS. A reaction-diffusion model of basic fibroblast growth factor interactions with cell surface receptors. Annals of Biomedical Engineering. 2004;32(5):645-63. doi: 10.1023/b:abme.0000030231.88326.78. PubMed PMID: WOS:000221817600002.

79.   Mac Gabhann F, Popel AS. Interactions of VEGF isoforms with VEGFR-1, VEGFR-2, and neuropilin in vivo: a computational model of human skeletal muscle. American Journal of Physiology-Heart and Circulatory Physiology. 2007;292(1). doi: 10.1152/ajpheart.00637.2006. PubMed PMID: WOS:000243383300055.

80.   Rohrbach DH, Wagner CW, Star VL, Martin GR, Brown KS, Yoon JW. Reduced synthesis of basement-membrane heparan-sulfate proteoglycans in streptozotocin-induced diabetic mice. Journal of Biological Chemistry. 1983;258(19):1672-7. PubMed PMID: WOS:A1983RL31600041.

81.   Yamamoto H, Rundqvist H, Branco C, Johnson RS. Autocrine VEGF Isoforms Differentially Regulate Endothelial Cell Behavior. Frontiers in Cell and Developmental Biology. 2016;4(99). doi: 10.3389/fcell.2016.00099.

82.   Carmeliet P, Ng YS, Nuyens D, Theilmeier G, Brusselmans K, Cornelissen I, et al. Impaired myocardial angiogenesis and ischemic cardiomyopathy in mice lacking the vascular endothelial growth factor isoforms VEGF(164) and VEGF(188). Nature Medicine. 1999;5(5):495-502. doi: 10.1038/8379. PubMed PMID: WOS:000081497400029.

83.   Pipp F, Heil M, Issbrucker K, Ziegelhoeffer T, Martin S, van den Heuvel J, et al. VEGFR-1-selective VEGF homologue PlGF is arteriogenic - Evidence for a monocyte-mediated mechanism. Circulation Research. 2003;92(4):378-85. doi: 10.1161/01.res.0000057997.77714.72. PubMed PMID: WOS:000181448700008.

84.   Escudero-Esparza A, Martin TA, Douglas-Jones A, Mansel RE, Jiang WG. PGF isoforms, PLGF-1 and PGF-2 and the PGF receptor, neuropilin, in human breast cancer: Prognostic significance. Oncology Reports. 2010;23(2):537-44. doi: 10.3892/or_00000667. PubMed PMID: WOS:000273873500032.

85.   Marcellini M, De Luca N, Riccioni T, Ciucci A, Orecchia A, Lacal PM, et al. Increased melanoma growth and metastasis spreading in mice overexpressing placenta growth factor. American Journal of Pathology.   2006;169(2):643-54.   doi: 10.2353/ajpath.2006.051041.   PubMed   PMID: WOS:000239471100028.

86.   Roy H, Bhardwaj S, Babu M, Jauhiainen S, Herzig KH, Bellu AR, et al. Adenovirus-mediated gene transfer of placental growth factor to perivascular tissue induces angiogenesis via upregulation of the expression of endogenous vascular endothelial growth factor-A. Human Gene Therapy. 2005;16(12):1422-8. doi: 10.1089/hum.2005.16.1422. PubMed PMID: WOS:000234253000007.

87.   Räsänen M, Degerman J, Nissinen TA, Miinalainen I, Kerkelä R, Siltanen A, et al. VEGF-B gene therapy inhibits doxorubicin-induced cardiotoxicity by endothelial protection. Proceedings of the National Academy of Sciences. 2016;113(46):13144-9.

88.   Hazarika S, Dokun AO, Li Y, Popel AS, Kontos CD, Annex BH. Impaired angiogenesis after Hindlimb ischemia in type 2 diabetes Mellitus - Differential regulation of vascular endothelial growth factor receptor 1 and soluble vascular endothelial growth factor receptor 1. Circulation Research. 2007;101(9):948-56. doi: 10.1161/circresaha.107.160630. PubMed PMID: WOS:000250617600016.

89.   Martino MM, Tortelli F, Mochizuki M, Traub S, Ben-David D, Kuhn GA, et al. Engineering the Growth Factor Microenvironment with Fibronectin Domains to Promote Wound and Bone Tissue Healing. Science Translational Medicine. 2011;3(100). doi: 10.1126/scitranslmed.3002614. PubMed PMID: WOS:000294841400004.

90.   Jakobsson L, Kreuger J, Holmborn K, Lundin L, Eriksson I, Kjellen L, et al. Heparan sulfate in trans potentiates VEGFR-mediated angiogenesis. Developmental Cell. 2006;10(5):625-34. doi: 10.1016/j.devcel.2006.03.009. PubMed PMID: WOS:000237648800012.

91.   Koch S, van Meeteren LA, Morin E, Testini C, Westrom S, Bjorkelund H, et al. NRP1 Presented in trans to the Endothelium Arrests VEGFR2 Endocytosis, Preventing Angiogenic Signaling and Tumor Initiation. Developmental Cell. 2014;28(6):633-46. doi: 10.1016/j.devcel.2014.02.010. PubMed PMID: WOS:000333765900005.

92.   Fong GH, Rossant J, Gertsenstein M, Breitman ML. ROLE OF THE FLT-1 RECEPTOR TYROSINE KINASE IN REGULATING THE ASSEMBLY OF VASCULAR ENDOTHELIUM. Nature. 1995;376(6535):66-70. doi: 10.1038/376066a0. PubMed PMID: WOS:A1995RH11100063.

93.   Bussolati B, Dunk C, Grohman M, Kontos CD, Mason J, Ahmed A. Vascular endothelial growth factor receptor-1 modulates vascular endothelial growth factor-mediated angiogenesis via nitric oxide. American Journal of Pathology. 2001;159(3):993-1008. doi: 10.1016/s0002-9440(10)61775-0. PubMed PMID: WOS:000170872400026.

94.   Kikuchi R, Nakamura K, MacLauchlan S, Doan Thi-Minh N, Shimizu I, Fuster JJ, et al. An antiangiogenic isoform of VEGF-A contributes to impaired vascularization in peripheral artery disease. Nature Medicine. 2014;20(12):1464-71. doi: 10.1038/nm.3703. PubMed PMID: WOS:000345817900023.

95.   Ngo DTM, Farb MG, Kikuchi R, Karki S, Tiwari S, Bigornia SJ, et al. Antiangiogenic Actions of Vascular Endothelial Growth Factor-A(165)b, an Inhibitory Isoform of Vascular Endothelial Growth Factor-A, in Human Obesity. Circulation. 2014;130(13):1072-80. doi: 10.1161/circulationaha.113.008171. PubMed PMID: WOS:000342685100012.

96.   Vempati P, Mac Gabhann F, Popel AS. Quantifying the Proteolytic Release of Extracellular Matrix-Sequestered VEGF with a Computational Model. Plos One. 2010;5(7). doi: 10.1371/journal.pone.0011860. PubMed PMID: WOS:000280520200024.

97.   Vempati P, Popel AS, Mac Gabhann F. Formation of VEGF isoform-specific spatial distributions governing angiogenesis: computational analysis. BMC Syst Biol. 2011;5:59. Epub 2011/05/04. doi: 10.1186/1752-0509-5-59. PubMed PMID: 21535871; PubMed Central PMCID: PMC3113235.

98.   Chappell JC, Cluceru JG, Nesmith JE, Mouillesseaux KP, Bradley VB, Hartland CM, et al. Flt-1 (VEGFR-1) coordinates discrete stages of blood vessel formation. Cardiovascular Research. 2016;111(1):84-93. doi: 10.1093/cvr/cvw091. PubMed PMID: WOS:000379811800013.

99.   Hashambhoy YL, Chappell JC, Peirce SM, Bautch VL, Mac Gabhann F. Computational modeling of interacting VEGF and soluble VEGF receptor concentration gradients. Front Physiol. 2011;2:62. Epub 2011/10/19. doi: 10.3389/fphys.2011.00062. PubMed PMID: 22007175; PubMed Central PMCID: PMC3185289.

100.   Ji JW, Mac Gabhann F, Popel AS. Skeletal muscle VEGF gradients in peripheral arterial disease: Simulations of rest and exercise. Am J Physiol Heart Circ Physiol. 2007;293:H3740-H9.

101.   Vempati P, Popel AS, Mac Gabhann F. Formation of VEGF isoform-specific spatial distributions governing angiogenesis: computational analysis. BMC Systems Biology. 2011;5. doi: 10.1186/1752-0509-5-59. PubMed PMID: WOS:000291881200001.

6.6 Supplemental Results

6.6.1 Pharmacokinetics & Pharmacodynamics

High immobilized growth factor concentrations in endothelial basement membrane. When the concentration of endothelial basement membrane immobilized growth factor is calculated using the volume of the basement membrane (instead of the total available interstitial space, as the concentration of free ligand is calculated), the concentration of BME-bound ligand is higher than the concentration of free ligand "seen" by endothelial cells for all growth factors (**Figure 6-S2A**). While $VEGF_{121}$ and PlGF1 are only bound to the EBM in complex with sR1, the local "available" (non-sR1-bound) $VEGF_{165}$, $VEGF_{189}$, and PlGF2 concentrations bound to the EBM are in the nanomolar range, far above the picomolar-range concentrations of free VEGF and PlGF in interstitial space. While spatial effects are not taken into account in this compartment model, this may have important implications for relative receptor ligation by free and immobilized growth factor, as well as spatial patterning due to ECM and basement membrane heterogeneity in vivo.

Fractional activation of ligated VEGFR2 is predicted to be VEGF isoform-specific. Our model predicts that the dephosphorylation rates are higher on the cell surface than in early endosomes, and very high in the NRP1-dependent Rab11 recycling pathway, altering the total amount of phosphorylated VEGFR2 in an isoform-specific manner (89.6% of total $VEGF_{121}$-R2, 58.0% of total $VEGF_{165}$-R2, 61.4% of total $VEGF_{189}$-R2) (**Figure 6-S2B**). This novel prediction, suggesting varying "potency" of different VEGF isoforms, is a direct consequence of isoform-specific NRP1- and matrix-binding leading to isoform-specific trafficking. The relative contributions of NRP1-binding and matrix-binding to isoform-specific signaling could be validated experimentally using VEGF isoforms engineered to bind ECM but not NRP1 (e.g.[1]) Note that, while a large quantity of ligated VEGFR2 is present in Rab11 recycling endosomes at steady-state, very little of this VEGFR2 pool is phosphorylated (**Figures 6-4 & 6-5**).

6.6.2 Single VEGF Isoform Expression

Interestingly, the model predicts changes in ligand distribution and receptor activation in our single isoform simulations, compared to the baseline case. Specifically, after fitting to maintain the same plasma VEGF levels as baseline, expression of only $VEGF_{121}$ is predicted to lead to higher tissue levels of

free VEGF (**Figure 6-8A**) than expression of only heparin-binding VEGF isoforms (**Figure 6-8B**). This leads to increased receptor ligation in the $VEGF_{121}$ only case, while $VEGF_{189}$ binds strongly to the ECM, increasing the proportion of surface M-V-R2 complexes substantially (27.1%, compared to 6.9% in baseline case) (**Figure 6-8D**), and retaining VEGFR2 at the cell surface longer. As a result, expression of only $VEGF_{189}$ leads to higher predicted cell surface pR2/R2 than $VEGF_{121}$ alone, while $VEGF_{165}$ alone leads to slightly lower-than-baseline pR2/R2 (**Figure 6-8B**). This is consistent with our baseline observations; when normalized by the fraction of VEGF production for each isoform, $VEGF_{121}$ is over-represented in VEGFR1 ligation, and both $VEGF_{121}$ and $VEGF_{189}$ are over-represented in VEGFR2 ligation (see **Figure 6-3E**). In summary, our model predicts that, compared to baseline, expression of only VEGF-$_{189}$ increases both pY1214/pY1175 and the relative activation of VEGFR2 compared to VEGFR1, while expression of $VEGF_{121}$ alone decreases these quantities. VEGFR1 loss or blockade results in a hyperproliferative vascular phenotype [2, 3], suggesting that the balance of VEGFR1 and VEGFR2 activation may contribute to the observed VEGF isoform-specific phenotypes.

6.6.3 Sensitivity of transport parameters and new reactions included in the model

We analyzed the sensitivity of our model to a few additional parameters whose values are not well-established, as well as a few reactions that have not been clearly demonstrated to occur. We started with NRP1 production, as NRP1 is clearly an important regulator of VEGF-family signaling, as well as the rates for bidirectional vascular permeability, lymphatic drainage, and clearance of growth factors and sR1 from the blood (**Figure 6-S3A**). We increased, then decreased, each rate by a factor of two, and averaged the change from baseline. As anticipated, both ligand distribution and receptor activation were quite sensitive to NRP1 production. The system was less sensitive to changes in transport parameters; perturbations of vascular permeability (k_p) and lymphatic drainage (k_L) resulted in similar changes in ligand distribution and VEGFR1 ligation. Clearance from the blood (k_{CL}) led to large changes only in plasma protein levels.

Next, we examined the effect of removing reactions that have not been proven to occur from the model (**Figure 6-S3B**). We calculated the fold changes in outputs from baseline when a given reaction was removed. Removing binding of sR1 to EC surface NRP1 (to form non-signaling complexes) had a large

256

effect on ligand distribution, as this is a key route of sR1 clearance, and (as a result) also affected receptor activation. Disallowing ligand-binding to sR1-NRP1 complexes had a smaller effect. As the binding properties of PlGF are less well-studied than those of VEGF, we assumed, similar to VEGF, that the shorter PlGF1 can bind to NRP1-VEGFR1 complexes, while PlGF2 cannot. If we remove binding of PlGF1 to NRP1-VEGFR1 complexes, we saw little change aside from the amount of PlGF1 binding to VEGFR1. While immobilized ligand has been shown to bind and activate VEGFR2, the same has not been proven for VEGFR1, or sR1. As such, we examined the effect of allowing these complexes to form with VEGFR2, but not with VEGFR1 or sR1. As expected, we saw large changes in VEGFR1 ligation. While all matrix-ligand-sR1 complexes were lost, there was relatively little change in the amount of ligand bound to matrix alone. As we found earlier that formation of immobilized ligand-sR1 complexes regulates ligand distribution, we looked to see if any of the particular paths to form these complexes were especially sensitive. The sensitivity for removal of any single path was relatively low; the maximum change to the concentration of matrix-ligand-sR1 complexes was 17%. This suggests that the combination of these routes, not a single path, contributes to formation of immobilized ligand-sR1 complexes and regulation of ligand distribution. Note the log scale in **Figure 6-S3B** when comparing these results to **Figure 6-7**.

6.7 Supplemental Figures

Figure 6-S1. Super-sensitivity of steady-state VEGF and VEGFR2 levels, compared to previous model set-up. These panels expands upon the results shown in **Fig 2** of the main manuscript. **(A)** In previous models, surface VEGFR2 levels were fixed (same internalization rate for free and VEGF-bound VEGFR2, no recycling), so increasing VEGF levels would lead to more VEGF-VEGFR2 binding and subsequent degradation of VEGF, keeping the net change in VEGF levels relatively small. **(B)** In this model, trafficking rates are different for free and ligand-bound VEGFR2, so endothelial cell surface VEGFR2 levels are not constant when VEGF levels change. If VEGF levels increase, more VEGFR2 becomes occupied, internalized, and degraded, reducing steady-state VEGFR2 levels and decreasing VEGF consumption via VEGFR2 (purple). Similarly, if VEGFR2 production increases, more VEGF is bound to VEGFR2, internalized, and degraded, reducing steady-state VEGF levels and as a result further increasing surface VEGFR2 (green).
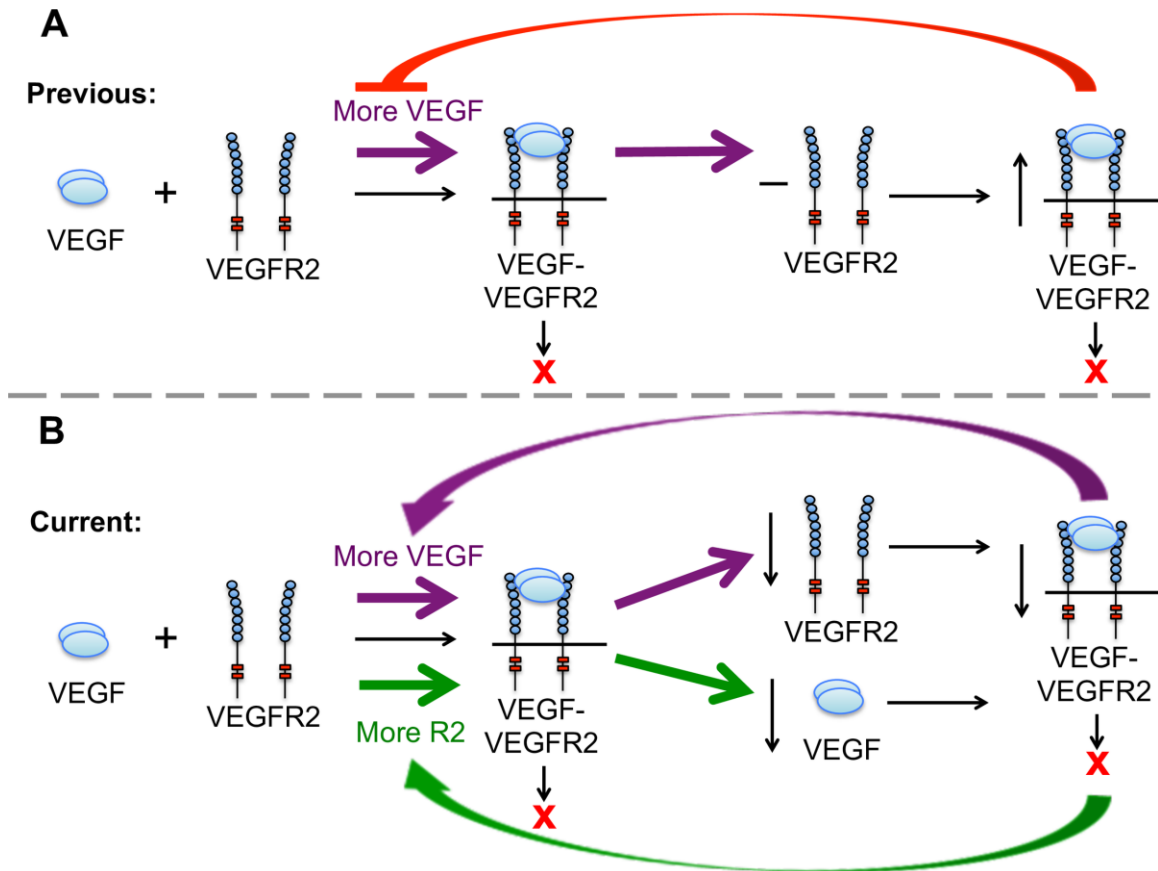
Figure 6-S2. Additional pharmacokinetic/pharmacodynamic predictions of the model. (A) This panel, which shows "local" concentrations of growth factor accessible to endothelial cell receptors, is related to **Fig 4A** of the main manuscript. EBM-bound growth factor concentrations are calculated using the EBM volume, while free levels are calculated using the total available interstitial space. **(B)** This panel expands upon the results shown in **Fig 5** of the main manuscript. For each isoform, total phosphorylated VEGFR2 (pR2) bound to the given ligand is divided by total VEGFR2 bound to the respective ligand.
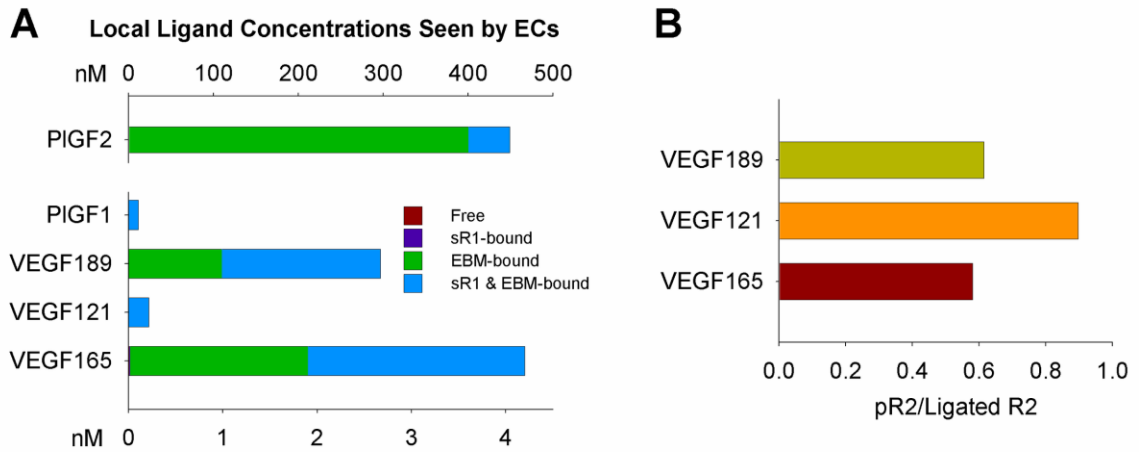
Figure 6-S3. Sensitivity of transport parameters and new or unconfirmed reactions. (A) Sensitivity of

ligand distribution and receptor activation to changes in, from left to right: NRP1 production rate (sN1),

vascular permeability (k_p), lymphatic drainage rate (k_L), and rate of clearance from the blood (k_{CL}). All

tissue quantities are taken from the "Main Body Mass" compartment. Values shown are the average

magnitude of change in a given quantity when the specified parameter is increased or decreased by a factor

of 10 (baseline = 0). Note the different scale on the NRP1 production rate than on the other panels. **(B)**

Changes to ligand distribution and receptor activation when k_{on} for different reactions is set to zero,

prohibiting the selected reactions from occurring. Values shown are fold change from baseline (baseline =

1). Examined reactions are, from left to right: binding of sR1 to EC NRP1 (with or without ligand), binding

of ligand to sR1-N1 complexes, binding of PlGF1 to NRP1-VEGFR1 and NRP1-sR1 complexes, formation

of immobilized ligand-VEGFR1 and immobilized ligand-sR1 complexes (in any form), binding of

$VEGF_{121}$ or PlGF1 to immobilized sR1, binding of free sR1 to matrix proteins (no ligand), binding of

immobilized ligands to sR1 (only), and binding of matrix proteins to $VEGF_{165}$, $VEGF_{189}$, or PlGF2 bound

to sR1. All tissue quantities taken from "Main Body Mass" compartment. Note the different scale on the

sR1-N1 and P1-(N1-R1) panels than on the other panels.
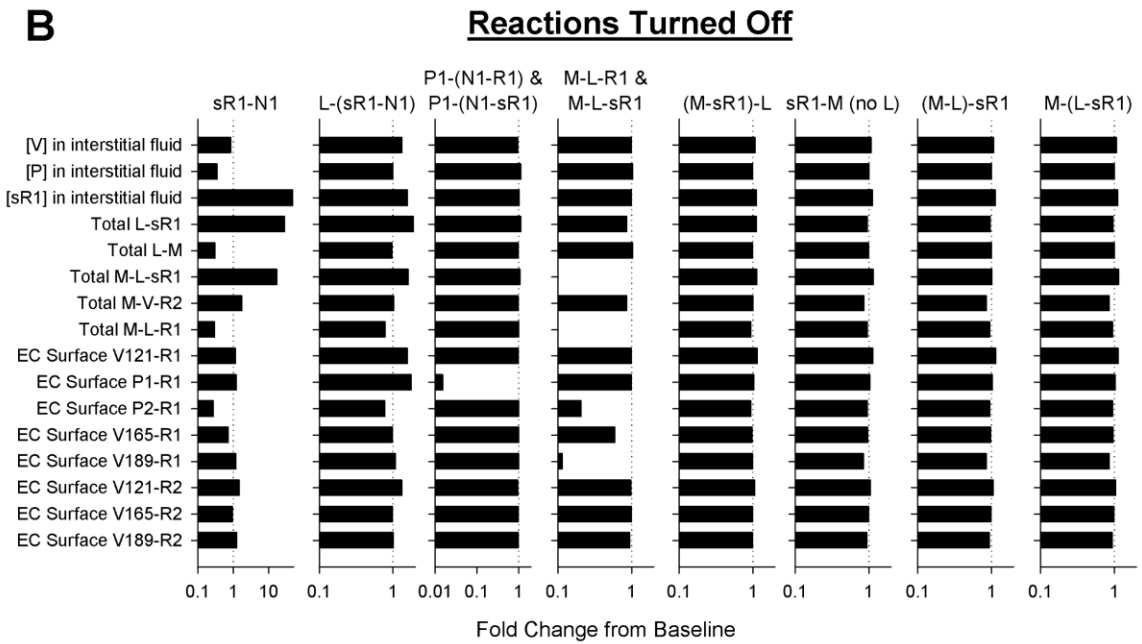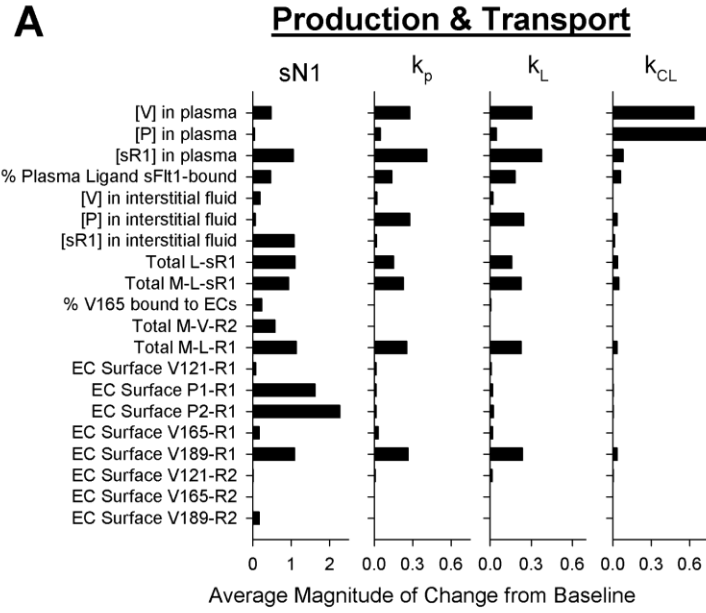
Figure 6-S3

6.8 Supplemental Tables

Table 6-S1. Binding/Unbinding Reactions: K_D in the main body mass.

$\underline{K_D}$	VEGF$_{165}$	VEGF$_{121}$	VEGF$_{189}$	PlGF1	PlGF2	Units	Ref
L-R1	1.0×10^{-15}	1.0×10^{-15}	1.0×10^{-15}	6.9×10^{-15}	6.9×10^{-15}	moles/cm³ tissue	[1, 2]
L-R2	3.0×10^{-15}	3.0×10^{-15}	3.0×10^{-15}	-	-	moles/cm³ tissue	[1, 2]
L-N1	3.6×10^{-14}	-	3.6×10^{-15}	-	1.0×10^{-7}	moles/cm³ tissue	[3, 4]
L-sR1	1.0×10^{-15}	1.0×10^{-15}	1.0×10^{-15}	6.9×10^{-15}	6.9×10^{-15}	moles/cm³ tissue	[1]
L-M	1.8×10^{-12}	-	1.8×10^{-13}	-	1.4×10^{-13}	moles/cm³ tissue	[5]
(M-L)-R1	1.0×10^{-15}	-	1.0×10^{-15}	-	6.9×10^{-15}	moles/cm³ tissue	
(M-L)-R2	3.0×10^{-15}	-	3.0×10^{-15}	-	-	moles/cm³ tissue	
(M-L)-sR1	1.0×10^{-15}	-	1.0×10^{-15}	-	6.9×10^{-15}	moles/cm³ tissue	
M-(L-R1)	1.8×10^{-12}	-	1.8×10^{-13}	-	1.4×10^{-13}	moles/cm³ tissue	
M-(L-R2)	1.8×10^{-12}	-	1.8×10^{-13}	-	-	moles/cm³ tissue	
M-(L-sR1)	1.8×10^{-12}	-	1.8×10^{-13}	-	1.4×10^{-13}	moles/cm³ tissue	
(L-sR1)-M	-	7.2×10^{-13}	-	7.2×10^{-13}	-	moles/cm³ tissue	
(M-sR1)-L	-	6.9×10^{-15}	-	6.9×10^{-15}	-	moles/cm³ tissue	
(N1-L)-R2	7.3×10^{-16}	-	7.3×10^{-16}	-	-	moles/cm³ tissue	
N1-(L-R2)	2.3×10^{-15}	-	2.3×10^{-15}	-	-	moles/cm³ tissue	
(L-R1)-N1	-	7.3×10^{-15}	-	7.3×10^{-15}	-	moles/cm³ tissue	
(L-sR1)-N1	-	5.4×10^{-14}	-	5.4×10^{-14}	-	moles/cm³ tissue	
(N1-R1)-L	-	1.0×10^{-15}	-	1.0×10^{-15}	-	moles/cm³ tissue	
(N1-sR1)-L	-	1.0×10^{-15}	-	1.0×10^{-15}	-	moles/cm³ tissue	
Other	N1-R1	7.3×10^{-15}	moles/cm³ tissue				[1]
	sR1-N1	5.4×10^{-14}	moles/cm³ tissue				[3, 4]
	sR1-M	7.2×10^{-13}	moles/cm³ tissue				

1.   Wu FTH, Stefanini MO, Gabhann FM, Popel AS. A Compartment Model of VEGF Distribution in Humans in the Presence of Soluble VEGF Receptor-1 Acting as a Ligand Trap. Plos One. 2009;4(4). doi: 10.1371/journal.pone.0005108. PubMed PMID: WOS:000265505700013.

2.   Mac Gabhann F, Popel AS. Model of competitive binding of vascular endothelial growth factor and placental growth factor to VEGF receptors on endothelial cells. American Journal of Physiology-Heart and Circulatory Physiology. 2004;286(1). doi: 10.1152/ajpheart.00254.2003. PubMed PMID: WOS:000187350500021.

3.   Vintonenko N, Pelaez-Garavito I, Buteau-Lozano H, Toullec A, Lidereau R, Perret GY, et al. Overexpression of VEGF189 in breast cancer cells induces apoptosis via NRP1 under stress conditions. Cell Adhesion & Migration. 2011;5(4):332-43. doi: 10.4161/cam.5.4.17287. PubMed PMID: WOS:000300713300008.

4.   Hoffmann DC, Willenborg S, Koch M, Zwolanek D, Mueller S, Becker A-KA, et al. Proteolytic Processing Regulates Placental Growth Factor Activities. Journal of Biological Chemistry. 2013;288(25):17976-89. doi: 10.1074/jbc.M113.451831. PubMed PMID: WOS:000320721900005.

5.   Martino MM, Briquez PS, Güç E, Tortelli F, Kilarski WW, Metzger S, et al. Growth Factors Engineered for Super-Affinity to the Extracellular Matrix Enhance Tissue Healing. Science. 2014;343(6173):885-8. doi: 10.1126/science.1247663.

Table 6-S2. Binding/Unbinding Reactions: K_D in healthy calf muscle.

K_D	VEGF$_{165}$	VEGF$_{121}$	VEGF$_{189}$	PlGF1	PlGF2	Units	Ref
L-R1	3.7×10^{-15}	3.7×10^{-15}	3.7×10^{-15}	2.5×10^{-14}	3.7×10^{-15}	moles/cm³ tissue	[1, 2]
L-R2	1.1×10^{-14}	1.1×10^{-14}	1.1×10^{-14}	-	-	moles/cm³ tissue	[1, 2]
L-N1	1.3×10^{-13}	-	1.3×10^{-14}	-	1.1×10^{-11}	moles/cm³ tissue	[3, 4]
L-sR1	3.7×10^{-15}	3.7×10^{-15}	3.7×10^{-15}	2.5×10^{-14}	2.5×10^{-14}	moles/cm³ tissue	[1]
L-M	6.7×10^{-12}	-	6.7×10^{-13}	-	5.1×10^{-13}	moles/cm³ tissue	[5]
(M-L)-R1	3.7×10^{-15}	-	3.7×10^{-15}	-	3.7×10^{-15}	moles/cm³ tissue	
(M-L)-R2	1.1×10^{-14}	-	1.1×10^{-14}	-	-	moles/cm³ tissue	
(M-L)-sR1	3.7×10^{-15}	-	3.7×10^{-15}	-	3.7×10^{-15}	moles/cm³ tissue	
M-(L-R1)	6.7×10^{-12}	-	6.7×10^{-13}	-	5.1×10^{-13}	moles/cm³ tissue	
M-(L-R2)	6.7×10^{-12}	-	6.7×10^{-13}	-	-	moles/cm³ tissue	
M-(L-sR1)	6.7×10^{-12}	-	6.7×10^{-13}	-	5.1×10^{-13}	moles/cm³ tissue	
(L-sR1)-M	-	2.6×10^{-12}	-	2.6×10^{-12}	-	moles/cm³ tissue	
(M-sR1)-L	-	3.7×10^{-15}	-	2.5×10^{-14}	-	moles/cm³ tissue	
(N1-L)-R2	4.4×10^{-16}	-	4.4×10^{-16}	-	-	moles/cm³ tissue	
N1-(L-R2)	1.4×10^{-15}	-	1.4×10^{-15}	-	-	moles/cm³ tissue	
(L-R1)-N1	-	4.4×10^{-15}	-	4.4×10^{-15}	-	moles/cm³ tissue	
(L-sR1)-N1	-	2.0×10^{-13}	-	2.0×10^{-13}	-	moles/cm³ tissue	
(N1-R1)-L	-	3.6×10^{-15}	-	3.6×10^{-15}	-	moles/cm³ tissue	
(N1-sR1)-L	-	3.6×10^{-15}	-	3.6×10^{-15}	-	moles/cm³ tissue	

Other		Units	Ref
N1-R1	4.4×10^{-15}	moles/cm³ tissue	[1]
sR1-N1	2.0×10^{-13}	moles/cm³ tissue	[3, 4]
sR1-M	2.6×10^{-12}	moles/cm³ tissue	

1.   Wu FTH, Stefanini MO, Gabhann FM, Popel AS. A Compartment Model of VEGF Distribution in Humans in the Presence of Soluble VEGF Receptor-1 Acting as a Ligand Trap. Plos One. 2009;4(4). doi: 10.1371/journal.pone.0005108. PubMed PMID: WOS:000265505700013.

2.   Mac Gabhann F, Popel AS. Model of competitive binding of vascular endothelial growth factor and placental growth factor to VEGF receptors on endothelial cells. American Journal of Physiology-Heart

and Circulatory Physiology. 2004;286(1). doi: 10.1152/ajpheart.00254.2003. PubMed PMID: WOS:000187350500021.

3.   Vintonenko N, Pelaez-Garavito I, Buteau-Lozano H, Toullec A, Lidereau R, Perret GY, et al. Overexpression of VEGF189 in breast cancer cells induces apoptosis via NRP1 under stress conditions. Cell Adhesion & Migration. 2011;5(4):332-43. doi: 10.4161/cam.5.4.17287. PubMed PMID: WOS:000300713300008.

4.   Hoffmann DC, Willenborg S, Koch M, Zwolanek D, Mueller S, Becker A-KA, et al. Proteolytic Processing Regulates Placental Growth Factor Activities. Journal of Biological Chemistry. 2013;288(25):17976-89. doi: 10.1074/jbc.M113.451831. PubMed PMID: WOS:000320721900005.

5.   Martino MM, Briquez PS, Güç E, Tortelli F, Kilarski WW, Metzger S, et al. Growth Factors Engineered for Super-Affinity to the Extracellular Matrix Enhance Tissue Healing. Science. 2014;343(6173):885-8. doi: 10.1126/science.1247663.

Table 6-S3. Binding/Unbinding Reactions: K_D in plasma.

K_D	$VEGF_{165}$	$VEGF_{121}$	$VEGF_{189}$	PlGF1	PlGF2	Units	Ref
L-sR1	2.0×10^{-14}	2.0×10^{-14}	2.0×10^{-14}	1.4×10^{-13}	1.4×10^{-13}	moles/cm^3 plasma	[1]

1.   Wu FTH, Stefanini MO, Gabhann FM, Popel AS. A Compartment Model of VEGF Distribution in Humans in the Presence of Soluble VEGF Receptor-1 Acting as a Ligand Trap. Plos One. 2009;4(4). doi: 10.1371/journal.pone.0005108. PubMed PMID: WOS:000265505700013.

Table 6-S4. Binding/Unbinding Reactions: k_{on} in the main body mass.

k_{on}	VEGF$_{165}$	VEGF$_{121}$	VEGF$_{189}$	PlGF1	PlGF2	Units
L-R1	1.0×10^{12}	1.0×10^{12}	1.0×10^{12}	5.0×10^{10}	5.0×10^{10}	(moles/cm^3 tissue)$^{-1}$ s^{-1}
L-R2	3.3×10^{11}	3.3×10^{11}	3.3×10^{11}	-	-	(moles/cm^3 tissue)$^{-1}$ s^{-1}
L-N1	1.7×10^{10}	-	4.7×10^{10}	-	3.3×10^{8}	(moles/cm^3 tissue)$^{-1}$ s^{-1}
L-sR1	1.0×10^{12}	1.0×10^{12}	1.0×10^{12}	5.0×10^{10}	5.0×10^{10}	(moles/cm^3 tissue)$^{-1}$ s^{-1}
L-M	5.3×10^{9}	-	5.3×10^{9}	-	7.3×10^{10}	(moles/cm^3 tissue)$^{-1}$ s^{-1}
(M-L)-R1	1.0×10^{12}	-	1.0×10^{12}	-	5.0×10^{10}	(moles/cm^3 tissue)$^{-1}$ s^{-1}
(M-L)-R2	3.3×10^{11}	-	3.3×10^{11}	-	-	(moles/cm^3 tissue)$^{-1}$ s^{-1}
(M-L)-sR1	1.0×10^{12}	-	1.0×10^{12}	-	5.0×10^{10}	(moles/cm^3 tissue)$^{-1}$ s^{-1}
M-(L-R1)	5.3×10^{9}	-	5.3×10^{9}	-	7.3×10^{9}	(moles/cm^3 tissue)$^{-1}$ s^{-1}
M-(L-R2)	5.3×10^{9}	-	5.3×10^{9}	-	-	(moles/cm^3 tissue)$^{-1}$ s^{-1}
M-(L-sR1)	5.3×10^{9}	-	5.3×10^{9}	-	7.3×10^{9}	(moles/cm^3 tissue)$^{-1}$ s^{-1}
(L-sR1)-M	-	1.4×10^{10}	-	1.4×10^{10}	-	(moles/cm^3 tissue)$^{-1}$ s^{-1}
(M-sR1)-L	-	1.0×10^{12}	-	1.0×10^{12}	-	(moles/cm^3 tissue)$^{-1}$ s^{-1}
(N1-L)-R2	1.4×10^{12}	-	1.4×10^{12}	-	-	(moles/cm^3 tissue)$^{-1}$ s^{-1}
N1-(L-R2)	4.2×10^{11}	-	4.2×10^{11}	-	-	(moles/cm^3 tissue)$^{-1}$ s^{-1}
(L-R1)-N1	-	1.4×10^{12}	-	1.4×10^{12}	-	(moles/cm^3 tissue)$^{-1}$ s^{-1}
(L-sR1)-N1	-	1.9×10^{11}	-	1.9×10^{11}	-	(moles/cm^3 tissue)$^{-1}$ s^{-1}
(N1-R1)-L	-	1.0×10^{12}	-	5.0×10^{10}	-	(moles/cm^3 tissue)$^{-1}$ s^{-1}
(N1-sR1)-L	-	1.0×10^{12}	-	5.0×10^{10}	-	(moles/cm^3 tissue)$^{-1}$ s^{-1}
Other	N1-R1	1.4×10^{12}	(moles/cm^3 tissue)$^{-1}$ s^{-1}			
	sR1-N1	1.9×10^{11}	(moles/cm^3 tissue)$^{-1}$ s^{-1}			
	sR1-M	1.4×10^{11}	(moles/cm^3 tissue)$^{-1}$ s^{-1}			

Table 6-S5. Binding/Unbinding Reactions: k_{on} in healthy calf muscle.

k_{on}	VEGF$_{165}$	VEGF$_{121}$	VEGF$_{189}$	PlGF1	PlGF2	Units
L-R1	2.7×10^{11}	2.7×10^{11}	2.7×10^{11}	1.4×10^{10}	1.4×10^{10}	(moles/cm^3 tissue)$^{-1}$ s^{-1}
L-R2	9.1×10^{10}	9.1×10^{10}	9.1×10^{10}	-	-	(moles/cm^3 tissue)$^{-1}$ s^{-1}
L-N1	4.5×10^{9}	-	1.3×10^{10}	-	9.1×10^{7}	(moles/cm^3 tissue)$^{-1}$ s^{-1}
L-sR1	2.7×10^{11}	2.7×10^{11}	2.7×10^{11}	1.4×10^{10}	1.4×10^{10}	(moles/cm^3 tissue)$^{-1}$ s^{-1}
L-M	1.5×10^{9}	-	1.5×10^{9}	-	2.0×10^{9}	(moles/cm^3 tissue)$^{-1}$ s^{-1}
(M-L)-R1	2.7×10^{11}	-	2.7×10^{11}	-	1.4×10^{10}	(moles/cm^3 tissue)$^{-1}$ s^{-1}
(M-L)-R2	9.1×10^{10}	-	9.1×10^{10}	-	-	(moles/cm^3 tissue)$^{-1}$ s^{-1}
(M-L)-sR1	2.7×10^{11}	-	2.7×10^{11}	-	1.4×10^{10}	(moles/cm^3 tissue)$^{-1}$ s^{-1}
M-(L-R1)	1.5×10^{9}	-	1.5×10^{9}	-	2.0×10^{9}	(moles/cm^3 tissue)$^{-1}$ s^{-1}
M-(L-R2)	1.5×10^{9}	-	1.5×10^{9}	-	-	(moles/cm^3 tissue)$^{-1}$ s^{-1}
M-(L-sR1)	1.5×10^{9}	-	1.5×10^{9}	-	2.0×10^{9}	(moles/cm^3 tissue)$^{-1}$ s^{-1}
(L-sR1)-M	-	3.8×10^{9}	-	3.8×10^{9}	-	(moles/cm^3 tissue)$^{-1}$ s^{-1}
(M-sR1)-L	-	2.7×10^{11}	-	1.4×10^{10}	-	(moles/cm^3 tissue)$^{-1}$ s^{-1}
(N1-L)-R2	2.3×10^{12}	-	2.3×10^{12}	-	-	(moles/cm^3 tissue)$^{-1}$ s^{-1}
N1-(L-R2)	7.0×10^{11}	-	7.0×10^{11}	-	-	(moles/cm^3 tissue)$^{-1}$ s^{-1}
(L-R1)-N1	-	2.3×10^{12}	-	2.3×10^{12}	-	(moles/cm^3 tissue)$^{-1}$ s^{-1}
(L-sR1)-N1	-	5.1×10^{10}	-	5.1×10^{10}	-	(moles/cm^3 tissue)$^{-1}$ s^{-1}
(N1-R1)-L	-	2.7×10^{11}	-	1.4×10^{10}	-	(moles/cm^3 tissue)$^{-1}$ s^{-1}
(N1-sR1)-L	-	2.7×10^{11}	-	1.4×10^{10}	-	(moles/cm^3 tissue)$^{-1}$ s^{-1}
Other	N1-R1	2.3×10^{12}	(moles/cm^3 tissue)$^{-1}$ s^{-1}			
	sR1-N1	5.1×10^{10}	(moles/cm^3 tissue)$^{-1}$ s^{-1}			
	sR1-M	3.8×10^{9}	(moles/cm^3 tissue)$^{-1}$ s^{-1}			

Table 6-S6. Binding/Unbinding Reactions: k_{on} in plasma.

k_{on}	$VEGF_{165}$	$VEGF_{121}$	$VEGF_{189}$	PlGF1	PlGF2	Units
L-sR1	3.3×10^{10}	3.3×10^{10}	3.3×10^{10}	2.5×10^{9}	2.5×10^{9}	(moles/cm^3 tissue)$^{-1}$ s^{-1}

Table 6-S7. Geometric Parameterization.

	Main Body Mass Value	Calf Muscle Value	Units
Compartment Volume	60,453	868	cm^3
Individual Muscle Fiber			
Diameter	71	73	μm
Perimeter correction factor	1.14	1.14	
Perimeter	253	261	μm
FCSA	3904	4173	$μm^2$
Myonuclear density	120	150	mm^{-1}
MDSA	2104	1740	$μm^2$/MD
Muscle Fiber Space			
Muscle fiber density	242	199	fibers/mm^2 tissue
FSAV	611	520	cm^2/cm^3 tissue
Muscle fiber space volume fraction	94.4%	83.1%	cm^3/cm^3 tissue
Individual Capillary			
Luminal diameter	4.86	3.97	μm
Endothelium thickness	0.77	0.78	μm
Abluminal diameter	6.39	5.53	μm
Perimeter correction factor	1.1	1.1	
Abluminal perimeter	22.1	19.1	μm
CCSA	32.1	24.0	$μm^2$
Lumen CSA	18.6	12.4	$μm^2$
Endothelium CSA	13.5	11.6	$μm^2$
ECSA (abluminal)	1000	1000	$μm^2$/EC
Capillary Space			
Capillary:fiber ratio	1.36	1.16	
Capillary density	329	231	capillaries/mm^2 tissue
ESAV (abluminal)	73	44	cm^2/cm^3 tissue
Capillary space volume fraction	1.1%	0.6%	cm^3/cm^3 tissue
Endothelium space	0.4%	0.3%	cm^3/cm^3 tissue
Vascular space	0.6%	0.3%	cm^3/cm^3 tissue
Interstitial Space			
IS volume fraction	4.5%	16.3%	cm^3/cm^3 tissue
IF volume fraction	3.7%	13.7%	cm^3/cm^3 tissue
Available IF volume fraction	3%	11%	cm^3/cm^3 tissue
Extracellular Matrix (ECM)			
ECM volume	3.9%	14.9%	cm^3/cm^3 tissue
	86.72%	91.24%	cm^3/cm^3 IS
Solid fraction	13.40%	13.40%	cm^3/cm^3 ECM
Fluid volume in ECM	3.38%	12.92%	cm^3/cm^3 tissue
	91.13%	94.25%	cm^3/cm^3 IF
Available fluid volume in ECM	2.87%	10.98%	cm^3/cm^3 tissue
Endothelial Basement Membrane (EBM)			
Thickness	87.5	254	nm
EBM volume	0.06%	0.11%	cm^3/cm^3 tissue
	1.41%	0.69%	cm^3/cm^3 IS
Solid fraction	45%	45%	cm^3/cm^3 BME
Fluid volume in EBM	0.03%	0.06%	cm^3/cm^3 tissue
	0.94%	0.45%	cm^3/cm^3 IF
Available fluid volume in EBM	0.01%	0.02%	cm^3/cm^3 tissue
EBM Thickness accessible to EC receptors*	**25**	**25**	**nm**

Fraction EBM accessible to EC receptors	**28.6%**	**9.84%**	**cm^3/cm^3 BME**
Parenchymal Basement Membrane (PBM)			
Thickness	87.5	254	nm
PBM volume	0.53%	1.32%	cm^3/cm^3 tissue
	11.87%	8.07%	cm^3/cm^3 IS
Solid fraction	45%	45%	cm^3/cm^3 BMP
Fluid volume in PBM	0.29%	0.73%	cm^3/cm^3 tissue
	7.92%	5.30%	cm^3/cm^3 IF
Available fluid volume in PBM	0.10%	0.24%	cm^3/cm^3 tissue
Blood Compartment			
Total Volume	5		L
Plasma Fraction	60%		cm^3/cm^3 blood

*Based on length of ErbB2 and ErbB3 extracellular domains (11.3-16.4nm [2-4]), assuming some

flexibility in cell shape and position.

Bold: new parameters

1.   Wu FTH, Stefanini MO, Gabhann FM, Popel AS. A Compartment Model of VEGF Distribution in Humans in the Presence of Soluble VEGF Receptor-1 Acting as a Ligand Trap. Plos One. 2009;4(4). doi: 10.1371/journal.pone.0005108. PubMed PMID: WOS:000265505700013.

2.   Hu S, Sun Y, Meng Y, Wang X, Yang W, Fu W, et al. Molecular architecture of the ErbB2 extracellular domain homodimer. Oncotarget. 2015;6(3):1695-706. PubMed PMID: WOS:000352689800031.

3.   Cho HS, Leahy DJ. Structure of the extracellular region of HER3 reveals an interdomain tether. Science. 2002;297(5585):1330-3. doi: 10.1126/science.1074611. PubMed PMID: WOS:000177573900042.

4.   Cho HS, Mason K, Ramyar KX, Stanley AM, Gabelli SB, Denney DW, et al. Structure of the extracellular region of HER2 alone and in complex with the Herceptin Fab. Nature. 2003;421(6924):756-60. doi: 10.1038/nature01392. PubMed PMID: WOS:000180938000047.

Table 6-S8. Trafficking Parameters (from [1]).

Species Units: s^{-1}	k$_{int}$ (from surface)	k$_{rec4}$ (from Rab4/5)	k$_{rec11}$ (from Rab11)	k$_{4to11}$ (from Rab4/5)	k$_{degr}$ (from Rab4/5)
R2	2.6×10^{-3}	3.8×10^{-3}	1.4×10^{-4}	1.0×10^{-5}	8.6×10^{-6}
V·R2	3.12×10^{-2}	3.8×10^{-3}	1.4×10^{-4}	1.0×10^{-5}	8.6×10^{-5}
M·V·R2	0	-	-	-	-
L	0	0	0	0	1.2×10^{-2}
N1	2.6×10^{-3}	3.8×10^{-5}	1.4×10^{-2}	1.9×10^{-2}	3.8×10^{-4}
V·N1	2.6×10^{-3}	3.8×10^{-5}	1.4×10^{-2}	1.9×10^{-2}	3.8×10^{-4}
V·N1·R2	3.12×10^{-2}	3.8×10^{-5}	1.4×10^{-2}	1.9×10^{-2}	6.8×10^{-4}
R1	2.6×10^{-3}	3.8×10^{-3}	1.4×10^{-4}	1.0×10^{-5}	8.6×10^{-5}
N1·R1	2.6×10^{-3}	3.8×10^{-5}	1.4×10^{-2}	1.9×10^{-2}	3.8×10^{-4}
L·R1	3.12×10^{-2}	3.8×10^{-3}	1.4×10^{-4}	1.0×10^{-5}	8.6×10^{-5}
L·N1·R1	3.12×10^{-2}	3.8×10^{-5}	1.4×10^{-2}	1.9×10^{-2}	3.8×10^{-4}
M·V·R1	0	-	-	-	-
L·sR1	0	0	0	0	1.2×10^{-2}
sR1·N1	2.6×10^{-3}	3.8×10^{-5}	1.4×10^{-2}	1.9×10^{-2}	3.8×10^{-4}
L·sR1·N1	2.6×10^{-3}	3.8×10^{-5}	1.4×10^{-2}	1.9×10^{-2}	3.8×10^{-4}

L: ligand- all trafficking parameters independent of ligand identify. Free sR1 trafficked with same rates as

L·sR1.

1.   Clegg LW, Mac Gabhann F. Site-Specific Phosphorylation of VEGFR2 Is Mediated by Receptor Trafficking: Insights from a Computational Model. PLoS Comput Biol. 2015;11(6):e1004158. doi: 10.1371/journal.pcbi.1004158.

Table 6-S9. Phosphorylation Parameters (from [1]).

	Free R2			V-R2 (not affected by N1 or M)		
	Cell Surface	Rab4/5 Endosomes	Rab11 Endosomes	Cell Surface	Rab4/5 Endosomes	Rab11 Endosomes
k_p (s^{-1})	0	0	0	1	1	1
$k_{dp,Y951}$ (s^{-1})	30	30	30	0.043	75	30
$k_{dp,Y1775}$ (s^{-1})	30	30	30	4.98	0.00972	30
$k_{dp,Y1214}$ (s^{-1})	30	30	30	1.06	0.0307	30

Notes:

k_p: phosphorylation rate constant for all tyrosine sites

k_{dp}: site-specific dephosphorylation rate constant

1.   Clegg LW, Mac Gabhann F. Site-Specific Phosphorylation of VEGFR2 Is Mediated by Receptor Trafficking: Insights from a Computational Model. PLoS Comput Biol. 2015;11(6):e1004158. doi: 10.1371/journal.pcbi.1004158.

Table 6-S10. Transport Parameters

	Permeability (bi-directional)	Lymphatic Drainage (main body mass to blood)	Lymphatic Drainage (calf muscle to blood)	Clearance from Blood
VEGF	4.39×10^{-8} cm/s	0.1418 cm^3/s	0.0026 cm^3/s	1.08×10^{-3} s^{-1}
PlGF	4.39×10^{-8} cm/s	0.1418 cm^3/s	0.0026 cm^3/s	1.08×10^{-3} s^{-1}
sFlt1	1.86×10^{-8} cm/s	0.1418 cm^3/s	0.0026 cm^3/s	5.0×10^{-6} s^{-1}
VEGF-sFlt1	1.86×10^{-8} cm/s	0.1418 cm^3/s	0.0026 cm^3/s	5.0×10^{-6} s^{-1}
PlGF-sFlt1	1.86×10^{-8} cm/s	0.1418 cm^3/s	0.0026 cm^3/s	5.0×10^{-6} s^{-1}

Note: Permeability rates apply to both calf muscle & main body mass. Geometric unit conversions applied

[1].

1.   Clegg LW, Mac Gabhann F. Site-Specific Phosphorylation of VEGFR2 Is Mediated by Receptor

Trafficking: Insights from a Computational Model. PLoS Comput Biol. 2015;11(6):e1004158. doi:

10.1371/journal.pcbi.1004158.

Table 6-S11. Available Matrix Site Densities

	ECM	EBM	PBM
Value (μM)	0.75	20	20
Main Body Mass (moles/cm^3 tissue)	2.15×10^{-11}	2.0×10^{-12}	2.0×10^{-11}
Calf Muscle (moles/cm^3 tissue)	8.24×10^{-11}	4.0×10^{-12}	4.8×10^{-11}

Note: Unit conversions described in [1, 2].

1.   Wu FTH, Stefanini MO, Gabhann FM, Popel AS. A Compartment Model of VEGF Distribution in Humans in the Presence of Soluble VEGF Receptor-1 Acting as a Ligand Trap. Plos One. 2009;4(4). doi: 10.1371/journal.pone.0005108. PubMed PMID: WOS:000265505700013.

2.   Wu FT, Stefanini MO, Mac Gabhann F, Kontos CD, Annex BH, Popel AS. VEGF and soluble VEGF receptor-1 (sFlt-1) distributions in peripheral arterial disease: an in silico model. Am J Physiol Heart Circ Physiol. 2010;298(6):H2174-91. Epub 2010/04/13. doi: ajpheart.00365.2009 [pii]

10.1152/ajpheart.00365.2009. PubMed PMID: 20382861; PubMed Central PMCID: PMC2886617.

Table 6-S12. Production and secretion rates for "MLR" cases (Figure 6-7).

Species	Target Location	Baseline	Cell Only	sR1 Only	No MLR	Production Units
VEGFR1	Main Body Mass	1.162	1.20	1.14	1.175	Change from No VEGF SS
	Calf	1.32	1.42	1.42	1.38	Change from No VEGF SS
VEGFR2	Main Body Mass	32.09	31.10	29.12	28.763	Change from No VEGF SS
	Calf	53.96	52.27	48.9	48.295	Change from No VEGF SS
NRP1	Main Body Mass	1.295	1.285	1.267	1.262	Change from No VEGF SS
	Calf	1.502	1.482	1.455	1.445	Change from No VEGF SS
sR1	Plasma	0.0893	0.0838	0.0856	0.0813	molec/EC/s
PlGF	Plasma	0.0146	0.0144	0.0142	0.0142	molec/MD/s
VEGF	Plasma	0.2830	0.2733	0.2560	0.2522	molec/MD/s

*Note: Both M-L-sR1 and L-sR1-M complexes are included/excluded in "sR1" reactions.

SS: steady-state

Table 6-S13. Production and secretion rates for Single VEGF Isoform cases (Figure 6-8)

Species	Target Location	Baseline	VEGF$_{121}$	VEGF$_{165}$	VEGF$_{189}$	Production Units
VEGFR1	Main Body Mass	1.162	3.40	0.93	0.93	Change from No VEGF SS
	Calf	1.32	5.51	0.932	0.935	Change from No VEGF SS
VEGFR2	Main Body Mass	32.09	14.3	31.465	52.91	Change from No VEGF SS
	Calf	53.96	30.2	52.81	89.42	Change from No VEGF SS
NRP1	Main Body Mass	1.295	1.195	1.285	1.485	Change from No VEGF SS
	Calf	1.502	1.27	1.482	1.823	Change from No VEGF SS
sR1	Plasma	0.0893	0.5564	0.0588	0.0588	molec/EC/s
PlGF	Plasma	0.0146	0.0144	0.0146	0.0146	molec/MD/s
VEGF	Plasma	0.2830	0.3080	0.2637	0.4485	molec/MD/s

SS: steady-state

Chapter 7. The Role of VEGF Splicing in Human Peripheral Artery Disease

Content from this chapter will be submitted for publication as:

L. E. Clegg, V.C. Ganta, B.H. Annex, & F. Mac Gabhann, "Systems pharmacology of VEGF165b in peripheral artery disease."

7.0 Summary

The role of the $VEGF_{165b}$ splice isoform in peripheral artery disease (PAD) has garnered recent interest, but remains poorly understood. $VEGF_{165b}$ lacks the ability to bind to Neuropilin-1 and HSPGs, and activates VEGF receptor 2 (VEGFR2) only weakly *in vitro*. Here, we use a computational systems pharmacology model that explicitly accounts for VEGF isoform ECM- and NRP1-binding, as well as VEGFR2 ligation and site-specific phosphorylation, to bridge from these experimental measurements to insight about $VEGF_{165b}$ distribution and VEGF receptor activation in human PAD. We use both published and previously unpublished experimental data, *in vitro* and in mouse and human skeletal muscle, to build and validate our model. The resulting computational model, which captures all known information about $VEGF_{165b}$ properties and distribution in the human body, provides several novel and non-intuitive insights into $VEGF_{165b}$ mechanism of action. First, the model suggests that blood levels of $VEGF_{165b}$ are not predictive of signaling in tissue. Consistent with *in vitro* observations, the model predicts that $VEGF_{165b}$ is a weak activator of VEGFR2 *in vivo*. Conversely, while the model agrees with experimental evidence of competition between $VEGF_{165a}$ and $VEGF_{165b}$ *in vitro*, simulations shows that these isoforms do not compete for VEGFR2 at much lower physiological concentrations. Instead, the model suggests that reduced $VEGF_{165a}$ expression, concomitant with increasing $VEGF_{165b}$, may drive impaired VEGFR2 signaling in PAD. Interestingly, the model predicts that $VEGF_{165b}$ does compete with other VEGF and PlGF isoforms for binding to VEGFR1, supporting the recently proposed role for VEGFR1 in the pro-angiogenic response to anti-$VEGF_{165b}$ treatment in murine hindlimb ischemia. All together, the model predicts a key role for $VEGF_{165b}$ in PAD, but in a different way than previously hypothesized. This mechanistic insight, which

could not have been obtained via experiment alone, is key to identifying effective pro-angiogenic strategies for PAD treatment.

7.1 Introduction

Peripheral artery disease (PAD) is a manifestation of chronic atherosclerotic disease in which occlusion of small arteries in the legs results in skeletal muscle ischemia, pain and limited mobility[1]. PAD leads to muscle atrophy, capillary rarefaction[2,3], and other anatomical changes to the tissue (e.g. endothelial basement membrane thickening[4]), and eventual below knee or higher amputation in many patients (25-40% 6-month risk with critical limb ischemia[5,6]). Despite this ischemia, sufficient angiogenesis (growth of new capillaries from the existing vascular network) to restore normal perfusion does not appear to occur in PAD. Interestingly, levels of vascular endothelial growth factor (VEGF), considered central to promoting angiogenesis in response to ischemia, are elevated three-fold in plasma[7-10] and are unchanged at rest in muscle biopsies[11] and interstitial fluid of PAD-afflicted muscle[12]. The primary treatments for PAD are: exercise, which can promote VEGF secretion[13] but is often difficult and painful for patients; and surgical revascularization, for which many patients are not suited and which is not always successful[1,5,14]. Following arterial occlusion, remaining blood flow to the foot occurs via new or remodeled collateral vessels; indeed, capillary density is a better predictor of functional performance than arterial-brachial index[2], and angiogenesis is known to precede increases in muscle oxygen uptake in PAD patients[15]. As such, promoting angiogenesis and vascular remodeling to improve muscle perfusion is considered a promising therapeutic avenue. Despite many clinical trials, there are no approved growth factor-based therapies (protein or gene-based delivery of VEGF or fibroblast growth factor-2, or upregulation of these through transcription factors), due to lack of efficacy and some side-effects of excessive vascular permeability[1,16]. While this failure can be partially attributed to poor, spatially inhomogeneous delivery of short duration[17-20], it is also clear that a lack of understanding of the mechanism behind the signaling impairment in PAD limits selection of appropriate therapeutic targets and strategies[21,22]. Computational models provide a unique potential to examine this signaling complexity, bridging observations in cell culture experiments, imperfect animal models of disease, and human PAD patients[23].

The VEGF family is complex, consisting of five ligand genes, including VEGFA and PlGF, three receptors (VEGFR1-3), and multiple coreceptors, including Neuropilin-1 (NRP1)[24]. The VEGF receptors can be alternatively spliced, producing soluble isoforms (e.g. soluble VEGFR1 (sR1)) that can be secreted into the interstitial space, binding to VEGF, PlGF, and heparin sulfate proteoglycans (HSPGs). sR1 levels

are increased in mice following hindlimb ischemia, but not in human PAD[25,26]. VEGFA (hereafter referred to as VEGF), considered the primary pro-angiogenic protein, can be spliced into numerous isoforms, each with different ability to bind to NRP1 and to HSPGs on the cell surface and in the extracellular matrix (ECM). The most prevalent in the human body are: $VEGF_{121}$, which binds to neither ECM nor NRP1; $VEGF_{165}$, which binds to both ECM and NRP1; and $VEGF_{189}$, which binds to ECM more strongly than $VEGF_{165}$[27,28]. These isoform-specific properties have physiological relevance; in murine systems and in human tumors implanted in mice, expression of $VEGF_{121}$ alone leads to formation of vascular networks consisting of small numbers of wide-diameter vessels; expression of $VEGF_{165}$ alone produces a relatively normal phenotype; and expression of $VEGF_{189}$ alone results in a highly branched network of thin vessels[29-35].

Recently, altered expression of additional splice isoforms – the "VEGFxxxb" isoforms, with different C-terminal six amino acids (exon 8) [36,37] – has been measured in several disease conditions, including PAD[38,39], cancer[36,40-42], systemic sclerosis[43], and pre-eclampsia[44]. Changes in VEGF splicing can be induced by specific growth factors[45,46], by exercise[47,48], and by ECM stiffness[49], though the mechanisms involved in disease-induced splicing, and even tissue-specific splicing[50,51], are not well-established. Despite only a small change in sequence, $VEGF_{165b}$, the counterpart of $VEGF_{165a}$, does not bind to NRP1, and did not bind to heparin or HSPGs in three independent *in vitro* studies[52-54]. Additionally, despite binding to VEGFR2 with the same affinity as $VEGF_{165a}$[53,54] (**Fig. 7-1B**), $VEGF_{165b}$ phosphorylates VEGFR2 only weakly, a property hypothesized to result from its lack of NRP1-binding[53]. This poor activation of VEGFR2 suggested that $VEGF_{165b}$ may be anti-angiogenic, acting as a "brake" to prevent binding of "a" isoforms to VEGFR2 and reduce signaling[37,39], though other studies have suggested that "b" isoforms are indeed weakly pro-angiogenic *in vitro* and in tumors[52,55]. Study of the "a" and "b" isoforms *in vivo* has been complicated by difficulties in achieving consistent measurements using current methods, detection of both classes of isoforms by commonly used antibodies, potential differences in splicing between mice and humans[50], and the difficulty of detecting $VEGF_{xxxb}$ mRNA in murine systems[56,57]. As such, while $VEGF_{165b}$ has been detected in healthy humans[58], is secreted at much higher levels by monocytes in the blood of PAD patients than healthy controls[39], and is increased in the adipose tissue of obese patients undergoing bariatric surgery[59], reliable quantification of the total levels of $VEGF_{165a}$ and $VEGF_{165b}$ in healthy and diseased

human tissues and blood remains elusive. Nonetheless, promising improvements in blood flow observed in diabetic mice subjected to hindlimb ischemia following treatment with an anti-VEGF$_{165b}$ antibody[39] suggest that VEGF$_{165b}$ may be an important, albeit poorly understood, missing piece in the PAD puzzle. Using a computational model, we can screen potential ranges of relative secretion of these isoforms, to understand the implications of splicing changes on VEGF distribution and endothelial receptor signaling. This will deepen our understanding of how signaling is perturbed in disease, a critical step in the design of the next generation of pro-angiogenic therapies. We also hope to determine if measurable quantities (e.g. in the plasma) are clinically predictive of disease state, disease progression, and/or therapy effectiveness.

7.1.1 Objectives

Our objective was to develop a systems pharmacology model of endogenous VEGF$_{165b}$ and other VEGF isoforms in peripheral artery disease that can be used to better understand: (1) the distribution of VEGF$_{165b}$ in the body, as compared to VEGF$_{165a}$; (2) the effects of VEGF$_{165b}$ on VEGFR1 and VEGFR2 activation; and (3) resulting signaling changes in PAD (due to altered VEGF$_{165b}$ expression) that may be responsible for the observed impaired angiogenic response to ischemia. We aim to develop a platform that can be used to screen a diverse range of potential pro-angiogenic therapies for PAD. In achieving these objectives, we improve greatly on a previous PK/PD model of PAD[60], which was unable to capture the VEGF distribution and signaling impairment observed in PAD, by incorporating separate simulation of VEGFR2 ligand-binding and site-specific phosphorylation[61,62], and by incorporating recent discoveries about VEGF$_{165b}$ (**Fig 7-1B**) and its relevance to PAD[11,39,59]. By iteratively building upon and validating our models using both previously unpublished and published data, *in vitro* and *in vivo*, we improve the predictive capabilities without adding many parameters at a time. These improvements allow us to predict clinically-relevant quantities that are difficult or impossible to measure *in vivo*, such as VEGF distribution and VEGFR1 and VEGFR2 signaling in muscle tissue, explicitly accounting for physiological processes such as vascular permeability, lymphatic drainage, and protein clearance from blood (**Fig 7-1A**), maintaining physiological levels of ligands and receptors.

Figure 7-1. Overview of model structure and VEGF$_{165b}$ properties. (A) Structure of multi-scale whole-body compartment model, incorporating PAD-specific changes in geometry and molecular expression of the calf muscle, and secretion of VEGF$_{165b}$ into the blood by monocytes. See **Fig 7-S1** for details. **(B)** Comparision of the properties of VEGF$_{165a}$ and VEGF$_{165b}$, which has been shown *in vitro* to lack the ability to bind to heparin/HSPGs and NRP1, and is a weak activator of VEGFR2.
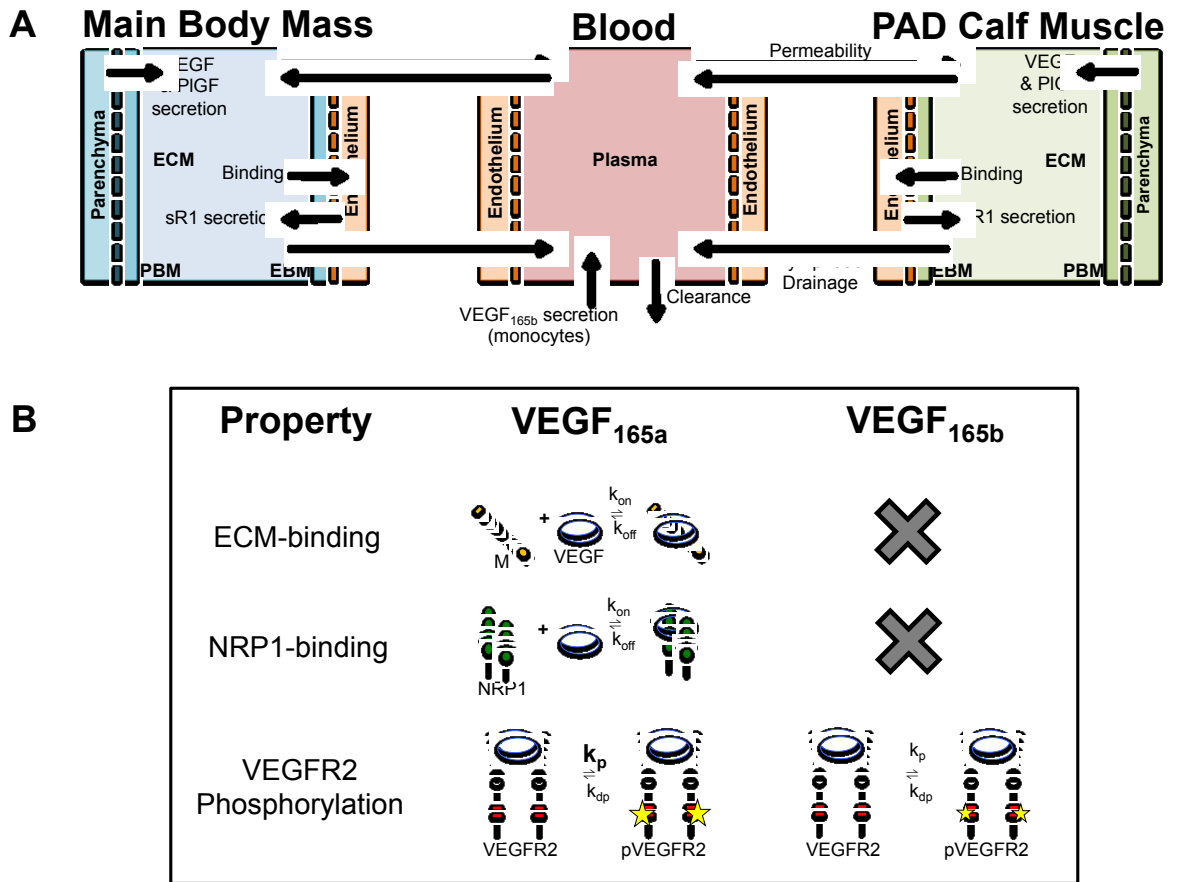
7.2 Results

7.2.1 Modeling the Role of VEGF165b in PAD

To capture the role of $VEGF_{165b}$ in PAD, we incorporated: (1) its measured binding properties (**Fig 7-1B**), (2) varying expression of $VEGF_{165a}$ and $VEGF_{165b}$ in tissue, and (3) secretion of $VEGF_{165b}$ into blood by monocytes. In the tissue compartments, we screened the possible range of relative $VEGF_{165a}$ and $VEGF_{165b}$ expression, maintaining constant free VEGF levels in plasma to mimic the roughly unchanged total VEGF protein and free VEGF in interstitial fluid in human PAD[11,12] (**Fig 7-S2D, Suppl. Model Fitting Section**). In the bloodstream, we then increased secretion of $VEGF_{165b}$ (by monocytes) to capture the roughly 3-fold higher observed serum VEGF in PAD patients than healthy human subjects[39]. Inclusion of this monocyte-derived $VEGF_{165b}$ secretion was necessary to achieve target plasma VEGF levels without the unrealistic tissue VEGF concentrations observed in previous models[60]. The resulting model matches all known information about VEGF distribution in PAD (**Fig 7-2A**).

7.2.2 Pharmacokinetics of $VEGF_{165b}$: Predicted Over-representation in Tissue and Blood

To understand the pharmacokinetics of $VEGF_{165b}$, as compared to $VEGF_{165a}$, we examined the predicted distributions of these isoforms in the PAD Calf Muscle and plasma at steady-state. When $VEGF_{165a}$ and $VEGF_{165b}$ were secreted at equal rates in tissue (fractional $VEGF_{165b}$ secretion = 50%), the model predicts that $VEGF_{165b}$ protein is over-represented compared to $VEGF_{165a}$ in tissue (**Fig 7-2B**), both in extracellular ligand (**Fig 7-S2C**) and endothelial cell-bound ligand (**Fig 7-2B**, orange). This over-representation results from: (a) lack of ECM-binding, leading to 2.4-fold more free $VEGF_{165b}$ than $VEGF_{165a}$ in the PAD Calf Muscle; combined with (b) lack of NRP1-binding slowing binding to VEGFR2 and subsequent recycling, and thus slowing turn-over of $VEGF_{165b}$-VEGFR2 complexes. The model predicts that this over-representation of $VEGF_{165b}$ in total tissue VEGF and free VEGF in blood (**Fig 7-2C**), is predicted to occur at all $VEGF_{165b}$ levels, with a larger difference in blood than tissue due to monocyte secretion of $VEGF_{165b}$ into the bloodstream.

To further probe the differential distribution of $VEGF_{165a}$ and $VEGF_{165b}$, we calculated the net steady-state secretion, transport, consumption, and clearance of each isoform in each compartment, at different fractional $VEGF_{165b}$ secretion rates in the PAD Calf Muscle and Main Body Mass (**Fig 7-2D**). The

first thing to note here is that, consistent with our previous models[60,62,63], most tissue-secreted VEGF is consumed by local endothelial cells. As such, VEGF isoform secretion in one tissue compartment has minimal effect on VEGF isoform concentrations in the other compartment, suggesting that local VEGF isoform secretion is the key driver of local tissue signaling. A small amount of intravasation of $VEGF_{165b}$ and $VEGF_{165a}$ from blood into tissues is predicted only when the two tissue compartments exclusively produce different VEGF isoforms. Over-representation of $VEGF_{165b}$ in free tissue VEGF is evident with equal secretion of the two isoforms (middle).

We next examined the potential of plasma $VEGF_{165b}$ as a biomarker of VEGFR signaling in the PAD Calf Muscle. We found that, due to its larger size, the Main Body Mass is predicted to contribute the bulk of tissue-derived VEGF in the bloodstream (**Fig 7-S2B**); thus blood VEGF isoform levels are likely a poor biomarker of VEGF isoform levels in the PAD Calf Muscle. This prediction is consistent with the lack of correlation between serum $VEGF_{165b}$ and ankle-brachial index in PAD patients as measured by Kikuchi et. al.[39], and highlights the need for tissue biopsy or microdialysis measurements to accurately predict patient-specific signaling state.

Figure 7-2. VEGF$_{165b}$ is predicted to be over-represented in tissue and blood compared to VEGF$_{165a}$.
(A) Comparison of model-predicted VEGF distribution to clinical measurements in PAD patients vs. healthy control subjects. **(B)** Predicted distribution of VEGF and PlGF isoforms and sR1 in the PAD Calf Muscle, with equal secretion of VEGF$_{165a}$ and VEGF$_{165b}$ by parenchymal cells. **(C)** Fraction of total VEGF in plasma and PAD Calf Muscle (Tissue) that is VEGF$_{165a}$ and VEGF$_{165b}$, as a function of the relative fraction of total VEGF$_{165}$ secretion (in both tissue compartments). Note that total free VEGF in plasma is held constant as the relative secretion ratio changes. **(D)** Steady-state net flow profiles for VEGF$_{165a}$ and VEGF$_{165b}$ between the PAD Calf Muscle, Blood, and Main Body Mass, with varying relative secretion of VEGF$_{165a}$ and VEGF$_{165b}$ in the PAD Calf Muscle and Main Body Mass.
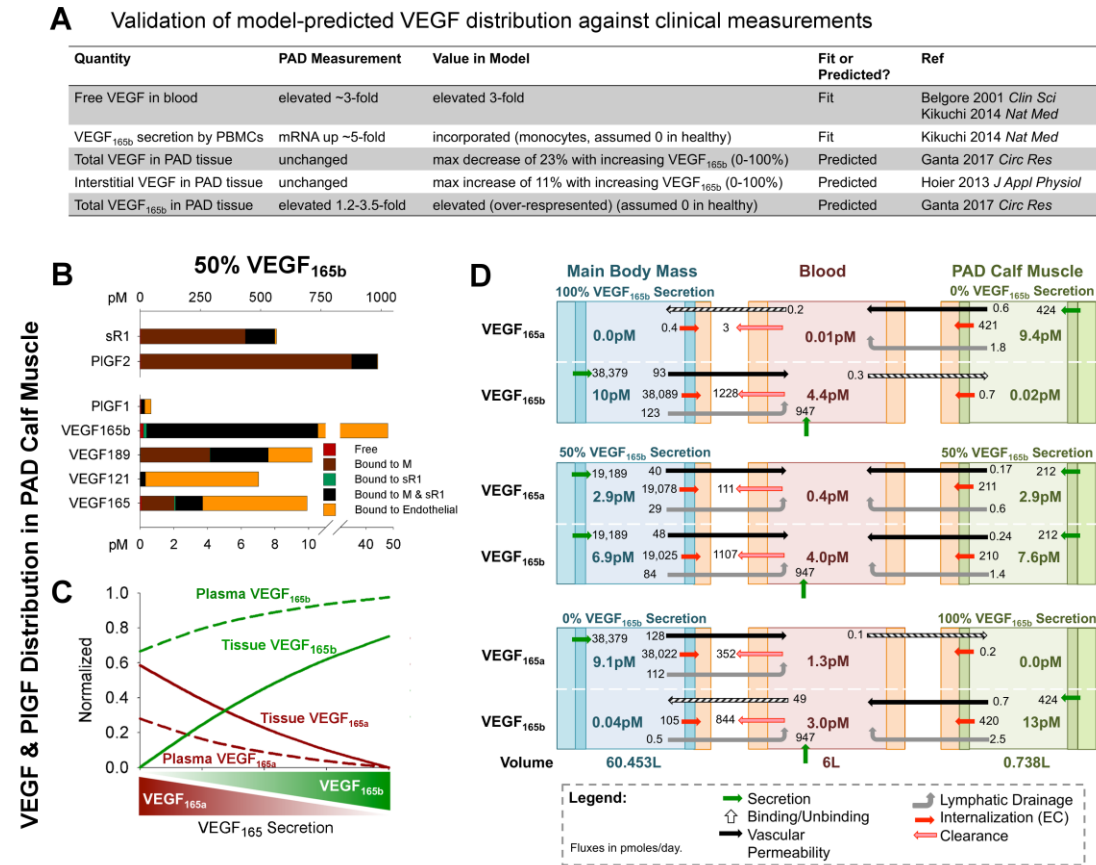
7.2.3 VEGF165b Is Over-represented in Binding to Endothelial VEGFR1 and VEGFR2

We next "zoomed in" on the endothelial-bound fraction of tissue VEGF and PlGF, to examine growth factor binding to endothelial VEGFR1 and VEGFR2. With equal secretion of $VEGF_{165b}$ and $VEGF_{165a}$ in the PAD Calf Muscle, $VEGF_{165b}$ is predicted to dominate binding to both VEGFR1 and VEGFR2 (**Fig 7-3A**), with higher (but still low) receptor occupancy than previously predicted in healthy tissue[62] (**Fig 7-S3A**). The majority of $VEGF_{165b}$-VEGFR2 is predicted to be in early signaling (Rab4/5) endosomes at steady-state, owing to slow recycling resulting from lack of NRP1-binding and subsequent NRP1-mediated recycling. This dominance of VEGFR2 binding by a non-NRP1-binding isoform (60% of total ligand) is in contrast to predicted domination by $VEGF_{165a}$ and $VEGF_{189}$ in healthy tissue in the absence of $VEGF_{165b}$[62]. In the model, we assume that, similar to $VEGF_{121}$, $VEGF_{165b}$ can bind to NRP1-VEGFR1 complexes, allowing $VEGF_{165b}$ to become the dominant VEGFR1 ligand (>80% of total ligand at 50% fractional secretion), a prediction in line with the important role for $VEGF_{165b}$ binding to VEGFR1 highlighted by Ganta et al[11], which would not occur in the absence of $VEGF_{165b}$-NRP1-VEGFR1 complex formation (**Fig 7-S8**). As fractional secretion of $VEGF_{165b}$ increases, the model predicts increasing dominance in receptor binding by $VEGF_{165b}$, with equivalent binding of $VEGF_{165a}$ and $VEGF_{165b}$ to VEGFR2 when only 25% of secreted $VEGF_{165}$ is $VEGF_{165b}$, and even more dramatic increases in $VEGF_{165b}$-VEGFR1 binding (**Fig 7-3B**). As $VEGF_{165b}$ increases, surface endothelial VEGFR1 occupancy is predicted to increase while surface VEGFR2 occupancy is predicted to decrease, and total VEGFR2 occupancy remains constant (**Fig 7-3C**), suggesting a shift in relative signaling by VEGFR2 vs. VEGFR1.

Figure 7-3. VEGF$_{165b}$ is predicted to dominate endothelial receptor binding. (A) Break-down of ligands bound to endothelial VEGFR2 on the cell surface, in early (Rab4/5) endosomes, and recycling (Rab11) endosomes, and cell surface VEGFR1 and NRP1. Unoccupied receptor not shown. Quantities are given in pM of total tissue in the PAD Calf Muscle. Complexes not listed in the legend are present at levels too low to be seen in the figure. **(B)** Fraction of ligand-bound endothelial cell surface VEGFR1 and VEGFR2 bound to VEGF$_{165a}$ and VEGF$_{165b}$, as a function of the relative fraction of total VEGF$_{165}$ secretion that is VEGF$_{165b}$. **(C)** Percentage of endothelial cell surface VEGFR1 and VEGFR2 bound to any ligand, as a function of fractional VEGF$_{165b}$ secretion.
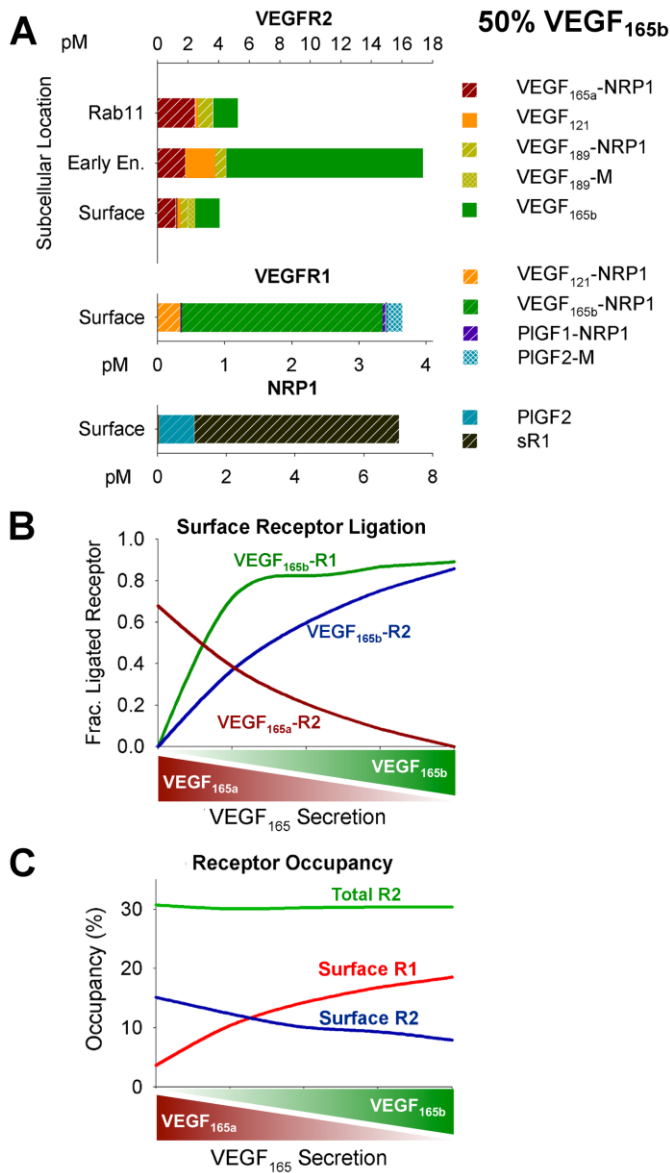
7.2.4 Novel Insight Gained by Testing Mechanistic Hypotheses

What appears to be conflicting information in the literature can sometimes be resolved by using a computational model to directly compare experiments performed under different conditions. Here we use our model to resolve confusion over two key VEGF$_{165b}$ hypotheses.

Hypothesis 1: VEGF$_{165b}$ is a weak activator of VEGFR2. By explicitly simulating VEGFR2 ligand-binding and phosphorylation as separate processes, we can now for the first time account for weak phosphorylation of VEGFR2 by VEGF$_{165b}$, and explore the *in vivo* endothelial signaling implications of increased VEGF$_{165b}$ expression in PAD. We fit the phosphorylation rate constant (k_p) for VEGFR2 upon binding of VEGF$_{165b}$ (as compared to VEGF$_{165a}$) to *in vitro* data from PAECs transfected with VEGFR2 and NRP1 by Kawamura et. al.[52] using our previously-published cell-level model[61] (**Fig 7-4A & Fig 7-S4A**). The required reduction in k_p to fit experimental data (from 1 s^{-1} for VEGF$_{165a}$ to 8×10^{-4} s^{-1} for VEGF$_{165b}$) demonstrates that lack of binding to NRP1 by VEGF$_{165b}$, which is accounted for in our simulations, is not sufficient to explain the weak activation of VEGFR2 observed following stimulation with VEGF$_{165b}$. Together, the experimental data and our model show that, while phosphorylation of VEGF$_{165a}$-VEGFR2 is fast, activation of VEGF$_{165b}$-VEGFR2 is slow compared to VEGF-VEGFR2 binding. We validated this prediction against independent data from *ex vivo* fat pads (**Fig 7-4B**) [59]; the optimized k_p from above (red line) captured a reduction in VEGFR2 phosphorylation as VEGF$_{165b}$ increased, demonstrating the need for this adjustment to accurately predict signaling in tissues.

To validate this mechanistic insight *in vivo*, we compared model predictions of VEGF and VEGF$_{165b}$ protein levels and VEGFR2 activation to measurements in human PAD and murine hindlimb ischemia from an extended analysis of the data presented in Ganta et al[11]. To match the roughly 3-fold increase in VEGF$_{165b}$ observed in human PAD and murine hindlimb ischemia, we compared simulation results for 75% fractional VEGF$_{165b}$ secretion to those for 25% fractional VEGF$_{165b}$ secretion. These simulations predict the effect of changing VEGF$_{165b}$ secretion only; we made no other changes in tissue anatomy or molecular expression. The model accurately captures the increase in VEGF$_{165b}$ without substantial increases in total VEGF or VEGF-R2 observed in PAD patient muscle biopsies, validating the model's predictive power for human PAD (**Fig 7-4C**), and suggesting altered VEGF splicing is a key driver of the observed signaling changes. We also compared these model predictions to murine hindlimb ischemia

(HLI); while tissue VEGF levels increase substantially in HLI, the model accurately captures trends in VEGF binding to VEGFR2 and the observed lack of increase (non-significant decrease) in VEGFR2 phosphorylation (**Fig 7-4D**). This suggests that, while there are many differences between human PAD and murine HLI, receptor-level signaling appear to be similar in this case, giving us confidence in the relevance of comparisons between model predictions and experimental data in mice.

Hypothesis 2: $VEGF_{165b}$ does not compete with $VEGF_{165a}$ for binding to VEGFR2 at physiological concentrations. We leveraged the newly fit and validated model to test the prevailing hypothesis that $VEGF_{165a}$ and $VEGF_{165b}$ compete for binding to VEGFR2, leading to observed reductions in VEGFR2 phosphorylation in some experiments. To do this, we simulated VEGFR2 phosphorylation in cultured endothelial cells following stimulation with $VEGF_{165a}$, $VEGF_{165b}$, or both (**Fig 7-4E**). The model captured experimentally-observed competition at *in vitro* concentrations of 1nM or higher [53,54]. However, competition is concentration-dependent, and the model predicts that, due to low receptor occupancy (**Fig 7-S4B**, dotted lines) at physiological concentrations (1-15pM), $VEGF_{165a}$ and $VEGF_{165b}$ do not compete for VEGFR2 activation *in vivo*. We then further examined signaling *in vivo* using the compartment model, with PAD-specific molecular expression and physiology in the calf muscle. This model predicted that the impaired VEGF receptor signaling with increasing $VEGF_{165b}$ expression observed in PAD results from reduced expression of other VEGF isoforms (as total VEGF levels are unchanged)**,** rather than from competition between VEGF isoforms for receptor binding, as observed *in vitro* (**Fig 7-4E & Fig 7-5D**). This conclusion, which could not have been reached with experiments alone, has important implications for therapy; it suggests strategies designed to increase local $VEGF_{xxxa}$ secretion or delivery will have a larger impact on VEGFR2 phosphorylation than antibody-based therapies designed to remove $VEGF_{165b}$

Putting the above together, we can conclude that: $VEGF_{165b}$ is a weak activator of VEGFR2, but does not compete with $VEGF_{165a}$ for binding to VEGFR2 at physiological concentrations.

Figure 7-4. Implications of weak VEGFR2 phosphorylation by VEGF$_{165b}$ *in vitro* and *in vivo*. (A) The phosphorylation rate for VEGFR2 bound to VEGF$_{165b}$ was fit to *in vitro* data from Kawamura et. al.[52], minimizing the least squared error between data and simulation for the ratio of pR2 when stimulated with VEGF$_{165b}$ or VEGF$_{165a}$ at different concentrations. Axes units: 10^{-4} s^{-1}. **(B)** Validation of optimized k$_p$ value for VEGF$_{165b}$ against measurements of pR2 as a function of relative VEGF$_{165b}$ in *ex vivo* human fat pads as measured by Ngo et. al.[59] **(C-D)** Validation of *in vivo* compartment model against human PAD and mouse hind-limb ischemia measurements from an extended analysis of the data set presented in Ganta et al.[11]. Simulations use values in the PAD calf muscle, with 75% secretion of VEGF$_{165b}$, normalized by the 25% VEGF$_{165b}$ secretion case. **(C)** Human data are total tissue measurements from PAD muscle biopsies, normalized by healthy patient values. Asterisks denote significance using an unpaired, two-tailed t-test with p≤0.05. n=10 PAD subjects, 5 normal subjects for VEGF protein measurements, 6 normal subjects for VEGF-VEGFR binding. **(D)** Mouse measurements are from muscle 3 days after femoral artery ligation, and represent total tissue measurements (receptor-bound ligand and VEGF protein) or CD31+ cells (pR2/R2), normalized by equivalent quantities in the contralateral leg. Asterisks denote significance using an unpaired, two-tailed t-test with p≤0.05. n=4. **(E)** Dose-dependent competition between VEGF$_{165a}$ and VEGF$_{165b}$. pR2 at 5 minutes after VEGF addition, normalized by VEGF$_{165a}$ at each concentration. Simulations performed using endothelial cell culture model including VEGFR2 and NRP1, but not VEGFR1[61].

A *in vitro* parameter fitting: pR2 by VEGF$_{165b}$/VEGF$_{165a}$

B *ex vivo* validation: fat pad explant data

in vivo validation: human PAD and mouse hindlimb ischemia

C Human

D Mouse

E Testing mechanistic hypotheses: Competition between VEGF$_{165a}$ and VEGF$_{165b}$?
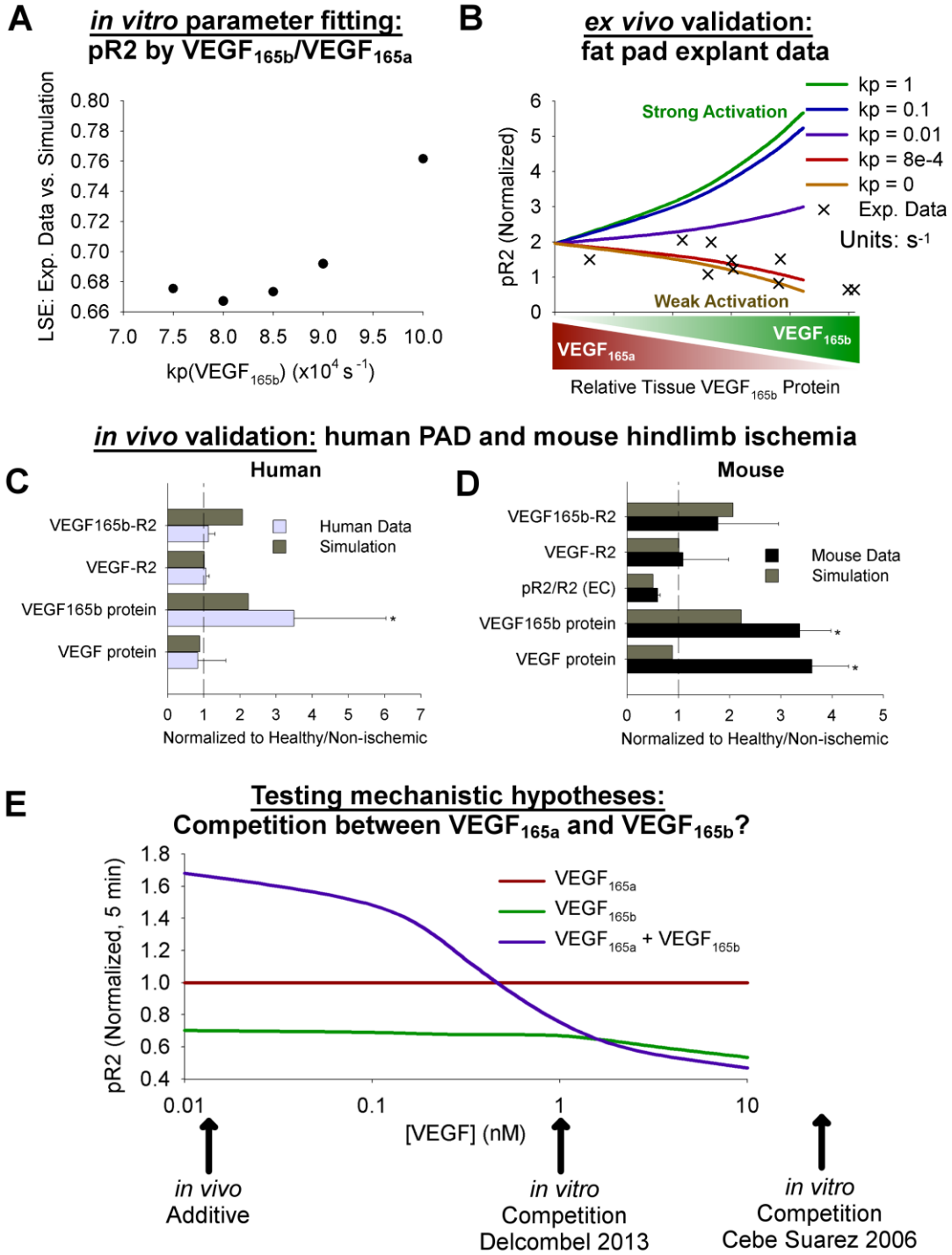
Figure 7-4

7.2.5 VEGF165b regulates signaling of both VEGFR2 and endothelial VEGFR1 in vivo

We next explored model predictions of VEGFR2 phosphorylation and VEGFR1 ligand-binding *in vivo*. Despite being the dominant ligand bound to VEGFR2, $VEGF_{165b}$ is predicted to contribute only modestly to pR2, even without competing with other isoforms for VEGFR2, due to its weak ability to phosphorylate VEGFR2. The fraction of ligand-bound VEGFR2 phosphorylated at steady-state decreasing from 62% with no $VEGF_{165b}$ secretion to 16% with 100% relative $VEGF_{165b}$ secretion (**Fig 7-5A&C, Fig 7-S5A**). Due to the differences in dephosphorylation rates on the cell surface and in endosomes [61], very little $VEGF_{165b}$-R2 is predicted to be phosphorylated on the cell surface, though some $VEGF_{165b}$-R2 phosphorylation in early endosomes is predicted. This leads to a dramatic predicted reduction in pY1214/pY1175 (and relative migratory vs. proliferative downstream signaling) when VEGFR2 is bound to $VEGF_{165b}$ compared to other VEGF isoforms (**Fig 7-5B & Fig 7-S5C**), an unvalidated but experimentally testable model prediction.

A lack of detailed understanding of VEGFR1 phosphorylation by different ligands makes explicit prediction of VEGFR1 signaling difficult, though VEGF and PlGF activate different tyrosine sites[64], and $VEGF_{165b}$ appears not to activate Y1333 on VEGFR1, upstream of STAT3 in PAD[11]. As a step towards this end, we examined the profile of ligands predicted to bind endothelial cell surface VEGFR1 at steady-state, with varying relative $VEGF_{165b}$ secretion (**Fig 7-5E & Fig 7-S5B**). With increasing $VEGF_{165b}$, ligation of VEGFR1 by other VEGF isoforms and by PlGF is predicted to decrease. While expression of $VEGF_{165a}$ is decreasing as $VEGF_{165b}$ increases, PlGF expression remains constant. Thus, this reduction in PlGF-VEGFR1 suggests that, unlike VEGFR2, and consistent with recent data from Ganta et al.[11], competition between $VEGF_{165b}$ and other ligands *does* occur on VEGFR1. This effect is likely magnified by the presence of VEGFR1 on other cell types that play a role in PAD (e.g. monocytes and macrophages), which are not included in this model. Comparing these model predictions of VEGFR1 binding to reduced VEGFR1 Y1333 phosphorylation in murine HLI[11] suggests that both PlGF and non-$VEGF_{165b}$ VEGF isoforms may contribute to VEGFR1 Y1333 phosphorylation (**Fig 7-5F**). The lack of close match in model predictions of VEGF binding to VEGFR1 are likely owing to our incomplete understanding of VEGFR1 signaling and expression on multiple cell types. This result emphasizes the need for careful quantitative

studies to discriminate between physiological and molecular conditions under which competition does or

does not play a role, and to further elucidate the role of VEGFR1 on endothelial and other cells in PAD.

Figure 7-5. *In vivo* **VEGFR activation varies with VEGF$_{165b}$ levels in simulated human PAD. (A)** VEGFR2 phosphorylation (on at least one tyrosine site) as a function of VEGF isoform and subcellular location in the PAD Calf Muscle, with 50% of VEGF$_{165}$ secretion being VEGF$_{165b}$. **(B)** VEGF isoform-specific, NRP1-dependent trafficking and subcellular location-specific dephosphorylation rates for Y1175 and Y1214 lead to isoform-specific predictions of relative activation on Y1175 and Y1214, with VEGF$_{165b}$ favoring pY1175. 50% of VEGF$_{165}$ secretion is VEGF$_{165b}$. **(C)** Comparison of changes in VEGFR2 ligation and phosphorylation by VEGF$_{165b}$, as a function of local fractional VEGF$_{165b}$ secretion. **(D)** Summary of total (cell surface + endosomes) VEGFR2 activation as a function of local fractional VEGF$_{165b}$ secretion. **(E)** Summary of endothelial surface VEGFR1 ligation as a function of local fractional VEGF$_{165b}$ secretion. **(F)** Comparison of experimental VEGF-VEGFR1 and pR1 in murine hindlimb ischemia and model predictions of VEGFR1 ligation. Simulations use values in the PAD Calf Muscle, with 75% secretion of VEGF$_{165b}$, normalized by the 25% VEGF$_{165b}$ secretion case. Mouse measurements are from muscle 3 days after femoral artery ligation, and represent CD31+ cells, normalized by equivalent quantities in the contralateral leg. Asterisks denote significance using an unpaired, two-tailed t-test with $p \leq 0.05$. n= 10.
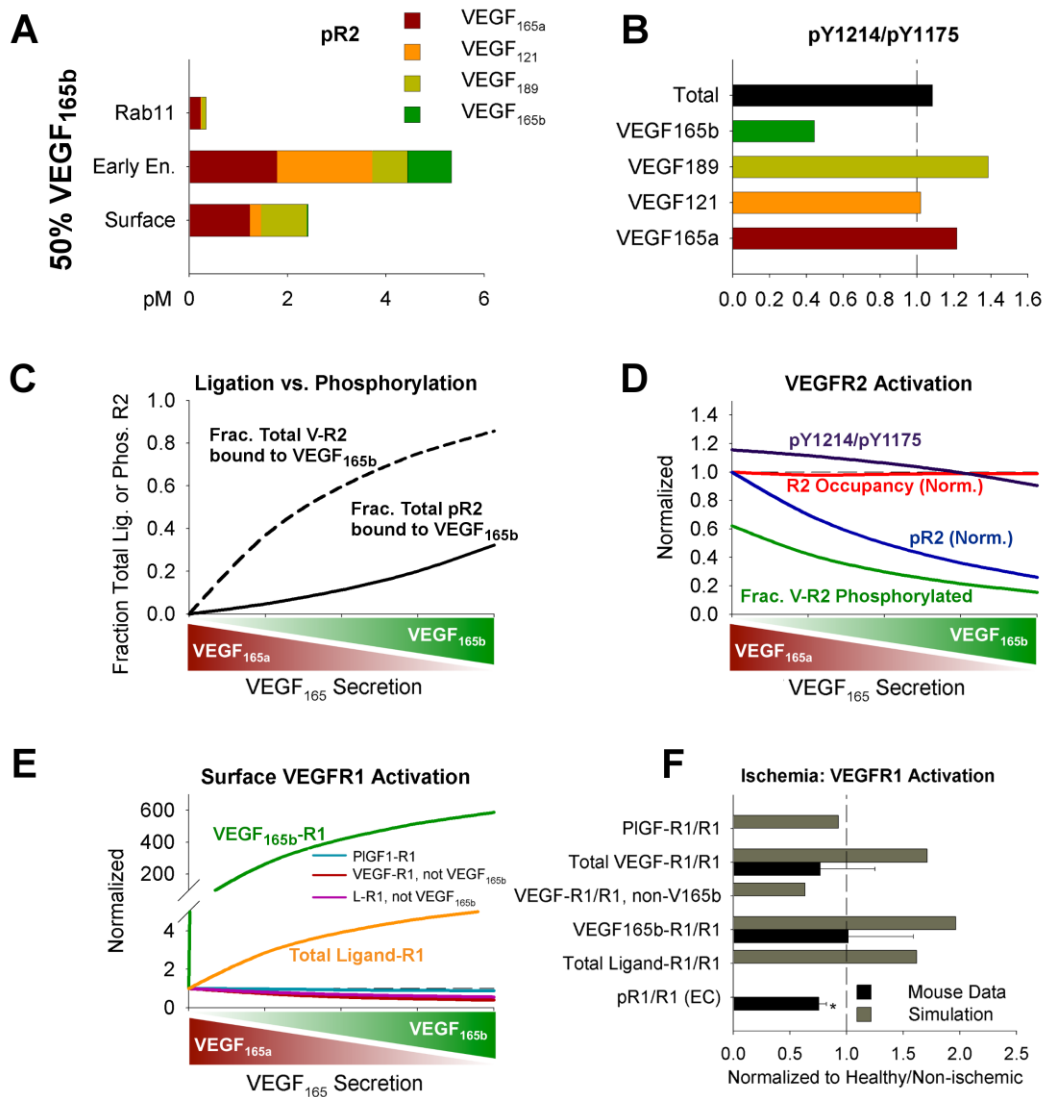
Figure 7-5

7.2.6 VEGF165b over-expression experiments confirm competition for VEGFR1, but not VEGFR2

To this point, we have focused on a switch in expression of $VEGF_{165a}$ and $VEGF_{165b}$, with total VEGF remaining constant. However, this is not an accurate reflection of murine hindlimb ischemia, where total VEGF increases, or time-varying changes in VEGF secretion in exercising humans or during intermittent claudication. As such, we studied the impact of changes in $VEGF_{165b}$ expression, independent of $VEGF_{165a}$ secretion. We first examined experimental over-expression of $VEGF_{165b}$. Using an extended analysis of the data presented in [11], and assuming changes in expression of $VEGF_{165b}$ only, measurements of total VEGFA and $VEGF_{165b}$ suggest that in non-ischemic Balb/c mouse muscle, $VEGF_{165b}$ represents approximately 24% of total VEGF, increasing to 64% in the $VEGF_{165b}$ overexpression experiment. As such, we used 25% fractional $VEGF_{165b}$ secretion as our model baseline, increasing $VEGF_{165b}$ secretion 3.5-fold to match experimental observations. The model mirrors the small (~10%), non-significant increase in VEGFR2 phosphorylation observed experimentally, and predicts decreased PlGF-VEGFR1 binding, potentially consistent with the non-significant decrease in VEGFR1 phosphorylation observed, and again supporting the hypothesis that ligands compete for VEGFR1 but not VEGFR2. We further investigated the sensitivity of VEGFR1 and VEGFR2 signaling to small changes in $VEGF_{165b}$ expression (**Fig 7-6C** & **Fig 7-S6A**). The model predicts that VEGFR1 is consistently more sensitive to changes in $VEGF_{165b}$ expression than VEGFR2, and that signaling changes less in response to varying $VEGF_{165b}$ than varying $VEGF_{165a}$ (**Fig 7-6C & Fig 7-S6B**).

An open question in the field is whether $VEGF_{165b}$ detected in serum is found in plasma or only in formed elements (e.g. PBMCs, platelets). To examine the impact of freely available VEGF in the bloodstream, we turned off secretion of $VEGF_{165b}$ by monocytes into the blood. The model predicts very little (<1%) change in VEGF levels or signaling in the PAD Calf Muscle (**Fig 7-6D**), reinforcing our earlier conclusion that tissue secretion is the key driver of local signaling, and suggesting that whether or not high free $VEGF_{165b}$ is present in plasma is not important for angiogenic impairment in PAD. We also explored the possibility that some monocyte-derived $VEGF_{165b}$ is secreted into tissues instead of the bloodstream (**Fig 7-S6D**).

Figure 7-6. Non-switch-like changes in VEGF$_{165b}$ expression affect VEGFR1 activation more than VEGFR2 activation. (A-B) Validation of *in vivo* compartment model against mouse VEGF$_{165b}$ overexpression, from an extended analysis of the data set presented in Ganta et al.[11]. Simulations use values in the PAD Calf Muscle, using the 25% VEGF$_{165b}$ secretion case as the non-ischemic baseline, and increasing VEGF$_{165b}$ expression to mirror the experimental increase in VEGF$_{165b}$ protein. Mouse measurements are taken from non-ischemic muscle 7 days after transfection with VEGF$_{165b}$ plasmid or a control plasmid, and represent total tissue measurements (receptor-bound ligand and VEGF protein) or CD31+ cells (pR1/R1), normalized by equivalent quantities in the control group. **(A)** VEGF protein and endothelial VEGFR2 phosphorylation. Asterisks denote significance using an unpaired, two-tailed t-test with $p \leq 0.05$. n=4. **(B)** Experimental endothelial VEGFR1 phosphorylation, compared to simulated break-down of VEGFR1 ligand-binding. n=4. **(C)** Simulation of direct increases or decreases in local VEGF$_{165b}$ secretion in the PAD Calf Muscle, at 50% fractional VEGF$_{165b}$ secretion in both tissue compartments, normalized to baseline quantities. **(D)** Predicted impact of removing monocyte secretion of VEGF$_{165b}$ into the bloodstream on quantities in the PAD Calf Muscle.
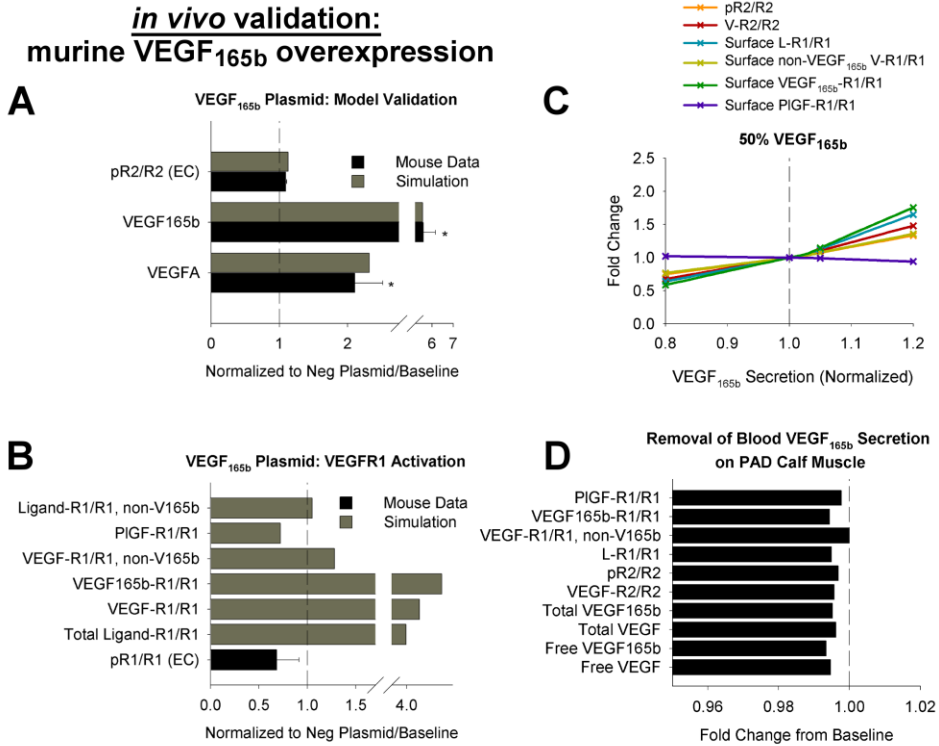
7.2.7 Other potential contributions to impaired angiogenesis in PAD

Finally, we examined other potential, non-VEGF$_{165b}$-related contributions to impaired signaling in PAD. We compared predicted signaling in a PAD Calf Muscle, a Healthy Calf Muscle[62], and a PAD Calf Muscle with healthy endothelial receptor expression, or healthy permeability levels (**Fig 7-S7**). We found that only receptor expression levels had a noticeable impact on VEGFR2 phosphorylation, suggesting potential value in receptor-targeted gene therapy. It, however, remains an open question whether the total number of phosphorylated receptors or activated fraction is key to signaling.

7.3 Discussion

Our objective in building this model was to investigate in detail the implications of the experimentally-measured properties of $VEGF_{165b}$ – lack of ECM-binding, lack of NRP1-binding, and weak phosphorylation of VEGFR2 – on the role of this isoform in peripheral artery disease. We leveraged a previously-built and validated computational model that accounts explicitly for differences in ECM- and NRP1-binding by VEGF isoforms, as well as simulating binding, trafficking, and tyrosine site-specific phosphorylation of VEGFR2 as distinct, though related, processes[62]. This framework enabled us to directly implement the unique properties of $VEGF_{165b}$, making predictions of disease-specific *in vivo* concentrations and signaling that are difficult, if not impossible, to quantify experimentally. In doing so, we built a model that is qualitatively consistent with all observed *in vitro* behaviors of $VEGF_{165b}$ and all available knowledge of VEGF distribution in human PAD (**Fig 7-2A**). This process sheds light onto the mechanism of action of $VEGF_{165b}$ in PAD (**Table 7-1**) more accurately and more completely than previous models have done[60,65] (**Table 7-S15**), providing insight that is critical for design of future pro-angiogenic therapies,

Table 7-1. Key Model Predictions

Prediction	Experimental Basis or Validation	Therapeutic Implications
$VEGF_{165b}$ is over-represented in tissue.	Elevated muscle $VEGF_{165b}$ in PAD and murine hindlimb ischemia[11,65]. **(Fig 2)**	Understand pharmacokinetics of $VEGF_{165b}$ to better predict its role in disease and therapy response.
$VEGF_{165b}$ secretion into the blood by monocytes has minimal effect on baseline VEGFR signaling.	Unchanged total muscle VEGFA in PAD[11,12]. **(Figs 2 & 6)**	Blood $VEGF_{165b}$ is neither a good biomarker nor a therapeutic target for pro-angiogenic therapy.
$VEGF_{165b}$ is a weak activator of VEGFR2 *in vivo*.	Consistent with *in vitro* observations[52-54], *ex vivo* measurements (fat pads)[59], and *in vivo* data[11]. (**Figs 4 & 6**)	Translate *in vitro* observations into an *in vivo,* physiological context to predict changes in signaling in disease.
Reduced $VEGF_{165a}$ in PAD contributes to reduced VEGFR2 phosphorylation.	Prediction is result of properties measured *in vitro*[52-54] placed in a physiological context. (**Fig 4**)	$VEGF_{165b}$-VEGFR2 binding alone is not responsible for reduced angiogenic signaling in PAD. Affects therapy design.
$VEGF_{165b}$ does not compete for binding to VEGFR2, but does compete for binding to VEGFR1.	VEGR1 phosphorylation is increased by delivery of anti-$VEGF_{165b}$ and decreased by overexpression of $VEGF_{165b}$, but VEGFR2 phosphorylation is not substantially affected[11]. (**Figs 4-6**)	Understand mechanism of action of $VEGF_{165b}$, and how anti-$VEGF_{165b}$ induces improved perfusion recovery in mice[39]. Leverage for design of pro-angiogenic therapies.

7.3.1 Interpretation of model predictions

The results presented in this paper demonstrate that $VEGF_{165b}$ does indeed play a role in the pathology of PAD, but in a different way than previously hypothesized. For example, the model predicts that, contrary to *in vitro* observations, $VEGF_{165b}$ does not compete with other VEGF isoforms for binding to VEGFR2 *in vivo*, due to the low VEGF concentrations and VEGFR2 occupancy predicted in physiological conditions. Instead, as total VEGF levels are roughly constant in PAD-afflicted tissue, the model suggests that reduced $VEGF_{165a}$ levels, concomitant with increasing $VEGF_{165b}$, is the source of reduced VEGFR2 phosphorylation observed in some studies[39,59]. As another example, consistent with experimental data[11], the model predicts that modest increases in $VEGF_{165b}$ will indeed slightly increase pR2, not reduce it, and decreased $VEGF_{165b}$ will decrease pR2 slightly. Interestingly, and again consistent with Ganta et. al.[11] and the previously unpublished data presented here, the model does predict competition between $VEGF_{165b}$ and other ligands for binding to VEGFR1, which appears to be poorly or not at all activated by $VEGF_{165b}$ on tyrosine-1333. This supports a VEGFR1-mediated pro-angiogenic response to anti-$VEGF_{165b}$ treatment, as opposed to a VEGFR2-mediated response. The model also predicts that increased secretion of $VEGF_{165b}$ into the bloodstream by monocytes does not play a major role in VEGFR signaling in tissue, with locally-produced VEGF dominating the local signaling environment. The model does predict over-representation of $VEGF_{165b}$ protein and $VEGF_{165b}$ receptor binding in tissue, suggesting that microdialysis or muscle biopsy measurements of $VEGF_{165b}$ may be a good predictor of local angiogenic impairment.

7.3.2 Open questions

There are still many open questions about the role and properties of $VEGF_{165b}$, which limit our ability to fully interpret our model predictions, but which, with new experimental data, this model can be leveraged to answer. These measurements would increase our ability to understand and confidently predict the effectiveness of potential pro-angiogenic therapies. At the *in vitro* scale, there is still uncertainty in some of the binding properties of $VEGF_{165b}$ (e.g. binding to NRP1-VEGFR1 complexes) and characterization of different length $VEGF_{xxxb}$ isoforms, which necessitated certain assumptions in the construction of this model. At the molecular level, a better understanding of how exactly $VEGF_{165b}$ binds with normal affinity to VEGFR2 but induces only weak activation would be instructive. A potential

hypothesis involves changes in homo- and hetero-dimerization of ligands or receptors. This study and the work of Ganta et. al.[11] motivate a better understanding of VEGFR1 binding, trafficking, and differences in activation by $VEGF_{165b}$, other VEGF isoforms, and PlGF, in order to better target this pathway in PAD and other human diseases. In this study we cannot make definitive statements about VEGFR1 signaling, owing to the incomplete mechanistic understanding of VEGFR1 upon which we can construct our model. Additionally, we focused here exclusively on endothelial VEGFR1. A better understanding of the role of VEGFR1 signaling on macrophages and monocytes, which are involved in arteriogenesis, and which populations of receptors may contribute to the observed competition between ligands for VEGFR1 binding, is also key to fully understand the role of VEGF receptors in PAD. The existence of VEGF-Ax read-though transcripts[66] also deserves further investigation, to see whether they play a physiological role similar to that of $VEGF_{165b}$.

Finally, and perhaps most critically, we are limited by available quantitative measurements of absolute and relative levels of $VEGF_{165a}$ and $VEGF_{165b}$ in blood, healthy tissue, and diseased tissue. While measurements of difference in total protein between healthy and diseased tissue are available, quantitative measurements are key to pin down the distribution of these isoforms. For example, how much $VEGF_{165b}$ is present in healthy tissue remains an open question, though we know it decreases in several types of cancer[36,37], and increases in PAD and white adipose tissue[11,39,59]. We used our model to explore the dynamic range of relative $VEGF_{165a}$ and $VEGF_{165b}$ secretion and the implications of this splicing switch for signaling in a way that has not been possible experimentally. However, to fully understand signaling in disease, we need to know where patients reside on this spectrum. In this model, we assumed high $VEGF_{165b}$ only in the blood and in a relatively small PAD calf muscle, while in real patients with extensive PAD or systemic cardiovascular disease and/or large quantities of adipose tissue, the relative amounts of "healthy" and "diseased" tissue with high $VEGF_{165b}$ expression may be very different, potentially altering the $VEGF_{165b}$ pharmacokinetic predictions presented here. While such reliable and quantitative measurements remain challenging, there is hope that the future will bring the required tools, which, with the help of quantitative frameworks to integrate the data, will continue to improve our understanding of PAD and $VEGF_{165b}$, leading to more successful therapy design and clinical outcomes.

7.3.3 Conclusions

This model, the first to translate *in vitro* observations of $VEGF_{165b}$ properties into the context of human PAD, provides novel insight into questions that have remained challenging to answer due to limited measurement feasibility and a lack of reliable, quantitative measurement techniques. In doing so, we were able to integrate existing knowledge and previously unpublished data to test prevailing hypotheses about $VEGF_{165b}$ mechanism of action in PAD, and highlight important future questions and measurements on the path towards more effective treatments for PAD. The model's ability to capture key aspects of VEGF signaling in human PAD and murine hindlimb ischemia, as well as predict response to perturbation ($VEGF_{165b}$ over-expression) gives us confidence that the insight elucidated here is meaningful and relevant. In the future, this work can be extended to examine the role of $VEGF_{165b}$ in other diseases (e.g. cancer, obesity, pre-eclampsia), and to examine the signaling effects of promising pro-angiogenic therapies.

7.4 Methods

7.4.1 Compartmental Model Formulation

To study the distribution of VEGF$_{165b}$, as compared to other VEGF and PlGF isoforms, within the human body, we modified our three-compartment model[62], including the blood, the main bulk of body tissue (Main Body Mass), and a calf muscle (gastrocnemius + soleus), to include PAD-specific changes in geometry and molecular expression in the calf compartment. In this model, VEGF, PlGF, and sR1 move between the compartments by way of bi-directional vascular permeability and lymphatic drainage of tissue mass into the blood. All complexes can also be cleared from the blood. Within the tissue compartments, the relative fractions of interstitial space filled with fluid, extracellular matrix, endothelial cells, other cells including myocytes, and basement membranes (both endothelial – "EBM" and parenchymal – "PBM"), are estimated based on histology and other measurements.

We simulate detailed molecular interactions within the tissue compartments to capture the pharmacodynamics of VEGF, PlGF, and sR1 interactions with VEGFR1, VEGFR2, and NRP1, as well as interstitial HSPGs. VEGF and PlGF are secreted by parenchymal cells, and sR1 by endothelial cells (EC), into the interstitial space, where they can bind to EC receptors or to HSPGs in the ECM and basement membranes. VEGF$_{165b}$ production by monocytes in the bloodstream is also included[39]. VEGF, PlGF, and sR1 can be removed from the tissue compartments via binding to EC receptors and subsequent intracellular degradation, or via vascular permeability and lymphatic drainage (**Fig 7-S1**). Isoform-specific growth factor binding affinities for HSPGs and NRP1 are included to capture the resulting differences in distribution and signaling of each VEGF and PlGF isoform. The details of growth factor and sR1 binding to EC receptors are as previously described[62] (summarized in **Tables 7-S1 through 7-S9**), with the addition of VEGF$_{165b}$, which binds to VEGFR1 and VEGFR2 with the same affinity as other VEGF isoforms, but does not bind to NRP1, due to the change in the six amino acids of exon 8[53]. Additionally, despite including the VEGF heparin-binding domain, VEGF$_{165b}$ fails to bind to heparin or HSPGs[52-54], presumably due to structural difference induced by the alternate exon 8. Thus, we assume that VEGF$_{165b}$ cannot bind to HSPGs in the ECM and basement membranes. As in our previous model, endothelial receptors are continually produced, internalized, recycled, and degraded, with rates that depend on ligand-binding and coupling with the co-receptor NRP1[61,67]. Production is tuned to maintain target surface receptor levels at

305

steady-state. Upon ligand-binding we simulate site-specific phosphorylation of VEGFR2 on tyrosines Y1175 (upstream of ERK1/2 and proliferation) and Y1214 (upstream of p38 MAPK and migration), with preferential activation of Y1214 at the cell surface and Y1175 in early signaling endosomes[61]. As $VEGF_{165b}$ has been shown to phosphorylate VEGFR2 poorly compared to other VEGF isoforms, we fitted the phosphorylation rate upon binding to VEGFR2 using *in vitro* data, and validated against *ex vivo* and *in vivo* data. This allows us to study VEGF isoform-specific, site-specific phosphorylation of VEGFR2.

We assume infinitely fast diffusion, thus neglecting spatial patterning and heterogeneity in distribution and signaling. This is a useful trade-off for speed on computation, and allows us to focus on average values for healthy tissue and a PAD calf, in the context of the whole body and changes in VEGF splicing. We neglect direct secretion of sR1 by ECs into the bloodstream, and the expression receptors on the luminal (blood-facing) side of endothelial cells, focusing on "tissue-side" (abluminal) signaling, as angiogenesis is directed outward into tissue from the existing vasculature.

The model, comprised of 749 equations, is simulated in Fortran using the Livermore Solver for Ordinary Differential Equations with Automatic method switching for stiff and nonstiff problems (LSODA) on a laptop PC, using a relative error tolerance of 10^{-6}.

7.4.2 Model Parameterization

Geometry. The tissue geometry and compartment sizes represent a 70kg healthy human as use previously[62], with the calf muscle parameters now reflecting the PAD parameterization used in [60] (**Table 7-S12**). These geometries are based on histological cross-sections of human muscle, as well as other data. PAD-specific changes incorporated include atrophy of calf muscle, leading to reduced total calf volume and increased fractional interstitial space, and thickening of endothelial basement membranes. The blood is assumed to be 60% plasma.

Binding and Coupling Kinetics. With the exception of $VEGF_{165b}$, all binding reactions are parameterized as described previously[62] (summarized in **Figure 7-S1B&E** and **Tables 7-S1 though 7-S9**). This includes binding of matrix-immobilized VEGF and PlGF to sR1, and to EC receptors (described recently in [61,62]). By incorporating isoform-specific binding to matrix proteins and NRP1, we can study differences between $VEGF_{165b}$ and other VEGF isoforms. While there are no published studies on binding of $VEGF_{165b}$ to

306

NRP1-VEGFR1 complexes, including this reaction improves match between predictions and experimental observations (see **Fig 7-S8**) [11]. We assume the same binding and unbinding rate constants for VEGF$_{165b}$ binding to VEGFR1 and VEGFR2 as for other VEGF isoforms. As before, we assume all ligands and receptors are pre-dimerized. We assume that immobilized ligand bound to the innermost 25nm of endothelial basement membrane is accessible to EC surface receptors[62].

Receptor Trafficking and VEGFR2 Phosphorylation: Fitting & validating k$_p$ for VEGF165b. We included receptor trafficking and site-specific phosphorylation of VEGFR2, as previously described (summarized in **Figure 7-S1C&D** and **Tables 7-S10 & 7-S11**). This allows us to explicitly predict VEGFR2 activation, and not just receptor occupancy, and is key to understanding the binding of matrix-immobilized VEGF isoforms to VEGFRs [61]. This is also of importance to explicitly account for weak phosphorylation of VEGFR2 when stimulated with VEGF$_{165b}$, despite normal binding affinity[53,54]. VEGFR1 trafficking is included, but as sufficient data is not available to confidently parameterize these processes at the same resolution as VEGFR2 trafficking, free and ligand-bound VEGFR1 quantities are shown only on the EC surface. For all VEGF isoforms except VEGF$_{165b}$, we assume the same constant phosphorylation rate (k$_p$) for ligand-bound VEGFR2. For VEGF$_{165b}$, we fit the phosphorylation rate using published *in vitro* data. This study, by Kawamura et. al.[52] measured VEGFR2 phosphorylation at 5 minutes after exposure to varying doses of VEGF$_{165a}$ or VEGF$_{165b}$ in PAECs transfected to express VEGFR2 and NRP1. In our simulation, we used our *in vitro* model (previously described [61]), now parameterized with the specific VEGFR2 and NRP1 levels for PAECs[61]. These experiments did not include ECM-binding, so the only differences between VEGF$_{165a}$ and VEGF$_{165b}$ in the simulation were NRP1-binding and the fit k$_p$ value. The k$_p$ value for VEGF$_{165b}$ was fitted to minimize the least squared error for the ratio of VEGFR2 phosphorylated in response to VEGF$_{165b}$ / VEGFR2 phosphorylated in response to VEGF$_{165a}$ at each concentration. For all isoforms, we assumed the same site-specific and subcellular location-specific dephosphorylation rates as fit in our previous *in vitro* model[61]. After fitting the VEGF$_{165b}$-specific VEGFR2 phosphorylation rate constant, we validated it qualitatively using data from explanted human fat pads[59]. To do this, we ran our compartment model to steady-state at different levels of relative VEGF$_{165a}$ and VEGF$_{165b}$ production. Then, we shut off intercompartmental transport to mimic the explant and simulated 24 hours (culture time). Finally, we analyzed the amount of phosphorylated VEGFR2, and compared this to

the trend of decreasing pR2 with increasing tissue $VEGF_{165b}$ levels in the fat pad measurements. While this data comes from obese, non-PAD patients, the matching trend in $VEGF_{165b}$ levels and pR2 between the experimental data and simulations, which does not occur with a higher k_p value, validates our fit estimate of this phosphorylation rate.

Transport. Transport parameters and PAD-specific changes in transport were taken directly from previous models, assuming a supine, awake 70kg human[60,63] (**Table 7-S13**).

Protein Expression. Interstitial matrix binding site densities in the ECM and basement membranes remained the same as in the previous PAD model[60] (**Table 7-S14**). Endothelial surface receptor levels in healthy tissue were also the same as our previous healthy model, while changes to receptor expression in the PAD calf muscle were based on measured changes in EC surface receptor numbers following hindlimb ischemia in a murine system[68], with VEGFR1 and NRP1 levels increasing and VEGFR2 levels decreasing (**Table 7-2**). The ratios of PlGF isoform secretion[69] were unchanged from our previous model, and tissue secretion ratios of $VEGF_{121}$, $VEGF_{165}$, and $VEGF_{189}$ were also unchanged[51] (**Table 7-2**). Given the uncertainty in the relative production of $VEGF_{165a}$ and $VEGF_{165b}$ in healthy and ischemic tissue, and microdialaysis measurements showing that interstitial VEGF levels are not significantly different in resting PAD muscle than in healthy tissue[12], we varied the relative splicing of $VEGF_{165}$ (77% of total VEGF production in the model) from "all $VEGF_{165a}$" (0%) to "all $VEGF_{165b}$" (100%), and examined the effects on VEGF distribution and VEGFR1 and VEGFR2 activation. Due to differences in the properties of $VEGF_{165a}$ and $VEGF_{165b}$, the VEGF secretion rate and the VEGFR1, VEGFR2, and NRP1 production rates had to be re-tuned for each case considered (0%, 25%, 50%, 75%, and 100%, see **Tables 7-SM1 & 7-SM2**). The PlGF and sR1 production rates were not altered; this resulted in only small changes in plasma measurements, and plasma PlGF levels are not known to change in PAD[70,71], while plasma sR1 levels have been observed to either remain unchanged or decrease[7-9,71] (in contrast to the increase in sR1 observed following hindlimb ischemia in murine systems[26]). Production rates for VEGFR1, VEGFR2, and NRP1 in the healthy Main Body Mass were not changed from the previous healthy model; only small changes in surface receptor levels occurred. Finally, we included for the first time production of $VEGF_{165b}$ in the bloodstream by monocytes, as demonstrated by Kikuchi et. al.[39] As tissue VEGF levels do not increase in PAD, but plasma levels are generally seen to increase roughly three-fold[7-10], after fitting tissue secretion

and production rates to maintain the healthy target level of 1.5pM VEGF in plasma and appropriate EC

receptor levels, we increased blood-located monocyte production of $VEGF_{165b}$ until the PAD target plasma

VEGF level of 4.5pM was achieved. This did not have a substantial effect on tissue ligand or receptor

levels (see **Suppl. Model Fitting**).

Table 7-2. Target Surface Receptor and Plasma Ligand Levels at Steady-State

Species	Target Location	PAD Target Value	Healthy Target Value	Units	Ref
VEGFR1	Main Body Mass	1800	1800	Surface receptors/EC	[49,59]
	PAD Calf Muscle	3150	1800	Surface receptors/EC	[49,59]
VEGFR2	Main Body Mass	5800	5800	Surface receptors/EC	[49,59]
	PAD Calf Muscle	4750	5800	Surface receptors/EC	[49,59]
NRP1	Main Body Mass	70,000	70,000	Surface receptors/EC	[49,59]
	PAD Calf Muscle	122,500	70,000	Surface receptors/EC	[49,59]
sR1	Plasma	100	100	pM	[7-9,71]
PlGF	Plasma	10	10	pM	[70,71]
PlGF1		15%	15%	% of tissue production	[69]
PlGF2		85%	85%	% of tissue production	[69]
VEGF	Plasma	4.5	1.5	pM	[7-10]
VEGF$_{165}$		0-77%	77%	% of tissue production	[51]
VEGF$_{121}$		8%	8%	% of tissue production	[51]
VEGF$_{189}$		15%	15%	% of tissue production	[51]
VEGF$_{165b}$		0-77%	0%	% of tissue production	

Notes:

*Receptor level fold changes based on fold changes following hindlimb ischemia in mice[68], applied to healthy human cell numbers.

*Unit conversions for receptor levels to molecules/cm^3 tissue:

$$[R] \text{ in } \frac{\text{moles}}{\text{cm}^3 \text{ tissue}} = \left([R] \text{ in } \frac{\#}{\text{EC}} \right) \cdot \frac{\text{ESAV}}{\text{ECSA}} \cdot \frac{1}{N_{Av}}$$, where N_{Av} is Avogadro's number, 6.023×10^{23}

molecules/mole.

Simulations of Human PAD and Murine Hindlimb Ischemia. To match the roughly 3-fold increase in $VEGF_{165b}$ observed in human PAD and murine hindlimb ischemia, we used 75% fractional $VEGF_{165b}$ secretion as our "PAD" case and 25% fractional $VEGF_{165b}$ secretion as our "normal" case. We did not make any other changes in tissue anatomy or molecular expression for these simulations. Note that we used our human-parameterized model for comparison to both human and mouse data, despite many differences in anatomy and molecular expression. Delivery of $VEGF_{165b}$ plasmid to non-ischemic mouse muscle was simulated using the 25% fractional $VEGF_{165b}$ secretion case, increasing $VEGF_{165b}$ secretion 3.51-fold to match experimental measurements of increased muscle $VEGF_{165b}$ protein.

Experimental Measurements of Human PAD and Murine Hindlimb Ischemia. The experimental data presented in this paper represent an extended analysis of the results presented in [11], and all methods are the same as those in [11]. Human data are total tissue measurements from muscle biopsies in PAD patients, normalized by healthy patient values. Western blot measurements of VEGF and $VEGF_{165b}$ were used as the $VEGF_{165b}$ ELISA used by Ganta et al. also detects other $VEGF_{xxxb}$ isoforms. For the ischemic vs. non-ischemic comparisons, mouse measurements are taken from muscle 3 days after femoral artery ligation, and represent total tissue measurements (receptor-bound ligand and VEGF protein) or CD31+ cells (pR2/R2, noted by (EC) in plots), normalized by equivalent quantities in the contralateral leg. In the $VEGF_{165b}$ over-expression experiments, mouse measurements were taken from non-ischemic muscle 7 days after transfection with $VEGF_{165b}$ plasmid or a control plasmid, and represent total tissue measurements (receptor-bound ligand and VEGF protein) or CD31+ cells (pR1/R1, noted by (EC) in plots), normalized by equivalent quantities in the control group.

7.5 References

1   Annex, B. H. Therapeutic angiogenesis for critical limb ischaemia. *Nature Reviews Cardiology* **10**, 387-396, doi:10.1038/nrcardio.2013.70 (2013).

2   Robbins, J. L. *et al.* Relationship between leg muscle capillary density and peak hyperemic blood flow with endurance capacity in peripheral artery disease. *Journal of Applied Physiology* **111**, 81-86, doi:10.1152/japplphysiol.00141.2011 (2011).

3   Askew, C. D. *et al.* Skeletal muscle phenotype is associated with exercise tolerance in patients with peripheral arterial disease. *Journal of Vascular Surgery* **41**, 802-807, doi:10.1016/j.jvs.2005.01.037 (2005).

4   Baum, O., Djonov, V., Ganster, M., Widmer, M. & Baumgartner, I. Arteriolization of capillaries and FGF-2 upregulation in skeletal muscles of patients with chronic peripheral arterial disease. *Microcirculation* **12**, 527-537, doi:10.1080/10739680591003413 (2005).

5   Norgren, L. *et al.* Inter-Society Consensus for the Management of Peripheral Arterial Disease (TASC II). *European journal of vascular and endovascular surgery : the official journal of the European Society for Vascular Surgery* **33 Suppl 1**, S1-75, doi:10.1016/j.ejvs.2006.09.024 (2007).

6   Dormandy, J. A. & Rutherford, R. B. Management of peripheral arterial disease (PAD). TASC Working Group. TransAtlantic Inter-Society Consensus (TASC). *Journal of vascular surgery* **31**, S1-S296 (2000).

7   Belgore, F. M., Blann, A. D. & Lip, G. Y. Measurement of free and complexed soluble vascular endothelial growth factor receptor, Flt-I, in fluid samples: development and application of two new immunoassays. *Clinical Science* **100**, 567-575, doi:10.1042/cs20000234 (2001).

8   Blann, A. D. *et al.* Vascular endothelial growth factor and its receptor, Flt-1, in the plasma of patients with coronary or peripheral atherosclerosis, or Type II diabetes. *Clinical Science* **102**, 187-194 (2002).

9   Makin, A. J., Chung, N. A. Y., Silverman, S. H. & Lip, G. Y. H. Vascular endothelial growth factor and tissue factor in patients with established peripheral artery disease: a link between angiogenesis and thrombogenesis? *Clinical Science* **104**, 397-404, doi:10.1042/cs20020182 (2003).

10   Lee, T. M., Su, S. F., Tsai, C. H., Lee, Y. T. & Wang, S. S. Differential effects of cilostazol and pentoxifylline on vascular endothelial growth factor in patients with intermittent claudication. *Clinical Science* **101**, 305-311, doi:10.1042/cs20000281 (2001).

11   Ganta, V. C., Choi, M., Kutateladze, A. & Annex, B. H. VEGF<sub>165</sub>b Modulates Endothelial VEGFR1-STAT3 Signaling Pathway and Angiogenesis in Human and Experimental Peripheral Arterial Disease. *Circulation Research* (2016).

12   Hoier, B. *et al.* Angiogenic response to passive movement and active exercise in individuals with peripheral arterial disease. *Journal of Applied Physiology* **115**, 1777-1787, doi:10.1152/japplphysiol.00979.2013 (2013).

13   Hoier, B. & Hellsten, Y. Exercise-Induced Capillary Growth in Human Skeletal Muscle and the Dynamics of VEGF. *Microcirculation* **21**, 301-314, doi:10.1111/micc.12117 (2014).

14   Hankey, G. J., Norman, P. E. & Eikelboom, J. W. MEdical treatment of peripheral arterial disease. *JAMA* **295**, 547-553, doi:10.1001/jama.295.5.547 (2006).

15   Duscha, B. D. *et al.* Angiogenesis in Skeletal Muscle Precede Improvements in Peak Oxygen Uptake in Peripheral Artery Disease Patients. *Arteriosclerosis Thrombosis and Vascular Biology* **31**, 2742-2748, doi:10.1161/atvbaha.111.230441 (2011).

16   Grochot-Przeczek, A., Dulak, J. & Jozkowicz, A. Therapeutic angiogenesis for revascularization in peripheral artery disease. *Gene* **525**, 220-228, doi:10.1016/j.gene.2013.03.097 (2013).

17   Ozawa, C. R. *et al.* Microenvironmental VEGF concentration, not total dose, determines a threshold between normal and aberrant angiogenesis. *Journal of Clinical Investigation* **113**, 516-527, doi:10.1172/jci200418420 (2004).

18   Gussoni, E., Blau, H. M. & Kunkel, L. M. The fate of individual myoblasts after transplantation into muscles of DMD patients. *Nature Medicine* **3**, 970-977, doi:10.1038/nm0997-970 (1997).

19   Yla-Herttuala, S. & Alitalo, K. Gene transfer as a tool to induce therapeutic vascular growth. *Nature Medicine* **9**, 694-701, doi:10.1038/nm0603-694 (2003).

20   Yla-Herttuala, S., Markkanen, J. E. & Rissanen, T. T. Gene therapy for ischemic cardiovascular disease: Somes lessons learned from the first clinical trials. *Trends in Cardiovascular Medicine* **14**, 295-300, doi:10.1016/j.tcm.2004.09.001 (2004).

21   Mac Gabhann, F., Qutub, A. A., Annex, B. H. & Popel, A. S. Systems biology of pro-angiogenic therapies targeting the VEGF system. *Wiley Interdisciplinary Reviews-Systems Biology and Medicine* **2**, 694-707, doi:10.1002/wsbm.92 (2010).

22   Briquez, P. S., Clegg, L. E., Martino, M. M., Gabhann, F. M. & Hubbell, J. A. Design principles for therapeutic angiogenic materials. *Nature Reviews Materials* **1**, 15006, doi:10.1038/natrevmats.2015.6 (2016).

23   Clegg, L. E. & Mac Gabhann, F. Molecular mechanism matters: Benefits of mechanistic computational models for drug development. *Pharmacological Research* **99**, 149-154, doi:http://dx.doi.org/10.1016/j.phrs.2015.06.002 (2015).

24   Mac Gabhann, F. & Popel, A. S. Systems biology of vascular endothelial growth factors. *Microcirculation (New York, N.Y. : 1994)* **15**, 715-738 (2008).

25   Wu, F. T. H. *et al.* A systems biology perspective on sVEGFR1: its biological function, pathogenic role and therapeutic use. *Journal of Cellular and Molecular Medicine* **14**, 528-552, doi:10.1111/j.1582-4934.2009.00941.x (2010).

26   Hazarika, S. *et al.* Impaired angiogenesis after Hindlimb ischemia in type 2 diabetes Mellitus - Differential regulation of vascular endothelial growth factor receptor 1 and soluble vascular endothelial growth factor receptor 1. *Circulation Research* **101**, 948-956, doi:10.1161/circresaha.107.160630 (2007).

27   Koch, S., Tugues, S., Li, X., Gualandi, L. & Claesson-Welsh, L. Signal transduction by vascular endothelial growth factor receptors. *Biochemical Journal* **437**, 169-183, doi:10.1042/bj20110301 (2011).

28   Koch, S. & Claesson-Welsh, L. Signal Transduction by Vascular Endothelial Growth Factor Receptors. *Cold Spring Harbor Perspectives in Medicine* **2**, doi:10.1101/cshperspect.a006502 (2012).

29   Vempati, P., Popel, A. S. & Mac Gabhann, F. Extracellular regulation of VEGF: Isoforms, proteolysis, and vascular patterning. *Cytokine & Growth Factor Reviews* **25**, 1-19, doi:http://dx.doi.org/10.1016/j.cytogfr.2013.11.002 (2014).

30   Park, J. E., Keller, G. A. & Ferrara, N. VASCULAR ENDOTHELIAL GROWTH-FACTOR (VEGF) ISOFORMS - DIFFERENTIAL DEPOSITION INTO THE SUBEPITHELIAL EXTRACELLULAR-MATRIX AND BIOACTIVITY OF EXTRACELLULAR MATRIX-BOUND VEGF. *Molecular Biology of the Cell* **4**, 1317-1326 (1993).

31   Ruhrberg, C. *et al.* Spatially restricted patterning cues provided by heparin-binding VEGF-A control blood vessel branching morphogenesis. *Genes & Development* **16**, 2684-2698, doi:10.1101/gad.242002 (2002).

32   Lee, S., Jilani, S. M., Nikolova, G. V., Carpizo, D. & Iruela-Arispe, M. L. Processing of VEGF-A by matrix metalloproteinases regulates bioavailability and vascular patterning in tumors. *Journal of Cell Biology* **169**, 681-691, doi:10.1083/jcb.200409115 (2005).

33   Grunstein, J., Masbad, J. J., Hickey, R., Giordano, F. & Johnson, R. S. Isoforms of vascular endothelial growth factor act in a coordinate fashion to recruit and expand tumor vasculature. *Molecular and Cellular Biology* **20**, 7282-7291, doi:10.1128/mcb.20.19.7282-7291.2000 (2000).

34   Carmeliet, P. *et al.* Abnormal blood vessel development and lethality in embryos lacking a single VEGF allele. *Nature* **380**, 435-439, doi:10.1038/380435a0 (1996).

35   Carmeliet, P. *et al.* Impaired myocardial angiogenesis and ischemic cardiomyopathy in mice lacking the vascular endothelial growth factor isoforms VEGF(164) and VEGF(188). *Nature Medicine* **5**, 495-502, doi:10.1038/8379 (1999).

36   Bates, D. O. *et al.* VEGF(165)b, an inhibitory splice variant of vascular endothelial growth factor, is down-regulated in renal cell carcinoma. *Cancer Research* **62**, 4123-4131 (2002).

37   Harper, S. J. & Bates, D. O. VEGF-A splicing: the key to anti-angiogenic therapeutics? *Nature Reviews Cancer* **8**, 880-887, doi:10.1038/nrc2505 (2008).

38   Jones, W. S. *et al.* Alteration in angiogenic and anti-angiogenic forms of vascular endothelial growth factor-A in skeletal muscle of patients with intermittent claudication following exercise training. *Vascular Medicine* **17**, 94-100, doi:10.1177/1358863x11436334 (2012).

39   Kikuchi, R. *et al.* An antiangiogenic isoform of VEGF-A contributes to impaired vascularization in peripheral artery disease. *Nature Medicine* **20**, 1464-1471, doi:10.1038/nm.3703 (2014).

40   Varey, A. H. R. *et al.* VEGF(165)b, an antiangiogenic VEGF-A isoform, binds and inhibits bevacizumab treatment in experimental colorectal carcinoma: balance of pro- and antiangiogenic VEGF-A isoforms has implications for therapy. *British Journal of Cancer* **98**, 1366-1379, doi:10.1038/sj.bjc.6604308 (2008).

41   Pritchard-Jones, R. O. *et al.* Expression of VEGF(xxx)b, the inhibitory isoforms of VEGF, in malignant melanoma. *British Journal of Cancer* **97**, 223-230, doi:10.1038/sj.bjc.6603839 (2007).

42   Wellmann, S. *et al.* Specific reverse transcription-PCR quantification of vascular endothelial growth factor (VEGF) splice variants by LightCycler technology. *Clinical Chemistry* **47**, 654-660 (2001).

43   Manetti, M. *et al.* Overexpression of VEGF(165)b, an Inhibitory Splice Variant of Vascular Endothelial Growth Factor, Leads to Insufficient Angiogenesis in Patients With Systemic Sclerosis. *Circulation Research* **109**, E14-U35, doi:10.1161/circresaha.111.242057 (2011).

44   Bills, V. L. *et al.* Failure to up-regulate VEGF(165)b in maternal plasma is a first trimester predictive marker for pre-eclampsia. *Clinical Science* **116**, 265-272, doi:10.1042/cs20080270 (2009).

45   Nowak, D. G. *et al.* Expression of pro- and anti-angiogenic isoforms of VEGF is differentially regulated by splicing and growth factors. *Journal of Cell Science* **121**, 3487-3495, doi:10.1242/jcs.016410 (2008).

46   Nowak, D. G. *et al.* Regulation of Vascular Endothelial Growth Factor (VEGF) Splicing from Pro-angiogenic to Anti-angiogenic Isoforms A NOVEL THERAPEUTIC STRATEGY FOR ANGIOGENESIS. *Journal of Biological Chemistry* **285**, 5532-5540, doi:10.1074/jbc.M109.074930 (2010).

47   Gustafsson, T. *et al.* VEGF-A splice variants and related receptor expression in human skeletal muscle following submaximal exercise. *Journal of Applied Physiology* **98**, 2137-2146, doi:10.1152/japplphysiol.01402.2004 (2005).

48   Jensen, L., Pilegaard, H., Neufer, P. D. & Hellsten, Y. Effect of acute exercise and exercise training on VEGF splice variants in human skeletal muscle. *American Journal of Physiology-Regulatory Integrative and Comparative Physiology* **287**, R397-R402, doi:10.1152/ajpregu.00071.2004 (2004).

49   Bordeleau, F. *et al.* Tissue stiffness regulates serine/arginine-rich protein-mediated splicing of the extra domain B-fibronectin isoform in tumors. *Proceedings of the National Academy of Sciences* (2015).

50   Xu, J. *et al.* The evolution of alternative splicing exons in vascular endothelial growth factor A. *Gene* **487**, 143-150, doi:10.1016/j.gene.2011.06.024 (2011).

51   Ng, Y. S., Rohan, R., Sunday, M. E., Demello, D. E. & D'Amore, P. A. Differential expression of VEGF isoforms in mouse during development and in the adult. *Developmental Dynamics* **220**, 112-121, doi:10.1002/1097-0177(2000) (2001).

52   Kawamura, H., Li, X., Harper, S. J., Bates, D. O. & Claesson-Welsh, L. Vascular endothelial growth factor (VEGF)-A165b is a weak in vitro agonist for VEGF receptor-2 due to lack of coreceptor binding and deficient regulation of kinase activity. *Cancer Research* **68**, 4683-4692, doi:10.1158/0008-5472.can-07-6577 (2008).

53   Suarez, S. C. *et al.* A VEGF-A splice variant defective for heparan sulfate and neuropilin-1 binding shows attenuated signaling through VEGFR-2. *Cellular and Molecular Life Sciences* **63**, 2067-2077, doi:10.1007/s00018-006-6254-9 (2006).

54   Delcombel, R. *et al.* New prospects in the roles of the C-terminal domains of VEGF-A and their cooperation for ligand binding, cellular signaling and vessels formation. *Angiogenesis* **16**, 353-371, doi:10.1007/s10456-012-9320-y (2013).

55   Catena, R. *et al.* VEGF(121)b and VEGF(165)b are weakly angiogenic isoforms of VEGF-A. *Molecular Cancer* **9**, doi:10.1186/1476-4598-9-320 (2010).

56   Bates, D. O. *et al.* Detection of VEGF-A(xxx)b Isoforms in Human Tissues. *Plos One* **8**, doi:10.1371/journal.pone.0068399 (2013).

57   Harris, S. *et al.* Do Anti-Angiogenic VEGF (VEGFxxxb) Isoforms Exist? A Cautionary Tale. *Plos One* **7**, doi:10.1371/journal.pone.0035231 (2012).

58   Woolard, J. *et al.* VEGF(165)b, an inhibitory vascular endothelial growth factor splice variant: Mechanism of action, in vivo effect on angiogenesis and endogenous protein expression. *Cancer Research* **64**, 7822-7835, doi:10.1158/0008-5472.can-04-0934 (2004).

59   Ngo, D. T. M. *et al.* Antiangiogenic Actions of Vascular Endothelial Growth Factor-A(165)b, an Inhibitory Isoform of Vascular Endothelial Growth Factor-A, in Human Obesity. *Circulation* **130**, 1072-1080, doi:10.1161/circulationaha.113.008171 (2014).

60   Wu, F. T. *et al.* VEGF and soluble VEGF receptor-1 (sFlt-1) distributions in peripheral arterial disease: an in silico model. *Am J Physiol Heart Circ Physiol* **298**, H2174-2191, doi:ajpheart.00365.2009 [pii] 10.1152/ajpheart.00365.2009 (2010).

61   Clegg, L. W. & Mac Gabhann, F. Site-Specific Phosphorylation of VEGFR2 Is Mediated by Receptor Trafficking: Insights from a Computational Model. *PLoS Comput Biol* **11**, e1004158, doi:10.1371/journal.pcbi.1004158 (2015).

62   Clegg, L. E. & Mac Gabhann, F. A computational analysis of in vivo VEGFR activation by multiple co-expressed ligands. *PLOS Computational Biology* **13**, e1005445, doi:10.1371/journal.pcbi.1005445 (2017).

63   Wu, F. T. H., Stefanini, M. O., Gabhann, F. M. & Popel, A. S. A Compartment Model of VEGF Distribution in Humans in the Presence of Soluble VEGF Receptor-1 Acting as a Ligand Trap. *Plos One* **4**, doi:10.1371/journal.pone.0005108 (2009).

64   Autiero, M. *et al.* Role of PlGF in the intra- and intermolecular cross talk between the VEGF receptors Flt1 and Flk1. *Nature Medicine* **9**, 936-943, doi:10.1038/nm884 (2003).

65   Chu, L.-H. *et al.* A multiscale computational model predicts distribution of anti-angiogenic isoform VEGF165b in peripheral arterial disease in human and mouse. *Scientific Reports* **6**, 37030, doi:10.1038/srep37030 http://www.nature.com/articles/srep37030 - supplementary-information (2016).

66   Xin, H., Zhong, C., Nudleman, E. & Ferrara, N. Evidence for Pro-angiogenic Functions of VEGF-Ax. *Cell* **167**, 275-284.e276, doi:10.1016/j.cell.2016.08.054.

67   Ballmer-Hofer, K., Andersson, A. E., Ratcliffe, L. E. & Berger, P. Neuropilin-1 promotes VEGFR-2 trafficking through Rab11 vesicles thereby specifying signal output. *Blood* **118**, doi:10.1182/blood-2011-01-328773 (2011).

68   Imoukhuede, P. I., Dokun, A. O., Annex, B. H. & Popel, A. S. Endothelial cell-by-cell profiling reveals the temporal dynamics of VEGFR1 and VEGFR2 membrane localization after murine hindlimb ischemia. *American Journal of Physiology-Heart and Circulatory Physiology* **304**, H1085-H1093, doi:10.1152/ajpheart.00514.2012 (2013).

69   Nucci, M., Poon, L. C., Demirdjian, G., Darbouret, B. & Nicolaides, K. H. Maternal Serum Placental Growth Factor (PlGF) Isoforms 1 and 2 at 11-13 Weeks' Gestation in Normal and Pathological Pregnancies. *Fetal Diagnosis and Therapy* **36**, 106-116, doi:10.1159/000357842 (2014).

70   Smadja, D. M. *et al.* Thrombospondin-1 Is a Plasmatic Marker of Peripheral Arterial Disease That Modulates Endothelial Progenitor Cell Angiogenic Properties. *Arteriosclerosis Thrombosis and Vascular Biology* **31**, 551-U189, doi:10.1161/atvbaha.110.220624 (2011).

71   Findley, C. M., Mitchell, R. G., Duscha, B. D., Annex, B. H. & Kontos, C. D. Plasma levels of soluble Tie2 and vascular endothelial growth factor distinguish critical limb ischemia from intermittent claudication in patients with peripheral arterial disease. *Journal of the American College of Cardiology* **52**, 387-393, doi:10.1016/j.jacc.2008.02.045 (2008).

7.6 Supplemental Model Fitting

7.6.1 Incorporation of VEGF165b Properties and Secretion into the Computational Model

We first adjusted our model to capture anatomical and molecular expression changes occurring in PAD (summarized in **Tables 7-2 & 7-S12)**, based on measurements of endothelial receptor levels in ischemia [4] and previous modeling work [1] with increased endothelial surface VEGFR1 and NRP1, and decreased endothelial surface VEGFR2 (**Table 7-2**). We then tuned the model to explore the implications of varying expression of $VEGF_{165b}$. We varied the fraction of total $VEGF_{165}$ secretion (which is 77% of total VEGF secretion, the rest being $VEGF_{121}$ and $VEGF_{189}$) that is $VEGF_{165b}$ from 0% to 100% in both the PAD Calf Muscle and the Main Body Mass, mimicking decreasing tissue and serum $VEGF_{165a}$ concurrent with increasing $VEGF_{165b}$ [3, 5]. As we varied the $VEGF_{165b}$ secretion fraction, we had to re-tune the receptor production and ligand secretion rates (**Table 7-SM1**) in the model to maintain target receptor levels and plasma ligand concentrations (**Table 7-SM2**). As $VEGF_{165b}$ secretion increased, we had to increase production of VEGFR1 and decrease production of VEGFR2 and total VEGF to meet these targets (**Fig 7-S2D**). Finally, we incorporated secretion of $VEGF_{165b}$ into the bloodstream by monocytes to reach the PAD target plasma VEGF level of 4.5pM. This is in line with the correlation between peripheral blood mononuclear cell $VEGF_{165b}$ mRNA and serum $VEGF_{165b}$ levels measured by Kikuchi et. al.[5], suggesting that this monocyte-derived $VEGF_{165b}$ likely represents a substantial portion of blood $VEGF_{165b}$.

Table 7-SM1. Receptor Production and Ligand Secretion Rates

| Species | Location | Local Tissue Fraction of $VEGF_{165}$ Production that is $VEGF_{165b}$ | | | | | |
		0.0	0.25	0.5	0.75	1.0	Units
VEGFR1	Main Body Mass	1.162	1.75	2.1	2.315	2.48	Change from No VEGF SS
	PAD Calf Muscle	1.14	1.805	2.188	2.44	2.615	Change from No VEGF SS
VEGFR2	Main Body Mass	32.09	23.11	17.145	13.13	10.19	Change from No VEGF SS
	PAD Calf Muscle	51.696	35.472	24.845	17.68	13.65	Change from No VEGF SS
NRP1	Main Body Mass	1.295	1.203	1.142	1.1	1.07	Change from No VEGF SS
	PAD Calf Muscle	1.23	1.1655	1.1214	1.091	1.069	Change from No VEGF SS
sR1	Main Body Mass	0.0893	0.0835	0.0793	0.0762	0.0740	molecules/EC/s
	PAD Calf Muscle	0.0893	0.0835	0.0793	0.0762	0.0740	
PlGF	Main Body Mass	0.0146	0.0146	0.0146	0.0146	0.0146	molecules/MD/s
	PAD Calf Muscle	0.0146	0.0146	0.0146	0.0146	0.0146	
VEGF	Main Body Mass	0.283	0.2214	0.1790	0.1502	0.1290	molecules/MD/s
	PAD Calf Muscle	0.283	0.2214	0.1790	0.1502	0.1290	
$VEGF_{165b}$	Plasma	3.33	3.33	3.33	3.33	3.33	molecules/monocyte/s

*SS: steady-state, MD: myonuclear domain

Table 7-SM2. Achieved Steady-state Plasma Ligand and Tissue Surface Receptor Levels

Species	Location	Tar-get	Local Tissue Fraction of VEGF$_{165}$ Production that is VEGF$_{165b}$					Units	Ref
			0.0	0.25	0.5	0.75	1.0		
VEGFR1	Main Body Mass	1800	1786	1780	1789	1779	1788	Surface receptors/EC	[6]
	PAD Calf Muscle	3150	3155	3154	3147	3148	3150	Surface receptors/EC	[4]
VEGFR2	Main Body Mass	5800	5710	5721	5720	5718	5712	Surface receptors/EC	[6]
	PAD Calf Muscle	4750	4748	4753	4751	4753	4753	Surface receptors/EC	[4]
NRP1	Main Body Mass	70,000	69,976	69,918	70,006	69,941	69,970	Surface receptors/EC	[6]
	PAD Calf Muscle	122,500	122,477	122,489	122,487	122,470	122,485	Surface receptors/EC	[4]
sR1	Plasma	100	92.49	92.55	92.57	92.44	92.5	pM	[7-10]
PlGF	Plasma	10	10.00	10.03	10.04	10.05	10.06	pM	[9, 11]
VEGF	Plasma	4.5	4.51	4.51	4.50	4.51	4.51	pM	[7, 8, 10, 12]

*Note: Receptor productions rates in the Main Body Mass and all tissue ligand secretion rates were fit in the healthy model [13], and were not changed for the PAD model, as there is no evidence of these values changing outside the affected tissue in PAD. This accounts for the small deviation in the Main Body Mass values from target values.

7.7 Supplemental Figures

Figure 7-S1. Detailed schematic of molecular interactions and whole body compartment model structure. This figure is related to **Fig 7-1**. **(A)** Structure of compartment model, which includes secretion of VEGF and PlGF by parenchymal cells and sR1 by endothelial cell in tissue, as well as $VEGF_{165b}$ in blood by monocytes, binding of VEGF, PlGF, and sR1 to receptors on endothelial cells and HSPGs in the ECM and basement membranes, clearance from the blood, and transport of VEGF, PlGF, and sR1 between compartments via vascular permeability or lymphatic drainage. The geometry and molecular expression levels in the calf compartment were modified to account for changes between healthy and PAD subjects [1]. **(B)** Interactions VEGF isoforms, PlGF isoforms, sR1, and extracellular HSPGs (M) in the interstitial space of tissues. **(C)** Summary of VEGFR2 trafficking reactions simulated in endothelial cells. **(D)** Tyrosine site-specific phosphorylation and dephosphorylation of VEGFR2. **(E)** Molecular interactions at the abluminal (tissue-facing) endothelial cell surface between VEGF isoforms, PlGF isoforms, sR1, VEGFR1, VEGFR2, NRP1, and HSPGs (M) in the endothelial basement membrane (EBM).

A Main Body Mass · Blood · PAD Calf Muscle

Extracellular Space

B

Endothelium

C

D

E EBM-bound ligands can bind VEGFR1 & VEGFR2

Figure 7-S1

325
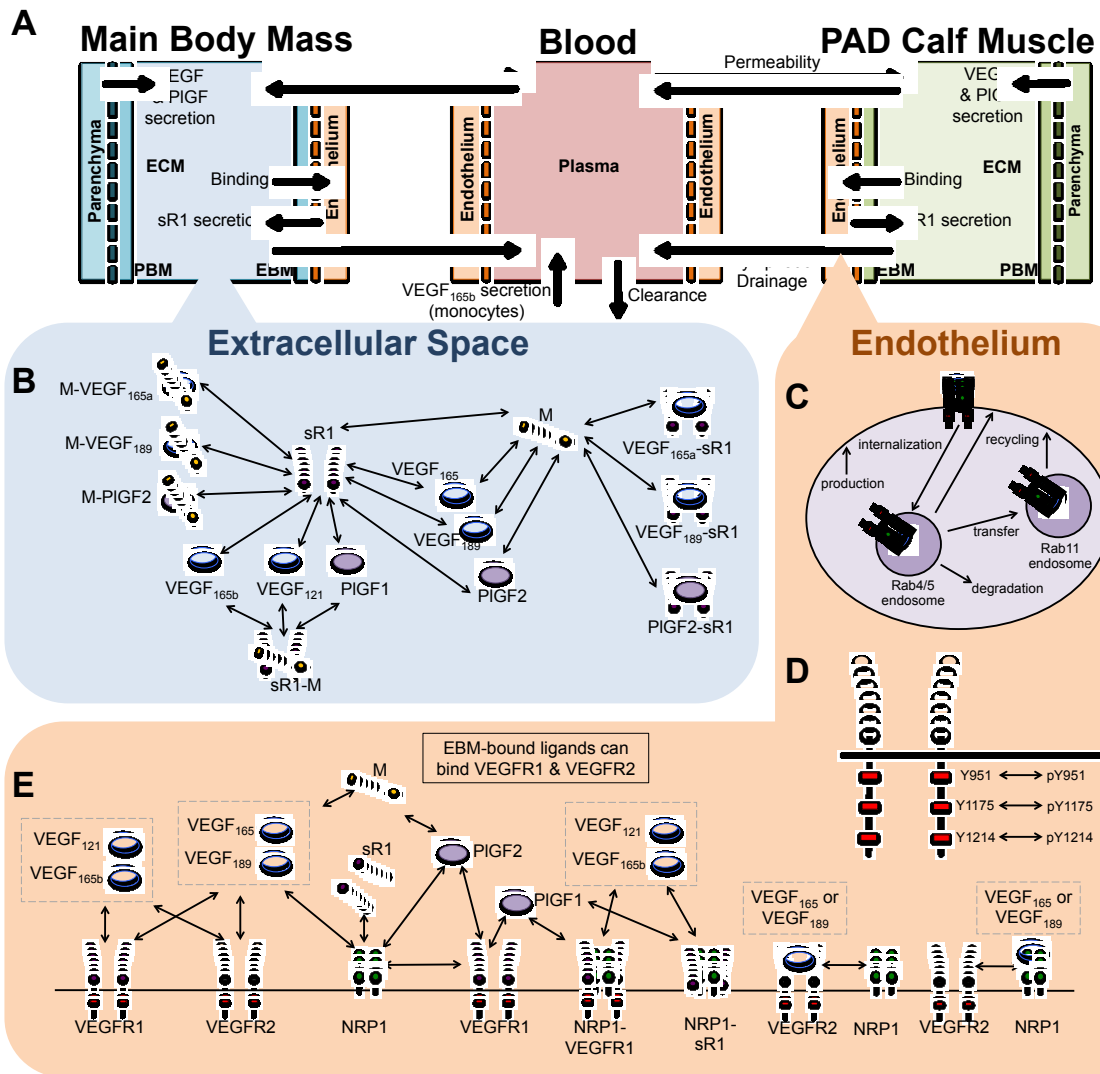
Figure 7-S2. Pharmacokinetics of VEGF$_{165a}$ and VEGF$_{165b}$ in PAD. This figure is related to **Fig 7-2**. **(A)** Predicted distribution of free and sR1-bound VEGF and PlGF isoforms in plasma at steady-state with equal secretion of VEGF$_{165a}$ and VEGF$_{165b}$ in both tissue compartments. Approximately 1/3 of plasma VEGF is tissue-derived (the same as in healthy subjects), and 2/3 is monocyte-secreted directly into the bloodstream. **(B)** Fraction of free plasma VEGF that is VEGF$_{165b}$, as a function of VEGF$_{165b}$ secretion fractions in the PAD Calf Muscle and the Main Body Mass. **(C)** Predicted distribution of VEGF isoforms, PlGF isoforms, and sR1 in the extracellular space (non-endothelial cell-bound) of the PAD Calf Muscle with equal secretion of VEGF$_{165a}$ and VEGF$_{165b}$. **(D)** Changes in ligand secretion and receptor production rates required to maintain target plasma ligand and endothelial cell surface receptor levels in the PAD Calf Muscle, as a function of the relative fraction of total VEGF$_{165}$ secretion that is VEGF$_{165b}$. Lack of NRP1-binding by VEGF$_{165b}$ slowing binding to VEGFR2 and subsequent recycling, and thus slowing turn-over of VEGF$_{165b}$-VEGFR2 complexes. The latter also leads to lower VEGF secretion and VEGFR2 production rates required to maintain target levels when VEGF$_{165b}$ is elevated. **(E)** VEGF distribution in plasma and the PAD Calf Muscle (Tissue), as a function of the relative fraction of total VEGF$_{165}$ secretion that is VEGF$_{165b}$ (versus VEGF$_{165a}$). Note that total free VEGF in plasma is held constant as the relative secretion ratio changes.

50% VEGF₁₆₅ᵦ

A Plasma

B Plasma VEGF₁₆₅ᵦ as a Biomarker?

C PAD Calf Extracellular

D Production

E VEGF Distribution
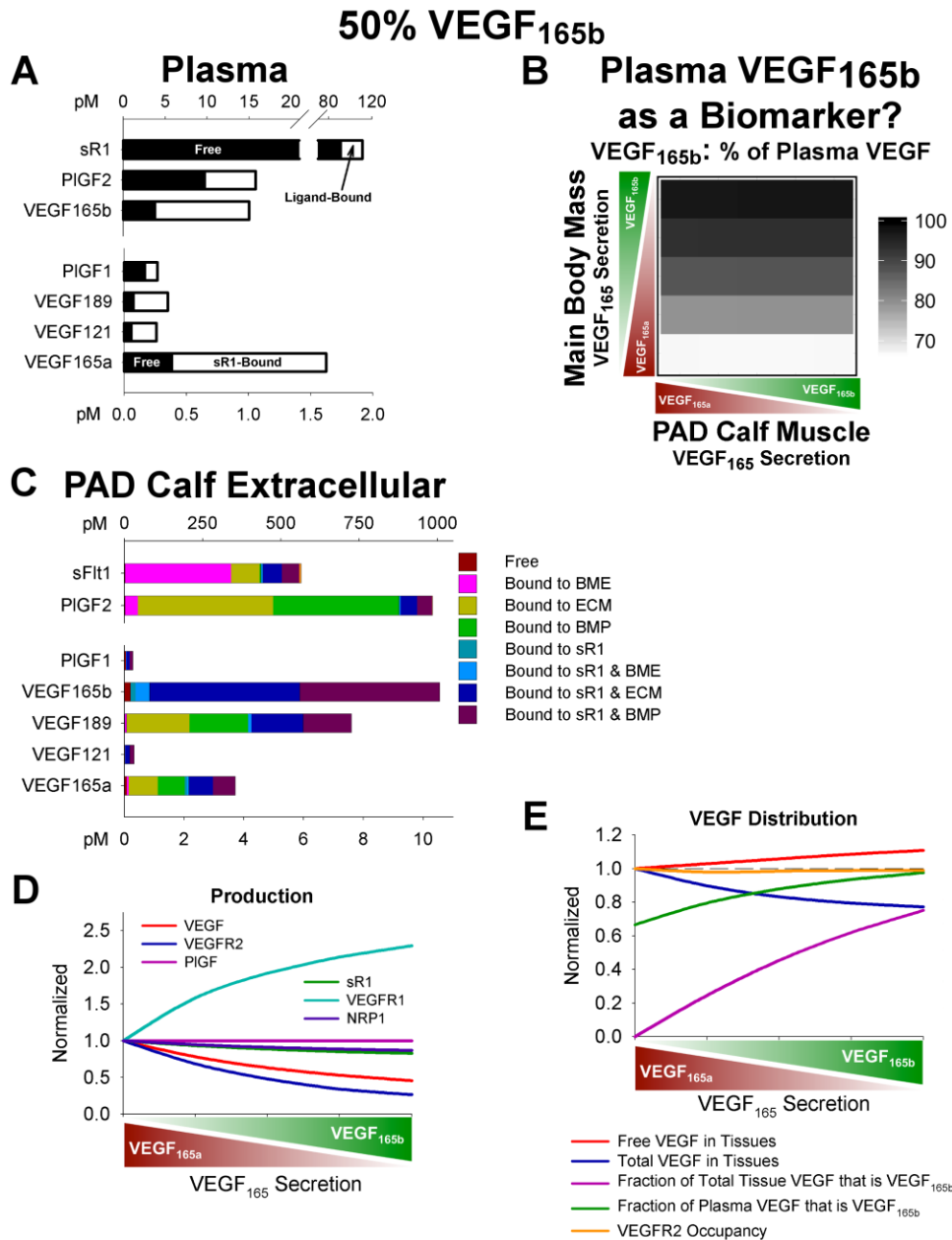
Figure 7-S2

Figure 7-S3. VEGFR occupancy in PAD Calf Muscle. This figure is related to **Fig 7-3**. **(A)** Break-down free and ligand-bound VEGFR2 on the cell surface, in early (Rab4/5) endosomes, and recycling (Rab11) endosomes, and cell surface VEGFR1 and NRP1. Quantities are given in pM of total tissue in the PAD Calf Muscle. Receptor occupancy for each subcellular location is shown in parentheses. **(B)** Break-down of EC surface-bound ligand, by isoform. Note the difference in quantities of total ligated VEGFR2, VEGFR1, and NRP1.
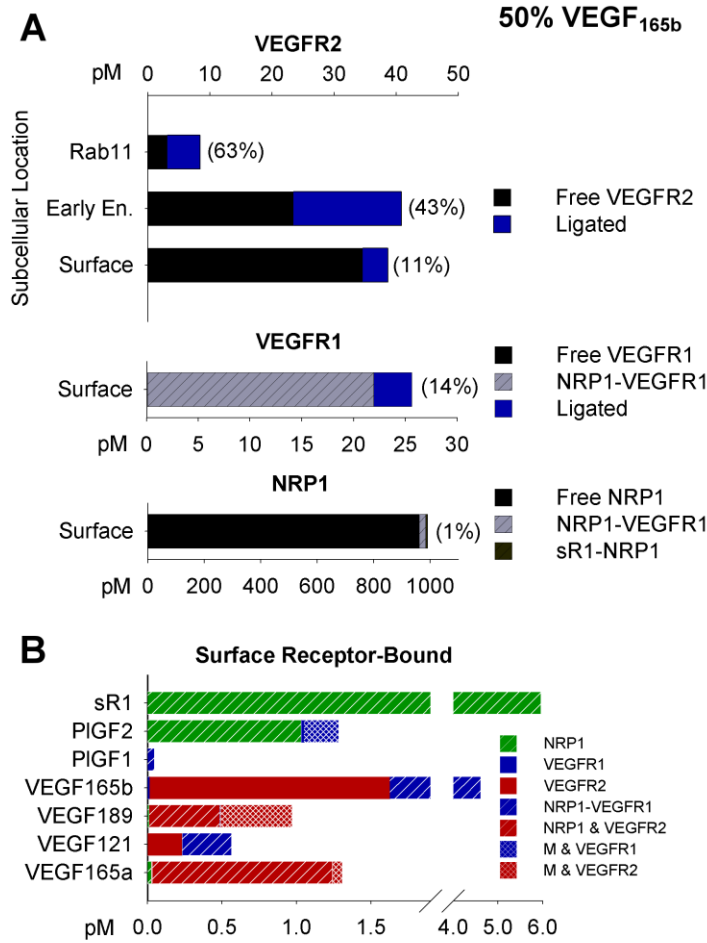
Figure 7-S4. *In vitro* **simulations of VEGFR2 phosphorylation by VEGF**$_{165b}$**.**This figure is related to **Fig 7-4**. **(A)** Comparison of simulated (solid lines) and experimental measurements (dashed lines) of VEGFR2 phosphorylation 5 minutes after stimulation with VEGF$_{165a}$ (red) and VEGF$_{165b}$ (green), using the optimized k_p value of 8×10^{-4} s^{-1} for VEGF$_{165b}$ and the normal phosphorylation rate for VEGF$_{165a}$ (1 s^{-1}). **(B)** Dose-dependent competition between VEGF$_{165a}$ and VEGF$_{165b}$. Solid lines: pR2, normalized by VEGF$_{165a}$ at each concentration (left axis). Dashed lines: VEGFR2 occupancy (right axis). Simulations performed using endothelial cell culture model including VEGFR2 and NRP1, but not VEGFR1 [2].
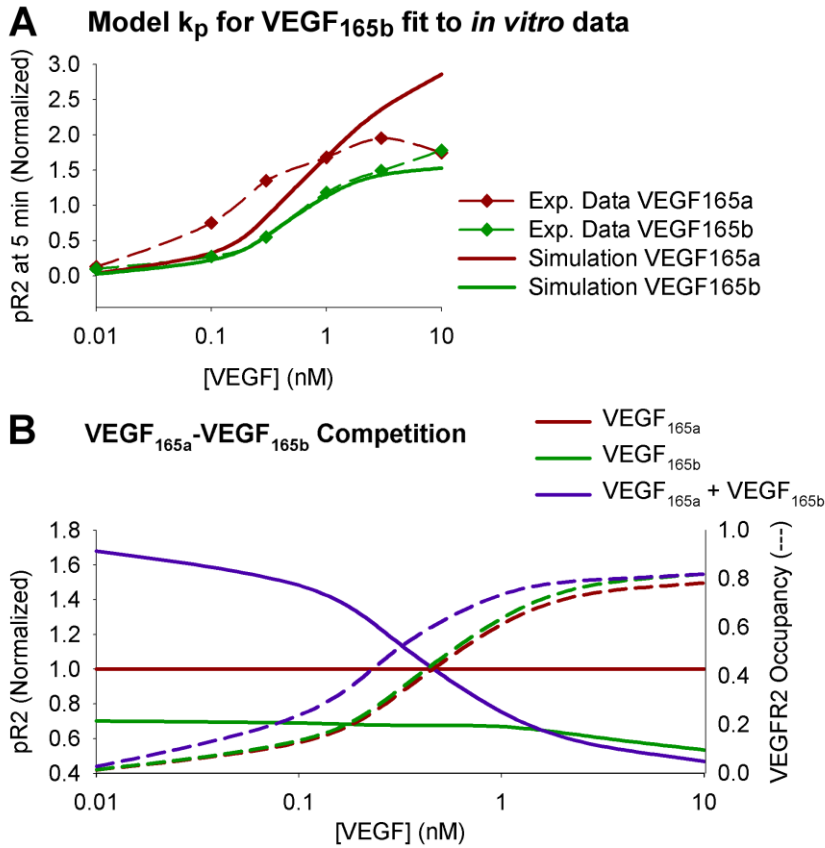
Figure 7-S5. *In vivo* **VEGFR activation varies with VEGF$_{165b}$ levels in simulated human PAD.** This figure is related to **Fig 7-5**. **(A)** Additional summary of VEGFR2 occupancy, ligation, and phosphorylation, as a function of local fractional VEGF$_{165b}$ secretion in the PAD Calf Muscle. **(B)** Summary of reduced endothelial surface VEGFR1 ligation by non-VEGF$_{165b}$ ligands with increasing VEGF$_{165b}$ secretion. **(C)** Further break-down of VEGFR2 phosphorylation as a function of VEGF isoform, subcellular location, and tyrosine site, with 50% fractional VEGF$_{165b}$ secretion in the PAD Calf Muscle.
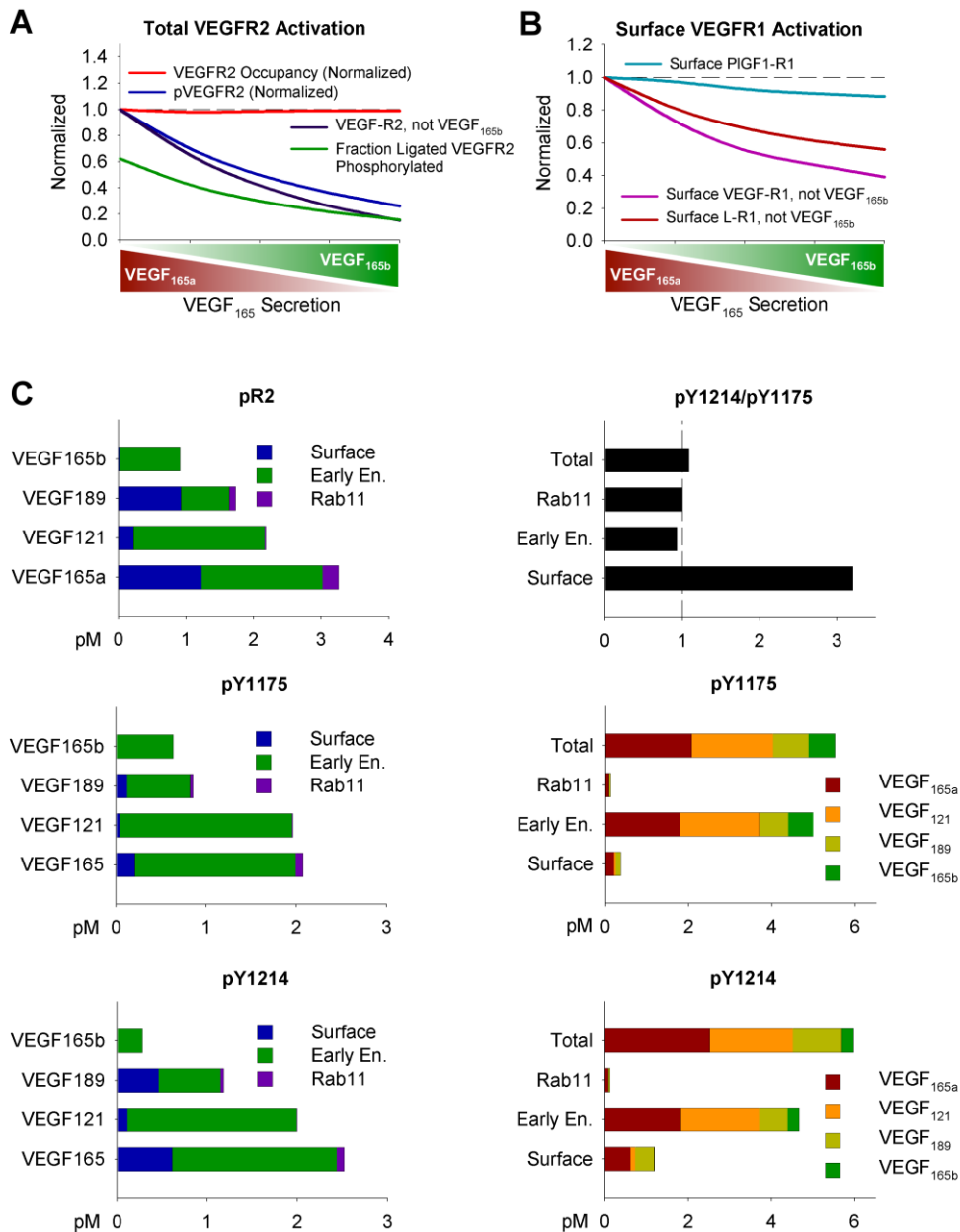
Figure 7-S6. Model-predicted changes in VEGF distribution and signaling in response to VEGF$_{165b}$ over-expression. This figure is related to **Fig 7-6**. **(A-B)** Simulation of direct increases or decreases in local VEGF$_{165b}$ **(A)** or VEGF$_{165a}$ **(B)** secretion in the PAD Calf Muscle, at 100% **(A)** or 50% **(B)** fractional VEGF$_{165b}$ secretion ratios, normalized to baseline quantities. **(C)** Additional model predictions for simulated VEGF$_{165b}$ over-expression experiment presented in **Fig 6A-B**. **(D)** Examination of the impact of a portion monocyte-derived VEGF$_{165b}$ secretion occurring into tissue instead of the bloodstream on VEGFR2 activation. The the model predicts increased pR2/R2, but reduced pR2/R2 and pR2/EC due to reduction in receptor levels and capillary rarefaction following increased local VEGF production.
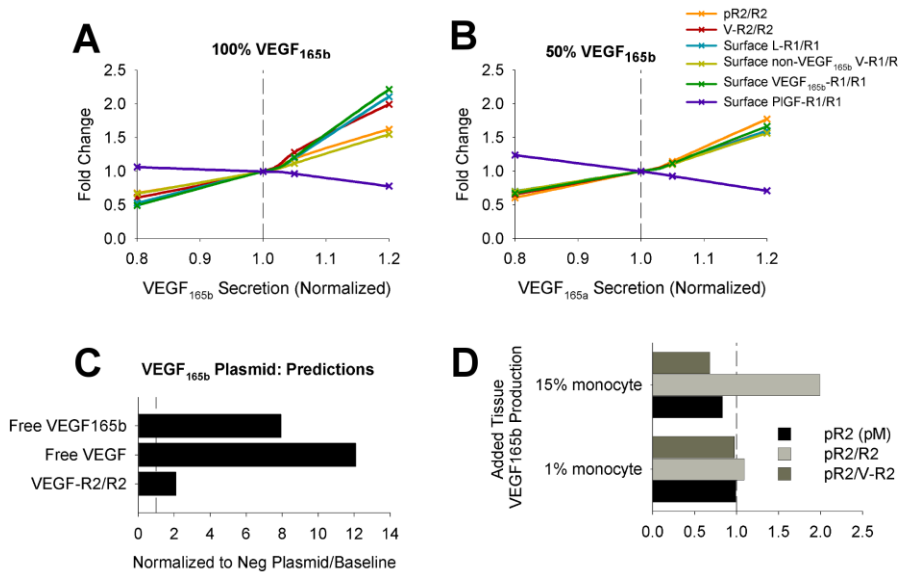
Figure 7-S7. Contributions of non-VEGF$_{165b}$ changes to reduced pR2 in PAD. (A) Comparison of total VEGFR2 phosphorylation, pR2/R2, and pR2/endothelial cell in the PAD Calf Muscle, a Healthy Calf Muscle, and three modified PAD Calf Muscle cases: no VEGF$_{165b}$ secretion by monocytes in the blood, healthy levels of VEGFR expression on endothelial cells, and healthy vascular permeability, to elucidate the impact on signaling of each change. 50% relative VEGF$_{165b}$ secretion in all cases. **(B)** Data from **(A)** displayed as percent change from PAD Calf Muscle baseline.
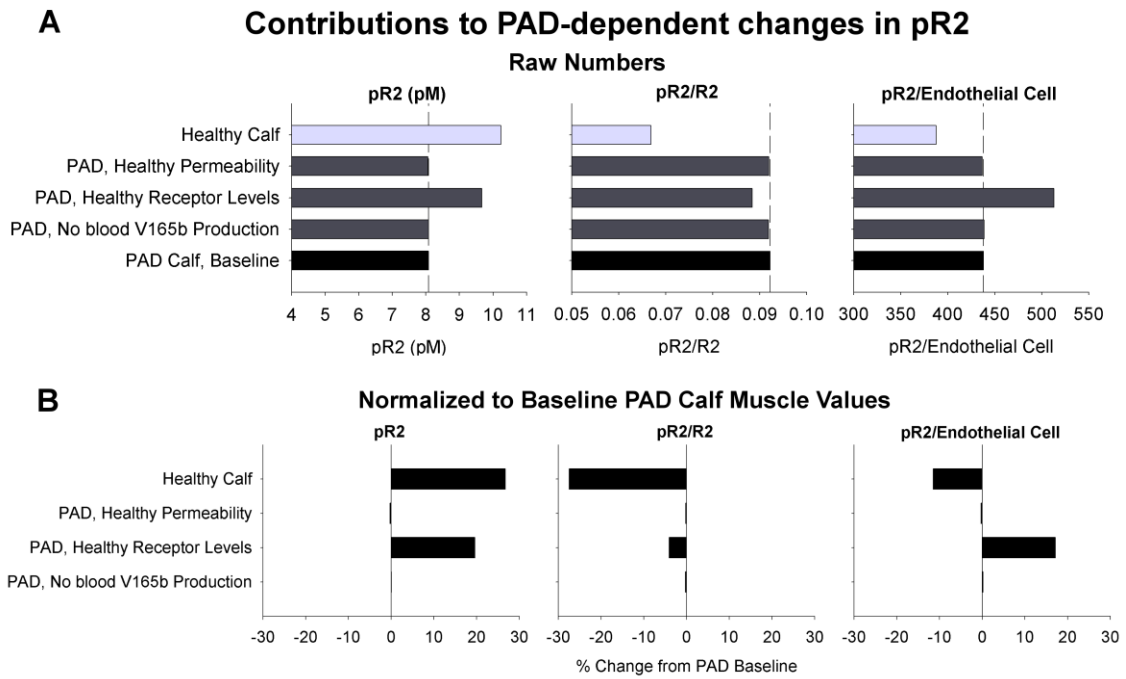
Figure 7-S8. Impact of excluding VEGF$_{165b}$ binding to NRP1-VEGFR1 complexes. (A) Changes in VEGF distribution, VEGFR1 ligation, and VEGFR2 activation if VEGF$_{165b}$-NRP1-VEGFR1 complexes are not included in the model. While ligated VEGFR2 would increases, pR2 decreases, owing to increased VEGF$_{165b}$R2 binding, and the amount of ligand bound to VEGFR1 decreases substantially, suggesting only a limited role of VEGF$_{165b}$ in VEGFR1 signaling if this were the case, contrary to the experimental results of Ganta et al. [3]. **(B)** In this case, the model had to be re-fit to maintain target endothelial surface receptor and plasma ligand levels. Those changes in secretion and production rates are shown here. MBM: Main Body Mass, PCM: PAD Calf Muscle.
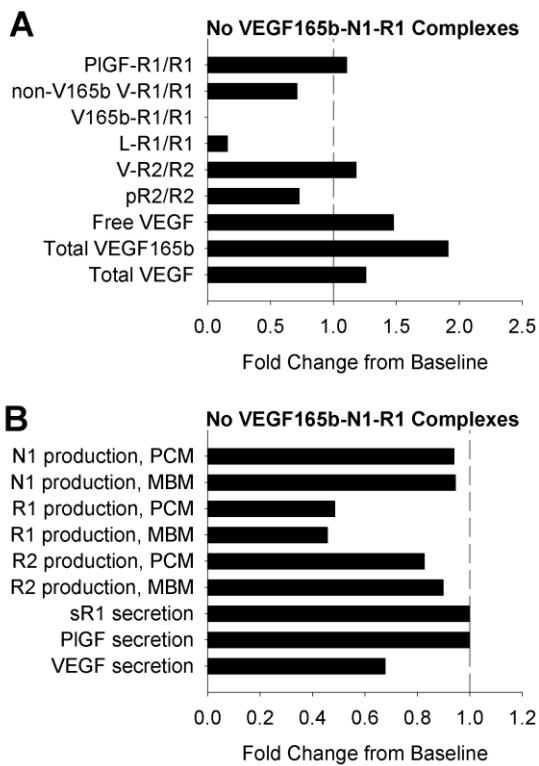
7.8 Supplemental Tables

Table 7-S1. Binding/Unbinding Reactions: K_D

K_D	VEGF$_{165}$	VEGF$_{121}$	VEGF$_{189}$	VEGF$_{165b}$	PlGF1	PlGF2	Units	
L-R1	3.3×10^{-11}	3.3×10^{-11}	3.3×10^{-11}	3.3×10^{-11}	2.3×10^{-10}	2.3×10^{-10}	M	[14-16]
L-R2	1.0×10^{-10}	1.0×10^{-10}	1.0×10^{-10}	1.0×10^{-10}	-	-	M	[14-16]
L-N1	1.2×10^{-9}	-	1.2×10^{-10}	-	-	1.0×10^{-7}	M	[17, 18]
L-sR1	3.3×10^{-11}	3.3×10^{-11}	3.3×10^{-11}	3.3×10^{-11}	2.3×10^{-10}	2.3×10^{-10}	M	[14]
L-M	6.1×10^{-8}	-	6.1×10^{-9}	-	-	4.6×10^{-9}	M	[19]
(M-L)-R1	3.3×10^{-11}	-	3.3×10^{-11}	-	-	2.3×10^{-10}	M	
(M-L)-R2	1.0×10^{-10}	-	1.0×10^{-10}	-	-	-	M	
(M-L)-sR1	3.3×10^{-11}	-	3.3×10^{-11}	-	-	2.3×10^{-10}	M	
M-(L-R1)	6.1×10^{-8}	-	6.1×10^{-9}	-	-	4.6×10^{-9}	M	
M-(L-R2)	6.1×10^{-8}	-	6.1×10^{-9}	-	-	-	M	
M-(L-sR1)	6.1×10^{-8}	-	6.1×10^{-9}	-	-	4.6×10^{-9}	M	
(L-sR1)-M	-	2.4×10^{-8}	-	2.4×10^{-8}	2.4×10^{-8}	-	M	
(M-sR1)-L	-	3.3×10^{-11}	-	3.3×10^{-11}	2.3×10^{-11}	-	M	
(N1-L)-R2	1.0×10^{-17}	-	1.0×10^{-17}	-	-	-	moles/cm^2	
N1-(L-R2)	3.2×10^{-17}	-	3.2×10^{-17}	-	-	-	moles/cm^2	
(L-R1)-N1	-	1.0×10^{-16}	-	1.0×10^{-16}	1.0×10^{-16}	-	moles/cm^2	
(L-sR1)-N1	-	1.8×10^{-9}	-	1.8×10^{-9}	1.8×10^{-9}	-	M	
(N1-R1)-L	-	3.3×10^{-11}	-	3.3×10^{-11}	2.3×10^{-10}	-	M	
(N1-sR1)-L	-	3.3×10^{-11}	-	3.3×10^{-11}	2.3×10^{-11}	-	M	

Other				
N1-R1	1.0×10^{-16}	moles/cm^2		[14]
sR1-N1	1.8×10^{-9}	M		[17, 18]
sR1-M	2.4×10^{-8}	M		

Notes:

1. L: ligand, column-specific

2. Ordering shows where the bond is. For example: in M-(L-sR1): M binding to L for VEGF$_{165}$, VEGF$_{189}$, & PlGF2. Whereas, in (L-sR1)-M, M binding to sR1 for VEGF$_{121}$, VEGF$_{165b}$, & PlGF1.

5. All rates are the same inside endosomes as on cell surface. Unit conversions (see [2, 13]) were required to convert all k_{on} (and thus K_D) into context-specific units, as in previous compartment models.

Table 7-S2. Binding/Unbinding Reactions: K_D in Main Body Mass

K_D	VEGF$_{165}$	VEGF$_{121}$	VEGF$_{189}$	VEGF$_{165b}$	PlGF1	PlGF2	Units	Ref
L-R1	1.0×10^{-15}	1.0×10^{-15}	1.0×10^{-15}	1.0×10^{-15}	6.9×10^{-15}	6.9×10^{-15}	moles/cm^3 tissue	[14-16]
L-R2	3.0×10^{-15}	3.0×10^{-15}	3.0×10^{-15}	3.0×10^{-15}	-	-	moles/cm^3 tissue	[14-16]
L-N1	3.6×10^{-14}	-	3.6×10^{-15}	-	-	1.0×10^{-7}	moles/cm^3 tissue	[17, 18]
L-sR1	1.0×10^{-15}	1.0×10^{-15}	1.0×10^{-15}	1.0×10^{-15}	6.9×10^{-15}	6.9×10^{-15}	moles/cm^3 tissue	[14]
L-M	1.8×10^{-12}	-	1.8×10^{-13}	-	-	1.4×10^{-13}	moles/cm^3 tissue	[19]
(M-L)-R1	1.0×10^{-15}	-	1.0×10^{-15}	-	-	6.9×10^{-15}	moles/cm^3 tissue	
(M-L)-R2	3.0×10^{-15}	-	3.0×10^{-15}	-	-	-	moles/cm^3 tissue	
(M-L)-sR1	1.0×10^{-15}	-	1.0×10^{-15}	-	-	6.9×10^{-15}	moles/cm^3 tissue	
M-(L-R1)	1.8×10^{-12}	-	1.8×10^{-13}	-	-	1.4×10^{-13}	moles/cm^3 tissue	
M-(L-R2)	1.8×10^{-12}	-	1.8×10^{-13}	-	-	-	moles/cm^3 tissue	
M-(L-sR1)	1.8×10^{-12}	-	1.8×10^{-13}	-	-	1.4×10^{-13}	moles/cm^3 tissue	
(L-sR1)-M	-	7.2×10^{-13}	-	7.2×10^{-13}	7.2×10^{-13}	-	moles/cm^3 tissue	
(M-sR1)-L	-	6.9×10^{-15}	-	6.9×10^{-15}	6.9×10^{-15}	-	moles/cm^3 tissue	
(N1-L)-R2	7.3×10^{-16}	-	7.3×10^{-16}	-	-	-	moles/cm^3 tissue	
N1-(L-R2)	2.3×10^{-15}	-	2.3×10^{-15}	-	-	-	moles/cm^3 tissue	
(L-R1)-N1	-	7.3×10^{-15}	-	7.3×10^{-15}	7.3×10^{-15}	-	moles/cm^3 tissue	
(L-sR1)-N1	-	5.4×10^{-14}	-	5.4×10^{-14}	5.4×10^{-14}	-	moles/cm^3 tissue	
(N1-R1)-L	-	1.0×10^{-15}	-	1.0×10^{-15}	1.0×10^{-15}	-	moles/cm^3 tissue	
(N1-sR1)-L	-	1.0×10^{-15}	-	1.0×10^{-15}	1.0×10^{-15}	-	moles/cm^3 tissue	
Other								
N1-R1	7.3×10^{-15}						moles/cm^3 tissue	[14]
sR1-N1	5.4×10^{-14}						moles/cm^3 tissue	
sR1-M	7.2×10^{-13}						moles/cm^3 tissue	[17, 18]

Table 7-S3. Binding/Unbinding Reactions: K_D in PAD Calf Muscle

K_D	VEGF$_{165}$	VEGF$_{121}$	VEGF$_{189}$	VEGF$_{165b}$	PlGF1	PlGF2	Units
L-R1	8.9×10^{-15}	8.9×10^{-15}	8.9×10^{-15}	8.9×10^{-15}	6.2×10^{-14}	6.2×10^{-14}	moles/cm^3 tissue [14-16]
L-R2	2.7×10^{-14}	2.7×10^{-14}	2.7×10^{-14}	2.7×10^{-14}	-	-	moles/cm^3 tissue [14-16]
L-N1	3.2×10^{-13}	-	3.2×10^{-14}	-	-	1.1×10^{-11}	moles/cm^3 tissue [17, 18]
L-sR1	8.9×10^{-15}	8.9×10^{-15}	8.9×10^{-15}	8.9×10^{-15}	6.2×10^{-14}	6.2×10^{-14}	moles/cm^3 tissue [14]
L-M	1.6×10^{-11}	-	1.6×10^{-12}	-	-	2.7×10^{-11}	moles/cm^3 tissue [19]
(M-L)-R1	8.9×10^{-15}	-	8.9×10^{-15}	-	-	6.2×10^{-14}	moles/cm^3 tissue
(M-L)-R2	2.7×10^{-14}	-	2.7×10^{-14}	-	-	-	moles/cm^3 tissue
(M-L)-sR1	8.9×10^{-15}	-	8.9×10^{-15}	-	-	6.2×10^{-14}	moles/cm^3 tissue
M-(L-R1)	1.6×10^{-11}	-	1.6×10^{-12}	-	-	2.7×10^{-11}	moles/cm^3 tissue
M-(L-R2)	1.6×10^{-11}	-	1.6×10^{-12}	-	-	-	moles/cm^3 tissue
M-(L-sR1)	1.6×10^{-11}	-	1.6×10^{-12}	-	-	2.7×10^{-11}	moles/cm^3 tissue
(L-sR1)-M	-	6.5×10^{-12}	-	6.5×10^{-12}	6.5×10^{-12}	-	moles/cm^3 tissue
(M-sR1)-L	-	8.9×10^{-15}	-	8.9×10^{-15}	6.2×10^{-14}	-	moles/cm^3 tissue
(N1-L)-R2	4.9×10^{-16}	-	4.9×10^{-16}	-	-	-	moles/cm^3 tissue
N1-(L-R2)	1.6×10^{-15}	-	1.6×10^{-15}	-	-	-	moles/cm^3 tissue
(L-R1)-N1	-	4.9×10^{-15}	-	4.9×10^{-15}	4.9×10^{-15}	-	moles/cm^3 tissue
(L-sR1)-N1	-	4.9×10^{-13}	-	4.9×10^{-13}	4.9×10^{-13}	-	moles/cm^3 tissue
(N1-R1)-L	-	8.9×10^{-15}	-	8.9×10^{-15}	6.2×10^{-14}	-	moles/cm^3 tissue
(N1-sR1)-L	-	8.9×10^{-15}	-	8.9×10^{-15}	6.2×10^{-14}	-	moles/cm^3 tissue
Other							
N1-R1	4.9×10^{-15}	moles/cm^3 tissue					[14]
sR1-N1	4.9×10^{-13}	moles/cm^3 tissue					
sR1-M	6.5×10^{-12}	moles/cm^3 tissue					[17, 18]

Table 7-S4. Binding/Unbinding Reactions: K_D in Plasma

$\underline{K_D}$	VEGF 165	VEGF 121	VEGF 189	VEGF$_{165b}$	PlGF1	PlGF2	Units	
L-sR1	2.0×10^{-14}	2.0×10^{-14}	2.0×10^{-14}	2.0×10^{-14}	1.4×10^{-13}	1.4×10^{-13}	moles/ cm^3 plasma	[14]

Table 7-S5. Binding/Unbinding Reactions: k_{on}

k_{on}	VEGF$_{165}$	VEGF$_{121}$	VEGF$_{189}$	VEGF$_{165b}$	PlGF1	PlGF2	Units
L-R1	3.0×10^7	3.0×10^7	3.0×10^7	3.0×10^7	1.5×10^6	1.5×10^6	$M^{-1} s^{-1}$
L-R2	1.0×10^7	1.0×10^7	1.0×10^7	1.0×10^7	-	-	$M^{-1} s^{-1}$
L-N1	5.0×10^5	-	1.4×10^6	-	-	1.0×10^4	$M^{-1} s^{-1}$
L-sR1	3.0×10^7	3.0×10^7	3.0×10^7	3.0×10^7	1.5×10^6	1.5×10^6	$M^{-1} s^{-1}$
L-M	1.6×10^5	-	1.6×10^5	-	-	2.2×10^5	$M^{-1} s^{-1}$
(M-L)-R1	3.0×10^7	-	3.0×10^7	-	-	1.5×10^6	$M^{-1} s^{-1}$
(M-L)-R2	1.0×10^7	-	1.0×10^7	-	-	-	$M^{-1} s^{-1}$
(M-L)-sR1	3.0×10^7	-	3.0×10^7	-	-	1.5×10^6	$M^{-1} s^{-1}$
M-(L-R1)	1.6×10^5	-	1.6×10^5	-	-	2.2×10^5	$M^{-1} s^{-1}$
M-(L-R2)	1.6×10^5	-	1.6×10^5	-	-	-	$M^{-1} s^{-1}$
M-(L-sR1)	1.6×10^5	-	1.6×10^5	-	-	2.2×10^5	$M^{-1} s^{-1}$
(L-sR1)-M	-	4.2×10^5	-	4.2×10^5	4.2×10^5	-	$M^{-1} s^{-1}$
(M-sR1)-L	-	3.0×10^7	-	3.0×10^7	1.5×10^6	-	$M^{-1} s^{-1}$
(N1-L)-R2	1.0×10^{14}	-	1.0×10^{14}	-	-	-	$(moles/cm^2)^{-1} s^{-1}$
N1-(L-R2)	3.1×10^{13}	-	3.1×10^{13}	-	-	-	$(moles/cm^2)^{-1} s^{-1}$
(L-R1)-N1	-	1.0×10^{14}	-	1.0×10^{14}	1.0×10^{14}	-	$(moles/cm^2)^{-1} s^{-1}$
(L-sR1)-N1	-	5.6×10^6	-	5.6×10^6	5.6×10^6	-	$M^{-1} s^{-1}$
(N1-R1)-L	-	3.0×10^7	-	3.0×10^7	1.5×10^6	-	$M^{-1} s^{-1}$
(N1-sR1)-L	-	3.0×10^7	-	3.0×10^7	1.5×10^6	-	$M^{-1} s^{-1}$

Other		
N1-R1	1.0×10^{14}	$(moles/cm^2)^{-1} s^{-1}$
sR1-N1	5.6×10^6	$M^{-1} s^{-1}$
sR1-M	4.2×10^5	$M^{-1} s^{-1}$

Table 7-S6. Binding/Unbinding Reactions: k_{on} in Main Body Mass

k_{on}	VEGF$_{165}$	VEGF$_{121}$	VEGF$_{189}$	VEGF$_{165b}$	PlGF1	PlGF2	Units
L-R1	1.0×10^{12}	1.0×10^{12}	1.0×10^{12}	1.0×10^{12}	5.0×10^{10}	5.0×10^{10}	$(\text{moles/cm}^3\ \text{tissue})^{-1}\ \text{s}^{-1}$
L-R2	3.3×10^{11}	3.3×10^{11}	3.3×10^{11}	3.3×10^{11}	-	-	$(\text{moles/cm}^3\ \text{tissue})^{-1}\ \text{s}^{-1}$
L-N1	1.7×10^{10}	-	4.7×10^{10}	-	-	3.3×10^{8}	$(\text{moles/cm}^3\ \text{tissue})^{-1}\ \text{s}^{-1}$
L-sR1	1.0×10^{12}	1.0×10^{12}	1.0×10^{12}	1.0×10^{12}	5.0×10^{10}	5.0×10^{10}	$(\text{moles/cm}^3\ \text{tissue})^{-1}\ \text{s}^{-1}$
L-M	5.3×10^{9}	-	5.3×10^{9}	-	-	7.3×10^{10}	$(\text{moles/cm}^3\ \text{tissue})^{-1}\ \text{s}^{-1}$
(M-L)-R1	1.0×10^{12}	-	1.0×10^{12}	-	-	5.0×10^{10}	$(\text{moles/cm}^3\ \text{tissue})^{-1}\ \text{s}^{-1}$
(M-L)-R2	3.3×10^{11}	-	3.3×10^{11}	-	-	-	$(\text{moles/cm}^3\ \text{tissue})^{-1}\ \text{s}^{-1}$
(M-L)-sR1	1.0×10^{12}	-	1.0×10^{12}	-	-	5.0×10^{10}	$(\text{moles/cm}^3\ \text{tissue})^{-1}\ \text{s}^{-1}$
M-(L-R1)	5.3×10^{9}	-	5.3×10^{9}	-	-	7.3×10^{9}	$(\text{moles/cm}^3\ \text{tissue})^{-1}\ \text{s}^{-1}$
M-(L-R2)	5.3×10^{9}	-	5.3×10^{9}	-	-	-	$(\text{moles/cm}^3\ \text{tissue})^{-1}\ \text{s}^{-1}$
M-(L-sR1)	5.3×10^{9}	-	5.3×10^{9}	-	-	7.3×10^{9}	$(\text{moles/cm}^3\ \text{tissue})^{-1}\ \text{s}^{-1}$
(L-sR1)-M	-	1.4×10^{10}	-	1.4×10^{10}	1.4×10^{10}	-	$(\text{moles/cm}^3\ \text{tissue})^{-1}\ \text{s}^{-1}$
(M-sR1)-L	-	1.0×10^{12}	-	1.0×10^{12}	5.0×10^{10}	-	$(\text{moles/cm}^3\ \text{tissue})^{-1}\ \text{s}^{-1}$
(N1-L)-R2	1.4×10^{12}	-	1.4×10^{12}	-	-	-	$(\text{moles/cm}^3\ \text{tissue})^{-1}\ \text{s}^{-1}$
N1-(L-R2)	4.2×10^{11}	-	4.2×10^{11}	-	-	-	$(\text{moles/cm}^3\ \text{tissue})^{-1}\ \text{s}^{-1}$
(L-R1)-N1	-	1.4×10^{12}	-	1.4×10^{12}	1.4×10^{12}	-	$(\text{moles/cm}^3\ \text{tissue})^{-1}\ \text{s}^{-1}$
(L-sR1)-N1	-	1.9×10^{11}	-	1.9×10^{11}	1.9×10^{11}	-	$(\text{moles/cm}^3\ \text{tissue})^{-1}\ \text{s}^{-1}$
(N1-R1)-L	-	1.0×10^{12}	-	1.0×10^{12}	5.0×10^{10}	-	$(\text{moles/cm}^3\ \text{tissue})^{-1}\ \text{s}^{-1}$
(N1-sR1)-L	-	1.0×10^{12}	-	1.0×10^{12}	5.0×10^{10}	-	$(\text{moles/cm}^3\ \text{tissue})^{-1}\ \text{s}^{-1}$

Other		Units
N1-R1	1.4×10^{12}	$(\text{moles/cm}^3\ \text{tissue})^{-1}\ \text{s}^{-1}$
sR1-N1	1.9×10^{11}	$(\text{moles/cm}^3\ \text{tissue})^{-1}\ \text{s}^{-1}$
sR1-M	1.4×10^{11}	$(\text{moles/cm}^3\ \text{tissue})^{-1}\ \text{s}^{-1}$

Table 7-S7. Binding/Unbinding Reactions: k_{on} in PAD Calf Muscle

k_{on}	$VEGF_{165}$	$VEGF_{121}$	$VEGF_{189}$	$VEGF_{165b}$	PlGF1	PlGF2	Units
L-R1	1.1×10^{11}	1.1×10^{11}	1.1×10^{11}	1.1×10^{11}	5.6×10^{9}	5.6×10^{9}	(moles/cm³ tissue)⁻¹ s⁻¹
L-R2	3.7×10^{10}	3.7×10^{10}	3.7×10^{10}	3.7×10^{10}	-	-	(moles/cm³ tissue)⁻¹ s⁻¹
L-N1	1.9×10^{9}	-	5.2×10^{9}	-	-	3.7×10^{7}	(moles/cm³ tissue)⁻¹ s⁻¹
L-sR1	1.1×10^{11}	1.1×10^{11}	1.1×10^{11}	1.1×10^{11}	5.6×10^{9}	5.6×10^{9}	(moles/cm³ tissue)⁻¹ s⁻¹
L-M	5.9×10^{8}	-	5.9×10^{8}	-	-	8.1×10^{8}	(moles/cm³ tissue)⁻¹ s⁻¹
(M-L)-R1	1.1×10^{11}	-	1.1×10^{11}	-	-	5.6×10^{9}	(moles/cm³ tissue)⁻¹ s⁻¹
(M-L)-R2	3.7×10^{10}	-	3.7×10^{10}	-	-	-	(moles/cm³ tissue)⁻¹ s⁻¹
(M-L)-sR1	1.1×10^{11}	-	1.1×10^{11}	-	-	5.6×10^{9}	(moles/cm³ tissue)⁻¹ s⁻¹
M-(L-R1)	5.9×10^{8}	-	5.9×10^{8}	-	-	8.1×10^{8}	(moles/cm³ tissue)⁻¹ s⁻¹
M-(L-R2)	5.9×10^{8}	-	5.9×10^{8}	-	-	-	(moles/cm³ tissue)⁻¹ s⁻¹
M-(L-sR1)	5.9×10^{8}	-	5.9×10^{8}	-	-	8.1×10^{8}	(moles/cm³ tissue)⁻¹ s⁻¹
(L-sR1)-M	-	1.6×10^{9}	-	1.6×10^{9}	1.6×10^{9}	-	(moles/cm³ tissue)⁻¹ s⁻¹
(M-sR1)-L	-	1.1×10^{11}	-	1.1×10^{11}	5.6×10^{9}	-	(moles/cm³ tissue)⁻¹ s⁻¹
(N1-L)-R2	2.0×10^{12}	-	2.0×10^{12}	-	-	-	(moles/cm³ tissue)⁻¹ s⁻¹
N1-(L-R2)	6.3×10^{11}	-	6.3×10^{11}	-	-	-	(moles/cm³ tissue)⁻¹ s⁻¹
(L-R1)-N1	-	2.0×10^{12}	-	2.0×10^{12}	2.0×10^{12}	-	(moles/cm³ tissue)⁻¹ s⁻¹
(L-sR1)-N1	-	2.1×10^{10}	-	2.1×10^{10}	2.1×10^{10}	-	(moles/cm³ tissue)⁻¹ s⁻¹
(N1-R1)-L	-	1.1×10^{11}	-	1.1×10^{11}	5.6×10^{9}	-	(moles/cm³ tissue)⁻¹ s⁻¹
(N1-sR1)-L	-	5.6×10^{9}	-	5.6×10^{9}	5.6×10^{9}	-	(moles/cm³ tissue)⁻¹ s⁻¹

Other		Units
N1-R1	2.0×10^{12}	(moles/cm³ tissue)⁻¹ s⁻¹
sR1-N1	2.1×10^{10}	(moles/cm³ tissue)⁻¹ s⁻¹
sR1-M	1.6×10^{9}	(moles/cm³ tissue)⁻¹ s⁻¹

Table 7-S8. Binding/Unbinding Reactions: k_{on} in Plasma

k_{on}	$VEGF_{165}$	$VEGF_{121}$	$VEGF_{189}$	$VEGF_{165b}$	PlGF1	PlGF2	Units
L-sR1	3.3×10^{10}	3.3×10^{10}	3.3×10^{10}	3.3×10^{10}	2.5×10^{9}	2.5×10^{9}	$(\text{moles/cm}^3 \text{ tissue})^{-1} \text{ s}^{-1}$

Table 7-S9. Binding/Unbinding Reactions: k_{off}

$\underline{k_{off}}$	VEGF$_{165}$	VEGF$_{121}$	VEGF$_{189}$	VEGF$_{165b}$	PlGF1	PlGF2	Units
L-R1	1.0×10^{-3}	1.0×10^{-3}	1.0×10^{-3}	1.0×10^{-3}	3.5×10^{-4}	3.5×10^{-4}	s^{-1}
L-R2	1.0×10^{-3}	1.0×10^{-3}	1.0×10^{-3}	1.0×10^{-3}	-	-	s^{-1}
L-N1	6.0×10^{-4}	-	1.7×10^{-4}	-	-	1.0×10^{-3}	s^{-1}
L-sR1	1.0×10^{-3}	1.0×10^{-3}	1.0×10^{-3}	1.0×10^{-3}	3.5×10^{-4}	3.5×10^{-4}	s^{-1}
L-M	1.0×10^{-2}	-	1.0×10^{-3}	-	-	1.0×10^{-3}	s^{-1}
(M-L)-R1	1.0×10^{-3}	-	1.0×10^{-3}	-	-	3.5×10^{-4}	s^{-1}
(M-L)-R2	1.0×10^{-3}	-	1.0×10^{-3}	-	-	-	s^{-1}
(M-L)-sR1	1.0×10^{-3}	-	1.0×10^{-3}	-	-	3.5×10^{-4}	s^{-1}
M-(L-R1)	1.0×10^{-2}	-	1.0×10^{-3}	-	-	1.0×10^{-3}	s^{-1}
M-(L-R2)	1.0×10^{-2}	-	1.0×10^{-3}	-	-	-	s^{-1}
M-(L-sR1)	1.0×10^{-2}	-	1.0×10^{-3}	-	-	1.0×10^{-3}	s^{-1}
(L-sR1)-M	-	1.0×10^{-2}	-	1.0×10^{-2}	1.0×10^{-2}	-	s^{-1}
(M-sR1)-L	-	1.0×10^{-3}	-	1.0×10^{-3}	3.5×10^{-4}	-	s^{-1}
(N1-L)-R2	1.0×10^{-3}	-	1.0×10^{-3}	-	-	-	s^{-1}
N1-(L-R2)	1.0×10^{-3}	-	1.0×10^{-3}	-	-	-	s^{-1}
(L-R1)-N1	-	1.0×10^{-2}	-	1.0×10^{-2}	1.0×10^{-3}	-	s^{-1}
(L-sR1)-N1	-	1.0×10^{-2}	-	1.0×10^{-2}	1.0×10^{-3}	-	s^{-1}
(N1-R1)-L	-	1.0×10^{-3}	-	1.0×10^{-3}	3.5×10^{-4}	-	s^{-1}
(N1-sR1)-L	-	1.0×10^{-3}	-	1.0×10^{-3}	3.5×10^{-4}	-	s^{-1}
Other	N1-R1	1.0×10^{-2}	s^{-1}				
	sR1-N1	1.0×10^{-2}	s^{-1}				
	sR1-M	1.0×10^{-2}	s^{-1}				

Table 7-S10. Trafficking Parameters

Species Units: s^{-1}	k_{int} (from surface)	k_{rec4} (from Rab4/5)	k_{rec11} (from Rab11)	k_{4to11} (from Rab4/5)	k_{degr} (from Rab4/5)
R2	2.6×10^{-3}	3.8×10^{-3}	1.4×10^{-4}	1.0×10^{-5}	8.6×10^{-6}
V·R2	3.12×10^{-2}	3.8×10^{-3}	1.4×10^{-4}	1.0×10^{-5}	8.6×10^{-5}
M·V·R2	0	-	-	-	-
V	0	0	0	0	1.2×10^{-2}
N1	2.6×10^{-3}	3.8×10^{-5}	1.4×10^{-2}	1.9×10^{-2}	3.8×10^{-4}
V·N1	2.6×10^{-3}	3.8×10^{-5}	1.4×10^{-2}	1.9×10^{-2}	3.8×10^{-4}
V·N1·R2	3.12×10^{-2}	3.8×10^{-5}	1.4×10^{-2}	1.9×10^{-2}	6.8×10^{-4}
R1	2.6×10^{-3}	3.8×10^{-3}	1.4×10^{-4}	1.0×10^{-5}	8.6×10^{-5}
N1·R1	2.6×10^{-3}	3.8×10^{-5}	1.4×10^{-2}	1.9×10^{-2}	3.8×10^{-4}
L·R1	3.12×10^{-2}	3.8×10^{-3}	1.4×10^{-4}	1.0×10^{-5}	8.6×10^{-5}
L·N1·R1	3.12×10^{-2}	3.8×10^{-5}	1.4×10^{-2}	1.9×10^{-2}	3.8×10^{-4}
M·V·R1	0	-	-	-	-
L·sR1	0	0	0	0	3.8×10^{-4}
sR1·N1	2.6×10^{-3}	3.8×10^{-5}	1.4×10^{-2}	1.9×10^{-2}	3.8×10^{-4}
L·sR1·N1	2.6×10^{-3}	3.8×10^{-5}	1.4×10^{-2}	1.9×10^{-2}	3.8×10^{-4}

L: ligand- all trafficking parameters independent of ligand identify

Table 7-S11. Phosphorylation Parameters

	Free R2			V-R2 (not affected by N1 or M)		
	Cell Surface	Rab4/5 Endosomes	Rab11 Endosomes	Cell Surface	Rab4/5 Endosomes	Rab11 Endosomes
k_p (normal) (s^{-1})	0	0	0	1	1	1
k_p for VEGF$_{165b}$ (s^{-1})	0	0	0	8.0×10^{-4}	8.0×10^{-4}	8.0×10^{-4}
$k_{dp,Y951}$ (s^{-1})	30	30	30	0.043	75	30
$k_{dp,Y1775}$ (s^{-1})	30	30	30	4.98	0.00972	30
$k_{dp,Y1214}$ (s^{-1})	30	30	30	1.06	0.0307	30

*The "normal" k_p value applies to all VEGF isoforms other than VEGR$_{165b}$. k_p is the same in all locations

for a given VEGF isoform.

Table 7-S12. Geometric Parameterization

	Main Body Mass Value	PAD Calf Muscle Value	Units
Compartment Volume	60,453	738	cm^3
Individual Muscle Fiber			
Diameter	71	66	μm
Perimeter correction factor	1.14	1.14	
Perimeter	253	238	μm
FCSA	3904	3464	μm^2
Myonuclear density	120	150	mm^{-1}
MDSA	2104	1586	μm^2/MD
Muscle Fiber Space			
Muscle fiber density	242	175	fibers/mm^2 tissue
FSAV	611	417	cm^2/cm^3 tissue
Muscle fiber space volume fraction	94.4%	60.8%	cm^3/cm^3 tissue
Individual Capillary			
Luminal diameter	4.86	3.17	μm
Endothelium thickness	0.77	0.91	μm
Abluminal diameter	6.39	4.98	μm
Perimeter correction factor	1.1	1.1	
Abluminal perimeter	22.1	17.2	μm
CCSA	32.1	19.5	μm^2
Lumen CSA	18.6	7.91	μm^2
Endothelium CSA	13.5	11.6	μm^2
ECSA (abluminal)	1000	1000	μm^2/EC
Capillary Space			
Capillary:fiber ratio	1.36	1.63	
Capillary density	329	286	capillaries/mm^2 tissue
ESAV (abluminal)	73	49	cm^2/cm^3 tissue
Capillary space volume fraction	1.1%	0.6%	cm^3/cm^3 tissue
Endothelium space	0.4%	0.3%	cm^3/cm^3 tissue
Vascular space	0.6%	0.2%	cm^3/cm^3 tissue
Interstitial Space			
IS volume fraction	4.5%	38.7%	cm^3/cm^3 tissue
IF volume fraction	3.7%	32.9%	cm^3/cm^3 tissue
Available IF volume fraction	3%	27%	cm^3/cm^3 tissue
Extracellular Matrix			
ECM volume	3.9%	36.8%	cm^3/cm^3 tissue
	86.72%	95.1%	cm^3/cm^3 IS
Solid fraction	13.40%	13.40%	cm^3/cm^3 ECM
Fluid volume in ECM	3.38%	31.87%	cm^3/cm^3 tissue
	91.13%	96.97%	cm^3/cm^3 IF
Available fluid volume in ECM	2.87%	27.09%	cm^3/cm^3 tissue
Endothelial Basement Membrane (EBM)			
Thickness	87.5	1650	nm
EBM volume	0.06%	0.81%	cm^3/cm^3 tissue
	1.41%	2.1%	cm^3/cm^3 IS
Solid fraction	45%	45%	cm^3/cm^3 BME
Fluid volume in EBM	0.03%	0.45%	cm^3/cm^3 tissue
	0.94%	1.36%	cm^3/cm^3 IF
Available fluid volume in EBM	0.01%	0.15%	cm^3/cm^3 tissue
EBM Thickness accessible to EC receptors*	25	25	nm

Fraction EBM accessible to EC receptors	28.6%	1.52%	cm^3/cm^3 BME
Parenchymal Basement Membrane (PBM)			
Thickness	87.5	254	nm
PBM volume	0.53%	1.06%	cm^3/cm^3 tissue
	11.87%	2.74%	cm^3/cm^3 IS
Solid fraction	45%	45%	cm^3/cm^3 BMP
Fluid volume in PBM	0.29%	0.58%	cm^3/cm^3 tissue
	7.92%	1.77%	cm^3/cm^3 IF
Available fluid volume in PBM	0.10%	0.19%	cm^3/cm^3 tissue
Blood Compartment			
Total Volume	5		L
Plasma Fraction	60%		cm^3/cm^3 blood
Monocyte Concentration	400		monocytes/µL
Total Monocytes	2×10^9		monocytes

*Based on length of ErbB2 and ErbB3 extracellular domains: 11.3-16.4nm [20-22], assuming some

flexibility in cell shape and position.

Table 7-S13. Transport Parameters

	Permeability (bi-directional)	Lymphatic Drainage (Mass Body Mass to Blood)	Lymphatic Drainage (PAD Calf Muscle to Blood)	Clearance from Blood
VEGF	4.39×10^{-8} cm/s	0.1418 cm^3/s	0.0022 cm^3/s	1.08×10^{-3} s^{-1}
PlGF	4.39×10^{-8} cm/s	0.1418 cm^3/s	0.0022 cm^3/s	1.08×10^{-3} s^{-1}
sFlt1	1.86×10^{-8} cm/s	0.1418 cm^3/s	0.0022 cm^3/s	5.0×10^{-6} s^{-1}
VEGF-sFlt1	1.86×10^{-8} cm/s	0.1418 cm^3/s	0.0022 cm^3/s	5.0×10^{-6} s^{-1}
PlGF-sFlt1	1.86×10^{-8} cm/s	0.1418 cm^3/s	0.0022 cm^3/s	5.0×10^{-6} s^{-1}

Notes: Permeability rates apply to both PAD Calf Muscle & Main Body Mass. Geometric unit conversions applied [1].

Permeability rate constant is multiplied by a recruitment factor, γ (See Supplemental Equations), which is 1 for the Main Body Mass, and 0.5 for the PAD Calf Muscle.

Table 7-S14. Available Matrix Site Densities

	ECM	EBM	PBM
Value (μM)	0.75	20/5 (Body/Calf)	20/5
Main Body Mass (moles/cm^3 tissue)	2.15×10^{-11}	2.0×10^{-12}	2.0×10^{-11}
PAD Calf Muscle (moles/cm^3 tissue)	2.03×10^{-10}	7.5×10^{-10}	9.5×10^{-12}

Note: Unit conversions described in [1, 13, 14].

Table 7-S15. Comparison of Model Predictions with Previous Model

Topic	Exp. Data	Wu 2010[1]	Current	Change
Plasma sR1	Decreased/ unchanged	Increased	Decreased	Monocyte-derived VEGF$_{165b}$ secretion, so lower tissue VEGF secretion required to achieve plasma target VEGF levels
Interstitial VEGF	Unchanged or slightly increased	Increased 24-fold	Increased a maximum of 11%	
Plasma sR1 bound to ligand	0.06%	13%	17%	- (Not fixed)
Plasma VEGF bound to sR1	4%	91%	75%	
Angiogenic response	Impaired	Increased VEGFR2/VEGFR1 balance	Decreased pR2 + increased VEGFR1 ligation	• Weak phosphorylation of R2 by VEGF$_{165b}$ • Lower tissue VEGF • Receptor expression: VEGFR2 decreased & VEGFR1 increased in ischemia

Chapter 8. A Computational Analysis of Pro-angiogenic Therapies

Content from this chapter will be submitted for publication as:

L. E. Clegg & F. Mac Gabhann, "A computational analysis of pro-angiogenic therapies for peripheral artery disease."

8.0 Summary

Development of pro-angiogenic therapies for tissue engineering applications and ischemic disease has been the subject of extensive research and multiple clinical trials. However, effective induction of angiogenesis to form hierarchical, non-leaky networks of perfused vessels has remained an unmet challenge. Here, we use a previously-developed, multi-scale, computational systems pharmacology model of human peripheral artery disease, to screen a diverse array of promising pro-angiogenic strategies. This previously-validated model explicitly accounts for VEGF immobilization, Neuropilin-1 binding, and weak activation of VEGF receptor 2 (VEGFR2) by the "$VEGF_{xxxb}$" isoforms. First, we compare biomaterial-based delivery of VEGF engineered for increased affinity to the extracellular matrix, showing that these constructs, which show promise in mice, maintain more physiological VEGF levels and extend duration of VEGFR2 activation compared to $VEGF_{165a}$ delivery. We also demonstrate the importance of sub-saturating VEGF dosing to prevent angioma formation. Next, we examine the potential of ligand- or receptor-based gene therapy to normalize VEGF receptor signaling, if uniform and sustained expression can be achieved. Finally, we explore the potential for antibody-based therapy. Our model supports recent observations that improvement in perfusion following treatment with anti-$VEGF_{165b}$ in murine hindlimb ischemia is mediated by VEGF-receptor 1, not VEGFR2. Further, the model predicts that the approved cancer agent bevacizumab (anti-VEGF) may improve signaling via both VEGFR1 and VEGFR2 via a novel 'antibody swapping' effect that we demonstrate here. Altogether, this model provides insight into the mechanisms of action of several classes of pro-angiogenic strategies, identifying molecular signaling differences between

promising and ineffective approaches, and highlighting key questions and considerations for design,

optimization, and translation of these therapeutics into humans.

8.1 Introduction

Inducing angiogenesis, the growth of new vessels from the existing vasculature, in order to establish collateral blood flow has long been a therapeutic strategy of interest for ischemic disease[1,2]. Peripheral artery disease (PAD), the manifestation of systemic atherosclerosis in the legs, leads to pain, limited mobility, and elevated risk of amputation, and is characterized by skeletal muscle ischemia without induction of sufficient angiogenesis to restore normal perfusion[3,4]. The molecular mechanisms underlying this insufficient vascular remodeling have not been fully elucidated[5]. Delivery of vascular endothelial growth factor (VEGF), a key angiogenic factor, via gene- or cell-based therapy has been tested in multiple clinical trials for PAD, but no constructs have proceeded to Phase III trials or regulatory approval, due to lack of efficacy at improving patient outcomes as well as occurrence of edema in some patients[5,6]. This failure, which could be attributed in part to inefficient, spatially heterogeneous, short duration gene delivery[7-10], has motivated development of newer therapeutic strategies to better induce and regulate angiogenesis in ischemia. Strategies to form functional vessel networks in thick engineered tissues are also of high interest[11]. Key to success of these strategies is a more in-depth understanding of both the underlying cause(s) of impaired angiogenic signaling in PAD, and the effect of these molecular mechanisms on therapy effectiveness.

The VEGF family consists of five ligands, with VEGFA (hereafter VEGF) considered the primary pro-angiogenic isoform, three receptors (VEGFR1-3), and the Neuropilins as co-receptors[12]. Both ligands and receptors can be alternatively spliced, the latter resulting in production of soluble receptors, most notably soluble VEGFR1 (sR1)[13], and the former VEGF isoforms with different binding affinities for HSPGs in the extracellular matrix (ECM) and for Neuropilin-1 (NRP1) [14,15]. VEGF splicing varies by tissue[16,17], with the most prominent isoforms in human being $VEGF_{121}$, $VEGF_{165}$, and $VEGF_{189}$[12]. Expression of single VEGF isoforms in mice or tumors leads to different vascular phenotypes; non-ECM-binding $VEGF_{121}$ promotes production of wide diameter vessels with few branch points, while expression of ECM-binding $VEGF_{165}$ alone leads to phenotypically normal vessels, and strong ECM-binding $VEGF_{189}$ induces networks of thin, highly branched vessels[18-24]. An alternate set of VEGF "b" isoforms with the same numbers of amino acids, but a switch in the last six amino acids (exon 8a to exon 8b) have recently been discovered and characterized[25,26]. Despite very similar sequences, these isoforms, the most-studied

being $VEGF_{165b}$ (as opposed to $VEGF_{165a}$), do not bind to NRP1 or to HSPGs, and induce only weak

phosphorylation of $VEGFR2^{26-28}$, despite binding to the receptor with the same affinity as other VEGF

isoforms. While VEGF is found at normal levels in resting PAD-afflicted skeletal muscle[29,30], and is

elevated in the plasma of patients with PAD[31-34], splicing of VEGF is different in PAD[35,36] (and other

diseases). Specifically, expression of $VEGF_{165b}$ increases in tissue, likely accompanied by reduced

expression of $VEGF_{165a}$ (to maintain unchanged total VEGF levels); secretion of $VEGF_{165b}$ in the

bloodstream by peripheral blood mononuclear cells (e.g. monocytes) also increases substantially[36]. Despite

these observations, quantitative measurements of absolute quantities of $VEGF_{165a}$ and $VEGF_{165b}$ in healthy

and ischemic tissue remain very limited[37]. We previous built and published a model of the role of $VEGF_{165b}$

in PAD in the absence of pro-angiogenic therapy (Chapter 7), which showed that, contrary to the prevailing

hypothesis in the field, $VEGF_{165b}$ does not compete with $VEGF_{165a}$ for binding to VEGFR2, but may

compete for binding to VEGFR1. This prediction is consistent with recently published data from Ganta et.

al.[29]

Several different approaches to pro-angiogenic therapy for PAD, tissue engineering, and wound

healing are currently under development, which leverage different aspects of the VEGF system. The first

uses biomaterials for tunable, extended release of VEGF protein and other growth factors *in vivo*[11]. The

groups of Jeff Hubbell and Andrea Banfi have engineered VEGF forms for increased affinity to the ECM

or covalent binding in fibrin gels with tunable proteolytic release to deliver low VEGF and/or PDGF doses

over the course of weeks[38,39]. With these constructs, which can be delivered in injectable fibrin gels, they

obtained improved wound healing, reduced permeability, angiogenesis without vessel regression, and/or

improved perfusion recovery in rodent models, compared to delivery of wild type $VEGF_{165}$ protein. We are

also learning more about how to effectively induce angiogenesis via VEGF overexpression[7,8]. In the future,

these concepts can be combined with efforts to improve gene delivery to induce controlled expression

levels with high efficiency, spatially homogeneous transfection, and tunable duration, targeted to specific

cell types[40,41]. Such optimized control of gene delivery would likely address many of the failures observed

in past clinical trials. Finally, Kikuchi et. al. recently showed that treatment with an antibody that binds

specifically to the $VEGF_{165b}$ isoform improves perfusion recovery in murine hindlimb ischemia models[36],

an observation that was confirmed by Ganta et. al.[29]. The mechanism of action of this therapeutic was

predicted by Kikuchi et. al. to involve an increase in VEGFR2 phosphorylation. However, Ganta et. al. showed that VEGFR2 phosphorylation was unchanged following antibody treatment, while VEGFR1 phosphorylation increased. Our previous model of PAD showed that, contrary to the prevailing hypothesis in the field, $VEGF_{165b}$ does not compete with $VEGF_{165a}$ for binding to VEGFR2, but may compete for binding to VEGFR1, a prediction that is consistent with recently published data from Ganta et. al.[29]

8.1.1 Objective

Our objective was to use a previously-developed systems pharmacology model of human peripheral artery disease to screen promising protein-, gene-, and antibody-based pro-angiogenic therapeutics. Our systems pharmacology model, which has been built using and validated against *in vitro*, *ex vivo*, *in vivo*, and clinical data, includes detailed molecular biology and physiology, allowing us to: (1) ask questions that are difficult or impossible to answer experimentally, (2) provide insight into the mechanisms of action of therapies, and (3) identify potentially non-intuitive side effects, toxicity, or challenges to efficacy that merit further study. Specifically, we can predict free VEGF concentrations and VEGFR2 phosphorylation in diseased tissue following therapy administration, accounting for differences in VEGFR2 signaling as a function of VEGF isoform ECM- and NRP1-binding properties by leveraging a computational model that was built using and validated against *in vitro* data[42], then translated to consider these reactions in an *in vivo* context. By simulating failed therapies and those that show promise in mice in a single quantitative framework, we aim to identify potential molecular drivers of therapy success or failure[43]. In elucidating these key rules, we hope to identify strategies most likely to be effective in the context of human disease, working with, and potentially leveraging, the underlying biology.

8.2 Results

8.2.1 Quantitative insight into design and dosing for biomaterial-based VEGF delivery in PAD

We used our computational systems pharmacology model (**Fig. 8-1**) to perform *in silico* screening of VEGF protein delivery strategies, including native VEGF$_{165a}$ (which has failed to produce benefit in clinical trials), and two engineered constructs that have shown promise in mice: VEGF engineered for "super affinity" to the ECM [38], and VEGF covalently bound for proteolytic release [39], at multiple doses (**Fig. 8-2B**). Calibrating against experimental release data in mice (see Methods), our model gives as outputs the predicted local VEGF concentration and VEGFR2 phosphorylation following therapy (**Fig. 8-2B**) in the context of human PAD, using allometric scaling to adjust the dose for our human model. We found that, unlike native VEGF$_{165a}$ (in red), the VEGF constructs engineered for increased ECM affinity (purple & green) maintain free VEGF levels within a physiological range of no more than ~5-fold baseline levels (**Fig. 8-2B**), likely reducing induction of permeability following treatment. The engineered constructs also elevate VEGFR2 phosphorylation for at least 2 weeks, a duration close to the range shown experimentally to prevent vessel regression[7,8]. Simulations also predict increased ligation of endothelial VEGFR1 by all three constructs, but to a smaller extent than the increase on VEGFR2 (**Fig. 8-S1**). For this analysis, we assumed that 100% of locally produced VEGF$_{165}$ is VEGF$_{165b}$; the action of these therapies was similar regardless of endogenous VEGF$_{165b}$ production (not shown).

Figure 8-1. Overview of model structure and therapy implementation. (A) Structure of multi-scale whole body compartment model of human PAD. Antibody delivery is simulated as a 90 minute intravenous infusion, while gene therapy is simulated to target either parenchymal cells (targeting ligands) or endothelial cells (receptors) specifically in the PAD Calf Muscle. Biomaterial-based VEGF delivery assumes delivery into the extracellular space (ECM) of the PAD Calf Muscle. **(B)** Overview of key PAD-specific features in model: $VEGF_{165b}$ properties (left), and changes in VEGF splicing and secretion occurring in PAD (right). The binding and VEGFR2 phosphorylation properties of $VEGF_{165b}$ are explicitly included in the model, and VEGF secretion is altered from the healthy baseline model to reflect changes in VEGF distribution observed in PAD (see Chapter 7).
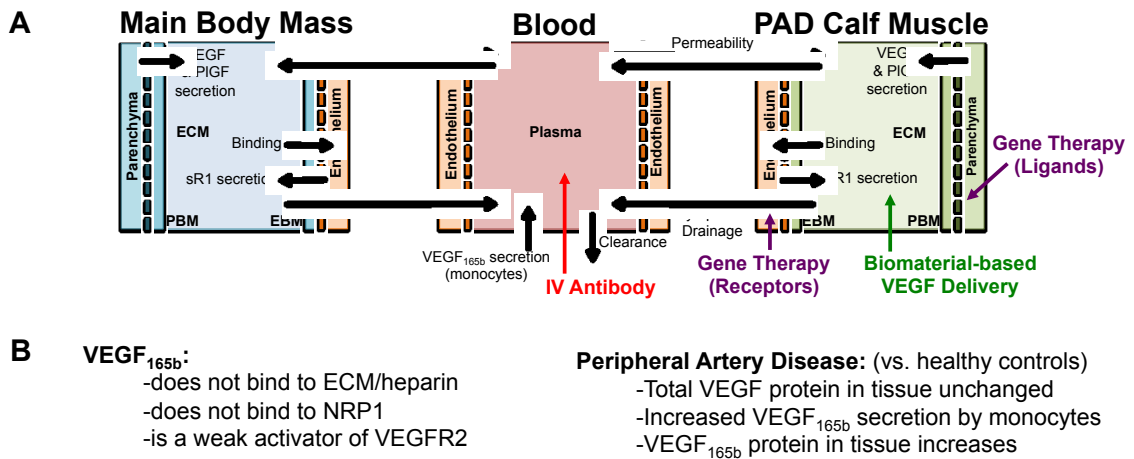
We next examined the important and challenging question of appropriate VEGF dosing. Simulations predict that VEGF doses leading to effective angiogenesis without angioma formation in mice correspond to sub-saturating VEGF receptor activation (**Fig. 8-2C**). Indeed, the lowest test dose in Ref. [39], 0.01 µg/mL, which was still able to induce stable angiogenesis by 3 months after gel implantation, is predicted to elevate VEGFR2 phosphorylation by only about 30%. This suggests that small increases in signaling, if sustained for a duration of weeks, are sufficient to induce and sustain therapeutic angiogenesis. Interestingly, only the highest dose (100 µg/mL) was predicted to saturate endothelial surface VEGFR1 (**Fig. 8-S2**). These predictions suggest that receptor saturation and VEGF-ECM binding affinity are both important considerations in dosing and translation of pro-angiogenic biomaterials.

Figure 8-2. ECM-binding affinity and dosing are key design considerations for effective VEGFR signaling following biomaterial-based VEGF delivery. (A) Summary of experimentally-tested VEGF constructs delivered in biomaterials and observed results in mice. **(B)** Calibrating against experimental data (left), we simulated the predicted magnitude and duration of increased local VEGF concentration (middle) and VEGFR2 phosphorylation (right) following delivery of 354μg (matched to mouse experiments, with allometric scaling to simulated human) of each VEGF construct delivered in a fibrin gel delivered at the same dose in the same system, assuming 100% local fractional VEGF$_{165b}$ secretion. **(C)** Simulation of delivery of the "Covalent VEGF w/ Proteolysis" construct at different doses, assuming 0% local fractional VEGF$_{165b}$ secretion.
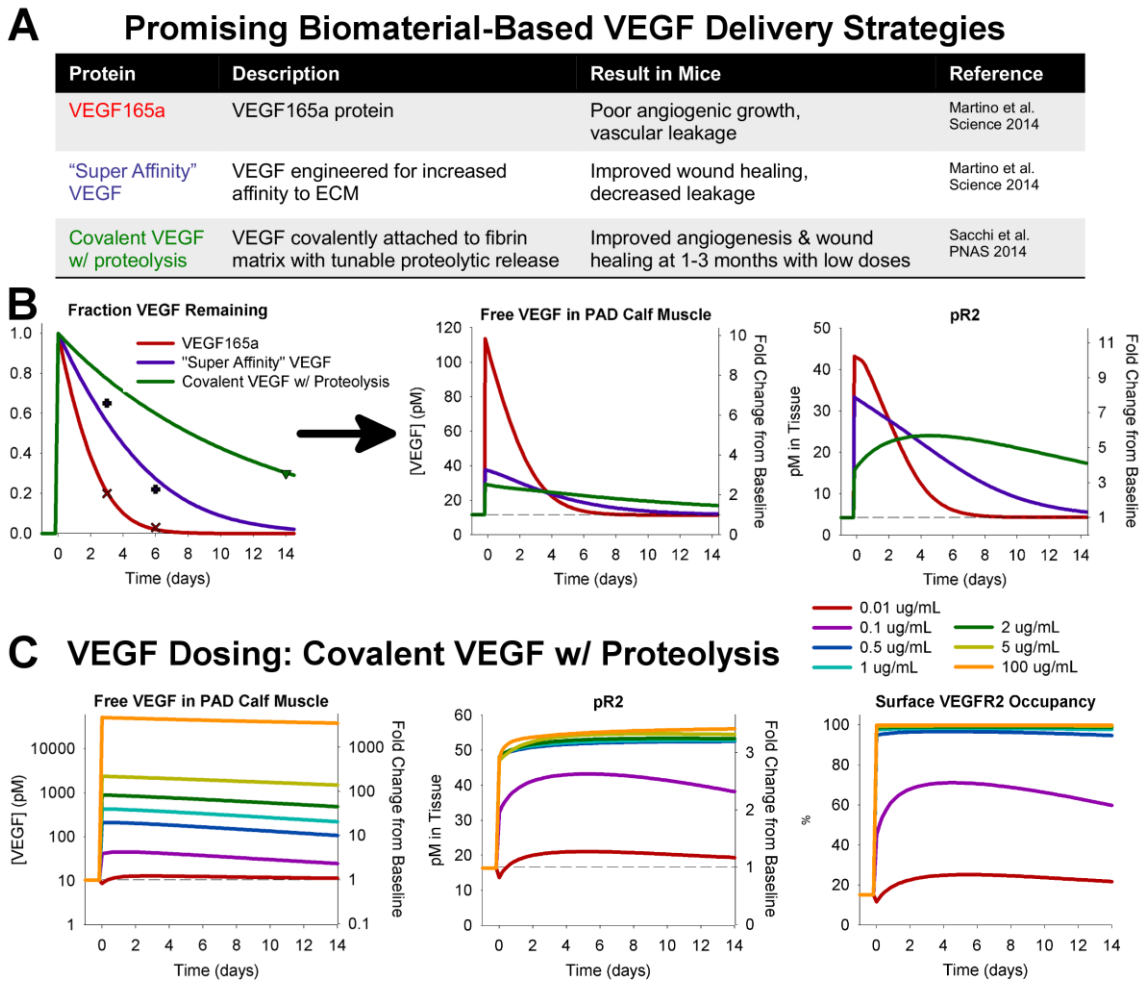
8.2.2 Gene therapy effectiveness depends on target and magnitude, as well as optimized delivery

We next examined delivery of VEGF family-related genes to the PAD Calf Muscle, assuming instant, 100% efficient, spatially homogeneous transfection of myocytes at a constant expression rate for the duration of the experiment, to examine if, with sufficient improvements in gene delivery, VEGF family gene therapy holds similar potential to biomaterial-based VEGF delivery to improve angiogenic signaling in PAD. We tested these therapies assuming high (100%) fractional production of $VEGF_{165b}$. While several trials in humans have delivered VEGF at levels sufficient to induce increased plasma or serum VEGF[44-46], based on our above results for VEGF protein delivery, we chose to examine smaller increases in VEGF expression, which do not induce any detectable systemic effects (**Fig. 8-3A**). We found that expression of $VEGF_{165a}$ at roughly 5-fold higher than endogenous $VEGF_{165}$ secretion resulted in changes to free VEGF and VEGFR2 phosphorylation in the PAD Calf Muscle in the same range as that induced by the engineered VEGF constructs in **Fig. 8-2**, while 20-fold increased expression was sufficient to saturate VEGFR2 (**Fig. 8-S4**). Interestingly, expression of the engineered super affinity VEGF construct increased predicted VEGFR2 phosphorylation more than $VEGF_{165a}$ expression (**Fig. 8-3C**), with a smaller increase in tissue free VEGF (**Fig. 8-3A**), suggesting that this construct would improve efficacy, delivered as either a protein or a gene construct.

We also tested several other approaches, to compare the effect of targeting VEGF family ligands vs. receptors. First, we simulated induction of a splicing switch for $VEGF_{165}$, from all $VEGF_{165b}$ to all $VEGF_{165a}$ in the PAD Calf Muscle only, which is currently of interest in the field[36]. This strategy increased pR2 slightly (**Fig. 8-3**), but resulted in predicted decreases in free VEGF and VEGFR1 occupancy, unlike direct delivery of $VEGF_{165a}$ gene (**Fig. 8-3**). Finally, we tested receptor-based therapy, over-expressing VEGFR2 or knocking down expression of sR1, a soluble receptor that modulates VEGFR ligation. Increased VEGFR2 expression is predicted to increased total pR2, but decrease the fraction of VEGFR2 phosphorylated (pR2/R2, **Fig. 8-3, bottom row**), as well as VEGFR1 ligation and free VEGF in the PAD Calf Muscle (**Fig. 8-3**) to a larger extent than the splicing switch. The magnitude of this effect is limited by available VEGF, and effectiveness depends on specific targeting of gene therapy to endothelial cells, and the assumption that total pR2, as opposed to relative pR2/R2 is a key driver of signaling. Conversely, while blocking sR1 in mice has shown promise, in human PAD minimal effect is predicted, suggesting that this is

not an effective strategy. These simulation results highlight the potential of several approaches to gene

therapy for PAD, as our clinical gene delivery toolkit gets better at targeting consistent, controlled

expression levels in specific cell populations *in vivo*[40,41].

Figure 8-3. Distinct patterns of VEGF distribution and receptor activation predicted following different gene therapy approaches. Panels show fold change from baseline following six forms of gene therapy (across top). Gray dashed lines are provided for references to more easily compare changes between the different gene therapy approaches. **Top row:** Changes in free VEGF (not bound to ECM, BM, or sR1) in the Blood, Main Body Mass, and PAD Calf Muscle) 6 days after treatment, assuming immediate and constant transgene over- or under-expression. **Middle row:** Predicted occupancy of endothelial VEGF receptors in the PAD Calf Muscle at day 6 following treatment. **Bottom row:** VEGFR2 phosphorylation in the PAD Calf Muscle 6 days after treatment.
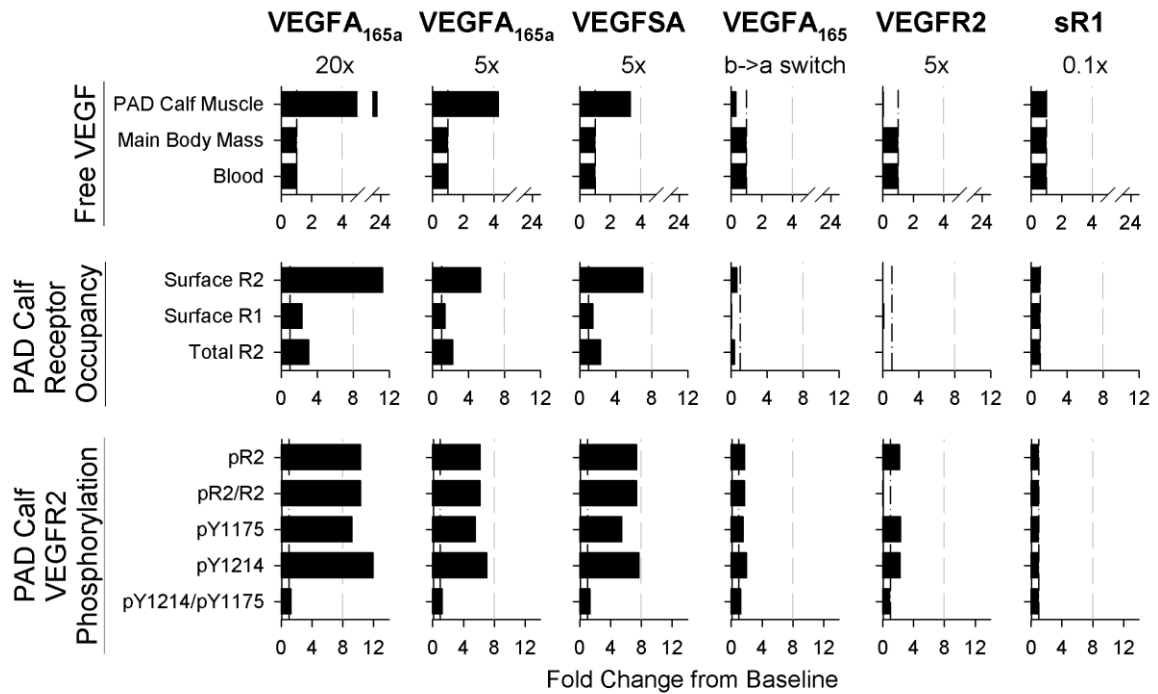
8.2.3 Non-intuitive, systemic effects with anti-VEGF treatment for peripheral artery disease

Model validation against murine experimental data. We then turned to a different therapeutic strategy, which has recently been shown to increase perfusion recovery in diabetic mice following femoral artery ligation (hindlimb ischemia): treatment with an antibody designed to bind only the $VEGF_{165b}$ isoform[36]. As our model predicts that $VEGF_{165b}$ does not compete with $VEGF_{165a}$ for binding to VEGFR2, we wanted to see whether a mechanism other than competition between ligands may be driving the observed effects in mice. We assumed the same intravenous dosing, antibody binding affinity, and pharmacokinetic properties as for bevacizumab, a non-isoform-specific VEGF antibody approved for use in several types of cancer.

First, we compared model predictions following anti-$VEGF_{165b}$ treatment to experimental measurements in murine hindlimb ischemia, in order to confirm that our model is predictive of therapeutic response. We found that the model is consistent with a lack of change in endothelial VEGFR2 phosphorylation following antibody treatment, while $VEGF_{165b}$ bound to VEGFR1 deceases (**Fig 8-4A**), supporting a VEGFR1-driven therapeutic response, as opposed to a VEGFR2-driven response. Owing to a lack of mechanistic understanding in the field, our model does not directly predict VEGFR1 phosphorylation. However, consistent with previous work, the model predicts increases in PlGF and non-$VEGF_{165b}$ VEGF isoforms binding to VEGFR1 (**Fig 8-4B**), while $VEGF_{165b}$-VEGFR1 decreases. This aligns with the results of Ganta et. al. [29], showing that $VEGF_{165b}$ appears to not induce phosphorylation of VEGFR1 on Y1333, and that VEGFR1 phosphorylation, presumably by PlGF and/or other VEGF isoforms, increases following antibody treatment (**Fig 8-4B**). This result provides confidence in our model predictions of signaling in response to anti-$VEGF_{165b}$ treatment, and supports the conclusion that improved perfusion following anti-$VEGF_{165b}$ is likely mediated by VEGFR1, not VEGFR2. Interestingly, the model predicts that $VEGF_{165b}$ secretion into the bloodstream by monocytes- included in our model thought it is not yet clear whether serum $VEGF_{165b}$ is free in plasma or confided to formed elements- would have minimal impact on PAD Calf Muscle response to anti-$VEGF_{165b}$ treatment (**Fig 8-4C**). This result suggests that the question of blood $VEGF_{165b}$ source is not critical to understand patient response to therapy.

Figure 8-4. Model captures experimental response to anti-VEGF$_{165b}$ in mice and predicts signaling *in vivo*. (A-B) Model-predicted response to Anti-VEGF$_{165b}$ treatment, compared to measurements in mouse hind-limb ischemia, from an extended analysis of the data set presented in Ganta et al.[11]. Total muscle VEGF and VEGF$_{165b}$ protein levels were unchanged. Simulations use values in the PAD Calf Muscle, with 75% secretion of VEGF$_{165b}$ in the PAD Calf Muscle and 25% VEGF$_{165b}$ secretion in the Main Body Mass, to roughly mimic the 3-fold increase in ischemic tissue VEGF$_{xxxb}$ measured experimentally, as done in our previous analysis. Mouse measurements are taken from muscle after antibody treatment, and represent total tissue measurements (receptor-bound ligand and VEGF protein) or CD31+ cells (pR2/R2), normalized by equivalent quantities in IgG-treated controls. Asterisks denote significance using an unpaired, two-tailed t-test with $p<0.05$. n= 3 for pR2/R2, n=5 for IgG group and n=7 for treatment group for VEGF binding to VEGFR1, and n=5 for pR1/R1. **(A)** Model validation. **(B)** Comparison of model-predicated ligand-VEGFR1 binding to experimental VEGFR1 phosphorylation in Y1333. **(C)** Model predictions of changes in PAD Calf Muscle in response to anti-VEGF$_{165b}$ treatment in the absence of VEGF$_{165b}$ secretion into the bloodstream by monocytes.
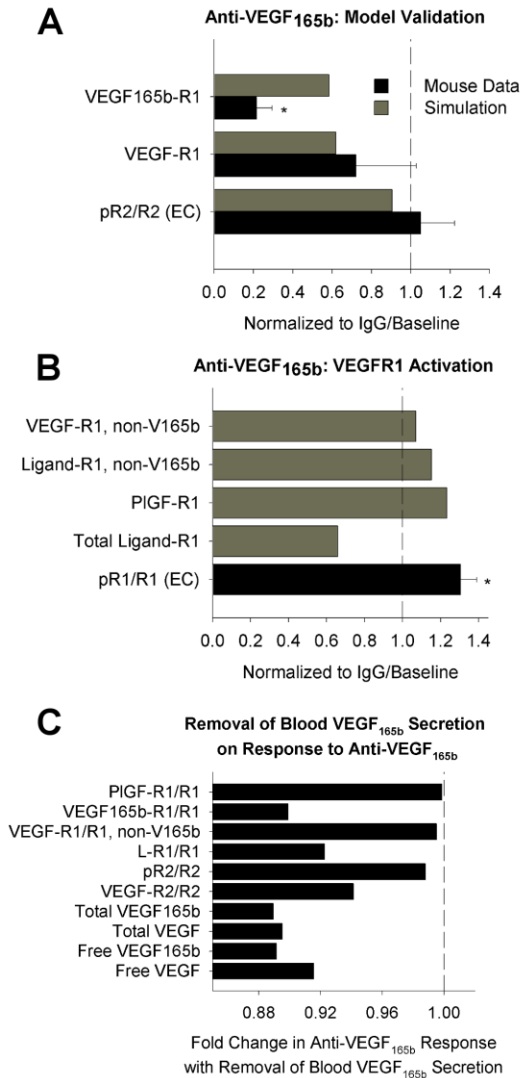
Figure 8-4

Translation to humans: implications of variable tissue VEGF$_{165b}$ secretion. Having validated our model against experimental data, we next screened the possible range of fractional VEGF$_{165b}$ production in both the Main Body Mass (healthy tissue) and the PAD Calf Muscle (ischemic tissue), that maybe occur in a variable human population. This allows us to explore the implications of changes in these ratios on potential antibody action. Such an analysis cannot be done easily in *in vivo* systems, but is important to understand before the drug is tested in human patients. Since total VEGF levels are held constant, secretion of VEGF$_{165a}$ and VEGF$_{165b}$ are inversely related.

Pre-treatment, our model predicts that tissue VEGF receptor signaling is driven by locally-secreted VEGF. In contrast, the model predicts important systemic effects following antibody administration. This occurs as a result of two antibody properties: (1) VEGF-antibody binding is reversible, and (2) the *in vivo* half-life of bevacizumab is 21 days, similar to that of other monoclonal antibodies. As such, the antibody does not simply bind to VEGF and remove it from the system, but rather continues to circulate. In tissue compartments with high target (VEGF$_{165b}$) concentration, the antibody will tend to bind to target. However, upon transport to a tissue with lower target concentration, the antibody-target complex will tend to dissociate, facilitating movement of target between compartments, and reducing the concentration difference between tissues (**Fig. 8-5A**).

PAD patients are expected to have high VEGF$_{165b}$ in the PAD Calf Muscle and low VEGF$_{165b}$ in the Main Body Mass. In simulating anti-VEGF$_{165b}$ treatment in this quadrant, local free VEGF in the PAD Calf Muscle was predicted to decrease to as low as 14% of baseline, as the antibody binds to VEGF$_{165b}$ (**Fig. 8-5B, lower right corner**). Levels of free VEGF$_{165a}$ in the PAD Calf Muscle were essentially unchanged (**Fig. 8-S5**). Conversely, free VEGF was predicted to increase in the PAD Calf Muscle with VEGF$_{165b}$ secretion low in PAD Calf Muscle and high in Main Body Mass (**Fig. 8-5B**). We also simulated treatment with a non-isoform-specific antibody (anti-VEGF), similar to bevacizumab. Because the antibody dose of 10mg/kg is in excess of available VEGF, the 'antibody shuttling' effect occurs independently for each VEGF isoform. As total free VEGF levels are similar in both tissue compartments, treatment with anti-VEGF is predicted to have a much smaller effect on total free VEGF levels in the PAD Calf Muscle; the antibody 'swaps' VEGF$_{165a}$ and VEGF$_{165b}$ between tissues (range: 65%-103% of baseline) (**Fig. 8-5B**). VEGF$_{165b}$ transport is predicted to be essentially identical for the two treatments, regardless of relative

$VEGF_{165b}$ secretion rates; the difference is almost entirely due to shuttling of $VEGF_{165a}$ (**Fig. 8-S5**). As such, anti-VEGF, a traditionally anti-angiogenic therapy, is predicted to bring additional, endogenous $VEGF_{165a}$ into the PAD Calf Muscle when $VEGF_{165b}$ secretion is higher in the PAD Calf Muscle than the Main Body Mass, the conditions we expect in PAD patients, based on mouse and human data. Due to the large size of the Main Body Mass, little effect on free VEGF levels is predicted for either antibody treatment in this compartment (**Fig. 8-S6**), though predicted changes in plasma VEGF levels do reflect fractional $VEGF_{165b}$ production in the Main Body Mass (**Fig. 8-S6**).

Figure 8-5. Mechanism of action of VEGF-targeting antibodies in PAD. (A) Schematic of antibody "shuttling" effect. When the antibody is in a compartment with high target concentration, it tends to bind to target. Upon moving (via vascular permeability or lymphatic drainage) to a compartment with lower target concentration, mass action kinetics dictate that the target-antibody complexes will tend to dissociate Thus, the antibody acts to reduce the concentration difference between two compartments. **(B)** Predicted fold change in free VEGF in the PAD Calf Muscle on Day 6 following treatment with Anti-VEGF$_{165b}$ (left) or a non-isoform-specific Anti-VEGF (right), as a function of the local fractional secretion of VEGF$_{165b}$ in the PAD Calf Muscle (x-axis) and the Main Body Mass (y-axis).
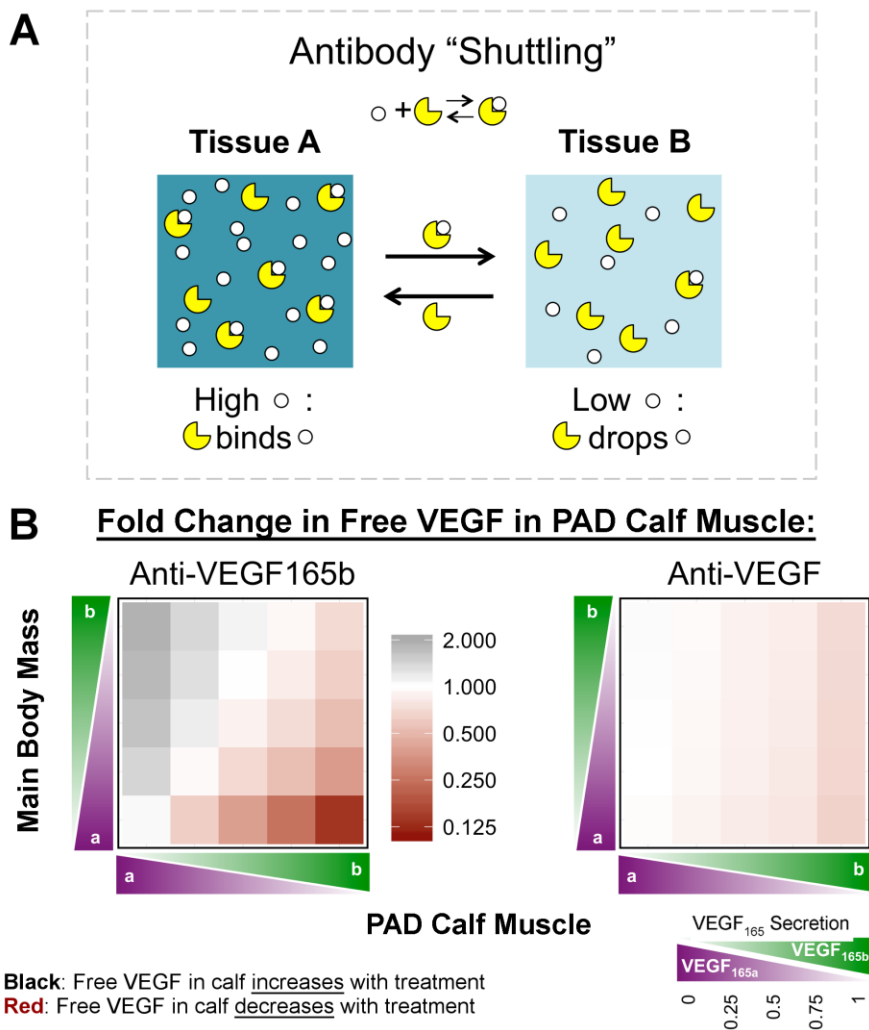
Next, we examined the effect of anti-VEGF$_{165b}$ or anti-VEGF treatment on endothelial VEGFR1 and VEGFR2 ligation and activation. The model predicts that anti-VEGF$_{165b}$ treatment would not increase VEGFR2 phosphorylation in any conditions, and may even decrease pR2 when local VEGF$_{165b}$ secretion is high (**Fig. 8-6**). Removal of VEGF$_{165b}$, a weak activator of VEGFR2, does not lead to increased VEGFR2 ligation by other VEGF isoforms (**Fig. 8-S8 & Fig. 8-S9**). The model predicts much larger changes in endothelial VEGFR1 ligation (**Fig. 8-6**); when VEGF$_{165b}$ is high in the PAD Calf Muscle and low in the Main Body Mass, cell surface VEGFR1 ligation is predicted to decrease to as low as 24% of baseline, with increased ligation of VEGFR1 by other VEGF isoforms (to 118% of baseline) and especially by PlGF (160% of baseline) (**Fig. 8-S10**).

Interestingly, treatment with the non-isoform-specific anti-VEGF is predicted to increase VEGFR2 phosphorylation in the PAD Calf Muscle (up to 366% of baseline) when VEGF$_{165b}$ production is higher in the PAD Calf Muscle than in the Main Body Mass (**Fig. 8-5**), owing to the increased VEGF$_{165a}$ (which is a strong activator of VEGFR2) brought into the calf by the antibody, as weak VEGFR2-activating VEGF$_{165b}$ is removed. Additionally, in these conditions, anti-VEGF is predicted to reduce VEGFR1 ligation (as low as 44% of baseline), with increasing binding by PlGF (up to 150% of baseline) and other VEGF isoforms (534%), similar to anti-VEGF$_{165b}$. This occurs because VEGF$_{165a}$ binds preferentially to VEGFR2 over VEGFR1, due to its NRP1-binding properties. Thus, while anti-VEGF$_{165b}$ is predicted to act via VEGFR1, anti-VEGF treatment is predicted to improve signaling via both VEGFR2 (increased phosphorylation) and VEGFR1 (decreased ligation) under conditions of higher VEGF$_{165b}$ production in the PAD Calf Muscle than in other tissues.

Figure 8-6. Effect of VEGF-targeting antibodies on endothelial VEGFR signaling *in vivo*. (Top) Predicted fold change from baseline (top row) and values of pR2/R2 in the PAD Calf Muscle on Day 6 following treatment with Anti-VEGF$_{165b}$ (middle) or a non-isoform-specific Anti-VEGF (right), as a function of the local fractional secretion of VEGF$_{165b}$ in the PAD Calf Muscle (x-axis) and the Main Body Mass (y-axis). **(Bottom)** Predicted changes in total endothelial surface VEGFR1 ligation in the PAD Calf Muscle on Day 6 following systemic antibody treatment.

VEGFR2 Phosphorylation in PAD Calf Muscle:
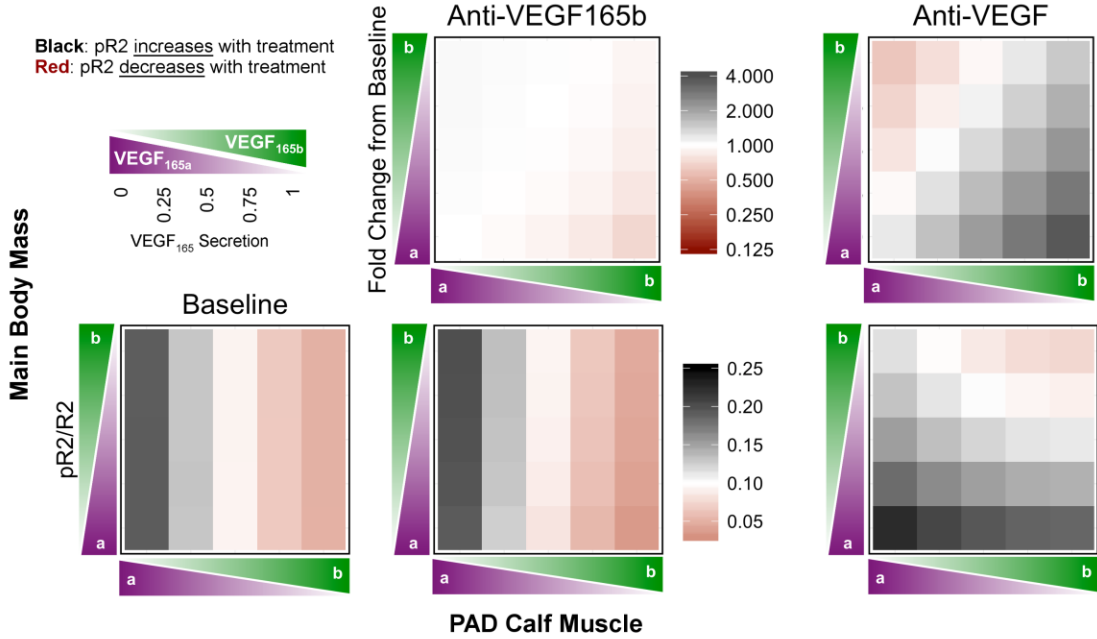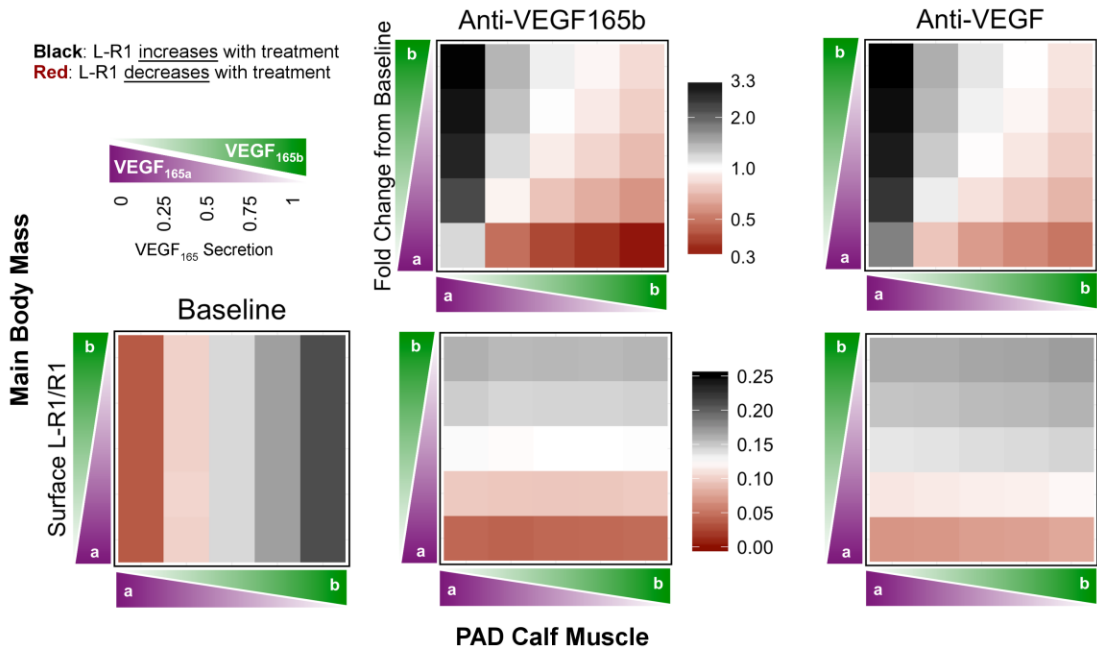

Surface VEGFR1 Ligation in PAD Calf Muscle:

Figure 8-6

8.2.4 Antibody treatment induces qualitatively different effects than VEGF gene or protein delivery

Finally, we leveraged our ability to simulate disparate therapeutic strategies in a single framework to compare the dynamics of therapy response following biomaterial-based protein therapy, gene therapy, or antibody therapy. We chose a promising representative therapy from each category: the "Covalent VEGF with Proteolysis" biomaterial construct; delivery of 'Super Affinity' VEGF gene at 5-fold normal VEGF expression levels; and the non-isoform-specific anti-VEGF. As the magnitude of change in signaling depends on the dose of gene or protein delivered, we were interested in the relative trends and time-courses of VEGF redistribution and endothelial signaling, more so than the relative magnitudes of change following therapy, though the antibody treatment simulations represent saturating levels of antibody, and thus the maximal predicted response for this strategy.

While protein and gene therapy are predicted to increase free VEGF levels in the PAD Calf Muscle but have little-to-no systemic effects at low doses, anti-VEGF is predicted to reduce free VEGF levels in the PAD Calf Muscle, but also increase free VEGF in the blood and slightly reduce free VEGF in the Main Body Mass (**Fig. 8-6A**), very similar to the changes predicted following anti-VEGF treatment in cancer[47]. For all three treatments, phosphorylation of VEGFR2 is predicted to increase, and remain elevated from more than two weeks, though the magnitude of increase is lower with anti-VEGF than could be achieved via VEGF delivery. However, while delivery of matrix-binding VEGF gene or protein is also predicted to increase VEGFR1 ligation, anti-VEGF is predicted to reduce VEGFR1 ligation (**Fig. 8-6B**). Our currently limited understanding of VEGFR1 signaling make it difficult to predict which of these signaling profiles would more effectively stimulate angiogenesis in PAD.

Figure 8-7. Anti-VEGF induces different VEGF distribution and endothelial VEGFR activation than biomaterial-based protein delivery or VEGF gene therapy. Therapies compared are: biomaterial-based delivery of the "Covalent VEGF with Proteolysis" construct to the PAD Calf Muscle at the dose used in **Fig. 8-2B** (green); therapeutic expression of the "Super Affinity VEGF" construct at 5-fold the normal expression level for VEGF (all isoforms combined) in the PAD Calf Muscle (blue); and intravenous injection of a non-isoform specific antibody to VEGF (Anti-VEGF, red). All therapies are delivered with fraction $VEGF_{165b}$ production of 100% in the PAD Calf Muscle and 0% in the Main Body Mass. **(A)** Changes in free VEGF (not bound to ECM, BM, sR1, or antibody) in the PAD Calf Muscle (left), blood (middle), and Main Body Mass (right) over time following therapy administration. **(B)** VEGFR2 phosphorylation (left), endothelial cell surface VEGFR2 occupancy (middle), and endothelial cell surface VEGFR1 occupancy (right) following treatment.
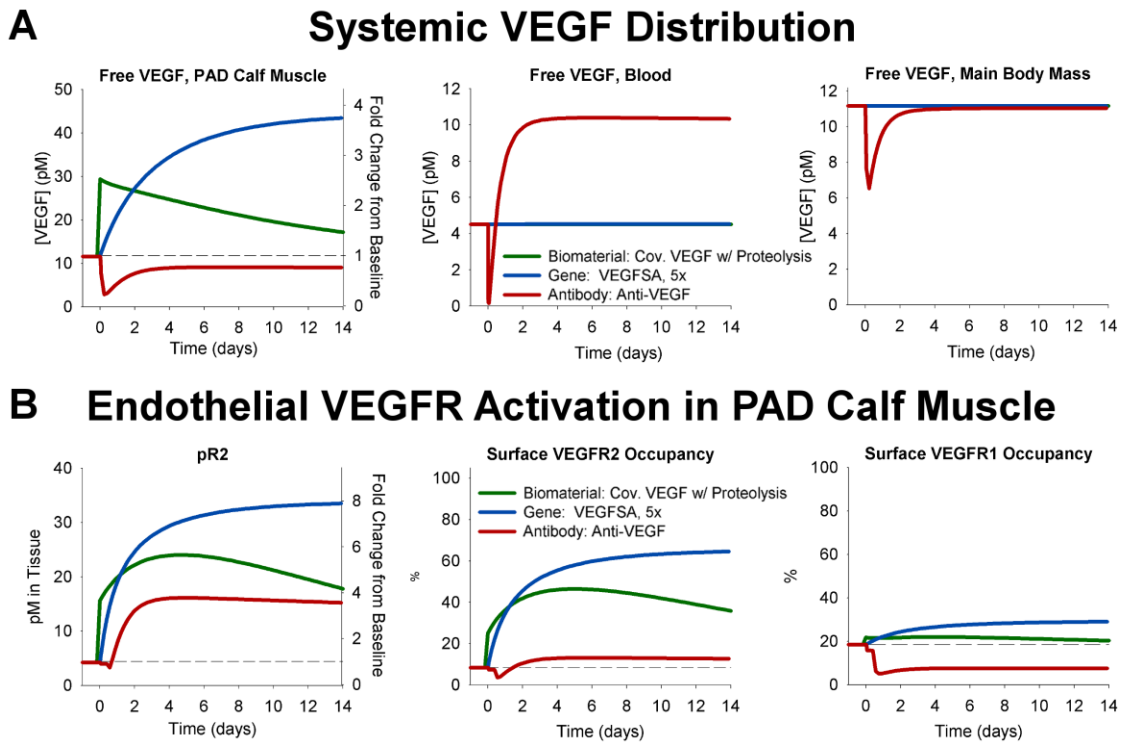
8.3 Discussion

8.3.1 In silico screening of therapeutics in a physiological context

In this paper, we used a systems pharmacology model of VEGF isoforms and VEGFR signaling in human peripheral artery disease to screen three types of promising therapies *in silico*: biomaterial-based VEGF delivery; gene therapy; and pro-angiogenic antibodies. The simulations provide insight into the mechanisms of action of these therapies, identifying molecular signaling differences between promising and ineffective approaches to predict drivers of therapy success or failure. The model also highlights key questions and considerations for design, optimization, and translation of these therapeutics into humans (**Table 8-1**). Along the way, we unearthed some common trends and open questions about the underlying biology that drives response to therapy. For example, a key unanswered question in dosing studies is: how much increase in pR2 is optimal? We showed that, while many past study designs have resulted in fully ligated VEGFR2, either throughout a tissue or in local areas, this saturation appears to be unnecessary, and likely detrimental to inducing stable collateral vessels. Rather, the model supports the hypothesis of the Banfi group that sufficient *duration* of VEGFR2 activation is a critical factor[7], and one which can potentially be achieved using biomaterial-based protein delivery, gene therapy, or antibody treatment with optimized therapy design and delivery.

Table 8-1. Summary of analyzed pro-angiogenic therapies.

	Biomaterial-based VEGF Delivery	Gene Therapy	Pro-angiogenic Antibodies
Pros	- No systemic effects - No dependence on underlying VEGF expression or splicing - Tunable, controlled duration and spatiotemporal patterning - Lower dose = lower cost - Likely applicable to multiple diseases (PAD, wound healing, etc.)	- With proper controlled dosing, no systemic effects predicted - Multiple potential targets: VEGF, VEGFR2 - Therapeutically inducing a VEGF splicing switch may be a relative safe, effective option without the magnitude control concerns of other approaches.	- Leverage underlying biology - Single factor, with easy (IV) delivery - Long half-life - Precedent for approved anti-VEGF therapy - Lower local VEGF levels than VEGF protein or gene delivery, so no concern about inducing VEGFR2 saturation
Cons	- How to deliver to large tissues with chronic, diffuse disease? (injectable?) - Cost of growth factor is high, especially for repeated delivery to large tissues. - Growth factor + gel both require regulatory approval	- Precise control of magnitude & duration critical for success - How to deliver to large tissues with chronic, diffuse disease? - Concerns over safety of long-term or permanent gene therapy	- Potential for systemic effects - Efficacy depends on underlying VEGF splicing in healthy & diseased tissue, and relative size of tissues with high vs. low $VEGF_{165b}$
Mechanism of Action	- Low initial VEGF spike (more physiological, less permeability, prevent angioma formation) - Extended pR2 elevation vs. native protein delivery (may prevent vessel regression)	- VEGF: elevate local VEGF protein - VEGF splicing: elevate local "strong" VEGFR2-activating $VEGF_{165a}$ - VEGFR2: increase number of VEGFR2 to be activated per endothelial cell	- Antibody 'shuttling' between tissues with different VEGF isoform expression - Improves VEGFR1 signaling (both) and could increase pR2 (anti-VEGF only)
Key Questions	- Need to understand *in vivo* receptor levels in each therapeutic case or experimental system of interest to select doses that avoid receptor saturation.	- Can induction of stable, high efficiency (but not permanent), spatially homogenous expression, potentially targeting specific cell types be achieved? - How can VEGF splicing be tuned therapeutically?	- What are the absolute levels of $VEGF_{165a}$ and $VEGF_{165b}$ in healthy and ischemic disease? In obese subjects and those with extensive CV disease, what fraction of tissue expresses high $VEGF_{165b}$ levels? - Need to better understand VEGFR1 signaling.

374

Fig 8-8. Comparisons of therapy profiles.

Therapeutic Strategy	Free VEGF	VEGFR2 Phosphorylation	VEGFR1 Ligation
VEGF gene or protein delivery	↑	↑	↑
VEGF b-> a splicing switch VEGFR2 overexpression Anti-VEGF	↓	↑	↓

This model captures important trends in observed data *in vitro*, *in vivo*, and in the clinic, and provides valuable and informative mechanistic insight that could not have been obtained with experiments alone. It is important to remember that, due to differences between our model system, experimental systems, and real (often highly variable) patients, along with assumptions used to simplify the model or account for lack of complete understanding of the underlying biology, precise match between simulations and observed experimental and clinical outcomes is challenging and should not be expected. Computational models have the advantage of easily implementing theoretical treatments that can be very challenging to effectively design. While this analysis does not address the practical or logistical issues associated with therapy production or delivery, the insight provided does facilitate decision making about which strategies are promising enough to merit further development.

8.3.2 Dosing and delivery leading to extended, sub-saturating VEGFR2 activation is key to successful biomaterial-based VEGF delivery

In simulating biomaterial-based VEGF delivery approaches leveraging engineered VEGF-ECM interactions, our model showed that the engineered constructs maintain more physiological free VEGF levels, likely accounting for reduced induction of permeability, and sustain VEGFR2 phosphorylation for weeks, promoting vessel stabilization following angiogenesis. We also simulated different doses of VEGF, finding that receptor saturation may be causative for angioma formation at high VEGF doses. This could occur via several different mechanisms: (1) saturation prevents cells from sensing VEGF gradients, allowing for cell proliferation but not directed migration, (2) VEGFR2 signaling is different at saturation than in sub-saturating regimes, or (3) high VEGF levels lead to depletion of available endothelial receptors, leading to changes in signaling. This result aligns with the pathogenic C482R VEGFR2 mutant, which is constitutively active in the absence of ligand, and induces hemangioma formation in infants[48], similar to the phenotype observed with delivery of high VEGF doses. It also provides insight into the need for tight natural regulation of endogenous VEGF secretion; VEGF haploinsufficiency is lethal[23,49], as is even 2-3x global overexpression during development[50].

The appropriate VEGF dose to stimulate angiogenesis without saturating VEGFR2 will likely vary depending on the species and tissue, as local capillary density (number of endothelial cells), interstitial

VEGF concentration, and expression of receptors and proteases vary. Nonetheless, quantification of these variables is feasible, and can be used with computational analyses such as this to inform appropriate doses for experiments in mice and initial trials in humans with varying disease states. It should be noted that the threshold between therapeutic angiogenesis and angioma formation in [39] varied by model system (mouse vs. rat, no injury vs. hindlimb ischemia vs. wound healing), from >0.5μg/mL to <25μg/mL. The threshold appears to occur at the lowest end of this range in our model (~0.5 μg/mL), owing to molecular, physiological, and geometric size differences[51], the approximate nature of allometric scaling between mouse and human doses, and mis-match in the systems being compared. VEGFR1, which is predicted to saturate at higher doses, could also play a role. Additionally, we set up our simulations to predict signaling within and in close proximity to the gel, the area imaged in the experimental study. To study gradients of VEGF concentration father from the gel, a spatial model including diffusion would be required. While diffusion would alter the shape of the release curves, the general match in release rate obtained in this study allows the model to predict relative magnitude and duration of VEGF delivery, and downstream effects. As such, the trends, rough magnitude, and mechanism of action highlighted by this modeling work are valuable and instructive. In the future we can build models with variable capillary density and receptor expression to further explore this issue, as well as building parallel mouse and human models for better matching of doses for similar signaling between species, and the potential to predict divergent effects in mice and humans.

8.3.3 Effective gene therapy depends on tight control of delivery and chosen target gene

It is believed that past VEGF gene therapy trials in PAD and CAD have failed largely due to insufficient and/or poorly controlled VEGF expression. Here, we asked: (1) what fold increase in expression would be effective at inducing pR2 without saturating VEGFR2, (2) what would the resulting changes in free VEGF and endothelial VEGFR signaling be, and (3) would the results be different if other VEGF-pathway targets were selected? We showed that approximately 5-fold (vs. total endogenous VEGF$_{165}$) over-expression of VEGF$_{165}$ or a super affinity VEGF construct produced similar signaling to the promising engineered VEGF protein constructs simulated above. It is of note that von Degenfeld et. al.[8] achieved effective angiogenesis following delivery of myoblast clones expressing uniform VEGF levels

using a myoblast clone that expresses VEGF at approximately 5-fold the expression level of control myocytes. While not a traditional gene therapy approach, inducing a splicing switch for $VEGF_{165}$, from all $VEGF_{165b}$ to $VEGF_{165a}$ in the PAD Calf Muscle showed promise. The success of even low doses of biomaterial-based VEGF delivery in inducing angiogenesis suggest that this modest increase in pR2 (180% of baseline) coupled with a predicted reduction in VEGFR1 ligation by $VEGF_{165b}$ (and increasing binding by PlGF and non-$VEGF_{165b}$, **Fig 8-S3A**) may be promising. Alternative splicing of $VEGF_{xxxa}$ and $VEGF_{xxxb}$ is known to be regulated by IGF1, TNFα, TGFβ[52], as well as noncanonical Wnt5a signaling[36]. Here we assumed a splicing switch only in the PAD Calf Muscle; our previous work predicts that blood-produced VEGF contributes very little to signaling in tissue, suggesting that targeting to a specific tissue may not be critical. However, levels of $VEGF_{165b}$ are decreased in several types of cancer (renal[25], colon[53], metastatic melanoma[54]) and in diabetic retinopathy[55], so detailed measurements of the ratio of "a" to "b" isoforms in healthy tissue will be necessary to determine the appropriate amount to shift splicing for optimal safety and efficacy.

8.3.4 'Anti-angiogenic' anti-VEGF treatment predicted to improve endothelial VEGFR signaling in PAD.

Finally, we simulated treatment of PAD with VEGF-binding antibodies. Our model supports the results from an extended analysis of the data in Ganta et. al. that perfusion recovery in murine hindlimb ischemia following anti-$VEGF_{165b}$ is mediated by VEGFR1, not VEGFR2[29], consistent with model predictions that VEGF isoforms compete for binding to VEGFR1, but not VEGFR2. This appears to be the case in both murine hindlimb ischemia, where VEGF is elevated, and human PAD, where VEGF levels are unchanged, suggesting potentially key similarities in response to anti-$VEGF_{165b}$ across species. This result motivates further study of the signaling induced by VEGFR1, to understand its role in PAD, and the therapeutic changes in VEGFR1 activation that would be most effective. It should be noted that this model considers only endothelial VEGFR1, while VEGFR1 expressed on monocytes and macrophages may also be relevant to PAD and contribute to ligand competition for binding to VEGFR1.

The model predicts that, due to reversible VEGF-antibody binding and the long half-life of monoclonal antibodies, a non-isoform-specific VEGF antibody would 'shuttle' VEGF isoforms between tissues with varying levels of VEGF isoform expression. This surprising mechanism of action has been

observed in cancer following bevacizumab treatment; a previous model showed that 'antibody shuttling' could explain the seemingly paradoxical increase in plasma VEGF observed following treatment[47]. This, combined with accurate prediction of response to anti-VEGF$_{165b}$ treatment by the model, give us confidence that such a mechanism is feasible; this prediction can be tested in mice in the future. Due to this 'antibody shuttling' effect, and the relatively high VEGF$_{165b}$ levels in ischemic PAD tissue, the model predicts that treatment with 'anti-angiogenic' anti-VEGF would improve signaling via both VEGFR1 and VEGFR2, potentially providing more therapeutic benefit than anti-VEGF$_{165b}$. Note that, while the largest predicted change in pR2 occurs with highest local VEGF$_{165b}$ production, the absolute quantity of pR2 is still highest with low local VEGF$_{165b}$ secretion, reinforcing the potential appeal of a therapeutic agent that can 'fix' impaired signaling in PAD by reverting splicing towards VEGF$_{165a}$ production.

This counter-intuitive prediction suggests that differences in the underlying biology in cancer and ischemic disease may lead to opposite responses to the same therapy. While VEGF levels are substantially elevated in cancer, in PAD ischemic tissues display a splicing switch, leading to relative differences of VEGF$_{165a}$ and VEGF$_{165b}$ between healthy and ischemic tissue. Interestingly, even in cancer, anti-VEGF is predicted to alter VEGFR1 ligation more than VEGFR2[47], though potential anti-VEGF-mediated redistribution of VEGF splice isoforms has not been investigated in cancer. Note that the efficacy and safety of this approach depends on a relatively small quantify of disease tissue expressing VEGF$_{165b}$ at higher levels than healthy tissue. This motivates further quantitative measurement of absolute VEGF isoform levels in healthy and ischemic tissue, and suggests that this approach may not be effective in patients with extensive ischemic disease or large quantities of white adipose tissue, which also has elevated VEGF$_{165b}$ expression[17]. Further work to establish the effect of antibody treatment on exercise-mediated increases in VEGF expression and signaling is also merited.

This prediction could not have been made based on cell culture experiments or measurements in mice alone, but is nonetheless consistent with observed signaling data and understanding of antibody properties, and is therapeutically relevant and actionable. This highlights the need for complex pharmacological models such as this to integrate detailed molecular interactions and signaling properties measured *in vitro*, observations in animal models, and knowledge of therapy pharmacokinetics into a single consistent framework, in order to predict the complex and sometimes surprising actions of therapeutics in

human subjects. Our model can also identify potential toxicity and unexpected side-effects prior to human studies, propose new purposes for existing drugs, and more efficiently guide therapy design and translation. This study demonstrates that consideration of systemic VEGF distribution and antibody pharmacokinetics, along with quantitative measurements of VEGF isoform protein levels in healthy and diseased tissue, are essential next steps for design of an effective antibody-based therapeutic for PAD.

8.3.5 Key Similarities Across Promising Therapeutic Strategies

We used a multiscale mechanistic computational model to study potential pro-angiogenic therapies for PAD. The mechanisms of action uncovered by this analysis may also be relevant to other pro-angiogenic applications, including wound healing and tissue engineering. Comparing the therapeutic strategies simulated here, we saw two distinct profiles of signaling following treatment with promising therapeutics: (1) elevated local free VEGF, pR2, and VEGFR1 ligation produced by delivery of matrix-binding VEGF protein or gene, and (2) reduced local free VEGF, moderate increases in pR2, and reduced endothelial VEGFR1 ligation produced by anti-VEGF, a splicing switch from $VEGF_{165b}$ to $VEGF_{165a}$ and VEGFR2 gene delivery (**Fig 8-8**). Further experiments are necessary to fully determine whether one or both of these profiles results in sustained improvements in perfusion in human PAD. The common theme across both of these profiles is small, non-saturating improvements in VEGFR signaling that are sustained for weeks. We propose that this is a key criteria to drive design and dosing of these therapeutics in experimental systems and human subjects, taking into account the underlying physiology, molecular biology, and ligand and receptor expression levels in each system during dose selection.

8.4 Methods

This whole body compartment model accounts for molecular and physiological processes, including growth factor secretion in tissues and blood, growth factor and soluble receptor binding to endothelial receptors and HSPGs in the ECM and basement membranes, trafficking and tyrosine site-specific phosphorylation of endothelial VEGFR2, transport between compartments via vascular permeability and lymphatic drainage, and clearance of growth factor and sR1 in the blood (via the liver and kidneys). Each tissue compartment is approximated using the properties of skeletal muscle, and contains physiological proportions of endothelial cells, ECM, interstitial space, and basement membrane, as well as molecular expression levels adjusted to account for measured changes in PAD, compared to healthy skeletal muscle (**Fig. 8-1**). By incorporating VEGF and PlGF isoform-specific ECM- and NRP1-binding properties, the model can predict the effect of splicing changes, such as those occurring in PAD, on signaling. Additionally, the ability to predict the effect of VEGF-ECM binding on VEGFR2 signaling makes our model an excellent platform to study biomaterial-based VEGF delivery. These model capabilities have been validated against *in vitro*, *ex vivo*, murine, and human data from multiple groups in several previous studies. For detailed model formulation, please see the previous chapter.

To simulate biomaterial-based protein, gene, or antibody therapy, we mimicked therapy delivery in experimental and clinical studies as closely as possible, in order to make model predictions as realistic and meaningful as possible.

8.4.1 Implementation of Biomaterial-based VEGF Delivery

The first therapeutic strategy we simulated was use of biomaterials to control and extend VEGF delivery. For these simulations, we modeled experiment constructs engineered by the groups of Jeff Hubbell and Andrea Banfi (**Fig. 8-2A**). In the Martino 2014 study, a dose of 200ng was delivered to a 5-6mm diameter punch biopsy wound[38]. To deliver a roughly equivalent dose to the PAD Calf Muscle of our simulated 70kg human, we used allometric scaling, with an exponent of 0.75 to account for differences in metabolic rate between mice and humans, then adjusted this value to account for differences in the size of the wound vs. PAD Calf Muscle relative to total body size, resulting in a human dose of 354µg VEGF. This dose was used for all three constructs in **Fig. 8-2B**, to provide an equivalent comparison. We used affinity

measurements from [38] for $VEGF_{165}$ and the engineered "Super Affinity" VEGF (VEGFSA) (**Table 8-2**).

Then, we tuned the model by adjusting the number of ECM binding sites added along with the VEGF (i.e.

in the fibrin gel), in order to match experimentally measured kinetics for VEGF release from the implanted

gels *in vivo* (**Table 8-2**), matching the fraction of VEGF retained in or within 2mm of the gel when

VEGFSA was delivered with fibrin. This adjustment helped to account for diffusion, which is not

considered in this model. As proteases are not included in this model, we also modeled release of the

"Covalent VEGF w/ Proteolysis" construct as a reversible VEGF-ECM bond, reducing the k_{off} rate constant

from Super Affinity VEGF until the release kinetics matched experimental data from [39].

For the dosing study presented in **Fig. 8-2C**, we assumed uniform delivery of the VEGF-

containing fibrin gel to the entire PAD Calf Muscle, at the same concentrations (in total tissue volume)

used in the experimental study, ranging from 0.01μg/mL to 100μg/mL[39], using the same added number of

ECM sites as for **Fig 8-2B** for all doses. To demonstrate similar therapy action regardless of underlying

$VEGF_{165b}$ secretion, these simulations were run with no local $VEGF_{165b}$ production (0%).

Table 8-2. Summary of parameters for biomaterial-based VEGF delivery.

Protein Construct	K_D(V-M) in nM	k_{on}(V-M) in $M^{-1}s^{-1}$	k_{off}(V-M) in s^{-1}	[ECM] added (*VEGF dose)	Ref.
VEGF$_{165}$	60.9	1.64×10^5	1.0×10^{-2}	425	38
Super Affinity VEGF	5.9	1.69×10^5	1.0×10^{-3}	150	38
Cov. VEGF w/ Prot.	0.002	1.69×10^5	3.3×10^{-7}	150	Tuned to match [39]

*All constructs assumed to bind NRP1, VEGFR1, VEGFR2, & sR1 with the same affinities as VEGF$_{165}$.

8.4.2 Implementation of Gene Therapy

Next, we simulated gene delivery-based pro-angiogenic therapeutic strategies, including delivery of $VEGF_{165}$ gene at moderate levels, VEGF engineered for increased affinity to the ECM (VEGFSA), increased VEGFR2 expression on endothelial cells, and decreased expression of sR1 (summarized in **Table 8-3**). We also examined the impact of switching $VEGF_{165}$ splicing from all $VEGF_{165b}$ to all $VEGF_{165a}$, another therapeutic strategy of interest. We assume ideal delivery: 100% transfection efficiency, spatially homogeneous delivery, with expression occurring instantly, at a constant level for an infinite duration, and only in the target tissue (PAD Calf Muscle).

Table 8-3. Summary of parameters for gene therapy.

Targeted Gene	Targeted Cells	Fold Change
VEGF$_{165}$	Parenchymal (e.g. skeletal muscle)	5x basal VEGF secretion
VEGF$_{165}$	Parenchymal (e.g. skeletal muscle)	20x basal VEGF secretion
Super Affinity VEGF	Parenchymal (e.g. skeletal muscle)	5x basal VEGF secretion
VEGF$_{165}$ b->a switch	Parenchymal*	-
VEGFR2	Endothelial cells	5x basal VEGFR2 prod.
sR1	Endothelial cells	0.1x basal sR1 secretion

*Splicing switch: assuming no change to VEGF$_{165b}$ secretion by monocytes into the blood. This has

minimal effect on tissue signaling anyway.

8.4.3 Implementation of Antibody Therapy

We modeled intravenous infusion of anti-VEGF$_{165b}$ in a single bolus over 90 minutes, at a dose of 10mg/kg (**Table 8-4**), using the same binding and pharmacokinetic properties as previously used for bevacizumab[47]. To provide a frame of reference against a similar approved antibody, we also simulated a non-isoform-specific antibody (anti-VEGF) using the same protocol and binding properties, assuming an equivalent binding affinity for all VEGF isoforms. Additionally, as done before, we assumed the antibodies bind only to free VEGF, not VEGF bound to HSPGs, sR1, or endothelial receptors, as well as neglecting multimeric binding of VEGF by antibodies.

Table 8-4. Summary of parameters for intravenous antibody infusion.

Parameter	Description	Value	Units	Ref.
K_D(V-AB)	Binding affinity for VEGF to AB	2.2	nM	[47,56]
k_{on}(V-AB)	on-rate constant for V-AB	9.2×10^4	$M^{-1}s^{-1}$	[47]
k_{off}(V-AB)	off-rate constant for V-AB	2.0×10^{-4}	s^{-1}	[47]
k_{perm}(AB)	vascular permeability of AB	3×10^{-8}	cm/s	[47]
k_{perm}(V-AB)	vascular permeability of V-AB	3×10^{-8}	cm/s	[47]
k_{lymph}(AB), MBM	lymphatic drainage of AB from MBM	0.1418	cm^2/s	[57]
k_{lymph}(V-AB), MBM	lymphatic drainage of V-AB from MBM	0.1418	cm^2/s	[57]
k_{lymph}(AB), PCM	lymphatic drainage of AB from PCM	0.0022	cm^2/s	[57]
k_{lymph}(V-AB), PCM	lymphatic drainage of V-AB from PCM	0.0022	cm^2/s	[57]
k_{CL}(AB)	clearance of AB from blood	3.2×10^{-7}	s^{-1}	[47]
k_{CL}(V-AB)	clearance of V-AB from blood	3.2×10^{-7}	s^{-1}	[47]
Bolus size	dose (70kg human subject)	10	mg/kg	[47]
Infusion duration		90	min	[47]

*All parameters assumed same for Anti-VEGF and Anti-VEGF$_{165b}$, aside from set of VEGF isoforms

bound by ligand.

*MBM = main body mass, PCM = PAD calf muscle

No therapy-induced remodeling

The model is simulated in Fortran using the Livermore Solver for Ordinary Differential Equations with Automatic method switching for stiff and nonstiff problems (LSODA) on a laptop PC, using a relative error tolerance of 10^{-6}.

8.4.4 Experimental anti-VEGF$_{165b}$ Treatment in Murine Hindlimb Ischemia

The experimental data presented in this paper represent an extended analysis of the results presented in [11], and all methods are the same. For the ischemic vs. non-ischemic comparisons, mouse measurements are taken from muscle 3 days after antibody administration in ischemic limbs, and represent total tissue measurements (receptor-bound ligand and VEGF protein) or CD31+ cells (pR2/R2 & pR1/R1, noted by (EC) in plots), normalized by equivalent quantities in the IgG-treated control.

8.5 References

1   Clegg, L. E. & Mac Gabhann, F. Systems biology of the microvasculature. *Integrative Biology*, doi:10.1039/C4IB00296B (2015).

2   Collinson, D. J. & Donnelly, R. Therapeutic angiogenesis in peripheral arterial disease: Can biotechnology produce an effective collateral circulation? *European Journal of Vascular and Endovascular Surgery* **28**, 9-23, doi:10.1016/j.ejvs.2004.03.021 (2004).

3   Norgren, L. *et al.* Inter-Society Consensus for the Management of Peripheral Arterial Disease (TASC II). *European journal of vascular and endovascular surgery : the official journal of the European Society for Vascular Surgery* **33 Suppl 1**, S1-75, doi:10.1016/j.ejvs.2006.09.024 (2007).

4   Dormandy, J. A. & Rutherford, R. B. Management of peripheral arterial disease (PAD). TASC Working Group. TransAtlantic Inter-Society Consensus (TASC). *Journal of vascular surgery* **31**, S1-S296 (2000).

5   Annex, B. H. Therapeutic angiogenesis for critical limb ischaemia. *Nature Reviews Cardiology* **10**, 387-396, doi:10.1038/nrcardio.2013.70 (2013).

6   Grochot-Przeczek, A., Dulak, J. & Jozkowicz, A. Therapeutic angiogenesis for revascularization in peripheral artery disease. *Gene* **525**, 220-228, doi:10.1016/j.gene.2013.03.097 (2013).

7   Ozawa, C. R. *et al.* Microenvironmental VEGF concentration, not total dose, determines a threshold between normal and aberrant angiogenesis. *Journal of Clinical Investigation* **113**, 516-527, doi:10.1172/jci200418420 (2004).

8   von Degenfeld, G. *et al.* Microenvironmental VEGF distribution is critical for stable and functional vessel growth in ischemia. *Faseb Journal* **20**, 2657-+, doi:10.1096/fj.06-6568fje (2006).

9   Yla-Herttuala, S., Markkanen, J. E. & Rissanen, T. T. Gene therapy for ischemic cardiovascular disease: Somes lessons learned from the first clinical trials. *Trends in Cardiovascular Medicine* **14**, 295-300, doi:10.1016/j.tcm.2004.09.001 (2004).

10   Yla-Herttuala, S., Rissanen, T. T., Vajanto, I. & Hartikainen, J. Vascular endothelial growth factors - Biology and current status of clinical applications in cardiovascular medicine. *Journal of the American College of Cardiology* **49**, 1015-1026, doi:10.1016/j.jace.2006.09.053 (2007).

11   Briquez, P. S., Clegg, L. E., Martino, M. M., Gabhann, F. M. & Hubbell, J. A. Design principles for therapeutic angiogenic materials. *Nature Reviews Materials* **1**, 15006, doi:10.1038/natrevmats.2015.6 (2016).

12   Mac Gabhann, F. & Popel, A. S. Systems biology of vascular endothelial growth factors. *Microcirculation (New York, N.Y. : 1994)* **15**, 715-738 (2008).

13   Wu, F. T. H. *et al.* A systems biology perspective on sVEGFR1: its biological function, pathogenic role and therapeutic use. *Journal of Cellular and Molecular Medicine* **14**, 528-552, doi:10.1111/j.1582-4934.2009.00941.x (2010).

14   Koch, S., Tugues, S., Li, X., Gualandi, L. & Claesson-Welsh, L. Signal transduction by vascular endothelial growth factor receptors. *Biochemical Journal* **437**, 169-183, doi:10.1042/bj20110301 (2011).

15   Koch, S. & Claesson-Welsh, L. Signal Transduction by Vascular Endothelial Growth Factor Receptors. *Cold Spring Harbor Perspectives in Medicine* **2**, doi:10.1101/cshperspect.a006502 (2012).

16   Ng, Y. S., Rohan, R., Sunday, M. E., Demello, D. E. & D'Amore, P. A. Differential expression of VEGF isoforms in mouse during development and in the adult. *Developmental Dynamics* **220**, 112-121, doi:10.1002/1097-0177(2000) (2001).

17   Ngo, D. T. M. *et al.* Antiangiogenic Actions of Vascular Endothelial Growth Factor-A(165)b, an Inhibitory Isoform of Vascular Endothelial Growth Factor-A, in Human Obesity. *Circulation* **130**, 1072-1080, doi:10.1161/circulationaha.113.008171 (2014).

18   Vempati, P., Popel, A. S. & Mac Gabhann, F. Extracellular regulation of VEGF: Isoforms, proteolysis, and vascular patterning. *Cytokine & Growth Factor Reviews* **25**, 1-19, doi:http://dx.doi.org/10.1016/j.cytogfr.2013.11.002 (2014).

19   Park, J. E., Keller, G. A. & Ferrara, N. VASCULAR ENDOTHELIAL GROWTH-FACTOR (VEGF) ISOFORMS - DIFFERENTIAL DEPOSITION INTO THE SUBEPITHELIAL EXTRACELLULAR-MATRIX AND BIOACTIVITY OF EXTRACELLULAR MATRIX-BOUND VEGF. *Molecular Biology of the Cell* **4**, 1317-1326 (1993).

20   Ruhrberg, C. *et al.* Spatially restricted patterning cues provided by heparin-binding VEGF-A control blood vessel branching morphogenesis. *Genes & Development* **16**, 2684-2698, doi:10.1101/gad.242002 (2002).

21   Lee, S., Jilani, S. M., Nikolova, G. V., Carpizo, D. & Iruela-Arispe, M. L. Processing of VEGF-A by matrix metalloproteinases regulates bioavailability and vascular patterning in tumors. *Journal of Cell Biology* **169**, 681-691, doi:10.1083/jcb.200409115 (2005).

22   Grunstein, J., Masbad, J. J., Hickey, R., Giordano, F. & Johnson, R. S. Isoforms of vascular endothelial growth factor act in a coordinate fashion to recruit and expand tumor vasculature. *Molecular and Cellular Biology* **20**, 7282-7291, doi:10.1128/mcb.20.19.7282-7291.2000 (2000).

23   Carmeliet, P. *et al.* Abnormal blood vessel development and lethality in embryos lacking a single VEGF allele. *Nature* **380**, 435-439, doi:10.1038/380435a0 (1996).

24   Carmeliet, P. *et al.* Impaired myocardial angiogenesis and ischemic cardiomyopathy in mice lacking the vascular endothelial growth factor isoforms VEGF(164) and VEGF(188). *Nature Medicine* **5**, 495-502, doi:10.1038/8379 (1999).

25   Bates, D. O. *et al.* VEGF(165)b, an inhibitory splice variant of vascular endothelial growth factor, is down-regulated in renal cell carcinoma. *Cancer Research* **62**, 4123-4131 (2002).

26   Delcombel, R. *et al.* New prospects in the roles of the C-terminal domains of VEGF-A and their cooperation for ligand binding, cellular signaling and vessels formation. *Angiogenesis* **16**, 353-371, doi:10.1007/s10456-012-9320-y (2013).

27   Kawamura, H., Li, X., Harper, S. J., Bates, D. O. & Claesson-Welsh, L. Vascular endothelial growth factor (VEGF)-A165b is a weak in vitro agonist for VEGF receptor-2 due to lack of

coreceptor binding and deficient regulation of kinase activity. *Cancer Research* **68**, 4683-4692, doi:10.1158/0008-5472.can-07-6577 (2008).

28   Suarez, S. C. *et al.* A VEGF-A splice variant defective for heparan sulfate and neuropilin-1 binding shows attenuated signaling through VEGFR-2. *Cellular and Molecular Life Sciences* **63**, 2067-2077, doi:10.1007/s00018-006-6254-9 (2006).

29   Ganta, V. C., Choi, M., Kutateladze, A. & Annex, B. H. VEGF<sub>165</sub>b Modulates Endothelial VEGFR1-STAT3 Signaling Pathway and Angiogenesis in Human and Experimental Peripheral Arterial Disease. *Circulation Research* (2016).

30   Hoier, B. *et al.* Angiogenic response to passive movement and active exercise in individuals with peripheral arterial disease. *Journal of Applied Physiology* **115**, 1777-1787, doi:10.1152/japplphysiol.00979.2013 (2013).

31   Belgore, F. M., Blann, A. D. & Lip, G. Y. Measurement of free and complexed soluble vascular endothelial growth factor receptor, Flt-I, in fluid samples: development and application of two new immunoassays. *Clinical Science* **100**, 567-575, doi:10.1042/cs20000234 (2001).

32   Blann, A. D. *et al.* Vascular endothelial growth factor and its receptor, Flt-1, in the plasma of patients with coronary or peripheral atherosclerosis, or Type II diabetes. *Clinical Science* **102**, 187-194 (2002).

33   Makin, A. J., Chung, N. A. Y., Silverman, S. H. & Lip, G. Y. H. Vascular endothelial growth factor and tissue factor in patients with established peripheral artery disease: a link between angiogenesis and thrombogenesis? *Clinical Science* **104**, 397-404, doi:10.1042/cs20020182 (2003).

34   Lee, T. M., Su, S. F., Tsai, C. H., Lee, Y. T. & Wang, S. S. Differential effects of cilostazol and pentoxifylline on vascular endothelial growth factor in patients with intermittent claudication. *Clinical Science* **101**, 305-311, doi:10.1042/cs20000281 (2001).

35   Jones, W. S. *et al.* Alteration in angiogenic and anti-angiogenic forms of vascular endothelial growth factor-A in skeletal muscle of patients with intermittent claudication following exercise training. *Vascular Medicine* **17**, 94-100, doi:10.1177/1358863x11436334 (2012).

36   Kikuchi, R. *et al.* An antiangiogenic isoform of VEGF-A contributes to impaired vascularization in peripheral artery disease. *Nature Medicine* **20**, 1464-1471, doi:10.1038/nm.3703 (2014).

37   Bates, D. O. *et al.* Detection of VEGF-A(xxx)b Isoforms in Human Tissues. *Plos One* **8**, doi:10.1371/journal.pone.0068399 (2013).

38   Martino, M. M. *et al.* Growth Factors Engineered for Super-Affinity to the Extracellular Matrix Enhance Tissue Healing. *Science* **343**, 885-888, doi:10.1126/science.1247663 (2014).

39   Sacchi, V. *et al.* Long-lasting fibrin matrices ensure stable and functional angiogenesis by highly tunable, sustained delivery of recombinant VEGF(164). *Proceedings of the National Academy of Sciences of the United States of America* **111**, 6952-6957, doi:10.1073/pnas.1404605111 (2014).

40   Curtin, J. F., Candolfi, M., Xiong, W., Lowenstein, P. R. & Castro, M. G. Turning the gene tap off; implications of regulating gene expression for cancer therapeutics. *Molecular Cancer Therapeutics* **7**, 439-448, doi:10.1158/1535-7163.mct-07-2328 (2008).

41   Buchholz, C. J., Friedel, T. & Buening, H. Surface-Engineered Viral Vectors for Selective and Cell Type-Specific Gene Delivery. *Trends in Biotechnology* **33**, 777-790, doi:10.1016/j.tibtech.2015.09.008 (2015).

42   Clegg, L. W. & Mac Gabhann, F. Site-Specific Phosphorylation of VEGFR2 Is Mediated by Receptor Trafficking: Insights from a Computational Model. *PLoS Comput Biol* **11**, e1004158, doi:10.1371/journal.pcbi.1004158 (2015).

43   Clegg, L. E. & Mac Gabhann, F. Molecular mechanism matters: Benefits of mechanistic computational models for drug development. *Pharmacological Research* **99**, 149-154, doi:http://dx.doi.org/10.1016/j.phrs.2015.06.002 (2015).

44   Shyu, K. G., Chang, H., Wang, B. W. & Kuan, P. L. Intramuscular vascular endothelial growth factor gene therapy in patients with chronic critical leg ischemia. *American Journal of Medicine* **114**, 85-92, doi:10.1016/s0002-9343(02)01392-x (2003).

45   Baumgartner, I. *et al.* Constitutive expression of phVEGF(165) after intramuscular gene transfer promotes collateral vessel development in patients with critical limb ischemia. *Circulation* **97**, 1114-1123 (1998).

46   Isner, J. M. *et al.* Treatment of thromboangiitis obliterans (Buerger's disease) by intramuscular gene transfer of vascular endothelial growth factor: Preliminary clinical results. *Journal of Vascular Surgery* **28**, 964-973, doi:10.1016/s0741-5214(98)70022-9 (1998).

47   Stefanini, M. O., Wu, F. T. H., Mac Gabhann, F. & Popel, A. S. Increase of Plasma VEGF after Intravenous Administration of Bevacizumab Is Predicted by a Pharmacokinetic Model. *Cancer Research* **70**, 9886-9894, doi:10.1158/0008-5472.can-10-1419 (2010).

48   Sarabipour, S., Ballmer-Hofer, K. & Hristova, K. VEGFR-2 conformational switch in response to ligand binding. *Elife* **5**, doi:10.7554/eLife.13876 (2016).

49   Ferrara, N. *et al.* Heterozygous embryonic lethality induced by targeted inactivation of the VEGF gene. *Nature* **380**, 439-442, doi:10.1038/380439a0 (1996).

50   Miquerol, L., Langille, B. L. & Nagy, A. Embryonic development is disrupted by modest increases in vascular endothelial growth factor gene expression. *Development* **127**, 3941-3946 (2000).

51   Yla-Herttuala, S. & Alitalo, K. Gene transfer as a tool to induce therapeutic vascular growth. *Nature Medicine* **9**, 694-701, doi:10.1038/nm0603-694 (2003).

52   Nowak, D. G. *et al.* Expression of pro- and anti-angiogenic isoforms of VEGF is differentially regulated by splicing and growth factors. *Journal of Cell Science* **121**, 3487-3495, doi:10.1242/jcs.016410 (2008).

53   Varey, A. H. R. *et al.* VEGF(165)b, an antiangiogenic VEGF-A isoform, binds and inhibits bevacizumab treatment in experimental colorectal carcinoma: balance of pro- and antiangiogenic VEGF-A isoforms has implications for therapy. *British Journal of Cancer* **98**, 1366-1379, doi:10.1038/sj.bjc.6604308 (2008).

54   Pritchard-Jones, R. O. *et al.* Expression of VEGF(xxx)b, the inhibitory isoforms of VEGF, in malignant melanoma. *British Journal of Cancer* **97**, 223-230, doi:10.1038/sj.bjc.6603839 (2007).

55   Perrin, R. M. *et al.* Diabetic retinopathy is associated with a switch in splicing from anti- to pro-angiogenic isoforms of vascular endothelial growth factor. *Diabetologia* **48**, 2422-2427, doi:10.1007/s00125-005-1951-8 (2005).

56   Liang, W. C. *et al.* Cross-species vascular endothelial growth factor (VEGF)-blocking antibodies completely inhibit the growth of human tumor xenografts and measure the contribution of stromal VEGF. *Journal of Biological Chemistry* **281**, 951-961 (2006).

57   Wu, F. T. *et al.* VEGF and soluble VEGF receptor-1 (sFlt-1) distributions in peripheral arterial disease: an in silico model. *Am J Physiol Heart Circ Physiol* **298**, H2174-2191, doi:ajpheart.00365.2009 [pii] 10.1152/ajpheart.00365.2009 (2010).

8.6 Supplemental Figures

Figure 8-S1. Detailed response to biomaterial-based delivery of engineered VEGF constructs to the PAD Calf Muscle. This figure is related to **Fig. 8-2**. Free VEGF levels in compartments (**A-B**), details of VEGFR2 phosphorylation (**C-F**), endothelial receptor occupancy (**G-I**), changes in surface receptor levels following treatment (**J-L**), and the dynamic changes in receptor production required to hold total receptor levels constant following treatment (**M-O**).
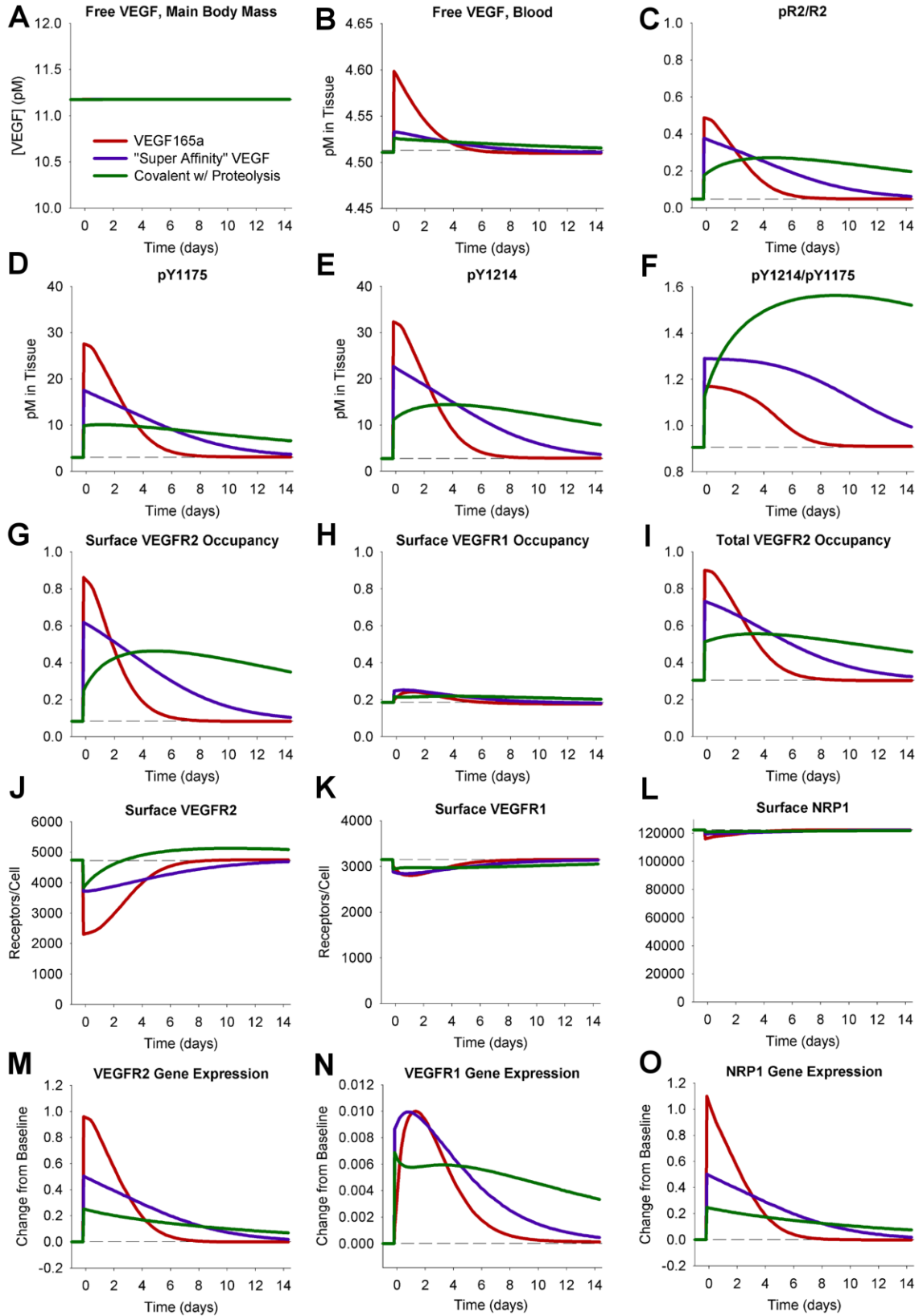
Figure 8-S1

Figure 8-S2. Detailed response to varying doses of "Covalent VEGF w/ Proteolysis" construct to the PAD Calf Muscle. This figure is related to **Fig. 2** of the main manuscript. Free VEGF levels in other compartments (**A-B**), details of VEGFR2 phosphorylation (**C-F**), endothelial receptor occupancy (**G-H**), changes in surface receptor levels following treatment (**I-K**), and the dynamic changes in receptor production required to hold total receptor levels constant following treatment (**L-N**).

Figure 8-S2

Figure 8-S3. Additional metrics of response to gene therapy at Day 6 following treatment. This figure is related to **Fig. 8-3**. Breakdown of ligands bound to VEGFR1 and VEGFR2 on endothelial cells (**top row**), endothelial surface receptor levels (**middle row**), and changes in receptor production required to hold total receptor levels constant (**bottom row**) following treatment at 6 days post-treatment.
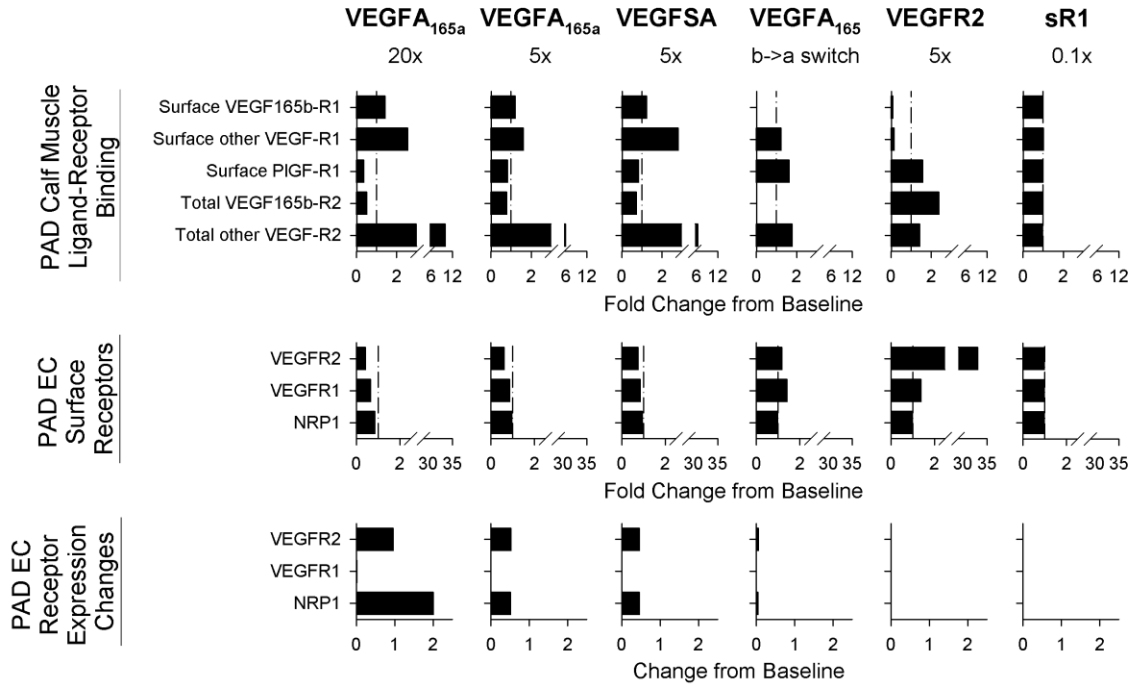
Figure 8-S4. Detailed time-course response to gene therapy strategies. This figure is related to **Fig. 8-3**.

Free VEGF levels in other compartments (**A-D**), details of VEGFR2 phosphorylation (**E-F,J-L**),

endothelial receptor occupancy (**G-I**), changes in surface receptor levels following treatment (**M-O**), and

the dynamic changes in receptor production required to hold total receptor levels constant following
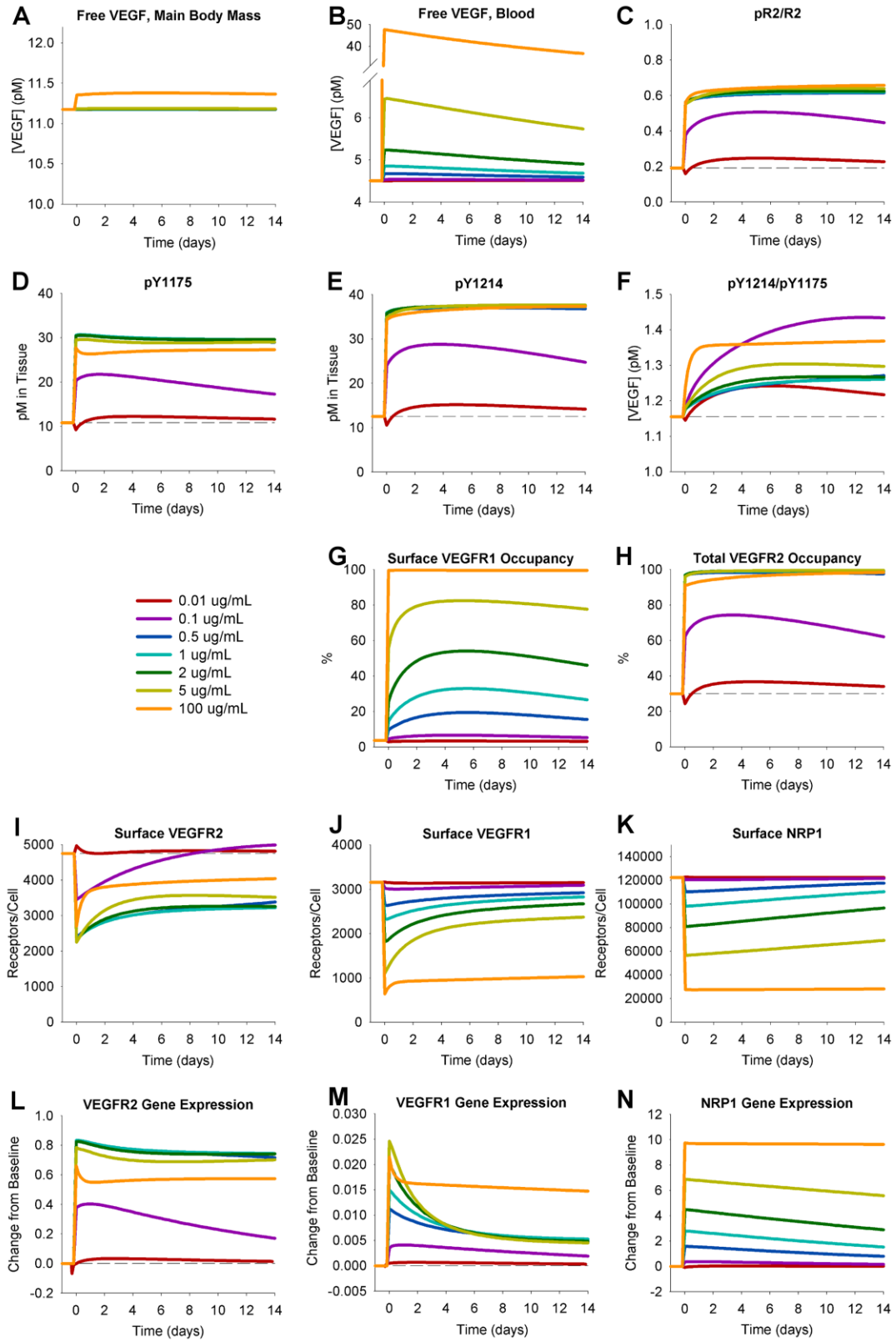
treatment (**P-R**).
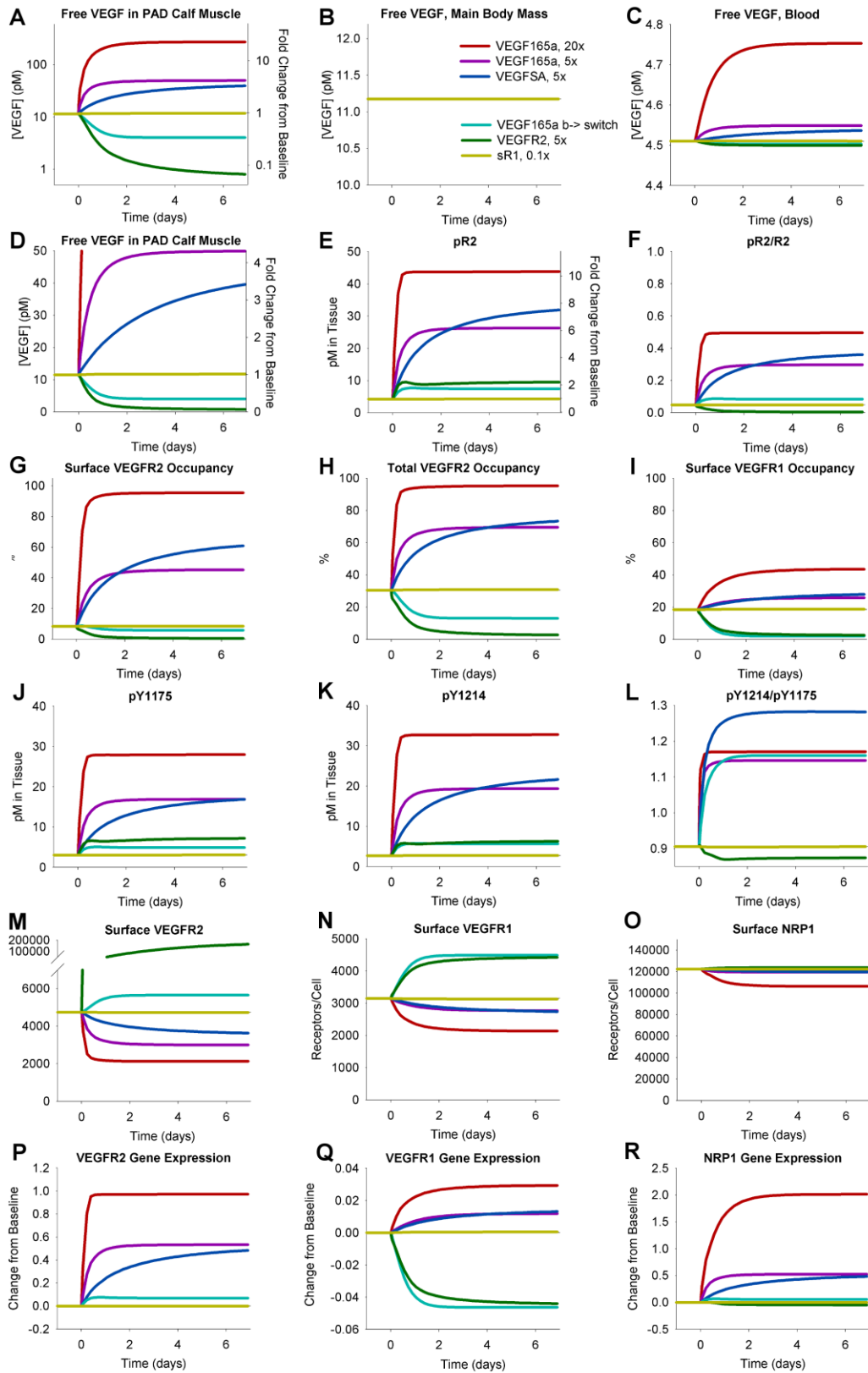
Figure 8-S4

Figure 8-S5. Analysis of predicted VEGF$_{165a}$ and VEGF$_{165b}$ distribution in human body following VEGF-targeted antibody therapy. This figure is related to **Fig. 8-4**. Concentration of free VEGF$_{165a}$ and VEGF$_{165b}$, free antibody, and VEGF-antibody complexes in the Main Body Mass, Blood, and PAD Calf Muscle at baseline (middle) and on Day 6 following IV infusion of Anti-VEGF$_{165b}$ (left) or Anti-VEGF (right), at different fractional VEGF$_{165b}$ secretion rates in the Main Body Mass and PAD Calf Muscle. Gray arrows indicate net association of antibody and VEGF, while gray arrows denote net dissociation. Note that, while at baseline only local VEGF secretion is important for signaling, upon treatment with antibody, systemic effects become important (i.e. the concentrations of VEGF$_{165a}$ and VEGF$_{165b}$ in the other tissue compartment affect local VEGF levels). Changes in flow directions between compartments also occur following antibody treatment. Note that VEGF$_{165b}$ distribution is similarly impacted by both Anti-VEGF$_{165b}$ and Anti-VEGF; the difference in effect arises from the concomitant redistribution of VEGF$_{165a}$ by Anti-VEGF.

Figure 8-S5

404
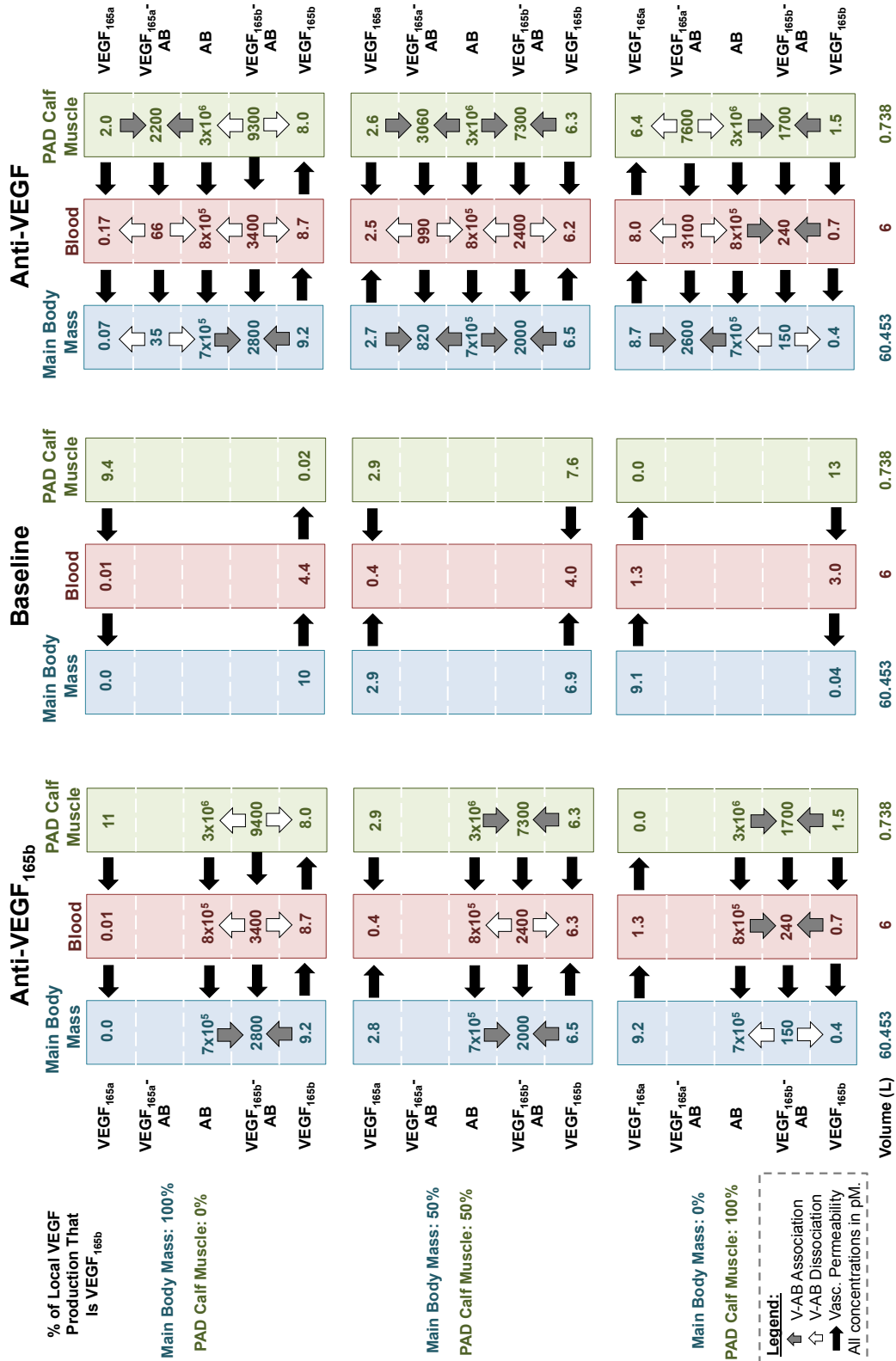
Figure 8-S6. Effect of VEGF-targeting antibodies on systemic free VEGF distribution. This figure is related to **Fig. 8-4**. Predicted fold change from baseline of total free VEGF in the PAD Calf Muscle (left), blood (middle) and Main Body Mass (right) on Day 6 following treatment with Anti-VEGF$_{165b}$ (top row) or a non-isoform-specific Anti-VEGF (bottom row), as a function of the local fractional secretion of VEGF$_{165b}$ in the PAD Calf Muscle (x-axis) and the Main Body Mass (y-axis).
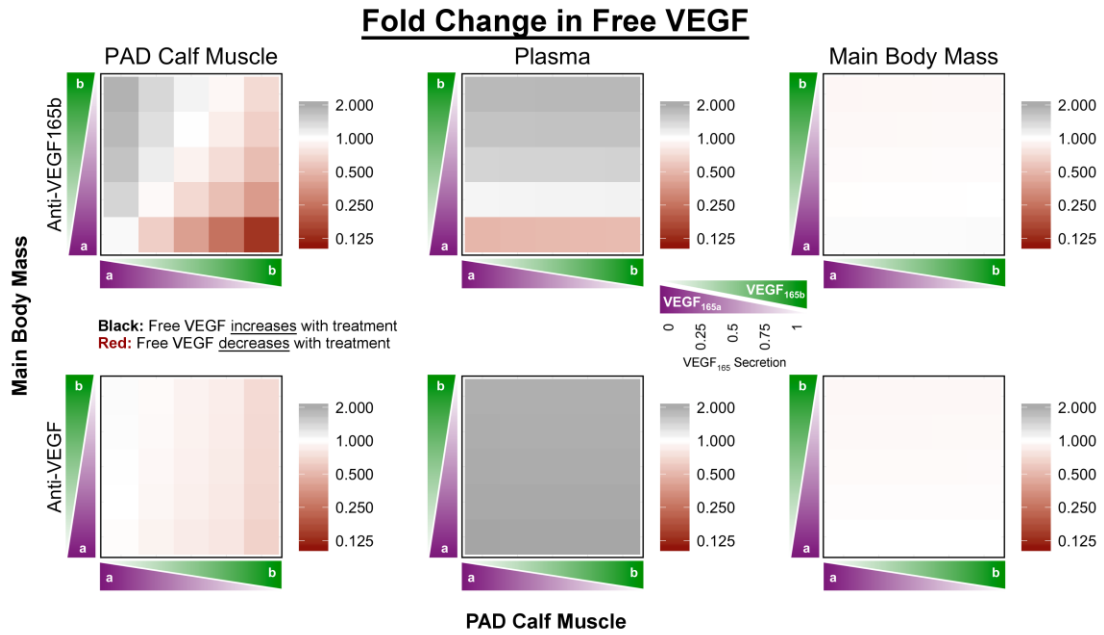
Figure 8-S7. Additional effects of VEGF-targeting antibodies on endothelial VEGFR signaling *in vivo*. This figure is related to **Fig. 8-5**. **(Top)** Predicted ratio of VEGFR2 phosphorylation on Y1214 to Y1175 in the PAD Calf Muscle at baseline (left), and on Day 6 following treatment with Anti-VEGF$_{165b}$ (middle) or a non-isoform-specific Anti-VEGF (right), as a function of the local fractional secretion of VEGF$_{165b}$ in the PAD Calf Muscle (x-axis) and the Main Body Mass (y-axis). **(Bottom)** Predicted fold change in VEGFR2 phosphorylation in the Main Body Mass on Day 6 following systemic antibody treatment.
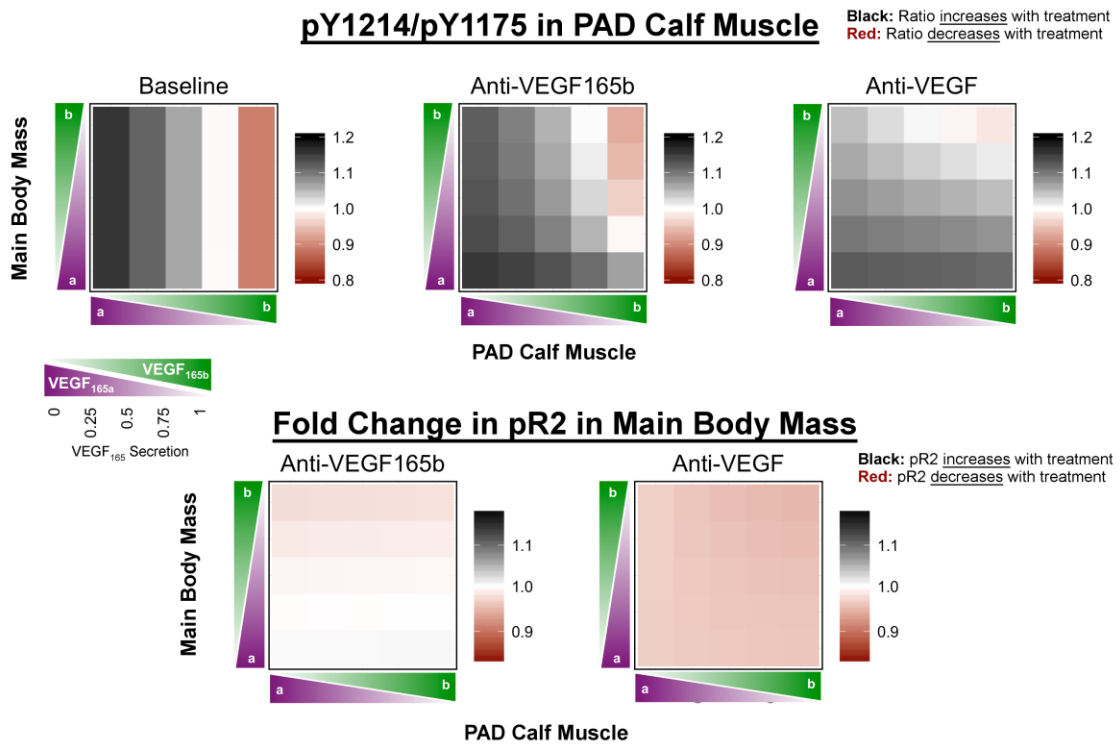
Fig 8-S8. Effects of VEGF-targeting antibodies on endothelial total VEGFR2 ligation *in vivo*. This figure is related to **Fig. 8-5**. Predicted total binding of VEGF to VEGFR2 (top row), VEGF$_{165b}$-R2 (middle row), and binding of other VEGF isoforms to VEGFR2 (bottom row) in the PAD Calf Muscle at baseline (left), and fold change from baseline on Day 6 following treatment with Anti-VEGF$_{165b}$ (middle) or a non-isoform-specific Anti-VEGF (right), as a function of the local fractional secretion of VEGF$_{165b}$ in the PAD Calf Muscle (x-axis) and the Main Body Mass (y-axis).
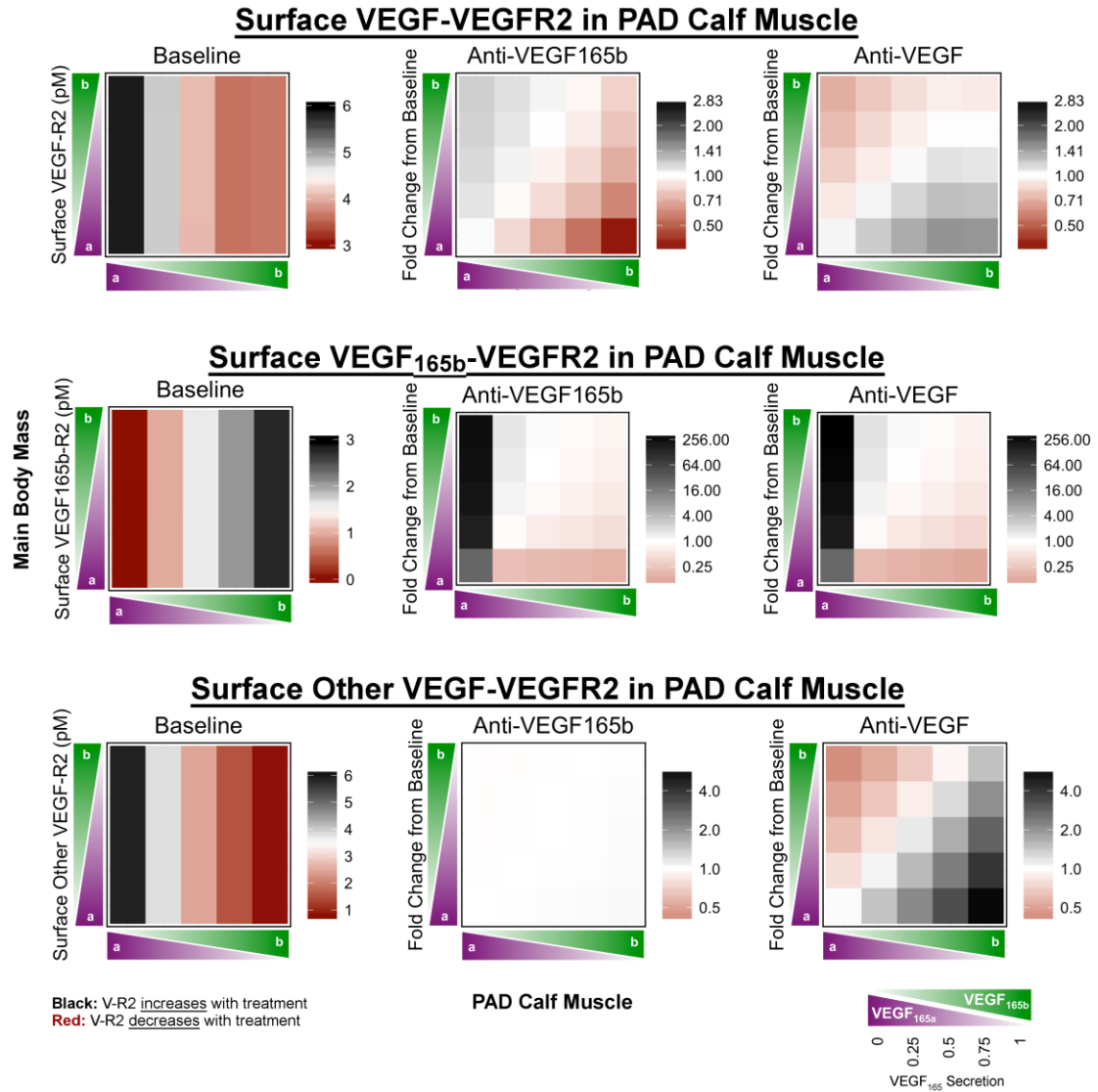
Fig 8-S9. Effects of VEGF-targeting antibodies on endothelial cell surface VEGFR2 ligation *in vivo*. This figure is related to **Fig. 8-5**. Predicted total binding of VEGF to VEGFR2 (top row), $VEGF_{165b}$-R2 (middle row), and binding of other VEGF isoforms to VEGFR2 (bottom row) in the PAD Calf Muscle at baseline (left), and fold change from baseline on Day 6 following treatment with Anti-$VEGF_{165b}$ (middle) or a non-isoform-specific Anti-VEGF (right), as a function of the local fractional secretion of $VEGF_{165b}$ in the PAD Calf Muscle (x-axis) and the Main Body Mass (y-axis).
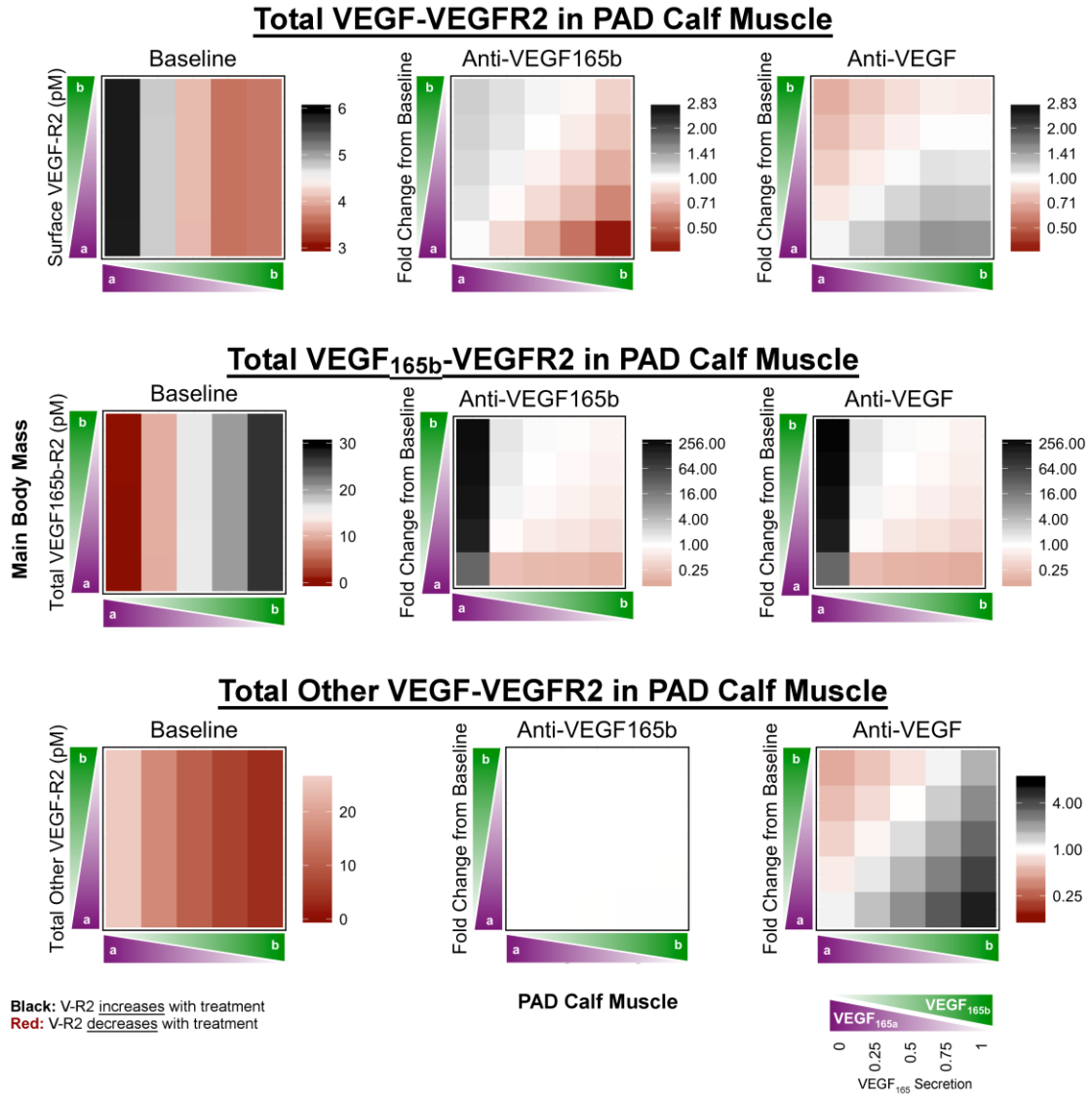
Figure 8-S10. Effects of VEGF-targeting antibodies on endothelial cell surface VEGFR1 ligation *in vivo*. This figure is related to **Fig. 8-5**. Predicted total binding of PlGF to VEGFR1 (top row), total VEGF to VEGFR1 (2nd row), $VEGF_{165b}$-R1 (3rd row), and binding of other VEGF isoforms to VEGFR1 (bottom row) in the PAD Calf Muscle at baseline (left), and fold change from baseline on Day 6 following treatment with Anti-$VEGF_{165b}$ (middle) or a non-isoform-specific Anti-VEGF (right), as a function of the local fractional secretion of $VEGF_{165b}$ in the PAD Calf Muscle (x-axis) and the Main Body Mass (y-axis).
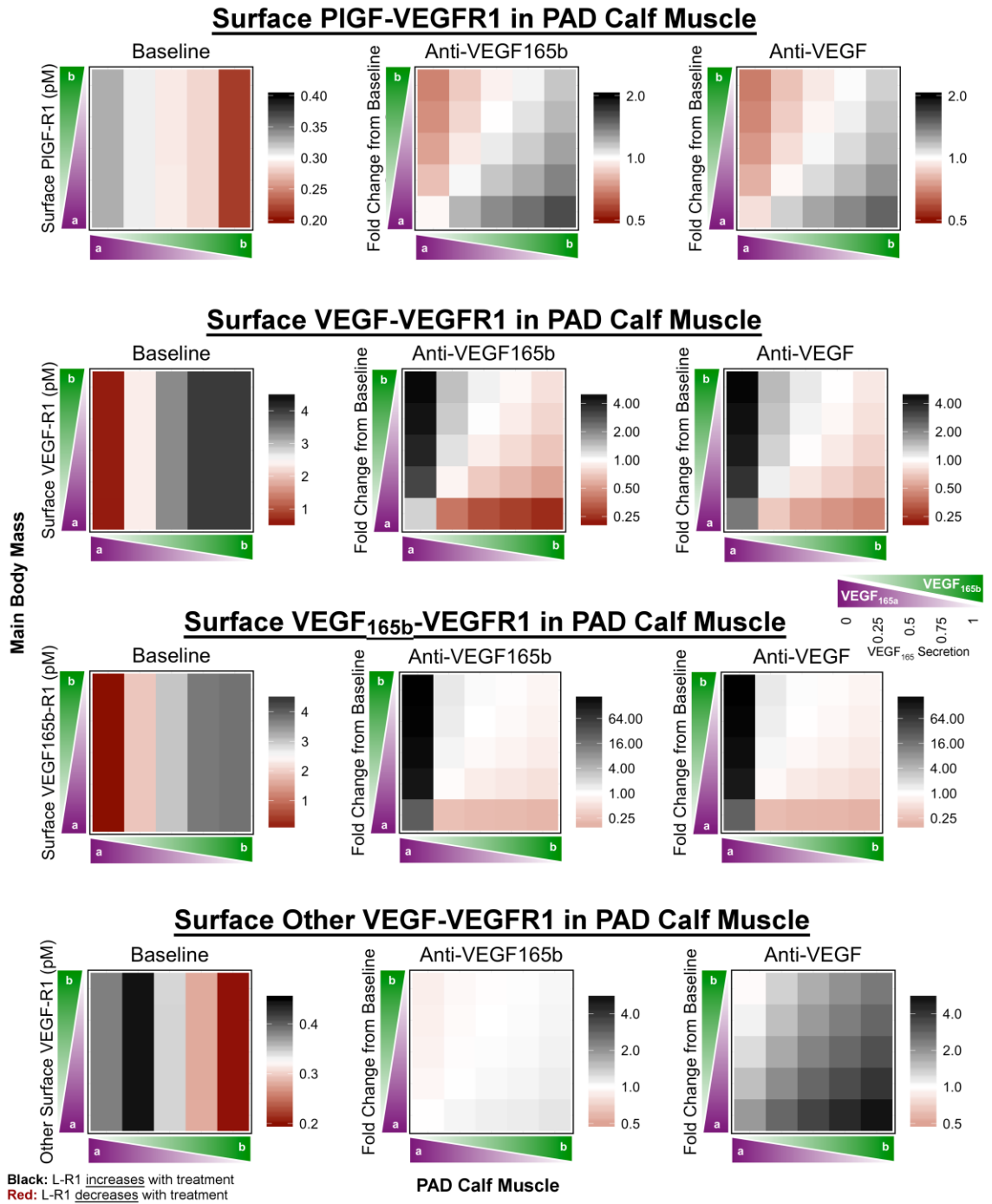
Figure 8-S10

Figure 8-S11. Relative antibody binding to VEGF$_{165a}$ and VEGF$_{165b}$ in the Main Body Mass and PAD Calf Muscle. This figure is related to **Fig. 8-4**. **(Top)** Predicted ratio of VEGF bound to the antibody in the PAD Calf Muscle as compared to the Main Body Mass on Day 6 following treatment, as a function of the local fractional secretion of VEGF$_{165b}$ in the PAD Calf Muscle (x-axis) and the Main Body Mass (y-axis). Left: VEGF$_{165b}$ bound to Anti-VEGF$_{165b}$, Middle: VEGF$_{165b}$ bound to Anti-VEGF, Right: VEGF$_{165a}$ bound to Anti-VEGF. **(Bottom)** Predicted ratio of VEGF$_{165b}$ to VEGF$_{165a}$ bound to Anti-VEGF in the PAD Calf Muscle (left), Blood (middle), and Main Body Mass (right) at Day 6 following treatment. In most cases, VEGF$_{165b}$ dominates due to its over-representation relative to its secretion fraction.
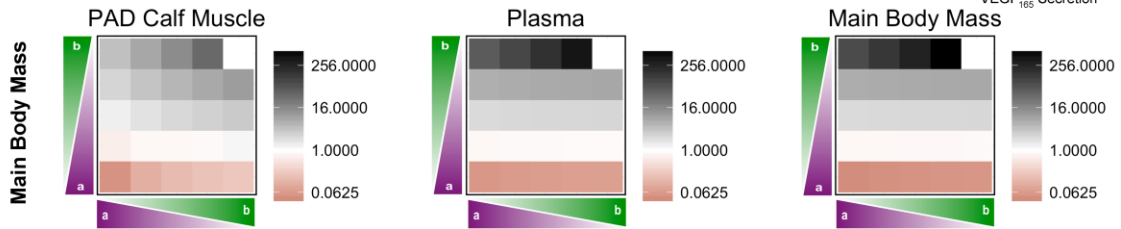
Figure 8-S12. Comparison of VEGFR2 activation following biomaterial-based protein delivery, gene therapy, or anti-VEGF treatment. This figure is related to **Fig. 8-6**. Fraction of total VEGFR2 phosphorylated (**A**), total VEGFR2 occupancy (**B**), and pY1214/pY1175 over time following treatment induction.
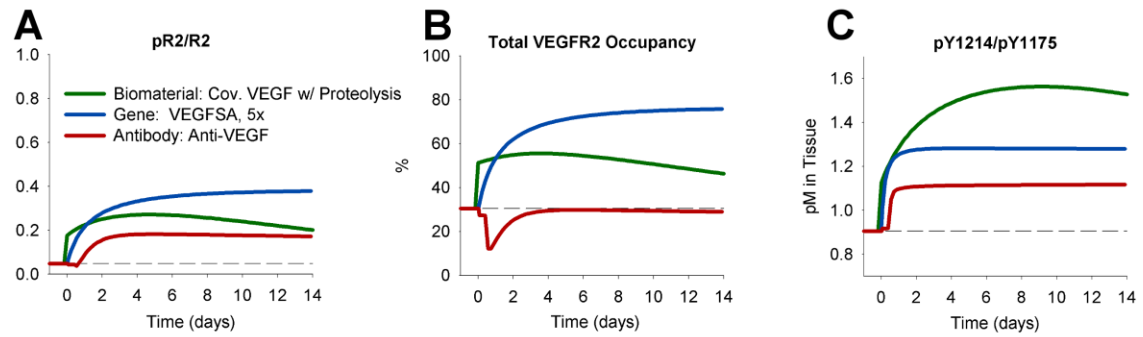
Chapter 9. A Generalized Analysis of Antibody Shuttling for Soluble Endogenous Paracrine Proteins

9.0 Summary

Here, we examined whether the 'antibody shuttling' effect observed in our complex human peripheral artery disease model (Chapter 8) was a more general phenomenon that may occur in other applications. We found that this effect requires only reversible binding of an antibody with a long half-life in the human body to a paracrine-acting target protein with multiple isoforms, which may be expressed at different levels in different tissue. This simple, generalized model captures both shuttling of a single ligand, as observed in cancer, and swapping of multiple ligands, as predicted in Chapter 8.

9.1 Introduction

Our objective was to create a simple compartment model to demonstrate an under-appreciated action of monoclonal antibodies targeting soluble paracrine factors (e.g. growth factors). Often, therapeutic antibodies are viewed as a means to remove a target endogenous protein from the body[1]. While this does occur, our model shows that they can also move target protein between compartments with different concentrations of endogenous protein, with potentially therapeutically-relevant consequences. Thus, we propose the importance of accounting not only for antibody pharmacokinetics, but also for antibody-mediated redistribution of endogenous proteins that may contribute to therapeutic response or off-target effects and toxicity.

The model results depend only on:

(1) the long (typically ~21 days) half-life of monoclonal antibodies

(2) reversible binding between antibody and target protein

(3) low transport of soluble target protein between compartments at baseline

The first two of these requirements hold generally for monoclonal antibodies. The third, a characteristic of

the underlying system, holds for growth factors and other cytokines that primarily act in a paracrine

manner; binding to receptors and being subsequently degraded in the same tissue in which they are

produced.

9.2 Methods

We created a simple, 2-compartment model containing two endogenous species: Red & Blue. Red & Blue are assumed to have identical properties; color simply enables tracking of two subsets of the endogenous target population (though this assumption can be relaxed). These may represent different isoforms of the target protein, or related proteins with which the antibody cross-reacts. The volumes of Compartment 1 and Compartment 2 are variable, as are the relative secretion of Red and Blue in each compartment. In this simple model, we assume constant clearance of Red & Blue from each compartment (e.g. via receptor-mediated endocytosis), with relatively low transport between compartments. An antibody with physiologically reasonably properties is delivered to Compartment 1 in excess at time=0, reversibly binding to Red & Blue, and moving between compartments at the same rate as free Red & Blue. The ten equations in the model are given below, followed by Tables detailing model parameters. R_i represents Red in compartment i, B_i is Blue in compartment I, and AB_i is free antibody.

$$\frac{d[R_1]}{dt} = q_{R1} - k_{c,R1}[R_1] - k_{on,R}[R_1][AB_1] + k_{off}[R_1 \times AB_1] - k_{t,R}[R_1] + k_{t,R}[R_2] * \frac{Vol_2}{Vol_1}$$

$$\frac{d[B_1]}{dt} = q_{B1} - k_{c,B1}[B_1] - k_{on,B}[B_1][AB_1] + k_{off}[B_1 \times AB_1] - k_{t,B}[B_1] + k_{t,B}[B_2] * \frac{Vol_2}{Vol_1}$$

$$\frac{d[AB_1]}{dt} = Dose_1(t) - k_{c,AB}[AB_1] - k_{on,R}[R_1][AB_1] + k_{off}[R_1 \times AB_1]$$
$$- k_{on,B}[B_1][AB_1] + k_{off}[B_1 \times AB_1] - k_{t,AB}[AB_1] + k_{t,AB}[AB_2] * \frac{Vol_2}{Vol_1}$$

$$\frac{d[R_1 \times AB_1]}{dt} = -k_{c,AB}[R_1 \times AB_1] + k_{on,R}[R_1][AB_1] - k_{off}[R_1 \times AB_1]$$
$$- k_{t,AB}[R_1 \times AB_1] + k_{t,AB}[R_2 \times AB_2] * \frac{Vol_2}{Vol_1}$$

$$\frac{d[B_1 \times AB_1]}{dt} = -k_{c,AB}[B_1 \times AB_1] + k_{on,B}[B_1][AB_1] - k_{off}[B_1 \times AB_1]$$
$$- k_{t,AB}[B_1 \times AB_1] + k_{t,AB}[B_2 \times AB_2] * \frac{Vol_2}{Vol_1}$$

$$\frac{d[R_2]}{dt} = q_{R2} - k_{c,R2}[R_2] - k_{on,R}[R_2][AB_2] + k_{off}[R_2 \times AB_2] - k_{t,R}[R_2] + k_{t,R}[R_1] * \frac{Vol_1}{Vol_2}$$

$$\frac{d[B_2]}{dt} = q_{B2} - k_{c,B2}[B_2] - k_{on,B}[B_2][AB_2] + k_{off}[B_2 \times AB_2] - k_{t,B}[B_2] + k_{t,B}[B_1] * \frac{Vol_1}{Vol_2}$$

$$\frac{d[AB_2]}{dt} = Dose_2(t) - k_{c,AB}[AB_2] - k_{on,R}[R_2][AB_2] + k_{off}[R_2 \times AB_2]$$

$$- k_{on,B}[B_2][AB_2] + k_{off}[B_2 \times AB_2] - k_{t,AB}[AB_2] + k_{t,AB}[AB_1] * \frac{Vol_1}{Vol_2}$$

$$\frac{d[R_2 \times AB_2]}{dt} = -k_{c,AB}[R_2 \times AB_2] + k_{on,R}[R_2][AB_2] - k_{off}[R_2 \times AB_2]$$

$$- k_{t,AB}[R_2 \times AB_2] + k_{t,AB}[R_1 \times AB_1] * \frac{Vol_1}{Vol_2}$$

$$\frac{d[B_2 \times AB_2]}{dt} = -k_{c,AB}[B_2 \times AB_2] + k_{on,B}[B_2][AB_2] - k_{off}[B_2 \times AB_2]$$

$$- k_{t,AB}[B_2 \times AB_2] + k_{t,AB}[B_1 \times AB_1] * \frac{Vol_1}{Vol_2}$$

The model was solved in R using the Livermore Solver for Ordinary Differential equations with Adaptive step size for stiff and non-stiff problems (LSODA), using an absolute tolerance of 10^{-10}.

Table 9-1. System Parameterization

Parameter	Description	Compartment 1	Compartment 2	Units
q_R	Secretion Rate, Red	0-10 (3)	0-10 (1)	nmoles/L/day
q_B	Secretion Rate, Blue	0-10 (1)	0-10 (3)	nmoles/L/day
Vol	Compartment Volume	0.1-10 (1)	0.1-10 (1)	L
$k_{c,R}$	Clearance Rate, Red	90	90	day^{-1}
$k_{c,B}$	Clearance Rate, Blue	90	90	day^{-1}
$k_{c,AB}$	Clearance Rate, Antibody	0.03	0.03	day^{-1}
$k_{t,R}$	Inter-compartment Transport, Red	10	10	day^{-1}
$k_{t,B}$	Inter-compartment Transport, Blue	10	10	day^{-1}
$k_{t,AB}$	Inter-compartment Transport, Antibody	10	10	day^{-1}

Notes: For variable parameters, default value given in parenthesis.

Table 9-2. Antibody-Binding Parameters

Parameter	Description	Red	Blue	Units
K_D	Antibody Binding Affinity	1.25	1.25	nmoles/L
k_{on}	Antibody Binding on-rate	8	8	(nmoles/L/day)$^{-1}$
k_{off}	Antibody Unbinding Rate	10	10	day^{-1}

Note: Antibody dose: compartment 1 only, 80 nmoles/L (in excess compared to ligand)

9.3 Results

Antibody Shuttling: Antibody facilitates movement of target protein, reducing concentration differences

We first examined a situation such as that found in cancer: a small compartment (e.g. tumor) expressing high levels of target protein compared to the main (e.g. central) compartment (**Fig 9-1A**). We showed that, following antibody administration (at a saturating concentration) into the main compartment, free target (Red) levels in the tumor drop as expected (**Fig 9-1B**). However, Red concentration is predicted to increase in the main compartment, as the antibody tends to bind Red in the high concentration small compartment, and tends to drop Red upon moving into the lower concentration environment of the main compartment. This effect has been predicted by a compartment model and confirmed via clinical observation in cancer, where plasma vascular endothelial growth factor (VEGF) levels can increase following treatment with an anti-VEGF antibody (bevacizumab)[2]. The extent of this effect depends on the relative volumes of the two compartments, but predicted free target generally increases in the low-baseline-concentration compartment, and decreases in the high-baseline-concentration compartment (**Fig 9-1C-D**), demonstrating the robustness of this 'shuttling' effect. The effect is not present if the compartment with high baseline target levels is much larger than compartment with low baseline target levels (discussed below).

Figure 9-1. Antibody shuttling effect leads to an increase in main compartment concentration when target protein is produced at high levels in a smaller compartment (e.g. tumor). (A) Schematic of model, including target protein section, clearance, and transport, as well as antibody dosing into compartment 1 (Main), transport, and clearance. The main compartment is 10L, with 1/10 the target secretion rate (per L) of the small compartment, which is 1L. **(B)** Following antibody administration, the concentration of free target protein decreases in the small compartment, but increases in the main compartment. **(C)** Analysis of fold change in free target protein in compartment 1 (low baseline) 10 days after antibody treatment, as a function of compartment volumes. **(D)** Fold change in free target protein concentration in compartment 2 (high baseline) 10 days after antibody treatment, as a function of compartment volumes.
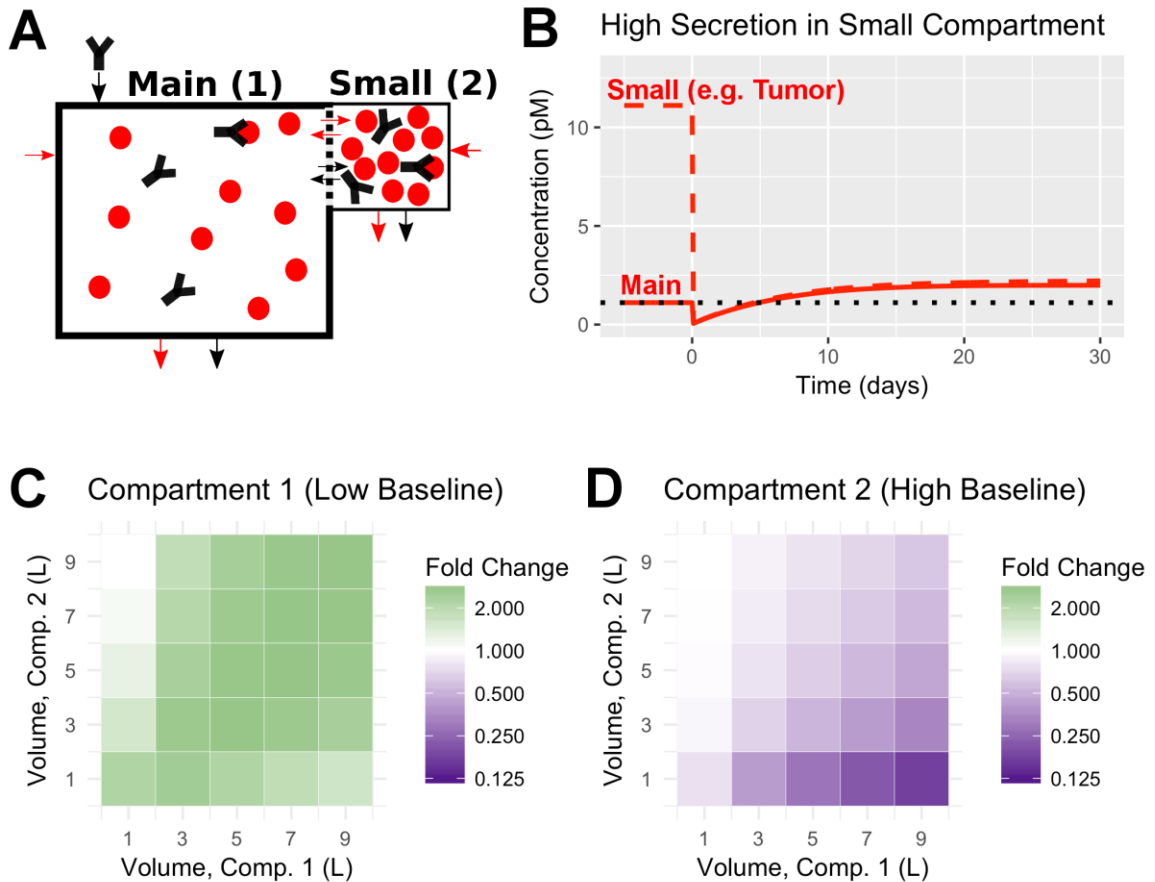
Antibody-Mediated Swapping: Shuttling occurs independently for multiple target proteins

We next examined a case where two identical target proteins, Red and Blue, are expressed at different levels in the two compartments (**Fig 9-2A**). This is representative of a case where an antibody binds to multiple isoforms of a target protein, which may have different signaling properties, or cross-reacts with related proteins. Such a scenario is quite common for antibodies targeting growth factors and other paracrine factors (e.g. cytokines). As the antibody is given in excess compared to target protein levels, it acts independently to shuttle Red and Blue between the compartments, leading to antibody-mediated swapping of Red and Blue, reducing the concentration differences between the two compartments (**Fig 9-2B-C**). Note that, because in this simulation total Red + Blue secretion is the same in each compartment, the antibody induces minimal change in total target protein concentration in either compartment (**Fig 9-2B-C**). Thus, while Red & Blue may have different signaling properties, if an assay is used that detects only total target concentration (e.g. a non-isoform-specific detection antibody), this effect will not be detected.

Figure 9-2. Antibody can 'swap' different target proteins between compartments, reducing concentration differences. (A) Schematic of model system, with two compartments of equal volume, with 10x higher secretion of Red than Blue in compartment 1, and 10x higher secretion of Blue than Red in compartment 2. Red and Blue have identical properties. **(B)** Comparison of concentration of Red and Blue in each compartment before and 10 days after antibody administration. Concentrations of Red and Blue in the two compartments become more similar following antibody treatment, demonstrating the 'swapping' effect. **(C)** Time-course of free Red and Blue following antibody treatment. Note minimal change in total (Red + Blue) concentrations (dashed line).
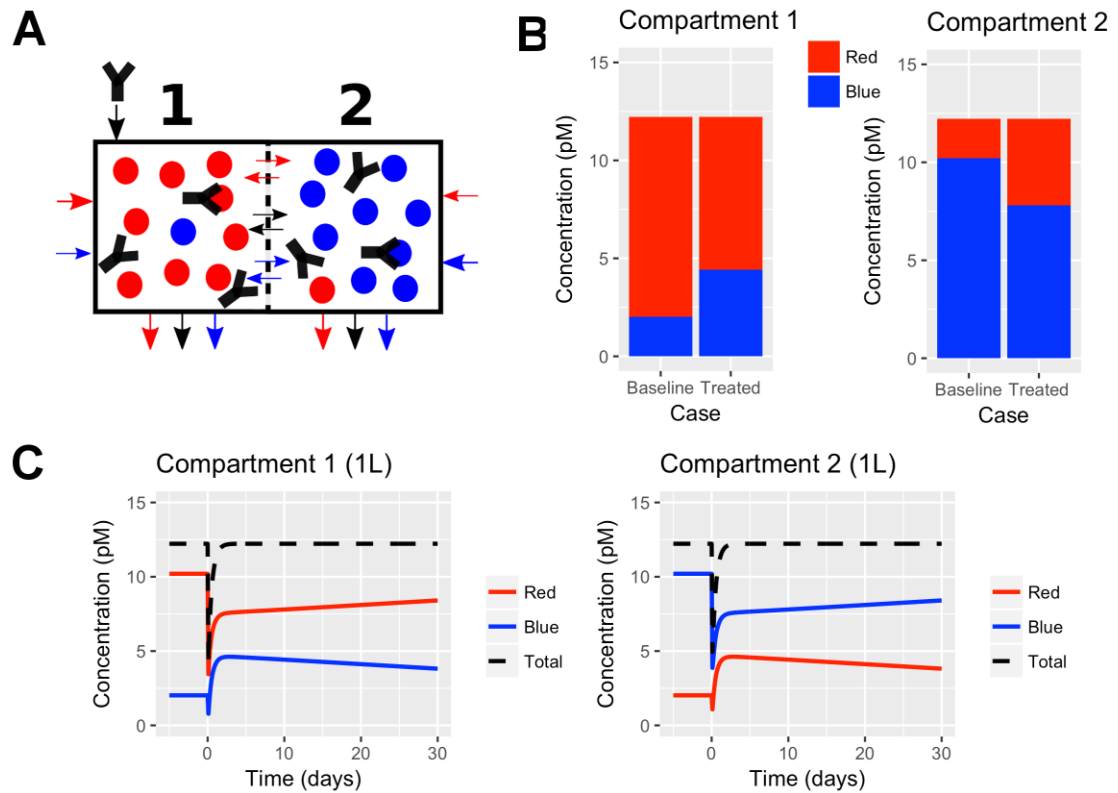
Antibody-Mediated Swapping: Effect of volume and relative secretion of Red & Blue

We next examined the robustness of this 'swapping' effect to changes in volume or initial concentration differences between compartments. While the effect is symmetric with equal size compartments (**Fig 9-2C**), asymmetry emerges for non-equal volume compartments, with larger changes in the concentrations of Red and Blue in the smaller compartment (**Fig 9-3A**). If the compartment with high baseline concentration of a target protein is sufficiently larger than the compartment with low baseline levels, significant 'leakage' of target protein from the large into the small compartment may occur, removing the concentration difference between compartments, and nullifying the antibody 'swapping' effect (**Fig 9-3B**, Red in Compartment 2).

Figure 9-3. Effect of compartment volume on antibody-mediated 'swapping' effect. (A) Time-course of free Red and Blue following antibody treatment when compartment 1 is twice as large as compartment 2. Note non-symmetric response. **(B)** Time-course of free Red and Blue following antibody treatment when compartment 1 is 10x as large as compartment 2. Note that, due to the disparate volumes, the baseline concentration of Red in compartment 2 matches that in the larger compartment 1, due to baseline 'leak' of Red between compartments. Due to this non-negligible basal transport, no 'swapping' effect is seen upon antibody administration.
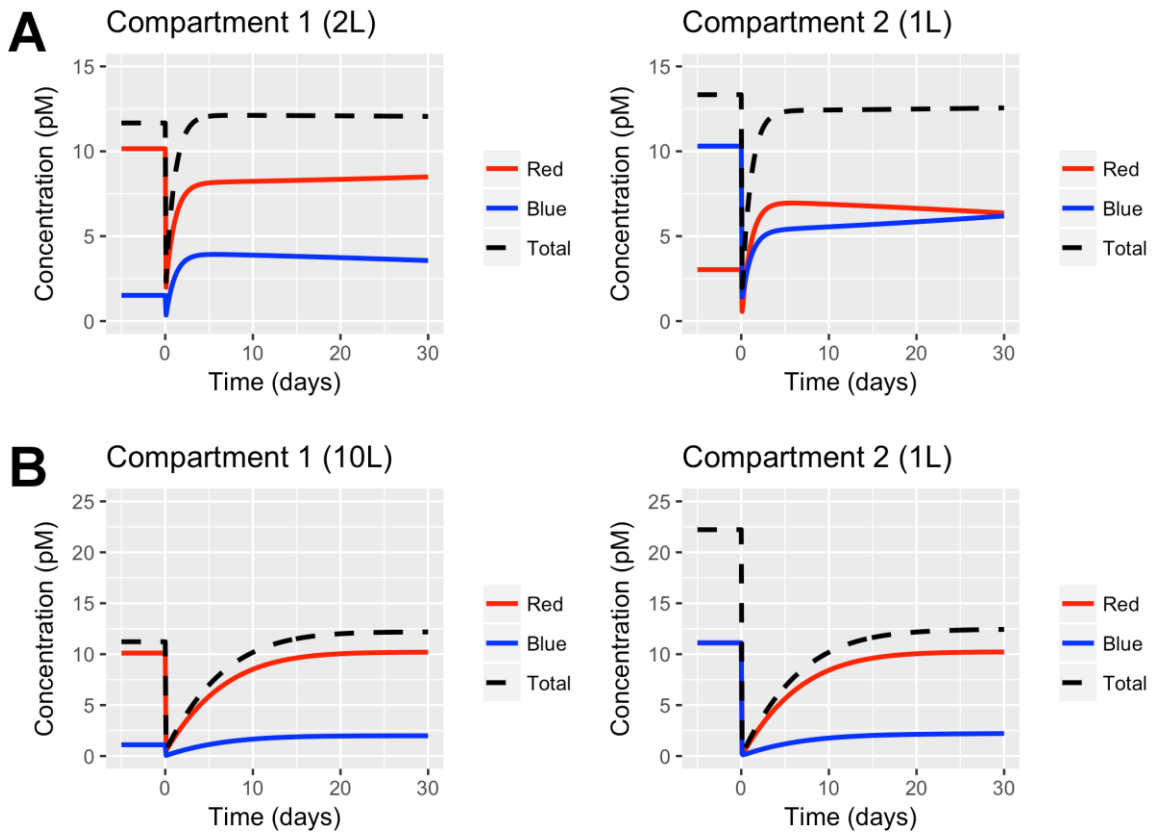
Examining the effect of compartment volume more broadly, we found, as for the single target protein case (**Fig 9-1C**), that following antibody administration, in each compartment the target protein that was high at baseline decreases, and the one was low in that compartment at baseline increases (**Fig 9-4**). As described in **Fig 9-3**, the effect disappears for very large volume differences.

Finally, we examined the effect of varying the concentration difference of Red and Blue between two equal-sized compartments. Holding total Red + Blue secretion constant, we found that the antibody would have little effect on total free target concentrations in each compartment (**Fig 9-5**, right column). The extent of Red/Blue swapping is proportional to the baseline concentration difference (**Fig 9-5**). We have observed this case in our systems pharmacology models of human peripheral artery disease, where total VEGF levels remain unchanged, but splicing changes in disease, from a 'strong' activator of signaling to increased expression of a 'weak' activator, leading to clinically-relevant changes in signaling, and impacting appropriate design of antibodies for this application.

We created a Shiny app that allows users to further explore these antibody-mediated 'shuttling' and 'swapping' effects, varying secretion of Red and Blue in each compartment, as well as compartment volumes.

Figure 9-4. Antibody swapping effect is not highly sensitive to compartment volumes. Fold change in free Red (left) and Blue (right) in compartment 1 (top) and compartment 2 (bottom) as a function of compartment volume. In all cases, upon antibody treatment, the target that was originally high in a compartment decreases (purple), while the target that was originally low increases (green). These simulations use the same model set-up as Figure 2 & 3, with 'high' denoting 10x higher secretion than the other target protein.
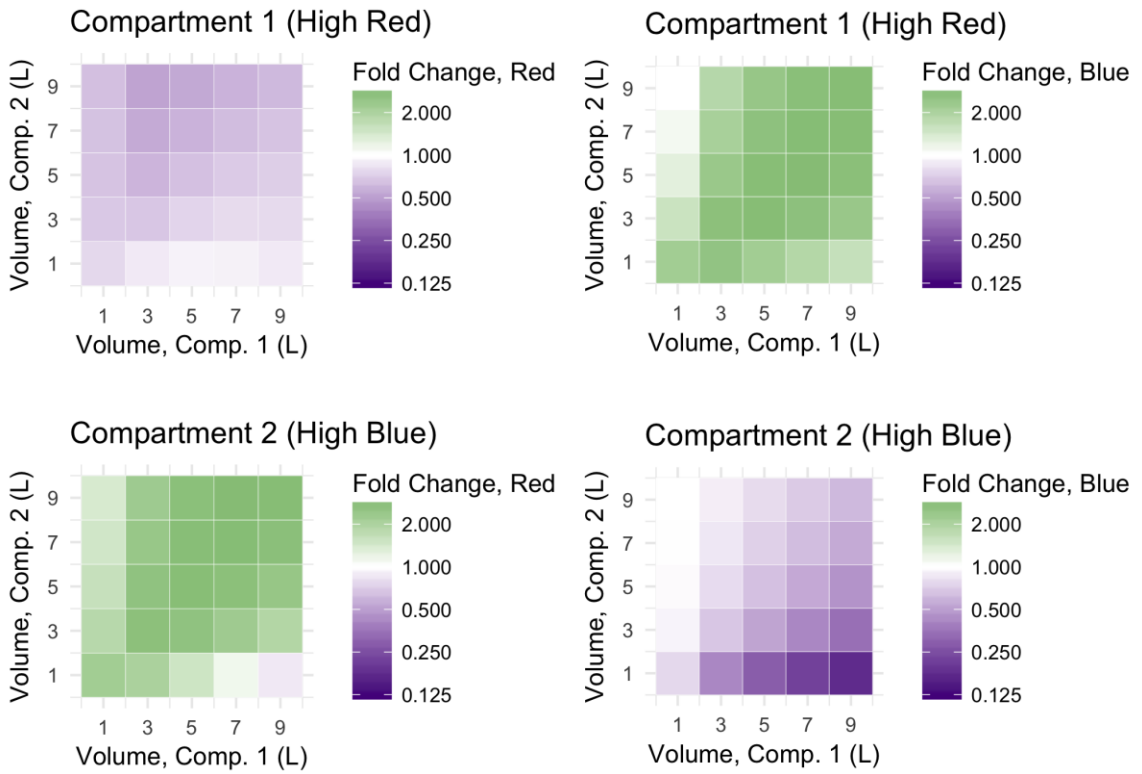
Figure 9-5. Antibody swapping effect magnitude is determined by relative secretion of Red and Blue in each compartment. Fold change in free Red (left), Blue (middle), and total target protein (right), in compartments 1 (top row) and 2 (bottom row). Total target secretion is held constant at 10 nmoles/L/day: as Red secretion increases, Blue secretion decreases proportionally.
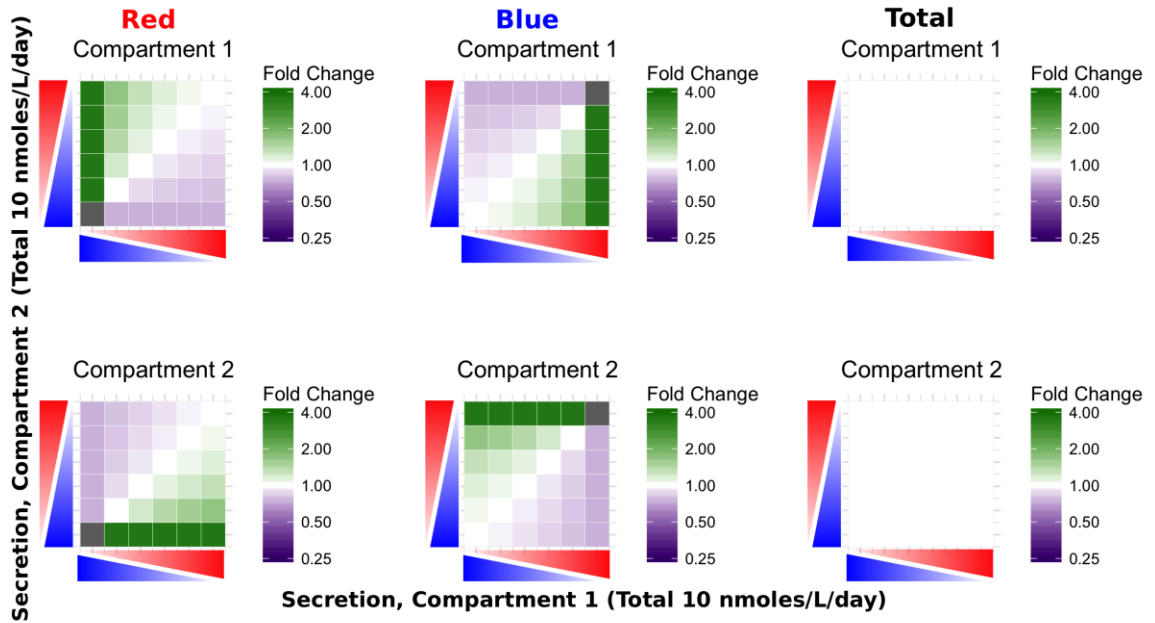
9.4 Conclusions

We have demonstrated here the generality of an un-appreciated mechanism of action of antibodies that bind to one or more isoforms of a soluble, paracrine-acting endogenous protein, which has been previously confirmed to occur in cancer[2] and is predicted to occur in human peripheral artery disease. We hypothesize that this effect may contribute to some of the observed off-target effects, toxicity, and unexpected actions observed clinically for this class of antibodies. This work motivates consideration of underlying target protein concentration differences between tissue in therapy design and in evaluation of drug pharmacokinetics and pharmacodynamics prior to first dosing in humans.

9.5 References

1   Davda, J. P. & Hansen, R. J. Properties of a general PK/PD model of antibody-ligand interactions for therapeutic antibodies that bind to soluble endogenous targets. *Mabs* **2**, 576-588, doi:10.4161/mabs.2.5.12833 (2010).

2   Stefanini, M. O., Wu, F. T. H., Mac Gabhann, F. & Popel, A. S. Increase of Plasma VEGF after Intravenous Administration of Bevacizumab Is Predicted by a Pharmacokinetic Model. *Cancer Research* **70**, 9886-9894, doi:10.1158/0008-5472.can-10-1419 (2010).

Chapter 10. Discussion & Future Directions

10.0 Summary

By building multi-scale mechanistic models firmly grounded in and validated against experimental data, we obtained unique mechanistic insight into a common biological process (growth factor immobilization) that could not have been arrived at through experiments alone. These models allow us to translate insight between cell culture, animal models, and human disease, overcoming barriers to effective design and translation of pro-angiogenic therapies. Specifically, we leveraged our mechanistic model to show how VEGF splicing changes contribute to impaired angiogenesis in peripheral artery disease (Chapter 8). We also provided quantitative evaluation of drivers of success or failure for biomaterial-based VEGF delivery, and identified a novel antibody-based therapeutic strategy using a clinically-approved drug (Chapter 9). This work provides a framework and motivation for study of immobilization of many other growth factors for tissue engineering applications [1, 2] (Chapter 3), by facilitating translation of experimental observations into predicted therapy effectiveness in human patients.

10.1 Bridging Scales: *in vitro* to Human Disease

A key feature of computational models is their ability to bridge scales (**Fig. 10-1**), facilitating interpretation of mechanistic detail observed *in vitro* in the context of human physiology, and improving understanding of how multiple perturbations contribute to signaling impairment in disease (Chapter 4). Here, we started with *in vitro* observations of VEGFR2 signaling in response to soluble or immobilized VEGF (Chapter 5), building a cell-level model to test mechanistic hypotheses about how immobilization alters signaling. We showed that a relatively simple mechanism – extended retention of immobilized VEGF-VEGFR2 complexes at the cell surface – can explain all experimental data to date.

Next, we wanted to study whether immobilized VEGF, which is predicted to be present at much higher levels than soluble VEGF *in vivo*, contributes to differential VEGF receptor signaling in the human body (Chapter 6). We found that the model does, in fact, predict signaling that varies as a function of VEGF isoform ECM-binding properties *in vivo*, and which aligns with the vascular morphologies observed in mice or tumors expressing single VEGF isoforms.

Having a predictive model, we next probed the contribution of changes in splicing of VEGF in peripheral artery disease to impaired angiogenic signaling (Chapter 7). Our model demonstrated that the VEGF$_{165b}$ isoform, which is elevated in PAD, does play a role in the disease, but not in the way previously hypothesized. While the prevailing hypothesis that VEGF$_{165b}$ competes for binding to VEGFR2 was based on *in vitro* observations, our model showed that, due to differences in concentration between *in vitro* and *in vivo* scenarios, this competition is not likely to occur *in vivo*. Instead, the model highlights the importance of reduction in expression of other VEGF isoforms to impaired VEGFR2 signaling, and confirms the observations of Ganta et. al. that VEGF$_{165b}$ can compete for binding to and alter the signaling of VEGFR1. These predictions, which could not have been reached via experiment alone, demonstrate the power of using models to translate across scales.

In building a model that captures all key aspects of VEGF distribution and VEGF receptor signaling in healthy subjects and peripheral artery disease patients, we created a framework that can be used to screen a broad array of different therapeutic strategies, evaluating their ability to induce more normal signaling in diseased tissue, and facilitating selection of appropriate doses (Chapter 8). These predictions are key to effective design and translation of therapies; in addition to identifying key rules for

biomaterial design, we predicted a new mechanism of action for antibody-based therapy, suggesting that an approved drug binding all VEGF isoforms may be more effective than an antibody tested in mice, which binds to only VEGF$_{165b}$ (Chapter 9). Further, we demonstrated that the newly identified mode of antibody action is generalizable to all antibodies designed to bind soluble paracrine-acting factors with multiple isoforms expressed at different levels in different tissues or in diseased vs. healthy tissue (Chapter 10). These predictions are novel, testable, and actionable during therapy development.

Figure 10-1. Overview of multi-scale modeling approach.
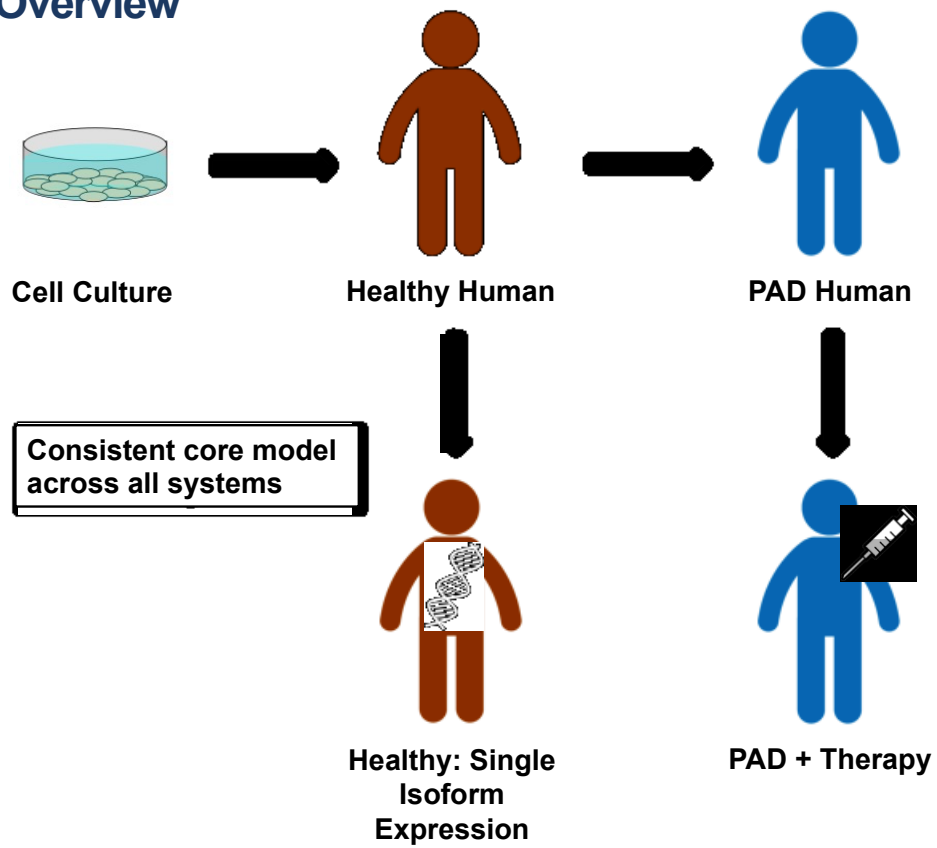
10.2 Future Directions

The work described here has further application in a variety of fields, and is far from exploring the full potential of this avenue of research to elucidate mechanisms underlying human disease and therapy.

10.2.1 Additional mechanistic detail on VEGF immobilization: integrins

Here, I explored the effect of physical retention of VEGF-VEGFR complexes at the cell surface. However, the complex interplay between integrins and growth factor receptors must be considered to fully understand the key role of the ECM in regulating growth factor-induced signaling in the body and in engineering tissues [1]. Co-stimulation of VEGFR2 and integrins leads to synergistic angiogenic signaling, reducing the amount of growth factor required to promote regeneration. However, the molecular mechanism behind this synergy, which also exists for other growth factor receptors, is poorly understood, making it difficult to predictively leverage for therapy. The effects of integrins on angiogenic signaling varies by integrin: $\alpha_5\beta_1$, which binds to fibronectin, is pro-angiogenic, while signaling of $\alpha_v\beta_3$, which binds to vitronectin and other ECM proteins, appears to be context-dependent. Building mechanistic models of co-regulation and signaling by VEGFR2 and integrins would allow for better predictions of effective ways to leverage this synergy therapeutically (Chapter 3). Incorporating this detail into multi-scale models will improve our ability to optimize VEGF & ECM co-presentation to predictably induce synergistic signaling *in vivo* [3].

10.2.2 Detailed trafficking and signaling of VEGFR1

While we have developed a detailed model of VEGFR2 trafficking and site-specific phosphorylation, sufficient mechanistic knowledge is not available to do the same for VEGFR1. Recent experimental data and the results presented here suggest that VEGFR1 may have an under-appreciated role in human disease [4-7], motivating such work. The framework here can easily be adapted and updated to incorporate such detailed mechanistic detail for VEGFR1, improving the model's ability to accurately capture and predict VEGFR1 signaling in different conditions.

10.2.3 VEGF splicing and immobilization in different disease applications

VEGF splicing changes and ECM remodeling occur not only in PAD, but also in diabetes and obesity [8], conditions characterized by impaired wound healing and poor angiogenic responses to ischemia. A quantitative understanding of how these changes affect VEGF signaling and microvascular dysfunction will lead to better strategies to prevent this damage and design tissue constructs to facilitate wound healing in these chronic conditions. Future work to quantify both local changes in VEGF and ECM in healthy vs. unhealing wounds [1], and systemic changes due to disease, in both mice and humans, will be important.

Building upon existing human and mouse whole-body human compartment models, models of diabetic and obese humans, and parallel computational models of diseased mice (e.g. ob/ob, C57BL/6 diet-induced obesity) can be created to probe key drivers of microvascular impairment in each disease. A chronic wound compartment can be incorporated to study the signaling underlying impaired wound healing, and to optimize VEGF delivery for improved regeneration, accounting for disease-specific changes in tissue-level physiology, VEGF splicing, and ECM protein expression and degradation by proteases, along with emerging research on the role of fat and glucose on microvascular dysfunction. Intruiging evidence on the role of VEGF splicing changes in cancer is also emerging [9-11], which could be explored using this model framework.

10.2.4 Spatiotemporal patterning of VEGFR signaling in tissue

Spatial and temporal patterning of cues is critical to formation of functional vascular networks; poor spatial control is believed to be a key cause of failure in gene- and cell-based VEGF delivery to date [12, 13]. A quantitative understanding of these dynamics, which are difficult to measure *in vivo*, is necessary to optimize delivery and presentation (e.g. ECM-binding) of VEGF. Building upon my thesis work, realistic 3D models of VEGF spatial distribution and VEGF receptor activation *in vivo* could be constructed [7, 14]. This framework could be used to simulate signaling in experimental systems of vascular development (e.g. embryoid body & fibrin bead assays), in which the vasculature can be imaged over time following a perturbation, to understand the minimal spatiotemporal requirements for vascular network formation. The level of molecular and physiological detail in the model allows us to extract key, experimentally testable readouts. These readouts include predicted microenvironmental variability in

VEGF concentration and VEGFR2 signaling, and spatial gradients in VEGFR2 activation at branching points vs. in quiescent vasculature.

The model could also be used to simulate signaling in healthy & ischemic skeletal muscle at baseline and following cell, gene, protein, antibody, and exercise therapy [15]. This will help to optimize therapy design, dosing, and delivery to mimic micropatterning of VEGF signaling in healthy and developmental tissues, reducing poor responses to due insufficient VEGF delivery and angioma formation due to receptor saturation by excess local VEGF.

10.2.5 VEGF immobilization in tissue engineering applications

A key next step for this work will be translation of these computational predictions towards application in engineered tissue constructs. The key rules for biomaterial-based VEGF delivery outlined in Chapter 9 can be used to design and test VEGF dosing and delivery mode in experimental tissues, developmental applications, and animal experiments. Results from these experiments can be used to further refine the model in an iterative fashion. Additionally, implementation of the 3D tissue model will allow explicit predictions of optimal VEGF, ECM, and endothelial cell patterning in tissue constructs to generate therapeutically optimal gradients in VEGF distribution and receptor signaling. 3D bioprinting technology can be used to build and test such systems. In this way, the computational modeling work presented here can have concrete and immediate impact on design of growth factor-incorporating tissue constructs and biomaterials, allowing for more rational and systematic optimization of these systems, as well as testing of key mechanistic hypotheses about response to VEGF gradients and VEGF immobilization in real tissues.

10.2.6 Immobilization of other growth factors: tissue engineering, stem cell differentiation

Differential cellular behavior following stimulation with soluble or immobilized growth factor is not limited to the VEGF family, and VEGF is not the only growth factor regulating angiogenesis [16, 17]. Indeed, co-delivery of VEGF and platelet-derived growth factor (PDGF) engineered for strong ECM-binding in fibrin gels improves growth and stability of angiogenic vascular networks [3, 18]. Therefore, it would be valuable, using the work presented here as a framework, to build detailed models of receptor activation by soluble and ECM-bound PDGF, which activates receptors on vascular smooth muscle cells

and pericytes to stabilize neovessels following VEGF-simulated angiogenesis [18-20]. This insight could be translated *in vivo* using our existing human body model framework. This work is key to design biomaterials that effectively co-deliver VEGF & PDGF in sequence to induce stable angiogenesis concurrent with tissue remodeling, a necessity for thick tissues.

While the ability of growth factors to bind ECM is broadly of interest to control growth factor delivery for regenerative medicine applications, the impact of immobilization on signaling is poorly understood for the majority of these factors. For example, BMP (osteogenesis), TGFβ (chondrogenesis and wound healing), GDNF (peripheral nerve regeneration), FGF and other growth factors (stem cell differentiation) all have isoforms that can bind to ECM proteins [2]. Therefore, similar analysis of immobilization of these growth factors would improve our ability to rational design delivery systems for growth factors in diverse applications.

10.3 References

1.   Briquez PS, Clegg LE, Martino MM, Gabhann FM, Hubbell JA. Design principles for therapeutic angiogenic materials. Nature Reviews Materials. 2016;1:15006. doi: 10.1038/natrevmats.2015.6.

2.   Salmeron-Sanchez M, Dalby MJ. Synergistic growth factor microenvironments. Chemical Communications.   2016;52(91):13327-36.   doi: 10.1039/c6cc06888j.   PubMed   PMID: WOS:000388102800002.

3.   Martino MM, Briquez PS, Güç E, Tortelli F, Kilarski WW, Metzger S, et al. Growth Factors Engineered for Super-Affinity to the Extracellular Matrix Enhance Tissue Healing. Science. 2014;343(6173):885-8. doi: 10.1126/science.1247663.

4.   Ganta VC, Choi M, Kutateladze A, Annex BH. VEGF₁₆₅b Modulates Endothelial VEGFR1-STAT3 Signaling Pathway and Angiogenesis in Human and Experimental Peripheral Arterial Disease. Circulation Research. 2016.

5.   Räsänen M, Degerman J, Nissinen TA, Miinalainen I, Kerkelä R, Siltanen A, et al. VEGF-B gene therapy inhibits doxorubicin-induced cardiotoxicity by endothelial protection. Proceedings of the National Academy of Sciences. 2016;113(46):13144-9.

6.   Robciuc MR, Kivela R, Williams IM, de Boer JF, van Dijk TH, Elamaa H, et al. VEGFB/VEGFR1-Induced Expansion of Adipose Vasculature Counteracts Obesity and Related Metabolic Complications. Cell Metabolism. 2016;23(4):712-24. doi: 10.1016/j.cmet.2016.03.004. PubMed PMID: WOS:000374123200018.

7.   Chappell JC, Cluceru JG, Nesmith JE, Mouillesseaux KP, Bradley VB, Hartland CM, et al. Flt-1 (VEGFR-1) coordinates discrete stages of blood vessel formation. Cardiovascular Research. 2016;111(1):84-93. doi: 10.1093/cvr/cvw091. PubMed PMID: WOS:000379811800013.

8.   Ngo DTM, Farb MG, Kikuchi R, Karki S, Tiwari S, Bigornia SJ, et al. Antiangiogenic Actions of Vascular Endothelial Growth Factor-A(165)b, an Inhibitory Isoform of Vascular Endothelial Growth Factor-A, in Human Obesity. Circulation. 2014;130(13):1072-80. doi: 10.1161/circulationaha.113.008171. PubMed PMID: WOS:000342685100012.

9.   English WR, Lunt SJ, Fisher M, Lefley DV, Dhingra M, Lee Y-C, et al. Differential Expression of VEGFA Isoforms Regulates Metastasis and Response to Anti-VEGFA Therapy in Sarcoma. Cancer Research. 2017.

10.   Bates DO, Cui TG, Doughty JM, Winkler M, Sugiono M, Shields JD, et al. VEGF(165)b, an inhibitory splice variant of vascular endothelial growth factor, is down-regulated in renal cell carcinoma. Cancer Research. 2002;62(14):4123-31. PubMed PMID: WOS:000176871500037.

11.   Nowak DG, Woolard J, Amin EM, Konopatskaya O, Saleem MA, Churchill AJ, et al. Expression of pro- and anti-angiogenic isoforms of VEGF is differentially regulated by splicing and growth factors. Journal of Cell Science. 2008;121(20):3487-95. doi: 10.1242/jcs.016410. PubMed PMID: WOS:000259912100021.

12.   Ozawa CR, Banfi A, Glazer NL, Thurston G, Springer ML, Kraft PE, et al. Microenvironmental VEGF concentration, not total dose, determines a threshold between normal and aberrant angiogenesis. Journal of Clinical Investigation. 2004;113(4):516-27. doi: 10.1172/jci200418420. PubMed PMID: WOS:000189008000007.

13.   von Degenfeld G, Banfi A, Springer ML, Wagner RA, Jacobi J, Ozawa CR, et al. Microenvironmental VEGF distribution is critical for stable and functional vessel growth in ischemia. Faseb Journal. 2006;20(14):2657-+. doi: 10.1096/fj.06-6568fje. PubMed PMID: WOS:000242490700056.

14.   Hashambhoy YL, Chappell JC, Peirce SM, Bautch VL, Mac Gabhann F. Computational modeling of interacting VEGF and soluble VEGF receptor concentration gradients. Front Physiol. 2011;2:62. Epub 2011/10/19. doi: 10.3389/fphys.2011.00062. PubMed PMID: 22007175; PubMed Central PMCID: PMC3185289.

15.   Vempati P, Popel AS, Mac Gabhann F. Formation of VEGF isoform-specific spatial distributions governing angiogenesis: computational analysis. BMC Syst Biol. 2011;5:59. Epub 2011/05/04. doi: 10.1186/1752-0509-5-59. PubMed PMID: 21535871; PubMed Central PMCID: PMC3113235.

16.   Clegg LE, Mac Gabhann F. Systems biology of the microvasculature. Integrative Biology. 2015. doi: 10.1039/C4IB00296B.

17.   Moulisová V, Gonzalez-García C, Cantini M, Rodrigo-Navarro A, Weaver J, Costell M, et al. Engineered microenvironments for synergistic VEGF – Integrin signalling during vascularization. Biomaterials. doi: http://dx.doi.org/10.1016/j.biomaterials.2017.02.024.

18.   Martino MM, Tortelli F, Mochizuki M, Traub S, Ben-David D, Kuhn GA, et al. Engineering the Growth Factor Microenvironment with Fibronectin Domains to Promote Wound and Bone Tissue Healing. Science Translational Medicine. 2011;3(100). doi: 10.1126/scitranslmed.3002614. PubMed PMID: WOS:000294841400004.

19.   Lindblom P, Gerhardt H, Liebner S, Abramsson A, Enge M, Hellstrom M, et al. Endothelial PDGF-B retention is required for proper investment of pericytes in the microvessel wall. Genes & Development. 2003;17(15):1835-40. doi: 10.1101/gad.266803. PubMed PMID: WOS:000184531500006.

20.   Xu JH, Clark RAF. Extracellular matrix alters PDGF regulation of fibroblast integrins. Journal of Cell Biology. 1996;132(1-2):239-49. doi: 10.1083/jcb.132.1.239. PubMed PMID: WOS:A1996TR59300019.

Appendix. Model Equations

A.1 Equations for Cell-level Model (Chapter 5)

A.1.1 Extracellular Molecular Complexes:

$$\frac{d[V]}{dt} = -k_{on,V\cdot M}[V][M] + k_{off,V\cdot M}[V\cdot M] - k_{on,V\cdot R2}[V][R2] + k_{off,V\cdot R2}[V\cdot R2] - k_{on,V\cdot N1}[V][N1]$$
$$+ k_{off,V\cdot N1}[V\cdot N1]$$

$$\frac{d[M]}{dt} = -k_{on,V\cdot M}[V][M] + k_{off,V\cdot M}[V\cdot M] - k_{on,M\cdot(V\cdot R2)}[M][V\cdot R2] + k_{off,M\cdot(V\cdot R2)}[M\cdot V\cdot R2]$$

$$\frac{d[V\cdot M]}{dt} = k_{on,V\cdot M}[V][M] - k_{off,V\cdot M}[V\cdot M] - k_{on,(V\cdot M)\cdot R2}[V\cdot M][R2] + k_{off,(M\cdot V)\cdot R2}[M\cdot V\cdot R2]$$

A.1.2 Cell Surface Molecular Complexes:

$$\frac{d[R2]}{dt} = -k_{on,V\cdot R2}[V][R2] + k_{off,V\cdot R2}[V\cdot R2] - k_{on,(V\cdot M)\cdot R2}[V\cdot M][R2] + k_{off,(M\cdot V)\cdot R2}[M\cdot V\cdot R2]$$
$$- k_{on,(V\cdot N1)\cdot R2}[V\cdot N1][R2] + k_{off,(V\cdot N1)\cdot R2}[V\cdot N1\cdot R2] - k_{intn,R2}[R2] + k_{rec4,R2}[R2_{rab45}]$$
$$+ k_{rec11,R2}[R2_{rab11}] + s_{R2}$$

$$\frac{d[V\cdot R2]}{dt} = k_{on,V\cdot R2}[V][R2] - k_{off,V\cdot R2}[V\cdot R2] - k_{on,M\cdot(V\cdot R2)}[M][V\cdot R2] + k_{off,M\cdot(V\cdot R2)}[M\cdot V\cdot R2]$$
$$- k_{on,(V\cdot R2)\cdot N1}[V\cdot R2][N1] + k_{off,(V\cdot R2)\cdot N1}[V\cdot N1\cdot R2] - k_{intn,V\cdot R2}[V\cdot R2]$$
$$+ k_{rec4,V\cdot R2}[(V\cdot R2)_{rab45}] + k_{rec11,V\cdot R2}[(V\cdot R2)_{rab11}]$$

$$\frac{d[V\cdot R2]}{dt} = k_{on,V\cdot R2}[V][R2] - k_{off,V\cdot R2}[V\cdot R2] - k_{on,M\cdot(V\cdot R2)}[M][V\cdot R2] + k_{off,M\cdot(V\cdot R2)}[M\cdot V\cdot R2]$$
$$- k_{on,(V\cdot R2)\cdot N1}[V\cdot R2][N1] + k_{off,(V\cdot R2)\cdot N1}[V\cdot N1\cdot R2] - k_{intn,V\cdot R2}[V\cdot R2] + k_{rec4,V\cdot R2}[(V\cdot R2)_{rab45}]$$
$$+ k_{rec11,V\cdot R2}[(V\cdot R2)_{rab11}]$$

$$\frac{d[M\cdot V\cdot R2]}{dt} = k_{on,(V\cdot M)\cdot R2}[V\cdot M][R2] - k_{off,(M\cdot V)\cdot R2}[M\cdot V\cdot R2] + k_{on,M\cdot(V\cdot R2)}[M][V\cdot R2]$$
$$- k_{off,M\cdot(V\cdot R2)}[M\cdot V\cdot R2]$$

$$\frac{d[N1]}{dt} = -k_{on,V \cdot N1}[V][N1] + k_{off,V \cdot N1}[V \cdot N1] - k_{on,(V \cdot R2) \cdot N1}[V \cdot R2][N1] + k_{off,(V \cdot R2) \cdot N1}[V \cdot N1 \cdot R2]$$
$$- k_{intn,N1}[N1] + k_{rec4,N1}[N1_{rab45}] + k_{rec11,N1}[N1_{rab11}] + s_{N1}$$

$$\frac{d[V \cdot N1]}{dt} = k_{on,V \cdot N1}[V][N1] - k_{off,V \cdot N1}[V \cdot N1] - k_{on,R2 \cdot (V \cdot N1)}[R2][V \cdot N1] + k_{off,R2 \cdot (V \cdot N1)}[V \cdot N1 \cdot R2]$$
$$- k_{intn,V \cdot N1}[V \cdot N1] + k_{rec4,V \cdot N1}[(V \cdot N1)_{rab45}] + k_{rec11,V \cdot N1}[(V \cdot N1)_{rab11}]$$

$$\frac{d[V \cdot N1 \cdot R2]}{dt} = k_{on,(V \cdot N1) \cdot R2}[V \cdot N1][R2] - k_{off,(V \cdot N1) \cdot R2}[V \cdot N1 \cdot R2] + k_{on,(V \cdot R2) \cdot N1}[V \cdot R2][N1]$$
$$- k_{off,(V \cdot R2) \cdot N1}[V \cdot N1 \cdot R2] - k_{intn,V \cdot N1 \cdot R2}[V \cdot N1 \cdot R2] + k_{rec4,V \cdot N1 \cdot R2}[(V \cdot N1 \cdot R2)_{rab45}]$$
$$+ k_{rec11,V \cdot N1 \cdot R2}[(V \cdot N1 \cdot R2)_{rab11}]$$

A.1.3 Rab 4/5 Molecular Complexes:

$$\frac{d[R2_{rab45}]}{dt} = -k_{on,V \cdot R2_{rab45}}[V_{rab45}][R2_{rab45}] + k_{off,V \cdot R2_{rab45}}[(V \cdot R2)_{rab45}]$$
$$- k_{on,(V \cdot N1) \cdot R2_{rab45}}[(V \cdot N1)_{rab45}][R2_{rab45}] + k_{off,(V \cdot N1) \cdot R2_{rab45}}[(V \cdot N1 \cdot R2)_{rab45}] + k_{intn,R2}[R2]$$
$$- k_{rec4,R2_{rab45}}[R2_{rab45}] - k_{4to11,R2_{rab45}}[R2_{rab45}] - k_{degr,R2_{rab45}}[R2_{rab45}]$$

$$\frac{d[(V \cdot R2)_{rab45}]}{dt} = k_{on,V \cdot R2_{rab45}}[V_{rab45}][R2_{rab45}] - k_{off,V \cdot R2_{rab45}}[(V \cdot R2)_{rab45}]$$
$$- k_{on,(V \cdot R2) \cdot N1_{rab45}}[(V \cdot R2)_{rab45}][N1_{rab45}] + k_{off,(V \cdot R2) \cdot N1_{rab45}}[(V \cdot N1 \cdot R2)_{rab45}]$$
$$+ k_{intn,V \cdot R2}[V \cdot R2] - k_{rec4,V \cdot R2_{rab45}}[(V \cdot R2)_{rab45}] - k_{4to11,4,V \cdot R2_{rab45}}[(V \cdot R2)_{rab45}]$$
$$- k_{degr,V \cdot R2_{rab45}}[(V \cdot R2)_{rab45}]$$

$$\frac{d[V_{rab45}]}{dt} = -k_{on,V \cdot R2_{rab45}}[V_{rab45}][R2_{rab45}] + k_{off,V \cdot R2_{rab45}}[(V \cdot R2)_{rab45}] - k_{on,V \cdot N1_{rab45}}[V_{rab45}][N1_{rab45}]$$
$$+ k_{off,V \cdot N1_{rab45}}[(V \cdot N1)_{rab45}] - k_{degr,V_{rab45}}[V_{rab45}]$$

$$\frac{d[N1_{rab45}]}{dt} = -k_{on,V \cdot N1_{rab45}}[V_{rab45}][N1_{rab45}] + k_{off,V \cdot N1_{rab45}}[(V \cdot N1)_{rab45}]$$
$$- k_{on,(V \cdot R2) \cdot N1_{rab45}}[(V \cdot R2)_{rab45}][N1_{rab45}] + k_{off,(V \cdot R2) \cdot N1_{rab45}}[(V \cdot N1 \cdot R2)_{rab45}] + k_{intn,N1}[N1]$$
$$- k_{rec4,N1_{rab45}}[N1_{rab45}] - k_{4to11,N1_{rab45}}[N1_{rab45}] - k_{degr,N1_{rab45}}[N1_{rab45}]$$

$$\frac{d\left[\left(V\cdot N1\right)_{rab45}\right]}{dt}=k_{on,V\cdot N1_{rab45}}\left[V_{rab45}\right]\left[N1_{rab45}\right]-k_{off,V\cdot N1_{rab45}}\left[\left(V\cdot N1\right)_{rab45}\right]$$

$$-k_{on,(V\cdot N1)\cdot R2_{rab45}}\left[\left(V\cdot N1\right)_{rab45}\right]\left[R2_{rab45}\right]+k_{off,(V\cdot N1)\cdot R2_{rab45}}\left[\left(V\cdot N1\cdot R2\right)_{rab45}\right]$$

$$+k_{intn,V\cdot N1}\left[V\cdot N1\right]-k_{rec4,V\cdot N1_{rab45}}\left[\left(V\cdot N1\right)_{rab45}\right]-k_{4to11,V\cdot N1_{rab45}}\left[\left(V\cdot N1\right)_{rab45}\right]$$

$$-k_{degr,V\cdot N1_{rab45}}\left[\left(V\cdot N1\right)_{rab45}\right]$$

$$\frac{d\left[\left(V\cdot N1\cdot R2\right)_{rab45}\right]}{dt}=k_{on,(V\cdot R2)\cdot N1_{rab45}}\left[\left(V\cdot R2\right)_{rab45}\right]\left[N1_{rab45}\right]-k_{off,(V\cdot R2)\cdot N1_{rab45}}\left[\left(V\cdot N1\cdot R2\right)_{rab45}\right]$$

$$+k_{on,(V\cdot N1)\cdot R2_{rab45}}\left[\left(V\cdot N1\right)_{rab45}\right]\left[R2_{rab45}\right]-k_{off,(V\cdot N1)\cdot R2_{rab45}}\left[\left(V\cdot N1\cdot R2\right)_{rab45}\right]$$

$$+k_{intn,V\cdot N1\cdot R2}\left[V\cdot N1\cdot R2\right]-k_{rec4,V\cdot N1\cdot R2_{rab45}}\left[\left(V\cdot N1\cdot R2\right)_{rab45}\right]$$

$$-k_{4to11,V\cdot N1\cdot R2_{rab45}}\left[\left(V\cdot N1\cdot R2\right)_{rab45}\right]-k_{degr,V\cdot N1\cdot R2_{rab45}}\left[\left(V\cdot N1\cdot R2\right)_{rab45}\right]$$

A.1.4 Rab 11 Molecular Complexes:

$$\frac{d\left[R2_{rab11}\right]}{dt}=-k_{on,V\cdot R2_{rab11}}\left[V_{rab11}\right]\left[R2_{rab11}\right]+k_{off,V\cdot R2_{rab11}}\left[\left(V\cdot R2\right)_{rab11}\right]$$

$$-k_{on,(V\cdot N1)\cdot R2_{rab11}}\left[\left(V\cdot N1\right)_{rab11}\right]\left[R2_{rab11}\right]+k_{off,(V\cdot N1)\cdot R2_{rab11}}\left[\left(V\cdot N1\cdot R2\right)_{rab11}\right]$$

$$+k_{4to11,R2_{rab45}}\left[R2_{rab45}\right]-k_{rec11,R2_{rab11}}\left[R2_{rab11}\right]$$

$$\frac{d\left[\left(V\cdot R2\right)_{rab11}\right]}{dt}=k_{on,V\cdot R2_{rab11}}\left[V_{rab11}\right]\left[R2_{rab11}\right]-k_{off,V\cdot R2_{rab11}}\left[\left(V\cdot R2\right)_{rab11}\right]$$

$$-k_{on,(V\cdot R2)\cdot N1_{rab11}}\left[\left(V\cdot R2\right)_{rab11}\right]\left[N1_{rab11}\right]+k_{off,(V\cdot R2)\cdot N1_{rab11}}\left[\left(V\cdot N1\cdot R2\right)_{rab11}\right]$$

$$+k_{4to11,V\cdot R2_{rab45}}\left[\left(V\cdot R2\right)_{rab45}\right]-k_{rec11,V\cdot R2_{rab11}}\left[\left(V\cdot R2\right)_{rab11}\right]$$

$$\frac{d\left[V_{rab11}\right]}{dt}=-k_{on,V\cdot R2_{rab11}}\left[V_{rab11}\right]\left[R2_{rab11}\right]+k_{off,V\cdot R2_{rab11}}\left[\left(V\cdot R2\right)_{rab11}\right]-k_{on,V\cdot N1_{rab11}}\left[V_{rab11}\right]\left[N1_{rab11}\right]$$

$$+k_{off,V\cdot N1_{rab11}}\left[\left(V\cdot N1\right)_{rab11}\right]$$

$$\frac{d\left[N1_{rab11}\right]}{dt}=-k_{on,V\cdot N1_{rab11}}\left[V_{rab11}\right]\left[N1_{rab11}\right]+k_{off,V\cdot N1_{rab11}}\left[\left(V\cdot N1\right)_{rab11}\right]$$

$$-k_{on,(V\cdot R2)\cdot N1_{rab11}}\left[\left(V\cdot R2\right)_{rab11}\right]\left[N1_{rab11}\right]+k_{off,(V\cdot R2)\cdot N1_{rab11}}\left[\left(V\cdot N1\cdot R2\right)_{rab11}\right]$$

$$+k_{4to11,N1_{rab45}}\left[N1_{rab45}\right]-k_{rec11,N1_{rab11}}\left[N1_{rab11}\right]$$

$$\frac{d\left[\left(V \cdot N1\right)_{rab11}\right]}{dt} = k_{on,V \cdot N1_{rab11}}\left[V_{rab11}\right]\left[N1_{rab11}\right] - k_{off,V \cdot N1_{rab11}}\left[\left(V \cdot N1\right)_{rab11}\right]$$

$$-k_{on,(V \cdot N1) \cdot R2_{rab11}}\left[\left(V \cdot N1\right)_{rab11}\right]\left[R2_{rab11}\right] + k_{off,(V \cdot N1) \cdot R2_{rab11}}\left[\left(V \cdot N1 \cdot R2\right)_{rab11}\right]$$

$$+k_{4to11,V \cdot N1_{rab45}}\left[\left(V \cdot N1\right)_{rab45}\right] - k_{rec11,V \cdot N1_{rab11}}\left[\left(V \cdot N1\right)_{rab11}\right]$$

$$\frac{d\left[\left(V \cdot N1 \cdot R2\right)_{rab11}\right]}{dt} = k_{on,(V \cdot R2) \cdot N1_{rab11}}\left[\left(V \cdot R2\right)_{rab11}\right]\left[N1_{rab11}\right] - k_{off,(V \cdot R2) \cdot N1_{rab11}}\left[\left(V \cdot N1 \cdot R2\right)_{rab11}\right]$$

$$+k_{on,(V \cdot N1) \cdot R2_{rab11}}\left[\left(V \cdot N1\right)_{rab11}\right]\left[R2_{rab11}\right] - k_{off,(V \cdot N1) \cdot R2_{rab11}}\left[\left(V \cdot N1 \cdot R2\right)_{rab11}\right]$$

$$+k_{4to11,V \cdot N1 \cdot R2_{rab45}}\left[\left(V \cdot N1 \cdot R2\right)_{rab45}\right] - k_{rec11,V \cdot N1 \cdot R2_{rab11}}\left[\left(V \cdot N1 \cdot R2\right)_{rab11}\right]$$

A.1.5 Degraded Molecular Complexes:

$$\frac{d\left[R2_{deg}\right]}{dt} = k_{degr,R2_{rab45}}\left[R2_{rab45}\right]$$

$$\frac{d\left[\left(V \cdot R2\right)_{deg}\right]}{dt} = k_{degr,V \cdot R2_{rab45}}\left[\left(V \cdot R2\right)_{rab45}\right]$$

$$\frac{d\left[V_{deg}\right]}{dt} = k_{degr,V_{rab45}}\left[V_{rab45}\right]$$

$$\frac{d\left[N1_{deg}\right]}{dt} = k_{degr,N1_{rab45}}\left[N1_{rab45}\right]$$

$$\frac{d\left[\left(V \cdot N1\right)_{deg}\right]}{dt} = k_{degr,V \cdot N1_{rab45}}\left[\left(V \cdot N1\right)_{rab45}\right]$$

$$\frac{d\left[\left(V \cdot N1 \cdot R2\right)_{deg}\right]}{dt} = k_{degr,V \cdot N1 \cdot R2_{rab45}}\left[\left(V \cdot N1 \cdot R2\right)_{rab45}\right]$$

A.2 Equations for Healthy Human Compartment Model (Chapter 6)

A.2.1 Unit Conversions

Due to the multi-compartment structure of the model, unit conversions are required to account for differences in compartment volumes (U), as well as reactions that occur in solution or on the two-dimensional cell surface. In the equations, concentrations are represented by $[X]_j$, where j represents the tissue compartment (calf muscle or main body mass) or $[X]_B$, where B is the blood. The units of concentration are moles/cm^3 of tissue or blood, as appropriate. In many cases (e.g. for transport), the relevant concentration is instead the concentration of ligand in available interstitial fluid (excluding spaces that are inaccessible to proteins), annotated $[X]_{IS,j}$ or the concentration of ligand in plasma, annotated $[X]_{pl}$. In the text and figures, the concentration being discussed is identified explicitly. Many outputs are shown in picomolar (pM), nanomolar (nM), or total picomoles of ligand in tissue, using simple unit conversions.

To convert between concentrations in total tissue and in interstitial fluid, the following equations are used:

$$[X]_{IS,j} = \frac{[X]_j}{K_{AV,j}} \text{ , where } K_{AV,j} = \frac{U_{IS,j}}{U_j} = \frac{\text{available interstitial volume}}{\text{total volume of tissue j}}$$

$$K_{AV,j} = \text{Available Volume Fraction} = \Phi \times f \times \varepsilon_{IS}$$

$$\Phi = \text{Partition Coefficient} = \frac{\text{available fluid volume}}{\text{interstitial fluid volume}}$$

$$f = \text{Fluid Fraction} = \frac{\text{interstitial fluid volume}}{\text{interstitial space}}$$

$$\varepsilon_{IS} = \text{Interstitial Fraction} = \frac{\text{interstitial space}}{\text{total tissue volume}}$$

Similarly, the conversion between total blood and plasma concentrations is:

$$[X]_{pl} = \frac{[X]_B}{K_{AV,B}} \text{ , where } K_{AV,B} = \frac{U_{pl}}{U_B} = \frac{\text{plasma volume}}{\text{total blood volume}}$$

To convert between measured receptor levels of number per cell to moles/cm^3 tissue:

$$[R] \text{ in } \frac{\text{moles}}{\text{cm}^3 \text{ tissue}} = \left([R] \text{ in } \frac{\#}{\text{EC}} \right) \cdot \frac{\text{ESAV}}{\text{ECSA}} \cdot \frac{1}{N_{Av}}$$, where N_{Av} is Avogadro's number, 6.023×10^{23}

molecules/mole.

A.2.2 Tissue Equations

This section lists the 112 equations that describe all reactions (excluding different VEGFR2 phospho-states) and transport within the tissue compartments.

Interstitial Matrix. These 30 equations describe the HSPGs site (M) in the ECM, endothelial basement membrane (EBM), and parenchymal basement membrane (PBM), either free, or bound to VEGF, PlGF, sR1, or sR1 and VEGF or PlGF. EBM-bound VEGF in the innermost 25nm of the EBM can bind to endothelial cell-surface VEGFR1, VEGFR2, and NRP1. We assume that, similar to cell-surface receptors, matrix-binding VEGF and PlGF isoforms ($VEGF_{165}$, $VEGF_{189}$, and PlGF), can bind to HSPGs sites and sR1 simultaneously, forming M-L-sR1 complexes, where L represents the ligand (either VEGF or PlGF). Since VEGFR1 can bind to NRP1 and $VEGF_{121}$ or PlGF1 simultaneously, and the NRP1 and matrix-binding sites on VEGFR1 overlap, we assume that these ligands can also bind to immobilized sR1, forming L-sR1-M complexes. Thus, complexes including VEGF or PlGF, matrix, and sR1 can form for all ligands, but in different ways (see **Figure 6-1B**). To reflect this, the ordering of species in the complexes described within the equations are ordered to show the actual binding partners next to each other. $[M_{ECM}]_j$ represents the concentration of free HSPG sites in the ECM, $[V_{165}]$ the interstitial concentration of free $VEGF_{165}$, $[P1]$ the interstitial concentration of free PlGF1, $[sR1]$ the interstitial concentration of free soluble VEGFR, and $[R1]$ the concentration of unoccupied EC surface VEGFR1. The binding rates (k_{on}) and unbinding rates (k_{off}) are given in **Tables 6-2 & 6-3**, with units of $M^{-1}s^{-1}$ and s^{-1}, respectively. To convert the binding rates (k_{on}) into an *in vivo* context (moles/cm^3 tissue/s for each compartment), the following conversions were applied, using geometric parameters from **Table 6-S7**, as previously described[1, 2].

$$k_{on} \text{ in } \frac{\text{moles}}{\text{cm}^3 \text{ tissue}}^{-1} \times s^{-1} = k_{on} \text{ in } M^{-1} \times s^{-1} \times \frac{1000}{\text{available IF volume fraction}}$$

$$k_{on} \text{ in } \frac{\text{moles}}{\text{cm}^3 \text{ tissue}}^{-1} \cdot s^{-1} = k_{on} \text{ in } \left(\frac{moles}{cm^2\ SA}\right)^{-1} \cdot s^{-1} \cdot \frac{1}{ESAV}$$

The resulting k_{on} values are given in **Tables S4-S6**.

$$
\begin{aligned}
d[M_{EBM}]_j / dt = &-k_{on,V165\times M,j}[V_{165}]_j[M_{EBM}]_j + k_{off,V165\times M,j}[V_{165}\times M_{EBM}]_j \\
&-k_{on,V189\times M,j}[V_{189}]_j[M_{EBM}]_j + k_{off,V189\times M,j}[V_{189}\times M_{EBM}]_j \\
&-k_{on,P2\times M,j}[P2]_j[M_{EBM}]_j + k_{off,P2\times M,j}[P2\times M_{EBM}]_j \\
&-k_{on,sR1\times M,j}[sR1]_j[M_{EBM}]_j + k_{off,sR1\times M,j}[sR1\times M_{EBM}]_j \\
&-k_{on,M\times(V165\times R2),j}[M_{EBM}]_j[V_{165}\times R2]_j + k_{off,M\times(V165\times R2),j}[M_{EBM}\times V_{165}\times R2]_j \\
&-k_{on,M\times(V165\times R1),j}[M_{EBM}]_j[V_{165}\times R1]_j + k_{off,M\times(V165\times R1),j}[M_{EBM}\times V_{165}\times R1]_j \\
&-k_{on,M\times(V189\times R2),j}[M_{EBM}]_j[V_{189}\times R2]_j + k_{off,M\times(V189\times R2),j}[M_{EBM}\times V_{189}\times R2]_j \\
&-k_{on,M\times(V189\times R1),j}[M_{EBM}]_j[V_{189}\times R1]_j + k_{off,M\times(V189\times R1),j}[M_{EBM}\times V_{189}\times R1]_j \\
&-k_{on,M\times(P2\times R1),j}[M_{EBM}]_j[P2\times R1]_j + k_{off,M\times(P2\times R1),j}[M_{EBM}\times P2\times R1]_j \\
&-k_{on,(V121\times R1)\times M,j}[V_{121}\times sR1]_j[M_{EBM}]_j + k_{off,(V121\times R1)\times M,j}[V_{121}\times sR1\times M_{EBM}]_j \\
&-k_{on,(P1\times R1)\times M,j}[P1\times sR1]_j[M_{EBM}]_j + k_{off,(P1\times R1)\times M,j}[P1\times sR1\times M_{EBM}]_j \\
&-k_{on,M\times(V165\times R1),j}[M_{EBM}]_j[V_{165}\times sR1]_j + k_{off,M\times(V165\times R1),j}[M_{EBM}\times V_{165}\times sR1]_j \\
&-k_{on,M\times(V189\times R1),j}[M_{EBM}]_j[V_{189}\times sR1]_j + k_{off,M\times(V189\times R1),j}[M_{EBM}\times V_{189}\times sR1]_j
\end{aligned}
$$

$$
\begin{aligned}
d[M_{ECM}]_j / dt = &-k_{on,V165\times M,j}[V_{165}]_j[M_{ECM}]_j + k_{off,V165\times M,j}[V_{165}\times M_{ECM}]_j \\
&-k_{on,V189\times M,j}[V_{189}]_j[M_{ECM}]_j + k_{off,V189\times M,j}[V_{189}\times M_{ECM}]_j \\
&-k_{on,P2\times M,j}[P2]_j[M_{ECM}]_j + k_{off,P2\times M,j}[P2\times M_{ECM}]_j \\
&-k_{on,sR1\times M,j}[sR1]_j[M_{ECM}]_j + k_{off,sR1\times M,j}[sR1\times M_{ECM}]_j \\
&-k_{on,(V121\times R1)\times M,j}[V_{121}\times sR1]_j[M_{ECM}]_j + k_{off,(V121\times R1)\times M,j}[V_{121}\times sR1\times M_{ECM}]_j \\
&-k_{on,(P1\times R1)\times M,j}[P1\times sR1]_j[M_{ECM}]_j + k_{off,(P1\times R1)\times M,j}[P1\times sR1\times M_{ECM}]_j \\
&-k_{on,M\times(V165\times R1),j}[M_{ECM}]_j[V_{165}\times sR1]_j + k_{off,M\times(V165\times R1),j}[M_{ECM}\times V_{165}\times sR1]_j \\
&-k_{on,M\times(V189\times R1),j}[M_{ECM}]_j[V_{189}\times sR1]_j + k_{off,M\times(V189\times R1),j}[M_{ECM}\times V_{189}\times sR1]_j
\end{aligned}
$$

$$d[M_{PBM}]_j / dt = -k_{on,V165\times M,j}[V_{165}]_j[M_{PBM}]_j + k_{off,V165\times M,j}[V_{165}\times M_{PBM}]_j$$
$$-k_{on,V189\times M,j}[V_{189}]_j[M_{PBM}]_j + k_{off,V189\times M,j}[V_{189}\times M_{PBM}]_j$$
$$-k_{on,P2\times M,j}[P2]_j[M_{PBM}]_j + k_{off,P2\times M,j}[P2\times M_{PBM}]_j$$
$$-k_{on,sR1\times M,j}[sR1]_j[M_{PBM}]_j + k_{off,sR1\times M,j}[sR1\times M_{PBM}]_j$$
$$-k_{on,(V121\times sR1)\times M,j}[V_{121}\times sR1]_j[M_{PBM}]_j + k_{off,(V121\times sR1)\times M,j}[V_{121}\times sR1\times M_{PBM}]_j$$
$$-k_{on,(P1\times sR1)\times M,j}[P1\times sR1]_j[M_{PBM}]_j + k_{off,(P1\times sR1)\times M,j}[P1\times sR1\times M_{PBM}]_j$$
$$-k_{on,M\times(V165\times sR1),j}[M_{PBM}]_j[V_{165}\times sR1]_j + k_{off,M\times(V165\times sR1),j}[M_{PBM}\times V_{165}\times sR1]_j$$
$$-k_{on,M\times(V189\times sR1),j}[M_{PBM}]_j[V_{189}\times sR1]_j + k_{off,M\times(V189\times sR1),j}[M_{PBM}\times V_{189}\times sR1]_j$$

$$d[V_{165}\times M_{EBM}]_j / dt = k_{on,V165\times M,j}[V_{165}]_j[M_{EBM}]_j - k_{off,V165\times M,j}[V_{165}\times M_{EBM}]_j$$
$$-k_{on,(M\times V165)\times R2,j}[M_{EBM}\times V_{165}]_j[R2]_j + k_{off,(M\times V165)\times R2,j}[M_{EBM}\times V_{165}\times R2]_j$$
$$-k_{on,(M\times V165)\times R1,j}[M_{EBM}\times V_{165}]_j[R1]_j + k_{off,(M\times V165)\times R1,j}[M_{EBM}\times V_{165}\times R1]_j$$
$$-k_{on,(M\times V165)\times sR1,j}[M_{EBM}\times V_{165}]_j[sR1]_j + k_{off,(M\times V165)\times sR1,j}[M_{EBM}\times V_{165}\times sR1]_j$$

$$d[V_{189}\times M_{EBM}]_j / dt = k_{on,V189\times M,j}[V_{189}]_j[M_{EBM}]_j - k_{off,V189\times M,j}[V_{189}\times M_{EBM}]_j$$
$$-k_{on,(M\times V189)\times R2,j}[M_{EBM}\times V_{189}]_j[R2]_j + k_{off,(M\times V189)\times R2,j}[M_{EBM}\times V_{189}\times R2]_j$$
$$-k_{on,(M\times V189)\times R1,j}[M_{EBM}\times V_{189}]_j[R1]_j + k_{off,(M\times V189)\times R1,j}[M_{EBM}\times V_{189}\times R1]_j$$
$$-k_{on,(M\times V189)\times sR1,j}[M_{EBM}\times V_{189}]_j[sR1]_j + k_{off,(M\times V189)\times sR1,j}[M_{EBM}\times V_{189}\times sR1]_j$$

$$d[P2\times M_{EBM}]_j / dt = k_{on,P2\times M,j}[P2]_j[M_{EBM}]_j - k_{off,P2\times M,j}[P2\times M_{EBM}]_j$$
$$-k_{on,(M\times P2)\times R1,j}[M_{EBM}\times P2]_j[R1]_j + k_{off,(M\times P2)\times R1,j}[M_{EBM}\times P2\times R1]_j$$
$$-k_{on,(M\times P2)\times sR1,j}[M_{EBM}\times P2]_j[sR1]_j + k_{off,(M\times P2)\times sR1,j}[M_{EBM}\times P2\times sR1]_j$$

$$d[V_{165}\times M_{ECM}]_j / dt = k_{on,V165\times M,j}[V_{165}]_j[M_{ECM}]_j - k_{off,V165\times M,j}[V_{165}\times M_{ECM}]_j$$
$$-k_{on,(M\times V165)\times sR1,j}[M_{ECM}\times V_{165}]_j[sR1]_j + k_{off,(M\times V165)\times sR1,j}[M_{ECM}\times V_{165}\times sR1]_j$$

$$d[V_{189}\times M_{ECM}]_j / dt = k_{on,V189\times M,j}[V_{189}]_j[M_{ECM}]_j - k_{off,V189\times M,j}[V_{189}\times M_{ECM}]_j$$
$$-k_{on,(M\times V189)\times sR1,j}[M_{ECM}\times V_{189}]_j[sR1]_j + k_{off,(M\times V189)\times sR1,j}[M_{ECM}\times V_{189}\times sR1]_j$$

$$d[P2\times M_{ECM}]_j / dt = k_{on,P2\times M,j}[P2]_j[M_{ECM}]_j - k_{off,P2\times M,j}[P2\times M_{ECM}]_j$$
$$-k_{on,(M\times P2)\times sR1,j}[M_{ECM}\times P2]_j[sR1]_j + k_{off,(M\times P2)\times sR1,j}[M_{ECM}\times P2\times sR1]_j$$

$$d[V_{165}\times M_{PBM}]_j / dt = k_{on,V165\times M,j}[V_{165}]_j[M_{PBM}]_j - k_{off,V165\times M,j}[V_{165}\times M_{PBM}]_j$$
$$-k_{on,(M\times V165)\times R1,j}[M_{PBM}\times V_{165}]_j[sR1]_j + k_{off,(M\times V165)\times R1,j}[M_{PBM}\times V_{165}\times R1]_j$$

$$d[V_{189}\times M_{PBM}]_j / dt = k_{on,V189\times M,j}[V_{189}]_j[M_{PBM}]_j - k_{off,V189\times M,j}[V_{189}\times M_{PBM}]_j$$
$$-k_{on,(M\times V189)\times R1,j}[M_{PBM}\times V_{189}]_j[sR1]_j + k_{off,(M\times V189)\times R1,j}[M_{PBM}\times V_{189}\times R1]_j$$

$$d[P2\times M_{PBM}]_j / dt = k_{on,P2\times M,j}[P2]_j[M_{PBM}]_j - k_{off,P2\times M,j}[P2\times M_{PBM}]_j$$
$$-k_{on,(M\times P2)\times R1,j}[M_{PBM}\times P2]_j[sR1]_j + k_{off,(M\times P2)\times R1,j}[M_{PBM}\times P2\times R1]_j$$

$$d[sR1\times M_{EBM}]_j / dt = k_{on,sR1\times M,j}[sR1]_j[M_{EBM}]_j - k_{off,sR1\times M,j}[sR1\times M_{EBM}]_j$$
$$-k_{on,(M\times R1)\times V121,j}[M_{EBM}\times R1]_j[V_{121}]_j + k_{off,(M\times R1)\times V121,j}[M_{EBM}\times R1\times V_{121}]_j$$
$$-k_{on,(M\times R1)\times P1,j}[M_{EBM}\times R1]_j[P1]_j + k_{off,(M\times R1)\times P1,j}[M_{EBM}\times R1\times P1]_j$$

$$d[sR1\times M_{ECM}]_j / dt = k_{on,sR1\times M,j}[sR1]_j[M_{ECM}]_j - k_{off,sR1\times M,j}[sR1\times M_{ECM}]_j$$
$$-k_{on,(M\times R1)\times V121,j}[M_{ECM}\times R1]_j[V_{121}]_j + k_{off,(M\times R1)\times V121,j}[M_{ECM}\times R1\times V_{121}]_j$$
$$-k_{on,(M\times R1)\times P1,j}[M_{ECM}\times R1]_j[P1]_j + k_{off,(M\times R1)\times P1,j}[M_{ECM}\times R1\times P1]_j$$

$$d[sR1\times M_{PBM}]_j / dt = k_{on,sR1\times M,j}[sR1]_j[M_{PBM}]_j - k_{off,sR1\times M,j}[sR1\times M_{PBM}]_j$$
$$-k_{on,(M\times R1)\times V121,j}[M_{PBM}\times R1]_j[V_{121}]_j + k_{off,(M\times R1)\times V121,j}[M_{PBM}\times R1\times V_{121}]_j$$
$$-k_{on,(M\times R1)\times P1,j}[M_{PBM}\times R1]_j[P1]_j + k_{off,(M\times R1)\times P1,j}[M_{PBM}\times R1\times P1]_j$$

$$d[M_{EBM}\times V_{165}\times R1]_j / dt = k_{on,M\times(V165\times R1),j}[M_{EBM}]_j[V_{165}\times R1]_j - k_{off,M\times(V165\times R1),j}[M_{EBM}\times V_{165}\times R1]_j$$
$$+k_{on,(M\times V165)\times R1,j}[M_{EBM}\times V_{165}]_j[sR1]_j - k_{off,(M\times V165)\times R1,j}[M_{EBM}\times V_{165}\times R1]_j$$

$$d[M_{EBM}\times V_{189}\times R1]_j / dt = k_{on,M\times(V189\times R1),j}[M_{EBM}]_j[V_{189}\times R1]_j - k_{off,M\times(V189\times R1),j}[M_{EBM}\times V_{189}\times R1]_j$$
$$+k_{on,(M\times V189)\times R1,j}[M_{EBM}\times V_{189}]_j[sR1]_j - k_{off,(M\times V189)\times R1,j}[M_{EBM}\times V_{189}\times R1]_j$$

$$d[M_{EBM}\times P2\times R1]_j / dt = k_{on,M\times(P2\times R1),j}[M_{EBM}]_j[P2\times R1]_j - k_{off,M\times(P2\times R1),j}[M_{EBM}\times P2\times R1]_j$$
$$+k_{on,(M\times P2)\times R1,j}[M_{EBM}\times P2]_j[sR1]_j - k_{off,(M\times P2)\times R1,j}[M_{EBM}\times P2\times R1]_j$$

$$d[V_{121}\times R1\times M_{EBM}]_j / dt = k_{on,(V121\times R1)\times M,j}[V_{121}\times R1]_j[M_{EBM}]_j - k_{off,(V121\times R1)\times M,j}[V_{121}\times R1\times M_{EBM}]_j$$
$$+k_{on,V121\times(sR1\times M),j}[V_{121}]_j[sR1\times M_{EBM}]_j - k_{off,V121\times(sR1\times M),j}[V_{121}\times R1\times M_{EBM}]_j$$

$$d[P1{\bullet}sR1{\bullet}M_{EBM}]_j\,/\,dt = k_{on,(P1{\bullet}R1){\bullet}M,j}[P1{\bullet}sR1]_j[M_{EBM}]_j - k_{off,(P1{\bullet}R1){\bullet}M,j}[P1{\bullet}sR1{\bullet}M_{EBM}]_j$$
$$+ k_{on,P1{\bullet}(sR1{\bullet}M),j}[P1]_j[sR1{\bullet}M_{EBM}]_j - k_{off,P1{\bullet}(sR1{\bullet}M),j}[P1{\bullet}sR1{\bullet}M_{EBM}]_j$$

$$d[M_{ECM}{\bullet}V_{165}{\bullet}sR1]_j\,/\,dt = k_{on,M{\bullet}(V165{\bullet}sR1),j}[M_{ECM}]_j[V_{165}{\bullet}sR1]_j - k_{off,M{\bullet}(V165{\bullet}sR1),j}[M_{ECM}{\bullet}V_{165}{\bullet}sR1]_j$$
$$+ k_{on,(M{\bullet}V165){\bullet}sR1,j}[M_{ECM}{\bullet}V_{165}]_j[sR1]_j - k_{off,(M{\bullet}V165){\bullet}sR1,j}[M_{ECM}{\bullet}V_{165}{\bullet}sR1]_j$$

$$d[M_{ECM}{\bullet}V_{165}{\bullet}sR1]_j\,/\,dt = k_{on,M{\bullet}(V165{\bullet}sR1),j}[M_{ECM}]_j[V_{165}{\bullet}sR1]_j - k_{off,M{\bullet}(V165{\bullet}sR1),j}[M_{ECM}{\bullet}V_{165}{\bullet}sR1]_j$$
$$+ k_{on,(M{\bullet}V165){\bullet}sR1,j}[M_{ECM}{\bullet}V_{165}]_j[sR1]_j - k_{off,(M{\bullet}V165){\bullet}sR1,j}[M_{ECM}{\bullet}V_{165}{\bullet}sR1]_j$$

$$d[M_{ECM}{\bullet}V_{189}{\bullet}sR1]_j\,/\,dt = k_{on,M{\bullet}(V189{\bullet}sR1),j}[M_{ECM}]_j[V_{189}{\bullet}sR1]_j - k_{off,M{\bullet}(V189{\bullet}sR1),j}[M_{ECM}{\bullet}V_{189}{\bullet}sR1]_j$$
$$+ k_{on,(M{\bullet}V189){\bullet}sR1,j}[M_{ECM}{\bullet}V_{189}]_j[sR1]_j - k_{off,(M{\bullet}V189){\bullet}sR1,j}[M_{ECM}{\bullet}V_{189}{\bullet}sR1]_j$$

$$d[M_{ECM}{\bullet}P2{\bullet}sR1]_j\,/\,dt = k_{on,M{\bullet}(P2{\bullet}sR1),j}[M_{ECM}]_j[P2{\bullet}sR1]_j - k_{off,M{\bullet}(P2{\bullet}sR1),j}[M_{ECM}{\bullet}P2{\bullet}sR1]_j$$
$$+ k_{on,(M{\bullet}P2){\bullet}sR1,j}[M_{ECM}{\bullet}P2]_j[sR1]_j - k_{off,(M{\bullet}P2){\bullet}sR1,j}[M_{ECM}{\bullet}P2{\bullet}sR1]_j$$

$$d[V_{121}{\bullet}sR1{\bullet}M_{ECM}]_j\,/\,dt = k_{on,(V121{\bullet}sR1){\bullet}M,j}[V_{121}{\bullet}sR1]_j[M_{ECM}]_j - k_{off,(V121{\bullet}sR1){\bullet}M,j}[V_{121}{\bullet}sR1{\bullet}M_{ECM}]_j$$
$$+ k_{on,V121{\bullet}(sR1{\bullet}M),j}[V_{121}]_j[sR1{\bullet}M_{ECM}]_j - k_{off,V121{\bullet}(sR1{\bullet}M),j}[V_{121}{\bullet}sR1{\bullet}M_{ECM}]_j$$

$$d[P1{\bullet}sR1{\bullet}M_{ECM}]_j\,/\,dt = k_{on,(P1{\bullet}R1){\bullet}M,j}[P1{\bullet}sR1]_j[M_{ECM}]_j - k_{off,(P1{\bullet}R1){\bullet}M,j}[P1{\bullet}sR1{\bullet}M_{ECM}]_j$$
$$+ k_{on,P1{\bullet}(sR1{\bullet}M),j}[P1]_j[sR1{\bullet}M_{ECM}]_j - k_{off,P1{\bullet}(sR1{\bullet}M),j}[P1{\bullet}sR1{\bullet}M_{ECM}]_j$$

$$d[M_{PBM}{\bullet}V_{165}{\bullet}sR1]_j\,/\,dt = k_{on,M{\bullet}(V165{\bullet}sR1),j}[M_{PBM}]_j[V_{165}{\bullet}sR1]_j - k_{off,M{\bullet}(V165{\bullet}sR1),j}[M_{PBM}{\bullet}V_{165}{\bullet}sR1]_j$$
$$+ k_{on,(M{\bullet}V165){\bullet}sR1,j}[M_{PBM}{\bullet}V_{165}]_j[sR1]_j - k_{off,(M{\bullet}V165){\bullet}sR1,j}[M_{PBM}{\bullet}V_{165}{\bullet}sR1]_j$$

$$d[M_{PBM}{\bullet}V_{189}{\bullet}sR1]_j\,/\,dt = k_{on,M{\bullet}(V189{\bullet}sR1),j}[M_{PBM}]_j[V_{189}{\bullet}sR1]_j - k_{off,M{\bullet}(V189{\bullet}sR1),j}[M_{PBM}{\bullet}V_{189}{\bullet}sR1]_j$$
$$+ k_{on,(M{\bullet}V189){\bullet}sR1,j}[M_{PBM}{\bullet}V_{189}]_j[sR1]_j - k_{off,(M{\bullet}V189){\bullet}sR1,j}[M_{PBM}{\bullet}V_{189}{\bullet}sR1]_j$$

$$d[M_{PBM}{\bullet}P2{\bullet}sR1]_j\,/\,dt = k_{on,M{\bullet}(P2{\bullet}sR1),j}[M_{PBM}]_j[P2{\bullet}sR1]_j - k_{off,M{\bullet}(P2{\bullet}sR1),j}[M_{PBM}{\bullet}P2{\bullet}sR1]_j$$
$$+ k_{on,(M{\bullet}P2){\bullet}sR1,j}[M_{PBM}{\bullet}P2]_j[sR1]_j - k_{off,(M{\bullet}P2){\bullet}sR1,j}[M_{PBM}{\bullet}P2{\bullet}sR1]_j$$

$$d[V_{121}{\bullet}sR1{\bullet}M_{PBM}]_j\,/\,dt = k_{on,(V121{\bullet}sR1){\bullet}M,j}[V_{121}{\bullet}sR1]_j[M_{PBM}]_j - k_{off,(V121{\bullet}sR1){\bullet}M,j}[V_{121}{\bullet}sR1{\bullet}M_{PBM}]_j$$
$$+ k_{on,V121{\bullet}(sR1{\bullet}M),j}[V_{121}]_j[sR1{\bullet}M_{PBM}]_j - k_{off,V121{\bullet}(sR1{\bullet}M),j}[V_{121}{\bullet}sR1{\bullet}M_{PBM}]_j$$

$$d[P1{\bullet}sR1{\bullet}M_{PBM}]_j\,/\,dt = k_{on,(P1{\bullet}R1){\bullet}M,j}[P1{\bullet}sR1]_j[M_{PBM}]_j - k_{off,(P1{\bullet}R1){\bullet}M,j}[P1{\bullet}sR1{\bullet}M_{PBM}]_j$$
$$+ k_{on,P1{\bullet}(sR1{\bullet}M),j}[P1]_j[sR1{\bullet}M_{PBM}]_j - k_{off,P1{\bullet}(sR1{\bullet}M),j}[P1{\bullet}sR1{\bullet}M_{PBM}]_j$$

Abluminal Endothelial Cell Surface. These 27 equations represent molecular species present on the surface of endothelial cells, as summarized in **Figure 6-1E**. The binding rates (k_{on}) and unbinding rates (k_{off}) are given in **Tables 6-2 & 6-3**, with units of $M^{-1}s^{-1}$ for binding of ligands to receptors, and $(moles/cm^2)^{-1}s^{-1}$ for coupling of cell surface receptors. The fraction of EBM accessible to endothelial cell receptors is f. The trafficking rates, which depend on receptor ligation and binding to NRP1 (**Table 6-S8**), are in units of s^{-1}, where k_{int} is the internalization rate, k_{rec4} is the recycling rate from early endosomes (Rab4/5) to the cell surface, and k_{rec11} is the recycling rate from recycling endosomes (Rab11) to the cell surface. $[R1_{rab45}]$ is the concentration of unoccupied VEGFR1 in early (Rab4/5) endosomes. s is the production rate for free (unoccupied) receptors delivered to the cell surface (#/cm²/s, converted), tuned to match experimental measurements of surface receptor densities at steady-state (**Table 6-4**).

$$
\begin{aligned}
d[R1]_j / dt = {} & s_{R1,j} - k_{int,R1,j}[R1]_j + k_{rec4,R1,j}[R1_{rab45}] + k_{rec11,R1,j}[R1_{rab11}] \\
& - k_{on,V165\times R1,j}[V_{165}]_j[R1]_j + k_{off,V165\times R1,j}[V_{165}\times R1]_j \\
& - k_{on,V189\times R1,j}[V_{189}]_j[R1]_j + k_{off,V189\times R1,j}[V_{189}\times R1]_j \\
& - k_{on,V121\times R1,j}[V_{121}]_j[R1]_j + k_{off,V121\times R1,j}[V_{121}\times R1]_j \\
& - k_{on,P1\times R1,j}[P1]_j[R1]_j + k_{off,P1\times R1,j}[P1\times R1]_j \\
& - k_{on,P2\times R1,j}[P2]_j[R1]_j + k_{off,P2\times R1,j}[P2\times R1]_j \\
& - k_{on,(M\times V165)\times R1,j}[M_{EBM}\times V_{165}]_j[R1]_j + k_{off,(M\times V165)\times R1,j}[M_{EBM}\times V_{165}\times R1]_j \\
& - k_{on,(M\times V189)\times R1,j}[M_{EBM}\times V_{189}]_j[R1]_j + k_{off,(M\times V189)\times R1,j}[M_{EBM}\times V_{189}\times R1]_j \\
& - k_{on,(M\times P2)\times R1,j}[M_{EBM}\times P2]_j[R1]_j + k_{off,(M\times P2)\times R1,j}[M_{EBM}\times P2\times R1]_j \\
& - k_{on,N1\times R1,j}[N1]_j[R1]_j + k_{off,N1\times R1,j}[N1\times R1]_j
\end{aligned}
$$

$$
\begin{aligned}
d[R2]_j / dt = {} & s_{R2,j} - k_{int,R2,j}[R2]_j + k_{rec4,R2,j}[R2_{rab45}] + k_{rec11,R2,j}[R2_{rab11}] \\
& - k_{on,V165\times R2,j}[V_{165}]_j[R2]_j + k_{off,V165\times R2,j}[V_{165}\times R2]_j \\
& - k_{on,V189\times R2,j}[V_{189}]_j[R2]_j + k_{off,V189\times R2,j}[V_{189}\times R2]_j \\
& - k_{on,V121\times R2,j}[V_{121}]_j[R2]_j + k_{off,V121\times R2,j}[V_{121}\times R2]_j \\
& - k_{on,(M\times V165)\times R2,j}[M_{EBM}\times V_{165}]_j[R2]_j + k_{off,(M\times V165)\times R2,j}[M_{EBM}\times V_{165}\times R2]_j \\
& - k_{on,(M\times V189)\times R2,j}[M_{EBM}\times V_{189}]_j[R2]_j + k_{off,(M\times V189)\times R2,j}[M_{EBM}\times V_{189}\times R2]_j \\
& - k_{on,(N1\times V165)\times R2,j}[N1\times V_{165}]_j[R2]_j + k_{off,(N1\times V165)\times R2,j}[N1\times V_{165}\times R2]_j \\
& - k_{on,(N1\times V189)\times R2,j}[N1\times V_{189}]_j[R2]_j + k_{off,(N1\times V189)\times R2,j}[N1\times V_{189}\times R2]_j
\end{aligned}
$$

$$d[N1]_j / dt = s_{N1,j} - k_{\text{int},N1,j}[N1]_j + k_{rec4,N1,j}[N1_{rab45}] + k_{rec11,N1,j}[N1_{rab11}]$$
$$- k_{on,V165\times N1,j}[V_{165}]_j[N1]_j + k_{off,V165\times N1,j}[V_{165}\times N1]_j$$
$$- k_{on,V189\times N1,j}[V_{189}]_j[N1]_j + k_{off,V189\times N1,j}[V_{189}\times N1]_j$$
$$- k_{on,P2\times N1,j}[P2]_j[N1]_j + k_{off,P2\times N1,j}[P2\times N1]_j$$
$$- k_{on,N1\times R1,j}[N1]_j[R1]_j + k_{off,N1\times R1,j}[N1\times R1]_j$$
$$- k_{on,N1\times sR1,j}[N1]_j[sR1]_j + k_{off,N1\times sR1,j}[N1\times sR1]_j$$
$$- k_{on,(V121\times R1)\times N1,j}[V_{121}\times R1]_j[N1]_j + k_{off,(V121\times R1)\times N1,j}[V_{121}\times R1\times N1]_j$$
$$- k_{on,(P1\times R1)\times N1,j}[P1\times R1]_j[N1]_j + k_{off,(P1\times R1)\times N1,j}[P1\times R1\times N1]_j$$
$$- k_{on,N1\times(V165\times R2),j}[N1]_j[V_{165}\times R2]_j + k_{off,N1\times(V165\times R2),j}[N1\times V_{165}\times R2]_j$$
$$- k_{on,N1\times(V189\times R2),j}[N1]_j[V_{189}\times R2]_j + k_{off,N1\times(V189\times R2),j}[N1\times V_{189}\times R2]_j$$

$$d[V_{165}\times R1]_j / dt = -k_{\text{int},V165\times R1,j}[V_{165}\times R1]_j + k_{rec4,V165\times R1,j}[V_{165}\times R1_{rab45}] + k_{rec11,V165\times R1,j}[V_{165}\times R1_{rab11}]$$
$$+ k_{on,V165\times R1,j}[V_{165}]_j[R1]_j - k_{off,V165\times R1,j}[V_{165}\times R1]_j$$
$$- k_{on,M\times(V165\times R1),j}[M_{EBM}]_j[V_{165}\times R1]_j + k_{off,M\times(V165\times R1),j}[M_{EBM}\times V_{165}\times R1]_j$$

$$d[V_{189}\times R1]_j / dt = -k_{\text{int},V189\times R1,j}[V_{189}\times R1]_j + k_{rec4,V189\times R1,j}[V_{189}\times R1_{rab45}] + k_{rec11,V189\times R1,j}[V_{189}\times R1_{rab11}]$$
$$+ k_{on,V189\times R1,j}[V_{189}]_j[R1]_j - k_{off,V189\times R1,j}[V_{189}\times R1]_j$$
$$- k_{on,M\times(V189\times R1),j}[M_{EBM}]_j[V_{189}\times R1]_j + k_{off,M\times(V189\times R1),j}[M_{EBM}\times V_{189}\times R1]_j$$

$$d[V_{121}\times R1]_j / dt = -k_{\text{int},V121\times R1,j}[V_{121}\times R1]_j + k_{rec4,V121\times R1,j}[V_{121}\times R1_{rab45}] + k_{rec11,V121\times R1,j}[V_{121}\times R1_{rab11}]$$
$$+ k_{on,V121\times R1,j}[V_{121}]_j[R1]_j - k_{off,V121\times R1,j}[V_{121}\times R1]_j$$
$$- k_{on,(V121\times R1)\times N1,j}[V_{121}\times R1]_j[N1]_j + k_{off,(V121\times R1)\times N1,j}[V_{121}\times R1\times N1]_j$$

$$d[P1\times R1]_j / dt = -k_{\text{int},P1\times R1,j}[P1\times R1]_j + k_{rec4,P1\times R1,j}[P1\times R1_{rab45}] + k_{rec11,P1\times R1,j}[P1\times R1_{rab11}]$$
$$+ k_{on,P1\times R1,j}[P1]_j[R1]_j - k_{off,P1\times R1,j}[P1\times R1]_j$$
$$- k_{on,(P1\times R1)\times N1,j}[P1\times R1]_j[N1]_j + k_{off,(P1\times R1)\times N1,j}[P1\times R1\times N1]_j$$

$$d[P2\times R1]_j / dt = -k_{\text{int},P2\times R1,j}[P2\times R1]_j + k_{rec4,P2\times R1,j}[P2\times R1_{rab45}] + k_{rec11,P2\times R1,j}[P2\times R1_{rab11}]$$
$$+ k_{on,P2\times R1,j}[P2]_j[R1]_j - k_{off,P2\times R1,j}[P2\times R1]_j$$
$$- k_{on,M\times(P2\times R1),j}[M_{EBM}]_j[P2\times R1]_j + k_{off,M\times(P2\times R1),j}[M_{EBM}\times P2\times R1]_j$$

$$d[V_{165}\times R2]_j / dt = -k_{\text{int},V165\times R2,j}[V_{165}\times R2]_j + k_{rec4,V165\times R2,j}[V_{165}\times R2_{rab45}] + k_{rec11,V165\times R2,j}[V_{165}\times R2_{rab11}]$$
$$+ k_{on,V165\times R2,j}[V_{165}]_j[R2]_j - k_{off,V165\times R2,j}[V_{165}\times R2]_j$$
$$- k_{on,M\times(V165\times R2),j}[M_{EBM}]_j[V_{165}\times R2]_j + k_{off,M\times(V165\times R2),j}[M_{EBM}\times V_{165}\times R2]_j$$
$$- k_{on,N1\times(V165\times R2),j}[N1]_j[V_{165}\times R2]_j + k_{off,N1\times(V165\times R2),j}[N1\times V_{165}\times R2]_j$$

$$d[V_{189}\times R2]_j / dt = -k_{\text{int},V189\times R2,j}[V_{189}\times R2]_j + k_{rec4,V189\times R2,j}[V_{189}\times R2_{rab45}] + k_{rec11,V189\times R2,j}[V_{189}\times R2_{rab11}]$$
$$+ k_{on,V189\times R2,j}[V_{189}]_j[R2]_j - k_{off,V189\times R2,j}[V_{189}\times R2]_j$$
$$- k_{on,M\times(V189\times R2),j}[M_{EBM}]_j[V_{189}\times R2]_j + k_{off,M\times(V189\times R2),j}[M_{EBM}\times V_{189}\times R2]_j$$
$$- k_{on,N1\times(V189\times R2),j}[N1]_j[V_{189}\times R2]_j + k_{off,N1\times(V189\times R2),j}[N1\times V_{189}\times R2]_j$$

$$d[V_{121}\times R2]_j / dt = -k_{\text{int},V121\times R2,j}[V_{121}\times R2]_j + k_{rec4,V121\times R2,j}[V_{121}\times R2_{rab45}] + k_{rec11,V121\times R2,j}[V_{121}\times R2_{rab11}]$$
$$+ k_{on,V121\times R2,j}[V_{121}]_j[R2]_j - k_{off,V121\times R2,j}[V_{121}\times R2]_j$$

$$d[V_{165}\times N1]_j / dt = -k_{\text{int},V165\times N1,j}[V_{165}\times N1]_j + k_{rec4,V165\times N1,j}[V_{165}\times N1_{rab45}] + k_{rec11,V165\times N1,j}[V_{165}\times N1_{rab11}]$$
$$+ k_{on,V165\times N1,j}[V_{165}]_j[N1]_j - k_{off,V165\times N1,j}[V_{165}\times N1]_j$$
$$- k_{on,(N1\times V165)\times R2,j}[N1\times V_{165}]_j[R2]_j + k_{off,(N1\times V165)\times R2,j}[N1\times V_{165}\times R2]_j$$

$$d[V_{189}\times N1]_j / dt = -k_{\text{int},V189\times N1,j}[V_{189}\times N1]_j + k_{rec4,V189\times N1,j}[V_{189}\times N1_{rab45}] + k_{rec11,V189\times N1,j}[V_{189}\times N1_{rab11}]$$
$$+ k_{on,V189\times N1,j}[V_{189}]_j[N1]_j - k_{off,V189\times N1,j}[V_{189}\times N1]_j$$
$$- k_{on,(N1\times V189)\times R2,j}[N1\times V_{189}]_j[R2]_j + k_{off,(N1\times V189)\times R2,j}[N1\times V_{189}\times R2]_j$$

$$d[P2\times N1]_j / dt = -k_{\text{int},P2\times N1,j}[P2\times N1]_j + k_{rec4,P2\times N1,j}[P2\times N1_{rab45}] + k_{rec11,P2\times N1,j}[P2\times N1_{rab11}]$$
$$+ k_{on,P2\times N1,j}[P2]_j[N1]_j - k_{off,P2\times N1,j}[P2\times N1]_j$$
$$- k_{on,(N1\times P2)\times R2,j}[N1\times P2]_j[R2]_j + k_{off,(N1\times P2)\times R2,j}[N1\times P2\times R2]_j$$

$$d[N1\times R1]_j / dt = -k_{\text{int},N1\times R1,j}[N1\times R1]_j + k_{rec4,N1\times R1,j}[N1\times R1_{rab45}] + k_{rec11,N1\times R1,j}[N1\times R1_{rab11}]$$
$$+ k_{on,N1\times R1,j}[N1]_j[R1]_j - k_{off,N1\times R1,j}[N1\times R1]_j$$
$$- k_{on,V121\times(N1\times R1),j}[V_{121}]_j[N1\times R1]_j + k_{off,V121\times(N1\times R1),j}[V_{121}\times R1\times N1]_j$$
$$- k_{on,P1\times(N1\times R1),j}[P1]_j[N1\times R1]_j + k_{off,P1\times(N1\times R1),j}[P1\times R1\times N1]_j$$

$$d[N1\times sR1]_j / dt = -k_{\text{int},N1\times sR1,j}[N1\times sR1]_j + k_{rec4,N1\times sR1,j}[N1\times sR1_{rab45}] + k_{rec11,N1\times sR1,j}[N1\times sR1_{rab11}]$$
$$+ k_{on,N1\times sR1,j}[N1]_j[sR1]_j - k_{off,N1\times sR1,j}[N1\times sR1]_j$$
$$- k_{on,V121\times(N1\times sR1),j}[V_{121}]_j[N1\times sR1]_j + k_{off,V121\times(N1\times sR1),j}[V_{121}\times sR1\times N1]_j$$
$$- k_{on,P1\times(N1\times sR1),j}[P1]_j[N1\times sR1]_j + k_{off,P1\times(N1\times sR1),j}[P1\times sR1\times N1]_j$$

453

$$d[N1{\times}V_{165}{\times}R2]_j/dt = -k_{\text{int},N1{\times}V165{\times}R2,j}[N1{\times}V_{165}{\times}R2]_j + k_{rec4,N1{\times}V165{\times}R2,j}[N1{\times}V_{165}{\times}R2_{rab45}]$$
$$+k_{rec11,N1{\times}V165{\times}R2,j}[N1{\times}V_{165}{\times}R2_{rab11}]$$
$$+k_{on,R2{\times}(N1{\times}V165),j}[R2]_j[V_{165}{\times}N1]_j - k_{off,R2{\times}(N1{\times}V165),j}[N1{\times}V_{165}{\times}R2]_j$$
$$+k_{on,N1{\times}(V165{\times}R2),j}[N1]_j[V_{165}{\times}R2]_j - k_{off,N1{\times}(V165{\times}R2),j}[N1{\times}V_{165}{\times}R2]_j$$

$$d[N1{\times}V_{189}{\times}R2]_j/dt = -k_{\text{int},N1{\times}V189{\times}R2,j}[N1{\times}V_{189}{\times}R2]_j + k_{rec4,N1{\times}V189{\times}R2,j}[N1{\times}V_{189}{\times}R2_{rab45}]$$
$$+k_{rec11,N1{\times}V189{\times}R2,j}[N1{\times}V_{189}{\times}R2_{rab11}]$$
$$+k_{on,R2{\times}(V189{\times}N1),j}[R2]_j[V_{189}{\times}N1]_j - k_{off,R2{\times}(N1{\times}V189),j}[N1{\times}V_{189}{\times}R2]_j$$
$$+k_{on,N1{\times}(V189{\times}R2),j}[N1]_j[V_{189}{\times}R2]_j - k_{off,N1{\times}(V189{\times}R2),j}[N1{\times}V_{189}{\times}R2]_j$$

$$d[V_{121}{\times}R1{\times}N1]_j/dt = -k_{\text{int},V121{\times}R1{\times}N1,j}[V_{121}{\times}R1{\times}N1]_j + k_{rec4,V121{\times}R1{\times}N1,j}[V_{121}{\times}R1{\times}N1_{rab45}]$$
$$+k_{rec11,V121{\times}R1{\times}N1,j}[V_{121}{\times}R1{\times}N1_{rab11}]$$
$$+k_{on,V121{\times}(R1{\times}N1),j}[V_{121}]_j[R1{\times}N1]_j - k_{off,V121{\times}(R1{\times}N1),j}[V_{121}{\times}R1{\times}N1]_j$$
$$+k_{on,(V121{\times}R1){\times}N1,j}[V_{121}{\times}R1]_j[N1]_j - k_{off,(V121{\times}R1){\times}N1,j}[V_{121}{\times}R1{\times}N1]_j$$

$$d[P1{\times}R1{\times}N1]_j/dt = -k_{\text{int},P1{\times}R1{\times}N1,j}[P1{\times}R1{\times}N1]_j + k_{rec4,P1{\times}R1{\times}N1,j}[P1{\times}R1{\times}N1_{rab45}]$$
$$+k_{rec11,P1{\times}R1{\times}N1,j}[P1{\times}R1{\times}N1_{rab11}]$$
$$+k_{on,P1{\times}(R1{\times}N1),j}[P1]_j[R1{\times}N1]_j - k_{off,P1{\times}(R1{\times}N1),j}[P1{\times}R1{\times}N1]_j$$
$$+k_{on,(P1{\times}R1){\times}N1,j}[P1{\times}R1]_j[N1]_j - k_{off,(P1{\times}R1){\times}N1,j}[P1{\times}R1{\times}N1]_j$$

$$d[V_{121}{\times}sR1{\times}N1]_j/dt = -k_{\text{int},V121{\times}sR1{\times}N1,j}[V_{121}{\times}sR1{\times}N1]_j + k_{rec4,V121{\times}sR1{\times}N1,j}[V_{121}{\times}sR1{\times}N1_{rab45}]$$
$$+k_{rec11,V121{\times}sR1{\times}N1,j}[V_{121}{\times}sR1{\times}N1_{rab11}]$$
$$+k_{on,V121{\times}(sR1{\times}N1),j}[V_{121}]_j[sR1{\times}N1]_j - k_{off,V121{\times}(sR1{\times}N1),j}[V_{121}{\times}sR1{\times}N1]_j$$
$$+k_{on,(V121{\times}sR1){\times}N1,j}[V_{121}{\times}sR1]_j[N1]_j - k_{off,(V121{\times}sR1){\times}N1,j}[V_{121}{\times}sR1{\times}N1]_j$$

$$d[P1{\times}sR1{\times}N1]_j/dt = -k_{\text{int},P1{\times}sR1{\times}N1,j}[P1{\times}sR1{\times}N1]_j + k_{rec4,P1{\times}sR1{\times}N1,j}[P1{\times}sR1{\times}N1_{rab45}]$$
$$+k_{rec11,P1{\times}sR1{\times}N1,j}[P1{\times}sR1{\times}N1_{rab11}]$$
$$+k_{on,P1{\times}(sR1{\times}N1),j}[P1]_j[sR1{\times}N1]_j - k_{off,P1{\times}(sR1{\times}N1),j}[P1{\times}sR1{\times}N1]_j$$
$$+k_{on,(P1{\times}sR1){\times}N1,j}[P1{\times}sR1]_j[N1]_j - k_{off,(P1{\times}sR1){\times}N1,j}[P1{\times}sR1{\times}N1]_j$$

$$d[M_{EBM}{\times}V_{165}{\times}R2]_j/dt = k_{on,(M{\times}V165){\times}R2,j}{\times}f{\times}[M_{EBM}{\times}V_{165}]_j[R2]_j - k_{off,(M{\times}V165){\times}R2,j}[M_{EBM}{\times}V_{165}{\times}R2]_j$$
$$+k_{on,M{\times}(V165{\times}R2),j}{\times}f{\times}[M_{EBM}]_j[V_{165}{\times}R2]_j - k_{off,M{\times}(V165{\times}R2),j}[M_{EBM}{\times}V_{165}{\times}R2]_j$$

$$d[M_{EBM} \times V_{189} \times R2]_j / dt = k_{on,(M \times V189) \times R2,j} \times f \times [M_{EBM} \times V_{189}]_j [R2]_j - k_{off,(M \times V189) \times R2,j} [M_{EBM} \times V_{189} \times R2]_j$$
$$+ k_{on,M \times (V189 \times R2),j} \times f \times [M_{EBM}]_j [V_{189} \times R2]_j - k_{off,M \times (V189 \times R2),j} [M_{EBM} \times V_{189} \times R2]_j$$

$$d[M_{EBM} \times V_{165} \times R1]_j / dt = k_{on,(M \times V165) \times R1,j} \times f \times [M_{EBM} \times V_{165}]_j [R1]_j - k_{off,(M \times V165) \times R1,j} [M_{EBM} \times V_{165} \times R1]_j$$
$$+ k_{on,M \times (V165 \times R1),j} \times f \times [M_{EBM}]_j [V_{165} \times R1]_j - k_{off,M \times (V165 \times R1),j} [M_{EBM} \times V_{165} \times R1]_j$$

$$d[M_{EBM} \times V_{189} \times R1]_j / dt = k_{on,(M \times V189) \times R1,j} \times f \times [M_{EBM} \times V_{189}]_j [R1]_j - k_{off,(M \times V189) \times R1,j} [M_{EBM} \times V_{189} \times R1]_j$$
$$+ k_{on,M \times (V189 \times R1),j} \times f \times [M_{EBM}]_j [V_{189} \times R1]_j - k_{off,M \times (V189 \times R1),j} [M_{EBM} \times V_{189} \times R1]_j$$

$$d[M_{EBM} \times P2 \times R1]_j / dt = k_{on,(M \times P2) \times R1,j} \times f \times [M_{EBM} \times P2]_j [R1]_j - k_{off,(M \times P2) \times R1,j} [M_{EBM} \times P2 \times R1]_j$$
$$+ k_{on,M \times (P2 \times R1),j} \times f \times [M_{EBM}]_j [P2 \times R1]_j - k_{off,M \times (P2 \times R1),j} [M_{EBM} \times P2 \times R1]_j$$

Detailed VEGFR2 Phosphorylation Reactions. Here we show one example equation (unoccupied cell surface VEGFR2 phosphorylated only on tyrosine Y1175) demonstrating the site-specific phosphorylation and dephosphorylation of VEGFR2 on tyrosines 951, 1175, and 1214 (**Figure 6-1D**). Phosphorylation is assumed to be independent on each site, giving 8 possible combinations: no phosphorylation, pY951 only, pY1175 only, pY1214 only, pY951 and pY1175, pY951 and pY1214, pY1175 and pY1214, and all three sites phosphorylated. VEGFR2 can be phosphorylated in any of these patterns on the cell surface, in early (Rab4/5) endosomes, or in recycling (Rab11) endosomes. The phosphorylation and dephosphorylation rates (**Table S9**) vary by subcellular location and with ligation, but are assumed to be independent of NRP1 and HSPG binding. The phosphorylation state of VEGFR2 is assumed not to alter is binding or trafficking properties. We focus here on pY1175 and pY1214 because the parameters for these sites are better constrained than those for pY951. Total phosphorylated VEGFR (pR2) is approximated as the sum of all VEGFR2 phosphorylated on at least one site. The full set of equations for phosphorylation of VEGFR2 in all complexes and all locations is omitted for the sake of brevity.

$$
\begin{aligned}
d[R2_{pY1175}]_j / dt =\ &-k_{\text{int},R2,j}[R2_{pY1175}]_j + k_{rec4,R2,j}[R2_{rab45,pY1175}] + k_{rec11,R2,j}[R2_{rab11,pY1175}] \\
&-k_{on,V165\times R2,j}[V_{165}]_j[R2_{pY1175}]_j + k_{off,V165\times R2,j}[V_{165}\times R2_{pY1175}]_j \\
&-k_{on,V189\times R2,j}[V_{189}]_j[R2_{pY1175}]_j + k_{off,V189\times R2,j}[V_{189}\times R2_{pY1175}]_j \\
&-k_{on,V121\times R2,j}[V_{121}]_j[R2_{pY1175}]_j + k_{off,V121\times R2,j}[V_{121}\times R2_{pY1175}]_j \\
&-k_{on,(M\times V165)\times R2,j}[M_{EBM}\times V_{165}]_j[R2_{pY1175}]_j + k_{off,(M\times V165)\times R2,j}[M_{EBM}\times V_{165}\times R2_{pY1175}]_j \\
&-k_{on,(M\times V189)\times R2,j}[M_{EBM}\times V_{189}]_j[R2_{pY1175}]_j + k_{off,(M\times V189)\times R2,j}[M_{EBM}\times V_{189}\times R2_{pY1175}]_j \\
&-k_{on,(N1\times V165)\times R2,j}[N1\times V_{165}]_j[R2_{pY1175}]_j + k_{off,(N1\times V165)\times R2,j}[N1\times V_{165}\times R2_{pY1175}]_j \\
&-k_{on,(N1\times V189)\times R2,j}[N1\times V_{189}]_j[R2_{pY1175}]_j + k_{off,(N1\times V189)\times R2,j}[N1\times V_{189}\times R2_{pY1175}]_j \\
&+k_{p,Y1175,R2,j}[R2]_j - k_{dp,Y1175,R2,j}[R2_{pY1175}]_j \\
&-k_{p,Y951,R2,j}[R2_{pY1175}]_j + k_{dp,Y951,R2,j}[R2_{pY951-pY1175}]_j \\
&-k_{p,Y1214,R2,j}[R2_{pY1175}]_j + k_{dp,Y1214,R2,j}[R2_{pY1175-pY1214}]_j
\end{aligned}
$$

Endothelial Endosomes. These 54 equations represent molecular species within early signaling (Rab4/5) or recycling (Rab11) endosomes in endothelial cells. Here, k_{4to11} is the trafficking rate from early (Rab45) to recycling (Rab11) endosomes, and k_{degr} is the rate of degradation of species from early Rab4/5 endosomes. $[R1_{rab45}]$ is the concentration of unoccupied VEGFR1 in early (Rab4/5) endosomes.

Rab4/5 Early Signaling Endosomes

$$
\begin{aligned}
d[R1_{rab45}]_j / dt =\ &k_{\text{int},R1,j}[R1]_j - k_{rec4,R1,j}[R1_{rab45}] - k_{4to11,R1,j}[R1_{rab45}] - k_{degr,R1,j}[R1_{rab45}] \\
&-k_{on,V165\times R1,j}[V_{165,rab45}]_j[R1_{rab45}]_j + k_{off,V165\times R1,j}[V_{165}\times R1_{rab45}]_j \\
&-k_{on,V189\times R1,j}[V_{189,rab45}]_j[R1_{rab45}]_j + k_{off,V189\times R1,j}[V_{189}\times R1_{rab45}]_j \\
&-k_{on,V121\times R1,j}[V_{121,rab45}]_j[R1_{rab45}]_j + k_{off,V121\times R1,j}[V_{121}\times R1_{rab45}]_j \\
&-k_{on,P1\times R1,j}[P1_{rab45}]_j[R1_{rab45}]_j + k_{off,P1\times R1,j}[P1\times R1_{rab45}]_j \\
&-k_{on,P2\times R1,j}[P2_{rab45}]_j[R1_{rab45}]_j + k_{off,P2\times R1,j}[P2\times R1_{rab45}]_j \\
&-k_{on,N1\times R1,j}[N1_{rab45}]_j[R1_{rab45}]_j + k_{off,N1\times R1,j}[N1\times R1_{rab45}]_j
\end{aligned}
$$

$$d[R2_{rab45}]_j / dt = k_{int,R2,j}[R2]_j - k_{rec4,R2,j}[R2_{rab45}] - k_{4to11,R2,j}[R2_{rab45}] - k_{degr,R2,j}[R2_{rab45}]$$

$$- k_{on,V165\times R2,j}[V_{165,rab45}]_j[R2_{rab45}]_j + k_{off,V165\times R2,j}[V_{165}\times R2_{rab45}]_j$$

$$- k_{on,V189\times R2,j}[V_{189,rab45}]_j[R2_{rab45}]_j + k_{off,V189\times R2,j}[V_{189}\times R2_{rab45}]_j$$

$$- k_{on,V121\times R2,j}[V_{121,rab45}]_j[R2_{rab45}]_j + k_{off,V121\times R2,j}[V_{121}\times R2_{rab45}]_j$$

$$- k_{on,(N1\times V165)\times R2,j}[N1\times V_{165,rab45}]_j[R2_{rab45}]_j + k_{off,(N1\times V165)\times R2,j}[N1\times V_{165}\times R2_{rab45}]_j$$

$$- k_{on,(N1\times V189)\times R2,j}[N1\times V_{189,rab45}]_j[R2_{rab45}]_j + k_{off,(N1\times V189)\times R2,j}[N1\times V_{189}\times R2_{rab45}]_j$$

$$d[N1_{rab45}]_j / dt = k_{int,N1,j}[N1]_j - k_{rec4,N1,j}[N1_{rab45}] - k_{4to11,N1,j}[N1_{rab45}] - k_{degr,N1,j}[N1_{rab45}]$$

$$- k_{on,V165\times N1,j}[V_{165,rab45}]_j[N1_{rab45}]_j + k_{off,V165\times N1,j}[V_{165}\times N1_{rab45}]_j$$

$$- k_{on,V189\times N1,j}[V_{189,rab45}]_j[N1_{rab45}]_j + k_{off,V189\times N1,j}[V_{189}\times N1_{rab45}]_j$$

$$- k_{on,P2\times N1,j}[P2_{rab45}]_j[N1_{rab45}]_j + k_{off,P2\times N1,j}[P2\times N1_{rab45}]_j$$

$$- k_{on,N1\times R1,j}[N1_{rab45}]_j[R1_{rab45}]_j + k_{off,N1\times R1,j}[N1\times R1_{rab45}]_j$$

$$- k_{on,N1\times sR1,j}[N1_{rab45}]_j[sR1_{rab45}]_j + k_{off,N1\times sR1,j}[N1\times sR1_{rab45}]_j$$

$$- k_{on,(V121\times R1)\times N1,j}[V_{121}\times R1_{rab45}]_j[N1_{rab45}]_j + k_{off,(V121\times R1)\times N1,j}[V_{121}\times R1\times N1_{rab45}]_j$$

$$- k_{on,(P1\times R1)\times N1,j}[P1\times R1_{rab45}]_j[N1_{rab45}]_j + k_{off,(P1\times R1)\times N1,j}[P1\times R1\times N1_{rab45}]_j$$

$$- k_{on,N1\times(V165\times R2),j}[N1_{rab45}]_j[V_{165}\times R2_{rab45}]_j + k_{off,N1\times(V165\times R2),j}[N1\times V_{165}\times R2_{rab45}]_j$$

$$- k_{on,N1\times(V189\times R2),j}[N1_{rab45}]_j[V_{189}\times R2_{rab45}]_j + k_{off,N1\times(V189\times R2),j}[N1\times V_{189}\times R2_{rab45}]_j$$

$$d[V_{165}\times R1_{rab45}]_j / dt = k_{int,V165\times R1,j}[V_{165}\times R1]_j - k_{rec4,V165\times R1,j}[V_{165}\times R1_{rab45}]$$

$$- k_{4to11,V165\times R1,j}[V_{165}\times R1_{rab45}] - k_{degr,V165\times R1,j}[V_{165}\times R1_{rab45}]$$

$$+ k_{on,V165\times R1,j}[V_{165,rab45}]_j[R1_{rab45}]_j - k_{off,V165\times R1,j}[V_{165}\times R1_{rab45}]_j$$

$$d[V_{189}\times R1_{rab45}]_j / dt = k_{int,V189\times R1,j}[V_{189}\times R1]_j - k_{rec4,V189\times R1,j}[V_{189}\times R1_{rab45}]$$

$$- k_{4to11,V189\times R1,j}[V_{189}\times R1_{rab45}] - k_{degr,V189\times R1,j}[V_{189}\times R1_{rab45}]$$

$$+ k_{on,V189\times R1,j}[V_{189,rab45}]_j[R1_{rab45}]_j - k_{off,V189\times R1,j}[V_{189}\times R1_{rab45}]_j$$

$$d[V_{121}\times R1_{rab45}]_j / dt = k_{int,V121\times R1,j}[V_{121}\times R1]_j - k_{rec4,V121\times R1,j}[V_{121}\times R1_{rab45}]$$

$$- k_{4to11,V121\times R1,j}[V_{121}\times R1_{rab45}] - k_{degr,V121\times R1,j}[V_{121}\times R1_{rab45}]$$

$$+ k_{on,V121\times R1,j}[V_{121,rab45}]_j[R1_{rab45}]_j - k_{off,V121\times R1,j}[V_{121}\times R1_{rab45}]_j$$

$$- k_{on,(V121\times R1)\times N1,j}[V_{121}\times R1_{rab45}]_j[N1_{rab45}]_j + k_{off,(V121\times R1)\times N1,j}[V_{121}\times R1\times N1_{rab45}]_j$$

$$d[P1{\times}R1_{rab45}]_j / dt = k_{\mathrm{int},P1{\times}R1,j}[P1{\times}R1]_j - k_{rec4,P1{\times}R1,j}[P1{\times}R1_{rab45}]$$
$$-k_{4to11,P1{\times}R1,j}[P1{\times}R1_{rab45}] - k_{\mathrm{deg}r,P1{\times}R1,j}[P1{\times}R1_{rab45}]$$
$$+k_{on,P1{\times}R1,j}[P1_{rab45}]_j[R1_{rab45}]_j - k_{off,P1{\times}R1,j}[P1{\times}R1_{rab45}]_j$$
$$-k_{on,(P1{\times}R1){\times}N1,j}[P1{\times}R1_{rab45}]_j[N1_{rab45}]_j + k_{off,(P1{\times}R1){\times}N1,j}[P1{\times}R1{\times}N1_{rab45}]_j$$

$$d[P2{\times}R1_{rab45}]_j / dt = k_{\mathrm{int},P2{\times}R1,j}[P2{\times}R1]_j - k_{rec4,P2{\times}R1,j}[P2{\times}R1_{rab45}]$$
$$-k_{4to11,P2{\times}R1,j}[P2{\times}R1_{rab45}] - k_{\mathrm{deg}r,P2{\times}R1,j}[P2{\times}R1_{rab45}]$$
$$+k_{on,P2{\times}R1,j}[P2_{rab45}]_j[R1_{rab45}]_j - k_{off,P2{\times}R1,j}[P2{\times}R1_{rab45}]_j$$

$$d[V_{165}{\times}sR1_{rab45}]_j / dt = -k_{\mathrm{deg}r,V165{\times}R1,j}[V_{165}{\times}sR1_{rab45}]$$
$$+k_{on,V165{\times}sR1,j}[V_{165,rab45}]_j[sR1_{rab45}]_j - k_{off,V165{\times}sR1,j}[V_{165}{\times}sR1_{rab45}]_j$$

$$d[V_{189}{\times}sR1_{rab45}]_j / dt = -k_{\mathrm{deg}r,V189{\times}R1,j}[V_{189}{\times}sR1_{rab45}]$$
$$+k_{on,V189{\times}sR1,j}[V_{189,rab45}]_j[sR1_{rab45}]_j - k_{off,V189{\times}sR1,j}[V_{189}{\times}sR1_{rab45}]_j$$

$$d[V_{121}{\times}sR1_{rab45}]_j / dt = -k_{\mathrm{deg}r,V121{\times}R1,j}[V_{121}{\times}sR1_{rab45}]$$
$$+k_{on,V121{\times}sR1,j}[V_{121,rab45}]_j[sR1_{rab45}]_j - k_{off,V121{\times}sR1,j}[V_{121}{\times}sR1_{rab45}]_j$$
$$-k_{on,(V121{\times}sR1){\times}N1,j}[V_{121}{\times}sR1_{rab45}]_j[N1_{rab45}]_j + k_{off,(V121{\times}sR1){\times}N1,j}[V_{121}{\times}sR1{\times}N1_{rab45}]_j$$

$$d[P1{\times}sR1_{rab45}]_j / dt = -k_{\mathrm{deg}r,P1{\times}sR1,j}[P1{\times}sR1_{rab45}]$$
$$+k_{on,P1{\times}sR1,j}[P1_{rab45}]_j[sR1_{rab45}]_j - k_{off,P1{\times}sR1,j}[P1{\times}sR1_{rab45}]_j$$
$$-k_{on,(P1{\times}sR1){\times}N1,j}[P1{\times}sR1_{rab45}]_j[N1_{rab45}]_j + k_{off,(P1{\times}sR1){\times}N1,j}[P1{\times}sR1{\times}N1_{rab45}]_j$$

$$d[P2{\times}sR1_{rab45}]_j / dt = -k_{\mathrm{deg}r,P2{\times}sR1,j}[P2{\times}sR1_{rab45}]$$
$$+k_{on,P2{\times}sR1,j}[P2_{rab45}]_j[sR1_{rab45}]_j - k_{off,P2{\times}sR1,j}[P2{\times}sR1_{rab45}]_j$$

$$d[V_{165}{\times}R2_{rab45}]_j / dt = k_{\mathrm{int},V165{\times}R2,j}[V_{165}{\times}R2]_j - k_{rec4,V165{\times}R2,j}[V_{165}{\times}R2_{rab45}]$$
$$-k_{4to11,V165{\times}R2,j}[V_{165}{\times}R2_{rab45}] - k_{\mathrm{deg}r,V165{\times}R2,j}[V_{165}{\times}R2_{rab45}]$$
$$+k_{on,V165{\times}R2,j}[V_{165,rab45}]_j[R2_{rab45}]_j - k_{off,V165{\times}R2,j}[V_{165}{\times}R2_{rab45}]_j$$
$$-k_{on,N1{\times}(V165{\times}R2),j}[N1_{rab45}]_j[V_{165}{\times}R2_{rab45}]_j + k_{off,N1{\times}(V165{\times}R2),j}[N1{\times}V_{165}{\times}R2_{rab45}]_j$$

$$\begin{aligned}
d[V_{189}{\times}R2_{rab45}]_j / dt &= k_{\mathrm{int},V189{\times}R2,j}[V_{189}{\times}R2]_j - k_{rec4,V189{\times}R2,j}[V_{189}{\times}R2_{rab45}] \\
&\quad - k_{4to11,V189{\times}R2,j}[V_{189}{\times}R2_{rab45}] - k_{\mathrm{deg}r,V189{\times}R2,j}[V_{189}{\times}R2_{rab45}] \\
&\quad + k_{on,V189{\times}R2,j}[V_{189,rab45}]_j[R2_{rab45}]_j - k_{off,V189{\times}R2,j}[V_{189}{\times}R2_{rab45}]_j \\
&\quad - k_{on,N1{\times}(V189{\times}R2),j}[N1_{rab45}]_j[V_{189}{\times}R2_{rab45}]_j + k_{off,N1{\times}(V189{\times}R2),j}[N1{\times}V_{189}{\times}R2_{rab45}]_j
\end{aligned}$$

$$\begin{aligned}
d[V_{121}{\times}R2_{rab45}]_j / dt &= k_{\mathrm{int},V121{\times}R2,j}[V_{121}{\times}R2]_j - k_{rec4,V121{\times}R2,j}[V_{121}{\times}R2_{rab45}] \\
&\quad - k_{4to11,V121{\times}R2,j}[V_{121}{\times}R2_{rab45}] - k_{\mathrm{deg}r,V121{\times}R2,j}[V_{121}{\times}R2_{rab45}] \\
&\quad + k_{on,V121{\times}R2,j}[V_{121,rab45}]_j[R2_{rab45}]_j - k_{off,V121{\times}R2,j}[V_{121}{\times}R2_{rab45}]_j
\end{aligned}$$

$$\begin{aligned}
d[V_{165}{\times}N1_{rab45}]_j / dt &= k_{\mathrm{int},V165{\times}N1,j}[V_{165}{\times}N1]_j - k_{rec4,V165{\times}N1,j}[V_{165}{\times}N1_{rab45}] \\
&\quad - k_{4to11,V165{\times}N1,j}[V_{165}{\times}N1_{rab45}] - k_{\mathrm{deg}r,V165{\times}N1,j}[V_{165}{\times}N1_{rab45}] \\
&\quad + k_{on,V165{\times}N1,j}[V_{165,rab45}]_j[N1_{rab45}]_j - k_{off,V165{\times}N1,j}[V_{165}{\times}N1_{rab45}]_j \\
&\quad - k_{on,(N1{\times}V165){\times}R2,j}[N1{\times}V_{165,rab45}]_j[R2_{rab45}]_j + k_{off,(N1{\times}V165){\times}R2,j}[N1{\times}V_{165}{\times}R2_{rab45}]_j
\end{aligned}$$

$$\begin{aligned}
d[V_{189}{\times}N1_{rab45}]_j / dt &= k_{\mathrm{int},V189{\times}N1,j}[V_{189}{\times}N1]_j - k_{rec4,V189{\times}N1,j}[V_{189}{\times}N1_{rab45}] \\
&\quad - k_{4to11,V189{\times}N1,j}[V_{189}{\times}N1_{rab45}] - k_{\mathrm{deg}r,V189{\times}N1,j}[V_{189}{\times}N1_{rab45}] \\
&\quad + k_{on,V189{\times}N1,j}[V_{189,rab45}]_j[N1_{rab45}]_j - k_{off,V189{\times}N1,j}[V_{189}{\times}N1_{rab45}]_j \\
&\quad - k_{on,(N1{\times}V189){\times}R2,j}[N1{\times}V_{189,rab45}]_j[R2_{rab45}]_j + k_{off,(N1{\times}V189){\times}R2,j}[N1{\times}V_{189}{\times}R2_{rab45}]_j
\end{aligned}$$

$$\begin{aligned}
d[P2{\times}N1_{rab45}]_j / dt &= k_{\mathrm{int},P2{\times}N1,j}[P2{\times}N1]_j - k_{rec4,P2{\times}N1,j}[P2{\times}N1_{rab45}] \\
&\quad - k_{4to11,P2{\times}N1,j}[P2{\times}N1_{rab45}] - k_{\mathrm{deg}r,P2{\times}N1,j}[P2{\times}N1_{rab45}] \\
&\quad + k_{on,P2{\times}N1,j}[P2_{rab45}]_j[N1_{rab45}]_j - k_{off,P2{\times}N1,j}[P2{\times}N1_{rab45}]_j
\end{aligned}$$

$$\begin{aligned}
d[N1{\times}R1_{rab45}]_j / dt &= k_{\mathrm{int},N1{\times}R1,j}[N1{\times}R1]_j - k_{rec4,N1{\times}R1,j}[N1{\times}R1_{rab45}] \\
&\quad - k_{4to11,N1{\times}R1,j}[N1{\times}R1_{rab45}] - k_{\mathrm{deg}r,N1{\times}R1,j}[N1{\times}R1_{rab45}] \\
&\quad + k_{on,N1{\times}R1,j}[N1_{rab45}]_j[R1_{rab45}]_j - k_{off,N1{\times}R1,j}[N1{\times}R1_{rab45}]_j \\
&\quad - k_{on,V121{\times}(N1{\times}R1),j}[V_{121,rab45}]_j[N1{\times}R1_{rab45}]_j + k_{off,V121{\times}(N1{\times}R1),j}[V_{121}{\times}R1{\times}N1_{rab45}]_j \\
&\quad - k_{on,P1{\times}(N1{\times}R1),j}[P1_{rab45}]_j[N1{\times}R1_{rab45}]_j + k_{off,P1{\times}(N1{\times}R1),j}[P1{\times}R1{\times}N1_{rab45}]_j
\end{aligned}$$

$$d[N1{\times}sR1_{rab45}]_j / dt = k_{\mathrm{int},N1{\times}R1,j}[N1{\times}R1]_j - k_{rec4,N1{\times}R1,j}[N1{\times}sR1_{rab45}]$$
$$-k_{4to11,N1{\times}R1,j}[N1{\times}sR1_{rab45}] - k_{\mathrm{deg}r,N1{\times}R1,j}[N1{\times}sR1_{rab45}]$$
$$+k_{on,N1{\times}R1,j}[N1_{rab45}]_j[sR1_{rab45}]_j - k_{off,N1{\times}R1,j}[N1{\times}sR1_{rab45}]_j$$
$$-k_{on,V121{\times}(N1{\times}R1),j}[V_{121,rab45}]_j[N1{\times}sR1_{rab45}]_j + k_{off,V121{\times}(N1{\times}R1),j}[V_{121}{\times}sR1{\times}N1_{rab45}]_j$$
$$-k_{on,P1{\times}(N1{\times}R1),j}[P1_{rab45}]_j[N1{\times}sR1_{rab45}]_j + k_{off,P1{\times}(N1{\times}R1),j}[P1{\times}sR1{\times}N1_{rab45}]_j$$

$$d[N1{\times}V_{165}{\times}R2_{rab45}]_j / dt = k_{\mathrm{int},N1{\times}V165{\times}R2,j}[N1{\times}V_{165}{\times}R2]_j - k_{rec4,N1{\times}V165{\times}R2,j}[N1{\times}V_{165}{\times}R2_{rab45}]$$
$$+k_{4to11,N1{\times}V165{\times}R2,j}[N1{\times}V_{165}{\times}R2_{rab45}] - k_{\mathrm{deg}r,N1{\times}V165{\times}R2,j}[N1{\times}V_{165}{\times}R2_{rab45}]$$
$$+k_{on,R2{\times}(N1{\times}V165),j}[R2_{rab45}]_j[V_{165}{\times}N1_{rab45}]_j - k_{off,R2{\times}(N1{\times}V165),j}[N1{\times}V_{165}{\times}R2_{rab45}]_j$$
$$+k_{on,N1{\times}(V165{\times}R2),j}[N1_{rab45}]_j[V_{165}{\times}R2_{rab45}]_j - k_{off,N1{\times}(V165{\times}R2),j}[N1{\times}V_{165}{\times}R2_{rab45}]_j$$

$$d[N1{\times}V_{189}{\times}R2_{rab45}]_j / dt = k_{\mathrm{int},N1{\times}V189{\times}R2,j}[N1{\times}V_{189}{\times}R2]_j - k_{rec4,N1{\times}V189{\times}R2,j}[N1{\times}V_{189}{\times}R2_{rab45}]$$
$$-k_{4to11,N1{\times}V189{\times}R2,j}[N1{\times}V_{189}{\times}R2_{rab45}] - k_{\mathrm{deg}r,N1{\times}V189{\times}R2,j}[N1{\times}V_{189}{\times}R2_{rab45}]$$
$$+k_{on,R2{\times}(V189{\times}N1),j}[R2_{rab45}]_j[V_{189}{\times}N1_{rab45}]_j - k_{off,R2{\times}(N1{\times}V189),j}[N1{\times}V_{189}{\times}R2_{rab45}]_j$$
$$+k_{on,N1{\times}(V189{\times}R2),j}[N1_{rab45}]_j[V_{189}{\times}R2_{rab45}]_j - k_{off,N1{\times}(V189{\times}R2),j}[N1{\times}V_{189}{\times}R2_{rab45}]_j$$

$$d[V_{121}{\times}R1{\times}N1_{rab45}]_j / dt = k_{\mathrm{int},V121{\times}R1{\times}N1,j}[V_{121}{\times}R1{\times}N1]_j - k_{rec4,V121{\times}R1{\times}N1,j}[V_{121}{\times}R1{\times}N1_{rab45}]$$
$$-k_{4to11,V121{\times}R1{\times}N1,j}[V_{121}{\times}R1{\times}N1_{rab45}] - k_{\mathrm{deg}r,V121{\times}R1{\times}N1,j}[V_{121}{\times}R1{\times}N1_{rab45}]$$
$$+k_{on,V121{\times}(R1{\times}N1),j}[V_{121,rab45}]_j[R1{\times}N1_{rab45}]_j - k_{off,V121{\times}(R1{\times}N1),j}[V_{121}{\times}R1{\times}N1_{rab45}]_j$$
$$+k_{on,(V121{\times}R1){\times}N1,j}[V_{121}{\times}R1_{rab45}]_j[N1_{rab45}]_j - k_{off,(V121{\times}R1){\times}N1,j}[V_{121}{\times}R1{\times}N1_{rab45}]_j$$

$$d[P1{\times}R1{\times}N1_{rab45}]_j / dt = k_{\mathrm{int},P1{\times}R1{\times}N1,j}[P1{\times}R1{\times}N1]_j - k_{rec4,P1{\times}R1{\times}N1,j}[P1{\times}R1{\times}N1_{rab45}]$$
$$-k_{4to11,P1{\times}R1{\times}N1,j}[P1{\times}R1{\times}N1_{rab45}] - k_{\mathrm{deg}r,P1{\times}R1{\times}N1,j}[P1{\times}R1{\times}N1_{rab45}]$$
$$+k_{on,P1{\times}(R1{\times}N1),j}[P1_{rab45}]_j[R1{\times}N1_{rab45}]_j - k_{off,P1{\times}(R1{\times}N1),j}[P1{\times}R1{\times}N1_{rab45}]_j$$
$$+k_{on,(P1{\times}R1){\times}N1,j}[P1{\times}R1_{rab45}]_j[N1_{rab45}]_j - k_{off,(P1{\times}R1){\times}N1,j}[P1{\times}R1{\times}N1_{rab45}]_j$$

$$d[V_{121}{\times}sR1{\times}N1_{rab45}]_j / dt = k_{\mathrm{int},V121{\times}R1{\times}N1,j}[V_{121}{\times}sR1{\times}N1]_j - k_{rec4,V121{\times}R1{\times}N1,j}[V_{121}{\times}sR1{\times}N1_{rab45}]$$
$$-k_{4to11,V121{\times}R1{\times}N1,j}[V_{121}{\times}sR1{\times}N1_{rab45}] - k_{\mathrm{deg}r,V121{\times}R1{\times}N1,j}[V_{121}{\times}sR1{\times}N1_{rab45}]$$
$$+k_{on,V121{\times}(sR1{\times}N1),j}[V_{121,rab45}]_j[sR1{\times}N1_{rab45}]_j - k_{off,V121{\times}(sR1{\times}N1),j}[V_{121}{\times}sR1{\times}N1_{rab45}]_j$$
$$+k_{on,(V121{\times}sR1){\times}N1,j}[V_{121}{\times}sR1_{rab45}]_j[N1_{rab45}]_j - k_{off,(V121{\times}sR1){\times}N1,j}[V_{121}{\times}sR1{\times}N1_{rab45}]_j$$

$$d[P1{\times}sR1{\times}N1_{rab45}]_j / dt = k_{\mathrm{int},P1{\times}sR1{\times}N1,j}[P1{\times}sR1{\times}N1]_j - k_{rec4,P1{\times}sR1{\times}N1,j}[P1{\times}sR1{\times}N1_{rab45}]$$

$$-k_{4to11,P1{\times}sR1{\times}N1,j}[P1{\times}sR1{\times}N1_{rab45}] - k_{\deg r,P1{\times}sR1{\times}N1,j}[P1{\times}sR1{\times}N1_{rab45}]$$

$$+k_{on,P1{\times}(sR1{\times}N1),j}[P1_{rab45}]_j[sR1{\times}N1_{rab45}]_j - k_{off,P1{\times}(sR1{\times}N1),j}[P1{\times}sR1{\times}N1_{rab45}]_j$$

$$+k_{on,(P1{\times}sR1){\times}N1,j}[P1{\times}sR1_{rab45}]_j[N1_{rab45}]_j - k_{off,(P1{\times}sR1){\times}N1,j}[P1{\times}sR1{\times}N1_{rab45}]_j$$

Rab11 Recycling Endosomes

$$d[R1_{rab11}]_j / dt = k_{4to11,R1,j}[R1_{rab45}] - k_{rec11,R1,j}[R1_{rab11}]$$

$$-k_{on,V165{\times}R1,j}[V_{165,rab11}]_j[R1_{rab11}]_j + k_{off,V165{\times}R1,j}[V_{165}{\times}R1_{rab11}]_j$$

$$-k_{on,V189{\times}R1,j}[V_{189,rab11}]_j[R1_{rab11}]_j + k_{off,V189{\times}R1,j}[V_{189}{\times}R1_{rab11}]_j$$

$$-k_{on,V121{\times}R1,j}[V_{121,rab45}]_j[R1_{rab11}]_j + k_{off,V121{\times}R1,j}[V_{121}{\times}R1_{rab11}]_j$$

$$-k_{on,P1{\times}R1,j}[P1_{rab11}]_j[R1_{rab11}]_j + k_{off,P1{\times}R1,j}[P1{\times}R1_{rab11}]_j$$

$$-k_{on,P2{\times}R1,j}[P2_{rab11}]_j[R1_{rab11}]_j + k_{off,P2{\times}R1,j}[P2{\times}R1_{rab11}]_j$$

$$-k_{on,N1{\times}R1,j}[N1_{rab11}]_j[R1_{rab11}]_j + k_{off,N1{\times}R1,j}[N1{\times}R1_{rab11}]_j$$

$$d[R2_{rab11}]_j / dt = k_{4to11,R2,j}[R2_{rab45}] - k_{rec11,R2,j}[R2_{rab11}]$$

$$-k_{on,V165{\times}R2,j}[V_{165,rab11}]_j[R2_{rab11}]_j + k_{off,V165{\times}R2,j}[V_{165}{\times}R2_{rab11}]_j$$

$$-k_{on,V189{\times}R2,j}[V_{189,rab11}]_j[R2_{rab11}]_j + k_{off,V189{\times}R2,j}[V_{189}{\times}R2_{rab11}]_j$$

$$-k_{on,V121{\times}R2,j}[V_{121,rab11}]_j[R2_{rab11}]_j + k_{off,V121{\times}R2,j}[V_{121}{\times}R2_{rab11}]_j$$

$$-k_{on,(N1{\times}V165){\times}R2,j}[N1{\times}V_{165,rab11}]_j[R2_{rab11}]_j + k_{off,(N1{\times}V165){\times}R2,j}[N1{\times}V_{165}{\times}R2_{rab11}]_j$$

$$-k_{on,(N1{\times}V189){\times}R2,j}[N1{\times}V_{189,rab11}]_j[R2_{rab11}]_j + k_{off,(N1{\times}V189){\times}R2,j}[N1{\times}V_{189}{\times}R2_{rab11}]_j$$

$$d[N1_{rab11}]_j / dt = k_{4to11,N1,j}[N1_{rab45}] - k_{rec11,N1,j}[N1_{rab11}]$$

$$-k_{on,V165{\times}N1,j}[V_{165,rab11}]_j[N1_{rab11}]_j + k_{off,V165{\times}N1,j}[V_{165}{\times}N1_{rab11}]_j$$

$$-k_{on,V189{\times}N1,j}[V_{189,rab11}]_j[N1_{rab11}]_j + k_{off,V189{\times}N1,j}[V_{189}{\times}N1_{rab11}]_j$$

$$-k_{on,P2{\times}N1,j}[P2_{rab11}]_j[N1_{rab11}]_j + k_{off,P2{\times}N1,j}[P2{\times}N1_{rab11}]_j$$

$$-k_{on,N1{\times}R1,j}[N1_{rab11}]_j[R1_{rab11}]_j + k_{off,N1{\times}R1,j}[N1{\times}R1_{rab11}]_j$$

$$-k_{on,N1{\times}sR1,j}[N1_{rab11}]_j[sR1_{rab11}]_j + k_{off,N1{\times}sR1,j}[N1{\times}sR1_{rab11}]_j$$

$$-k_{on,(V121{\times}R1){\times}N1,j}[V_{121}{\times}R1_{rab11}]_j[N1_{rab11}]_j + k_{off,(V121{\times}R1){\times}N1,j}[V_{121}{\times}R1{\times}N1_{rab11}]_j$$

$$-k_{on,(P1{\times}R1){\times}N1,j}[P1{\times}R1_{rab11}]_j[N1_{rab11}]_j + k_{off,(P1{\times}R1){\times}N1,j}[P1{\times}R1{\times}N1_{rab11}]_j$$

$$-k_{on,N1{\times}(V165{\times}R2),j}[N1_{rab11}]_j[V_{165}{\times}R2_{rab11}]_j + k_{off,N1{\times}(V165{\times}R2),j}[N1{\times}V_{165}{\times}R2_{rab11}]_j$$

$$-k_{on,N1{\times}(V189{\times}R2),j}[N1_{rab11}]_j[V_{189}{\times}R2_{rab11}]_j + k_{off,N1{\times}(V189{\times}R2),j}[N1{\times}V_{189}{\times}R2_{rab11}]_j$$

$$d[V_{165} \times R1_{rab11}]_j / dt = k_{4to11,V165 \times R1,j}[V_{165} \times R1_{rab45}] - k_{rec11,V165 \times R1,j}[V_{165} \times R1_{rab11}]$$
$$+ k_{on,V165 \times R1,j}[V_{165,rab11}]_j[R1_{rab11}]_j - k_{off,V165 \times R1,j}[V_{165} \times R1_{rab11}]_j$$

$$d[V_{189} \times R1_{rab11}]_j / dt = k_{4to11,V189 \times R1,j}[V_{189} \times R1_{rab45}] - k_{rec11,V189 \times R1,j}[V_{189} \times R1_{rab11}]$$
$$+ k_{on,V189 \times R1,j}[V_{189,rab11}]_j[R1_{rab11}]_j - k_{off,V189 \times R1,j}[V_{189} \times R1_{rab11}]_j$$

$$d[V_{121} \times R1_{rab11}]_j / dt = k_{4to11,V121 \times R1,j}[V_{121} \times R1_{rab45}] - k_{rec11,V121 \times R1,j}[V_{121} \times R1_{rab11}]$$
$$+ k_{on,V121 \times R1,j}[V_{121,rab11}]_j[R1_{rab11}]_j - k_{off,V121 \times R1,j}[V_{121} \times R1_{rab11}]_j$$
$$- k_{on,(V121 \times R1) \times N1,j}[V_{121} \times R1_{rab11}]_j[N1_{rab11}]_j + k_{off,(V121 \times R1) \times N1,j}[V_{121} \times R1 \times N1_{rab11}]_j$$

$$d[P1 \times R1_{rab11}]_j / dt = k_{4to11,P1 \times R1,j}[P1 \times R1_{rab45}] - k_{rec11,P1 \times R1,j}[P1 \times R1_{rab11}]$$
$$+ k_{on,P1 \times R1,j}[P1_{rab11}]_j[R1_{rab11}]_j - k_{off,P1 \times R1,j}[P1 \times R1_{rab11}]_j$$
$$- k_{on,(P1 \times R1) \times N1,j}[P1 \times R1_{rab11}]_j[N1_{rab11}]_j + k_{off,(P1 \times R1) \times N1,j}[P1 \times R1 \times N1_{rab11}]_j$$

$$d[P2 \times R1_{rab11}]_j / dt = k_{4to11,P2 \times R1,j}[P2 \times R1_{rab45}] - k_{rec11,P2 \times R1,j}[P2 \times R1_{rab11}]$$
$$+ k_{on,P2 \times R1,j}[P2_{rab11}]_j[R1_{rab11}]_j - k_{off,P2 \times R1,j}[P2 \times R1_{rab11}]_j$$

$$d[V_{165} \times sR1_{rab11}]_j / dt = k_{on,V165 \times sR1,j}[V_{165,rab11}]_j[sR1_{rab11}]_j - k_{off,V165 \times sR1,j}[V_{165} \times sR1_{rab11}]_j$$

$$d[V_{121} \times sR1_{rab11}]_j / dt = k_{on,V121 \times sR1,j}[V_{121,rab11}]_j[sR1_{rab11}]_j - k_{off,V121 \times sR1,j}[V_{121} \times sR1_{rab11}]_j$$
$$- k_{on,(V121 \times sR1) \times N1,j}[V_{121} \times sR1_{rab11}]_j[N1_{rab11}]_j + k_{off,(V121 \times sR1) \times N1,j}[V_{121} \times sR1 \times N1_{rab11}]_j$$

$$d[V_{189} \times sR1_{rab11}]_j / dt = k_{on,V189 \times sR1,j}[V_{189,rab11}]_j[sR1_{rab11}]_j - k_{off,V189 \times sR1,j}[V_{189} \times sR1_{rab11}]_j$$

$$d[P1 \times sR1_{rab11}]_j / dt = k_{on,P1 \times sR1,j}[P1_{rab11}]_j[sR1_{rab11}]_j - k_{off,P1 \times sR1,j}[P1 \times sR1_{rab11}]_j$$
$$- k_{on,(P1 \times sR1) \times N1,j}[P1 \times sR1_{rab11}]_j[N1_{rab11}]_j + k_{off,(P1 \times sR1) \times N1,j}[P1 \times sR1 \times N1_{rab11}]_j$$

$$d[P2 \times sR1_{rab11}]_j / dt = k_{on,P2 \times sR1,j}[P2_{rab11}]_j[sR1_{rab11}]_j - k_{off,P2 \times sR1,j}[P2 \times sR1_{rab11}]_j$$

$$d[V_{165} \times R2_{rab11}]_j / dt = k_{4to11,V165 \times R2,j}[V_{165} \times R2_{rab45}] - k_{rec11,V165 \times R2,j}[V_{165} \times R2_{rab11}]$$
$$+ k_{on,V165 \times R2,j}[V_{165,rab45}]_j[R2_{rab11}]_j - k_{off,V165 \times R2,j}[V_{165} \times R2_{rab11}]_j$$
$$- k_{on,N1 \times (V165 \times R2),j}[N1_{rab11}]_j[V_{165} \times R2_{rab11}]_j + k_{off,N1 \times (V165 \times R2),j}[N1 \times V_{165} \times R2_{rab11}]_j$$

$$d[V_{189}{\times}R2_{rab11}]_j\,/\,dt = k_{4to11,V189{\times}R2,j}[V_{189}{\times}R2_{rab45}] - k_{rec11,V189{\times}R2,j}[V_{189}{\times}R2_{rab11}]$$
$$+ k_{on,V189{\times}R2,j}[V_{189,rab11}]_j[R2_{rab11}]_j - k_{off,V189{\times}R2,j}[V_{189}{\times}R2_{rab11}]_j$$
$$- k_{on,N1{\times}(V189{\times}R2),j}[N1_{rab11}]_j[V_{189}{\times}R2_{rab11}]_j + k_{off,N1{\times}(V189{\times}R2),j}[N1{\times}V_{189}{\times}R2_{rab11}]_j$$

$$d[V_{121}{\times}R2_{rab11}]_j\,/\,dt = k_{4to11,V121{\times}R2,j}[V_{121}{\times}R2_{rab45}] - k_{rec11,V121{\times}R2,j}[V_{121}{\times}R2_{rab11}]$$
$$+ k_{on,V121{\times}R2,j}[V_{121,rab11}]_j[R2_{rab11}]_j - k_{off,V121{\times}R2,j}[V_{121}{\times}R2_{rab11}]_j$$

$$d[V_{165}{\times}N1_{rab11}]_j\,/\,dt = k_{4to11,V165{\times}N1,j}[V_{165}{\times}N1_{rab45}] - k_{rec11,V165{\times}N1,j}[V_{165}{\times}N1_{rab11}]$$
$$+ k_{on,V165{\times}N1,j}[V_{165,rab11}]_j[N1_{rab11}]_j - k_{off,V165{\times}N1,j}[V_{165}{\times}N1_{rab11}]_j$$
$$- k_{on,(N1{\times}V165){\times}R2,j}[N1{\times}V_{165,rab11}]_j[R2_{rab11}]_j + k_{off,(N1{\times}V165){\times}R2,j}[N1{\times}V_{165}{\times}R2_{rab11}]_j$$

$$d[V_{189}{\times}N1_{rab11}]_j\,/\,dt = k_{4to11,V189{\times}N1,j}[V_{189}{\times}N1_{rab11}] - k_{rec11,V189{\times}N1,j}[V_{189}{\times}N1_{rab11}]$$
$$+ k_{on,V189{\times}N1,j}[V_{189,rab11}]_j[N1_{rab11}]_j - k_{off,V189{\times}N1,j}[V_{189}{\times}N1_{rab11}]_j$$
$$- k_{on,(N1{\times}V189){\times}R2,j}[N1{\times}V_{189,rab11}]_j[R2_{rab11}]_j + k_{off,(N1{\times}V189){\times}R2,j}[N1{\times}V_{189}{\times}R2_{rab11}]_j$$

$$d[P2{\times}N1_{rab11}]_j\,/\,dt = k_{4to11,P2{\times}N1,j}[P2{\times}N1_{rab45}] - k_{rec11,P2{\times}N1,j}[P2{\times}N1_{rab11}]$$
$$+ k_{on,P2{\times}N1,j}[P2_{rab11}]_j[N1_{rab11}]_j - k_{off,P2{\times}N1,j}[P2{\times}N1_{rab11}]_j$$

$$d[N1{\times}R1_{rab11}]_j\,/\,dt = k_{4to11,N1{\times}R1,j}[N1{\times}R1_{rab45}] - k_{rec11,N1{\times}R1,j}[N1{\times}R1_{rab11}]$$
$$+ k_{on,N1{\times}R1,j}[N1_{rab11}]_j[R1_{rab11}]_j - k_{off,N1{\times}R1,j}[N1{\times}R1_{rab11}]_j$$
$$- k_{on,V121{\times}(N1{\times}R1),j}[V_{121,rab11}]_j[N1{\times}R1_{rab11}]_j + k_{off,V121{\times}(N1{\times}R1),j}[V_{121}{\times}R1{\times}N1_{rab11}]_j$$
$$- k_{on,P1{\times}(N1{\times}R1),j}[P1_{rab11}]_j[N1{\times}R1_{rab11}]_j + k_{off,P1{\times}(N1{\times}R1),j}[P1{\times}R1{\times}N1_{rab11}]_j$$

$$d[N1{\times}sR1_{rab11}]_j\,/\,dt = k_{4to11,N1{\times}sR1,j}[N1{\times}sR1_{rab45}] - k_{rec11,N1{\times}sR1,j}[N1{\times}sR1_{rab11}]$$
$$+ k_{on,N1{\times}sR1,j}[N1_{rab11}]_j[sR1_{rab11}]_j - k_{off,N1{\times}sR1,j}[N1{\times}sR1_{rab11}]_j$$
$$- k_{on,V121{\times}(N1{\times}sR1),j}[V_{121,rab11}]_j[N1{\times}sR1_{rab11}]_j + k_{off,V121{\times}(N1{\times}sR1),j}[V_{121}{\times}sR1{\times}N1_{rab11}]_j$$
$$- k_{on,P1{\times}(N1{\times}sR1),j}[P1_{rab11}]_j[N1{\times}sR1_{rab11}]_j + k_{off,P1{\times}(N1{\times}sR1),j}[P1{\times}sR1{\times}N1_{rab11}]_j$$

$$d[N1{\times}V_{165}{\times}R2_{rab11}]_j\,/\,dt = k_{4to11,N1{\times}V165{\times}R2,j}[N1{\times}V_{165}{\times}R2_{rab45}] - k_{rec11,N1{\times}V165{\times}R2,j}[N1{\times}V_{165}{\times}R2_{rab11}]$$
$$+ k_{on,R2{\times}(N1{\times}V165),j}[R2_{rab11}]_j[V_{165}{\times}N1_{rab11}]_j - k_{off,R2{\times}(N1{\times}V165),j}[N1{\times}V_{165}{\times}R2_{rab11}]_j$$
$$+ k_{on,N1{\times}(V165{\times}R2),j}[N1_{rab11}]_j[V_{165}{\times}R2_{rab11}]_j - k_{off,N1{\times}(V165{\times}R2),j}[N1{\times}V_{165}{\times}R2_{rab11}]_j$$

$$d[N1{\times}V_{189}{\times}R2_{rab11}]_j / dt = k_{4to11,N1{\times}V189{\times}R2,j}[N1{\times}V_{189}{\times}R2_{rab45}] - k_{rec11,N1{\times}V189{\times}R2,j}[N1{\times}V_{189}{\times}R2_{rab11}]$$
$$+ k_{on,R2{\times}(V189{\times}N1),j}[R2_{rab11}]_j[V_{189}{\times}N1_{rab11}]_j - k_{off,R2{\times}(N1{\times}V189),j}[N1{\times}V_{189}{\times}R2_{rab11}]_j$$
$$+ k_{on,N1{\times}(V189{\times}R2),j}[N1_{rab11}]_j[V_{189}{\times}R2_{rab11}]_j - k_{off,N1{\times}(V189{\times}R2),j}[N1{\times}V_{189}{\times}R2_{rab11}]_j$$

$$d[V_{121}{\times}R1{\times}N1_{rab11}]_j / dt = k_{4to11,V121{\times}R1{\times}N1,j}[V_{121}{\times}R1{\times}N1_{rab45}] - k_{rec11,V121{\times}R1{\times}N1,j}[V_{121}{\times}R1{\times}N1_{rab11}]$$
$$+ k_{on,V121{\times}(R1{\times}N1),j}[V_{121,rab11}]_j[R1{\times}N1_{rab11}]_j - k_{off,V121{\times}(R1{\times}N1),j}[V_{121}{\times}R1{\times}N1_{rab11}]_j$$
$$+ k_{on,(V121{\times}R1){\times}N1,j}[V_{121}{\times}R1_{rab11}]_j[N1_{rab11}]_j - k_{off,(V121{\times}R1){\times}N1,j}[V_{121}{\times}R1{\times}N1_{rab11}]_j$$

$$d[P1{\times}R1{\times}N1_{rab11}]_j / dt = k_{4to11,P1{\times}R1{\times}N1,j}[P1{\times}R1{\times}N1_{rab45}] - k_{rec11,P1{\times}R1{\times}N1,j}[P1{\times}R1{\times}N1_{rab11}]$$
$$+ k_{on,P1{\times}(R1{\times}N1),j}[P1_{rab11}]_j[R1{\times}N1_{rab11}]_j - k_{off,P1{\times}(R1{\times}N1),j}[P1{\times}R1{\times}N1_{rab11}]_j$$
$$+ k_{on,(P1{\times}R1){\times}N1,j}[P1{\times}R1_{rab11}]_j[N1_{rab11}]_j - k_{off,(P1{\times}R1){\times}N1,j}[P1{\times}R1{\times}N1_{rab11}]_j$$

$$d[V_{121}{\times}sR1{\times}N1_{rab11}]_j / dt = k_{4to11,V121{\times}sR1{\times}N1,j}[V_{121}{\times}sR1{\times}N1_{rab45}] - k_{\deg r,V121{\times}sR1{\times}N1,j}[V_{121}{\times}sR1{\times}N1_{rab11}]$$
$$+ k_{on,V121{\times}(sR1{\times}N1),j}[V_{121,rab11}]_j[sR1{\times}N1_{rab11}]_j - k_{off,V121{\times}(sR1{\times}N1),j}[V_{121}{\times}sR1{\times}N1_{rab11}]_j$$
$$+ k_{on,(V121{\times}sR1){\times}N1,j}[V_{121}{\times}sR1_{rab11}]_j[N1_{rab11}]_j - k_{off,(V121{\times}sR1){\times}N1,j}[V_{121}{\times}sR1{\times}N1_{rab11}]_j$$

$$d[P1{\times}sR1{\times}N1_{rab11}]_j / dt = k_{4to11,P1{\times}sR1{\times}N1,j}[P1{\times}sR1{\times}N1_{rab45}] - k_{rec11,P1{\times}sR1{\times}N1,j}[P1{\times}sR1{\times}N1_{rab11}]$$
$$+ k_{on,P1{\times}(sR1{\times}N1),j}[P1_{rab11}]_j[sR1{\times}N1_{rab11}]_j - k_{off,P1{\times}(sR1{\times}N1),j}[P1{\times}sR1{\times}N1_{rab11}]_j$$
$$+ k_{on,(P1{\times}sR1){\times}N1,j}[P1{\times}sR1_{rab11}]_j[N1_{rab11}]_j - k_{off,(P1{\times}sR1){\times}N1,j}[P1{\times}sR1{\times}N1_{rab11}]_j$$

Interstitial Fluid. These 11 equations describe the free species found in the interstitial fluid in tissues, including free VEGF, PlGF, and sR1, and complexes of sR1 with ligands. q_X is the constant secretion of VEGF or PlGF isoforms from myocytes (molecules/myonuclear domain/s), or of sR1 from endothelial cells (molecules/EC/s), as given in **Table 6-4**, and converted into moles/cm^3 tissue. All molecular species in the interstitial fluid can be transported into the blood via lymphatic drainage (k_L in cm^3/s), or moved between the blood and tissue via bi-directional vascular permeability (k_p in cm/s). (See **Table 6-S10** for transport parameter values.) Vascular permeability depends on the total abluminal EC surface area, S_{jB} (cm^2). The endothelial cell surface recruitment factor γ is always one in this study, but can be used to account for changes in transport as a result of altered perfusion or vasodilation. As detailed above, U represents a volume, while K_{Av} is the fraction of the volume that is available. These geometric factors are included to account for the relevant volumes in the tissue and blood for exchange of molecular species; when one molecule is transported between tissue j and the blood, the concentration changes in j and the blood depend on the respective volumes.

$$
\begin{aligned}
d[V_{165}]_j / dt = {} & q_{V165,j} - \frac{k_{L,j}}{U_j} \frac{[V_{165}]_j}{K_{Av,j}} + \frac{\gamma_j \cdot S_{jB}}{U_j} \cdot \left(k_{p,V}^{B \to j} \frac{[V_{165}]_B}{K_{AV,B}} - k_{p,V}^{j \to B} \frac{[V_{165}]_j}{K_{AV,j}} \right) \\
& - k_{on,V165 \cdot M,j}[V_{165}]_j[M_{EBM}]_j + k_{off,V165 \cdot M,j}[V_{165} \cdot M_{EBM}]_j \\
& - k_{on,V165 \cdot M,j}[V_{165}]_j[M_{ECM}]_j + k_{off,V165 \cdot M,j}[V_{165} \cdot M_{ECM}]_j \\
& - k_{on,V165 \cdot M,j}[V_{165}]_j[M_{PBM}]_j + k_{off,V165 \cdot M,j}[V_{165} \cdot M_{PBM}]_j \\
& - k_{on,V165 \cdot N1,j}[V_{165}]_j[N1]_j + k_{off,V165 \cdot N1,j}[V_{165} \cdot N1]_j \\
& - k_{on,V165 \cdot R2,j}[V_{165}]_j[R2]_j + k_{off,V165 \cdot R2,j}[V_{165} \cdot R2]_j \\
& - k_{on,V165 \cdot R1,j}[V_{165}]_j[R1]_j + k_{off,V165 \cdot R1,j}[V_{165} \cdot R1]_j \\
& - k_{on,V165 \cdot sR1,j}[V_{165}]_j[sR1]_j + k_{off,V165 \cdot sR1,j}[V_{165} \cdot sR1]_j
\end{aligned}
$$

$$d[V_{189}]_j / dt = q_{V189,j} - \frac{k_{L,j}}{U_j} \frac{[V_{189}]_j}{K_{Av,j}} + \frac{\gamma_j \cdot S_{jB}}{U_j} \cdot \left(k_{p,V}^{B \to j} \frac{[V_{189}]_B}{K_{AV,B}} - k_{p,V}^{j \to B} \frac{[V_{189}]_j}{K_{AV,j}} \right)$$

$$- k_{on,V189\cdot M,j}[V_{189}]_j[M_{EBM}]_j + k_{off,V189\cdot M,j}[V_{189} \cdot M_{EBM}]_j$$

$$- k_{on,V189\cdot M,j}[V_{189}]_j[M_{ECM}]_j + k_{off,V189\cdot M,j}[V_{189} \cdot M_{ECM}]_j$$

$$- k_{on,V189\cdot M,j}[V_{189}]_j[M_{PBM}]_j + k_{off,V189\cdot M,j}[V_{189} \cdot M_{PBM}]_j$$

$$- k_{on,V189\cdot N1,j}[V_{189}]_j[N1]_j + k_{off,V189\cdot N1,j}[V_{189} \cdot N1]_j$$

$$- k_{on,V189\cdot R2,j}[V_{189}]_j[R2]_j + k_{off,V189\cdot R2,j}[V_{189} \cdot R2]_j$$

$$- k_{on,V189\cdot R1,j}[V_{189}]_j[R1]_j + k_{off,V189\cdot R1,j}[V_{189} \cdot R1]_j$$

$$- k_{on,V189\cdot sR1,j}[V_{189}]_j[sR1]_j + k_{off,V189\cdot sR1,j}[V_{189} \cdot sR1]_j$$

$$d[V_{121}]_j / dt = q_{V121,j} - \frac{k_{L,j}}{U_j} \frac{[V_{121}]_j}{K_{Av,j}} + \frac{\gamma_j \cdot S_{jB}}{U_j} \cdot \left(k_{p,V}^{B \to j} \frac{[V_{121}]_B}{K_{AV,B}} - k_{p,V}^{j \to B} \frac{[V_{121}]_j}{K_{AV,j}} \right)$$

$$- k_{on,V121\cdot R2,j}[V_{121}]_j[R2]_j + k_{off,V121\cdot R2,j}[V_{121} \cdot R2]_j$$

$$- k_{on,V121\cdot R1,j}[V_{121}]_j[R1]_j + k_{off,V121\cdot R1,j}[V_{121} \cdot R1]_j$$

$$- k_{on,V121\cdot(R1\cdot N1),j}[V_{121}]_j[R1 \cdot N1]_j + k_{off,V121\cdot(R1\cdot N1),j}[V_{121} \cdot R1 \cdot N1]_j$$

$$- k_{on,V121\cdot sR1,j}[V_{121}]_j[sR1]_j + k_{off,V121\cdot sR1,j}[V_{121} \cdot sR1]_j$$

$$- k_{on,V121\cdot(sR1\cdot N1),j}[V_{121}]_j[sR1 \cdot N1]_j + k_{off,V121\cdot(sR1\cdot N1),j}[V_{121} \cdot sR1 \cdot N1]_j$$

$$- k_{on,V121\cdot(sR1\cdot M),j}[V_{121}]_j[sR1 \cdot M_{EBM}]_j + k_{off,V121\cdot(sR1\cdot M),j}[V_{121} \cdot sR1 \cdot M_{EBM}]_j$$

$$- k_{on,V121\cdot(sR1\cdot M),j}[V_{121}]_j[sR1 \cdot M_{ECM}]_j + k_{off,V121\cdot(sR1\cdot M),j}[V_{121} \cdot sR1 \cdot M_{ECM}]_j$$

$$- k_{on,V121\cdot(sR1\cdot M),j}[V_{121}]_j[sR1 \cdot M_{PBM}]_j + k_{off,V121\cdot(sR1\cdot M),j}[V_{121} \cdot sR1 \cdot M_{PBM}]_j$$

$$d[P1]_j / dt = q_{P1,j} - \frac{k_{L,j}}{U_j} \frac{[P1]_j}{K_{Av,j}} + \frac{\gamma_j \cdot S_{jB}}{U_j} \cdot \left(k_{p,P}^{B \to j} \frac{[P1]_B}{K_{AV,B}} - k_{p,P}^{j \to B} \frac{[P]_j}{K_{AV,j}} \right)$$

$$- k_{on,P1\cdot R1,j}[P1]_j[R1]_j + k_{off,P1\cdot R1,j}[P1 \cdot R1]_j$$

$$- k_{on,P1\cdot(R1\cdot N1),j}[P1]_j[R1 \cdot N1]_j + k_{off,P1\cdot(R1\cdot N1),j}[P1 \cdot R1 \cdot N1]_j$$

$$- k_{on,P1\cdot sR1,j}[P1]_j[sR1]_j + k_{off,P1\cdot sR1,j}[P1 \cdot sR1]_j$$

$$- k_{on,P1\cdot(sR1\cdot N1),j}[P1]_j[sR1 \cdot N1]_j + k_{off,P1\cdot(sR1\cdot N1),j}[P1 \cdot sR1 \cdot N1]_j$$

$$- k_{on,P1\cdot(sR1\cdot M),j}[P1]_j[sR1 \cdot M_{EBM}]_j + k_{off,P1\cdot(sR1\cdot M),j}[P1 \cdot sR1 \cdot M_{EBM}]_j$$

$$- k_{on,P1\cdot(sR1\cdot M),j}[P1]_j[sR1 \cdot M_{ECM}]_j + k_{off,P1\cdot(sR1\cdot M),j}[P1 \cdot sR1 \cdot M_{ECM}]_j$$

$$- k_{on,P1\cdot(sR1\cdot M),j}[P1]_j[sR1 \cdot M_{PBM}]_j + k_{off,P1\cdot(sR1\cdot M),j}[P1 \cdot sR1 \cdot M_{PBM}]_j$$

$$d[P2]_j / dt = q_{P2,j} - \frac{k_{L,j}}{U_j}\frac{[P2]_j}{K_{Av,j}} + \frac{\gamma_j \cdot S_{jB}}{U_j} \cdot \left(k_{p,P}^{B \to j}\frac{[P2]_B}{K_{AV,B}} - k_{p,P}^{j \to B}\frac{[P2]_j}{K_{AV,j}} \right)$$

$$-k_{on,P2 \cdot M,j}[P2]_j[M_{EBM}]_j + k_{off,P2 \cdot M,j}[P2 \cdot M_{EBM}]_j$$

$$-k_{on,P2 \cdot M,j}[P2]_j[M_{ECM}]_j + k_{off,P2 \cdot M,j}[P2 \cdot M_{ECM}]_j$$

$$-k_{on,P2 \cdot M,j}[P2]_j[M_{PBM}]_j + k_{off,P2 \cdot M,j}[P2 \cdot M_{PBM}]_j$$

$$-k_{on,P2 \cdot N1,j}[P2]_j[N1]_j + k_{off,P2 \cdot N1,j}[P2 \cdot N1]_j$$

$$-k_{on,P2 \cdot R1,j}[P2]_j[R1]_j + k_{off,P2 \cdot R1,j}[P2 \cdot R1]_j$$

$$-k_{on,P2 \cdot sR1,j}[P2]_j[sR1]_j + k_{off,P2 \cdot sR1,j}[P2 \cdot sR1]_j$$

$$d[sR1]_j / dt = q_{sR1,j} - \frac{k_{L,j}}{U_j}\frac{[sR1]_j}{K_{Av,j}} + \frac{\gamma_j \cdot S_{jB}}{U_j} \cdot \left(k_{p,sR1}^{B \to j}\frac{[sR1]_B}{K_{AV,B}} - k_{p,sR1}^{j \to B}\frac{[sR1]_j}{K_{AV,j}} \right)$$

$$-k_{on,V165 \cdot sR1,j}[V_{165}]_j[sR1]_j + k_{off,V165 \cdot sR1,j}[V_{165} \cdot sR1]_j$$

$$-k_{on,V189 \cdot sR1,j}[V_{189}]_j[sR1]_j + k_{off,V189 \cdot sR1,j}[V_{189} \cdot sR1]_j$$

$$-k_{on,V121 \cdot sR1,j}[V_{121}]_j[sR1]_j + k_{off,V121 \cdot sR1,j}[V_{121} \cdot sR1]_j$$

$$-k_{on,P1 \cdot sR1,j}[P1]_j[sR1]_j + k_{off,P1 \cdot sR1,j}[P1 \cdot sR1]_j$$

$$-k_{on,P2 \cdot sR1,j}[P2]_j[sR1]_j + k_{off,P2 \cdot sR1,j}[P2 \cdot sR1]_j$$

$$-k_{on,sR1 \cdot M,j}[sR1]_j[M_{EBM}]_j + k_{off,sR1 \cdot M,j}[sR1 \cdot M_{EBM}]_j$$

$$-k_{on,sR1 \cdot M,j}[sR1]_j[M_{ECM}]_j + k_{off,sR1 \cdot M,j}[sR1 \cdot M_{ECM}]_j$$

$$-k_{on,sR1 \cdot M,j}[sR1]_j[M_{PBM}]_j + k_{off,sR1 \cdot M,j}[sR1 \cdot M_{PBM}]_j$$

$$-k_{on,sR1 \cdot N1,j}[sR1]_j[N1]_j + k_{off,sR1 \cdot N1,j}[sR1 \cdot N1]_j$$

$$-k_{on,sR1 \cdot (V165 \cdot M),j}[sR1]_j[V_{165} \cdot M_{EBM}]_j + k_{off,sR1 \cdot (V165 \cdot M),j}[sR1 \cdot V_{165} \cdot M_{EBM}]_j$$

$$-k_{on,sR1 \cdot (V189 \cdot M),j}[sR1]_j[V_{189} \cdot M_{EBM}]_j + k_{off,sR1 \cdot (V189 \cdot M),j}[sR1 \cdot V_{189} \cdot M_{EBM}]_j$$

$$-k_{on,sR1 \cdot (P2 \cdot M),j}[sR1]_j[P2 \cdot M_{EBM}]_j + k_{off,sR1 \cdot (P2 \cdot M),j}[sR1 \cdot P2 \cdot M_{EBM}]_j$$

$$-k_{on,sR1 \cdot (V165 \cdot M),j}[sR1]_j[V_{165} \cdot M_{ECM}]_j + k_{off,sR1 \cdot (V165 \cdot M),j}[sR1 \cdot V_{165} \cdot M_{ECM}]_j$$

$$-k_{on,sR1 \cdot (V189 \cdot M),j}[sR1]_j[V_{189} \cdot M_{ECM}]_j + k_{off,sR1 \cdot (V189 \cdot M),j}[sR1 \cdot V_{189} \cdot M_{ECM}]_j$$

$$-k_{on,sR1 \cdot (P2 \cdot M),j}[sR1]_j[P2 \cdot M_{ECM}]_j + k_{off,sR1 \cdot (P2 \cdot M),j}[sR1 \cdot P2 \cdot M_{ECM}]_j$$

$$-k_{on,sR1 \cdot (V165 \cdot M),j}[sR1]_j[V_{165} \cdot M_{PBM}]_j + k_{off,sR1 \cdot (V165 \cdot M),j}[sR1 \cdot V_{165} \cdot M_{PBM}]_j$$

$$-k_{on,sR1 \cdot (V189 \cdot M),j}[sR1]_j[V_{189} \cdot M_{PBM}]_j + k_{off,sR1 \cdot (V189 \cdot M),j}[sR1 \cdot V_{189} \cdot M_{PBM}]_j$$

$$-k_{on,sR1 \cdot (P2 \cdot M),j}[sR1]_j[P2 \cdot M_{PBM}]_j + k_{off,sR1 \cdot (P2 \cdot M),j}[sR1 \cdot P2 \cdot M_{PBM}]_j$$

$$d[V_{165} \cdot sR1]_j / dt = -\frac{k_{L,j}}{U_j} \frac{[V_{165} \cdot sR1]_j}{K_{Av,j}} + \frac{\gamma_j \cdot S_{jB}}{U_j} \cdot \left(k_{p,sR1}^{B \to j} \frac{[V_{165} \cdot sR1]_B}{K_{AV,B}} - k_{p,sR1}^{j \to B} \frac{[V_{165} \cdot sR1]_j}{K_{AV,j}} \right)$$

$$+ k_{on,V165 \cdot sR1,j}[V_{165}]_j[sR1]_j - k_{off,V165 \cdot sR1,j}[V_{165} \cdot sR1]_j$$

$$- k_{on,M \cdot (V165 \cdot sR1),j}[M_{EBM}]_j[V_{165} \cdot sR1]_j + k_{off,M \cdot (V165 \cdot sR1),j}[M_{EBM} \cdot V_{165} \cdot sR1]_j$$

$$- k_{on,M \cdot (V165 \cdot sR1),j}[M_{ECM}]_j[V_{165} \cdot sR1]_j + k_{off,M \cdot (V165 \cdot sR1),j}[M_{ECM} \cdot V_{165} \cdot sR1]_j$$

$$- k_{on,M \cdot (V165 \cdot sR1),j}[M_{PBM}]_j[V_{165} \cdot sR1]_j + k_{off,M \cdot (V165 \cdot sR1),j}[M_{PBM} \cdot V_{165} \cdot sR1]_j$$

$$d[V_{189} \cdot sR1]_j / dt = -\frac{k_{L,j}}{U_j} \frac{[V_{189} \cdot sR1]_j}{K_{Av,j}} + \frac{\gamma_j \cdot S_{jB}}{U_j} \cdot \left(k_{p,sR1}^{B \to j} \frac{[V_{189} \cdot sR1]_B}{K_{AV,B}} - k_{p,sR1}^{j \to B} \frac{[V_{189} \cdot sR1]_j}{K_{AV,j}} \right)$$

$$+ k_{on,V189 \cdot sR1,j}[V_{189}]_j[sR1]_j - k_{off,V189 \cdot sR1,j}[V_{189} \cdot sR1]_j$$

$$- k_{on,M \cdot (V189 \cdot sR1),j}[M_{EBM}]_j[V_{189} \cdot sR1]_j + k_{off,M \cdot (V189 \cdot sR1),j}[M_{EBM} \cdot V_{189} \cdot sR1]_j$$

$$- k_{on,M \cdot (V189 \cdot sR1),j}[M_{ECM}]_j[V_{189} \cdot sR1]_j + k_{off,M \cdot (V189 \cdot sR1),j}[M_{ECM} \cdot V_{189} \cdot sR1]_j$$

$$- k_{on,M \cdot (V189 \cdot sR1),j}[M_{PBM}]_j[V_{189} \cdot sR1]_j + k_{off,M \cdot (V189 \cdot sR1),j}[M_{PBM} \cdot V_{189} \cdot sR1]_j$$

$$d[V_{121} \cdot sR1]_j / dt = -\frac{k_{L,j}}{U_j} \frac{[V_{121} \cdot sR1]_j}{K_{Av,j}} + \frac{\gamma_j \cdot S_{jB}}{U_j} \cdot \left(k_{p,sR1}^{B \to j} \frac{[V_{121} \cdot sR1]_B}{K_{AV,B}} - k_{p,sR1}^{j \to B} \frac{[V_{121} \cdot sR1]_j}{K_{AV,j}} \right)$$

$$+ k_{on,V121 \cdot sR1,j}[V_{121}]_j[sR1]_j - k_{off,V121 \cdot sR1,j}[V_{121} \cdot sR1]_j$$

$$- k_{on,(M \cdot sR1) \cdot V121,j}[M_{EBM} \cdot sR1]_j[V_{121}]_j + k_{off,(M \cdot sR1) \cdot V121,j}[M_{EBM} \cdot sR1 \cdot V_{121}]_j$$

$$- k_{on,(M \cdot sR1) \cdot V121,j}[M_{ECM} \cdot sR1]_j[V_{121}]_j + k_{off,(M \cdot sR1) \cdot V121,j}[M_{ECM} \cdot sR1 \cdot V_{121}]_j$$

$$- k_{on,(M \cdot sR1) \cdot V121,j}[M_{PBM} \cdot sR1]_j[V_{121}]_j + k_{off,(M \cdot sR1) \cdot V121,j}[M_{PBM} \cdot sR1 \cdot V_{121}]_j$$

$$d[P1 \cdot sR1]_j / dt = -\frac{k_{L,j}}{U_j} \frac{[P1 \cdot sR1]_j}{K_{Av,j}} + \frac{\gamma_j \cdot S_{jB}}{U_j} \cdot \left(k_{p,sR1}^{B \to j} \frac{[P1 \cdot sR1]_B}{K_{AV,B}} - k_{p,sR1}^{j \to B} \frac{[P1 \cdot sR1]_j}{K_{AV,j}} \right)$$

$$+ k_{on,P1 \cdot sR1,j}[P1]_j[sR1]_j - k_{off,P1 \cdot sR1,j}[P1 \cdot sR1]_j$$

$$- k_{on,(M \cdot sR1) \cdot P1,j}[M_{EBM} \cdot sR1]_j[P1]_j + k_{off,(M \cdot sR1) \cdot P1,j}[M_{EBM} \cdot sR1 \cdot P1]_j$$

$$- k_{on,(M \cdot sR1) \cdot P1,j}[M_{ECM} \cdot sR1]_j[P1]_j + k_{off,(M \cdot sR1) \cdot P1,j}[M_{ECM} \cdot sR1 \cdot P1]_j$$

$$- k_{on,(M \cdot sR1) \cdot P1,j}[M_{PBM} \cdot sR1]_j[P1]_j + k_{off,(M \cdot sR1) \cdot P1,j}[M_{PBM} \cdot sR1 \cdot P1]_j$$

$$d[P2 \cdot sR1]_j / dt = -\frac{k_{L,j}}{U_j}\frac{[P2 \cdot sR1]_j}{K_{Av,j}} + \frac{\gamma_j \cdot S_{jB}}{U_j} \cdot \left(k_{p,sR1}^{B \to j}\frac{[P2 \cdot sR1]_B}{K_{AV,B}} - k_{p,sR1}^{j \to B}\frac{[P2 \cdot sR1]_j}{K_{AV,j}} \right)$$

$$+ k_{on,P2 \cdot sR1,j}[P2]_j[sR1]_j - k_{off,P2 \cdot sR1,j}[P2 \cdot sR1]_j$$

$$- k_{on,M \cdot (P2 \cdot sR1),j}[M_{EBM}]_j[P2 \cdot sR1]_j + k_{off,M \cdot (P2 \cdot sR1),j}[M_{EBM} \cdot P2 \cdot sR1]_j$$

$$- k_{on,M \cdot (P2 \cdot sR1),j}[M_{ECM}]_j[P2 \cdot sR1]_j + k_{off,M \cdot (P2 \cdot sR1),j}[M_{ECM} \cdot P2 \cdot sR1]_j$$

$$- k_{on,M \cdot (P2 \cdot sR1),j}[M_{PBM}]_j[P2 \cdot sR1]_j + k_{off,M \cdot (P2 \cdot sR1),j}[M_{PBM} \cdot P2 \cdot sR1]_j$$

A.2.3 Blood Equations

The final set of 11 equations describes the binding and unbinding of molecular species in the blood, as well as clearance (k_{CL} in s^{-1}, see **Table 6-S10**). In this model, we assume no secretion of any molecular species directly into the blood.

$$d[V_{165}]_B / dt = -k_{CL,V165} + \frac{k_{L,N}}{U_B}\frac{[V_{165}]_N}{K_{Av,N}} + \frac{k_{L,D}}{U_B}\frac{[V_{165}]_D}{K_{Av,D}}$$

$$+ \frac{\gamma_N \cdot S_{NB}}{U_B} \cdot \left(k_{p,V}^{N \to B}\frac{[V_{165}]_N}{K_{AV,N}} - k_{p,V}^{B \to N}\frac{[V_{165}]_B}{K_{AV,B}} \right)$$

$$+ \frac{\gamma_D \cdot S_{DB}}{U_B} \cdot \left(k_{p,V}^{D \to B}\frac{[V_{165}]_D}{K_{AV,D}} - k_{p,V}^{B \to D}\frac{[V_{165}]_B}{K_{AV,B}} \right)$$

$$- k_{on,V165 \cdot sR1}[V_{165}]_B[sR1]_B + k_{off,V165 \cdot sR1,j}[V_{165} \cdot sR1]_B$$

$$d[V_{189}]_B / dt = -k_{CL,V189} + \frac{k_{L,N}}{U_B}\frac{[V_{189}]_N}{K_{Av,N}} + \frac{k_{L,D}}{U_B}\frac{[V_{189}]_D}{K_{Av,D}}$$

$$+ \frac{\gamma_N \cdot S_{NB}}{U_B} \cdot \left(k_{p,V}^{N \to B}\frac{[V_{189}]_N}{K_{AV,N}} - k_{p,V}^{B \to N}\frac{[V_{189}]_B}{K_{AV,B}} \right)$$

$$+ \frac{\gamma_D \cdot S_{DB}}{U_B} \cdot \left(k_{p,V}^{D \to B}\frac{[V_{189}]_D}{K_{AV,D}} - k_{p,V}^{B \to D}\frac{[V_{189}]_B}{K_{AV,B}} \right)$$

$$- k_{on,V189 \cdot sR1}[V_{189}]_B[sR1]_B + k_{off,V189 \cdot sR1,j}[V_{189} \cdot sR1]_B$$

$$d[V_{121}]_B / dt = -k_{CL,V121} + \frac{k_{L,N}}{U_B} \frac{[V_{121}]_N}{K_{Av,N}} + \frac{k_{L,D}}{U_B} \frac{[V_{121}]_D}{K_{Av,D}}$$

$$+ \frac{\gamma_N \cdot S_{NB}}{U_B} \cdot \left(k_{p,V}^{N \to B} \frac{[V_{121}]_N}{K_{AV,N}} - k_{p,V}^{B \to N} \frac{[V_{121}]_B}{K_{AV,B}} \right)$$

$$+ \frac{\gamma_D \cdot S_{DB}}{U_B} \cdot \left(k_{p,V}^{D \to B} \frac{[V_{121}]_D}{K_{AV,D}} - k_{p,V}^{B \to D} \frac{[V_{121}]_B}{K_{AV,B}} \right)$$

$$- k_{on,V121 \cdot sR1}[V_{121}]_B[sR1]_B + k_{off,V121 \cdot sR1,j}[V_{121} \cdot sR1]_B$$

$$d[P1]_B / dt = -k_{CL,P1} + \frac{k_{L,N}}{U_B} \frac{[P1]_N}{K_{Av,N}} + \frac{k_{L,D}}{U_B} \frac{[P1]_D}{K_{Av,D}}$$

$$+ \frac{\gamma_N \cdot S_{NB}}{U_B} \cdot \left(k_{p,P}^{N \to B} \frac{[P1]_N}{K_{AV,N}} - k_{p,P}^{B \to N} \frac{[P1]_B}{K_{AV,B}} \right)$$

$$+ \frac{\gamma_D \cdot S_{DB}}{U_B} \cdot \left(k_{p,P}^{D \to B} \frac{[P1]_D}{K_{AV,D}} - k_{p,P}^{B \to D} \frac{[P1]_B}{K_{AV,B}} \right)$$

$$- k_{on,P1 \cdot sR1}[P1]_B[sR1]_B + k_{off,P1 \cdot sR1,j}[P1 \cdot sR1]_B$$

$$d[P2]_B / dt = -k_{CL,P2} + \frac{k_{L,N}}{U_B} \frac{[P2]_N}{K_{Av,N}} + \frac{k_{L,D}}{U_B} \frac{[P2]_D}{K_{Av,D}}$$

$$+ \frac{\gamma_N \cdot S_{NB}}{U_B} \cdot \left(k_{p,P}^{N \to B} \frac{[P2]_N}{K_{AV,N}} - k_{p,P}^{B \to N} \frac{[P2]_B}{K_{AV,B}} \right)$$

$$+ \frac{\gamma_D \cdot S_{DB}}{U_B} \cdot \left(k_{p,P}^{D \to B} \frac{[P2]_D}{K_{AV,D}} - k_{p,P}^{B \to D} \frac{[P2]_B}{K_{AV,B}} \right)$$

$$- k_{on,P2 \cdot sR1}[P2]_B[sR1]_B + k_{off,P2 \cdot sR1,j}[P2 \cdot sR1]_B$$

$$d[sR1]_B / dt = -k_{CL,sR1} + \frac{k_{L,N}}{U_B} \frac{[sR1]_N}{K_{Av,N}} + \frac{k_{L,D}}{U_B} \frac{[sR1]_D}{K_{Av,D}}$$

$$+ \frac{\gamma_N \cdot S_{NB}}{U_B} \cdot \left(k_{p,sR1}^{N \to B} \frac{[sR1]_N}{K_{AV,N}} - k_{p,sR1}^{B \to N} \frac{[sR1]_B}{K_{AV,B}} \right)$$

$$+ \frac{\gamma_D \cdot S_{DB}}{U_B} \cdot \left(k_{p,sR1}^{D \to B} \frac{[sR1]_D}{K_{AV,D}} - k_{p,sR1}^{B \to D} \frac{[sR1]_B}{K_{AV,B}} \right)$$

$$- k_{on,V165 \cdot sR1}[V_{165}]_B[sR1]_B + k_{off,V165 \cdot sR1,j}[V_{165} \cdot sR1]_B$$

$$- k_{on,V189 \cdot sR1}[V_{189}]_B[sR1]_B + k_{off,V189 \cdot sR1,j}[V_{189} \cdot sR1]_B$$

$$- k_{on,V121 \cdot sR1}[V_{121}]_B[sR1]_B + k_{off,V121 \cdot sR1,j}[V_{121} \cdot sR1]_B$$

$$- k_{on,P1 \cdot sR1}[P1]_B[sR1]_B + k_{off,P1 \cdot sR1,j}[P1 \cdot sR1]_B$$

$$- k_{on,P2 \cdot sR1}[P2]_B[sR1]_B + k_{off,P2 \cdot sR1,j}[P2 \cdot sR1]_B$$

$$d[V_{165} \cdot sR1]_B / dt = -k_{CL,V165 \cdot sR1} + \frac{k_{L,N}}{U_B} \frac{[V_{165} \cdot sR1]_N}{K_{Av,N}} + \frac{k_{L,D}}{U_B} \frac{[V_{165} \cdot sR1]_D}{K_{Av,D}}$$

$$+ \frac{\gamma_N \cdot S_{NB}}{U_B} \cdot \left(k_{p,sR1}^{N \to B} \frac{[V_{165} \cdot sR1]_N}{K_{AV,N}} - k_{p,sR1}^{B \to N} \frac{[V_{165} \cdot sR1]_B}{K_{AV,B}} \right)$$

$$+ \frac{\gamma_D \cdot S_{DB}}{U_B} \cdot \left(k_{p,sR1}^{D \to B} \frac{[V_{165} \cdot sR1]_D}{K_{AV,D}} - k_{p,sR1}^{B \to D} \frac{[V_{165} \cdot sR1]_B}{K_{AV,B}} \right)$$

$$+ k_{on,V165 \cdot sR1}[V_{165}]_B[sR1]_B - k_{off,V165 \cdot sR1,j}[V_{165} \cdot sR1]_B$$

$$d[V_{189} \cdot sR1]_B / dt = -k_{CL,V189 \cdot sR1} + \frac{k_{L,N}}{U_B} \frac{[V_{189} \cdot sR1]_N}{K_{Av,N}} + \frac{k_{L,D}}{U_B} \frac{[V_{189} \cdot sR1]_D}{K_{Av,D}}$$

$$+ \frac{\gamma_N \cdot S_{NB}}{U_B} \cdot \left(k_{p,sR1}^{N \to B} \frac{[V_{189} \cdot sR1]_N}{K_{AV,N}} - k_{p,sR1}^{B \to N} \frac{[V_{189} \cdot sR1]_B}{K_{AV,B}} \right)$$

$$+ \frac{\gamma_D \cdot S_{DB}}{U_B} \cdot \left(k_{p,sR1}^{D \to B} \frac{[V_{189} \cdot sR1]_D}{K_{AV,D}} - k_{p,sR1}^{B \to D} \frac{[V_{189} \cdot sR1]_B}{K_{AV,B}} \right)$$

$$+ k_{on,V189 \cdot sR1}[V_{189}]_B[sR1]_B - k_{off,V189 \cdot sR1,j}[V_{189} \cdot sR1]_B$$

$$d[V_{121} \cdot sR1]_B / dt = -k_{CL,V121 \cdot sR1} + \frac{k_{L,N}}{U_B} \frac{[V_{121} \cdot sR1]_N}{K_{Av,N}} + \frac{k_{L,D}}{U_B} \frac{[V_{121} \cdot sR1]_D}{K_{Av,D}}$$

$$+ \frac{\gamma_N \cdot S_{NB}}{U_B} \cdot \left(k_{p,sR1}^{N \to B} \frac{[V_{121} \cdot sR1]_N}{K_{AV,N}} - k_{p,sR1}^{B \to N} \frac{[V_{121} \cdot sR1]_B}{K_{AV,B}} \right)$$

$$+ \frac{\gamma_D \cdot S_{DB}}{U_B} \cdot \left(k_{p,sR1}^{D \to B} \frac{[V_{121} \cdot sR1]_D}{K_{AV,D}} - k_{p,sR1}^{B \to D} \frac{[V_{121} \cdot sR1]_B}{K_{AV,B}} \right)$$

$$+ k_{on,V121 \cdot sR1}[V_{121}]_B [sR1]_B - k_{off,V121 \cdot sR1,j}[V_{121} \cdot sR1]_B$$

$$d[P1 \cdot sR1]_B / dt = -k_{CL,P1 \cdot sR1} + \frac{k_{L,N}}{U_B} \frac{[P1 \cdot sR1]_N}{K_{Av,N}} + \frac{k_{L,D}}{U_B} \frac{[P1 \cdot sR1]_D}{K_{Av,D}}$$

$$+ \frac{\gamma_N \cdot S_{NB}}{U_B} \cdot \left(k_{p,sR1}^{N \to B} \frac{[P1 \cdot sR1]_N}{K_{AV,N}} - k_{p,sR1}^{B \to N} \frac{[P1 \cdot sR1]_B}{K_{AV,B}} \right)$$

$$+ \frac{\gamma_D \cdot S_{DB}}{U_B} \cdot \left(k_{p,sR1}^{D \to B} \frac{[P1 \cdot sR1]_D}{K_{AV,D}} - k_{p,sR1}^{B \to D} \frac{[P1 \cdot sR1]_B}{K_{AV,B}} \right)$$

$$+ k_{on,P1 \cdot sR1}[P1]_B [sR1]_B - k_{off,P1 \cdot sR1,j}[P1 \cdot sR1]_B$$

$$d[P2 \cdot sR1]_B / dt = -k_{CL,P2 \cdot sR1} + \frac{k_{L,N}}{U_B} \frac{[P2 \cdot sR1]_N}{K_{Av,N}} + \frac{k_{L,D}}{U_B} \frac{[P2 \cdot sR1]_D}{K_{Av,D}}$$

$$+ \frac{\gamma_N \cdot S_{NB}}{U_B} \cdot \left(k_{p,sR1}^{N \to B} \frac{[P2 \cdot sR1]_N}{K_{AV,N}} - k_{p,sR1}^{B \to N} \frac{[P2 \cdot sR1]_B}{K_{AV,B}} \right)$$

$$+ \frac{\gamma_D \cdot S_{DB}}{U_B} \cdot \left(k_{p,sR1}^{D \to B} \frac{[P2 \cdot sR1]_D}{K_{AV,D}} - k_{p,sR1}^{B \to D} \frac{[P2 \cdot sR1]_B}{K_{AV,B}} \right)$$

$$+ k_{on,P2 \cdot sR1}[P2]_B [sR1]_B - k_{off,P2 \cdot sR1,j}[P2 \cdot sR1]_B$$

A.2.4 References

1.   Stefanini MO, Wu FT, Mac Gabhann F, Popel AS. A compartment model of VEGF distribution in blood, healthy and diseased tissues. BMC Systems Biology. 2008;2. doi: 10.1186/1752-0509-2-77. PubMed PMID: WOS:000259952700001.

2.   Wu FTH, Stefanini MO, Gabhann FM, Popel AS. A Compartment Model of VEGF Distribution in Humans in the Presence of Soluble VEGF Receptor-1 Acting as a Ligand Trap. Plos One. 2009;4(4). doi: 10.1371/journal.pone.0005108. PubMed PMID: WOS:000265505700013.

A.3 Equations for Human PAD Compartment Model (Chapter 7)

A.3.1 Unit Conversions

To convert between concentrations in total tissue and in interstitial fluid, the following equations are used:

$$[X]_{IS,j} = \frac{[X]_j}{K_{AV,j}} \text{ , where } K_{AV,j} = \frac{U_{IS,j}}{U_j} = \frac{\text{available interstitial volume}}{\text{total volume of tissue j}}$$

$$K_{AV,j} = \text{Available Volume Fraction} = \Phi \times f \times \varepsilon_{IS}$$

$$\Phi = \text{Partition Coefficient} = \frac{\text{available fluid volume}}{\text{interstitial fluid volume}}$$

$$f = \text{Fluid Fraction} = \frac{\text{interstitial fluid volume}}{\text{interstitial space}}$$

$$\varepsilon_{IS} = \text{Interstitial Fraction} = \frac{\text{interstitial space}}{\text{total tissue volume}}$$

Similarly, the conversion between total blood and plasma concentrations is:

$$[X]_{pl} = \frac{[X]_B}{K_{AV,B}} \text{ , where } K_{AV,B} = \frac{U_{pl}}{U_B} = \frac{\text{plasma volume}}{\text{total blood volume}}$$

A.3.2 Tissue Equations

This section lists the 152 equations (not included phospho-states) that describe all molecular interactions and transport within the tissue compartments.

Interstitial Matrix– These 34 equations describe changes in HSPG site (M) density over time in the ECM, endothelial basement membrane (EBM), and parenchymal basement membrane (PBM), either free, or bound to VEGF, PlGF, sR1, or sR1 and VEGF or PlGF. EBM-bound VEGF in the innermost 25nm of the EBM can bind to endothelial cell-surface VEGFR1, VEGFR2, and NRP1. We assume that, similar to cell-surface receptors, matrix-binding VEGF and PlGF isoforms (VEGF$_{165}$, VEGF$_{189}$, and PlGF2) can bind to HSPGs sites and sR1 simultaneously, forming M-L-sR1 complexes, where L represents the ligand (either

VEGF or PlGF). Since VEGFR1 can bind to NRP1 and $VEGF_{121}$ or PlGF1 simultaneously (and we assume also $VEGF_{165b}$), and the NRP1 and matrix-binding sites on VEGFR1 overlap, we assume that these ligands can also bind to immobilized sR1, forming L-sR1-M complexes. Thus, complexes including VEGF or PlGF, matrix, and sR1 can form for all ligands, but in different ways (see **Figure 7-S1**). To reflect this, the species in the complexes described within the equations are ordered to show the actual binding partners next to each other. $[M_{ECM}]_j$ represents the concentration of free HSPG sites in the ECM, $[V_{165}]$ the interstitial concentration of free $VEGF_{165}$, $[P1]$ the interstitial concentration of free PlGF1, $[sR1]$ the interstitial concentration of free soluble VEGFR, and $[R1]$ the concentration of unoccupied EC surface VEGFR1 (units converted to match- see [13]). The binding rates (k_{on}) and unbinding rates (k_{off}) are given in **Tables 7-S1 though 7-S9**, with units of $M^{-1}s^{-1}$ and s^{-1}, respectively. To convert the binding rates (k_{on}) into an *in vivo* context (moles/cm^3 tissue/s for each compartment), the following conversions were applied, using geometric parameters from **Table 7-S12**, as previously described [13, 14, 23]:

$$k_{on} \text{ in } \left(\frac{\text{moles}}{\text{cm}^3 \text{ tissue}}\right)^{-1} \times s^{-1} = k_{on} \text{ in } M^{-1} \times s^{-1} \times \frac{1000}{\text{available IF volume fraction}}$$

$$k_{on} \text{ in } \left(\frac{\text{moles}}{\text{cm}^3 \text{ tissue}}\right)^{-1} \cdot s^{-1} = k_{on} \text{ in } \left(\frac{moles}{cm^2 \ SA}\right)^{-1} \cdot s^{-1} \cdot \frac{1}{ESAV}$$

The resulting k_{on} values are given in **Tables S5-S7**.

$$d[M_{EBM}]_j / dt = -k_{on,V165 \times M,j}[V_{165}]_j[M_{EBM}]_j + k_{off,V165 \times M,j}[V_{165} \times M_{EBM}]_j$$

$$-k_{on,V189 \times M,j}[V_{189}]_j[M_{EBM}]_j + k_{off,V189 \times M,j}[V_{189} \times M_{EBM}]_j$$

$$-k_{on,P2 \times M,j}[P2]_j[M_{EBM}]_j + k_{off,P2 \times M,j}[P2 \times M_{EBM}]_j$$

$$-k_{on,sR1 \times M,j}[sR1]_j[M_{EBM}]_j + k_{off,sR1 \times M,j}[sR1 \times M_{EBM}]_j$$

$$-k_{on,M \times (V165 \times R2),j}[M_{EBM}]_j[V_{165} \times R2]_j + k_{off,M \times (V165 \times R2),j}[M_{EBM} \times V_{165} \times R2]_j$$

$$-k_{on,M \times (V165 \times R1),j}[M_{EBM}]_j[V_{165} \times R1]_j + k_{off,M \times (V165 \times R1),j}[M_{EBM} \times V_{165} \times R1]_j$$

$$-k_{on,M \times (V189 \times R2),j}[M_{EBM}]_j[V_{189} \times R2]_j + k_{off,M \times (V189 \times R2),j}[M_{EBM} \times V_{189} \times R2]_j$$

$$-k_{on,M \times (V189 \times R1),j}[M_{EBM}]_j[V_{189} \times R1]_j + k_{off,M \times (V189 \times R1),j}[M_{EBM} \times V_{189} \times R1]_j$$

$$-k_{on,M \times (P2 \times R1),j}[M_{EBM}]_j[P2 \times R1]_j + k_{off,M \times (P2 \times R1),j}[M_{EBM} \times P2 \times R1]_j$$

$$-k_{on,(V121 \times sR1) \times M,j}[V_{121} \times sR1]_j[M_{EBM}]_j + k_{off,(V121 \times sR1) \times M,j}[V_{121} \times sR1 \times M_{EBM}]_j$$

$$-k_{on,(V165b \times sR1) \times M,j}[V_{165b} \times sR1]_j[M_{EBM}]_j + k_{off,(V165b \times sR1) \times M,j}[V_{165b} \times sR1 \times M_{EBM}]_j$$

$$-k_{on,(P1 \times sR1) \times M,j}[P1 \times sR1]_j[M_{EBM}]_j + k_{off,(P1 \times sR1) \times M,j}[P1 \times sR1 \times M_{EBM}]_j$$

$$-k_{on,M \times (V165 \times sR1),j}[M_{EBM}]_j[V_{165} \times sR1]_j + k_{off,M \times (V165 \times sR1),j}[M_{EBM} \times V_{165} \times sR1]_j$$

$$-k_{on,M \times (V189 \times sR1),j}[M_{EBM}]_j[V_{189} \times sR1]_j + k_{off,M \times (V189 \times sR1),j}[M_{EBM} \times V_{189} \times sR1]_j$$

$$-k_{on,M \times (P2 \times sR1),j}[M_{EBM}]_j[P2 \times sR1]_j + k_{off,M \times (P2 \times sR1),j}[M_{EBM} \times P2 \times sR1]_j$$

$$d[M_{ECM}]_j / dt = -k_{on,V165 \times M,j}[V_{165}]_j[M_{ECM}]_j + k_{off,V165 \times M,j}[V_{165} \times M_{ECM}]_j$$

$$-k_{on,V189 \times M,j}[V_{189}]_j[M_{ECM}]_j + k_{off,V189 \times M,j}[V_{189} \times M_{ECM}]_j$$

$$-k_{on,P2 \times M,j}[P2]_j[M_{ECM}]_j + k_{off,P2 \times M,j}[P2 \times M_{ECM}]_j$$

$$-k_{on,sR1 \times M,j}[sR1]_j[M_{ECM}]_j + k_{off,sR1 \times M,j}[sR1 \times M_{ECM}]_j$$

$$-k_{on,(V121 \times sR1) \times M,j}[V_{121} \times sR1]_j[M_{ECM}]_j + k_{off,(V121 \times sR1) \times M,j}[V_{121} \times sR1 \times M_{ECM}]_j$$

$$-k_{on,(V165b \times sR1) \times M,j}[V_{165b} \times sR1]_j[M_{ECM}]_j + k_{off,(V165b \times sR1) \times M,j}[V_{165b} \times sR1 \times M_{ECM}]_j$$

$$-k_{on,(P1 \times sR1) \times M,j}[P1 \times sR1]_j[M_{ECM}]_j + k_{off,(P1 \times sR1) \times M,j}[P1 \times sR1 \times M_{ECM}]_j$$

$$-k_{on,M \times (V165 \times sR1),j}[M_{ECM}]_j[V_{165} \times sR1]_j + k_{off,M \times (V165 \times sR1),j}[M_{ECM} \times V_{165} \times sR1]_j$$

$$-k_{on,M \times (V189 \times sR1),j}[M_{ECM}]_j[V_{189} \times sR1]_j + k_{off,M \times (V189 \times sR1),j}[M_{ECM} \times V_{189} \times sR1]_j$$

$$-k_{on,M \times (P2 \times sR1),j}[M_{ECM}]_j[P2 \times sR1]_j + k_{off,M \times (P2 \times sR1),j}[M_{ECM} \times P2 \times sR1]_j$$

$$d[M_{PBM}]_j / dt = -k_{on,V165\times M,j}[V_{165}]_j[M_{PBM}]_j + k_{off,V165\times M,j}[V_{165}\times M_{PBM}]_j$$
$$-k_{on,V189\times M,j}[V_{189}]_j[M_{PBM}]_j + k_{off,V189\times M,j}[V_{189}\times M_{PBM}]_j$$
$$-k_{on,P2\times M,j}[P2]_j[M_{PBM}]_j + k_{off,P2\times M,j}[P2\times M_{PBM}]_j$$
$$-k_{on,sR1\times M,j}[sR1]_j[M_{PBM}]_j + k_{off,sR1\times M,j}[sR1\times M_{PBM}]_j$$
$$-k_{on,(V121\times sR1)\times M,j}[V_{121}\times sR1]_j[M_{PBM}]_j + k_{off,(V121\times sR1)\times M,j}[V_{121}\times sR1\times M_{PBM}]_j$$
$$-k_{on,(V165b\times sR1)\times M,j}[V_{165b}\times sR1]_j[M_{PBM}]_j + k_{off,(V165b\times sR1)\times M,j}[V_{165b}\times sR1\times M_{PBM}]_j$$
$$-k_{on,(P1\times sR1)\times M,j}[P1\times sR1]_j[M_{PBM}]_j + k_{off,(P1\times sR1)\times M,j}[P1\times sR1\times M_{PBM}]_j$$
$$-k_{on,M\times(V165\times sR1),j}[M_{PBM}]_j[V_{165}\times sR1]_j + k_{off,M\times(V165\times sR1),j}[M_{PBM}\times V_{165}\times sR1]_j$$
$$-k_{on,M\times(V189\times sR1),j}[M_{PBM}]_j[V_{189}\times sR1]_j + k_{off,M\times(V189\times sR1),j}[M_{PBM}\times V_{189}\times sR1]_j$$
$$-k_{on,M\times(P2\times sR1),j}[M_{PBM}]_j[P2\times sR1]_j + k_{off,M\times(P2\times sR1),j}[M_{PBM}\times P2\times sR1]_j$$

$$d[V_{165}\times M_{EBM}]_j / dt = k_{on,V165\times M,j}[V_{165}]_j[M_{EBM}]_j - k_{off,V165\times M,j}[V_{165}\times M_{EBM}]_j$$
$$-k_{on,(M\times V165)\times R2,j}[M_{EBM}\times V_{165}]_j[R2]_j + k_{off,(M\times V165)\times R2,j}[M_{EBM}\times V_{165}\times R2]_j$$
$$-k_{on,(M\times V165)\times R1,j}[M_{EBM}\times V_{165}]_j[R1]_j + k_{off,(M\times V165)\times R1,j}[M_{EBM}\times V_{165}\times R1]_j$$
$$-k_{on,(M\times V165)\times sR1,j}[M_{EBM}\times V_{165}]_j[sR1]_j + k_{off,(M\times V165)\times sR1,j}[M_{EBM}\times V_{165}\times sR1]_j$$

$$d[V_{189}\times M_{EBM}]_j / dt = k_{on,V189\times M,j}[V_{189}]_j[M_{EBM}]_j - k_{off,V189\times M,j}[V_{189}\times M_{EBM}]_j$$
$$-k_{on,(M\times V189)\times R2,j}[M_{EBM}\times V_{189}]_j[R2]_j + k_{off,(M\times V189)\times R2,j}[M_{EBM}\times V_{189}\times R2]_j$$
$$-k_{on,(M\times V189)\times R1,j}[M_{EBM}\times V_{189}]_j[R1]_j + k_{off,(M\times V189)\times R1,j}[M_{EBM}\times V_{189}\times R1]_j$$
$$-k_{on,(M\times V189)\times sR1,j}[M_{EBM}\times V_{189}]_j[sR1]_j + k_{off,(M\times V189)\times sR1,j}[M_{EBM}\times V_{189}\times sR1]_j$$

$$d[P2\times M_{EBM}]_j / dt = k_{on,P2\times M,j}[P2]_j[M_{EBM}]_j - k_{off,P2\times M,j}[P2\times M_{EBM}]_j$$
$$-k_{on,(M\times P2)\times R1,j}[M_{EBM}\times P2]_j[R1]_j + k_{off,(M\times P2)\times R1,j}[M_{EBM}\times P2\times R1]_j$$
$$-k_{on,(M\times P2)\times sR1,j}[M_{EBM}\times P2]_j[sR1]_j + k_{off,(M\times P2)\times sR1,j}[M_{EBM}\times P2\times sR1]_j$$

$$d[V_{165}\times M_{ECM}]_j / dt = k_{on,V165\times M,j}[V_{165}]_j[M_{ECM}]_j - k_{off,V165\times M,j}[V_{165}\times M_{ECM}]_j$$
$$-k_{on,(M\times V165)\times sR1,j}[M_{ECM}\times V_{165}]_j[sR1]_j + k_{off,(M\times V165)\times sR1,j}[M_{ECM}\times V_{165}\times sR1]_j$$

$$d[V_{189}\times M_{ECM}]_j / dt = k_{on,V189\times M,j}[V_{189}]_j[M_{ECM}]_j - k_{off,V189\times M,j}[V_{189}\times M_{ECM}]_j$$
$$-k_{on,(M\times V189)\times sR1,j}[M_{ECM}\times V_{189}]_j[sR1]_j + k_{off,(M\times V189)\times sR1,j}[M_{ECM}\times V_{189}\times sR1]_j$$

$$d[P2 \times M_{ECM}]_j / dt = k_{on,P2 \times M,j}[P2]_j[M_{ECM}]_j - k_{off,P2 \times M,j}[P2 \times M_{ECM}]_j$$
$$-k_{on,(M \times P2) \times sR1,j}[M_{ECM} \times P2]_j[sR1]_j + k_{off,(M \times P2) \times sR1,j}[M_{ECM} \times P2 \times sR1]_j$$

$$d[V_{165} \times M_{PBM}]_j / dt = k_{on,V165 \times M,j}[V_{165}]_j[M_{PBM}]_j - k_{off,V165 \times M,j}[V_{165} \times M_{PBM}]_j$$
$$-k_{on,(M \times V165) \times sR1,j}[M_{PBM} \times V_{165}]_j[sR1]_j + k_{off,(M \times V165) \times sR1,j}[M_{PBM} \times V_{165} \times sR1]_j$$

$$d[V_{189} \times M_{PBM}]_j / dt = k_{on,V189 \times M,j}[V_{189}]_j[M_{PBM}]_j - k_{off,V189 \times M,j}[V_{189} \times M_{PBM}]_j$$
$$-k_{on,(M \times V189) \times sR1,j}[M_{PBM} \times V_{189}]_j[sR1]_j + k_{off,(M \times V189) \times sR1,j}[M_{PBM} \times V_{189} \times sR1]_j$$

$$d[P2 \times M_{PBM}]_j / dt = k_{on,P2 \times M,j}[P2]_j[M_{PBM}]_j - k_{off,P2 \times M,j}[P2 \times M_{PBM}]_j$$
$$-k_{on,(M \times P2) \times sR1,j}[M_{PBM} \times P2]_j[sR1]_j + k_{off,(M \times P2) \times sR1,j}[M_{PBM} \times P2 \times sR1]_j$$

$$d[sR1 \times M_{EBM}]_j / dt = k_{on,sR1 \times M,j}[sR1]_j[M_{EBM}]_j - k_{off,sR1 \times M,j}[sR1 \times M_{EBM}]_j$$
$$-k_{on,(M \times sR1) \times V121,j}[M_{EBM} \times sR1]_j[V_{121}]_j + k_{off,(M \times sR1) \times V121,j}[M_{EBM} \times sR1 \times V_{121}]_j$$
$$-k_{on,(M \times sR1) \times P1,j}[M_{EBM} \times sR1]_j[P1]_j + k_{off,(M \times sR1) \times P1,j}[M_{EBM} \times sR1 \times P1]_j$$

$$d[sR1 \times M_{ECM}]_j / dt = k_{on,sR1 \times M,j}[sR1]_j[M_{ECM}]_j - k_{off,sR1 \times M,j}[sR1 \times M_{ECM}]_j$$
$$-k_{on,(M \times sR1) \times V121,j}[M_{ECM} \times sR1]_j[V_{121}]_j + k_{off,(M \times sR1) \times V121,j}[M_{ECM} \times sR1 \times V_{121}]_j$$
$$-k_{on,(M \times sR1) \times P1,j}[M_{ECM} \times sR1]_j[P1]_j + k_{off,(M \times sR1) \times P1,j}[M_{ECM} \times sR1 \times P1]_j$$

$$d[sR1 \times M_{PBM}]_j / dt = k_{on,sR1 \times M,j}[sR1]_j[M_{PBM}]_j - k_{off,sR1 \times M,j}[sR1 \times M_{PBM}]_j$$
$$-k_{on,(M \times sR1) \times V121,j}[M_{PBM} \times sR1]_j[V_{121}]_j + k_{off,(M \times sR1) \times V121,j}[M_{PBM} \times sR1 \times V_{121}]_j$$
$$-k_{on,(M \times sR1) \times P1,j}[M_{PBM} \times sR1]_j[P1]_j + k_{off,(M \times sR1) \times P1,j}[M_{PBM} \times sR1 \times P1]_j$$

$$d[M_{EBM} \times V_{165} \times sR1]_j / dt = k_{on,M \times (V165 \times sR1),j}[M_{EBM}]_j[V_{165} \times sR1]_j - k_{off,M \times (V165 \times sR1),j}[M_{EBM} \times V_{165} \times sR1]_j$$
$$+k_{on,(M \times V165) \times sR1,j}[M_{EBM} \times V_{165}]_j[sR1]_j - k_{off,(M \times V165) \times sR1,j}[M_{EBM} \times V_{165} \times sR1]_j$$

$$d[M_{EBM} \times V_{189} \times sR1]_j / dt = k_{on,M \times (V189 \times sR1),j}[M_{EBM}]_j[V_{189} \times sR1]_j - k_{off,M \times (V189 \times sR1),j}[M_{EBM} \times V_{189} \times sR1]_j$$
$$+k_{on,(M \times V189) \times sR1,j}[M_{EBM} \times V_{189}]_j[sR1]_j - k_{off,(M \times V189) \times sR1,j}[M_{EBM} \times V_{189} \times sR1]_j$$

$$d[M_{EBM} \times P2 \times sR1]_j / dt = k_{on,M \times (P2 \times sR1),j}[M_{EBM}]_j[P2 \times sR1]_j - k_{off,M \times (P2 \times sR1),j}[M_{EBM} \times P2 \times sR1]_j$$
$$+k_{on,(M \times P2) \times sR1,j}[M_{EBM} \times P2]_j[sR1]_j - k_{off,(M \times P2) \times sR1,j}[M_{EBM} \times P2 \times sR1]_j$$

$$d[V_{121} \cdot sR1 \cdot M_{EBM}]_j / dt = k_{on,(V121 \cdot sR1) \cdot M,j}[V_{121} \cdot sR1]_j[M_{EBM}]_j - k_{off,(V121 \cdot sR1) \cdot M,j}[V_{121} \cdot sR1 \cdot M_{EBM}]_j$$
$$+ k_{on,V121 \cdot (sR1 \cdot M),j}[V_{121}]_j[sR1 \cdot M_{EBM}]_j - k_{off,V121 \cdot (sR1 \cdot M),j}[V_{121} \cdot sR1 \cdot M_{EBM}]_j$$

$$d[V_{165b} \cdot sR1 \cdot M_{EBM}]_j / dt = k_{on,(V165b \cdot sR1) \cdot M,j}[V_{165b} \cdot sR1]_j[M_{EBM}]_j - k_{off,(V165b \cdot sR1) \cdot M,j}[V_{165b} \cdot sR1 \cdot M_{EBM}]_j$$
$$+ k_{on,V165b \cdot (sR1 \cdot M),j}[V_{165b}]_j[sR1 \cdot M_{EBM}]_j - k_{off,V165b \cdot (sR1 \cdot M),j}[V_{165b} \cdot sR1 \cdot M_{EBM}]_j$$

$$d[P1 \cdot sR1 \cdot M_{EBM}]_j / dt = k_{on,(P1 \cdot sR1) \cdot M,j}[P1 \cdot sR1]_j[M_{EBM}]_j - k_{off,(P1 \cdot sR1) \cdot M,j}[P1 \cdot sR1 \cdot M_{EBM}]_j$$
$$+ k_{on,P1 \cdot (sR1 \cdot M),j}[P1]_j[sR1 \cdot M_{EBM}]_j - k_{off,P1 \cdot (sR1 \cdot M),j}[P1 \cdot sR1 \cdot M_{EBM}]_j$$

$$d[M_{ECM} \cdot V_{165} \cdot sR1]_j / dt = k_{on,M \cdot (V165 \cdot sR1),j}[M_{ECM}]_j[V_{165} \cdot sR1]_j - k_{off,M \cdot (V165 \cdot sR1),j}[M_{ECM} \cdot V_{165} \cdot sR1]_j$$
$$+ k_{on,(M \cdot V165) \cdot sR1,j}[M_{ECM} \cdot V_{165}]_j[sR1]_j - k_{off,(M \cdot V165) \cdot sR1,j}[M_{ECM} \cdot V_{165} \cdot sR1]_j$$

$$d[M_{ECM} \cdot V_{165} \cdot sR1]_j / dt = k_{on,M \cdot (V165 \cdot sR1),j}[M_{ECM}]_j[V_{165} \cdot sR1]_j - k_{off,M \cdot (V165 \cdot sR1),j}[M_{ECM} \cdot V_{165} \cdot sR1]_j$$
$$+ k_{on,(M \cdot V165) \cdot sR1,j}[M_{ECM} \cdot V_{165}]_j[sR1]_j - k_{off,(M \cdot V165) \cdot sR1,j}[M_{ECM} \cdot V_{165} \cdot sR1]_j$$

$$d[M_{ECM} \cdot V_{189} \cdot sR1]_j / dt = k_{on,M \cdot (V189 \cdot sR1),j}[M_{ECM}]_j[V_{189} \cdot sR1]_j - k_{off,M \cdot (V189 \cdot sR1),j}[M_{ECM} \cdot V_{189} \cdot sR1]_j$$
$$+ k_{on,(M \cdot V189) \cdot sR1,j}[M_{ECM} \cdot V_{189}]_j[sR1]_j - k_{off,(M \cdot V189) \cdot sR1,j}[M_{ECM} \cdot V_{189} \cdot sR1]_j$$

$$d[M_{ECM} \cdot P2 \cdot sR1]_j / dt = k_{on,M \cdot (P2 \cdot sR1),j}[M_{ECM}]_j[P2 \cdot sR1]_j - k_{off,M \cdot (P2 \cdot sR1),j}[M_{ECM} \cdot P2 \cdot sR1]_j$$
$$+ k_{on,(M \cdot P2) \cdot sR1,j}[M_{ECM} \cdot P2]_j[sR1]_j - k_{off,(M \cdot P2) \cdot sR1,j}[M_{ECM} \cdot P2 \cdot sR1]_j$$

$$d[V_{121} \cdot sR1 \cdot M_{ECM}]_j / dt = k_{on,(V121 \cdot sR1) \cdot M,j}[V_{121} \cdot sR1]_j[M_{ECM}]_j - k_{off,(V121 \cdot sR1) \cdot M,j}[V_{121} \cdot sR1 \cdot M_{ECM}]_j$$
$$+ k_{on,V121 \cdot (sR1 \cdot M),j}[V_{121}]_j[sR1 \cdot M_{ECM}]_j - k_{off,V121 \cdot (sR1 \cdot M),j}[V_{121} \cdot sR1 \cdot M_{ECM}]_j$$

$$d[V_{165b} \cdot sR1 \cdot M_{ECM}]_j / dt = k_{on,(V165b \cdot sR1) \cdot M,j}[V_{165b} \cdot sR1]_j[M_{ECM}]_j - k_{off,(V165b \cdot sR1) \cdot M,j}[V_{165b} \cdot sR1 \cdot M_{ECM}]_j$$
$$+ k_{on,V165b \cdot (sR1 \cdot M),j}[V_{165b}]_j[sR1 \cdot M_{ECM}]_j - k_{off,V165b \cdot (sR1 \cdot M),j}[V_{165b} \cdot sR1 \cdot M_{ECM}]_j$$

$$d[P1 \cdot sR1 \cdot M_{ECM}]_j / dt = k_{on,(P1 \cdot sR1) \cdot M,j}[P1 \cdot sR1]_j[M_{ECM}]_j - k_{off,(P1 \cdot sR1) \cdot M,j}[P1 \cdot sR1 \cdot M_{ECM}]_j$$
$$+ k_{on,P1 \cdot (sR1 \cdot M),j}[P1]_j[sR1 \cdot M_{ECM}]_j - k_{off,P1 \cdot (sR1 \cdot M),j}[P1 \cdot sR1 \cdot M_{ECM}]_j$$

$$d[M_{PBM} \cdot V_{165} \cdot sR1]_j / dt = k_{on,M \cdot (V165 \cdot sR1),j}[M_{PBM}]_j[V_{165} \cdot sR1]_j - k_{off,M \cdot (V165 \cdot sR1),j}[M_{PBM} \cdot V_{165} \cdot sR1]_j$$
$$+ k_{on,(M \cdot V165) \cdot sR1,j}[M_{PBM} \cdot V_{165}]_j[sR1]_j - k_{off,(M \cdot V165) \cdot sR1,j}[M_{PBM} \cdot V_{165} \cdot sR1]_j$$

$$d[M_{PBM} \times V_{189} \times sR1]_j / dt = k_{on,M \times (V189 \times sR1),j}[M_{PBM}]_j[V_{189} \times sR1]_j - k_{off,M \times (V189 \times sR1),j}[M_{PBM} \times V_{189} \times sR1]_j$$
$$+ k_{on,(M \times V189) \times sR1,j}[M_{PBM} \times V_{189}]_j[sR1]_j - k_{off,(M \times V189) \times sR1,j}[M_{PBM} \times V_{189} \times sR1]_j$$

$$d[M_{PBM} \times P2 \times sR1]_j / dt = k_{on,M \times (P2 \times sR1),j}[M_{PBM}]_j[P2 \times sR1]_j - k_{off,M \times (P2 \times sR1),j}[M_{PBM} \times P2 \times sR1]_j$$
$$+ k_{on,(M \times P2) \times sR1,j}[M_{PBM} \times P2]_j[sR1]_j - k_{off,(M \times P2) \times sR1,j}[M_{PBM} \times P2 \times sR1]_j$$

$$d[V_{121} \times sR1 \times M_{PBM}]_j / dt = k_{on,(V121 \times sR1) \times M,j}[V_{121} \times sR1]_j[M_{PBM}]_j - k_{off,(V121 \times sR1) \times M,j}[V_{121} \times sR1 \times M_{PBM}]_j$$
$$+ k_{on,V121 \times (sR1 \times M),j}[V_{121}]_j[sR1 \times M_{PBM}]_j - k_{off,V121 \times (sR1 \times M),j}[V_{121} \times sR1 \times M_{PBM}]_j$$

$$d[V_{165b} \times sR1 \times M_{PBM}]_j / dt = k_{on,(V165b \times sR1) \times M,j}[V_{165b} \times sR1]_j[M_{PBM}]_j - k_{off,(V165b \times sR1) \times M,j}[V_{165b} \times sR1 \times M_{PBM}]_j$$
$$+ k_{on,V165b \times (sR1 \times M),j}[V_{165b}]_j[sR1 \times M_{PBM}]_j - k_{off,V165b \times (sR1 \times M),j}[V_{165b} \times sR1 \times M_{PBM}]_j$$

$$d[P1 \times sR1 \times M_{PBM}]_j / dt = k_{on,(P1 \times sR1) \times M,j}[P1 \times sR1]_j[M_{PBM}]_j - k_{off,(P1 \times sR1) \times M,j}[P1 \times sR1 \times M_{PBM}]_j$$
$$+ k_{on,P1 \times (sR1 \times M),j}[P1]_j[sR1 \times M_{PBM}]_j - k_{off,P1 \times (sR1 \times M),j}[P1 \times sR1 \times M_{PBM}]_j$$

Abluminal Endothelial Cell Surface – These 31 equations represent molecular species present on the surface of endothelial cells, as summarized in **Figure 7-S1E**. The binding rates (k_{on}) are given in **Table 7-S5 though 7-S7**, with units of $M^{-1}s^{-1}$ for binding of ligands to receptors, and $(moles/cm^2)^{-1}s^{-1}$ for coupling of cell surface receptors. The fraction of EBM accessible to endothelial cell receptors is f. The trafficking rates, which depend on receptor ligation and binding to NRP1 (**Table 7-S10**), are in units of s^{-1}, where k_{int} is the internalization rate, k_{rec4} is the recycling rate from early endosomes (Rab4/5) to the cell surface, and k_{rec11} is the recycling rate from recycling endosomes (Rab11) to the cell surface. $[R1_{rab45}]$ is the concentration of unoccupied VEGFR1 in early (Rab4/5) endosomes. s is the production rate for free (unoccupied) receptors delivered to the cell surface ($\#/cm^2/s$, converted), tuned to match experimental measurements of surface receptor densities at steady-state (**Table 7-2**).

$$d[R1]_j / dt = s_{R1,j} - k_{\text{int},R1,j}[R1]_j + k_{rec4,R1,j}[R1_{rab45}] + k_{rec11,R1,j}[R1_{rab11}]$$

$$-k_{on,V165\times R1,j}[V_{165}]_j[R1]_j + k_{off,V165\times R1,j}[V_{165}\times R1]_j$$

$$-k_{on,V189\times R1,j}[V_{189}]_j[R1]_j + k_{off,V189\times R1,j}[V_{189}\times R1]_j$$

$$-k_{on,V121\times R1,j}[V_{121}]_j[R1]_j + k_{off,V121\times R1,j}[V_{121}\times R1]_j$$

$$-k_{on,V165b\times R1,j}[V_{165b}]_j[R1]_j + k_{off,V165b\times R1,j}[V_{165b}\times R1]_j$$

$$-k_{on,P1\times R1,j}[P1]_j[R1]_j + k_{off,P1\times R1,j}[P1\times R1]_j$$

$$-k_{on,P2\times R1,j}[P2]_j[R1]_j + k_{off,P2\times R1,j}[P2\times R1]_j$$

$$-k_{on,(M\times V165)\times R1,j}[M_{EBM}\times V_{165}]_j[R1]_j + k_{off,(M\times V165)\times R1,j}[M_{EBM}\times V_{165}\times R1]_j$$

$$-k_{on,(M\times V189)\times R1,j}[M_{EBM}\times V_{189}]_j[R1]_j + k_{off,(M\times V189)\times R1,j}[M_{EBM}\times V_{189}\times R1]_j$$

$$-k_{on,(M\times P2)\times R1,j}[M_{EBM}\times P2]_j[R1]_j + k_{off,(M\times P2)\times R1,j}[M_{EBM}\times P2\times R1]_j$$

$$-k_{on,N1\times R1,j}[N1]_j[R1]_j + k_{off,N1\times R1,j}[N1\times R1]_j$$

$$d[R2]_j / dt = s_{R2,j} - k_{\text{int},R2,j}[R2]_j + k_{rec4,R2,j}[R2_{rab45}] + k_{rec11,R2,j}[R2_{rab11}]$$

$$-k_{on,V165\times R2,j}[V_{165}]_j[R2]_j + k_{off,V165\times R2,j}[V_{165}\times R2]_j$$

$$-k_{on,V189\times R2,j}[V_{189}]_j[R2]_j + k_{off,V189\times R2,j}[V_{189}\times R2]_j$$

$$-k_{on,V121\times R2,j}[V_{121}]_j[R2]_j + k_{off,V121\times R2,j}[V_{121}\times R2]_j$$

$$-k_{on,V165b\times R2,j}[V_{165b}]_j[R2]_j + k_{off,V165b\times R2,j}[V_{165b}\times R2]_j$$

$$-k_{on,(M\times V165)\times R2,j}[M_{EBM}\times V_{165}]_j[R2]_j + k_{off,(M\times V165)\times R2,j}[M_{EBM}\times V_{165}\times R2]_j$$

$$-k_{on,(M\times V189)\times R2,j}[M_{EBM}\times V_{189}]_j[R2]_j + k_{off,(M\times V189)\times R2,j}[M_{EBM}\times V_{189}\times R2]_j$$

$$-k_{on,(N1\times V165)\times R2,j}[N1\times V_{165}]_j[R2]_j + k_{off,(N1\times V165)\times R2,j}[N1\times V_{165}\times R2]_j$$

$$-k_{on,(N1\times V189)\times R2,j}[N1\times V_{189}]_j[R2]_j + k_{off,(N1\times V189)\times R2,j}[N1\times V_{189}\times R2]_j$$

$$d[N1]_j / dt = s_{N1,j} - k_{int,N1,j}[N1]_j + k_{rec4,N1,j}[N1_{rab45}] + k_{rec11,N1,j}[N1_{rab11}]$$

$$- k_{on,V165\times N1,j}[V_{165}]_j[N1]_j + k_{off,V165\times N1,j}[V_{165}\times N1]_j$$

$$- k_{on,V189\times N1,j}[V_{189}]_j[N1]_j + k_{off,V189\times N1,j}[V_{189}\times N1]_j$$

$$- k_{on,P2\times N1,j}[P2]_j[N1]_j + k_{off,P2\times N1,j}[P2\times N1]_j$$

$$- k_{on,N1\times R1,j}[N1]_j[R1]_j + k_{off,N1\times R1,j}[N1\times R1]_j$$

$$- k_{on,N1\times sR1,j}[N1]_j[sR1]_j + k_{off,N1\times sR1,j}[N1\times sR1]_j$$

$$- k_{on,(V121\times R1)\times N1,j}[V_{121}\times R1]_j[N1]_j + k_{off,(V121\times R1)\times N1,j}[V_{121}\times R1\times N1]_j$$

$$- k_{on,(V165b\times R1)\times N1,j}[V_{165b}\times R1]_j[N1]_j + k_{off,(V165b\times R1)\times N1,j}[V_{165b}\times R1\times N1]_j$$

$$- k_{on,(P1\times R1)\times N1,j}[P1\times R1]_j[N1]_j + k_{off,(P1\times R1)\times N1,j}[P1\times R1\times N1]_j$$

$$- k_{on,N1\times(V165\times R2),j}[N1]_j[V_{165}\times R2]_j + k_{off,N1\times(V165\times R2),j}[N1\times V_{165}\times R2]_j$$

$$- k_{on,N1\times(V189\times R2),j}[N1]_j[V_{189}\times R2]_j + k_{off,N1\times(V189\times R2),j}[N1\times V_{189}\times R2]_j$$

$$d[V_{165}\times R1]_j / dt = -k_{int,V165\times R1,j}[V_{165}\times R1]_j + k_{rec4,V165\times R1,j}[V_{165}\times R1_{rab45}] + k_{rec11,V165\times R1,j}[V_{165}\times R1_{rab11}]$$

$$+ k_{on,V165\times R1,j}[V_{165}]_j[R1]_j - k_{off,V165\times R1,j}[V_{165}\times R1]_j$$

$$- k_{on,M\times(V165\times R1),j}[M_{EBM}]_j[V_{165}\times R1]_j + k_{off,M\times(V165\times R1),j}[M_{EBM}\times V_{165}\times R1]_j$$

$$d[V_{189}\times R1]_j / dt = -k_{int,V189\times R1,j}[V_{189}\times R1]_j + k_{rec4,V189\times R1,j}[V_{189}\times R1_{rab45}] + k_{rec11,V189\times R1,j}[V_{189}\times R1_{rab11}]$$

$$+ k_{on,V189\times R1,j}[V_{189}]_j[R1]_j - k_{off,V189\times R1,j}[V_{189}\times R1]_j$$

$$- k_{on,M\times(V189\times R1),j}[M_{EBM}]_j[V_{189}\times R1]_j + k_{off,M\times(V189\times R1),j}[M_{EBM}\times V_{189}\times R1]_j$$

$$d[V_{121}\times R1]_j / dt = -k_{int,V121\times R1,j}[V_{121}\times R1]_j + k_{rec4,V121\times R1,j}[V_{121}\times R1_{rab45}] + k_{rec11,V121\times R1,j}[V_{121}\times R1_{rab11}]$$

$$+ k_{on,V121\times R1,j}[V_{121}]_j[R1]_j - k_{off,V121\times R1,j}[V_{121}\times R1]_j$$

$$- k_{on,(V121\times R1)\times N1,j}[V_{121}\times R1]_j[N1]_j + k_{off,(V121\times R1)\times N1,j}[V_{121}\times R1\times N1]_j$$

$$d[V_{165b}\times R1]_j / dt = -k_{int,V165b\times R1,j}[V_{165b}\times R1]_j + k_{rec4,V165b\times R1,j}[V_{165b}\times R1_{rab45}] + k_{rec11,V165b\times R1,j}[V_{165b}\times R1_{rab11}]$$

$$+ k_{on,V165b\times R1,j}[V_{165b}]_j[R1]_j - k_{off,V165b\times R1,j}[V_{165b}\times R1]_j$$

$$- k_{on,(V165b\times R1)\times N1,j}[V_{165b}\times R1]_j[N1]_j + k_{off,(V165b\times R1)\times N1,j}[V_{165b}\times R1\times N1]_j$$

$$d[P1\times R1]_j / dt = -k_{int,P1\times R1,j}[P1\times R1]_j + k_{rec4,P1\times R1,j}[P1\times R1_{rab45}] + k_{rec11,P1\times R1,j}[P1\times R1_{rab11}]$$

$$+ k_{on,P1\times R1,j}[P1]_j[R1]_j - k_{off,P1\times R1,j}[P1\times R1]_j$$

$$- k_{on,(P1\times R1)\times N1,j}[P1\times R1]_j[N1]_j + k_{off,(P1\times R1)\times N1,j}[P1\times R1\times N1]_j$$

$$d[P2{\times}R1]_j / dt = -k_{\text{int},P2{\times}R1,j}[P2{\times}R1]_j + k_{rec4,P2{\times}R1,j}[P2{\times}R1_{rab45}] + k_{rec11,P2{\times}R1,j}[P2{\times}R1_{rab11}]$$
$$+ k_{on,P2{\times}R1,j}[P2]_j[R1]_j - k_{off,P2{\times}R1,j}[P2{\times}R1]_j$$
$$- k_{on,M{\times}(P2{\times}R1),j}[M_{EBM}]_j[P2{\times}R1]_j + k_{off,M{\times}(P2{\times}R1),j}[M_{EBM}{\times}P2{\times}R1]_j$$

$$d[V_{165}{\times}R2]_j / dt = -k_{\text{int},V165{\times}R2,j}[V_{165}{\times}R2]_j + k_{rec4,V165{\times}R2,j}[V_{165}{\times}R2_{rab45}] + k_{rec11,V165{\times}R2,j}[V_{165}{\times}R2_{rab11}]$$
$$+ k_{on,V165{\times}R2,j}[V_{165}]_j[R2]_j - k_{off,V165{\times}R2,j}[V_{165}{\times}R2]_j$$
$$- k_{on,M{\times}(V165{\times}R2),j}[M_{EBM}]_j[V_{165}{\times}R2]_j + k_{off,M{\times}(V165{\times}R2),j}[M_{EBM}{\times}V_{165}{\times}R2]_j$$
$$- k_{on,N1{\times}(V165{\times}R2),j}[N1]_j[V_{165}{\times}R2]_j + k_{off,N1{\times}(V165{\times}R2),j}[N1{\times}V_{165}{\times}R2]_j$$

$$d[V_{189}{\times}R2]_j / dt = -k_{\text{int},V189{\times}R2,j}[V_{189}{\times}R2]_j + k_{rec4,V189{\times}R2,j}[V_{189}{\times}R2_{rab45}] + k_{rec11,V189{\times}R2,j}[V_{189}{\times}R2_{rab11}]$$
$$+ k_{on,V189{\times}R2,j}[V_{189}]_j[R2]_j - k_{off,V189{\times}R2,j}[V_{189}{\times}R2]_j$$
$$- k_{on,M{\times}(V189{\times}R2),j}[M_{EBM}]_j[V_{189}{\times}R2]_j + k_{off,M{\times}(V189{\times}R2),j}[M_{EBM}{\times}V_{189}{\times}R2]_j$$
$$- k_{on,N1{\times}(V189{\times}R2),j}[N1]_j[V_{189}{\times}R2]_j + k_{off,N1{\times}(V189{\times}R2),j}[N1{\times}V_{189}{\times}R2]_j$$

$$d[V_{121}{\times}R2]_j / dt = -k_{\text{int},V121{\times}R2,j}[V_{121}{\times}R2]_j + k_{rec4,V121{\times}R2,j}[V_{121}{\times}R2_{rab45}] + k_{rec11,V121{\times}R2,j}[V_{121}{\times}R2_{rab11}]$$
$$+ k_{on,V121{\times}R2,j}[V_{121}]_j[R2]_j - k_{off,V121{\times}R2,j}[V_{121}{\times}R2]_j$$

$$d[V_{165b}{\times}R2]_j / dt = -k_{\text{int},V165b{\times}R2,j}[V_{165b}{\times}R2]_j + k_{rec4,V165b{\times}R2,j}[V_{165b}{\times}R2_{rab45}] + k_{rec11,V165b{\times}R2,j}[V_{165b}{\times}R2_{rab11}]$$
$$+ k_{on,V165b{\times}R2,j}[V_{165b}]_j[R2]_j - k_{off,V165b{\times}R2,j}[V_{165b}{\times}R2]_j$$

$$d[V_{165}{\times}N1]_j / dt = -k_{\text{int},V165{\times}N1,j}[V_{165}{\times}N1]_j + k_{rec4,V165{\times}N1,j}[V_{165}{\times}N1_{rab45}] + k_{rec11,V165{\times}N1,j}[V_{165}{\times}N1_{rab11}]$$
$$+ k_{on,V165{\times}N1,j}[V_{165}]_j[N1]_j - k_{off,V165{\times}N1,j}[V_{165}{\times}N1]_j$$
$$- k_{on,(N1{\times}V165){\times}R2,j}[N1{\times}V_{165}]_j[R2]_j + k_{off,(N1{\times}V165){\times}R2,j}[N1{\times}V_{165}{\times}R2]_j$$

$$d[V_{189}{\times}N1]_j / dt = -k_{\text{int},V189{\times}N1,j}[V_{189}{\times}N1]_j + k_{rec4,V189{\times}N1,j}[V_{189}{\times}N1_{rab45}] + k_{rec11,V189{\times}N1,j}[V_{189}{\times}N1_{rab11}]$$
$$+ k_{on,V189{\times}N1,j}[V_{189}]_j[N1]_j - k_{off,V189{\times}N1,j}[V_{189}{\times}N1]_j$$
$$- k_{on,(N1{\times}V189){\times}R2,j}[N1{\times}V_{189}]_j[R2]_j + k_{off,(N1{\times}V189){\times}R2,j}[N1{\times}V_{189}{\times}R2]_j$$

$$d[P2{\times}N1]_j / dt = -k_{\text{int},P2{\times}N1,j}[P2{\times}N1]_j + k_{rec4,P2{\times}N1,j}[P2{\times}N1_{rab45}] + k_{rec11,P2{\times}N1,j}[P2{\times}N1_{rab11}]$$
$$+ k_{on,P2{\times}N1,j}[P2]_j[N1]_j - k_{off,P2{\times}N1,j}[P2{\times}N1]_j$$
$$- k_{on,(N1{\times}P2){\times}R2,j}[N1{\times}P2]_j[R2]_j + k_{off,(N1{\times}P2){\times}R2,j}[N1{\times}P2{\times}R2]_j$$

$$d[N1{\times}R1]_j/dt = -k_{\text{int},N1{\times}R1,j}[N1{\times}R1]_j + k_{rec4,N1{\times}R1,j}[N1{\times}R1_{rab45}] + k_{rec11,N1{\times}R1,j}[N1{\times}R1_{rab11}]$$
$$+ k_{on,N1{\times}R1,j}[N1]_j[R1]_j - k_{off,N1{\times}R1,j}[N1{\times}R1]_j$$
$$- k_{on,V121{\times}(N1{\times}R1),j}[V_{121}]_j[N1{\times}R1]_j + k_{off,V121{\times}(N1{\times}R1),j}[V_{121}{\times}R1{\times}N1]_j$$
$$- k_{on,V165b{\times}(N1{\times}R1),j}[V_{165b}]_j[N1{\times}R1]_j + k_{off,V165b{\times}(N1{\times}R1),j}[V_{165b}{\times}R1{\times}N1]_j$$
$$- k_{on,P1{\times}(N1{\times}R1),j}[P1]_j[N1{\times}R1]_j + k_{off,P1{\times}(N1{\times}R1),j}[P1{\times}R1{\times}N1]_j$$

$$d[N1{\times}sR1]_j/dt = -k_{\text{int},N1{\times}sR1,j}[N1{\times}sR1]_j + k_{rec4,N1{\times}sR1,j}[N1{\times}sR1_{rab45}] + k_{rec11,N1{\times}sR1,j}[N1{\times}sR1_{rab11}]$$
$$+ k_{on,N1{\times}sR1,j}[N1]_j[sR1]_j - k_{off,N1{\times}sR1,j}[N1{\times}sR1]_j$$
$$- k_{on,V121{\times}(N1{\times}sR1),j}[V_{121}]_j[N1{\times}sR1]_j + k_{off,V121{\times}(N1{\times}sR1),j}[V_{121}{\times}sR1{\times}N1]_j$$
$$- k_{on,P1{\times}(N1{\times}sR1),j}[P1]_j[N1{\times}sR1]_j + k_{off,P1{\times}(N1{\times}sR1),j}[P1{\times}sR1{\times}N1]_j$$

$$d[N1{\times}V_{165}{\times}R2]_j/dt = -k_{\text{int},N1{\times}V165{\times}R2,j}[N1{\times}V_{165}{\times}R2]_j + k_{rec4,N1{\times}V165{\times}R2,j}[N1{\times}V_{165}{\times}R2_{rab45}]$$
$$+ k_{rec11,N1{\times}V165{\times}R2,j}[N1{\times}V_{165}{\times}R2_{rab11}]$$
$$+ k_{on,R2{\times}(N1{\times}V165),j}[R2]_j[V_{165}{\times}N1]_j - k_{off,R2{\times}(N1{\times}V165),j}[N1{\times}V_{165}{\times}R2]_j$$
$$+ k_{on,N1{\times}(V165{\times}R2),j}[N1]_j[V_{165}{\times}R2]_j - k_{off,N1{\times}(V165{\times}R2),j}[N1{\times}V_{165}{\times}R2]_j$$

$$d[N1{\times}V_{189}{\times}R2]_j/dt = -k_{\text{int},N1{\times}V189{\times}R2,j}[N1{\times}V_{189}{\times}R2]_j + k_{rec4,N1{\times}V189{\times}R2,j}[N1{\times}V_{189}{\times}R2_{rab45}]$$
$$+ k_{rec11,N1{\times}V189{\times}R2,j}[N1{\times}V_{189}{\times}R2_{rab11}]$$
$$+ k_{on,R2{\times}(V189{\times}N1),j}[R2]_j[V_{189}{\times}N1]_j - k_{off,R2{\times}(N1{\times}V189),j}[N1{\times}V_{189}{\times}R2]_j$$
$$+ k_{on,N1{\times}(V189{\times}R2),j}[N1]_j[V_{189}{\times}R2]_j - k_{off,N1{\times}(V189{\times}R2),j}[N1{\times}V_{189}{\times}R2]_j$$

$$d[V_{121}{\times}R1{\times}N1]_j/dt = -k_{\text{int},V121{\times}R1{\times}N1,j}[V_{121}{\times}R1{\times}N1]_j + k_{rec4,V121{\times}R1{\times}N1,j}[V_{121}{\times}R1{\times}N1_{rab45}]$$
$$+ k_{rec11,V121{\times}R1{\times}N1,j}[V_{121}{\times}R1{\times}N1_{rab11}]$$
$$+ k_{on,V121{\times}(R1{\times}N1),j}[V_{121}]_j[R1{\times}N1]_j - k_{off,V121{\times}(R1{\times}N1),j}[V_{121}{\times}R1{\times}N1]_j$$
$$+ k_{on,(V121{\times}R1){\times}N1,j}[V_{121}{\times}R1]_j[N1]_j - k_{off,(V121{\times}R1){\times}N1,j}[V_{121}{\times}R1{\times}N1]_j$$

$$d[V_{165b}{\times}R1{\times}N1]_j/dt = -k_{\text{int},V165b{\times}R1{\times}N1,j}[V_{165b}{\times}R1{\times}N1]_j + k_{rec4,V165b{\times}R1{\times}N1,j}[V_{165b}{\times}R1{\times}N1_{rab45}]$$
$$+ k_{rec11,V165b{\times}R1{\times}N1,j}[V_{165b}{\times}R1{\times}N1_{rab11}]$$
$$+ k_{on,V165b{\times}(R1{\times}N1),j}[V_{165b}]_j[R1{\times}N1]_j - k_{off,V165b{\times}(R1{\times}N1),j}[V_{165b}{\times}R1{\times}N1]_j$$
$$+ k_{on,(V165b{\times}R1){\times}N1,j}[V_{165b}{\times}R1]_j[N1]_j - k_{off,(V165b{\times}R1){\times}N1,j}[V_{165b}{\times}R1{\times}N1]_j$$

$$d[P1{\times}R1{\times}N1]_j/dt = -k_{\text{int},P1{\times}R1{\times}N1,j}[P1{\times}R1{\times}N1]_j + k_{rec4,P1{\times}R1{\times}N1,j}[P1{\times}R1{\times}N1_{rab45}]$$
$$+k_{rec11,P1{\times}R1{\times}N1,j}[P1{\times}R1{\times}N1_{rab11}]$$
$$+k_{on,P1{\times}(R1{\times}N1),j}[P1]_j[R1{\times}N1]_j - k_{off,P1{\times}(R1{\times}N1),j}[P1{\times}R1{\times}N1]_j$$
$$+k_{on,(P1{\times}R1){\times}N1,j}[P1{\times}R1]_j[N1]_j - k_{off,(P1{\times}R1){\times}N1,j}[P1{\times}R1{\times}N1]_j$$

$$d[V_{121}{\times}sR1{\times}N1]_j/dt = -k_{\text{int},V121{\times}sR1{\times}N1,j}[V_{121}{\times}sR1{\times}N1]_j + k_{rec4,V121{\times}sR1{\times}N1,j}[V_{121}{\times}sR1{\times}N1_{rab45}]$$
$$+k_{rec11,V121{\times}sR1{\times}N1,j}[V_{121}{\times}sR1{\times}N1_{rab11}]$$
$$+k_{on,V121{\times}(sR1{\times}N1),j}[V_{121}]_j[sR1{\times}N1]_j - k_{off,V121{\times}(sR1{\times}N1),j}[V_{121}{\times}sR1{\times}N1]_j$$
$$+k_{on,(V121{\times}sR1){\times}N1,j}[V_{121}{\times}sR1]_j[N1]_j - k_{off,(V121{\times}sR1){\times}N1,j}[V_{121}{\times}sR1{\times}N1]_j$$

$$d[V_{165b}{\times}sR1{\times}N1]_j/dt = -k_{\text{int},V165b{\times}sR1{\times}N1,j}[V_{165b}{\times}sR1{\times}N1]_j + k_{rec4,V165b{\times}sR1{\times}N1,j}[V_{165b}{\times}sR1{\times}N1_{rab45}]$$
$$+k_{rec11,V165b{\times}sR1{\times}N1,j}[V_{165b}{\times}sR1{\times}N1_{rab11}]$$
$$+k_{on,V165b{\times}(sR1{\times}N1),j}[V_{165b}]_j[sR1{\times}N1]_j - k_{off,V165b{\times}(sR1{\times}N1),j}[V_{165b}{\times}sR1{\times}N1]_j$$
$$+k_{on,(V165b{\times}sR1){\times}N1,j}[V_{165b}{\times}sR1]_j[N1]_j - k_{off,(V165b{\times}sR1){\times}N1,j}[V_{165b}{\times}sR1{\times}N1]_j$$

$$d[P1{\times}sR1{\times}N1]_j/dt = -k_{\text{int},P1{\times}sR1{\times}N1,j}[P1{\times}sR1{\times}N1]_j + k_{rec4,P1{\times}sR1{\times}N1,j}[P1{\times}sR1{\times}N1_{rab45}]$$
$$+k_{rec11,P1{\times}sR1{\times}N1,j}[P1{\times}sR1{\times}N1_{rab11}]$$
$$+k_{on,P1{\times}(sR1{\times}N1),j}[P1]_j[sR1{\times}N1]_j - k_{off,P1{\times}(sR1{\times}N1),j}[P1{\times}sR1{\times}N1]_j$$
$$+k_{on,(P1{\times}sR1){\times}N1,j}[P1{\times}sR1]_j[N1]_j - k_{off,(P1{\times}sR1){\times}N1,j}[P1{\times}sR1{\times}N1]_j$$

$$d[M_{EBM}{\times}V_{165}{\times}R2]_j/dt = k_{on,(M{\times}V165){\times}R2,j}{\times}f{\times}[M_{EBM}{\times}V_{165}]_j[R2]_j - k_{off,(M{\times}V165){\times}R2,j}[M_{EBM}{\times}V_{165}{\times}R2]_j$$
$$+k_{on,M{\times}(V165{\times}R2),j}{\times}f{\times}[M_{EBM}]_j[V_{165}{\times}R2]_j - k_{off,M{\times}(V165{\times}R2),j}[M_{EBM}{\times}V_{165}{\times}R2]_j$$

$$d[M_{EBM}{\times}V_{189}{\times}R2]_j/dt = k_{on,(M{\times}V189){\times}R2,j}{\times}f{\times}[M_{EBM}{\times}V_{189}]_j[R2]_j - k_{off,(M{\times}V189){\times}R2,j}[M_{EBM}{\times}V_{189}{\times}R2]_j$$
$$+k_{on,M{\times}(V189{\times}R2),j}{\times}f{\times}[M_{EBM}]_j[V_{189}{\times}R2]_j - k_{off,M{\times}(V189{\times}R2),j}[M_{EBM}{\times}V_{189}{\times}R2]_j$$

$$d[M_{EBM}{\times}V_{165}{\times}R1]_j/dt = k_{on,(M{\times}V165){\times}R1,j}{\times}f{\times}[M_{EBM}{\times}V_{165}]_j[R1]_j - k_{off,(M{\times}V165){\times}R1,j}[M_{EBM}{\times}V_{165}{\times}R1]_j$$
$$+k_{on,M{\times}(V165{\times}R1),j}{\times}f{\times}[M_{EBM}]_j[V_{165}{\times}R1]_j - k_{off,M{\times}(V165{\times}R1),j}[M_{EBM}{\times}V_{165}{\times}R1]_j$$

$$d[M_{EBM}{\times}V_{189}{\times}R1]_j/dt = k_{on,(M{\times}V189){\times}R1,j}{\times}f{\times}[M_{EBM}{\times}V_{189}]_j[R1]_j - k_{off,(M{\times}V189){\times}R1,j}[M_{EBM}{\times}V_{189}{\times}R1]_j$$
$$+k_{on,M{\times}(V189{\times}R1),j}{\times}f{\times}[M_{EBM}]_j[V_{189}{\times}R1]_j - k_{off,M{\times}(V189{\times}R1),j}[M_{EBM}{\times}V_{189}{\times}R1]_j$$

$$d[M_{EBM}{\times}P2{\times}R1]_j/dt = k_{on,(M{\times}P2){\times}R1,j}{\times}f{\times}[M_{EBM}{\times}P2]_j[R1]_j - k_{off,(M{\times}P2){\times}R1,j}[M_{EBM}{\times}P2{\times}R1]_j$$
$$+k_{on,M{\times}(P2{\times}R1),j}{\times}f{\times}[M_{EBM}]_j[P2{\times}R1]_j - k_{off,M{\times}(P2{\times}R1),j}[M_{EBM}{\times}P2{\times}R1]_j$$

Detailed VEGFR2 Phosphorylation Reactions – Here we show one example equation (unoccupied cell surface VEGFR2 phosphorylated only on tyrosine Y1175) demonstrating the site-specific phosphorylation and dephosphorylation of VEGFR2 on tyrosines 951, 1175, and 1214 (**Figure 7-S1D**). Phosphorylation is assumed to be independent on each site, giving 8 possible combinations: no phosphorylation, pY951 only, pY1175 only, pY1214 only, pY951 and pY1175, pY951 and pY1214, pY1175 and pY1214, and all three sites phosphorylated. VEGFR2 can be phosphorylated in any of these patterns on the cell surface, in early (Rab4/5) endosomes, or in recycling (Rab11) endosomes. The phosphorylation and dephosphorylation rates (**Table 7-S11**) vary by subcellular location and with ligation, but are assumed to be independent of NRP1- and HSPG-binding. The phosphorylation state of VEGFR2 is assumed not to alter its binding or trafficking properties. We focus here on pY1175 and pY1214 because the parameters for these sites are better constrained than those for pY951. Total phosphorylated VEGFR2 (pR2) is approximated as the sum of all VEGFR2 phosphorylated on at least one site. The full set of equations for phosphorylation of VEGFR2 in all complexes and all locations is omitted for the sake of brevity.

$$
\begin{aligned}
d[R2_{pY1175}]_j / dt = &-k_{\mathrm{int},R2,j}[R2_{pY1175}]_j + k_{rec4,R2,j}[R2_{rab45,pY1175}] + k_{rec11,R2,j}[R2_{rab11,pY1175}] \\
&-k_{on,V165\times R2,j}[V_{165}]_j[R2_{pY1175}]_j + k_{off,V165\times R2,j}[V_{165}\times R2_{pY1175}]_j \\
&-k_{on,V189\times R2,j}[V_{189}]_j[R2_{pY1175}]_j + k_{off,V189\times R2,j}[V_{189}\times R2_{pY1175}]_j \\
&-k_{on,V121\times R2,j}[V_{121}]_j[R2_{pY1175}]_j + k_{off,V121\times R2,j}[V_{121}\times R2_{pY1175}]_j \\
&-k_{on,V1165b\times R2,j}[V_{165b}]_j[R2_{pY1175}]_j + k_{off,V165b\times R2,j}[V_{165b}\times R2_{pY1175}]_j \\
&-k_{on,(M\times V165)\times R2,j}[M_{EBM}\times V_{165}]_j[R2_{pY1175}]_j + k_{off,(M\times V165)\times R2,j}[M_{EBM}\times V_{165}\times R2_{pY1175}]_j \\
&-k_{on,(M\times V189)\times R2,j}[M_{EBM}\times V_{189}]_j[R2_{pY1175}]_j + k_{off,(M\times V189)\times R2,j}[M_{EBM}\times V_{189}\times R2_{pY1175}]_j \\
&-k_{on,(N1\times V165)\times R2,j}[N1\times V_{165}]_j[R2_{pY1175}]_j + k_{off,(N1\times V165)\times R2,j}[N1\times V_{165}\times R2_{pY1175}]_j \\
&-k_{on,(N1\times V189)\times R2,j}[N1\times V_{189}]_j[R2_{pY1175}]_j + k_{off,(N1\times V189)\times R2,j}[N1\times V_{189}\times R2_{pY1175}]_j \\
&+k_{p,Y1175,R2,j}[R2]_j - k_{dp,Y1175,R2,j}[R2_{pY1175}]_j \\
&-k_{p,Y951,R2,j}[R2_{pY1175}]_j + k_{dp,Y951,R2,j}[R2_{pY951-pY1175}]_j \\
&-k_{p,Y1214,R2,j}[R2_{pY1175}]_j + k_{dp,Y1214,R2,j}[R2_{pY1175-pY1214}]_j
\end{aligned}
$$

Endothelial Endosomes- These 64 equations represent molecular species within early signaling (Rab4/5) or recycling (Rab11) endosomes in endothelial cells. Here, k_{4to11} is the trafficking rate from early (Rab45) to

recycling (Rab11) endosomes, and k_{degr} is the rate of degradation of species from early Rab4/5 endosomes. $[R1_{rab45}]$ is the concentration of unoccupied VEGFR1 in early (Rab4/5) endosomes.

Rab4/5 Early Signaling Endosomes

$$d[R1_{rab45}]_j / dt = k_{int,R1,j}[R1]_j - k_{rec4,R1,j}[R1_{rab45}] - k_{4to11,R1,j}[R1_{rab45}] - k_{degr,R1,j}[R1_{rab45}]$$
$$- k_{on,V165\times R1,j}[V_{165,rab45}]_j[R1_{rab45}]_j + k_{off,V165\times R1,j}[V_{165}\times R1_{rab45}]_j$$
$$- k_{on,V189\times R1,j}[V_{189,rab45}]_j[R1_{rab45}]_j + k_{off,V189\times R1,j}[V_{189}\times R1_{rab45}]_j$$
$$- k_{on,V121\times R1,j}[V_{121,rab45}]_j[R1_{rab45}]_j + k_{off,V121\times R1,j}[V_{121}\times R1_{rab45}]_j$$
$$- k_{on,V165b\times R1,j}[V_{165b,rab45}]_j[R1_{rab45}]_j + k_{off,V165b\times R1,j}[V_{165b}\times R1_{rab45}]_j$$
$$- k_{on,P1\times R1,j}[P1_{rab45}]_j[R1_{rab45}]_j + k_{off,P1\times R1,j}[P1\times R1_{rab45}]_j$$
$$- k_{on,P2\times R1,j}[P2_{rab45}]_j[R1_{rab45}]_j + k_{off,P2\times R1,j}[P2\times R1_{rab45}]_j$$
$$- k_{on,N1\times R1,j}[N1_{rab45}]_j[R1_{rab45}]_j + k_{off,N1\times R1,j}[N1\times R1_{rab45}]_j$$

$$d[R2_{rab45}]_j / dt = k_{int,R2,j}[R2]_j - k_{rec4,R2,j}[R2_{rab45}] - k_{4to11,R2,j}[R2_{rab45}] - k_{degr,R2,j}[R2_{rab45}]$$
$$- k_{on,V165\times R2,j}[V_{165,rab45}]_j[R2_{rab45}]_j + k_{off,V165\times R2,j}[V_{165}\times R2_{rab45}]_j$$
$$- k_{on,V189\times R2,j}[V_{189,rab45}]_j[R2_{rab45}]_j + k_{off,V189\times R2,j}[V_{189}\times R2_{rab45}]_j$$
$$- k_{on,V121\times R2,j}[V_{121,rab45}]_j[R2_{rab45}]_j + k_{off,V121\times R2,j}[V_{121}\times R2_{rab45}]_j$$
$$- k_{on,V165b\times R2,j}[V_{165b,rab45}]_j[R2_{rab45}]_j + k_{off,V165b\times R2,j}[V_{165b}\times R2_{rab45}]_j$$
$$- k_{on,(N1\times V165)\times R2,j}[N1\times V_{165,rab45}]_j[R2_{rab45}]_j + k_{off,(N1\times V165)\times R2,j}[N1\times V_{165}\times R2_{rab45}]_j$$
$$- k_{on,(N1\times V189)\times R2,j}[N1\times V_{189,rab45}]_j[R2_{rab45}]_j + k_{off,(N1\times V189)\times R2,j}[N1\times V_{189}\times R2_{rab45}]_j$$

$$d[N1_{rab45}]_j / dt = k_{int,N1,j}[N1]_j - k_{rec4,N1,j}[N1_{rab45}] - k_{4to11,N1,j}[N1_{rab45}] - k_{degr,N1,j}[N1_{rab45}]$$
$$- k_{on,V165\times N1,j}[V_{165,rab45}]_j[N1_{rab45}]_j + k_{off,V165\times N1,j}[V_{165}\times N1_{rab45}]_j$$
$$- k_{on,V189\times N1,j}[V_{189,rab45}]_j[N1_{rab45}]_j + k_{off,V189\times N1,j}[V_{189}\times N1_{rab45}]_j$$
$$- k_{on,P2\times N1,j}[P2_{rab45}]_j[N1_{rab45}]_j + k_{off,P2\times N1,j}[P2\times N1_{rab45}]_j$$
$$- k_{on,N1\times R1,j}[N1_{rab45}]_j[R1_{rab45}]_j + k_{off,N1\times R1,j}[N1\times R1_{rab45}]_j$$
$$- k_{on,N1\times sR1,j}[N1_{rab45}]_j[sR1_{rab45}]_j + k_{off,N1\times sR1,j}[N1\times sR1_{rab45}]_j$$
$$- k_{on,(V121\times R1)\times N1,j}[V_{121}\times R1_{rab45}]_j[N1_{rab45}]_j + k_{off,(V121\times R1)\times N1,j}[V_{121}\times R1\times N1_{rab45}]_j$$
$$- k_{on,(V165b\times R1)\times N1,j}[V_{165b}\times R1_{rab45}]_j[N1_{rab45}]_j + k_{off,(V165b\times R1)\times N1,j}[V_{165b}\times R1\times N1_{rab45}]_j$$
$$- k_{on,(P1\times R1)\times N1,j}[P1\times R1_{rab45}]_j[N1_{rab45}]_j + k_{off,(P1\times R1)\times N1,j}[P1\times R1\times N1_{rab45}]_j$$
$$- k_{on,N1\times(V165\times R2),j}[N1_{rab45}]_j[V_{165}\times R2_{rab45}]_j + k_{off,N1\times(V165\times R2),j}[N1\times V_{165}\times R2_{rab45}]_j$$
$$- k_{on,N1\times(V189\times R2),j}[N1_{rab45}]_j[V_{189}\times R2_{rab45}]_j + k_{off,N1\times(V189\times R2),j}[N1\times V_{189}\times R2_{rab45}]_j$$

$$d[V_{165}\times R1_{rab45}]_j / dt = k_{int,V165\times R1,j}[V_{165}\times R1]_j - k_{rec4,V165\times R1,j}[V_{165}\times R1_{rab45}]$$
$$- k_{4to11,V165\times R1,j}[V_{165}\times R1_{rab45}] - k_{degr,V165\times R1,j}[V_{165}\times R1_{rab45}]$$
$$+ k_{on,V165\times R1,j}[V_{165,rab45}]_j[R1_{rab45}]_j - k_{off,V165\times R1,j}[V_{165}\times R1_{rab45}]_j$$

$$d[V_{189}\times R1_{rab45}]_j / dt = k_{int,V189\times R1,j}[V_{189}\times R1]_j - k_{rec4,V189\times R1,j}[V_{189}\times R1_{rab45}]$$
$$- k_{4to11,V189\times R1,j}[V_{189}\times R1_{rab45}] - k_{degr,V189\times R1,j}[V_{189}\times R1_{rab45}]$$
$$+ k_{on,V189\times R1,j}[V_{189,rab45}]_j[R1_{rab45}]_j - k_{off,V189\times R1,j}[V_{189}\times R1_{rab45}]_j$$

$$d[V_{121}\times R1_{rab45}]_j / dt = k_{int,V121\times R1,j}[V_{121}\times R1]_j - k_{rec4,V121\times R1,j}[V_{121}\times R1_{rab45}]$$
$$- k_{4to11,V121\times R1,j}[V_{121}\times R1_{rab45}] - k_{degr,V121\times R1,j}[V_{121}\times R1_{rab45}]$$
$$+ k_{on,V121\times R1,j}[V_{121,rab45}]_j[R1_{rab45}]_j - k_{off,V121\times R1,j}[V_{121}\times R1_{rab45}]_j$$
$$- k_{on,(V121\times R1)\times N1,j}[V_{121}\times R1_{rab45}]_j[N1_{rab45}]_j + k_{off,(V121\times R1)\times N1,j}[V_{121}\times R1\times N1_{rab45}]_j$$

$$d[V_{165b}\times R1_{rab45}]_j / dt = k_{int,V165b\times R1,j}[V_{165b}\times R1]_j - k_{rec4,V165b\times R1,j}[V_{165b}\times R1_{rab45}]$$
$$- k_{4to11,V165b\times R1,j}[V_{165b}\times R1_{rab45}] - k_{degr,V165b\times R1,j}[V_{165b}\times R1_{rab45}]$$
$$+ k_{on,V165b\times R1,j}[V_{165b,rab45}]_j[R1_{rab45}]_j - k_{off,V165b\times R1,j}[V_{165b}\times R1_{rab45}]_j$$
$$- k_{on,(V165b\times R1)\times N1,j}[V_{165b}\times R1_{rab45}]_j[N1_{rab45}]_j + k_{off,(V165b\times R1)\times N1,j}[V_{165b}\times R1\times N1_{rab45}]_j$$

$$d[P1 \times R1_{rab45}]_j / dt = k_{\text{int},P1 \times R1,j}[P1 \times R1]_j - k_{rec4,P1 \times R1,j}[P1 \times R1_{rab45}]$$
$$-k_{4to11,P1 \times R1,j}[P1 \times R1_{rab45}] - k_{\deg r,P1 \times R1,j}[P1 \times R1_{rab45}]$$
$$+k_{on,P1 \times R1,j}[P1_{rab45}]_j[R1_{rab45}]_j - k_{off,P1 \times R1,j}[P1 \times R1_{rab45}]_j$$
$$-k_{on,(P1 \times R1) \times N1,j}[P1 \times R1_{rab45}]_j[N1_{rab45}]_j + k_{off,(P1 \times R1) \times N1,j}[P1 \times R1 \times N1_{rab45}]_j$$

$$d[P2 \times R1_{rab45}]_j / dt = k_{\text{int},P2 \times R1,j}[P2 \times R1]_j - k_{rec4,P2 \times R1,j}[P2 \times R1_{rab45}]$$
$$-k_{4to11,P2 \times R1,j}[P2 \times R1_{rab45}] - k_{\deg r,P2 \times R1,j}[P2 \times R1_{rab45}]$$
$$+k_{on,P2 \times R1,j}[P2_{rab45}]_j[R1_{rab45}]_j - k_{off,P2 \times R1,j}[P2 \times R1_{rab45}]_j$$

$$d[V_{165} \times sR1_{rab45}]_j / dt = -k_{\deg r,V165 \times R1,j}[V_{165} \times R1_{rab45}]$$
$$+k_{on,V165 \times R1,j}[V_{165,rab45}]_j[sR1_{rab45}]_j - k_{off,V165 \times R1,j}[V_{165} \times R1_{rab45}]_j$$

$$d[V_{189} \times sR1_{rab45}]_j / dt = -k_{\deg r,V189 \times R1,j}[V_{189} \times R1_{rab45}]$$
$$+k_{on,V189 \times R1,j}[V_{189,rab45}]_j[sR1_{rab45}]_j - k_{off,V189 \times R1,j}[V_{189} \times R1_{rab45}]_j$$

$$d[V_{121} \times sR1_{rab45}]_j / dt = -k_{\deg r,V121 \times R1,j}[V_{121} \times R1_{rab45}]$$
$$+k_{on,V121 \times R1,j}[V_{121,rab45}]_j[sR1_{rab45}]_j - k_{off,V121 \times R1,j}[V_{121} \times R1_{rab45}]_j$$
$$-k_{on,(V121 \times R1) \times N1,j}[V_{121} \times R1_{rab45}]_j[N1_{rab45}]_j + k_{off,(V121 \times R1) \times N1,j}[V_{121} \times R1 \times N1_{rab45}]_j$$

$$d[V_{165b} \times sR1_{rab45}]_j / dt = -k_{\deg r,V165b \times R1,j}[V_{165b} \times R1_{rab45}]$$
$$+k_{on,V165b \times R1,j}[V_{165b,rab45}]_j[sR1_{rab45}]_j - k_{off,V165b \times R1,j}[V_{165b} \times R1_{rab45}]_j$$
$$-k_{on,(V165b \times R1) \times N1,j}[V_{165b} \times R1_{rab45}]_j[N1_{rab45}]_j + k_{off,(V165b \times R1) \times N1,j}[V_{165b} \times R1 \times N1_{rab45}]_j$$

$$d[P1 \times sR1_{rab45}]_j / dt = -k_{\deg r,P1 \times R1,j}[P1 \times sR1_{rab45}]$$
$$+k_{on,P1 \times R1,j}[P1_{rab45}]_j[sR1_{rab45}]_j - k_{off,P1 \times R1,j}[P1 \times sR1_{rab45}]_j$$
$$-k_{on,(P1 \times R1) \times N1,j}[P1 \times sR1_{rab45}]_j[N1_{rab45}]_j + k_{off,(P1 \times R1) \times N1,j}[P1 \times sR1 \times N1_{rab45}]_j$$

$$d[P2 \times sR1_{rab45}]_j / dt = -k_{\deg r,P2 \times R1,j}[P2 \times sR1_{rab45}]$$
$$+k_{on,P2 \times R1,j}[P2_{rab45}]_j[sR1_{rab45}]_j - k_{off,P2 \times R1,j}[P2 \times sR1_{rab45}]_j$$

$$d[V_{165} \times R2_{rab45}]_j / dt = k_{\text{int},V165 \times R2,j}[V_{165} \times R2]_j - k_{rec4,V165 \times R2,j}[V_{165} \times R2_{rab45}]$$
$$- k_{4to11,V165 \times R2,j}[V_{165} \times R2_{rab45}] - k_{\deg r,V165 \times R2,j}[V_{165} \times R2_{rab45}]$$
$$+ k_{on,V165 \times R2,j}[V_{165,rab45}]_j[R2_{rab45}]_j - k_{off,V165 \times R2,j}[V_{165} \times R2_{rab45}]_j$$
$$- k_{on,N1 \times (V165 \times R2),j}[N1_{rab45}]_j[V_{165} \times R2_{rab45}]_j + k_{off,N1 \times (V165 \times R2),j}[N1 \times V_{165} \times R2_{rab45}]_j$$

$$d[V_{189} \times R2_{rab45}]_j / dt = k_{\text{int},V189 \times R2,j}[V_{189} \times R2]_j - k_{rec4,V189 \times R2,j}[V_{189} \times R2_{rab45}]$$
$$- k_{4to11,V189 \times R2,j}[V_{189} \times R2_{rab45}] - k_{\deg r,V189 \times R2,j}[V_{189} \times R2_{rab45}]$$
$$+ k_{on,V189 \times R2,j}[V_{189,rab45}]_j[R2_{rab45}]_j - k_{off,V189 \times R2,j}[V_{189} \times R2_{rab45}]_j$$
$$- k_{on,N1 \times (V189 \times R2),j}[N1_{rab45}]_j[V_{189} \times R2_{rab45}]_j + k_{off,N1 \times (V189 \times R2),j}[N1 \times V_{189} \times R2_{rab45}]_j$$

$$d[V_{121} \times R2_{rab45}]_j / dt = k_{\text{int},V121 \times R2,j}[V_{121} \times R2]_j - k_{rec4,V121 \times R2,j}[V_{121} \times R2_{rab45}]$$
$$- k_{4to11,V121 \times R2,j}[V_{121} \times R2_{rab45}] - k_{\deg r,V121 \times R2,j}[V_{121} \times R2_{rab45}]$$
$$+ k_{on,V121 \times R2,j}[V_{121,rab45}]_j[R2_{rab45}]_j - k_{off,V121 \times R2,j}[V_{121} \times R2_{rab45}]_j$$

$$d[V_{165b} \times R2_{rab45}]_j / dt = k_{\text{int},V165b \times R2,j}[V_{165b} \times R2]_j - k_{rec4,V165b \times R2,j}[V_{165b} \times R2_{rab45}]$$
$$- k_{4to11,V165b \times R2,j}[V_{165b} \times R2_{rab45}] - k_{\deg r,V165b \times R2,j}[V_{165b} \times R2_{rab45}]$$
$$+ k_{on,V165b \times R2,j}[V_{165b,rab45}]_j[R2_{rab45}]_j - k_{off,V165b \times R2,j}[V_{165b} \times R2_{rab45}]_j$$

$$d[V_{165} \times N1_{rab45}]_j / dt = k_{\text{int},V165 \times N1,j}[V_{165} \times N1]_j - k_{rec4,V165 \times N1,j}[V_{165} \times N1_{rab45}]$$
$$- k_{4to11,V165 \times N1,j}[V_{165} \times N1_{rab45}] - k_{\deg r,V165 \times N1,j}[V_{165} \times N1_{rab45}]$$
$$+ k_{on,V165 \times N1,j}[V_{165,rab45}]_j[N1_{rab45}]_j - k_{off,V165 \times N1,j}[V_{165} \times N1_{rab45}]_j$$
$$- k_{on,(N1 \times V165) \times R2,j}[N1 \times V_{165,rab45}]_j[R2_{rab45}]_j + k_{off,(N1 \times V165) \times R2,j}[N1 \times V_{165} \times R2_{rab45}]_j$$

$$d[V_{189} \times N1_{rab45}]_j / dt = k_{\text{int},V189 \times N1,j}[V_{189} \times N1]_j - k_{rec4,V189 \times N1,j}[V_{189} \times N1_{rab45}]$$
$$- k_{4to11,V189 \times N1,j}[V_{189} \times N1_{rab45}] - k_{\deg r,V189 \times N1,j}[V_{189} \times N1_{rab45}]$$
$$+ k_{on,V189 \times N1,j}[V_{189,rab45}]_j[N1_{rab45}]_j - k_{off,V189 \times N1,j}[V_{189} \times N1_{rab45}]_j$$
$$- k_{on,(N1 \times V189) \times R2,j}[N1 \times V_{189,rab45}]_j[R2_{rab45}]_j + k_{off,(N1 \times V189) \times R2,j}[N1 \times V_{189} \times R2_{rab45}]_j$$

$$d[P2 \times N1_{rab45}]_j / dt = k_{\text{int},P2 \times N1,j}[P2 \times N1]_j - k_{rec4,P2 \times N1,j}[P2 \times N1_{rab45}]$$
$$- k_{4to11,P2 \times N1,j}[P2 \times N1_{rab45}] - k_{\deg r,P2 \times N1,j}[P2 \times N1_{rab45}]$$
$$+ k_{on,P2 \times N1,j}[P2_{rab45}]_j[N1_{rab45}]_j - k_{off,P2 \times N1,j}[P2 \times N1_{rab45}]_j$$

$$d[N1{\times}R1_{rab45}]_j / dt = k_{\text{int},N1{\times}R1,j}[N1{\times}R1]_j - k_{rec4,N1{\times}R1,j}[N1{\times}R1_{rab45}]$$

$$-k_{4to11,N1{\times}R1,j}[N1{\times}R1_{rab45}] - k_{\deg r,N1{\times}R1,j}[N1{\times}R1_{rab45}]$$

$$+k_{on,N1{\times}R1,j}[N1_{rab45}]_j[R1_{rab45}]_j - k_{off,N1{\times}R1,j}[N1{\times}R1_{rab45}]_j$$

$$-k_{on,V121{\times}(N1{\times}R1),j}[V_{121,rab45}]_j[N1{\times}R1_{rab45}]_j + k_{off,V121{\times}(N1{\times}R1),j}[V_{121}{\times}R1{\times}N1_{rab45}]_j$$

$$-k_{on,V165b{\times}(N1{\times}R1),j}[V_{165b,rab45}]_j[N1{\times}R1_{rab45}]_j + k_{off,V165b{\times}(N1{\times}R1),j}[V_{165b}{\times}R1{\times}N1_{rab45}]_j$$

$$-k_{on,P1{\times}(N1{\times}R1),j}[P1_{rab45}]_j[N1{\times}R1_{rab45}]_j + k_{off,P1{\times}(N1{\times}R1),j}[P1{\times}R1{\times}N1_{rab45}]_j$$

$$d[N1{\times}sR1_{rab45}]_j / dt = k_{\text{int},N1{\times}sR1,j}[N1{\times}sR1]_j - k_{rec4,N1{\times}sR1,j}[N1{\times}sR1_{rab45}]$$

$$-k_{4to11,N1{\times}sR1,j}[N1{\times}sR1_{rab45}] - k_{\deg r,N1{\times}sR1,j}[N1{\times}sR1_{rab45}]$$

$$+k_{on,N1{\times}sR1,j}[N1_{rab45}]_j[sR1_{rab45}]_j - k_{off,N1{\times}sR1,j}[N1{\times}sR1_{rab45}]_j$$

$$-k_{on,V121{\times}(N1{\times}sR1),j}[V_{121,rab45}]_j[N1{\times}sR1_{rab45}]_j + k_{off,V121{\times}(N1{\times}sR1),j}[V_{121}{\times}sR1{\times}N1_{rab45}]_j$$

$$-k_{on,V165b{\times}(N1{\times}sR1),j}[V_{165b,rab45}]_j[N1{\times}sR1_{rab45}]_j + k_{off,V165b{\times}(N1{\times}sR1),j}[V_{165b}{\times}sR1{\times}N1_{rab45}]_j$$

$$-k_{on,P1{\times}(N1{\times}sR1),j}[P1_{rab45}]_j[N1{\times}sR1_{rab45}]_j + k_{off,P1{\times}(N1{\times}sR1),j}[P1{\times}sR1{\times}N1_{rab45}]_j$$

$$d[N1{\times}V_{165}{\times}R2_{rab45}]_j / dt = k_{\text{int},N1{\times}V165{\times}R2,j}[N1{\times}V_{165}{\times}R2]_j - k_{rec4,N1{\times}V165{\times}R2,j}[N1{\times}V_{165}{\times}R2_{rab45}]$$

$$+k_{4to11,N1{\times}V165{\times}R2,j}[N1{\times}V_{165}{\times}R2_{rab45}] - k_{\deg r,N1{\times}V165{\times}R2,j}[N1{\times}V_{165}{\times}R2_{rab45}]$$

$$+k_{on,R2{\times}(N1{\times}V165),j}[R2_{rab45}]_j[V_{165}{\times}N1_{rab45}]_j - k_{off,R2{\times}(N1{\times}V165),j}[N1{\times}V_{165}{\times}R2_{rab45}]_j$$

$$+k_{on,N1{\times}(V165{\times}R2),j}[N1_{rab45}]_j[V_{165}{\times}R2_{rab45}]_j - k_{off,N1{\times}(V165{\times}R2),j}[N1{\times}V_{165}{\times}R2_{rab45}]_j$$

$$d[N1{\times}V_{189}{\times}R2_{rab45}]_j / dt = k_{\text{int},N1{\times}V189{\times}R2,j}[N1{\times}V_{189}{\times}R2]_j - k_{rec4,N1{\times}V189{\times}R2,j}[N1{\times}V_{189}{\times}R2_{rab45}]$$

$$-k_{4to11,N1{\times}V189{\times}R2,j}[N1{\times}V_{189}{\times}R2_{rab45}] - k_{\deg r,N1{\times}V189{\times}R2,j}[N1{\times}V_{189}{\times}R2_{rab45}]$$

$$+k_{on,R2{\times}(V189{\times}N1),j}[R2_{rab45}]_j[V_{189}{\times}N1_{rab45}]_j - k_{off,R2{\times}(N1{\times}V189),j}[N1{\times}V_{189}{\times}R2_{rab45}]_j$$

$$+k_{on,N1{\times}(V189{\times}R2),j}[N1_{rab45}]_j[V_{189}{\times}R2_{rab45}]_j - k_{off,N1{\times}(V189{\times}R2),j}[N1{\times}V_{189}{\times}R2_{rab45}]_j$$

$$d[V_{121}{\times}R1{\times}N1_{rab45}]_j / dt = k_{\text{int},V121{\times}R1{\times}N1,j}[V_{121}{\times}R1{\times}N1]_j - k_{rec4,V121{\times}R1{\times}N1,j}[V_{121}{\times}R1{\times}N1_{rab45}]$$

$$-k_{4to11,V121{\times}R1{\times}N1,j}[V_{121}{\times}R1{\times}N1_{rab45}] - k_{\deg r,V121{\times}R1{\times}N1,j}[V_{121}{\times}R1{\times}N1_{rab45}]$$

$$+k_{on,V121{\times}(R1{\times}N1),j}[V_{121,rab45}]_j[R1{\times}N1_{rab45}]_j - k_{off,V121{\times}(R1{\times}N1),j}[V_{121}{\times}R1{\times}N1_{rab45}]_j$$

$$+k_{on,(V121{\times}R1){\times}N1,j}[V_{121}{\times}R1_{rab45}]_j[N1_{rab45}]_j - k_{off,(V121{\times}R1){\times}N1,j}[V_{121}{\times}R1{\times}N1_{rab45}]_j$$

$$
\begin{aligned}
d[V_{165b}\times R1\times N1_{rab45}]_j / dt =\ & k_{\mathrm{int},V165b\times R1\times N1,j}[V_{165b}\times R1\times N1]_j - k_{rec4,V165b\times R1\times N1,j}[V_{165b}\times R1\times N1_{rab45}] \\
& -k_{4to11,V165b\times R1\times N1,j}[V_{165b}\times R1\times N1_{rab45}] - k_{\deg r,V165b\times R1\times N1,j}[V_{165b}\times R1\times N1_{rab45}] \\
& +k_{on,V165b\times(R1\times N1),j}[V_{165b,rab45}]_j[R1\times N1_{rab45}]_j - k_{off,V165b\times(R1\times N1),j}[V_{165b}\times R1\times N1_{rab45}]_j \\
& +k_{on,(V165b\times R1)\times N1,j}[V_{165b}\times R1_{rab45}]_j[N1_{rab45}]_j - k_{off,(V165b\times R1)\times N1,j}[V_{165b}\times R1\times N1_{rab45}]_j
\end{aligned}
$$

$$
\begin{aligned}
d[P1\times R1\times N1_{rab45}]_j / dt =\ & k_{\mathrm{int},P1\times R1\times N1,j}[P1\times R1\times N1]_j - k_{rec4,P1\times R1\times N1,j}[P1\times R1\times N1_{rab45}] \\
& -k_{4to11,P1\times R1\times N1,j}[P1\times R1\times N1_{rab45}] - k_{\deg r,P1\times R1\times N1,j}[P1\times R1\times N1_{rab45}] \\
& +k_{on,P1\times(R1\times N1),j}[P1_{rab45}]_j[R1\times N1_{rab45}]_j - k_{off,P1\times(R1\times N1),j}[P1\times R1\times N1_{rab45}]_j \\
& +k_{on,(P1\times R1)\times N1,j}[P1\times R1_{rab45}]_j[N1_{rab45}]_j - k_{off,(P1\times R1)\times N1,j}[P1\times R1\times N1_{rab45}]_j
\end{aligned}
$$

$$
\begin{aligned}
d[V_{121}\times sR1\times N1_{rab45}]_j / dt =\ & k_{\mathrm{int},V121\times sR1\times N1,j}[V_{121}\times sR1\times N1]_j - k_{rec4,V121\times sR1\times N1,j}[V_{121}\times sR1\times N1_{rab45}] \\
& -k_{4to11,V121\times sR1\times N1,j}[V_{121}\times sR1\times N1_{rab45}] - k_{\deg r,V121\times sR1\times N1,j}[V_{121}\times sR1\times N1_{rab45}] \\
& +k_{on,V121\times(sR1\times N1),j}[V_{121,rab45}]_j[sR1\times N1_{rab45}]_j - k_{off,V121\times(sR1\times N1),j}[V_{121}\times sR1\times N1_{rab45}]_j \\
& +k_{on,(V121\times sR1)\times N1,j}[V_{121}\times sR1_{rab45}]_j[N1_{rab45}]_j - k_{off,(V121\times sR1)\times N1,j}[V_{121}\times sR1\times N1_{rab45}]_j
\end{aligned}
$$

$$
\begin{aligned}
d[V_{165b}\times sR1\times N1_{rab45}]_j / dt =\ & k_{\mathrm{int},V165b\times sR1\times N1,j}[V_{165b}\times sR1\times N1]_j - k_{rec4,V165b\times sR1\times N1,j}[V_{165b}\times sR1\times N1_{rab45}] \\
& -k_{4to11,V165b\times sR1\times N1,j}[V_{165b}\times sR1\times N1_{rab45}] - k_{\deg r,V165b\times sR1\times N1,j}[V_{165b}\times sR1\times N1_{rab45}] \\
& +k_{on,V165b\times(sR1\times N1),j}[V_{165b,rab45}]_j[sR1\times N1_{rab45}]_j - k_{off,V165b\times(sR1\times N1),j}[V_{165b}\times sR1\times N1_{rab45}]_j \\
& +k_{on,(V165b\times sR1)\times N1,j}[V_{165b}\times sR1_{rab45}]_j[N1_{rab45}]_j - k_{off,(V165b\times sR1)\times N1,j}[V_{165b}\times sR1\times N1_{rab45}]_j
\end{aligned}
$$

$$
\begin{aligned}
d[P1\times sR1\times N1_{rab45}]_j / dt =\ & k_{\mathrm{int},P1\times sR1\times N1,j}[P1\times sR1\times N1]_j - k_{rec4,P1\times sR1\times N1,j}[P1\times sR1\times N1_{rab45}] \\
& -k_{4to11,P1\times sR1\times N1,j}[P1\times sR1\times N1_{rab45}] - k_{\deg r,P1\times sR1\times N1,j}[P1\times sR1\times N1_{rab45}] \\
& +k_{on,P1\times(sR1\times N1),j}[P1_{rab45}]_j[sR1\times N1_{rab45}]_j - k_{off,P1\times(sR1\times N1),j}[P1\times sR1\times N1_{rab45}]_j \\
& +k_{on,(P1\times sR1)\times N1,j}[P1\times sR1_{rab45}]_j[N1_{rab45}]_j - k_{off,(P1\times sR1)\times N1,j}[P1\times sR1\times N1_{rab45}]_j
\end{aligned}
$$

Rab11 Recycling Endosomes

$$d[R1_{rab11}]_j / dt = k_{4to11,R1,j}[R1_{rab45}] - k_{rec11,R1,j}[R1_{rab11}]$$

$$-k_{on,V165\times R1,j}[V_{165,rab11}]_j[R1_{rab11}]_j + k_{off,V165\times R1,j}[V_{165}\times R1_{rab11}]_j$$

$$-k_{on,V189\times R1,j}[V_{189,rab11}]_j[R1_{rab11}]_j + k_{off,V189\times R1,j}[V_{189}\times R1_{rab11}]_j$$

$$-k_{on,V121\times R1,j}[V_{121,rab45}]_j[R1_{rab11}]_j + k_{off,V121\times R1,j}[V_{121}\times R1_{rab11}]_j$$

$$-k_{on,V165b\times R1,j}[V_{165b,rab45}]_j[R1_{rab11}]_j + k_{off,V165b\times R1,j}[V_{165b}\times R1_{rab11}]_j$$

$$-k_{on,P1\times R1,j}[P1_{rab11}]_j[R1_{rab11}]_j + k_{off,P1\times R1,j}[P1\times R1_{rab11}]_j$$

$$-k_{on,P2\times R1,j}[P2_{rab11}]_j[R1_{rab11}]_j + k_{off,P2\times R1,j}[P2\times R1_{rab11}]_j$$

$$-k_{on,N1\times R1,j}[N1_{rab11}]_j[R1_{rab11}]_j + k_{off,N1\times R1,j}[N1\times R1_{rab11}]_j$$

$$d[R2_{rab11}]_j / dt = k_{4to11,R2,j}[R2_{rab45}] - k_{rec11,R2,j}[R2_{rab11}]$$

$$-k_{on,V165\times R2,j}[V_{165,rab11}]_j[R2_{rab11}]_j + k_{off,V165\times R2,j}[V_{165}\times R2_{rab11}]_j$$

$$-k_{on,V189\times R2,j}[V_{189,rab11}]_j[R2_{rab11}]_j + k_{off,V189\times R2,j}[V_{189}\times R2_{rab11}]_j$$

$$-k_{on,V121\times R2,j}[V_{121,rab11}]_j[R2_{rab11}]_j + k_{off,V121\times R2,j}[V_{121}\times R2_{rab11}]_j$$

$$-k_{on,V165b\times R2,j}[V_{165b,rab11}]_j[R2_{rab11}]_j + k_{off,V165b\times R2,j}[V_{165b}\times R2_{rab11}]_j$$

$$-k_{on,(N1\times V165)\times R2,j}[N1\times V_{165,rab11}]_j[R2_{rab11}]_j + k_{off,(N1\times V165)\times R2,j}[N1\times V_{165}\times R2_{rab11}]_j$$

$$-k_{on,(N1\times V189)\times R2,j}[N1\times V_{189,rab11}]_j[R2_{rab11}]_j + k_{off,(N1\times V189)\times R2,j}[N1\times V_{189}\times R2_{rab11}]_j$$

$$d[N1_{rab11}]_j / dt = k_{4to11,N1,j}[N1_{rab45}] - k_{rec11,N1,j}[N1_{rab11}]$$

$$-k_{on,V165\times N1,j}[V_{165,rab11}]_j[N1_{rab11}]_j + k_{off,V165\times N1,j}[V_{165}\times N1_{rab11}]_j$$

$$-k_{on,V189\times N1,j}[V_{189,rab11}]_j[N1_{rab11}]_j + k_{off,V189\times N1,j}[V_{189}\times N1_{rab11}]_j$$

$$-k_{on,P2\times N1,j}[P2_{rab11}]_j[N1_{rab11}]_j + k_{off,P2\times N1,j}[P2\times N1_{rab11}]_j$$

$$-k_{on,N1\times R1,j}[N1_{rab11}]_j[R1_{rab11}]_j + k_{off,N1\times R1,j}[N1\times R1_{rab11}]_j$$

$$-k_{on,N1\times sR1,j}[N1_{rab11}]_j[sR1_{rab11}]_j + k_{off,N1\times sR1,j}[N1\times sR1_{rab11}]_j$$

$$-k_{on,(V121\times R1)\times N1,j}[V_{121}\times R1_{rab11}]_j[N1_{rab11}]_j + k_{off,(V121\times R1)\times N1,j}[V_{121}\times R1\times N1_{rab11}]_j$$

$$-k_{on,(V165b\times R1)\times N1,j}[V_{165b}\times R1_{rab11}]_j[N1_{rab11}]_j + k_{off,(V165b\times R1)\times N1,j}[V_{165b}\times R1\times N1_{rab11}]_j$$

$$-k_{on,(P1\times R1)\times N1,j}[P1\times R1_{rab11}]_j[N1_{rab11}]_j + k_{off,(P1\times R1)\times N1,j}[P1\times R1\times N1_{rab11}]_j$$

$$-k_{on,N1\times(V165\times R2),j}[N1_{rab11}]_j[V_{165}\times R2_{rab11}]_j + k_{off,N1\times(V165\times R2),j}[N1\times V_{165}\times R2_{rab11}]_j$$

$$-k_{on,N1\times(V189\times R2),j}[N1_{rab11}]_j[V_{189}\times R2_{rab11}]_j + k_{off,N1\times(V189\times R2),j}[N1\times V_{189}\times R2_{rab11}]_j$$

$$d[V_{165} \times R1_{rab11}]_j / dt = k_{4to11,V165 \times R1,j}[V_{165} \times R1_{rab45}] - k_{rec11,V165 \times R1,j}[V_{165} \times R1_{rab11}]$$
$$+ k_{on,V165 \times R1,j}[V_{165,rab11}]_j[R1_{rab11}]_j - k_{off,V165 \times R1,j}[V_{165} \times R1_{rab11}]_j$$

$$d[V_{189} \times R1_{rab11}]_j / dt = k_{4to11,V189 \times R1,j}[V_{189} \times R1_{rab45}] - k_{rec11,V189 \times R1,j}[V_{189} \times R1_{rab11}]$$
$$+ k_{on,V189 \times R1,j}[V_{189,rab11}]_j[R1_{rab11}]_j - k_{off,V189 \times R1,j}[V_{189} \times R1_{rab11}]_j$$

$$d[V_{121} \times R1_{rab11}]_j / dt = k_{4to11,V121 \times R1,j}[V_{121} \times R1_{rab45}] - k_{rec11,V121 \times R1,j}[V_{121} \times R1_{rab11}]$$
$$+ k_{on,V121 \times R1,j}[V_{121,rab11}]_j[R1_{rab11}]_j - k_{off,V121 \times R1,j}[V_{121} \times R1_{rab11}]_j$$
$$- k_{on,(V121 \times R1) \times N1,j}[V_{121} \times R1_{rab11}]_j[N1_{rab11}]_j + k_{off,(V121 \times R1) \times N1,j}[V_{121} \times R1 \times N1_{rab11}]_j$$

$$d[V_{165b} \times R1_{rab11}]_j / dt = k_{4to11,V165b \times R1,j}[V_{165b} \times R1_{rab45}] - k_{rec11,V165b \times R1,j}[V_{165b} \times R1_{rab11}]$$
$$+ k_{on,V165b \times R1,j}[V_{165b,rab11}]_j[R1_{rab11}]_j - k_{off,V165b \times R1,j}[V_{165b} \times R1_{rab11}]_j$$
$$- k_{on,(V165b \times R1) \times N1,j}[V_{165b} \times R1_{rab11}]_j[N1_{rab11}]_j + k_{off,(V165b \times R1) \times N1,j}[V_{165b} \times R1 \times N1_{rab11}]_j$$

$$d[P1 \times R1_{rab11}]_j / dt = k_{4to11,P1 \times R1,j}[P1 \times R1_{rab45}] - k_{rec11,P1 \times R1,j}[P1 \times R1_{rab11}]$$
$$+ k_{on,P1 \times R1,j}[P1_{rab11}]_j[R1_{rab11}]_j - k_{off,P1 \times R1,j}[P1 \times R1_{rab11}]_j$$
$$- k_{on,(P1 \times R1) \times N1,j}[P1 \times R1_{rab11}]_j[N1_{rab11}]_j + k_{off,(P1 \times R1) \times N1,j}[P1 \times R1 \times N1_{rab11}]_j$$

$$d[P2 \times R1_{rab11}]_j / dt = k_{4to11,P2 \times R1,j}[P2 \times R1_{rab45}] - k_{rec11,P2 \times R1,j}[P2 \times R1_{rab11}]$$
$$+ k_{on,P2 \times R1,j}[P2_{rab11}]_j[R1_{rab11}]_j - k_{off,P2 \times R1,j}[P2 \times R1_{rab11}]_j$$

$$d[V_{165} \times sR1_{rab11}]_j / dt = k_{on,V165 \times sR1,j}[V_{165,rab11}]_j[sR1_{rab11}]_j - k_{off,V165 \times sR1,j}[V_{165} \times sR1_{rab11}]_j$$

$$d[V_{121} \times sR1_{rab11}]_j / dt = k_{on,V121 \times sR1,j}[V_{121,rab11}]_j[sR1_{rab11}]_j - k_{off,V121 \times sR1,j}[V_{121} \times sR1_{rab11}]_j$$
$$- k_{on,(V121 \times sR1) \times N1,j}[V_{121} \times sR1_{rab11}]_j[N1_{rab11}]_j + k_{off,(V121 \times sR1) \times N1,j}[V_{121} \times sR1 \times N1_{rab11}]_j$$

$$d[V_{165b} \times sR1_{rab11}]_j / dt = k_{on,V165b \times sR1,j}[V_{165b,rab11}]_j[sR1_{rab11}]_j - k_{off,V165b \times sR1,j}[V_{165b} \times sR1_{rab11}]_j$$
$$- k_{on,(V165b \times sR1) \times N1,j}[V_{165b} \times sR1_{rab11}]_j[N1_{rab11}]_j + k_{off,(V165b \times sR1) \times N1,j}[V_{165b} \times sR1 \times N1_{rab11}]_j$$

$$d[V_{189} \times sR1_{rab11}]_j / dt = k_{on,V189 \times sR1,j}[V_{189,rab11}]_j[sR1_{rab11}]_j - k_{off,V189 \times sR1,j}[V_{189} \times sR1_{rab11}]_j$$

$$d[P1 \times sR1_{rab11}]_j / dt = k_{on,P1 \times sR1,j}[P1_{rab11}]_j[sR1_{rab11}]_j - k_{off,P1 \times sR1,j}[P1 \times sR1_{rab11}]_j$$
$$- k_{on,(P1 \times sR1) \times N1,j}[P1 \times sR1_{rab11}]_j[N1_{rab11}]_j + k_{off,(P1 \times sR1) \times N1,j}[P1 \times sR1 \times N1_{rab11}]_j$$

$$d[P2 \times sR1_{rab11}]_j / dt = k_{on,P2 \times R1,j}[P2_{rab11}]_j[sR1_{rab11}]_j - k_{off,P2 \times R1,j}[P2 \times sR1_{rab11}]_j$$

$$d[V_{165} \times R2_{rab11}]_j / dt = k_{4to11,V165 \times R2,j}[V_{165} \times R2_{rab45}] - k_{rec11,V165 \times R2,j}[V_{165} \times R2_{rab11}]$$
$$+ k_{on,V165 \times R2,j}[V_{165,rab45}]_j[R2_{rab11}]_j - k_{off,V165 \times R2,j}[V_{165} \times R2_{rab11}]_j$$
$$- k_{on,N1 \times (V165 \times R2),j}[N1_{rab11}]_j[V_{165} \times R2_{rab11}]_j + k_{off,N1 \times (V165 \times R2),j}[N1 \times V_{165} \times R2_{rab11}]_j$$

$$d[V_{189} \times R2_{rab11}]_j / dt = k_{4to11,V189 \times R2,j}[V_{189} \times R2_{rab45}] - k_{rec11,V189 \times R2,j}[V_{189} \times R2_{rab11}]$$
$$+ k_{on,V189 \times R2,j}[V_{189,rab11}]_j[R2_{rab11}]_j - k_{off,V189 \times R2,j}[V_{189} \times R2_{rab11}]_j$$
$$- k_{on,N1 \times (V189 \times R2),j}[N1_{rab11}]_j[V_{189} \times R2_{rab11}]_j + k_{off,N1 \times (V189 \times R2),j}[N1 \times V_{189} \times R2_{rab11}]_j$$

$$d[V_{121} \times R2_{rab11}]_j / dt = k_{4to11,V121 \times R2,j}[V_{121} \times R2_{rab45}] - k_{rec11,V121 \times R2,j}[V_{121} \times R2_{rab11}]$$
$$+ k_{on,V121 \times R2,j}[V_{121,rab11}]_j[R2_{rab11}]_j - k_{off,V121 \times R2,j}[V_{121} \times R2_{rab11}]_j$$

$$d[V_{165b} \times R2_{rab11}]_j / dt = k_{4to11,V165b \times R2,j}[V_{165b} \times R2_{rab45}] - k_{rec11,V165b \times R2,j}[V_{165b} \times R2_{rab11}]$$
$$+ k_{on,V165b \times R2,j}[V_{165b,rab11}]_j[R2_{rab11}]_j - k_{off,V165b \times R2,j}[V_{165b} \times R2_{rab11}]_j$$

$$d[V_{165} \times N1_{rab11}]_j / dt = k_{4to11,V165 \times N1,j}[V_{165} \times N1_{rab45}] - k_{rec11,V165 \times N1,j}[V_{165} \times N1_{rab11}]$$
$$+ k_{on,V165 \times N1,j}[V_{165,rab11}]_j[N1_{rab11}]_j - k_{off,V165 \times N1,j}[V_{165} \times N1_{rab11}]_j$$
$$- k_{on,(N1 \times V165) \times R2,j}[N1 \times V_{165,rab11}]_j[R2_{rab11}]_j + k_{off,(N1 \times V165) \times R2,j}[N1 \times V_{165} \times R2_{rab11}]_j$$

$$d[V_{189} \times N1_{rab11}]_j / dt = k_{4to11,V189 \times N1,j}[V_{189} \times N1_{rab11}] - k_{rec11,V189 \times N1,j}[V_{189} \times N1_{rab11}]$$
$$+ k_{on,V189 \times N1,j}[V_{189,rab11}]_j[N1_{rab11}]_j - k_{off,V189 \times N1,j}[V_{189} \times N1_{rab11}]_j$$
$$- k_{on,(N1 \times V189) \times R2,j}[N1 \times V_{189,rab11}]_j[R2_{rab11}]_j + k_{off,(N1 \times V189) \times R2,j}[N1 \times V_{189} \times R2_{rab11}]_j$$

$$d[P2 \times N1_{rab11}]_j / dt = k_{4to11,P2 \times N1,j}[P2 \times N1_{rab45}] - k_{rec11,P2 \times N1,j}[P2 \times N1_{rab11}]$$
$$+ k_{on,P2 \times N1,j}[P2_{rab11}]_j[N1_{rab11}]_j - k_{off,P2 \times N1,j}[P2 \times N1_{rab11}]_j$$

$$d[N1 \times R1_{rab11}]_j / dt = k_{4to11,N1 \times R1,j}[N1 \times R1_{rab45}] - k_{rec11,N1 \times R1,j}[N1 \times R1_{rab11}]$$
$$+ k_{on,N1 \times R1,j}[N1_{rab11}]_j[R1_{rab11}]_j - k_{off,N1 \times R1,j}[N1 \times R1_{rab11}]_j$$
$$- k_{on,V121 \times (N1 \times R1),j}[V_{121,rab11}]_j[N1 \times R1_{rab11}]_j + k_{off,V121 \times (N1 \times R1),j}[V_{121} \times R1 \times N1_{rab11}]_j$$
$$- k_{on,V165b \times (N1 \times R1),j}[V_{165b,rab11}]_j[N1 \times R1_{rab11}]_j + k_{off,V165b \times (N1 \times R1),j}[V_{165b} \times R1 \times N1_{rab11}]_j$$
$$- k_{on,P1 \times (N1 \times R1),j}[P1_{rab11}]_j[N1 \times R1_{rab11}]_j + k_{off,P1 \times (N1 \times R1),j}[P1 \times R1 \times N1_{rab11}]_j$$

$$d[N1{\times}sR1_{rab11}]_j / dt = k_{4to11,N1{\times}sR1,j}[N1{\times}sR1_{rab45}] - k_{rec11,N1{\times}sR1,j}[N1{\times}sR1_{rab11}]$$
$$+ k_{on,N1{\times}sR1,j}[N1_{rab11}]_j[sR1_{rab11}]_j - k_{off,N1{\times}sR1,j}[N1{\times}sR1_{rab11}]_j$$
$$- k_{on,V121{\times}(N1{\times}sR1),j}[V_{121,rab11}]_j[N1{\times}sR1_{rab11}]_j + k_{off,V121{\times}(N1{\times}sR1),j}[V_{121}{\times}sR1{\times}N1_{rab11}]_j$$
$$- k_{on,V165b{\times}(N1{\times}sR1),j}[V_{165b,rab11}]_j[N1{\times}sR1_{rab11}]_j + k_{off,V165b{\times}(N1{\times}sR1),j}[V_{165b}{\times}sR1{\times}N1_{rab11}]_j$$
$$- k_{on,P1{\times}(N1{\times}sR1),j}[P1_{rab11}]_j[N1{\times}sR1_{rab11}]_j + k_{off,P1{\times}(N1{\times}sR1),j}[P1{\times}sR1{\times}N1_{rab11}]_j$$

$$d[N1{\times}V_{165}{\times}R2_{rab11}]_j / dt = k_{4to11,N1{\times}V165{\times}R2,j}[N1{\times}V_{165}{\times}R2_{rab45}] - k_{rec11,N1{\times}V165{\times}R2,j}[N1{\times}V_{165}{\times}R2_{rab11}]$$
$$+ k_{on,R2{\times}(N1{\times}V165),j}[R2_{rab11}]_j[V_{165}{\times}N1_{rab11}]_j - k_{off,R2{\times}(N1{\times}V165),j}[N1{\times}V_{165}{\times}R2_{rab11}]_j$$
$$+ k_{on,N1{\times}(V165{\times}R2),j}[N1_{rab11}]_j[V_{165}{\times}R2_{rab11}]_j - k_{off,N1{\times}(V165{\times}R2),j}[N1{\times}V_{165}{\times}R2_{rab11}]_j$$

$$d[N1{\times}V_{189}{\times}R2_{rab11}]_j / dt = k_{4to11,N1{\times}V189{\times}R2,j}[N1{\times}V_{189}{\times}R2_{rab45}] - k_{rec11,N1{\times}V189{\times}R2,j}[N1{\times}V_{189}{\times}R2_{rab11}]$$
$$+ k_{on,R2{\times}(V189{\times}N1),j}[R2_{rab11}]_j[V_{189}{\times}N1_{rab11}]_j - k_{off,R2{\times}(N1{\times}V189),j}[N1{\times}V_{189}{\times}R2_{rab11}]_j$$
$$+ k_{on,N1{\times}(V189{\times}R2),j}[N1_{rab11}]_j[V_{189}{\times}R2_{rab11}]_j - k_{off,N1{\times}(V189{\times}R2),j}[N1{\times}V_{189}{\times}R2_{rab11}]_j$$

$$d[V_{121}{\times}R1{\times}N1_{rab11}]_j / dt = k_{4to11,V121{\times}R1{\times}N1,j}[V_{121}{\times}R1{\times}N1_{rab45}] - k_{rec11,V121{\times}R1{\times}N1,j}[V_{121}{\times}R1{\times}N1_{rab11}]$$
$$+ k_{on,V121{\times}(R1{\times}N1),j}[V_{121,rab11}]_j[R1{\times}N1_{rab11}]_j - k_{off,V121{\times}(R1{\times}N1),j}[V_{121}{\times}R1{\times}N1_{rab11}]_j$$
$$+ k_{on,(V121{\times}R1){\times}N1,j}[V_{121}{\times}R1_{rab11}]_j[N1_{rab11}]_j - k_{off,(V121{\times}R1){\times}N1,j}[V_{121}{\times}R1{\times}N1_{rab11}]_j$$

$$d[V_{165b}{\times}R1{\times}N1_{rab11}]_j / dt = k_{4to11,V165b{\times}R1{\times}N1,j}[V_{165b}{\times}R1{\times}N1_{rab45}] - k_{rec11,V165b{\times}R1{\times}N1,j}[V_{165b}{\times}R1{\times}N1_{rab11}]$$
$$+ k_{on,V165b{\times}(R1{\times}N1),j}[V_{165b,rab11}]_j[R1{\times}N1_{rab11}]_j - k_{off,V165b{\times}(R1{\times}N1),j}[V_{165b}{\times}R1{\times}N1_{rab11}]_j$$
$$+ k_{on,(V165b{\times}R1){\times}N1,j}[V_{165b}{\times}R1_{rab11}]_j[N1_{rab11}]_j - k_{off,(V165b{\times}R1){\times}N1,j}[V_{165b}{\times}R1{\times}N1_{rab11}]_j$$

$$d[P1{\times}R1{\times}N1_{rab11}]_j / dt = k_{4to11,P1{\times}R1{\times}N1,j}[P1{\times}R1{\times}N1_{rab45}] - k_{rec11,P1{\times}R1{\times}N1,j}[P1{\times}R1{\times}N1_{rab11}]$$
$$+ k_{on,P1{\times}(R1{\times}N1),j}[P1_{rab11}]_j[R1{\times}N1_{rab11}]_j - k_{off,P1{\times}(R1{\times}N1),j}[P1{\times}R1{\times}N1_{rab11}]_j$$
$$+ k_{on,(P1{\times}R1){\times}N1,j}[P1{\times}R1_{rab11}]_j[N1_{rab11}]_j - k_{off,(P1{\times}R1){\times}N1,j}[P1{\times}R1{\times}N1_{rab11}]_j$$

$$d[V_{121}{\times}sR1{\times}N1_{rab11}]_j / dt = k_{4to11,V121{\times}sR1{\times}N1,j}[V_{121}{\times}sR1{\times}N1_{rab45}] - k_{degr,V121{\times}sR1{\times}N1,j}[V_{121}{\times}sR1{\times}N1_{rab11}]$$
$$+ k_{on,V121{\times}(sR1{\times}N1),j}[V_{121,rab11}]_j[sR1{\times}N1_{rab11}]_j - k_{off,V121{\times}(sR1{\times}N1),j}[V_{121}{\times}sR1{\times}N1_{rab11}]_j$$
$$+ k_{on,(V121{\times}sR1){\times}N1,j}[V_{121}{\times}sR1_{rab11}]_j[N1_{rab11}]_j - k_{off,(V121{\times}sR1){\times}N1,j}[V_{121}{\times}sR1{\times}N1_{rab11}]_j$$

$$d[V_{165b} \times R1 \times N1_{rab11}]_j / dt = k_{4to11,V165b \times R1 \times N1,j}[V_{165b} \times R1 \times N1_{rab45}] - k_{degr,V165b \times R1 \times N1,j}[V_{165b} \times R1 \times N1_{rab11}]$$

$$+ k_{on,V165b \times (sR1 \times N1),j}[V_{165b,rab11}]_j[sR1 \times N1_{rab11}]_j - k_{off,V165b \times (sR1 \times N1),j}[V_{165b} \times R1 \times N1_{rab11}]_j$$

$$+ k_{on,(V165b \times R1) \times N1,j}[V_{165b} \times R1_{rab11}]_j[N1_{rab11}]_j - k_{off,(V165b \times R1) \times N1,j}[V_{165b} \times R1 \times N1_{rab11}]_j$$

$$d[P1 \times R1 \times N1_{rab11}]_j / dt = k_{4to11,P1 \times R1 \times N1,j}[P1 \times R1 \times N1_{rab45}] - k_{rec11,P1 \times R1 \times N1,j}[P1 \times R1 \times N1_{rab11}]$$

$$+ k_{on,P1 \times (sR1 \times N1),j}[P1_{rab11}]_j[sR1 \times N1_{rab11}]_j - k_{off,P1 \times (sR1 \times N1),j}[P1 \times R1 \times N1_{rab11}]_j$$

$$+ k_{on,(P1 \times R1) \times N1,j}[P1 \times R1_{rab11}]_j[N1_{rab11}]_j - k_{off,(P1 \times R1) \times N1,j}[P1 \times R1 \times N1_{rab11}]_j$$

Interstitial Fluid- These 13 equations describe the free species found in the interstitial fluid in tissues, including free VEGF, PlGF, and sR1, and complexes of sR1 with ligands. q_X is the constant secretion of VEGF or PlGF isoforms from myocytes (molecules/myonuclear domain/s), or of sR1 from endothelial cells (molecules/EC/s), as given in **Table 7-SM1**, and converted into moles/cm^3 tissue as detailed in [13]. All molecular species in the interstitial fluid can be transported into the blood via lymphatic drainage (k_L in cm^3/s), or moved between the blood and tissue via bi-directional vascular permeability (k_p in cm/s). Vascular permeability depends on the total abluminal EC surface area, S_{jB} (cm^2). The endothelial cell surface recruitment factor γ is 1 in the Main Body Mass and 0.5 in the PAD Calf Muscle. As detailed above, U represents a volume, while K_{Av} is the fraction of the volume that is available. These geometric factors are included to account for the relevant volumes in the tissue and blood for exchange of molecular species; when one molecule is transported between tissue j and the blood, the concentration changes in j and the blood depend on the respective volumes.

$$d[V_{165}]_j / dt = q_{V165,j} - \frac{k_{L,j}}{U_j}\frac{[V_{165}]_j}{K_{Av,j}} + \frac{\gamma_j \cdot S_{jB}}{U_j} \cdot \left(k_{p,V}^{B \to j}\frac{[V_{165}]_B}{K_{AV,B}} - k_{p,V}^{j \to B}\frac{[V_{165}]_j}{K_{AV,j}} \right)$$

$$- k_{on,V165 \cdot M,j}[V_{165}]_j[M_{EBM}]_j + k_{off,V165 \cdot M,j}[V_{165} \cdot M_{EBM}]_j$$

$$- k_{on,V165 \cdot M,j}[V_{165}]_j[M_{ECM}]_j + k_{off,V165 \cdot M,j}[V_{165} \cdot M_{ECM}]_j$$

$$- k_{on,V165 \cdot M,j}[V_{165}]_j[M_{PBM}]_j + k_{off,V165 \cdot M,j}[V_{165} \cdot M_{PBM}]_j$$

$$- k_{on,V165 \cdot N1,j}[V_{165}]_j[N1]_j + k_{off,V165 \cdot N1,j}[V_{165} \cdot N1]_j$$

$$- k_{on,V165 \cdot R2,j}[V_{165}]_j[R2]_j + k_{off,V165 \cdot R2,j}[V_{165} \cdot R2]_j$$

$$- k_{on,V165 \cdot R1,j}[V_{165}]_j[R1]_j + k_{off,V165 \cdot R1,j}[V_{165} \cdot R1]_j$$

$$- k_{on,V165 \cdot sR1,j}[V_{165}]_j[sR1]_j + k_{off,V165 \cdot sR1,j}[V_{165} \cdot sR1]_j$$

$$d[V_{189}]_j / dt = q_{V189,j} - \frac{k_{L,j}}{U_j}\frac{[V_{189}]_j}{K_{Av,j}} + \frac{\gamma_j \cdot S_{jB}}{U_j}\cdot\left(k_{p,V}^{B\to j}\frac{[V_{189}]_B}{K_{AV,B}} - k_{p,V}^{j\to B}\frac{[V_{189}]_j}{K_{AV,j}} \right)$$

$$-k_{on,V189\cdot M,j}[V_{189}]_j[M_{EBM}]_j + k_{off,V189\cdot M,j}[V_{189}\cdot M_{EBM}]_j$$

$$-k_{on,V189\cdot M,j}[V_{189}]_j[M_{ECM}]_j + k_{off,V189\cdot M,j}[V_{189}\cdot M_{ECM}]_j$$

$$-k_{on,V189\cdot M,j}[V_{189}]_j[M_{PBM}]_j + k_{off,V189\cdot M,j}[V_{189}\cdot M_{PBM}]_j$$

$$-k_{on,V189\cdot N1,j}[V_{189}]_j[N1]_j + k_{off,V189\cdot N1,j}[V_{189}\cdot N1]_j$$

$$-k_{on,V189\cdot R2,j}[V_{189}]_j[R2]_j + k_{off,V189\cdot R2,j}[V_{189}\cdot R2]_j$$

$$-k_{on,V189\cdot R1,j}[V_{189}]_j[R1]_j + k_{off,V189\cdot R1,j}[V_{189}\cdot R1]_j$$

$$-k_{on,V189\cdot sR1,j}[V_{189}]_j[sR1]_j + k_{off,V189\cdot sR1,j}[V_{189}\cdot sR1]_j$$

$$d[V_{121}]_j / dt = q_{V121,j} - \frac{k_{L,j}}{U_j}\frac{[V_{121}]_j}{K_{Av,j}} + \frac{\gamma_j \cdot S_{jB}}{U_j}\cdot\left(k_{p,V}^{B\to j}\frac{[V_{121}]_B}{K_{AV,B}} - k_{p,V}^{j\to B}\frac{[V_{121}]_j}{K_{AV,j}} \right)$$

$$-k_{on,V121\cdot R2,j}[V_{121}]_j[R2]_j + k_{off,V121\cdot R2,j}[V_{121}\cdot R2]_j$$

$$-k_{on,V121\cdot R1,j}[V_{121}]_j[R1]_j + k_{off,V121\cdot R1,j}[V_{121}\cdot R1]_j$$

$$-k_{on,V121\cdot(R1\cdot N1),j}[V_{121}]_j[R1\cdot N1]_j + k_{off,V121\cdot(R1\cdot N1),j}[V_{121}\cdot R1\cdot N1]_j$$

$$-k_{on,V121\cdot sR1,j}[V_{121}]_j[sR1]_j + k_{off,V121\cdot sR1,j}[V_{121}\cdot sR1]_j$$

$$-k_{on,V121\cdot(sR1\cdot N1),j}[V_{121}]_j[sR1\cdot N1]_j + k_{off,V121\cdot(sR1\cdot N1),j}[V_{121}\cdot sR1\cdot N1]_j$$

$$-k_{on,V121\cdot(sR1\cdot M),j}[V_{121}]_j[sR1\cdot M_{EBM}]_j + k_{off,V121\cdot(sR1\cdot M),j}[V_{121}\cdot sR1\cdot M_{EBM}]_j$$

$$-k_{on,V121\cdot(sR1\cdot M),j}[V_{121}]_j[sR1\cdot M_{ECM}]_j + k_{off,V121\cdot(sR1\cdot M),j}[V_{121}\cdot sR1\cdot M_{ECM}]_j$$

$$-k_{on,V121\cdot(sR1\cdot M),j}[V_{121}]_j[sR1\cdot M_{PBM}]_j + k_{off,V121\cdot(sR1\cdot M),j}[V_{121}\cdot sR1\cdot M_{PBM}]_j$$

$$d[V_{165b}]_j / dt = q_{V165b,j} - \frac{k_{L,j}}{U_j}\frac{[V_{165b}]_j}{K_{Av,j}} + \frac{\gamma_j \cdot S_{jB}}{U_j}\cdot\left(k_{p,V}^{B\to j}\frac{[V_{165b}]_B}{K_{AV,B}} - k_{p,V}^{j\to B}\frac{[V_{165b}]_j}{K_{AV,j}} \right)$$

$$-k_{on,V165b\cdot R2,j}[V_{165b}]_j[R2]_j + k_{off,V165b\cdot R2,j}[V_{165b}\cdot R2]_j$$

$$-k_{on,V165b\cdot R1,j}[V_{165b}]_j[R1]_j + k_{off,V165b\cdot R1,j}[V_{165b}\cdot R1]_j$$

$$-k_{on,V165b\cdot(R1\cdot N1),j}[V_{165b}]_j[R1\cdot N1]_j + k_{off,V165b\cdot(R1\cdot N1),j}[V_{165b}\cdot R1\cdot N1]_j$$

$$-k_{on,V165b\cdot sR1,j}[V_{165b}]_j[sR1]_j + k_{off,V165b\cdot sR1,j}[V_{165b}\cdot sR1]_j$$

$$-k_{on,V165b\cdot(sR1\cdot N1),j}[V_{165b}]_j[sR1\cdot N1]_j + k_{off,V165b\cdot(sR1\cdot N1),j}[V_{165b}\cdot sR1\cdot N1]_j$$

$$-k_{on,V121\cdot(sR1\cdot M),j}[V_{121}]_j[sR1\cdot M_{EBM}]_j + k_{off,V121\cdot(sR1\cdot M),j}[V_{121}\cdot sR1\cdot M_{EBM}]_j$$

$$-k_{on,V121\cdot(sR1\cdot M),j}[V_{121}]_j[sR1\cdot M_{ECM}]_j + k_{off,V121\cdot(sR1\cdot M),j}[V_{121}\cdot sR1\cdot M_{ECM}]_j$$

$$-k_{on,V121\cdot(sR1\cdot M),j}[V_{121}]_j[sR1\cdot M_{PBM}]_j + k_{off,V121\cdot(sR1\cdot M),j}[V_{121}\cdot sR1\cdot M_{PBM}]_j$$

$$d[P1]_j / dt = q_{P1,j} - \frac{k_{L,j}}{U_j}\frac{[P1]_j}{K_{Av,j}} + \frac{\gamma_j \cdot S_{jB}}{U_j} \cdot \left(k_{p,P}^{B \to j} \frac{[P1]_B}{K_{AV,B}} - k_{p,P}^{j \to B} \frac{[P]_j}{K_{AV,j}} \right)$$

$$-k_{on,P1 \cdot R1,j}[P1]_j[R1]_j + k_{off,P1 \cdot R1,j}[P1 \cdot R1]_j$$

$$-k_{on,P1 \cdot (R1 \cdot N1),j}[P1]_j[R1 \cdot N1]_j + k_{off,P1 \cdot (R1 \cdot N1),j}[P1 \cdot R1 \cdot N1]_j$$

$$-k_{on,P1 \cdot sR1,j}[P1]_j[sR1]_j + k_{off,P1 \cdot sR1,j}[P1 \cdot sR1]_j$$

$$-k_{on,P1 \cdot (sR1 \cdot N1),j}[P1]_j[sR1 \cdot N1]_j + k_{off,P1 \cdot (sR1 \cdot N1),j}[P1 \cdot sR1 \cdot N1]_j$$

$$-k_{on,P1 \cdot (sR1 \cdot M),j}[P1]_j[sR1 \cdot M_{EBM}]_j + k_{off,P1 \cdot (sR1 \cdot M),j}[P1 \cdot sR1 \cdot M_{EBM}]_j$$

$$-k_{on,P1 \cdot (sR1 \cdot M),j}[P1]_j[sR1 \cdot M_{ECM}]_j + k_{off,P1 \cdot (sR1 \cdot M),j}[P1 \cdot sR1 \cdot M_{ECM}]_j$$

$$-k_{on,P1 \cdot (sR1 \cdot M),j}[P1]_j[sR1 \cdot M_{PBM}]_j + k_{off,P1 \cdot (sR1 \cdot M),j}[P1 \cdot sR1 \cdot M_{PBM}]_j$$

$$d[P2]_j / dt = q_{P2,j} - \frac{k_{L,j}}{U_j}\frac{[P2]_j}{K_{Av,j}} + \frac{\gamma_j \cdot S_{jB}}{U_j} \cdot \left(k_{p,P}^{B \to j} \frac{[P2]_B}{K_{AV,B}} - k_{p,P}^{j \to B} \frac{[P2]_j}{K_{AV,j}} \right)$$

$$-k_{on,P2 \cdot M,j}[P2]_j[M_{EBM}]_j + k_{off,P2 \cdot M,j}[P2 \cdot M_{EBM}]_j$$

$$-k_{on,P2 \cdot M,j}[P2]_j[M_{ECM}]_j + k_{off,P2 \cdot M,j}[P2 \cdot M_{ECM}]_j$$

$$-k_{on,P2 \cdot M,j}[P2]_j[M_{PBM}]_j + k_{off,P2 \cdot M,j}[P2 \cdot M_{PBM}]_j$$

$$-k_{on,P2 \cdot N1,j}[P2]_j[N1]_j + k_{off,P2 \cdot N1,j}[P2 \cdot N1]_j$$

$$-k_{on,P2 \cdot R1,j}[P2]_j[R1]_j + k_{off,P2 \cdot R1,j}[P2 \cdot R1]_j$$

$$-k_{on,P2 \cdot sR1,j}[P2]_j[sR1]_j + k_{off,P2 \cdot sR1,j}[P2 \cdot sR1]_j$$

$$d[sR1]_j / dt = q_{sR1,j} - \frac{k_{L,j}}{U_j} \frac{[sR1]_j}{K_{Av,j}} + \frac{\gamma_j \cdot S_{jB}}{U_j} \cdot \left(k_{p,sR1}^{B \to j} \frac{[sR1]_B}{K_{AV,B}} - k_{p,sR1}^{j \to B} \frac{[sR1]_j}{K_{AV,j}} \right)$$

$$- k_{on,V165 \cdot sR1,j}[V_{165}]_j[sR1]_j + k_{off,V165 \cdot sR1,j}[V_{165} \cdot sR1]_j$$

$$- k_{on,V189 \cdot sR1,j}[V_{189}]_j[sR1]_j + k_{off,V189 \cdot sR1,j}[V_{189} \cdot sR1]_j$$

$$- k_{on,V121 \cdot sR1,j}[V_{121}]_j[sR1]_j + k_{off,V121 \cdot sR1,j}[V_{121} \cdot sR1]_j$$

$$- k_{on,V165b \cdot sR1,j}[V_{165b}]_j[sR1]_j + k_{off,V165b \cdot sR1,j}[V_{165b} \cdot sR1]_j$$

$$- k_{on,P1 \cdot sR1,j}[P1]_j[sR1]_j + k_{off,P1 \cdot sR1,j}[P1 \cdot sR1]_j$$

$$- k_{on,P2 \cdot sR1,j}[P2]_j[sR1]_j + k_{off,P2 \cdot sR1,j}[P2 \cdot sR1]_j$$

$$- k_{on,sR1 \cdot M,j}[sR1]_j[M_{EBM}]_j + k_{off,sR1 \cdot M,j}[sR1 \cdot M_{EBM}]_j$$

$$- k_{on,sR1 \cdot M,j}[sR1]_j[M_{ECM}]_j + k_{off,sR1 \cdot M,j}[sR1 \cdot M_{ECM}]_j$$

$$- k_{on,sR1 \cdot M,j}[sR1]_j[M_{PBM}]_j + k_{off,sR1 \cdot M,j}[sR1 \cdot M_{PBM}]_j$$

$$- k_{on,sR1 \cdot N1,j}[sR1]_j[N1]_j + k_{off,sR1 \cdot N1,j}[sR1 \cdot N1]_j$$

$$- k_{on,sR1 \cdot (V165 \cdot M),j}[sR1]_j[V_{165} \cdot M_{EBM}]_j + k_{off,sR1 \cdot (V165 \cdot M),j}[sR1 \cdot V_{165} \cdot M_{EBM}]_j$$

$$- k_{on,sR1 \cdot (V189 \cdot M),j}[sR1]_j[V_{189} \cdot M_{EBM}]_j + k_{off,sR1 \cdot (V189 \cdot M),j}[sR1 \cdot V_{189} \cdot M_{EBM}]_j$$

$$- k_{on,sR1 \cdot (P2 \cdot M),j}[sR1]_j[P2 \cdot M_{EBM}]_j + k_{off,sR1 \cdot (P2 \cdot M),j}[sR1 \cdot P2 \cdot M_{EBM}]_j$$

$$- k_{on,sR1 \cdot (V165 \cdot M),j}[sR1]_j[V_{165} \cdot M_{ECM}]_j + k_{off,sR1 \cdot (V165 \cdot M),j}[sR1 \cdot V_{165} \cdot M_{ECM}]_j$$

$$- k_{on,sR1 \cdot (V189 \cdot M),j}[sR1]_j[V_{189} \cdot M_{ECM}]_j + k_{off,sR1 \cdot (V189 \cdot M),j}[sR1 \cdot V_{189} \cdot M_{ECM}]_j$$

$$- k_{on,sR1 \cdot (P2 \cdot M),j}[sR1]_j[P2 \cdot M_{ECM}]_j + k_{off,sR1 \cdot (P2 \cdot M),j}[sR1 \cdot P2 \cdot M_{ECM}]_j$$

$$- k_{on,sR1 \cdot (V165 \cdot M),j}[sR1]_j[V_{165} \cdot M_{PBM}]_j + k_{off,sR1 \cdot (V165 \cdot M),j}[sR1 \cdot V_{165} \cdot M_{PBM}]_j$$

$$- k_{on,sR1 \cdot (V189 \cdot M),j}[sR1]_j[V_{189} \cdot M_{PBM}]_j + k_{off,sR1 \cdot (V189 \cdot M),j}[sR1 \cdot V_{189} \cdot M_{PBM}]_j$$

$$- k_{on,sR1 \cdot (P2 \cdot M),j}[sR1]_j[P2 \cdot M_{PBM}]_j + k_{off,sR1 \cdot (P2 \cdot M),j}[sR1 \cdot P2 \cdot M_{PBM}]_j$$

$$d[V_{165} \cdot sR1]_j / dt = - \frac{k_{L,j}}{U_j} \frac{[V_{165} \cdot sR1]_j}{K_{Av,j}} + \frac{\gamma_j \cdot S_{jB}}{U_j} \cdot \left(k_{p,sR1}^{B \to j} \frac{[V_{165} \cdot sR1]_B}{K_{AV,B}} - k_{p,sR1}^{j \to B} \frac{[V_{165} \cdot sR1]_j}{K_{AV,j}} \right)$$

$$+ k_{on,V165 \cdot sR1,j}[V_{165}]_j[sR1]_j - k_{off,V165 \cdot sR1,j}[V_{165} \cdot sR1]_j$$

$$- k_{on,M \cdot (V165 \cdot sR1),j}[M_{EBM}]_j[V_{165} \cdot sR1]_j + k_{off,M \cdot (V165 \cdot sR1),j}[M_{EBM} \cdot V_{165} \cdot sR1]_j$$

$$- k_{on,M \cdot (V165 \cdot sR1),j}[M_{ECM}]_j[V_{165} \cdot sR1]_j + k_{off,M \cdot (V165 \cdot sR1),j}[M_{ECM} \cdot V_{165} \cdot sR1]_j$$

$$- k_{on,M \cdot (V165 \cdot sR1),j}[M_{PBM}]_j[V_{165} \cdot sR1]_j + k_{off,M \cdot (V165 \cdot sR1),j}[M_{PBM} \cdot V_{165} \cdot sR1]_j$$

$$d[V_{189} \cdot sR1]_j / dt = -\frac{k_{L,j}}{U_j} \frac{[V_{189} \cdot sR1]_j}{K_{Av,j}} + \frac{\gamma_j \cdot S_{jB}}{U_j} \cdot \left(k_{p,sR1}^{B \to j} \frac{[V_{189} \cdot sR1]_B}{K_{AV,B}} - k_{p,sR1}^{j \to B} \frac{[V_{189} \cdot sR1]_j}{K_{AV,j}} \right)$$

$$+ k_{on,V189 \cdot sR1,j}[V_{189}]_j[sR1]_j - k_{off,V189 \cdot sR1,j}[V_{189} \cdot sR1]_j$$

$$- k_{on,M \cdot (V189 \cdot sR1),j}[M_{EBM}]_j[V_{189} \cdot sR1]_j + k_{off,M \cdot (V189 \cdot sR1),j}[M_{EBM} \cdot V_{189} \cdot sR1]_j$$

$$- k_{on,M \cdot (V189 \cdot sR1),j}[M_{ECM}]_j[V_{189} \cdot sR1]_j + k_{off,M \cdot (V189 \cdot sR1),j}[M_{ECM} \cdot V_{189} \cdot sR1]_j$$

$$- k_{on,M \cdot (V189 \cdot sR1),j}[M_{PBM}]_j[V_{189} \cdot sR1]_j + k_{off,M \cdot (V189 \cdot sR1),j}[M_{PBM} \cdot V_{189} \cdot sR1]_j$$

$$d[V_{121} \cdot sR1]_j / dt = -\frac{k_{L,j}}{U_j} \frac{[V_{121} \cdot sR1]_j}{K_{Av,j}} + \frac{\gamma_j \cdot S_{jB}}{U_j} \cdot \left(k_{p,sR1}^{B \to j} \frac{[V_{121} \cdot sR1]_B}{K_{AV,B}} - k_{p,sR1}^{j \to B} \frac{[V_{121} \cdot sR1]_j}{K_{AV,j}} \right)$$

$$+ k_{on,V121 \cdot sR1,j}[V_{121}]_j[sR1]_j - k_{off,V121 \cdot sR1,j}[V_{121} \cdot sR1]_j$$

$$- k_{on,(M \cdot sR1) \cdot V121,j}[M_{EBM} \cdot sR1]_j[V_{121}]_j + k_{off,(M \cdot sR1) \cdot V121,j}[M_{EBM} \cdot sR1 \cdot V_{121}]_j$$

$$- k_{on,(M \cdot sR1) \cdot V121,j}[M_{ECM} \cdot sR1]_j[V_{121}]_j + k_{off,(M \cdot sR1) \cdot V121,j}[M_{ECM} \cdot sR1 \cdot V_{121}]_j$$

$$- k_{on,(M \cdot sR1) \cdot V121,j}[M_{PBM} \cdot sR1]_j[V_{121}]_j + k_{off,(M \cdot sR1) \cdot V121,j}[M_{PBM} \cdot sR1 \cdot V_{121}]_j$$

$$d[V_{165b} \cdot sR1]_j / dt = -\frac{k_{L,j}}{U_j} \frac{[V_{165b} \cdot sR1]_j}{K_{Av,j}} + \frac{\gamma_j \cdot S_{jB}}{U_j} \cdot \left(k_{p,sR1}^{B \to j} \frac{[V_{165b} \cdot sR1]_B}{K_{AV,B}} - k_{p,sR1}^{j \to B} \frac{[V_{165b} \cdot sR1]_j}{K_{AV,j}} \right)$$

$$+ k_{on,V165b \cdot sR1,j}[V_{165b}]_j[sR1]_j - k_{off,V165b \cdot sR1,j}[V_{165b} \cdot sR1]_j$$

$$- k_{on,(M \cdot sR1) \cdot V165b,j}[M_{EBM} \cdot sR1]_j[V_{165b}]_j + k_{off,(M \cdot sR1) \cdot V165b,j}[M_{EBM} \cdot sR1 \cdot V_{165b}]_j$$

$$- k_{on,(M \cdot sR1) \cdot V165b,j}[M_{ECM} \cdot sR1]_j[V_{165b}]_j + k_{off,(M \cdot sR1) \cdot V165b,j}[M_{ECM} \cdot sR1 \cdot V_{165b}]_j$$

$$- k_{on,(M \cdot sR1) \cdot V165b,j}[M_{PBM} \cdot sR1]_j[V_{165b}]_j + k_{off,(M \cdot sR1) \cdot V165b,j}[M_{PBM} \cdot sR1 \cdot V_{165b}]_j$$

$$d[P1 \cdot sR1]_j / dt = -\frac{k_{L,j}}{U_j} \frac{[P1 \cdot sR1]_j}{K_{Av,j}} + \frac{\gamma_j \cdot S_{jB}}{U_j} \cdot \left(k_{p,sR1}^{B \to j} \frac{[P1 \cdot sR1]_B}{K_{AV,B}} - k_{p,sR1}^{j \to B} \frac{[P1 \cdot sR1]_j}{K_{AV,j}} \right)$$

$$+ k_{on,P1 \cdot sR1,j}[P1]_j[sR1]_j - k_{off,P1 \cdot sR1,j}[P1 \cdot sR1]_j$$

$$- k_{on,(M \cdot sR1) \cdot P1,j}[M_{EBM} \cdot sR1]_j[P1]_j + k_{off,(M \cdot sR1) \cdot P1,j}[M_{EBM} \cdot sR1 \cdot P1]_j$$

$$- k_{on,(M \cdot sR1) \cdot P1,j}[M_{ECM} \cdot sR1]_j[P1]_j + k_{off,(M \cdot sR1) \cdot P1,j}[M_{ECM} \cdot sR1 \cdot P1]_j$$

$$- k_{on,(M \cdot sR1) \cdot P1,j}[M_{PBM} \cdot sR1]_j[P1]_j + k_{off,(M \cdot sR1) \cdot P1,j}[M_{PBM} \cdot sR1 \cdot P1]_j$$

$$d[P2 \cdot sR1]_j / dt = -\frac{k_{L,j}}{U_j} \frac{[P2 \cdot sR1]_j}{K_{Av,j}} + \frac{\gamma_j \cdot S_{jB}}{U_j} \cdot \left(k_{p,sR1}^{B \to j} \frac{[P2 \cdot sR1]_B}{K_{AV,B}} - k_{p,sR1}^{j \to B} \frac{[P2 \cdot sR1]_j}{K_{AV,j}} \right)$$

$$+ k_{on,P2 \cdot sR1,j}[P2]_j[sR1]_j - k_{off,P2 \cdot sR1,j}[P2 \cdot sR1]_j$$

$$- k_{on,M \cdot (P2 \cdot sR1),j}[M_{EBM}]_j[P2 \cdot sR1]_j + k_{off,M \cdot (P2 \cdot sR1),j}[M_{EBM} \cdot P2 \cdot sR1]_j$$

$$- k_{on,M \cdot (P2 \cdot sR1),j}[M_{ECM}]_j[P2 \cdot sR1]_j + k_{off,M \cdot (P2 \cdot sR1),j}[M_{ECM} \cdot P2 \cdot sR1]_j$$

$$- k_{on,M \cdot (P2 \cdot sR1),j}[M_{PBM}]_j[P2 \cdot sR1]_j + k_{off,M \cdot (P2 \cdot sR1),j}[M_{PBM} \cdot P2 \cdot sR1]_j$$

A.3.3 Blood Equations

The final set of 13 equations describes the binding and unbinding of molecular species in the blood, as well as clearance (k_{CL} in s^{-1}). $q_{165b,mono}$ represents secretion of $VEGF_{165b}$ into the blood by monocytes.

$$d[V_{165}]_B / dt = -k_{CL,V165} + \frac{k_{L,N}}{U_B} \frac{[V_{165}]_N}{K_{Av,N}} + \frac{k_{L,D}}{U_B} \frac{[V_{165}]_D}{K_{Av,D}}$$

$$+ \frac{\gamma_N \cdot S_{NB}}{U_B} \cdot \left(k_{p,V}^{N \to B} \frac{[V_{165}]_N}{K_{AV,N}} - k_{p,V}^{B \to N} \frac{[V_{165}]_B}{K_{AV,B}} \right)$$

$$+ \frac{\gamma_D \cdot S_{DB}}{U_B} \cdot \left(k_{p,V}^{D \to B} \frac{[V_{165}]_D}{K_{AV,D}} - k_{p,V}^{B \to D} \frac{[V_{165}]_B}{K_{AV,B}} \right)$$

$$- k_{on,V165 \cdot sR1}[V_{165}]_B[sR1]_B + k_{off,V165 \cdot sR1,j}[V_{165} \cdot sR1]_B$$

$$d[V_{189}]_B / dt = -k_{CL,V189} + \frac{k_{L,N}}{U_B} \frac{[V_{189}]_N}{K_{Av,N}} + \frac{k_{L,D}}{U_B} \frac{[V_{189}]_D}{K_{Av,D}}$$

$$+ \frac{\gamma_N \cdot S_{NB}}{U_B} \cdot \left(k_{p,V}^{N \to B} \frac{[V_{189}]_N}{K_{AV,N}} - k_{p,V}^{B \to N} \frac{[V_{189}]_B}{K_{AV,B}} \right)$$

$$+ \frac{\gamma_D \cdot S_{DB}}{U_B} \cdot \left(k_{p,V}^{D \to B} \frac{[V_{189}]_D}{K_{AV,D}} - k_{p,V}^{B \to D} \frac{[V_{189}]_B}{K_{AV,B}} \right)$$

$$- k_{on,V189 \cdot sR1}[V_{189}]_B[sR1]_B + k_{off,V189 \cdot sR1,j}[V_{189} \cdot sR1]_B$$

$$d[V_{121}]_B / dt = -k_{CL,V121} + \frac{k_{L,N}}{U_B}\frac{[V_{121}]_N}{K_{Av,N}} + \frac{k_{L,D}}{U_B}\frac{[V_{121}]_D}{K_{Av,D}}$$

$$+ \frac{\gamma_N \cdot S_{NB}}{U_B} \cdot \left(k_{p,V}^{N\to B}\frac{[V_{121}]_N}{K_{AV,N}} - k_{p,V}^{B\to N}\frac{[V_{121}]_B}{K_{AV,B}} \right)$$

$$+ \frac{\gamma_D \cdot S_{DB}}{U_B} \cdot \left(k_{p,V}^{D\to B}\frac{[V_{121}]_D}{K_{AV,D}} - k_{p,V}^{B\to D}\frac{[V_{121}]_B}{K_{AV,B}} \right)$$

$$- k_{on,V121\cdot sR1}[V_{121}]_B[sR1]_B + k_{off,V121\cdot sR1,j}[V_{121}\cdot sR1]_B$$

$$d[V_{165b}]_B / dt = q_{V165b,mono} - k_{CL,V165b} + \frac{k_{L,N}}{U_B}\frac{[V_{165b}]_N}{K_{Av,N}} + \frac{k_{L,D}}{U_B}\frac{[V_{165b}]_D}{K_{Av,D}}$$

$$+ \frac{\gamma_N \cdot S_{NB}}{U_B} \cdot \left(k_{p,V}^{N\to B}\frac{[V_{165b}]_N}{K_{AV,N}} - k_{p,V}^{B\to N}\frac{[V_{165b}]_B}{K_{AV,B}} \right)$$

$$+ \frac{\gamma_D \cdot S_{DB}}{U_B} \cdot \left(k_{p,V}^{D\to B}\frac{[V_{165b}]_D}{K_{AV,D}} - k_{p,V}^{B\to D}\frac{[V_{165b}]_B}{K_{AV,B}} \right)$$

$$- k_{on,V165b\cdot sR1}[V_{165b}]_B[sR1]_B + k_{off,V165b\cdot sR1,j}[V_{165b}\cdot sR1]_B$$

$$d[P1]_B / dt = -k_{CL,P1} + \frac{k_{L,N}}{U_B}\frac{[P1]_N}{K_{Av,N}} + \frac{k_{L,D}}{U_B}\frac{[P1]_D}{K_{Av,D}}$$

$$+ \frac{\gamma_N \cdot S_{NB}}{U_B} \cdot \left(k_{p,P}^{N\to B}\frac{[P1]_N}{K_{AV,N}} - k_{p,P}^{B\to N}\frac{[P1]_B}{K_{AV,B}} \right)$$

$$+ \frac{\gamma_D \cdot S_{DB}}{U_B} \cdot \left(k_{p,P}^{D\to B}\frac{[P1]_D}{K_{AV,D}} - k_{p,P}^{B\to D}\frac{[P1]_B}{K_{AV,B}} \right)$$

$$- k_{on,P1\cdot sR1}[P1]_B[sR1]_B + k_{off,P1\cdot sR1,j}[P1\cdot sR1]_B$$

$$d[P2]_B / dt = -k_{CL,P2} + \frac{k_{L,N}}{U_B}\frac{[P2]_N}{K_{Av,N}} + \frac{k_{L,D}}{U_B}\frac{[P2]_D}{K_{Av,D}}$$

$$+ \frac{\gamma_N \cdot S_{NB}}{U_B} \cdot \left(k_{p,P}^{N\to B}\frac{[P2]_N}{K_{AV,N}} - k_{p,P}^{B\to N}\frac{[P2]_B}{K_{AV,B}} \right)$$

$$+ \frac{\gamma_D \cdot S_{DB}}{U_B} \cdot \left(k_{p,P}^{D\to B}\frac{[P2]_D}{K_{AV,D}} - k_{p,P}^{B\to D}\frac{[P2]_B}{K_{AV,B}} \right)$$

$$- k_{on,P2\cdot sR1}[P2]_B[sR1]_B + k_{off,P2\cdot sR1,j}[P2\cdot sR1]_B$$

$$d[sR1]_B / dt = -k_{CL,sR1} + \frac{k_{L,N}}{U_B}\frac{[sR1]_N}{K_{Av,N}} + \frac{k_{L,D}}{U_B}\frac{[sR1]_D}{K_{Av,D}}$$

$$+ \frac{\gamma_N \cdot S_{NB}}{U_B} \cdot \left(k_{p,sR1}^{N\to B}\frac{[sR1]_N}{K_{AV,N}} - k_{p,sR1}^{B\to N}\frac{[sR1]_B}{K_{AV,B}} \right)$$

$$+ \frac{\gamma_D \cdot S_{DB}}{U_B} \cdot \left(k_{p,sR1}^{D\to B}\frac{[sR1]_D}{K_{AV,D}} - k_{p,sR1}^{B\to D}\frac{[sR1]_B}{K_{AV,B}} \right)$$

$$- k_{on,V165\cdot sR1}[V_{165}]_B[sR1]_B + k_{off,V165\cdot sR1,j}[V_{165}\cdot sR1]_B$$

$$- k_{on,V189\cdot sR1}[V_{189}]_B[sR1]_B + k_{off,V189\cdot sR1,j}[V_{189}\cdot sR1]_B$$

$$- k_{on,V121\cdot sR1}[V_{121}]_B[sR1]_B + k_{off,V121\cdot sR1,j}[V_{121}\cdot sR1]_B$$

$$- k_{on,V165b\cdot sR1}[V_{165b}]_B[sR1]_B + k_{off,V165b\cdot sR1,j}[V_{165b}\cdot sR1]_B$$

$$- k_{on,P1\cdot sR1}[P1]_B[sR1]_B + k_{off,P1\cdot sR1,j}[P1\cdot sR1]_B$$

$$- k_{on,P2\cdot sR1}[P2]_B[sR1]_B + k_{off,P2\cdot sR1,j}[P2\cdot sR1]_B$$

$$d[V_{165}\cdot sR1]_B / dt = -k_{CL,V165\cdot sR1} + \frac{k_{L,N}}{U_B}\frac{[V_{165}\cdot sR1]_N}{K_{Av,N}} + \frac{k_{L,D}}{U_B}\frac{[V_{165}\cdot sR1]_D}{K_{Av,D}}$$

$$+ \frac{\gamma_N \cdot S_{NB}}{U_B} \cdot \left(k_{p,sR1}^{N\to B}\frac{[V_{165}\cdot sR1]_N}{K_{AV,N}} - k_{p,sR1}^{B\to N}\frac{[V_{165}\cdot sR1]_B}{K_{AV,B}} \right)$$

$$+ \frac{\gamma_D \cdot S_{DB}}{U_B} \cdot \left(k_{p,sR1}^{D\to B}\frac{[V_{165}\cdot sR1]_D}{K_{AV,D}} - k_{p,sR1}^{B\to D}\frac{[V_{165}\cdot sR1]_B}{K_{AV,B}} \right)$$

$$+ k_{on,V165\cdot sR1}[V_{165}]_B[sR1]_B - k_{off,V165\cdot sR1,j}[V_{165}\cdot sR1]_B$$

$$d[V_{189}\cdot sR1]_B / dt = -k_{CL,V189\cdot sR1} + \frac{k_{L,N}}{U_B}\frac{[V_{189}\cdot sR1]_N}{K_{Av,N}} + \frac{k_{L,D}}{U_B}\frac{[V_{189}\cdot sR1]_D}{K_{Av,D}}$$

$$+ \frac{\gamma_N \cdot S_{NB}}{U_B} \cdot \left(k_{p,sR1}^{N\to B}\frac{[V_{189}\cdot sR1]_N}{K_{AV,N}} - k_{p,sR1}^{B\to N}\frac{[V_{189}\cdot sR1]_B}{K_{AV,B}} \right)$$

$$+ \frac{\gamma_D \cdot S_{DB}}{U_B} \cdot \left(k_{p,sR1}^{D\to B}\frac{[V_{189}\cdot sR1]_D}{K_{AV,D}} - k_{p,sR1}^{B\to D}\frac{[V_{189}\cdot sR1]_B}{K_{AV,B}} \right)$$

$$+ k_{on,V189\cdot sR1}[V_{189}]_B[sR1]_B - k_{off,V189\cdot sR1,j}[V_{189}\cdot sR1]_B$$

$$d[V_{121} \cdot sR1]_B / dt = -k_{CL,V121 \cdot sR1} + \frac{k_{L,N}}{U_B} \frac{[V_{121} \cdot sR1]_N}{K_{Av,N}} + \frac{k_{L,D}}{U_B} \frac{[V_{121} \cdot sR1]_D}{K_{Av,D}}$$

$$+ \frac{\gamma_N \cdot S_{NB}}{U_B} \cdot \left(k_{p,sR1}^{N \to B} \frac{[V_{121} \cdot sR1]_N}{K_{AV,N}} - k_{p,sR1}^{B \to N} \frac{[V_{121} \cdot sR1]_B}{K_{AV,B}} \right)$$

$$+ \frac{\gamma_D \cdot S_{DB}}{U_B} \cdot \left(k_{p,sR1}^{D \to B} \frac{[V_{121} \cdot sR1]_D}{K_{AV,D}} - k_{p,sR1}^{B \to D} \frac{[V_{121} \cdot sR1]_B}{K_{AV,B}} \right)$$

$$+ k_{on,V121 \cdot sR1} [V_{121}]_B [sR1]_B - k_{off,V121 \cdot sR1,j} [V_{121} \cdot sR1]_B$$

$$d[V_{165b} \cdot sR1]_B / dt = -k_{CL,V165b \cdot sR1} + \frac{k_{L,N}}{U_B} \frac{[V_{165b} \cdot sR1]_N}{K_{Av,N}} + \frac{k_{L,D}}{U_B} \frac{[V_{165b} \cdot sR1]_D}{K_{Av,D}}$$

$$+ \frac{\gamma_N \cdot S_{NB}}{U_B} \cdot \left(k_{p,sR1}^{N \to B} \frac{[V_{165b} \cdot sR1]_N}{K_{AV,N}} - k_{p,sR1}^{B \to N} \frac{[V_{165b} \cdot sR1]_B}{K_{AV,B}} \right)$$

$$+ \frac{\gamma_D \cdot S_{DB}}{U_B} \cdot \left(k_{p,sR1}^{D \to B} \frac{[V_{165b} \cdot sR1]_D}{K_{AV,D}} - k_{p,sR1}^{B \to D} \frac{[V_{165b} \cdot sR1]_B}{K_{AV,B}} \right)$$

$$+ k_{on,V165b \cdot sR1} [V_{165b}]_B [sR1]_B - k_{off,V165b \cdot sR1,j} [V_{165b} \cdot sR1]_B$$

$$d[P1 \cdot sR1]_B / dt = -k_{CL,P1 \cdot sR1} + \frac{k_{L,N}}{U_B} \frac{[P1 \cdot sR1]_N}{K_{Av,N}} + \frac{k_{L,D}}{U_B} \frac{[P1 \cdot sR1]_D}{K_{Av,D}}$$

$$+ \frac{\gamma_N \cdot S_{NB}}{U_B} \cdot \left(k_{p,sR1}^{N \to B} \frac{[P1 \cdot sR1]_N}{K_{AV,N}} - k_{p,sR1}^{B \to N} \frac{[P1 \cdot sR1]_B}{K_{AV,B}} \right)$$

$$+ \frac{\gamma_D \cdot S_{DB}}{U_B} \cdot \left(k_{p,sR1}^{D \to B} \frac{[P1 \cdot sR1]_D}{K_{AV,D}} - k_{p,sR1}^{B \to D} \frac{[P1 \cdot sR1]_B}{K_{AV,B}} \right)$$

$$+ k_{on,P1 \cdot sR1} [P1]_B [sR1]_B - k_{off,P1 \cdot sR1,j} [P1 \cdot sR1]_B$$

$$d[P2 \cdot sR1]_B / dt = -k_{CL,P2 \cdot sR1} + \frac{k_{L,N}}{U_B} \frac{[P2 \cdot sR1]_N}{K_{Av,N}} + \frac{k_{L,D}}{U_B} \frac{[P2 \cdot sR1]_D}{K_{Av,D}}$$

$$+ \frac{\gamma_N \cdot S_{NB}}{U_B} \cdot \left(k_{p,sR1}^{N \to B} \frac{[P2 \cdot sR1]_N}{K_{AV,N}} - k_{p,sR1}^{B \to N} \frac{[P2 \cdot sR1]_B}{K_{AV,B}} \right)$$

$$+ \frac{\gamma_D \cdot S_{DB}}{U_B} \cdot \left(k_{p,sR1}^{D \to B} \frac{[P2 \cdot sR1]_D}{K_{AV,D}} - k_{p,sR1}^{B \to D} \frac{[P2 \cdot sR1]_B}{K_{AV,B}} \right)$$

$$+ k_{on,P2 \cdot sR1} [P2]_B [sR1]_B - k_{off,P2 \cdot sR1,j} [P2 \cdot sR1]_B$$

Curriculum Vitae

Lindsay Clegg (née Wendel) was born in St. Louis, Missouri on March 13th, 1989. She grew up in Florissant, Missouri, attending Hazelwood Central High School, and graduating as valedictorian of her class in 2007. She then headed east to Indiana to attend Purdue University. At Purdue, along with meeting her future husband in a freshman calculus class, she studied Biomedical Engineering and minored in German. During her college summers, Lindsay participated in an academic exchange to Boğaziçi Üniversitesi in Istanbul, Turkey, worked as an intern at GE Healthcare in Waukesha, Wisconsin and built mathematical models at Roche Diagnostics in Indianapolis, Indiana. Through a combination of coursework and research, Lindsay discovered a passion for using mathematical models to understand biology and better predict optimal treatment for human disease. She dove headfirst into computational modeling and controls her senior year, under the guidance of Dr. Ann Rundell. Lindsay graduated from Purdue with highest distinction in 2011, recognized as the student commencement responder for the College of Engineering, and as the top junior across the Colleges of Science & Engineering in 2010. Following her interest in computational modeling, Lindsay joined the Biomedical Engineering PhD program at Johns Hopkins University in Baltimore, Maryland, dragging her new husband to Maryland along with her. She was immediately attracted to the Institute for Computational Medicine, where she worked under the mentorship of Dr. Feilim Mac Gabhann for six years. While Lindsay was occasionally to be found dabbling in the wet lab, her primary contributions to the fields of angiogenesis and tissue engineering are the molecularly-detailed, multi-scale models she built. This work, along with her dedication to STEM outreach through the FIRST Robotics Program, were recognized in 2017 with both a Siebel Scholarship and the Michael A. Shanoff Research Award at the Johns Hopkins Young Investigator's Day. During her PhD, Lindsay also designed and twice taught a freshman seminar course, developed curriculum on interactive visualization of large data sets for a 400-level biomedical engineering course, and spent a summer performing research at the Technische Universität München in Munich, Germany. Next, Lindsay is headed down the road to Gaithersburg, Maryland for an industry postdoc with the Quantitative Clinical Pharmacology group at AstraZeneca. She hopes to apply her computational modeling skills to new and immediately clinically-relevant problems, and to bridge her skills and knowledge between the academic and industry settings.